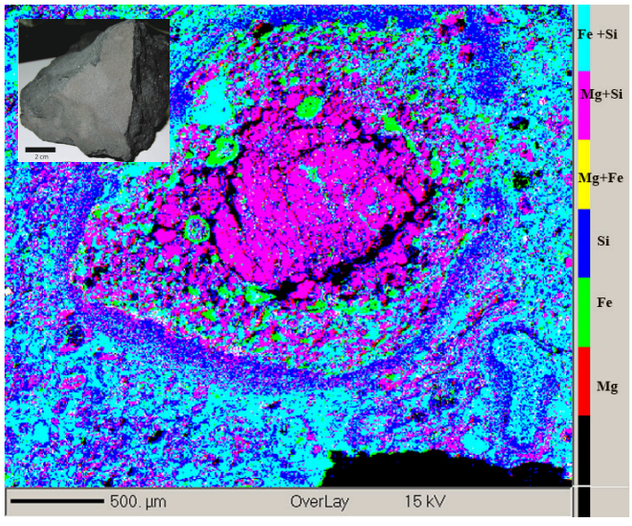
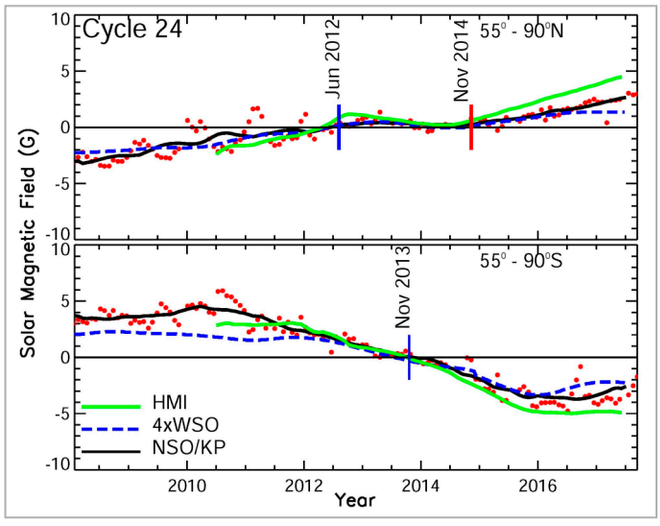
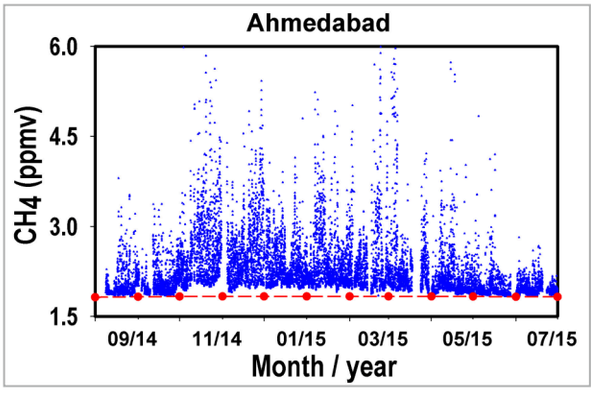
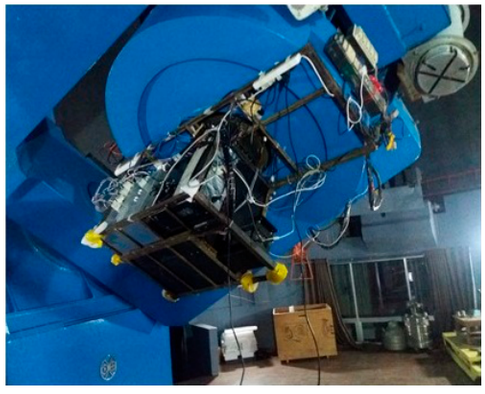
भौतिक अनुसंधान प्रयोगशाला, अहमदाबाद
Physical Research Laboratory, Ahmedabad

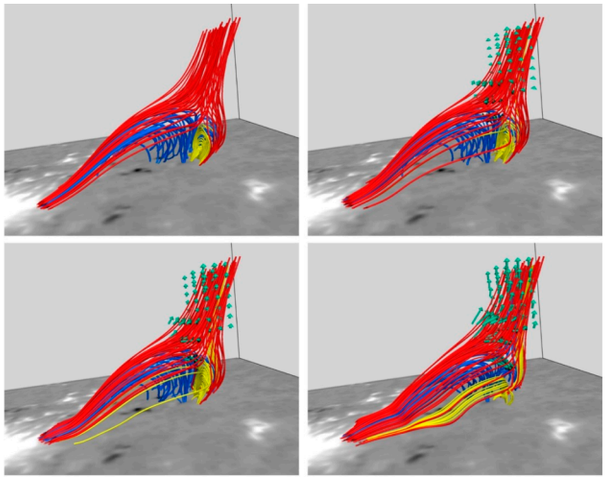


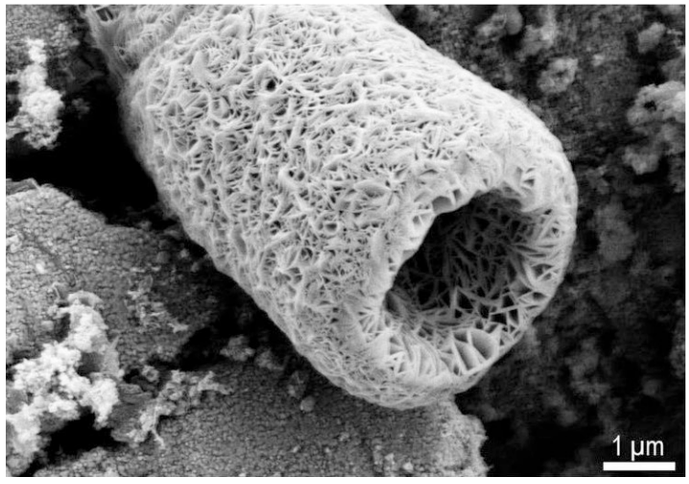












वार्षिक प्रतिवेदन
Annual Report
2018-2019



Front cover page:

Top Right Panel: Solar cycle 24: An unusual polar field reversal in the Solar Northern and Southern hemispheres

Top Left Panel: X-ray map of Fe, Mg, Si of the Mukundpura meteorite

Center Right Panel: Mt. Abu Faint Object Spectrograph and Camera-Pathfinder (MFOSC-P), a pathfinder instrument built in PRL for a bigger and more complex next generation instrument on upcoming PRL 2.5m telescope. The optics has been designed to provide 'seeing limited imaging' in astronomy standard Bessell's B, V, R and I filters

Center Middle Panel: e-CALLISTO: It is used for the observations of solar radio bursts and radio frequency interference monitoring for astronomical science, installed and operational at Udaipur Solar Observatory

Center Left Panel: Methane time series observed at Ahmedabad for the period of August 2014 to July 2015

Bottom Left Panel: Simulated dynamics of magnetic field lines for an observed coronal jet co-located with the solar active region NOAA AR 12615

Bottom right Panel: SEM image of residues obtained after shock processing of amino acid, the porous cylindrical feature, evidence for the formation of complex macrostructures when the molecular building blocks of life are subjected to impact conditions that commonly prevail in the solar system

Inside back cover pages: Events at PRL

Back cover page:

Dr. Vikram Sarabhai Birth Centenary Logo

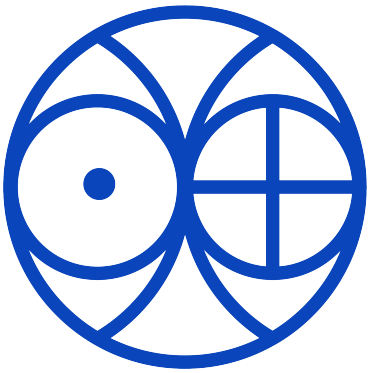
Compilation and Layout by:
Office of the Dean, PRL.

Published by:
Physical Research Laboratory, Ahmedabad.

Contact:
Physical Research Laboratory
Navrangpura
Ahmedabad - 380 009, India
Phone: +91-79-2631 4000 / 4855
Fax: +91-79-2631 4900
Email: info@prl.res.in
Website: https://www.prl.res.in/

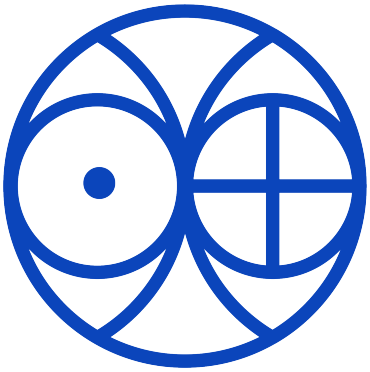
Contact

Website



Annual Report

2018 – 2019



PRL research

encompasses

the Earth, the Sun

Immersed in the fields

and radiations

reaching from and to infinity,

all that man’s curiosity

and intellect can reveal

PRL Council of Management

Three nominees of the Government of India

Shri A. S. Kiran Kumar Antariksh Bhavan, New BEL Road Bengaluru-560231	Chairman
Dr. K. Sivan, Secretary, Department of Space, Govt. of India Chairman, ISRO Bengaluru-560231	Member
Shri Anoop Srivastava, JS & FA, DoS Antariksh Bhavan, New BEL Road Bengaluru-560231	Member

A nominee of the Karmakshetra Education Foundation

Shri Kartikeya V. Sarabhai Director, Centre for Environment Education Ahmedabad-380054	Member

A nominee of Ahmedabad Education Society

Shri Sanjay S. Lalbhai Chancellor & Chairman, Board of Governors, Ahmedabad University, Ahmedabad-380009	Member

A nominee of the Govt. of Gujarat, Gandhinagar

Smt. Anju Sharma, I.A.S. The Principal Secretary, Higher and Technical Education Government of Gujarat, Gandhinagar	Member

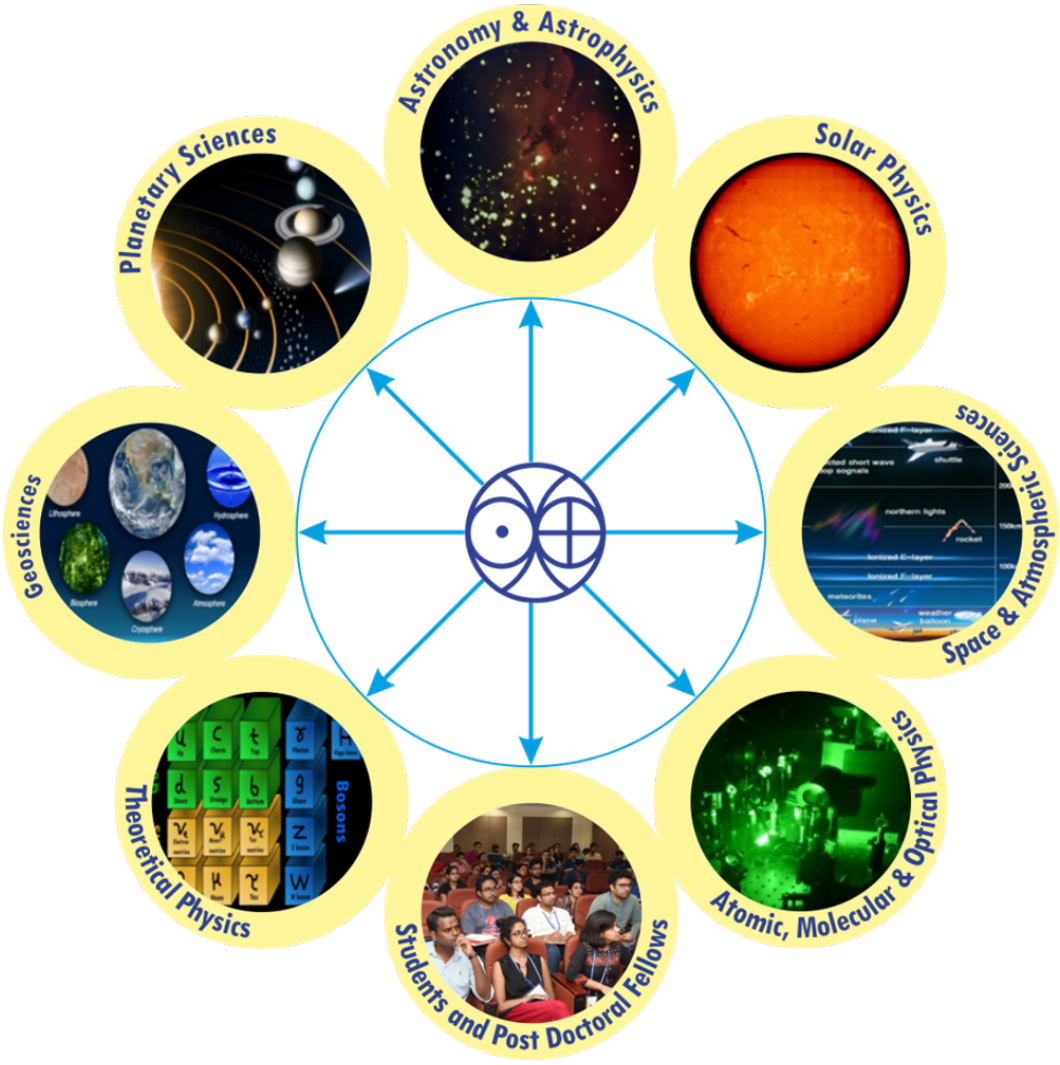
Director, Physical Research Laboratory

Dr. Anil Bhardwaj	Member (Ex-Officio)

Registrar, Physical Research Laboratory

Mr. C. V. R. G. Deekshitulu	Member (Ex-Officio)

Areas of Scientific Research and Activities



Contents

PRL Council of Management . . . i
From The Director's Desk . . . 1
Decadal Scientific Review of PRL . . . 3
PRL in News . . . 4
Science Highlights . . . 5
Awards and Honors . . . 11
Recognition, Best paper & Thesis awards . . . 13
Human Resource Development . . . 17
Ph.D. Awarded . . . 19
Colloquia/Public Lectures by Visitors . . . 20
Conference/Symposium/Workshop organized by PRL . . . 21
Invited Talks at Conferences / Symposia / Workshops . . . 22
Lectures at Universities / Institutions . . . 28
Science Outreach Talks by PRL Scientists . . . 30
Area Seminar by visitors . . . 31
Student Training . . . 32
Division Visitor Details . . . 36
Science . . . 38
- Astronomy and Astrophysics . . . 38
- Solar Physics . . . 57
- Planetary Sciences . . . 66
- Space and Atmospheric Sciences . . . 98
- Geosciences . . . 112
- Theoretical Physics . . . 129
- Atomic, Molecular and Optical Physics . . . 134

Publications . . . 141
- Journals . . . 141
- Proceedings of Conference/ Symposia/ Workshops . . . 149
- Books Edited / Review Articles / Other Publications . . . 152

Papers Presented in National/ International Conferences . . . 153
Various Events, and Outreach Activities at PRL . . . 160
Capacity Building Programmes . . . 168
Official Language promotion at PRL . . . 169
Facilities and Services . . . 170
Honorary Fellows & Faculty . . . 177
PRL Faculty . . . 178



From The Director's Desk

As I write this in 2019, I am reminded of the fact that 12 August 2019 is an important landmark in the history of PRL as it is the birth centenary of our Founder Prof. Vikram Sarabhai – who established both PRL and ISRO. This is therefore an opportune time to look back and reflect on scientific achievements and to chart a future course for PRL that will be in keeping with Prof. Sarabhai's vision of PRL conducting research at the cutting edge of the frontiers of the fields. Hence, the year 2019 began with a thorough scientific review of PRL covering the scientific achievements in the past decade by 15 eminent scientists of high stature and global repute from leading research institutes and well-known centre of excellence across the world. The research highlights achieved were deliberated threadbare and a road map for research during the next decade was laid out. The reviewing experts had a high opinion about the quality of research in PRL, which can be summarized in their own words as "The PRL science and technology is of the highest level, when compared to similar institutions on a global scale. The scope of the research is breathtaking. The engagement and training of junior scientists and students is superb".

Over the last one year, PRL has produced close to two hundred research publications in high impact peer-reviewed journals, and 10 PhD theses apart from contributing very significantly to development of payloads for Chandrayaan-2 mission, and the upcoming Aditya-L1 and future space and planetary missions. The level of commitment displayed by the PRL faculty and staff in carrying out research and societal obligations through producing high quality space-borne experiments, in-house instrumentation, detailed laboratory analysis, along with intense academic and scientific programs has been recognized through several awards and honours that they have received. Several PRL research scholars have also received awards for their presentation in national and international scientific conferences, and won best thesis award. PRL faculty have received more than two hundred invitations to give lectures at conferences, symposia, workshops, and other academic and research institutions. For me, this is a matter of great pride and honour to be heading such a committed and talented group of researchers.

Several new and vital scientific findings have been obtained and a good progress has been made in the establishment of a new 2.5m telescope facility at Mt. Abu, along with the development of appropriate back-end instruments. One of the major scientific highlights of the year was a study that has established that Giant flares took place from the embryonic Sun. Such super-flares has been calculated to be about a million times stronger in intensity compared to the highest X-class flare observed from the modern Sun.

The periodic solar polar field reversal that occurs at every solar maximum displayed an unusual and probably unprecedented pattern of reversal during the ongoing solar cycle 24, with the solar northern hemisphere reversing polarity 2.5 years after the southern hemisphere. Signatures of this unusual field reversal were also clearly identifiable in the solar wind. A study of the effects of the declining solar wind dynamic pressure has shown that the Earth's magnetosphere has expanded outward by one Earth radii since 1995, when solar polar fields began to decline. In other study, on the basis of near-Sun flux rope properties obtained from observational parameters, an analytical model has been developed for predicting the magnetic field vectors of coronal mass ejections at 1 AU. This shows promising results in forecasting of the southward component of the interplanetary magnetic field Bz and hence useful for the space weather prediction.

The building blocks of life, amino acids and nucleobases, are believed to have been synthesized in the extreme conditions that prevail in space starting from simple molecules containing hydrogen, carbon, oxygen and nitrogen. Work at PRL has established, for the first time, that shock processed amino acids and nucleobases tend to form complex macro-scale structures. This discovery suggests that the building blocks of life could have polymerized not just on Earth but on other planetary bodies. Further, microbial survivability in the Mukundpura meteorite impact crater has been studied, by recreating the condition using a low-intensity shock tube. The microbes isolated from a rock taken from the impact crater were subjected to conditions similar to that of impact. Microbes were observed to survive the impact and this is the first work carried out on microbial survivability on a fresh impact crater.

Near IR observations of star forming molecular clouds, using large telescope facilities across the globe, have strongly supported the cloud-cloud collision hypothesis for the formations of massive OB stars ($>$ 8 MSun). The first-overtone carbon monoxide emission in near infrared K-band spectrum was discovered in supernova SN2016adj at 58.2 days after its initial appearance, one of the earliest detections of CO in an erupting supernova. Detailed modelling of the CO emission provided the first constraint on the 12C/13C ratio determined from near-infrared observations. Broadband timing and spectral studies of X-ray pulsars GX 1+4 in 2015 October have revealed a spin period of 176.778 s, the highest values since its discovery. The phase-resolved spectroscopy showed a strong blackbody emission component in a narrow pulse phase range, which is interpreted as the origin of the peculiar peak in the pulse, profiles below 25 keV.

Global ocean circulation has undergone major changes during glacial and interglacial periods. Radiocarbon ages of planktonic and benthic foraminifera species has revealed that Indian Ocean show changes which establish a slowing down of global deep-water circulation.

Geological evolution of Grimaldi Basin on the Moon has been deciphered using remote sensing datasets from Chandrayaan-1 M3, and LRO-WAC, NAC. It has been found that the basin was experiencing volcanism and tectonic activities during the Copernican period. Thus, late stage volcanism on the Moon has a greater spatial span than understood earlier. Long term (4.5 years) ground-based high spectral resolution measurements of OH and O_2 nightglow emission intensities and corresponding temperatures from Gurushikhar, Mt. Abu, obtained using in-house developed near-infrared imaging spectrograph have been used to study the upper mesospheric temperature inversions (MTIs). Investigation of causative mechanisms for the upper MTIs revealed that although both breaking of vertically propagating gravity waves and chemical heating by the exothermic reactions do work together, the in situ chemical heating process seems to be more effective as compared to the vertical transport of energy from lower below.

Researchers at PRL have explored the synergy between the proposed atmospheric neutrino experiment INO and long baseline experiment ESSνSB. The later experiment is designed for discovering CP violation in lepton sector with high sensitivity. We have shown how the hierarchy sensitivity of ESSνSB can be enhanced by adding data from INO and ongoing experiments T2K and NOνA. Models of neutrino mixing were explored at the proposed long baseline experiments DUNE, T2HK and T2HKK and model correlations between the unknown parameters namely 2-3 mixing angle of neutrinos and the CP phase were tested.

A few selected highly charged ions, such as Ni^{12+}, Cu^{13+}, Pd^{12+}, and Ag^{13+}, are investigated and they are proposed for making very accurate optical clocks with the fractional uncertainties below 10^{-19} level. To support the recently developed multi photon ionization technique by laser ablation process, we carried out very accurate calculations of hyper fine structure constants of the 113, 115 in isotopes and combining these calculations with the measurements nuclear magnetic and quadrupole moments of these isotopes were inferred.

In its responsibility towards popularization of Science, PRL has always put its best foot forward. About 900 students participated in the World Space Week celebrations at USO-PRL during 8-9 October 2018. In addition, PRL celebrated National Science Day on 2 March 2019 by conducting various competitive events for students selected through a screening test conducted on 20 January 2019. Five students were awarded the Aruna Lal Fellowship selected through personal interview. Importantly, this year the screening test was both in online and offline mode with the aim to facilitate student participation without having to travel to distant exam centres. Additionally, to popularize girl child education PRL invited 151 girl students from schools across Gujarat to PRL.

As a part of societal commitment and capacity building, PRL contributes by providing highly skilled researchers through its vibrant Doctoral and Post-Doctoral programmes. In addition, PRL conducts a Visiting Scientist programme for university teachers, and project training for graduate and post graduate students in both engineering and science to conduct long-term project work. PRL organizes intensive summer programmes for students as well as college and university teachers every year and also partake through its association with similar programmes conducted by the Indian Science Academies. More than sixty graduate and undergraduate students participated this year in the PRL Summer Research Programme. PRL is entrusted with the responsibility of conducting United Nations CSSTEAP course on Space and Atmospheric Sciences for the Asia-Pacific region. The eleventh course with 15 students completes on 30 April 2019. PRL continues its strong academic association with many universities and institutes in Gujarat and all over the country.

The 15^{th} International Symposium on Equatorial Aeronomy (ISEA-15) was hosted by PRL during 22–26 October 2018, which was attended by about 200 delegates from around the world. PRL also hosted the 84^{th} Anniversary General Meeting of INSA during 26-28 December 2018 where about 250 participants gathered for the meeting. Other major meetings organized by PRL include SCOP, YAM, ISRO-STP, YPM, and Conference on Condensed Matter Physics. PRL also contribute in a big-way in the organization of several national and international meetings.

PRL ensures use of Hindi in all areas of administration and official communications and takes adequate steps in this direction. The website of PRL is bilingual. Work done at PRL in implementation of Hindi in various domains has been recognized by the Town Official Language Committee and DOS.

I am indebted to all the members of the PRL Council for their constant encouragement, invaluable advice and whole-hearted support for all the scientific activities pursued at PRL. In particular, I am grateful to Shri A. S. Kiran Kumar, Chairman, PRL Council, and Dr. K. Sivan, Chairman, ISRO and Secretary Department of Space for their sage advice, unstinted support and encouragement.

Anil Bhardwaj

Director

Decadal Scientific Review of Physical Research Laboratory

15-18 January, 2019

The Decadal Scientific Review of PRL was conducted during 15-18 January, 2019 at PRL, Ahmedabad. The decadal review is one of the most important organizational events of PRL in which the scientific performance during the past one decade is evaluated by the top-class scientists of respective disciplines and road map for research during next one decade is deliberated. Since the decadal review is the most significant evaluation activity, it was directly coordinated by Chairman, PRL Council of Management, who also chaired the Decadal Review Committee. The Decadal Review process was executed and organised by Director, PRL under the guidance of Chairman, PRL Council of Management.

This decadal review was conducted by 15 eminent scientists of high stature and global repute, invited from different countries as reviewing experts. These scientists belonged to leading research institutes and well-known centre of excellence in science from USA, Spain, Switzerland, Sweden, Taiwan, France, Italy and India. There were two experts from each of the seven disciplines pursued in PRL. The chairman of ADCOS, ISRO/DOS was also one of the reviewers. Each scientific area had prepared composite Decadal Scientific Report covering important scientific results obtained during last one decade. This scientific report was submitted to the experts in advance for their study and review.

The entire decadal review was comprehensively organized in the following eight segments.

1. An inaugural close-door meeting of Chairman, PRL Council of Management and the Director, PRL with experts and all Division Chairpersons.

2. Visit of all experts to all major laboratories of PRL to see the facilities to interact with scientists, engineers, students and PDFs.

3. Detailed scientific presentations by each scientific area before the experts of concerned fields.

4. Presentation of Overview of each scientific area to all the experts of different fields

5. Open feedback of experts in presence of all scientists.

6. Informal interaction of scientists with experts over a dinner.

7. A close-door feedback meeting.

8. Confidential Report writing session for experts

With a view to showcase typical cultural and architectural heritage of the Ahmedabad City, which is the UNESCO's first World Heritage City in India, a coordinated heritage walk was organised for the experts.

Excerpts from PRL Decadal Review Experts' Comments

"The PRL science and technology is of the highest level, when compared to similar institutions on a global scale. The scope of the research is breathtaking. The engagement and training of junior scientists and students is superb."

"PRL has an impressive array of new programs and advanced facilities that are attractive to the research community. PRL researchers are regularly making important new discoveries and breakthroughs as a result of exciting experimental and theoretical science programs."

"PRL is bustling with an impressive array of activities in theory, modeling, and observations from space and ground, a truly physical research institute."

"We wish to congratulate the staff of PRL on the breadth and depth of all the research being done in all disciplines. We are glad to see the emphasis is still on basic, curiosity-driven science at PRL, though we also note that there is a mix, a good balance, between this and more immediately societal-relevant research."

"PRL is unique not just because of the excellence in various scientific fields it has chosen to advance but also in its dual role as a national laboratory (under Department of Space) and a - training ground of young talents for the new generation of planetary science and space exploration."

"The PRL group has successfully developed a world class high resolution spectrograph (PARAS) with capability of measuring radial velocity to a precession of around one meter which is a very creditable achievement."

PRL in News

1. Sun's reversed polarity field may affect Earth's climate. An international team including scientists from the Physical Research Laboratory in Ahmedabad, Gujarat, detected the unusual pattern of reversal of magnetic fields in the Sun during the ongoing 11-year solar cycle. [Ref: Janardhan, P. et al. Solar cycle 24: an unusual polar field reversal. Astron. Astrophys. 618, A148 (2018)] They showed that the Sun's southern hemisphere reversed its polarity in mid-2013 whereas the reversal of the field in its northern hemisphere occurred 2.5 years later, after a sustained period of near-zero field strength. 10.1038/nindia.2018.153. News: Nature India

2. Martian dust detector: Scientists from the Physical Research Laboratory in Ahmedabad, India, have invented a prototype device that contains a target material made of a gold plate and different electronic components. [Ref: Pabari, J. P. et al. Orbital altitude dust at Mars, its implication and a prototype for its detection. Planet. Space. Sci. 161, 68-75 (2018)]. 10.1038/nindia.2018.111. News: Nature India

3. How spacecraft landings damage the Moon's surface: Scientists from the Physical Research Laboratory in Ahmedabad, India, assessed the spacecraft-landing-induced lunar surface damage by numerically evaluating the hovering time and altitude of a spacecraft, and the velocity and mass of the dust particles that it ejects during landing. They found that the hovering time determines the extent of damage done to the surface. The ejected mass of dust increases by almost three times as the hovering duration increases from 25 seconds to 45 seconds. [Ref: Mishra, S. K. et al. Numerical evaluation of surface modifications at landing site due to spacecraft (soft) landing on the moon. Planet. Space. Sci.156, 57-61 (2018)]. 10.1038/nindia.2018.89. News: Nature India.

4. The first results and performance of PRL's Accelerator Mass Spectrometer facility has been published in Current Science & Nuclear Instruments and Methods in Physics Research B. It is a matter of pride for PRL, Dr. Ravi Bhushan and his team that the February 10, 2019 issue of Current Science featured an image of the PRL AMS instrument on its cover page. The Link to the Paper published in Nuclear Instruments and Methods on Physics Research B is available through link https://doi.org/10.1016/j.nimb.2018.12.003

5. Super flares in Nascent Sun: Evidence from Meteorites: Scientists at Physical Research Laboratory, Ahmedabad working in collaboration with University of Heidelberg, Germany, have recently reported Giant flares from the embryonic Sun. The super-flare has been calculated to be about a million times stronger in intensity compared to the highest X-class flare observed from the modern Sun. The work is published in Nature Astronomy -https://www.nature.com/articles/s41550-019-0716-0 and also as ISRO story of the week https://www.isro.gov.in/super-flares-nascent-sun-evidence-meteorites.

6. Research paper "A comparative study of the eruptive and non-eruptive flares produced by the largest active region of solar cycle 24" highlighted in HMI Science Nugget (http://hmi.stanford.edu/hminuggets/?p=2333) by HMI Science Team.

Science Highlights

Astronomy and Astrophysics

- The Sun, like the earth, has a magnetic field with magnetic poles. However unlike the earth's magnetic field, which reverses or flips polarity over tens of millennia, the Sun does so every 11 years, at a time when its sunspot number peaks or the solar cycle reaches its maximum amplitude. Predicting the strength or amplitude of the oncoming or next solar cycle, is a complex task involving a deep understanding of how the Sun and the so called solar dynamo, that generates solar magnetic fields, behaves. We have discovered an unusual pattern in the reversal of solar magnetic fields during the ongoing solar cycle. Analysing solar activity during the past four solar cycles, we have detected an unusual and probably unprecedented pattern of reversal of magnetic fields in the poles of the Sun during the ongoing solar cycle 24. It has been shown that the Sun's southern hemisphere reversed its polarity in mid-2013 whereas, the reversal of the field in its northern hemisphere started in 2012, was followed by a sustained period of near-zero field strength for 2.5 years, lasting till the end of 2014 before it finally reversed polarity. Such an asymmetry in the reversal times of the two hemispheres is probably unprecedented since solar observations first began about 400 years ago. In combination with declining solar fields, this suggests that the onset of a Maunder like solar minimum is probably underway. Signatures of this unusual field reversal were also clearly identifiable in the solar wind.

- Massive OB stars ($\geq$ 8 $M_{\odot}$) are the major and ultimate sources of mechanical and radiative energy in galaxies, which are produced from their birth until their death. The understanding of the formation processes of such stars is still one of the outstanding topics in star formation research. In recent years, to explain the origin of massive stars and young clusters, a cloud-cloud collision process has been proposed as an interesting alternative against the existing competing theories of massive star formation (i.e. "Turbulent core accretion" and "Competitive accretion"). The cloud-cloud collision process has ability to trigger massive OB stars and young stellar clusters at the junction of molecular clouds. We found the observational signatures of the cloud-cloud collision in two Galactic star-forming regions, which are IRAS 18223-1243 and bubble N36. In both these sites, we investigated two molecular clouds along the line of sight, which are physically connected in both space and velocity. In the bubble N36, a complementary fit between the blueshifted and redshifted clouds was found, which indicates the interaction of these two clouds. In both these sites, we find that the collision of the molecular clouds seems to be occurred in the past, and may have influenced the birth of embedded protostars and massive stars.

- The birth of massive stars ($\geq$ 8 $M_{\odot}$) is still an open research question in astrophysics. In this context, we investigated the inner- and large-scales physical environment of a promising young massive protostar candidate in a star-forming site IRAS 17008-4040 (distance $\sim$2.4 kpc). In the IRAS site, an infrared counterpart of the 6.7 GHz methanol maser emission is identified, and is not associated with any radio continuum emission at GMRT 1.28 GHz, confirming its earliest stage in massive star formation. Based on the ESO-VLT/NACO adaptive-optics image at 3.8 μm (resolution $\sim 0''.1$), the source IRcmme is resolved into two objects (i.e. IRcmme1 and IRcmme2) within a scale of 900 AU that are found to be associated with the Atacama Large Millimeter/submillimeter Array (ALMA) core G345.50M. Considering the separation between IRcmme1 and IRcmme2 (i.e. $\sim$900 AU), the core fragmentation process is likely mechanism for these sources in the IRcmme system. We find that the source IRcmme1 is a rare accreting massive protostar candidate before the onset of an ultracompact Hii region.

- Understanding the role of filaments in the formation of dense star-forming clumps and the feedback of massive OB stars ($\geq$ 8 $M_{\odot}$) in their vicinity are still open research topics in the area of star formation. In this connection, we performed a detailed multi-wavelength study of a star-forming site S234,

which contains filaments and several massive OB stars. In the site S234, two filaments (i.e. ns1 and ns2) are identified as thermally supercritical. An extended temperature structure at 27-30 K surrounds a relatively cold ($\sim$19 K) $\sim$8.9 pc long filament ns1. At least four condensations (M_{clump} $\sim$70–300 $M_{\odot}$) are seen in ns1, and are devoid of the radio continuum emission at GMRT 610 MHz. The filament ns2 hosting clumps is devoid of ongoing star formation, and could be at an early stage of fragmentation. An intense star formation activity, having the star formation efficiency $\sim$3.3% and star formation rate $\sim$40–20 $M_{\odot}$ Myr^{-1}, is observed in ns1. We find that the feedback of massive stars in S234 seems to explain the observed star formation in the filament ns1.

- It is widely accepted that stars do not form in isolation and about 70-90% of the stars form in clusters. However recent $Spitzer$ observations have shown that a significant fraction of stars do form in isolated mode. The origin of this distributed mode of star formation is unclear. In a recent work, we investigated clustered and distributed modes of star formation in a massive star forming cloud complex. Using mid-infrared 24 micron observations we found 50% of the newly formed protostars to be isolated. We found these protostars are located at the tips of elephant trunks or pillars like structures present in the complex. These structures are long column of cold gas and dust with their tips pointing toward the older generation massive stars of the complex. We identified 38 such structures in the region and found that a majority of which consist of one or a few low-mass protostars at their tips. We suggest that in massive star forming environment, radiation and winds from the old generation massive stars results in such structures and star formation in such structures can be induced by the compression of the cold material to dense clumps and cores, which eventually fragments to form new stars. We argued that star formation in small-scale structures such as pillars, elephant trunks, or globulettes is likely an important ingredient for the formation of isolated low-mass stars and one of the viable mechanisms for forming isolated low-mass stars in molecular clouds.

- A comprehensive timing and spectral studies of accretion powered X-ray pulsar 2S 1417-624 has been carried out by using all RXTE observations during a giant outburst in 2009. Pulsations were detected in the light curves obtained from all epochs of observations. The pulsar was found to be spinning-up during the outburst. The pulse profiles were observed to be strongly dependent on photon energy and luminosity. A double-peaked profile at lower luminosity evolved into a triple-peaked profile at the peak of the outburst which is further reverted back to a double-peaked structure during the decay of the outburst. An anticorrelation was also observed between the pulse fraction and the source flux. The 3-70 keV energy spectrum of pulsar was well described with a power law modified with high-energy cut-off model along with an iron line at 6.4 keV. Based on the evolution of pulse profile, pulse fraction, and spectral parameters across observed luminosity, we interpreted our results in terms of changes in the pulsar beam configuration from sub-critical to super-critical regimes.

- Broad-band timing and spectral studies of X-ray pulsars provide important information regarding the geometry, magnetic field and emission mechanism of the neutron star in the binary systems. NuSTAR and Swift observations of GX 1+4 in 2015 October, during an intermediate-intensity state, were used to study the properties of the pulsar. The measured spin period of 176.778 s is found to be one of the highest values since its discovery. In contrast to a broad sinusoidal-like pulse profile, a peculiar sharp peak is observed in profiles below 25 keV. Broad-band energy spectra of GX 1+4, obtained from NuSTAR and Swift observations, are described with various continuum models. Among these, a two-component model consisting of a bremsstrahlung and a blackbody component is found to best fit the phase-averaged and phase-resolved spectra. Physical models are also used to investigate the emission mechanism in the pulsar, which allows us to estimate the magnetic field strength to be in (5-10)$\times10^{12}$ G range. Phase-resolved spectroscopy of NuSTAR observation shows a strong blackbody emission component in a narrow pulse phase range. This component is interpreted as the origin of the peculiar peak in the pulse profiles below 25 keV.

- A total of 110 ks $Chandra$ observations of the bright FRII radio galaxy 3C 320 showed a pair of huge X-ray cavities at an average distance of $\sim$38 kpc along East and West directions from the center of the galaxy. The cavity energy, age and total power are estimated to be 7.7$\times10^{59}$ erg, 7$\times10^{7}$ yr and 3.5$\times10^{44}$ erg s^{-1}, respectively. The cooling luminosity within the cooling radius of 100 kpc was found to be L_{cool} $\sim$ 8.5$\times10^{43}$ erg s^{-1}. Comparison of these two estimates (total cavity power and cooling luminosity) implies that the cavity power is sufficiently high to balance radiative loss. A pair of weak shocks with Mach numbers of 1.6 and 1.8 has also been detected at distances of 47 and 76 kpc surrounding the radio bubbles. A sharp surface-brightness edge was also detected at a relatively larger radius ($\sim$80 kpc) along the south direction. The far-infrared luminosity yielded a star formation rate of 51 $M_{\odot}$ yr^{-1}, which is a quarter of the cooling rate.

- Narrow-line Seyfert 1 galaxies (NLS1s) are a subclass of active galactic nuclei (AGN) and are generally considered to be radio-quiet. We made one of the first attempts to probe the nature of kilo-parsec (kpc) radio emission in NLS1s using the largest sample of 11000 optically-selected NLS1s. Our study based on GMRT and VLA radio surveys showed that the radio detection rate of NLS1s is merely 5 percent. But the use of largest sample resulted the largest sample of radio-loud NLS1s. Notably, our sample of 407 RL-NLS1s shows that the RL-NLS1s are much more common than thought earlier. We also found that the radio jets in NLS1s are either in the early evolutionary phase or possibly remain confined within the nuclear region due to low-power or intermittent AGN activity.

Solar Physics

- A new observing facility-Compound Astronomical Low cost Low frequency Instrument for Spectroscopy and Transportable Observatory (CALLISTO) has been set up at USO to observe the Sun in radio wavelengths. CALLISTO is a radio spectrograph operating in the range between 45–870 MHz with a frequency resolution of 62.5 KHz which will be useful to monitor the solar origins of space weather.

- Analysis of high resolution magnetograms and Dopplergrams during an observed M-class flare provides evidence that the transient Lorentz forces associated with the abrupt changes in the magnetic fields could drive the localized oscillations in the active region. This is important for the transport of wave energy to the higher solar atmospheric layers.

- Multi-wavelength analysis of the largest solar flare of the solar cycle 24 that occurred on September 6, 2017 showed that magnetic reconnection responsible for the flare, occurred at two coronal heights which was manifested by two sets of well-separated flare-ribbons.
- Role of Alfvén wave in the heating of coronal loop of more than a million degree temperature is explored. For the purpose, electron number density, temperature and velocity amplitude of Alfvén wave i.e. non-thermal velocity along the coronal loop were calculated using the spectroscopic techniques. The study shows that Alfvén wave carries sufficient energy to heat the coronal loop and also provides the spectroscopic evidence of damping of Alfvén wave along the loop.
- Using Proba2 mission observations, the evolution of a coronal cavity from quiescent to eruptive phase in association with a CME was studied. The results reveal that the decay-index value at the cavity centroid height can be used as a good indicator to predict the eruption of the cavity in context of torus instability.
- Analysis of the source region of a major geo–effective CME on June 21, 2015 suggests tether cutting reconnection as the primary trigger behind two M–class flares which led to two consecutive CMEs whose interaction led to a strong geomagnetic storm at the Earth.
- On the basis of near-Sun flux rope properties obtained from observational parameters, an analytical model has been developed for predicting the magnetic field vectors of CMEs at 1 AU. This shows promising results in forecasting of the southward component of the magnetic field Bz and hence useful for the space weather prediction.
- A data-constrained MHD simulation of a coronal blowout jet was performed which highlights the role of complex magnetic topology in the form of 3D nulls and magnetic flux ropes in the initiation of coronal jet.
- The investigation of mass loss from the Sun via solar wind and CMEs for two solar cycle (SC) 23 and 24 suggests a decrease in solar wind mass rate, CME mass loss rate, X-ray luminosity and sunspot number for the SC24 as compared to the values for the SC23. The study also shows that X-ray luminosity is a better proxy of CME mass loss rate over the solar cycle than the sunspot number. These results will be helpful to understand the mass loss from other solar-type stars.

Planetary Sciences

- We have studied the effects of dust storms on the electron density profiles in the magnetic anomaly regions of Mars. We identified strong oblique echoes from MARSIS instrument aboard the Mars Express (MEX) on four days in the year 2007. From the echo on 15^{th} July 2007, maximum electron density of 3.75 $\times 10^5$ cm^{-3} at $\sim$ 88 km was estimated. The causative mechanism of these oblique echoes were studied, it was found that they were observed at the initial phase and during the progression of a planet-encircling dust storm in Martian year 28.
- Convective vortices can lift dust on Mars thereby contributing to the total dust loading the atmosphere, as seen for example in large dust storms. We identify 91 short ($\sim$15 s) pressure drops ($\geq$0.3 Pa) that likely indicate the passage of convective vortices or dust devils in the data measured by the Environmental Monitoring Station on board the Mars Science Laboratory. Our estimates of the tangential wind velocities are well below the Martian dust lifting threshold, indicating that dust lifting may not have occurred by tangential winds alone.
- The first observational evidence for the transport of the solar wind protons scattered from the lunar magnetic anomaly (LMA) into the near wake region from SWIM/Sub-keV Atom Reflecting Analyzer (SARA) aboard Chandrayaan-1 is reported. Using our back-tracing model, the source region of these protons is found to be the large Lunar Magnetic Anomaly (LMA) at South Pole-Aitken basin on the dayside, suggesting that these are solar wind protons forward-scattered from LMA at the South Pole-Aitken.
- Lunar craters with uplifted central region/convex up floor are classified as domical craters. Only 16 craters are present on Moon, and their distinctive uplift revealed a new perspective about the presence and characteristic of intrusion processes. The chronological analysis suggested that domical formation peaked during Imbrium epoch and spreads from Pre-Nectarian to Eratosthenian epoch.
- Geological evolution of Grimaldi Basin on the Moon has been deciphered using remote sensing datasets from Chandrayaan-1 M3, and LRO-WAC, NAC. It has been found that the basin was experiencing volcanism and tectonic activities during the Copernican period. Thus, late stage volcanism on the Moon has a greater spatial span than understood earlier. KREEP may not be essential for producing the magma during the Copernican time.
- We have conducted geomorphic investigation utilizing the HiRISE images of the gullies formed inside the craters emplaced mid to high latitudes on Mars. Our study suggests that liquid water played a major role in formation of Martian lobate deposits and gullies vis-a-vis the present-day dry processes may not hold explaining the formation and evolution of entire string of gullies on Mars.
- Lunar feldspathic meteorites offer a global representation of lunar crust and provides an insight into the origin and evolution of primordial crust. Analysis of pristine lunar anorthositic meteorite - Dhofar 081 suggests its formation by serial magmatism, a process not consistent with the popular global magma ocean model. The parent magma of the Dhofar 081 envisaged a low-SiO_2 (40-47 wt$\%$) melt generated during partial melting of the lunar chondritic precursor and therefore involves complex magmatic process.
- The eucrite meteorites Vissannapeta and Piplia Kalan have been studied to find the cosmic ray exposure age and to understand signature of trapped gases. Distinct nitrogen components and depletion of halogens is observed in the eucrites. The HED meteorites contain extraneous components along with an evolved component of indigenous Vesta. Short ^{40}Ar ages support the gas loss during a thermal event in the history of eucrites.
- Lightning is a transient electrical discharge occurring in planetary atmosphere, which generates optical, electromagnetic and acoustic signals. A theoretical model is developed for calculating the Schuman Resonance profiles of modes l=1, 2 and 3 in the non-homogeneous, surface-ionosphere cavity, during a major dust storm in the Martian Year 25. It is found that lightning can occur within the

accumulated dust layer at ∼20-30 km altitudes. In addition, we have proposed an instrument to study the lightning on Venus in ELF-VLF frequency range. A laboratory model for the same has been developed and demonstrated working successfully for natural lightning on Earth.

- We have numerically investigated the disturbance caused to the lunar surface during soft landing and its effect on the lander subsystems and surroundings. This work gains significance in view of the upcoming landing of Chandrayaan-2 Vikram Lander. Results show that the blown out dust due to landing may have less impact on the lander sub-systems and operations of the lander. For the present configuration of Chandrayaan-2 landing, it is expected that a total of ∼7-10 kg of mass would be ejected during the landing which could disturb a surface upto 4 m^2 thereby removing surficial layer of ∼1.5 mm to 2 mm in the vicinity.

Space and Atmospheric Sciences

- Surface and column aerosol characteristics were strongly influenced by atmospheric dynamics and meteorology over urban region. Clear days or low aerosol amount days were marked with a smaller mixed-layer height, positive vertical velocity and higher aerosol scale height (>3 km), while hazy/smoky days were marked with a greater mixed-layer height, negative vertical velocity and lower aerosol scale height (≈1 km).
- Study revealed that externally mixed and internally core-shell mixed refractory black carbon aerosol population decrease with the increase in particle size while the trend reversed for the nonrefractory aerosol over an urban region. Aerosol population near 100 nm has relatively equal number of refractory and nonrefractory particles but the populations differ below and above 100 nm. Particles below 100 nm show different mixing trend compared to higher size ($\geq$ 100 nm) particles. These results highlight that particles near 100 nm size could be a barrier for equilibrium mixing of refractory and nonrefractory aerosol populations.
- Measurements of an important class of VOCs namely biogenic-VOCs (BVOCs) were made using a high resolution and high sensitivity proton-transfer-reaction time-of-flight mass spectrometer (PTR-TOF-MS) at an urban site of Ahmedabad during winter-to-summer transition period. Contributions of biogenic emissions from local vegetation to ambient levels of BVOCs during winter-to-summer transition period were estimated at a semi-arid urban site in India. It was found that the contributions of biogenic sources to monoterpenes increased from ∼31% in February to ∼67% in March implying global warming can significantly affect air quality through temperature stress related biogenic emissions.
- The first study over the semi-arid region focusing on the occurrence frequency of clouds, their seasonal variability and dynamics has been carried out using continuous measurements from ground-based ceilometer (Lidar) over Ahmedabad. Although, the annual cloud occurrence frequency is found to be around 64%, not many of the clouds observed are precipitating in nature. Multi-layer clouds are present during the southwest (SW) monsoon period which can modulate the net surface rainfall in this region.
- The sudden stratospheric warming (SSW) is generally found to be prominent in the winter Northern hemisphere. However, a strong SSW event occurred in the Southern hemisphere in September 2002. The reasons for such occurrence and the dynamical condition of the atmospheric regions during that event were investigated which illustrate the dominant tide-planetary (quasi-16-day) wave interaction supported by the migrating diurnal tide (DW1) and nonmigrating semidiurnal tide (SW1) during that warming episode.
- Long term (4.5 years) ground-based high spectral resolution measurements of OH and O_2 nightglow emission intensities and corresponding temperatures from Gurushikhar obtained using in-house developed near-infrared imaging spectrograph have been used to study the upper mesospheric temperature inversions (MTIs). Investigation of causative mechanisms for the upper MTIs revealed that although both gravity wave breaking of vertically propagating gravity waves and chemical heating by the exothermic reactions do work together, the in situ chemical heating process seems to be more effective as compared to the vertical transport of energy from lower below.
- A new approach by monitoring the isoelectron density contours are monitored as a function of time, wherein, vertical propagation of gravity waves, if any, shows up clearly enabling unambiguous information of propagation of gravity waves. Other radio method, such as the incoherent scatter radar can also be used to investigate this. However, there is only one incoherent scatter radar available over the dip equatorial region over the south American sector. Therefore, this method using digisonde measurements provides an easy effective and inexpensive (as compared to incoherent scatter radars) way to investigate the vertical propagation of gravity waves.
- Equatorial electrodynamics plays a crucial role in governing the large-scale equatorial and low-latitude phenomena and hence its determination assumes enormous importance. The vertical plasma drifts. which are direct consequence of equatorial electric fields, have been conventionally measured using ground-based incoherent scatter radars, however, such information is sparse. Using an indirect approach of monitoring the diurnal pattern of optical dayglow emissions over a low-latitude location, Hyderabad, an attempt has been made to quantify the asymmetric nature of dayglow with vertical drifts. The results from this approach match closely with empirical climatological models. This approach presents a potent method to carry out systematic study of vertical drifts that vary from day-to-day.
- Medium scale traveling ionospheric disturbances (MSTIDs) are generated over mid-latitudes and on some occasions these propagate to low latitudes. The existing paradigm is that the ingression of MSTID into low latitudes during low solar activity period can generate/modify the plasma irregularity structures present therein. In this investigation, it is shown that MSTIDs can penetrate closer to even dip equatorial latitudes during moderate solar activity period under favorable background conditions. These observations have important ramifications for the understanding of the mid- and low-latitude coupling.
- During disturbed space weather conditions, low-latitude ionosphere is affected by the delayed electric field perturbations generated by the disturbance dynamo mechanism. In general, the magnitude of disturbance dynamo electric field (DDEF) is expected to be greater during nighttime than during day time. Using 16 years of magnetic data, it is shown that the magnitude of the DDEF during daytime can be much stronger than expected based on the earlier observations

or model predictions. This has important implications for the low latitude ionosphere as an enhanced-than-usual disturbance dynamo electric field will significantly alter the plasma distribution over low-latitudes.

Geosciences

- An innovative approach has been developed to estimate Ground level vapour isotopic composition through liquid condensation and non-linear regression. From isotopic composition of liquid condensate on ice-cooled surface, the isotopic composition of vapour can be estimated with uncertainty of 1.83 ‰for δ^{18}O and 10 ‰for δD. In spite of this uncertainty, the estimated isotopic composition of vapour is more accurate than that based on satellite based observations.
- One of the most relevant climate systems of the tropical region driving the biogeochemistry of the Indian Ocean is the Indian Monsoon systems. The unique geographical feature of the northern Indian Ocean unlike Pacific and Atlantic Ocean leads to varying oceanic processes which regulates its biogeochemistry. The effect of Indian Monsoon either currently or during the past has always remained topic of immense interest for climate scientists. As part of the GEOTRACES project, various trace elements were studied in water column of the northern Indian Ocean. Methodology and protocol was developed for measurement of Fe, Zn, Mn, Ni, Co and Cu for their measurement in seawater from the Indian Ocean at ultra-low level concentrations using Seafast-HR-ICPMS duly taking care of the salt matrix of seawater with minimal contamination. Dissolved aluminum (DAl) concentration in the Bay of Bengal seawater is largely affected by Ganga-Brahmaputra river system and Indian Peninsular rivers with its fractional solubility from lithogenic sediments ranging from $\sim$1-5%
- Several paleoclimatic archives have been studied from the Indian Ocean region to decipher the past monsoonal variation and paleo-ocean circulation. In the northern Indian Ocean, Lakshadweep and Andaman and Nicobar Islands are potential locations with abundant coral growth. Corals are colourful invertebrate marine organism growing in shallow seawater and records sea surface properties. Paleotemperature reconstruction from annual bands of corals from the Lakshadweep Islands shows inverse relation of δ^{18}O with Sea Surface Temperature (SST). The Lakshadweep corals show lowest growth in 1998, year when ENSO was at extreme, which led to wide spread bleaching of corals due to high SST and increased cloudiness, together causing stressed conditions for coral growth. The corals from the Andaman Islands show enriched values of δ^{18}O and δ^{14}C indicative of enhanced winter monsoon and mixed layer deepening. Andaman and Nicobar archipelago is known for its pristine environment and mega biodiversity. Large symbiont bearing foraminiferal assemblages reported from this region show decreasing species diversity with increasing water depths.
- Global ocean circulation has undergone major changes during glacial and interglacial periods. Radiocarbon ages of planktonic and benthic formainifera species has revealed that Indian Ocean show changes in ventilation age shift from interglacial to glacial period, inferred as slowing down of global deep water circulation. Several sediments cores from the northern Indian Ocean provide past climatic information ranging from decades to millennial scale. Multiproxy approach on a core from the Arabian Sea demonstrated variation in redox conditions due to changes in deep water ventilation during interstadial and LGM events. Coastal east Arabian Sea sediments show enriched δ^{13}C and δ^{15}N signatures indicative of enhanced ISM with both overhead productivity and sediment provenance playing role in sedimentation. Results have shown that High latitude Daansgard-Oeschger and Heinrich events are significant components of low latitude monsoon climate variability. Based on studies from active mudflats from Saurashtra, monsoonal fluctuations during Meghalayan Age (last 4.2 ka) were found to be in unison with the global climatic events as a function of changing ISM.
- Linear relationship between oxygen isotope (δ^{18}O) and salinity in ocean water is not constant. We need to consider dynamic relationship to estimate palaeo-salinity in the proxy records.
- The palaeoglaciation study carried out in the southern Zanskar ranges which is located in the transitional climatic zone (between the Indian Summer monsoon (ISM) and westerlies) indicates preservation of four major glacial advances. These are dated to Marine Isotopic Stage-4 (MIS-4), Last Glacial Maximum (LGM), late glacial and mid-Holocene. The study implicates multi-millennial/millennial-scale cooling events associated with the phases of enhanced westerlies, thus, suggesting a synoptic scale climate coupling between southern Zanskar ranges and the north latitude climatic perturbations and negate the suggestion of earlier studies in which ISM was considered as the major driver of glacier advances in this region.
- Highly time-resolved measurements of non-refractory submicron particulate matter (NR-PM_1) were performed using a high-resolution time-of-flight aerosol mass spectrometer (HR-ToF-AMS) over Ahmedabad during post-monsoon. All the components of NR-PM_1 [i.e., organic aerosol (OA), SO_4^{2-}, NO_3^--, NH_4^+ and Cl^-] showed a strong diurnal variation with the overall dominance of OA (58%) in NR-PM1. A strong diurnal variation in O/C ratio caused a large variability in OA/OC ratio (ranging from 1.2 to 2.3) during the study period, which suggests that a constant conversion factor for OA estimation (from OC) can be a source of large uncertainty in their load assessment over the study region. Three distinct sources of OA [i.e., primary OA (POA), semi-volatile oxygenated OA (SV-OOA), and low volatility OOA (LV-OOA)] were identified via positive matrix factorization (PMF) analysis. The OA mass was dominated by POA (42%), followed by LV-OOA (33%) and SV-OOA (25%). This study provides new insights on the atmospheric aging of OA, for the first time, over western India.

Theoretical Physics

- CMS and ATLAS at Large Hadrons Collider (LHC) already accumulated more that $150fb^{-1}$ of 13 TeV data significant for Higgs study as well as new physics search. Although new physics limits are pushed towards at the range of TeV energy, there are several possibility evading these strong bounds. Detailed study carried out to entangle such scenario from overwhelming QCD and top backgrounds.
- Explored the synergy between the proposed atmospheric neutrino experiment INO and long baseline experiment

ESSnuSB. The later experiment is designed for discovering CP violation in lepton sector with high sensitivity. We have shown how the hierarchy sensitivity of ESSnuSB can be enhanced by adding data from INO and ongoing experiments T2K and NOVA.

- Models of neutrino mixing were explored at the proposed long baseline experiments DUNE, T2HK and T2HKK and model correlations between the unknown parameters namely 2-3 mixing angle of neutrinos and the CP phase were tested.
- The stability of the electroweak vacuum in the context of TeV seesaw models with triplet fermions was studied.
- An additional resistivity due to a novel mechanism is predicted in which momentum randomization of Zeeman split electrons happen via bosonic excitations (spin fluctuations). Our novel mechanism consists of a new channel of momentum relaxation in which electrons in upper Zeeman level can deexcite to lower Zeeman level by generating spin fluctuation excitation in the lattice. An order of magnitude of this additional resistivity is calculated and an experiment is proposed to check this novel effect.

Atomic, Molecular and Optical Physics

- Aluminum nano particles(Al-np) enhanced laser induced breakdown spectroscopy study of brass samples has been investigated. The 2-5 times optical signal enhancement has been observed due to Al-nano particles.
- The C_{60} and C_{70} fullerene coated on brass and copper targets for studying the surface plasmonic effect on optical signal enhancement in laser produced plasma. The enhancement of optical emission has been observed. The role of concentration, wavelengths and intensity of lasers on this enhancement has been investigated.
- We have studied the microbial survivability in a fresh impact crater, Mukundpura meteorite impact crater, by recreating the condition using a low-intensity shock tube. The microbes isolated from a rock taken from the impact crater were subjected to experience similar conditions of impact. Microbes were observed to survive the impact and this is the first work carried out on microbial survivability on a fresh impact crater.
- The Vacuum UltraViolet (VUV) photoabsorption spectra of few of the astrochemical important molecules, such as hydroxylamine, in the ice phase remain a challenge to experimental astrochemist due to the difficulty in synthesizing them in-situ and maintaining a block of pure ice. Here we report the VUV photoasborption spectra of hydroxylamine synthesized in-situ using VUV irradiation of ammonia-oxygen ice mixture and then warming the irradiated mixture to get pure hydroxylamine. The spectra recorded in astrochemical conditions will help us identify this molecule in the icy bodies of the solar system.
- The discovery of reversible phase change using ethanethiol ices led us to identify other molecules that show such reversible phase changes. While investigating 1-hexyne we stumbled upon reversible phase around 140 K while warming the ice formed at 10 K. However, upon depositing the ice well below the reversible phase change temperatures, we could observe the morphology change from crystalline to amorphous well below the actual reversible phase change temperature which is supposed to be at 140 K. Upon subjecting the ice to temperature cycle the ice was observed to exhibit a crystalline nature at the same temperature where it was amorphous before beginning the temperature cycle. Such behaviour in the morphology of astrochemical ices is quite new.
- Upon focusing, the truncated vector vortex beam is found to regain its original intensity structure within the Rayleigh range. The results hold importance as vector vortex modes are eigenmodes of the optical fibre.
- It has been shown that nonlinear optical properties of Au-TiO_2 nano composite can be tuned by changing the concentration of Au nano particles.
- Increasing dating limits for quartz using violet stimulated luminescence (VSL).
- Estimation of luminescence sensitivity changes in single grains of natural quartz during OSL measurements.
- A few selected highly charged ions (HCIs) such as Ni^{12+}, Cu^{13+}, Pd^{12+}, and Ag^{13+} are investigated for making very accurate optical clocks. We developed and applied normal coupled-cluster (RNCC) method to calculate electric dipole moment (EDM) of the 199Hg atom due to parity and time-reversal symmetry violations very reliably. To support the recently developed multi photon ionization technique by laser ablation process, we carried out very accurate calculations of hyperfine structure constants of the 113,115 In isotopes and combining these calculations with the measurements nuclear magnetic and quadrupole moments of these isotopes were inferred.

Awards and Honors

A. S. Kiran Kumar

1. International von Karman Wings Award 2018 by the Aerospace Historical Society, in collaboration with the Graduate Aerospace Laboratories in recognition of contribution to the development of India's economy through aerospace technology and telecommunication.
2. Chevalier de l'Ordre national de la Legion d'Honneur (or National Order of the Legion of Honour) by the Government of France, 2019.
3. Santokbaa Humanitarian Manav Ratna Award 2018 by SRKKF Surat received from the President of India.

Anil Bhardwaj

4. Elected Academician (Full Member), International Academy of Astronautics, 2018.
5. First PRL-IAPT Dr. Vikram Sarabahi Lecture-2019, PRL, Ahmedabad, 7 Feb., 2019.

Ashok K. Singhvi

6. DST-SERB Year of Science Chair Professorship 2019-2024.

S. A. Haider

7. Awarded 'ISRO Merit Award' for the year 2017 from Indian Space Research Organization.

Man Mohan Sarin

8. DST-SERB Distinguished Fellowship Award, Science & Engineering Research Board, New Delhi.

Srubabati Goswami

9. Awarded a Visiting Professorship from Leverhulme trust, UK to visit Imperial College London for three months.

Abhijit Chakraborty

10. Gujarat Science Academy: Lunar and Planetary Science Society's Gold Medal and Endowment Lecture on The Science, Observations and Implications of Exo-Planets.

Bijaya K. Sahoo

11. Selected as an Outstanding Reviewer for 2018 by J. Phys. B: Atomic, Mol. and Opt. Physics

Dibyendu Chakrabarty

12. Received Certificates for Outstanding contribution in reviewing from Elsevier for the journals "Journal of Atmospheric and Solar Terrestrial Physics" and "Advances in Space Research" (2019).

Lokesh K. Sahu

13. Certificate of Appreciation from Chhattisgarh Young Scientist Congress, Pt. Ravishankar Shukla University Raipur, March 2019.

S. Vijayan

14. Young Scientist Award, by the Indian National Science Academy (INSA), 2018.

Sivakandan Mani

15. Selected and awarded full financial support to present two research papers at SPARC General Assembly 2018 (1-5, October 2018), Kyoto, Japan.

Priyanka Ghosh

16. Selected and awarded full financial support to present two research papers at Stratosphere-troposphere Process And their Role in Climate (SPARC) General Assembly 2018, 1-5 October 2018, Kyoto, Japan.

Subir Mandal

17. Selected and awarded full financial support for the Incoherent Scatter Radar (ISR) School held in University of Massachusetts, Lowell, USA during 21-27 July, 2018.

Nidhi Tripathi

18. Stratosphere-troposphere Processes And their Role in Climate (SPARC) Travel Grant Award, SPARC General Assembly, Kyoto, Japan, 1-5 October 2018.

Kuldeep Pandey

19. Selected and awarded full financial support for the Heliophysics Summer School-2018 held at High Altitude Observatory, Boulder, Colorado (USA) during 22-31 July, 2018.

Varun Sharma

20. Received travel grant student award in recognition of his outstanding scientific contribution to Europhoton Conference 2018 from European Physical Society (EPS) and EPS Young Minds.
21. Received the best student poster contribution award at the Europhoton Conference, Barcelona, Spain during 02 - 07 September 2018.

Kaustav Chakraborty

22. Awarded the DST Indo-French Raman-Charpak Fellowship to visit University of Strasbourg, France for two months, 2018.

Recognition, Best paper & Thesis awards

Faculty

Anil Bhardwaj

1. Member, National Committee, Centre for Co-operation in Science and Technology among Developing Societies (CCSTDS), Chennai, 2018.
2. Member, National Advisory Committee (NAC) for the IAGA-IASPEI Joint Scientific Assembly in 2021.
3. Member, Governing Council, Indian Institute Astrophysics, Bangalore, 2019.
4. Chief Guest, 18^{th} Convocation of Karunya Institute of Technology and Science, Coimbatore, 30 June, 2018.
5. Guest of Honour, Inauguration of Gujarat Science Congress, L. J. Institute of Applied Sciences, L. J. Campus, Ahmedabad, 02 Feb. 2019.
6. Co-Convener, Session PS15 "Future and Current Space Missions and Instrumentation for Space and Planetary Science", AOGS 15^{th} Annual Meeting, Honolulu, Hawaii, USA, 3–8 June, 2018.
7. Deputy Organiser (DO), Session C3.2 "Planetary Upper Atmospheres, Ionospheres, Magnetospheres", 42^{nd} COSPAR Scientific Assembly, Pasadena, CA, USA, 14–22 July, 2018.
8. Member, Science Organizing Committee, "52^{nd} ESLAB-52 Symposium: Comparative aeronomy and plasma environment of terrestrial planets", ESTEC, Noordwijk, The Netherlands, 14-18 May, 2018.
9. Co-Convener, Session MT15 "Future Planetary missions and instrumentation (L class, M class, New frontiers, Discovery, etc.)", European Planetary Science Congress 2018, Technische Universität Berlin, Germany, 16-21 September, 2018.

Ashok K. Singhvi

10. Distinguished Lecturer, University of Peking, Beijing, China

S. A. Haider

11. Elected as "Main Scientific Organizer (MSO) of C3.2 session-Planetary upper Atmospheres, Ionospheres and Magnetospheres" of 43^{rd} COSPAR assembly 2020 to be held in Sydney, Australia.
12. Elected as "Chairman of Sub-Commission C3 of COSPAR" for the period 2018-2022.

Manmohan Sarin

13. Vice-Chairman (2018-19), United Nations Group of Experts on Scientific Aspects of Marine Environmental Protection (UN/GESAMP) - An interagency advisory body of the United Nations providing guidance on the design and execution of marine environmental assessments.
14. Co-Convener, Special Session on "Air-sea exchanges: Impacts on Biogeochemistry and Climate", European Geophysical Union-2018 Vienna (Austria), 8 - 13 April, 2018.
15. Co-Chair, UN/GESAMP Annual Session hosted by Food & Agricultural Organization (FAO), Rome (Italy), 17- 21 September, 2018.
16. Member, CSIR-Standing Committee for Emeritus Scientists and one-time research grant.
17. Member, Programme Advisory Committee for Earth & Atmospheric Sciences, DST- Science & Engineering Research Board.
18. Chair, Expert panel of MoES-DBT (India)-NERC-MRC (UK) on "Atmospheric Pollution and Human Health in Indian megacity", Review Meeting, 1 - 2 March, 2019, New Delhi.
19. Member, Review Panel of International GEOTRACES Programme - funded by International Scientific Committee on Oceanic Research (SCOR).
20. External Expert, CSIR Assessment Committee constituted in the area of "Physical, Earth and Environmental Sciences".
21. Member, Evaluation Committee of IITM (Pune) for Biennial Golden Jubilee Award for excellence in research.

Shyam Lal

22. Member, Panel of experts for review of Atmospheric Pollution and Human Health (APHH) programme of MoES, New Delhi

Harish Chandra

23. Chair for a scientific session in Structured Training Program (STP), PRL, 4-8 February 2019.

P. Janardhan

24. Member, Local organizing committee, APRASC- 2019: URSI Asia-Pacific Radio Science Conference (AP-RASC 2019), 9-15 March, 2019, New Delhi.

D. Pallamraju

25. Invited as an Expert in the field of Solar Terrestrial Physics to design the New Science Program of SCOSTEP, called

PRESTO (Predictability of Solar Terrestrial Environment) at International Space Science Institute-Beijing, 14-16 November 2018.

26. Mentor, Project on "Techniques for upper atmospheric measurements" in the Structured Training Program, held at PRL during 4-8 February 2019.
27. Chair, Scientific Session in Structured Training Program on 4 February 2019. STP was held at PRL during 4-8 February 2019.
28. Chair, International Scientific Organizing Committee and Convener for the 15^{th} International Symposium on Equatorial Aeronomy (ISEA-15), hosted by PRL, Ahmedabad, India during 22-26 October 2018.
29. Member, Local Organizing Committee, 84th Anniversary General Meeting of the Indian National Science Academy (INSA) held at PRL during 22-26 December, 2018.
30. Chair, Session PS2 on 29 January 2019 in the 20th National Space Science Symposium held at Savitribai Phule Pune University, Pune, India during 29-31 January 2019.
31. Chair, Session PS3 on 31 January 2019 in the 20^{th} National Space Science Symposium held at Savitribai Phule Pune University, Pune, India during 29-31 January 2019.

S. Ramachandran

32. Received certificate in recognition of his outstanding contributions to reviewing for Atmospheric Environment - Elsevier Publishers, The Netherlands (November 2018)
33. Received certificate in recognition of his outstanding contributions to reviewing for Atmospheric Research - Elsevier Publishers, The Netherlands (June 2018).

Nandita Srivastava

34. Guest Investigator, ESA-Proba2 mission for study on Evolution of coronal cavities using SWAP observations, Royal Observatory of Belgium, Brussels, April, 2018
35. SOC member, 42^{nd} COSPAR Scientific Assembly (Pasadena)-Session D2.3 "Solar transients: From solar origin to Earth impact and the outer heliosphere", $14-28$ July, 2018.
36. Member of the National Advisory Board, 6^{th} PSSI Plasma Scholars Colloquium 2018, 24-26 August, 2018, SMIT, Sikkim.
37. Session chair, Session-9 Basic Plasma (Theory & Experiment) 6^{th} PSSI Plasma Scholars Colloquium 2018, August 24-26, 2018, SMIT, Sikkim.
38. SOC member & Session chair, ISEST 2018, Hvar, Croatia, $24-28$ September, 2018
39. Invited as an expert "Variability and Predictability of Solar-Terrestrial Coupling: the next scientific program of SCOSTEP" by the International Council for Science (ICSU) Beijing, November 2018.
40. Appointed as Review Editor for Frontiers in Science since 2018.

Srubabati Goswami

41. Member in the Programme Advisory Committee of DST-SERB Physics - II.
42. Member, Executive Committee of Indian Physics Association .
43. Advisor in NASI Ahmedabad Chapter.

Varun Sheel

44. 2016-2018: President, Planetary Science section, Asia Oceania Geosciences Society (AOGS)
45. 2018-2019: Vice-President, Planetary Science section, AOGS.
46. Convener of Mars and Venus session, 15^{th} AOGS annual meeting, Hawaii, 03-08 June 2018.

Bijaya Kumar Sahoo

47. Buti Foundation Award in 2018 for Excellence in Theoretical Physics, Astrophysics and Biophysics by Indian Physics Association.

Dibyendu Chakrabarty

48. Convener, PS-3 session (Sun-Earth interactive phenomena, Magnetosphere, Ionosphere, Thermosphere, Middle Atmosphere and their interactions) in the 20^{th} National Space Science Symposium, Savitribai Phule Pune University, Pune, during 29-31 January, 2019.
49. Convener, S5 (Space weather effects on low- and mid-latitudes) session of the forthcoming 15^{th} International Symposium on Equatorial Aeronomy (ISEA15) during October 22-26, 2018 at Physical Research Laboratory, India.
50. Invited as External examiner for a Ph.D thesis defence at University of Mumbai in February, 2019.
51. Invited to be a panel member of the interaction session with the school students of Gujarat on the National Science Day held at PRL on 02 March, 2019.
52. Member, LOC, International Symposium on Equatorial Aeronomy (ISEA-15) held at PRL during 22-26 October, 2018.
53. Co-Convener (LOC), 84th Anniversary General Meeting of the Indian National Science Academy (INSA) held at PRL during 22-26 December, 2018.
54. Member of a committee for the inauguration of the Absolute Quality Programme (AQP) of ISRO at PRL

Som Kumar Sharma

55. Main convener: Exploration and Science of the Earth's Lower and Middle Atmosphere: Past, Present and Future perspectives, 15^{th} annual meeting of the Asia Oceania Geosciences Society (AOGS), 03-08 June, 2018 Honolulu, Hawaii
56. Co-convenor of the session PS2- Middle atmosphere, Coupling, Dynamics and Climate Change, 20^{th} National Space Sciences Symposium 2019 (NSSS-2019), Savitribai Phule Pune University, Pune, 29-31 January 2019.

57. Member, panel of judges to select Best Paper Awards during NSSS-2019, for the oral and poster papers of the Parallel Session PS2- Middle atmosphere, Coupling, Dynamics and Climate Change, 20^{th} National Space Sciences Symposium 2019 (NSSS-2019), Savitribai Phule Pune University, Pune, 29-31 January 2019.
58. An expert member of the review panel of the NASA Postdoctoral Programme (NPP)-2018.
59. Member, Local Organizing Committee, 15^{th} International Symposium on the Equatorial Aeronomy (ISEA-15), Physical Research Laboratory, Ahmedabad, October 22-26, 2018.
60. Chair, Local Organizing Committee, Indian Space Research Organization -Structured Training programme (ISRO-STP) on "Recent Advances in Scientific Research in the Earth, Planetary and Space Sciences using Ground and space based data: Global perspectives" Physical Research Laboratory, Ahmedabad, February 4-8, 2019

Kuljeet Kaur Marhas

61. Nominated and elected as Council member of Meteoritical Society for session 2019-2020

Shashikiran Ganesh

62. Membership of the International Astronomical Union
63. Co-convener, PS08 "Polarization as a Tool for Exploration of Earth, Solar System and Beyond " session at AOGS, Hawaii, 3 - 8 June 2018

Harish S. Gadhavi

64. Session Chair, Aerosols and Climate, Biennial Conference of Indian Aerosol Science and Technology Association (IASTA), IIT Delhi, 26-28th November 2018

Neeraj Rastogi

65. First prize for the presentation entitled "Reactive oxygen species generation capability of ambient aerosol over the Arabian Sea", in the conference of Indian Aerosol Science and Technology Association (IASTA-2018) on 'Aerosol Impacts: Human Health to Climate Change' held at Indian Institute of Technology, Delhi, 26 - 28 November, 2018.
66. Session Chair, 'Aerosol Processes', in Indian Aerosol Science and Technology Association (IASTA) 2018 conference, IIT-Delhi, India, 26-28 November, 2018.

Lokesh K. Sahu

67. Member organizing committee, Indian Space Research Organization-Structured Training Programme (ISRO-STP) on "Recent Advances in Scientific Research in the Earth, Planetary and Space Sciences using Ground and Spaced based data: Global Perspectives", Physical Research Laboratory (PRL), Ahmedabad, India February 4-8, 2019.
68. Member organizing committee, Two Day Technical Workshop on Ozone Precursors (VOCs & Carbonyls) Monitoring, CPCB, Delhi, India, December 6-7, 2018.

Bhalamurugan Sivaraman

69. Member of the Organizing committee of Frontiers of Science, Hyderabad, India.9th to 11th December 2018
70. Session Chair, Astrochemistry – Bridging Astrophysics and Astrobiology, Frontiers of Science, Hyderabad, India.9th to 11th December 2018
71. Member of the Scientific Organizing committee of the International Conference on Astrobiology, Pune, India.15th – 16th December 2018
72. Session Chair, National Conference on Advances in Spectroscopy – Molecules to Materials,IITRAM, Ahmedabad4th – 6th October 2018
73. Guest of honour, International Conference on Chemical Sciences and Nanomaterials 2019, VIT, Vellore.7th – 9th March 2019.

Amit Basu Sarbadhikari

74. Section (Mineralogy, Petrology and Geochemistry of the surface of the Moon) Editor for "Encyclopedia of Lunar Science", Springer Publishing

Kinsuk Acharyya

75. Chaired a session (The Evolving Chemical Universe: from proto-stars to the origin of life (F3.2)) in 42th COSPAR Scientific Assembly, 14 - 22 July 2018, Pasadena, USA.

Neeraj Srivastava

76. Session Co-chair, NSSS 2019, Parallel Session 5 Theme: Planetary Geology

Rishitosh Kumar Sinha

77. First prize in the poster category for the paper titled "Study of layered deposits in the East Melas Chasma, Mars using MCC, HiRISE, THEMIS and MOLA data" in the National symposium on Advancements in Geospatial Technology for Societal Benefits and Annual Conventions of Indian Society of Geomatics (ISG) & Indian Society of Remote Sensing held in Space Applications Center Ahmedabad during December 05-07, 2018.

Bhuwan Joshi

78. Member of Scientific Advisory Committee for 33^{rd} National Symposium on Plasma Science &Technology (PLASMA-2017) organized by Plasma Science Society of India (PSSI), Department of Physics and Astrophysics, University of Delhi, $4-7$ December 2018

Brajesh Kumar

79. Invited to evaluate the oral presentations given by the young scientists in the parallel session PS-4 (Astronomy and Astrophysics) on the theme “The Sun and Stellar Systems, Planetary Systems, and Galaxies and Cosmology” at the 20^{th} National Space Science Symposium 2019 jointly organized by SPPU/IUCAA/NCRA, Pune, India, during 29−31 January, 2019.

Amitava Guharay

80. Member, Local organizing committee,15^{th} International symposium on equatorial aeronomy (ISEA-15), Physical Research Laboratory, Ahmedabad, October 22-26, 2018

Manash Ranjan Samal

81. Member, Science Organizing Committee, “International Conference on Formation and Evolution of Star Clusters, Maulana Azad National Urdu University (MANUU), Hyderabad”, 21-24 January, 2019

Veeresh Singh

82. Elected as the member of International Astronomical Union (IAU), 2018.

83. Co-convener, Session J6 “Radio Astronomy Instrumentation and Techniques - II (Data Processing : Imaging, Big Data)” in International Union of Radio Science (URSI) Asia Pacific Radio Science Conference (AP-RASC), New Delhi, 9 - 15 March 2019

Post Doctoral Fellows and Research Scholars

Diptiranjan Rout

84. Among top 5 awardees of Best Young Scientist Paper for the work entitled “Extreme impacts over low latitude ionosphere during a space weather event” by Diptiranjan Rout, D. Chakrabarty and R. Sekar in the 15^{th} International Symposium on Equatorial Aeronomy (ISEA-15) held at Physical Research Laboratory, India during 22-26 October 2018.

Kuldeep Pandey

85. Among top 5 awardees of Best Young Scientist Paper for the work entitled “Effect of disturbance dynamo on equatorial ionosphere during daytime” by Kuldeep Pandey, D. Chakrabarty, and R. Sekar in the 15^{th} International Symposium on Equatorial Aeronomy (ISEA-15) held at Physical Research Laboratory, India during 22-26 October 2018.

Sivakandan Mani

86. Among top 5 awardees of Best Young Scientist Paper for the work entitled “Evidence for the presence of MSTID and Quasi-Periodic Southward Moving Waves over 6° Magnetic latitude” in the 15^{th} International Symposium on Equatorial Aeronomy (ISEA-15) held at Physical Research Laboratory, India during 22-26 October 2018.

Prabir Kumar Mitra

87. Best poster award in the category of “The Sun and the Solar System” in the 37^{th} Meeting of Astronomical Society of India, Bengaluru during February 18−22 , 2019 on the “Evolution of solar magnetic fields and large-scale reconnection events in extremely complex solar active region NOAA 12673”.

Srinivasa Prasannaa V

88. ISAMP Best Thesis Award, awarded at the biennial conference of Indian Society of Atomic and Molecular Physics, NCAMP 2019, held at IIT Kanpur.

Sushree Sangeeta Nayak

89. Received best talk award, Young Astronomers’ Meet at Physical Research Laboratory, Ahmedabad during September 24−28, 2018 for the talk on ”Investigation of the magnetohydrodynamic evolution of a solar coronal jet”.

Neeraj Kumari

90. Best Poster award for the paper titled ”Complex Craters Within Lunar Basin and Their Implication” in the 20th National Space Science Symposium held in Savitribai Phule Pune University during 29 January 2019 to 31 January 2019.

Deepak Kumar

91. Won the first prize in the Young Scientist Paper competition in the 15^{th} International Symposium on Equatorial Aeronomy (ISEA-15) held at Physical Research Laboratory, India during 22-26 October 2018 for the work entitled “Estimation of Daytime F-region Vertical (E x B) Drift Velocities from Neutral Optical Oxygen Dayglow Measurements.

Ranadeep Sarkar

92. Selected as SCOSTEP Visiting Scholar to visit NASA/GSFC, Maryland, USA during 1 October−31 December, 2018 for the research project entitled “Observationally constrained global MHD and semi-analytical modelings of space-weather events to forecast Bz at 1 A.U.”

93. Selected as Guest Investigator for PROBA2 project entitled “Evolution of coronal cavities leading to CMEs” at Royal Observatory of Belgium, Brussels, Belgium, 9 April–4 May, 2018.

Human Resource Development

Human Resource Development at PRL The laboratory has a strong Human Resource Development (HRD) component with Doctoral, Post-Doctoral, Visiting Scientist programs. In addition we have an Associate program for university teachers and project training for graduate and post graduate students in both science and engineering. PRL organizes intensive summer programmes for students as well as college teachers every year. The purpose is to provide them an insight into current research activities being pursued at PRL which they can continue even after returning back to their colleges. It is also aimed at motivating them to take up research in basic sciences. Brief details of scientific output and staff details in numbers during the reporting year are reported here.

Research Programmes One of the important aims of the laboratory is to serve as a post-graduate and post-doctoral study centre in physics, earth & planetary sciences and chemistry to train research students in experimental and theoretical physics. With this in view, PRL offers a graduate programme through Research Fellowship leading to Ph. D. degree. It also provides opportunities for carrying out post-doctoral research. The strength of fellows under these programmes are presented in figure 1.

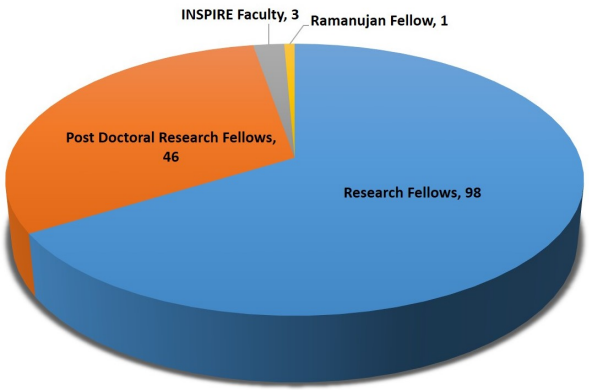


Figure 1: Research Programmes.

Training Opportunities PRL provides summer training programme to students doing their Bachlor's and Master's degree in Physics, Chemistry, Earth Sciences to acquaint them with the research programmes and opportunities available at PRL. This includes the internship of students selected through three national science academies and Indian Institute of Space Science and Technology, Thiruvananthapuram.

PRL also provides project training in engineering disciplines like computer engineering, electronics & communication, instrumentation & control, information technology to graduate/post-graduate students. Details of the same are presented in figure 2.

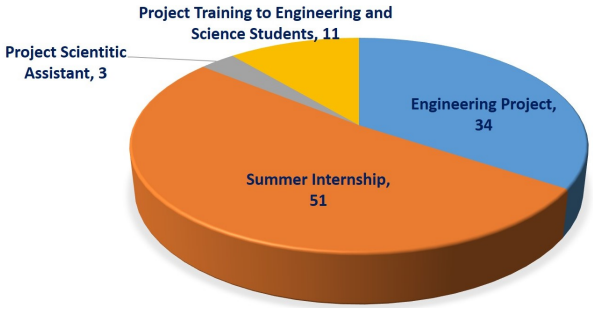


Figure 2: Internship Training Programmes.

PRL also offers training programmes in computers, electronics, library science, engineering and administrative services (Fig. 3).

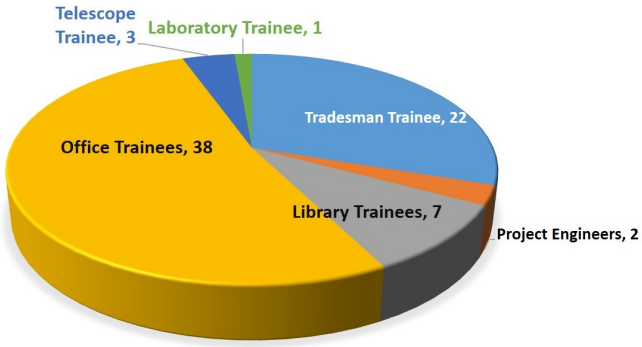


Figure 3: Training Programmes in technical and administrative areas.

Research Contributions The research work carried out by PRL scientists are published in reputed and peer reviewed national and international journals. Few of our scientists are also invited to write review articles in the field of their specialization. Some of our scientists have also edited books.

Many of our scientists attend conferences and symposia at home and abroad where they present the results of their research investigations. Some of them are invited to present review talks. Few of them serve as chairmen and members of scientific committees for organizing national conferences and symposia. They are also invited to convene and chair sessions during symposia and meetings. The research output during the reporting year are shown in figure 4.



Figure 4: Research Contributions.

Administrative Support

Behind the scientific achievements of PRL is the able and efficient support given by the administrative and the technical staff.

The administrative section of our laboratory continues to plays a pivotal role in providing an excellent management support to carry out our scientific activities. In addition, it also provides management support to the Solar Observatory at Udaipur and the Infrared Observatory al Mt. Abu. The staff structure of PRL are shown in figure 5.

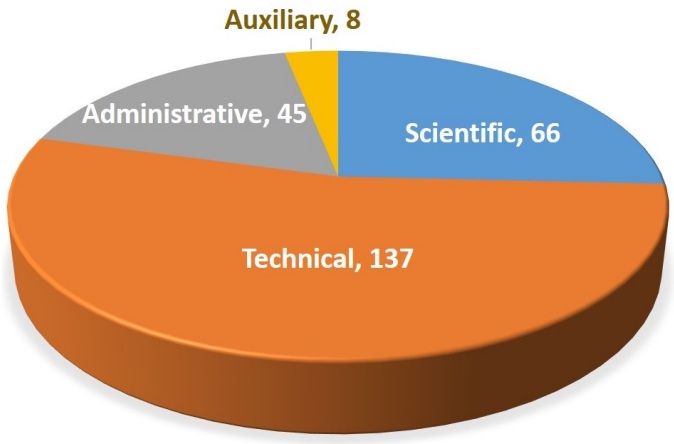


Figure 5: The distribution of PRL staff.

Ph.D. Awarded

[**PRL students/project associates/employees**]

Pandey Kuldeep Rambabu

1. "Investigations on Ionospheric Electrodynamics over Low Latitudes in Indian Sector", Indian Institute of Technology, Gandhinagar, November, 2018. [Supervisor: Dr. D. Chakrabarty, SPASC]

Alok Ranjan Tiwary

2. "Measurement of Solar magnetic fields: Development of a polarimeter for Multi-Application Solar Telescope", Indian Institute of Technology, Gandhinagar, June, 2018. [Supervisor: Dr. S K Mathew, USO]

Rahul Yadav

3. "Spectropolarimetric studies of sunspot and its fine-structure", Mohanlal Sukhadia University, Udaipur, March, 2019. [Supervisor: Dr. S K Mathew, USO]

Ali Anwar M A

4. "Characterization of Quantum Sources of Light Generated By Parametric Down Conversion Processes", Mohanlal Sukhadia University, Udaipur, November, 2018. [Supervisor: Dr. R P Singh, AMOPH]

Jabir M V

5. "Generation and characterization of quantum entanglement using SPDC photons", Mohanlal Sukhadia University, Udaipur, October, 2018. [Supervisor: Dr. G K Samanta, AMOPH]

P. R. Shreedevi

6. "A study on the impact of space weather events on the ionosphere over the Antarctic station Bharati and the Indian subcontinent", CUSAT, Kochi, July, 2018. [Supervisor: Dr. Anil Bhardwaj]

Vrinda Mukundan

7. "Modelling the Dayside Ionosphere of Titan: Application of Electron Degradation Model for Methane", CUSAT, Kochi, December, 2018. [Supervisor: Dr. Anil Bhardwaj]

Venkatesh Chinni

8. "Distributions of dissolved Iron and Zinc in the Indian Ocean: Implications to their sources, sinks and internal cycling.", Mohanlal Sukhadia University, Udaipur, July, 2018. [Supervisor: Dr. S K Singh]

Prahlad R. Epili

9. "Investigation of the Properties of X-ray Pulsars During Outbursts", Mohanlal Sukhadia University, Udaipur, June, 2018. [Supervisor: Dr. S K Naik, A&A]

Dipak Panda

10. "Development of Scintillation Gamma Ray Spectrometers for Planetary Missions and Methodological Investigations of Infrared Stimulated Luminescence Signals from Feldspars", Sardar Patel University, January, 2019. [Supervisor: Dr. K K Marhas, PSDN]

Colloquia/Public Lectures by Visitors

1. Dr. Shanti Pappu
Sharma Centre for Heritage Education, Chennai, Tamilnadu
Tools, Time and Transitions: New Perspectives on Early Prehistoric Populations in South Asia
23 May 2018

2. Dr. Nikku Madhusudhan
Institute of Astronomy, University of Cambridge
Chemical Characterization of Extrasolar Planets
12 July 2018

3. Prof. Deshdeep Sahdev
QuazarTech/(Ex-)IIT Kanpur
A Practical Approach To Strengthening Our Scientific Ecosystem
01 August 2018

4. Prof. Raghavendra Gadagkar
Centre for Ecological Science Indian Institute of Science, Bangalore
How and Why I do my Research: Some Reflections on the Pursuit and Evaluation of Science
23 August 2018

5. Prof. Debabrata Goswami
Prof. S. Sampath Chair Professor of Chemistry, IIT Kanpur
Femtosecond Laser Induced Spatiotemporal Control and Photothermal Spectroscopy for Remote Sensing and Computing at Nanoscale
03 October 2018

6. Prof. Rajesh Gopakumar
ICTS-TIFR, Bengaluru
Down-To-Earth String Theory
19 November 2018

7. Prof. Sushil Atreya
Planetary Science Laboratory, University of Michigan, Ann Arbor, USA
Formation of the Icy Giant Planets: In Situ Exploration
18 January 2019

8. Prof. Wing-Huen Ip
National Central University, Taiwan
Ice Skating on the Moon
19 January 2019

9. Dr. Shailesh Nayak
National Institute of Advanced Studies (NIAS), Bengaluru
Environmental Changes and Future Earth: An Indian Perspective
08 February 2019

10. Prof. Dr. Hermann W. Bange
GEOMAR Helmholtz Centre for Ocean Research Kiel, Germany
Non-CO2 Trace Gases in the Ocean
18 February 2019

11. Dr. N. Purnachandra Rao
National Centre for Earth Science Studies, Ministry of Earth Sciences, Thiruvananthapuram
Earthquakes and Tsunamis in the Indian Subcontinent
19 February 2019

12. Dr. G. D. Reeves
Los Alamos National Laboratory, USA
Space Sciences at Los Alamos National Laboratory – A Personal Perspective
20 March 2019

13. Prof. Debasis Sengupta
Centre for Atmospheric and Oceanic Sciences (CAOS), IISc Bangalore.
Biweekly Monsoon mode in the Bay of Bengal
27 March 2019

Conference/Symposium/Workshop organized by PRL

1. "YAM-2018", 15^{th} Young Astronomers' Meet, 24-28 September, 2018, PRL, Ahmedabad.
2. "SCOP-2018", The Students' conference in optics and photonics, PRL Ahmedabad, 4-6 October 2018.
3. "15^{th} International Symposium on Equatorial Aeronomy (ISEA-15)", held at PRL 22-26, October, 2018.
4. "84^{th} Anniversary General meeting of the Indian National Science Academy, New Delhi, held at PRL during 26-28 December, 2018.
5. "Indian Space Research Organization -Structured Training programme (ISRO-STP) on "Recent Advances in Scientific Research in the Earth, Planetary and Space Sciences using Ground and space based data: Global perspectives"", held at PRL 04-08, February, 2019.
6. "Young Physicists' Meet(YPM)", PRL, Ahmedabad 18-20 March 2019.

Invited Talks at Conference / Symposia / Workshops

Astronomy and Astrophysics

P. Janardhan

1. "The Sun-Earth Connection", National Symposium on Advancements in Geospatial Technology for Societal Benefits., Space Application Centre, Ahmedabad, 5-7 December, 2018.
2. "Solar Activity - Past, Present and Near Future", ISRO Structured Training Program (STP) in Space Sciences, Physical Research Laboratory, Ahmedabad, 5-9 March, 2018.
3. "Beyond the Mini Solar Maximum of Cycle 24: The Amplitude of Solar Cycle 25 and the Evolution of the Terrestrial Magnetosphere", National Space Science Symposium, Savitri Bhai Phule University, Pune, 29-31 January, 2019.

Shanwlee Sow Mondal

4. "Understanding the solar spicules through numerical simulation", 37th meeting of Astronomical Society of India, Christ College, Bangaluru, 18-22 Feb, 2019.

Aveek Sarkar

5. "Understanding the solar atmosphere using numerical simulations - progress and difficulties", CMNA conference, IIT, Indore, 1-3 Nov , 2018.
6. "Magnetohydrodynamics and solar dynamo", IUCAA Solar Physics Workshop, Aluva, Kerala, 1-2 Mar , 2019.
7. "ASPEX Science and operations", 37th Astronomical Society of India workshop, Christ College, Bangaluru, 18 Feb, 2019.

Navpreet Kaur

8. "Solar system studies with Indo-Belgian Telescopes", 2nd BINA Workshop, BINA as an Expanding International Collboration, Royal Observatory of Belgium, Brussels, Belgium, 9-12 October, 2018.

Manash Ranjan Samal

9. "Jets and Outflows from the UWISH2 survey", International Conference on Exploring the Universe: Near Earth Space Science to Extragalactic Astronmy, S. N. Bose National Centre for Basic Sciences, Kolkata, 14-17 November, 2018..
10. "New insights into formation and evolution of bipolar HII regions with Herschel", International Workshop on Formation and Evolution of Star Clusters, Maulana Azad Urdu University, Hyderabad, 21-24 January, 2019.

Sachindranatha Naik

11. "Complex X-ray/Ultraviolet/Optical variabilities of the Seyfert 1 galaxy NGC 4593", 2nd BINA Workshop, BINA as an Expanding International Collboration, Royal Observatory of Belgium, Brussels, Belgium, 9-12 October 2018.
12. "Properties of high mass Xray binary pulsars at different luminosities", Exploring the Universe: Near Earth space science to extragalactic astronomy, S. N. Bose National Centre for Basic Sciences, Kolkata, 14-17 November, 2018.

Subhajeet Karmakar

13. "Activity of Young Dwarfs with Planetary Systems: EPIC 211901114 and K2-33", Exploring the Universe: Near Earth space science to extragalactic astronomy, S. N. Bose National Centre for Basic Sciences, Kolkata, 14-17 November, 2018.
14. "Evolution of magnetic activities on active solar-type stars: starspot modulation, surface differential rotation, and flares", 2nd BINA Workshop, BINA as an Expanding International Collboration, Royal Observatory of Belgium, Brussels, Belgium, 09-12 October, 2018.

Neeraj Kumari

15. "Soft X-ray Excess in Narrow Line Seyfert 1 Galaxy Mrk 766", Exploring the Universe: Near Earth space science to extragalactic astronomy, S. N. Bose National Centre for Basic Sciences, Kolkata, 14-17 November, 2018.
16. "X-ray Excess in Active Galactic Nuclei Mrk 766", Young Astronomers Meet, Physical Research Laboratory, Ahmedabad, 24-28 September, 2018.

Veeresh Singh

17. "Unveiling the new population of AGN using deep multi-wavelength surveys", AGN science meeting, Indian Institute of Astrophysics, Bangalore, India, 6 October 2018.
18. "Radio outflows in AGN and their feedback : An observational perspective", Conference on bubbles big & small, Indian Institute of Science, Bangalore, India, 11 - 14 June 2018.

19. “AGN science interests with uGMRT - MIGHTEE deep radio continuum survey”, uGMRT - MIGHTEE : Indo-South Africa collaboration meeting, NCRA-TIFR Pune, 2 - 6 April 2018.
20. “Kpc-scale radio jets in NLS1s”, Conference on revisiting narrow-line Seyfert 1 galaxies and their place in the Universe, University of Padova, Italy, 10 - 13 April 2018.

J. N. H. S. Aditya

21. “HI absorbers at intermediate redshifts”, Metre Wavelength Sky - II conference, NCRA-TIFR Pune, India, 20 March 2019.

Mudit Kumar Srivastava

22. “Aspects of Optical Instrumentation in Astronomy”, Young Astronomers’ Meet, Physical Research Laboratory, Ahmedabad, 28 September 2018.
23. “Design and Development of Mt. Abu Faint Object Spectrograph and Camera-Pathfinder (MFOSC-P) on PRL 1.2m Telescope Mt. Abu”, 20th National Space Science Symposium (NSSS), Savitri Bhai Phule University, Pune, 29-31 January 2019.
24. “Design and Development of Mt. Abu Faint Object Spectrograph and Camera-Pathfinder (MFOSC-P) on PRL 1.2m Telescope Mt. Abu”, 37th Astronomical Society of India (ASI) meeting, Christ College, Bangaluru, 18-22 Feb, 2019.

Santosh Vadawale

25. “AstroSat-CZTI and Hard X-ray Polarimetry”, COSPAR Capacity Building Workshop, IISER Mohali, 9 - 20 March 2019.
26. “Elemental Composition with APXS on-board Chandrayaan-2 Rover”, Lunar Science Meet, ISRO Head Quarters, Banglore, 27 September 2018.

Solar Physics

Nandita Srivastava

27. “Solar physics research using ground and space-based observations”, ISRO-Structured Training Program (STP), PRL, Ahmedabad, PRL, Ahmedabad, 5−9 March, 2018.
28. “Interaction between coronal mass ejections and impact on space weather”, 6^{th} PSSI Plasma scholars colloquium 2018, Department of Physics, SMIT, Sikkim, 24−26 August, 2018.
29. “Current activities at USO and future outlook”, USO Foundation Day, Udaipur Solar Observatory, Udaipur, 20 September, 2018.

Brajesh Kumar

30. “On the magnetic-jerk driven acoustic oscillations in the solar atmosphere observed during major solar flares”, parallel session PS-4 (Astronomy and Astrophysics), 20^{th} National Space Science Symposium 2019, 20^{th} National Space Science Symposium 2019, Pune, 9−31 January, 2019.

Ashok Ambastha

31. “The first 25 Years of USO from its inception”, USO Foundation Day, Udaipur Solar Observatory, Udaipur, 20 September, 2018.

Bhuwan Joshi

32. “Role of magnetic reconnection in solar flares: An observational overview”, DAE-BRNS sponsored National Conference on Advances in Plasma Science and Technology, Sri Shakti Institute of Science and Technology, Coimbatore, Tamilnadu, 24 − 26 October, 2018.
33. “Solar eruptive phenomena and their low-frequency radio observations by e-CALLISTO”, Symposium on Advances in Physics from small to large scales, Department of Physics (UGC-centre of advanced study), Kumaun University, Nainital, Uttarakhand, 14 − 16 March, 2019.

Planetary Sciences

Anil Bhardwaj

34. “Key-Note Speaker”, International Symposium on Lunar and Planetary Science (2018), Macau University of Science and Technology, Macau., 12 − 15 June 2018.
35. “Special Invited Talk: Indian Mars Program”, MUAN - 10^{th} Mars Upper Atmosphere Network Workshop, Nicosia, Cyprus, 15 − 18 Oct 2018.
36. “Special Invited Lecture: A New Perspective on Solar Wind Interaction with Moon after Chandrayaan-1 Mission”, Celebrating 125^{th} Birth Anniversary of Professor Meghnad Saha, NASI, Allahabad, 6 − 7 October, 2018.
37. “Comparative Planetary Aeronomy”, 15^{th} International Symposium on Equatorial Aeronomy (ISEA-15), PRL, Ahmedabad, 22 October 2018.
38. “Deep Space Missions and Cutting Edge Technologies for Space Explorations”, 10 Years of Deep Space Network, ISTRAC, Bangalore, 24 October 2018.
39. “Highlights of Indian Planetary Missions and Future Plan”, International Conference on Computational Mathematics in Nano-electronics and Astrophysics (CMNA 2018), IIT Indore, Nov. 2, 2018.
40. “The Solar System and Beyond”, APRSAF ISRO-JAXA Seminar on Space Education for Educators, IIRS, Dehradun, 15 − 16 Nov, 2018.
41. “Science at PRL”, INSA Annual General Meeting, PRL, 26 Dec, 2018.
42. “Chandrayaan-2: Indian Second Lunar Mission”, Special Plenary Session (SPS) - 1: Future Space Science Missions, 20^{th} National Space Science Symposium, Savitribai Phule Pune University (SPPU), Pune, 29 − 31 Jan., 2019.
43. “Radio Probing of Planetary Bodies using GMRT and Science”, 2019 URSI Asia Pacific Radio Science Conference, Delhi, 9 − 15 March 2019.
44. “A New Perspective on Solar Wind Interaction with Moon after Chandrayaan-1 Mission”, 2019 URSI Asia Pacific Radio Science Conference, Delhi, 9 − 15 March 2019.

Amit Basu Sarbadhikari

45. "Alkali enrichment on the Lunar surface: Implications and Petrogenetic significance", Understanding lunar composition - utilizing different wavelength regions, PRL, 23 — 24 July 2018.
46. "Melting and Differentiation in Planetary Bodies of the Solar System: Mars evolution processes as revealed by meteorites", -, Presidency University, Kolkata, 24 August 2018.
47. "Lunar composition, evolution – current understanding and science from Ch-2", Lunar Science Meet, ISRO HQ Bengaluru, 27 September 2018.
48. "Alkaline rocks of the Moon: Recent Discoveries and Implications for Formation", JSPS-DST Japan-India Forum for Advanced Study, Nagoya University, Japan, 10 March 2019.

S. A. Haider

49. "First coupled model of D and E regions of Mars' ionosphere for flare and non-flare electron density profiles", 15^{th} annual meeting of the Asia Oceania Geosciences Society (AOGS), Honolulu, Hawaii, USA, 3 — 8 June, 2018.
50. "Martian aurora and its causative mechanisms: MAVEN observations", National Space Science Symposium 2019, Savitribhai Phule Pune University, Pune, 29 — 31 Jan 2019.

Kinsuk Acharyya

51. "Molecular Complexity at low metallicity", Exploring the Universe: Near Earth Space Science to Extra-Galactic Astronomy, S N Bose National Centre for Basic Sciences, Kolkata, 14 — 17 November 2018.
52. "Fluorine and Chlorine Chemistry in the Interstellar Medium", 42^{th} COSPAR Scientific Assembly, Pasadena, USA, 14 — 22 July 2018.

Kuljeet Kaur Marhas

53. "Shortlived nuclides in early solar system", Workshop on the theme "Role of sample return in addressing major outstanding questions in Planetary Sciences, Bern, Switzerland, 5 — 9 Feb 2018.
54. "The observed planetary architecture in the solar system and the evolution of the early solar system", UK-India Frontiers of Science (FoS) meeting organised by the Royal Society (UK) and the Department of Science and Technology of India (DST)., London, May 2018.
55. "Infrastructure of Solar System", International conference on exoplanets, Indian Institute of AstroPhysics, Bengaluru, 7 — 9 February 2019.
56. "Secondary Ion Imaging with nanoSIMS", Workshop on Atom Probe Tomography, Indian Institute of Technology, Chennai, 8 — March 2019.

Sanjay Kumar Mishra

57. "Photoelectron sheath on lunar sunlit regolith and fine particle levitation", 2019 URSI Asia-Pacific Radio Science Conference (AP-RASC 2019), New Delhi, 09-15 March 2019.

S. Vijayan

58. "Impact craters and Volatiles on Mars", 1^{st} Indian National Young Academy of Science - Frontiers of Science (INYAS-FoS) Brainstorming Meeting, Hyderabad, 9 — 11 December 2018.
59. "Remote sensing based analysis for identifying potential target on Mars", International Conference on Astrobiology, Pune, 15 — 16 December 2018.

Rajiv Ranjan Bharti

60. "Radar evidence of episodic lava flow near Mangala Fossa, Mars", NASA MARSIS-SHARAD Science Team meeting 2018, Grenoble, France, 2018.

Shiv Kumar Goyal

61. "STEPS: an instrument to understand the anisotropy of the high-energy particles in the interplanetary medium", AOGS 2018, Honolulu, Hawaii, USA, June 2018.

Jayesh P. Pabari

62. "Study of Interplanetary Dust from a Satellite", Keynote Talk at International Conference ETEST, CSPIT, Changa, 14 Dec 2018.

Space and Atmospheric Sciences

D. Pallamraju

63. "Overview of Aeronomy research in India", 15^{th} International Symposium on Equatorial Aeronomy, Physical Research Laboratory, Ahmedabad, 22-26 Oct, 2018.
64. "Space Weather and vertical and latitudinal coupling of ionosphere thermosphere", 15 November 2018, in Next Science Program of SCOSTEP, ISSI-Beijing forum, National Space Science Center, Beijing, China, 14-16 Nov, 2018.
65. "ISRO's Aeronomy Mission- DISHA (Disturbed and quite time Ionosphere-thermosphere System at High Altitudes)", 20^{th} National Space Science Symposium, Special Plenary Lecture, at Savitribai Phule Pune University, Pune, 29-31 Jan, 2019.
66. "Space Weather and Upper Atmospheric Dynamics", Ashok & Rita Patel Institute of Integrated Study and Research in Biotechnology and Allied Sciences (ARIBAS), New Vallabh Vidyanagar, 13-14 Mar, 2019.

Shyam Lal

67. "Greenhouse gases over the Indian region", International Workshop on Chemistry Climate Interaction, Indian Institute of Tropical Meteorology (IITM), Pune, 14 Mar, 2019.

S. Ramachandran

68. “Stratospheric sulfur injections: Benefits and Risks”, National Roundtable Discussion on Geoengineering and India: Science and Policy, Indian Institute of Science, Bengaluru, 26 Jul, 2018.
69. “Aerosols and Climate”, UN-CSSTEAP SAS and SATMET Course, Space Applications Centre (SAC), Ahmedabad, 7 Aug, 2018.
70. “Ozone: Past, Present and Future”, International Ozone Day, Space Applications Centre (SAC), Ahmedabad, 14 Sep, 2018.
71. “Ozone”, International Ozone Day, Gujarat Science City, Ahmedabad, 16 Sep, 2018..
72. “Aerosol Characterization: Challenges”, Conference of Indian Aerosol Science and Technology Association (IASTA) 2018, Indian Institute of Technology, Delhi, 26-28 Nov, 2018.

Harish S. Gadhavi

73. “Balloon borne measurements of Asian Tropopause Aerosol Layer (BATAL): An Overview”, Biennial Conference of Indian Aerosol Science and Technology Association, Indian Institute of Technology, Delhi, 26-28 Nov, 2018.

Dibyendu Chakrabarty

74. “New results on the effects of prompt penetration electric field on equatorial ionosphere”, 42^{nd} COSPAR Assembly in Pasadena, California, 14-22 Jul, 2018.
75. “Space weather”, ISRO Structured Training Programme (ISRO-STP, 05-09 March, 2019) on “Recent Advances in Scientific Research in the Earth, Planetary and Space Sciences using Ground and Space Based data: Global Perspective“, Physical Research Laboratory (PRL), Ahmedabad, 06 Mar, 2019.

Som Kumar Sharma

76. “Atmospheric Monitoring using Laser Systems”, Future Prospects of Space Technology in Forest and Environmental Applications, Space Applications Centre (SAC), Ahmedabad, 27-28 Jun, 2018.
77. “Applications of LIDAR in Industry, Science, and Society”, National Symposium on Industry-Academia Collaboration for Geospatial Technologies (IACGT), CEPT University, Ahmedabad, 14-15 Dec, 2018.
78. “Tropospheric and Stratospheric Investigations using Laser based Instruments and Satellites”, Max Planck Institute for Chemistry, Max Planck Institute for Chemistry (MPIC), Mainz, Germany, 16 Apr, 2018.
79. “Atmospheric Studies using Lidar”, UN-CSSTEAP SAS and SATMET Course, Space Applications Centre (SAC), Ahmedabad, 09 Aug, 2018.

Lokesh K. Sahu

80. “”Measurements of biogenic volatile organic compounds (BVOCs) in marine boundary layer of Arabian Sea (OMZ): Role of carbon cycle in pre-monsoon season””, International Ocean Deoxygenation Conference, Kiel, Germany, Kiel, Germany, 02-07 Sept, 2018.
81. “”Atmospheric Measurements of VOCs over India and surrounding ocean regions””, Two Day Technical Workshop on Ozone Precursors (VOCs & Carbonyls) Monitoring, Central Pollution Control Board (CPCB), Delhi, India, 06-07 Dec, 2018.

Geosciences

Jyotiranjan S. Ray

82. “Geochemical evolution of the Andaman Back Arc: A window to the Indian Ocean Mantle”, IODP Proposal Nurturing Workshop - SPADE, National Centre for Antarctic and Ocean Research, Goa, India, 17 September, 2018.
83. “Learning from volcanoes: the story of Barren Island”, ISRO Structured Training Programme (STP) - 2019, Physical Research Laboratory, Ahmedabad, India, 6 February, 2019.

Rajendra. D. Deshpande

84. “Oxygen and Hydrogen Isotope Systematics for Hydrological Applications”, National Level Short Term Training course on’ Application for Isotope techniques for Water Resources Management’, Centre for Water Resource Development and Management (CWRDM), Kzhikode, Kerala, India, 30 July , 2018.
85. “Isotope Tracer Applications for Hydrology”, National Workshop on ‘Isotopes in Earth, Ocean & Atmospheric Sciences’ Organized jointly by Inter-University Accelerator Centre, Delhi & NIO, Goa (Under the aegis of Geochronology project supported by Ministry of Earth Sciences Govt. of India), CSIR-National Institute of Oceanography (NIO), Goa, India, 18 - 20 February, 2019.
86. “Tracing surface-ground water interaction in the context of climate change using isotope tracers”, National Symposium on Environment (NSE-20), IIT Gandhinagar, Gujarat, India, 13-15 December, 2018.
87. “Isotope Applications for Groundwater Resources in Kachchh”, Second National Conference and Field Workshop on ‘Recent Studies on the Geology of Kachchh Basin, Krantiguru Shyamji Krishna Verma Kachchh University, Bhuj, Gujarat, India, 30 December, 2018 - 1 January, 2019.
88. “Isotope Tracers for Hydrology Research”, Session Talk, Manipal Academy of Higher Education, Manipal, Karnataka, India, 21 February, 2019.
89. “Indian Hydrological Scenario and Importance of Isotope Tracers”, ISRO-Structured Training Programme - 2019, Physical Research Laboratory, Ahmedabad, India, 4 - 8 February, 2019.

Neeraj Rastogi

90. “Brown Carbon Aerosol: Measurements and Climatic Implications”, International Workshop on Climate Chemistry Interaction (IWCCI), Indian Institute of Tropical Meteorology (IITM), Pune, 12-15 March, 2019..

91. “High Time-Resolved Characteristics and Composition of Ambient Organic Aerosol”, Indian Aerosol Science and Technology Association (IASTA) 2018, Indian Institute of Technology, Delhi, 26 - 28 November, 2018.

Arvind Singh

92. “High Rates of Nitrogen Fixation in the Arabian Sea”, workshop on “Advances in Earth System Science”, Banaras Hindu University, Varanasi, India, 31 October - 1 November, 2018..
93. “Early Career Scientists Network (ECSN) of IIOE-2”, 2^{nd} International Indian Ocean Expedition Working Group Meeting, Keil, Germany., 28 -30 November, 2018..
94. “IIOE-2 (ECSN) research activities”, 2^{nd} International Indian Ocean Expedition Working Group Meeting, Keil, Germany., 28 -30 November, 2018.
95. “Impact of climate change on the biogeochemistry of coastal wetlands in India”, World Wetlands Day, Gujarat Ecological Education and Research (GEER) Foundation, Gandhinagar , Gujarat, India, 2 February, 2019.

A.K. Sudheer

96. “Chemistry of Atmospheric Aerosol”, National Seminar on Current Trends and Advancement in Chemical, Physical and Life Sciences (CTACPLS-2019), J.N.V. University, Jodhpur, India, 15 - 17 March, 2019.
97. “Neutralization of aerosol acidity by ambient ammonia: Implication to aqueous phase SO_2 oxidation”, IASTA-2018 on ‘Aerosol Impacts: Human Health to Climate Change’, Indian Institute of Technology, Delhi, India, 26 - 28 November, 2018.

Manmohan Sarin

98. “Carbonaceous aerosols from biomass burning emissions in Northern India: Implications to atmospheric radiative forcing and climate”, Indian Academy of Sciences Workshop on “Advances in Earth System Science”, Banaras Hindu University, Varanasi, India, 31 October - 1 November, 2018.

Theoretical Physics

Partha Konar

99. “Boosted objects - Fat jet and jet-substructure at the LHC”, HEP activity week: HRI, HRI , Allahabad, 14-15 March 2019.
100. “Unmasking obscure events at the LHC”, Free Meson seminar at TIFR, TIFR,Mumbai, 15 Nov, 2018.

Srubabati Goswami

101. “Synergy between Long baseline and Atmospheric Neutrino Experiments”, PANE 2018, ICTP, Trieste, May 2018.
102. “Neutrino-less double beta decay”, Nu HORIzons, HRI Allahabad, February 2018.
103. “Discovering CP violation in the lepton sector: Challenges and possibilities”, 84th Annual General Meeting of Indian Academy of Sciences, BHU, Varanasi, November 2018.

Hiranmaya Mishra

104. “Superconductivity in magnetized quark matter”, Colloquium, Institute for Mathematical Sciences (IMSc.),Chennai, 28 March 2019.
105. “Properties of matter under extreme conditions”, 3rd Goa Researchers meet,, Goa University, 2nd March 2019.
106. “Hot and dense matter”, Invited talk, Department Physics IIT Goa, November 2018.
107. “Matter under extreme condition”, conference on “Frontiers in experimental and theoretical physics”, Center of Engineering and Technology, Bhubaneswar, 24 -27 April 2018.

Angom Dilipkumar Singh

108. “Ultracold atoms in optical lattices with disorder”, IISER Kolkata, Dept. of Physics Seminar, IISER Kolkata, Dept. of Physics Seminar, 22 November, 2018.
109. “Ultracold atoms in optical lattices with disorder”, Asian International Seminar on Atomic and Molecular Physics 2018, IIT Bombay-TIFR, December 3, 2018.

Atomic, Molecular and Optical Physics

Goutam Kumar Samanta

110. “Structured beams coherent radiation and their applications”, Recent Advances in Photonics, Manipal University, Manipal, Karnataka, 22nd September, 2018.
111. “Nonlinear interaction of structured beams”, Workshop on Experimental Techniques in Physics, Institute of Advanced Research (IAR), Gandhinagar, 4-14 June, 2018.

Ravindra Pratap Singh

112. “Role of physics in information and communication technology: Emergence of quantum computer and quantum communication”, IAPT program, Science City, Ahmedabad, 7th July, 2018.
113. “Statistics of heralded twisted single photons”, OSI-International Symposium on Optics (OSI-ISO 2018), IIT Kanpur, 20-22 Sept, 2018.
114. “Non-separable states of light: classical and quantum”, Meeting on Quantum Information Processing and Applications (QIPA 2018), HRI Allahabad, 02-08 Dec, 2018.
115. “Parametric down-conversion of structured beams and its applications”, International Conference on Fiber Optics and Photonics (PHOTONICS-2018), IIT Delhi, 12th – 15th December 2018.
116. “Orbital angular momentum entangled photons and their applications”, International Conference on Quantum and Atom Optics (ICQAO – 2108), IIT Patna, 16th – 18th Dec, 2018.

Rajesh Kumar Kushawaha

117. “Photoionization and dissociation of polyatomic molecules: Chasing ultrafast dynamics for molecular movie”, International workshop on atomic and molecular collisions, Udaipur, 10-12 December, 2018.
118. “Probing ultrafast dynamics in molecules: Towards Molecular Movies”, Discussion meeting on AMO S&T, IIT Tirupati, 20 March 2019.
119. “Ultrafast molecular physics: Towards Molecular Movies”, National Conference on Advances in Spectroscopy: Molecules to Materials NCASMM-2018, IITRAM Ahmedabad, 4-6 October, 2018.

Bijaya K. Sahoo

120. “Advances in Relativistic Atomic Coupled-Cluster Theory for High Precision Calculations”, The 6th International Workshop on Quantum Chemistry/Quantum Chemical Calculations on Quantum Computers (QC/QCC on QCs): Quantum Algorithms, Osaka City University, Osaka, Japan, 28 March, 2019..
121. “Atomic Clocks: precise time keeping devices to probing fundamental physics”, National Conference on Nonlinear Phenomena in Physics (NCNLPP -2019), Guru Nanak Dev University, Amritsar, India, 1-2 March, 2019.
122. “Recent Advances in the Relativistic Atomic Many-body The- ory”, International Conference on Quantum and Atom (ICQAO18), Indian Institute of Technology Patna, Bihar, India, 16-18 December, 2018.
123. “Relativistic Normal Coupled-cluster Theory of Electric Dipole Moments and Polarizabilities of Atoms”, The 3rd Highly Charged Ions (HCI - III), Wuhan Institute of Physics and Mathematics (WIPM), Wuhan, China, 23-27 April, 2018.

Bhalamurugan Sivaraman

124. “Laboratory Astrobiology”, International Conference on Astrobiology, University of Pune, Pune – India, 15th – 16th December 2018.
125. “VUV spectroscopy of astrochemical ices”, International Workshop on Atomic and Molecular Collisions, Udaipur, 10th – 12th December 2018..
126. “IR and VUV spectroscopy of Astrochemical Ices”, National Conference on Advances in Spectroscopy – Molecules to Materials, IITRAM, Ahmedabad, 4th – 6th October 2018.
127. “Shocks in nature – impact induced shock”, Recent Advances in Hypersonic and Shockwave Research, IISc, Bangalore, 20th July 2018.

Lectures at Universities / Institutions

Astronomy and Astrophysics

Navpreet Kaur

1. "Study of variability in AGN", KTH, Stockholm Sweden,, June 17, 2018

Manash Ranjan Samal

2. "Early Phases of Star Formation and Star Cluster", Aryabhatta Research Institute of Observational Sciences, Nainital., 28 November, 2018
3. "New insights into the structure of the Galactic bubbles and their role in the subsequent star formation with the Herschel Space Observatory", Indian Institute of Science Education and Research, Tirupati., 01 March, 2019.

Veeresh Singh

4. "New population of Active Galactic Nuclei from deep radio surveys", Instituto di Radio Astronomia - INAF, Bologna, Italy, 9th April 2018

Lokesh Dewangan

5. "Probing Observational Signatures of Cloud-Cloud Collision in Massive Star-Forming Regions", Radioastronomy Group, Nagoya University, Nagoya, Japan, 10-21 September, 2018.

Solar Physics

Ashok Ambastha

6. "Peeping through the interior of our Sun using solar oscillations as a tool", DST−Inspire camp, Aishwarya College of Education Sansthan, Udaipur, September 25, 2018
7. "Elements of Solar Physics", A course of 20 Lectures delivered at 11^{th} Post Graduate Course in Space and Atmospheric Sciences, Center for Space Science and Technology Education in Asia and the Pacific (CSSTEAP), Space Applications Center, Bopal Campus, Ahmedabad, December 3−7, 2018 and December 17−21, 2018
8. "Sounding the hidden interior of our day-time star: The Sun", DST–Inspire camp, Sir Padampat Singhania University, Bhatewar, Udaipur, January 17, 2019

Bhuwan Joshi

9. "Magnetic field configuration of the active region corona and energy release during solar flares", at School of Space Research, Kyung Hee University, Suwon, South Korea, June 12, 2018
10. "Triggering and evolution of eruptive phenomena on the Sun: A Multi-wavelength perspective", Colloquium at Korea Astronomy and Space Science Institute (KASI), Daejeon, South Korea, June 20, 2018
11. "Structure and evolution of interplanetary coronal mass ejections (ICMEs) during solar cycles 23 and 24", Invited seminar talk at Korea Astronomy and Space Science Institute (KASI), Daejeon, South Korea, June 21, 2018
12. "Solar activity and eruptive phenomena", Course lectures (10 lectures) at Aryabhatta Research Institute of Observational Science (ARIES), Nainital, India, December 24−29, 2018
13. "Origin and evolution of solar coronal transients", Astrophysics Colloquium, Institute of Physics, University of Graz, Graz, Austria, January 29, 2019

Naveen Chandra Joshi

14. "Generalization of the magnetic field configuration of typical and atypical confined flares", at Kyung Hee University, Yongin, Gyeonggi, Republic of Korea, October 25, 2018

Ranadeep Sarkar

15. "Recent advancements and challenges in solar astronomy", Salesian College, Siliguri, India, August 30, 2018
16. "A comparative study of the eruptive and non-eruptive flares produced by the largest active region of solar cycle 24", Royal Observatory of Belgium, Brussels, Belgium, May 4, 2018

Planetary Sciences

Anil Bhardwaj

17. "Indian Planetary Mission", Birbal Sahni Institute of Palaeosciences, Lucknow, January 23, 2019
18. "Indian Planetary Missions : Challenges And Science", Talk at Teachers Meet of Indian Academy of Sciences, Infosys Campus, Mysore, June 28, 2018

19. “Indian Planetary Missions ”, Young Astronomers’ Meet, PRL, Ahmedabad, September 24, 2018
20. “An Outlook on Planetary Science ”, World Space Week-2018 Popular Lecture, Space Application Centre, Ahmedabad, October 4, 2018
21. “Indian Planetary Mission”, In Face to Face with Frontiers in Science, at India International Science Festival (IISF), Indira Gandhi Prathishthan, Lucknow, 07 Oct, 2018., October 07, 2018
22. “Indian Space Missions”, at Sanshodhan - 3^{rd} Pune SciFi Fest, at National Film Archive of India, Pune, January 28, 2019
23. “Indian Planetary Exploration”, for M.Sc. students talk at Fergusson College, Pune, 31 Jan. 2019, January 31, 2019

Jayesh P. Pabari

24. “Interplanetary Dust Particles in Solar System”, An Invited Talk at Parul Institute of Engineering and Technology, Waghodia, January 28, 2019

Space and Atmospheric Sciences

Harish Chandra

25. “36 lectures: UN Course on Space and Atmospheric Science”, Space and Atmospheric Sciences Course (SAS11) at PRL, August-October, 2018.

Som Kumar Sharma

26. “Atmospheric Studies using LIDAR”, CEPT University, Ahmedabad, October 12 , 2018
27. “Atmospheric investigation using Ceilometers and LIDAR Systems”, NE-SAC, Shillong, February 22, 2019

Shyam Lal

28. “11 lectures on Concepts of Earth’s Atmosphere and Effects of Solar Radiation on Atmosphere”, Space and Atmospheric Sciences Course (SAS11) at PRL, 7 and 13-31, August, 2018.
29. “Inspire Research (INSPIRE) Science Internship Camp ”, Uka Tarsadia University, Surat, September 8 , 2018
30. “INSPIRE Internship camp ”, Aishwarya College of Education Sansthan, Udaipur, September 26 , 2018
31. “3 lectures on ”Ozone and other trace gases and atmospheric Chemistry””, Satellite Meteorology and Global Climate (SATMET -11) course at Space Applications Centre (SAC), Ahmedabad, December 24-27, 2018

Dibyendu Chakrabarty

32. “PRL experience of implementing quality assurance in Processing software”, Absolute Quality Programme (AQP) inaugurated at PRL, February 15, 2019

Geosciences

Madhusudan G. Yadava

33. “Greenhouse effect, and Global Warming, Paleoclimatology, and future climate scenario”, CSSTEAP, SATMET-11, SAC, Bopal Campus, Ahmedabad, 19 - 21 December, 2018. (3 Lectures)

Arvind Singh

34. “‘International Earth Science Olympiad (IESO) 2018’”, Anna University, (both the Indian students secured silver and bronze medals for India during 8 -17 August, 2018 in IESO Taiwan), 15 -17 May, 2018 & 7 August, 2018.
35. “‘Introduction to Paleoclimatology’”, M.Sc.(SEMESTER I) students, Gujarat University, Ahmedabad, August – October, 2018. (6 Lectures)
36. “‘Sustainable forest management’ and ‘Coastal zone management’”, M.Sc.(SEMESTER I) students, Gujarat University, Ahmedabad, August – October, 2018.(8 Lecture)

Theoretical Physics

Srubabati Goswami

37. “Mystery of the Missing Solar Neutrinos”, INSPIRE INTERNSHIP SCIENCE CAMP, organized by the UKA Tarsadia University, Surat, July 2018., July 2018
38. “Neutrinos: The Invisible Messengers”, St. Stephens College, Delhi, February 8, 2019

Atomic, Molecular and Optical Physics

Bhalamurugan Sivaraman

39. “Role of Chemical Engineering to Planetary Sciences”, Department of Chemical Engineering, VIT, Vellore., 19th July 2018
40. “Biography of molecules beyond Earth – Role of Astrochemical Ices”, Department of Chemistry, VIT, Vellore, 19th July 2018
41. “Biography of Molecules Beyond Earth”, Indian Association of Physics Teachers, Rajkot Science Center, Rajkot., 10th June 2018

Science Outreach Talks by PRL Scientists

Anil Bhardwaj

1. "Interacted with students", Pune Muktangan Exploratory Science Centre (MESC), January 30, 2019.

Vishal Joshi

2. "An interactive introduction to the Sun", G H Patel College of Engineering & Technology, Anand, Gujarat, on 30-03-2019.
3. "Workshop on Basic Astronomy", Community Science Centre, Gujarat Narmada Fartilizer Company, Bharuch, Gujarat, on 16-02-2019.

Ashok Ambastha

4. "Probing the hidden interior and outer atmosphere of our Sun", Special Multidisciplinary Webinar, Science Education and Research Foundation (SERF), Ahmedabad (Lecture's slides and YouTube video's link are available in `http://www.ser.foundation`)., on 06-09-2018.
5. "A Course of Solar Physics", A series of 8 Webinar lectures delivered under 10^{th} scientific program, Science Education and Research Foundation (SERF), Ahmedabad (Lecture's slides and YouTube links of videos are available `http://www.ser.foundation`) during February 19-22, and February 25-28, 2019, on 19-02-2018.

Rohan Eugene Louis

6. "Introduction to the Sun", at Kendra Vidyalaya Eklinggarh, Udaipur, on the occasion of Astronomical Telescope Making Workshop organized by Vigyan Prasar and Kendriya Vidyalaya Sangathan, on 09-04-2019.

Brajesh Kumar

7. "Science at PRL and USO, the various dynamic activities in the Sun and their effect in the near−earth environment", Science Express exhibition at Govt. Senior Secondary School, Badgaon, Udaipur, on 23-01-2019.

Nandita Srivastava

8. "Importance of international day of women and girls in science", at Heritage Girls School, Udaipur, India, on 11-02-2019.

Sushree Sangeeta Nayak

9. "Introduction to our star : The Sun", at Heritage Girls School, Udaipur, India, on 11-02-2019.

Bireddy Ramya

10. "Women's contribution to science and technology development", at Heritage Girls School, Udaipur, India, on 11-02-2019.

Kamlesh Bora

11. "Career options in science ", at Heritage Girls School, Udaipur, India, on 11-02-2019.

Anil Bhardwaj

12. "Interaction with Schools students", Muktangan Exploratory Science Centre (MESC), on 30-01-2019.

D. Pallamraju

13. "Space Weather and Upper Atmospheric Dynamics", Part of Faculty development program organized under the auspices of Kaizen Initiative for Academics, held at ARIBAS, New Vallabh Vidyanagar, Gujarat, on 14-03-2019.

Lokesh Kumar Sahu

14. "Future challenges in Atmospheric Measurements: Study of Climate and Environment", Workshop on Experimental Techniques in Physics, Institute of Advanced Research, Gandhinagar, India, on 07-06-2018.

Partha Konar

15. "Artificial Intelligence in research", for Advanced BSc Programme run by Gujarat Science Academy, 31st May, 2018, on 31-05-2018.

Srubabati Goswami

16. "Mystery of the Missing Solar Neutrinos ", Popular talk at the INSPIRE INTERNSHIP SCIENCE CAMP, organized by the UKA Tarsadia University, Surat, on 12-07-2018.

Namit Mahajan

17. "Leptoquark: An excellent candidate to probe new physics in flavor and dark matter sectors", National Institute of Science Education and Research, on 23-01-2019.

Area Seminar by visitors

Astronomy & Astrophysics

1. **Dr. Kamlesh Rajpurohit**, “The Largest Particle Accelerators of the Universe”, TLS Observatory, Germany, on 13-09-2018.
2. **Dr. C.S. Stalin** , “Gamma-ray emitting narrow-line seyfert 1 galaxies”, IIA, Bangaluru, on 01-11-2018.
3. **Dr. K. Sasikumar Raja** , “Density turbulence in the solar wind using low frequency angular broadening observations ”, IISER, Pune, on 15-11-2018.
4. **Prof. R.K. Manchanda**, , “History of Astronomy in TIFR and making of AstroSat mission”, TIFR, Mumbai / University of Mumbai, on 10-01-2019.
5. **Dr. Subhash Bose**, “Understanding supernovae diversity and exploring the rare and unusuals”, Kavli Institute for Astronomy and Astrophysics, China, on 21-02-2019.
6. **Dr. Susanta Kumar Bisoi**, “Where the energy during solar flare is released?”, National Astronomical Observatories, Beijing, China, on 07-03-2019.

Space and Atmospheric Sciences

7. **Dr. S. Tulasiram**, “A new ANN based global 3D dimensional Ionospheric Model (ANNIM-3D) - Approach, Merits, Limitations and scope for improvements”, Indian Institute of Geomagnetism, Navi Mumbai, on 18-03-2019.
8. **Dr. G. D. Reeves**, “The Radiation Belt Revolution”, Los Alamos National Laboratory, USA, on 22-03-2019

Geosciences

9. **Dr. Ishmohan Bahuguna**, “Monitoring of Himalayan and Polar Cryosphere using Earth observation data from orbiting satellites.”, Cryosphere Sciences Division (CSD), SAC, Ahmedabad, on 29-05-2018.
10. **Dr. Ajit Singh**, “Geological and archaeological implications of drainage morpho–dynamics in NW Indo–Gangetic plains”, Indian Institute of Technology, Gandhinagar, on 12-02-2019.
11. **Prof. Gh. Jeelani**, “Application of Stable Isotopes in delineating recharge areas and identifying the sources of recharge”, University of Kashmir, Srinagar, Jammu and Kashmir, on 26-02-2019.
12. **Dr. Satyajit Seth**, “Higgs+n-gluon one-loop amplitude: an analytical approach”, Johannes Gutenberg University of Mainz Rhineland Palatinate, Germany, on 29-10-2018.

Theoretical Physics

13. **Mr. Avdhesh Kumar**, “Thermodynamic versus kinetic approach to polarization-vorticity coupling and hydrodynamics with spin”, Institute of Nuclear Physics PAN, Krakow, Poland, on 31-10-2018.

Atomic, Molecular and Optical Physics

14. **Dr. Suchinder Sharma**, “Laser-induced fluorescence imaging for identification and recovery of rare earth elements”, Institut für Angewandte Physik, Germany, on 21-06-2018.
15. **Mr. Vishal Sharma**, “Analysis of atmospheric effects on satellite-based quantum communication: A comparative study”, IIT Jodhpur, Rajasthan, on 02-08-2018.
16. **Dr. Pranav R. Shirhatti**, “Understanding elementary processes in surface chemistry using state resolved molecular beam surface scattering experiments”, TIFR, Hyderabad, on 16-08-2018.
17. **Dr. Apurv Chaitanya N**, “Circular differential scattering of achiral structures”, School of Engineering and Sciences,Tecnológico de Monterrey, Maxico, on 31-08-2018.
18. **Dr. Rupesh Kumar**, “Continuous variables quantum communications ”, Quantum Communications Hub, University of York, on 04-09-2018.
19. **Dr. Sanjit Karmakar**, “Quantum Ghost Imaging, Quantum Microscope and Entanglement Generation in Telecommunication regime”, University of Maryland, Baltimore County (UMBC), USA, on 17-09-2018.
20. **Dr. V Jayaram**, “Shockwaves in materials research”, Solid State Chemistry Unit, IISc, Bangalore, on 17-09-2018.
21. **Prof. K Viswanathan**, “Why and How Do You Experimentally Locate Local Minima? Some Case Studies using Matrix Isolation Infrared Spectroscopy”, Department of Chemistry, IISER Mohali, on 20-09-2018.
22. **Dr. S. Chaitanya Kumar**, “Parametric source: Trends and applications ”, ICFO, Barcelona, Spain, on 10-12-2018.
23. **Dr. Jasleen Lugani**, “Integrated photonics technology for quantum information”, Postdoctoral Scholar at University of Oxford, on 11-01-2019.
24. **Dr. Muhammed Shameem K. M**, “Design and Development of a Hybrid Laser-Induced Breakdown Spectroscopy (LIBS)-Raman System using Echelle Spectrograph for Material Characterization”, Research Scholar, Manipal Academy of Higher Education, Manipal, India, on 27-02-2019.
25. **Mr. Amit Rai**, “Quantum walk of light in optical waveguides”, NIT Rourkela, Odisha, on 08-03-2019.

Student Training

Astronomy and Astrophysics

1. Ms. Niyati Shah, Indus University Ahmedabad , B.Tech, “Module development to understand the atmospheric properties of exoplanets”, from February 2019 to May 2019, [Supervisor: Dr. Arvind Singh Rajpurohit].
2. Ms. Ritu Rani , Indian Institute Of Technology, Delhi, “Wavefronyt sensing in astronomy: modal wavefront reconstruction with shack hartmann sensor”, from May 2018 to July 2018, [Supervisor: Dr. Mudit Srivastava].
3. Mr. Vipin Kumar, Indian Institute Of Technology, Thiruvanathpurram, “Polarimetry of active galactic nuclei”, from June 2018 to July 2018, [Supervisor: Dr. Shashikiran Ganesh].
4. Mr. Maharshi Doshi, Ahmedabad University, B.Tech, “Applications of machine learning for stellar light curves”, from February 2019 to April 2019, [Supervisor: Dr. Vishal Joshi]
5. Ms. Vishwa Shah, Ahmedabad University, B.Tech, “Applications of machine learning for stellar light curves”, from February 2019 to April 2019, [Supervisor: Dr. Vishal Joshi]
6. Mr. Arnav Tamrakar, Indian Institute of Space Science and Technology, Thiruvananthapuram, “Near-infrared properties of Be/X-ray binary pulsars”, from June 2018 to July 2018, [Supervisor: S. Naik].
7. Ms. Saili Keshari, Vishvabharati University, West Bengal, “Multiwavelength Study of Seyfert Galaxy NGC 4151”, from May 2018 to July 2018, [Supervisor: V. Singh].
8. Mr. Shubham Khokar, IIT-Bombay, “Understanding thermal design aspects for the proposed DAKSHA mission”, from December 2018 to December 2018, [Supervisor: S. Vadawale].
9. Ms. Shreeya Singh, IIT-Bombay, “Understanding thermal design aspects for the proposed DAKSHA mission”, from December 2018 to December 2018, [Supervisor: S. Vadawale].
10. Mr. Nevil Shal, IISER, Mohali, “NIR study of Seyfert galaxies”, from May 2018 to July 2018, [Supervisor: V. Joshi].
11. Mr. Hiren Kelaiya, PDPIAS, Charusat, Anand, “NIR study of Nova Oph 2017”, from December 2018 to May 2019, [Supervisor: V. Joshi].
12. Ms. Ashlin Varghese, Christ University, Banglore, “Understanding the roles of outflows on the growth and evolution of protostars”, from October 2018 to December 2018, [Supervisor: M. R. Samal].
13. Mr. Ronit Patel, Charotar University of Science and Technology, “Understanding physical conditions of star forming clouds with far-infrared observations”, from March 2019 to May 2019, [Supervisor: M. R. Samal].
14. Ms. Aditi Pathak, Charotar University of Science and Technology, Ahmedabad, “Understanding physical conditions of star forming cloud with far-infrared observations”, from March 2019 to May 2019, [Supervisor: M. R. Samal].
15. Mr. Ajay Potdar, Indian Institute of Space Science & Technology, “Solving radiative transfer using Monte Carlo simulation”, June - July 2018, Supervisor: Dr. Avik Sarkar.

Solar Physics

16. Kartik Chhajed, Indian Institutes Of Science Education And Research Mohali, “Magnetohydrodynamics Of The Solar Corona”, from May 2018 to July 2018, [Supervisor: Dr. Ramitendranath Bhattacharya]
17. Divya Thomas and Pranav Singhal, St. Stephen’s College and Venkateshwara College, University of Delhi, “Study of Solar Activity cycle and the Oscillations in the Solar Atmosphere”, from 7 June 2018 to 13 July 2018, [Supervisor: B. Kumar].
18. Nayantara Rose Jose, Mahatma Gandhi University, Kottayam, Kerala, “Study of the phase lag among the solar activity indicators over the solar cycles”, from 15 December 2018 to 15 March 2018, [Supervisor: B. Kumar].
19. Hitaishi K. Bhatt, Department of Physics, M & N Virani Science College, Rajkot, Gujarat, “Estimation of solar rotation using GONG observations”, from 10-20 May 2018 to 15-22 November 2018, [Supervisor: B. Kumar].
20. Jaidev Sharma, Department of Physics, CCS University, Meerut, U.P., “Long-term study of the diferential roation of the solar atmosphere using multi-wavelength observations”, from 15 November 2018 to 22 November 2018, [Supervisor: B. Kumar].
21. Aditya Jaypal, University of Waterloo, Canada, “Using multiple-point observations & analysis of ICMEs to test existing interplanetary propagation models”, from 15 May 2018 to 15 June 2018, [Supervisor: Nandita Srivastava].
22. Kush Kumar Sharma, Department of Aerospace Engineering, University of Petroleum and Energy Studies, Dehradun, “Study and Analysis of Solar Radio Flux at Multiple Frequencies”, from 5 July, 2018 to 5 August, 2018, [Supervisor: B. Joshi].
23. Pooja, Dept. of Physics, Kumaun University, Nainital, “Multi-wavelength analysis of a circular ribbon flare”, from 10 September 2018 to 31 October 2018, [Supervisor: B. Joshi].

Planetary Sciences

24. Ashutosh Choudhary, Indian Institute of Technology, Roorkee, “Classification and characterization of Mount Abu granites based on microscopic and geochemical studies”, from May 2018 to July 2018, [Supervisor: Dr. Dipak Kumar Panda]
25. Siddharth Rajpriye, “Indian Institute of Technology, Roorkee, Petrography, Mineralogy And Thermal History Of Ordinary Chondrite (Mahadevpur Meteorite)”, from May 2018 to July 2018, [Supervisor: Dr. Dwijesh Ray]
26. Shakti Ray, Pune University, “A Study On Thermophysical Characterisation Of Lunar Analogous Samples”, from May 2018 to July 2018, [Supervisor: Dr. Karnam Durga Prasad]
27. Veneela Mandala, Andhra University, “Topography and Temperature Study of Some Important Sites On The Moon”, from May 2018 to July 2018, [Supervisor: Dr. Karnam Durga Prasad]
28. Nikita Pithadiya, Indus University Ahmedabad , B.Tech, “Study, Design And Development of Technique For Measurement Of Dielectric Permittivity Measurement Of Liquid And Semi-Solid Samples”, from February 2019 to May 2019, [Supervisor: Dr. Karnam Durga Prasad]
29. Aitreyi Patel, Indus University, Ahmedabad , B.Tech, “Detection and Measurement of Gaseaus Matter In Atmosphere Leading to Air Pollution”, from February 2019 to May 2019, [Supervisor: Dr. Kinsuk Acharyya]
30. Rojal Bhandari, Indus University, Ahmedabad , B.Tech, “Detection And Measurement Of Particulate Matter In Atmosphere Leading To Air Pollution”, from February 2019 to May 2019, [Supervisor: Dr. Kinsuk Acharyya]
31. T. M. Nandakishor, Amrita Vishwa Vidyapeetham, Kollam, “Modal and structural analysis of Mechanical systems (Student from science academy)”, from May 2018 to July 2018, [Supervisor: A. Bhardwaj].
32. Chandra Reddeiah, Rajiv Gandhi University of Knowledge Technologies - APIIIT, Kadapa, “Simulating the effect of probe properties on in-situ lunar thermophysical measurements”, from May 2018 to July 2018, [Supervisor: A. Bhardwaj].
33. Viral Patel, Indus University, Ahmedabad, “Classification and mapping of lunar basalts using machine learning techniques”, from February 2019 to May 2019, [Supervisor: Megha Bhatt].
34. Harsh Kathiriya, Indus University, Ahmedabad, “Classification and mapping of lunar basalts using machine learning techniques”, from February 2019 to May 2019, [Supervisor: Megha Bhatt].
35. Aniruddha Sinha, Symbiosis Institute of Geoinformatics, Pune, “Geological assessment of probable landing sites from lunar southern pole”, from April 2019 to May 2019, [Supervisor: Megha Bhatt].
36. Shreya Natrajan, IIST, “Thermal alteration in meteorites based on studies of Insoluble organic matter”, from August 2018 to April 2019, [Supervisor: K. K. Marhas].
37. Aniket Saighwal, Kurushetra University, “Search of chlorine rich phases in CV CAIs”, from January 2019 to May 2019, [Supervisor: K. K. Marhas].
38. Vivek Kewalramani, Gujarat Technology University, Ahmedabad, “Gas grain condensation in protoplanetary disk atmosphere”, from January 2019 to April 2019, [Supervisor: K. K. Marhas].
39. Mittal Patel, Dharmsinh Desai University, Nadiad, “Gas grain condensation in protoplanetary disk atmosphere”, from January 2019 to April 2019, [Supervisor: K. K. Marhas].
40. J. Praveen, -, “Space radiation and detection (Student from science academy)”, from May 2018 to July 2018, [Supervisor: S. K. Goyal].
41. Akshit Gupta, Nirma University Of Science And Technology, Ahmedabad, “LabVIEW data acquisition for mass spectrometer”, from January 2019 to May 2019, [Supervisor: S. K. Goyal].
42. Harima Patel, Dharmsinh Desai University, “: LabVIEW data acquisition for mass spectrometer”, from January 2019 to May 2019, [Supervisor: S. K. Goyal].
43. Hnin Ei Lwin, Lecturer, University in Myanmar (under UN course), “GEANT4 simulation for the silicon detectors in ΔE-E mode”, from January 2019 to May 2019, [Supervisor: S. K. Goyal].
44. Htet Htet Linn, Lecturer, University in Myanmar (under UN course), “Modal and structural analysis of quadrupole mass spectrometer”, from January 2019 to May 2019, [Supervisor: S. K. Goyal].
45. Pushkala K., Pondicherry University, Pondicherry, “Study of ablation altitude of micrometeorites in Martian atmosphere”, from May 2018 to July 2018, [Supervisor: J. P. Pabari].
46. V. R. Dinesh Kumar, Birla Institute of Technology and Science, Hyderabad Campus, “Distance and Source Information Retrieval based on Lightning Measurement”, from July 2018 to November 2018, [Supervisor: J. P. Pabari].
47. Bhautik D. Patel, Charusat University, Changa, “Processing electronics of interplanetary dust particles detector”, from January 2019 to April 2019, [Supervisor: J. P. Pabari].
48. Dhruvang P. Shah, Charusat University, Changa, “Processing electronics of interplanetary dust particles detector”, from January 2019 to April 2019, [Supervisor: J. P. Pabari].
49. Uzma W. Shaikh, Charusat University, Changa, “Processing electronics of interplanetary dust particles detector”, from January 2019 to April 2019, [Supervisor: J. P. Pabari].
50. Adeetya Patel, U.V. Patel College of Engineering, Ganpat University, “Planet Weather Research and Forecast Modeling System”, from Jan 2019 to April 2019, [Supervisor: V. Sheel].
51. Hemangini Katara, Nirma University, “Probing Planetary Atmospheres by Radio Signal”, from Jan 2019 to April 2019, [Supervisor: V. Sheel].

Space and Atmospheric Sciences

52. Devanshi Dave, Indus University, Ahmedabad, B.Tech, “Design And Implementation Of Bipolar Temperature Controller For Optical Interference Filter Applications”, from February 2019 to May 2019, [Supervisor: Dr. D. Chakrabarty]
53. Krima Rohela, Indus University, Ahmedabad, B.Tech, “Design And Fabrication Of Back-End Electronics Of Space Borne Langmuir Probe”, from February 2019 to May 2019, [Supervisor: Dr. D. Chakrabarty]
54. Pragnesh Dave, Vallabh Vidynagar, “Volatile Organic Compound Emissions From A Pirana Landfill, Ahmedabad, India”, from May 2018 to July 2018, [Supervisor: Dr. Lokesh Kumar Sahu]

55. Aditya Anand, Indian Institute Of Technology, Gandhinagar, “Portable Meteorological Data Logger System”, from May 2018 to July 2018, [Supervisor: Dr. S. Ramachandran]

56. Mahir Shah, VVP Engineering College, Gujarat , B.E. , “Development Of Algorithm For Visualisation Of Atmospheric Parameters Using Satellite Ground Based Remote Sensing Instruments And Model Data”, from February 2019 to April 2019, [Supervisor: Dr. Som Kumar Sharma]

57. Esha Varshney, Banasthali Vidyapith, Rajasthan , B.Tech. , “Development Of Algorithm For Visualisation Of Atmospheric Parameters Using Satellite, Ground Based Remote Sensing Instruments And Model Data”, from February 2019 to May 2019, [Supervisor: Dr. Som Kumar Sharma]

58. Anand Chauhan, Indian Institute of Technology, Gandhinagar, “Ethernet Based Data Acquisition System”, from May 2018 to July 2018, [Supervisor: Dr. T. A. Rajesh]

59. Kalgi Soladhara, School of Sciences, Gujarat University, “Long-term trends of sulphur dioxide over Gujarat using satellite data”, from January 2019 to April 2019, [Supervisor: Harish Gadhavi].

60. Meenal Dhanetwal, Devi Ahilya Vishwavidyalaya, Indore, “hydroxyl (OH) airglow emission and it’s rotational temperature”, from May 2018 to 09 July 2018 , [Supervisor: Ravindra Pratap Singh].

61. Khyati Godhani, Dharmsinh Desai University, Nadiad, “To design software for automatic acquisition from a grating based spectrograph”, from January 2019 to April 2019, [Supervisor: Ravindra Pratap Singh].

62. Bhargav Lad, Dharmsinh Desai University, Nadiad, “To design software for automatic acquisition from a grating based spectrograph”, from January 2019 to April 2019, [Supervisor: Ravindra Pratap Singh].

63. Kaman Ansari, Pt. Ravisankar Shukla Shukla University, Raipur, Chhattisgarh, India., “Investigation of Middle Atmospheric Temperature and Ozone over Indian Region”, from May 2018 to June 2018, [Supervisor: Som Kumar Sharma].

64. Shubham Chaturvedi, Banaras Hindu University, “Meteorological Variations and Air Trajectories”, from May 2018 to July 2018, [Supervisor: Lokesh Kumar Sahu].

65. Hiram Khan, Ahmedabad, “Ionosphere over Ahmedabad”, from February 2019 to April 2019, [Supervisor: Som Kumar Sharma and H. Chandra].

Geosciences

66. Ms. Divyanshi Shukla, Lucknow University, “Developing a method to measure the Radiocarbon Activity of Modern Atmospheric CO_2”, from May 2018 to July 2018, [Supervisor: Dr. M.G. Yadava].

67. Ms. Lekshmi P Kumar, Cochin University Of Science And Technology (CUSAT), “Ambient Aerosol and Reactive Oxygen Species”, from May 2018 to July 2018, [Supervisor: Dr. Neeraj Rastogi].

68. Mr. Aditya Singh, IIT (ISM) Dhanbad, “Geochemical methods to estimate ocean nitrogen fluxes.”, from May 2018 to July 2018, [Supervisor: Dr. Arvind Singh].

69. Ms. Riddhi Siddhpura, M.sc. Analytical Chemistry, “Analysis of a selected major elements (Ca , Al ,Fe,K and Mg) in a proglacial Taroo lake sediment , Ladakh Himalaya”, from May 2018 to July 2018, [Supervisor: Dr. A.D. Shukla].

70. Ms. Aashita Rana, M.sc. Analytical Chemistry, “Behaviour of a few major elements in high altitude relict lake (Shey) sediments , Ladakh Himalaya”, from May 2018 to July 2018, [Supervisor: Dr. A.D. Shukla].

71. Mr. Pratik Chavda, M.Sc., “Reactive Oxygen Species Generation Capability of Ambient Aerosol”, from December 2018 to April 2019, [Supervisor: Dr. Neeraj Rastogi].

72. Ms. Krishna Rasaniya, M.Sc., “Brown Carbon in the Ambient Aerosol”, from December 2018 to April 2019, [Supervisor: Dr. Neeraj Rastogi].

73. Avinesh Kumar, Indian Institutes Of Science Education And Research, Mohali, “Geochemistry of partially active mud flats of gulf of Kutch: implication towards sea level reconstruction”, from May 2018 to July 2018, [Supervisor: Dr. A. D. Shukla]

74. Anisha Ganaxama Naique Verencar, Goa University, “Geochemistry and Petrography of Panjal volcanics, In Zanskar valley, Ladakh Himalayas”, from May 2018 to July 2018, [Supervisor: Dr. A. D. Shukla]

75. Naga Santosh Sree Bhuvan G, Pondicherry University, “Trace element behaviour during melting of a multicomponent mantle source”, from May 2018 to July 2018, [Supervisor: Dr. Arvind Singh]

Theoretical Physics

76. Prajjwal Yash, Indian Institute of Space Science & Technology, Thiruvanathpurram, “Theory Of Classical And Quantum Phase Transitions”, from June 2018 to July 2018, [Supervisor: Dr. Angom Dilip Kumar Singh]

77. Sairam Ithineni, Indian Institutes Of Science Education And Research, Thiruvananthapura, “Study Of Optical Lattice & Landau Theory For Bose Hubbard Model”, from May 2018 to July 2018, [Supervisor: Dr. Angom Dilip Kumar Singh]

78. Kiran M. Jayasurya, Indian Institute of Space Science & Technology, Thiruvanathpurram, “Accretion Disks Around Compact Objects: Their Evolution, High Luminosity, And Instabilities”, from June 2018 to July 2018, [Supervisor: Dr. J. R. Bhatt]

79. Sabyasachi Das, National Institute of Science Education and Research, Bhubaneswar, “Experimental Tests Of General Relativity”, from May 2018 to July 2018, [Supervisor: Dr. Namit Mahajan]

80. Maithresh Palemkota, Centre For Excellence In Basic Sciences, Mumbai, “Generalised Nyquist Equation And Power Dissipation In A Quantum Dot”, from May 2018 to July 2018, [Supervisor: Dr. Navinder Singh]

81. Mathin Yadav, Indian Institute of Space Science & Technology, Thiruvanathpurram, “Magneto-Resistance Due To Spin Fluctuation Generation”, from June 2018 to July 2018, [Supervisor: Dr. Navinder Singh]

82. Pooja V R, Calicut University, “Integer Quantum Hall Effect”, from May 2018 to July 2018,[Supervisor: Dr. Navinder Singh]

83. Mehak Bindra, Birla Institute of Technology & Science, Pilani, “Scattering Theory”, from May 2018 to July 2018, [Supervisor: Dr. Partha Konar]

84. Niharika Sonar, Indus Institute of Technology And Engineering, Ahmedabad, B.Tech. , “PRLconnect- An Event Management Android Application”, from February 2019 to April 2019, [Supervisor: Dr. Partha Konar]
85. Sagar Vadhel, Sardar Patel University, “Gravitational Wave From Binaries Masses Without General Relativity”, from May 2018 to July 2018, [Supervisor: Dr. Partha Konar]
86. Kushan Dharmadarshi, National Institute of Technology, (Rec), Surat, “Propagation Of Gravitational Waves In Linearised Gravity And Second Order Corrections To It”, from May 2018 to July 2018, [Supervisor: Dr. S. Mohanty]
87. Ayush Paliwal, Delhi Technological University, “Schwarzschild And Kerr Black Holes”, from May 2018 to July 2018, [Supervisor: Prof. S. Mohanty]
88. Siddhartha Poddar, IISER Bhopal, “Neutrino Oscillation”, from May 2018 to July 2018, [Supervisor: Prof. S. Goswami].

Atomic, Molecular and Optical Physics

89. Sandhya Iyer, Indus University, Ahmedabad, B.Tech, “Development of stable currents source and automation of entanglement characterization scheme”, from February 2019 to April 2019, [Supervisor: Dr. Goutam Kumar Samanta]
90. Ishan Varma, Centre for excellence in basic sciences , “Generation and propagation of optical vortices and hollow gaussian beams”, from May 2018 to July 2018, [Supervisor: Dr. Ravindra Pratap Singh]
91. Pranav Tiwari, Indian Institute Of Technology, Thiruvanathpurram, “Generation and propagation properties of optical vortex and hollow gaussian beam”, from June 2018 to July 2018, [Supervisor: Dr. Ravindra Pratap Singh]
92. Shiva Karthik, B.E - University Visvesvaraya College of Engineering, Bangalore, “Shock processing of microbes, membranes and amino acids.”, from June 2018 to Present, [Supervisor: B. Sivaraman].
93. Hari krishnan, MSc Chemistry, VIT – Vellore, “Infrared spectroscopy of mercaptoethanol in ISM conditions”, from Dec 2018 to April 2019, [Supervisor: B. Sivaraman].
94. Ashish, MSc Chemistry, VIT – Vellore, “Reversible phase change in astrochemical ices ”, from Dec 2018 to April 2019, [Supervisor: B. Sivaraman].
95. Neha Jitkar, MSc. Physics, Fergusson college, Pune, “To Study Effect Of Annealing On LM-OSL Component In Quartz”, from April 2018 to June 2018, [Supervisor: Naveen Chauhah].

Computer Center

96. Viraj Khatri, U. V. Patel College Of Engineering , B.Tech, “Scientific Software’s Log Analysis System”, from February 2019 to May 2019, [Supervisor: Mr. Hitendra Mishra] - CC

Division Visitor Details

Astronomy and Astrophysics

1. Prof. A. R. Rao, TIFR, Mumbai, “Discussion meeting”, from 30-08-2018 to 01-09-2018.
2. Prof. Dipankar Bhattacharya, IUCAA, Pune, “Discussion Meeting”, from 30-08-2018 to 01-09-2018.
3. Varun Bhalerao, IIT-Bombay, Mumbai, “Discussion Meeting”, from 30-08-2018 to 01-09-2018.
4. Hiromitsu Takahashi, Hiroshima University, Hiroshima, Japan, “Discussion Meeting”, from 04-03-2019 to 04-03-2019.

Solar Physics

5. Mr. Christian Monstein, ETH Switzerland, “Installation of e-CALLISTO at USO”, from 02-10-2018 to 05-10-2018,[Seminar : “Solar Radio Astronomy ”CALLISTO instrument and the e-CALLISTO network”].
6. Dr. A. Shanmugaraju, Arul Anandar College, Madurai Kamaraj University, “Collaborative work and area seminar”, from 12-11-2018 to 16-11-2018,[Seminar : “Type II radio bursts, coronal mass ejections and geoeffectiveness”].
7. Dr. K. Sasikumar Raja, A & A Division, PRL, Ahmedabad, “Inter divisional A & A & USO seminar”, from 28-11-2018 to 29-11-2018,[Seminar : “Solar Wind Density Turbulence from 2 to 45 Rsun”].
8. Dr. Jayant Joshi, The Institute of Theoretical Astrophysics (ITA), University of Oslo, “Area seminar”, from 22-01-2019 to 22-01-2019,[Seminar : “Properties of Chromospheric Magnetic Field of Sunspots”].
9. Dr. K. Kasturirangan, Raman Research Institute, Bangalore, “Udaipur Solar Observatory visit”, from 11-03-2019 to 11-03-2019.
10. Mr. Rahul Yadav, The Institute for Solar Physics, Stockholm, Sweden, “Thesis defense and area seminar”, from 15-03-2019 to 19-03-2019,[Seminar : “The magnetic structure of a flux emerging region in the photosphere and the chromosphere”].

Planetary Sciences

11. Munmun Chakarvorty, University of Allahabad, “collaborative research”, from 03-01-2019 to 14-01-2019.

Space and Atmospheric Sciences

12. S. Tulasi Ram, Indian Institute of Geomagnetism, Navi Mumbai, “To deliver a SPASC division seminar and to participate in the discussion on the possible research collaborations on space weather physics.”, from 18-03-2019 to 19-03-2019,[Seminar : “A new ANN based global 3D dimensional ionospheric Model (ANNIM-3D) - Approach, Merits, Limitations and scope for improvements”].
13. G. D. Reeves, Los Alamos National Laboratory, New Mexico, USA, “To deliver a SPASC division seminar, a PRL colloquium and to interact with the faculty, students and post-doctoral fellows.”, from 19-03-2019 to 24-03-2019,[Seminar : “Space sciences at Los Alamos National Laboratory - A Personal Perspective”].

Geosciences

14. Dr.Douthitt Charles Brown, M/s. ThermoFisher Scientific IOMS group, Branchburg, NJ 08876, USA, “To discuss new updates with endusers of Mass Spectrometers”, from 25-05-2018 to 25-05-2018.
15. Dr.Nathan Saetveit, M/s. Elemental Scientific, NE 68122, USA, “Installation of SeaFAST system of HR-ICP-MS laboratory.”, from 15-10-2018 to 18-10-2018.
16. Mr.Yoshiki Taisuke, M/s. Rigaku Corporation, Japan, “For technical discussions on Benchtop WD/XRF Fluorescence Analysers.”, from 05-12-2018 to 05-12-2018.
17. Mr.Wayne Edward Mozer, M/s. Teledyne Technologies, CA 91360, USA, “For discussion with the end user of the instrument i.e. Mass Spectrometers & Auto Samplers.”, from 11-12-2018 to 11-12-2018.
18. Mr.Barbula James Bryan, M/s. Teledyne Technologies, CA 91360, USA, “To give training on operation & maintenance of laser ablation system, with respect to HR-ICPMS.”, from 10-12-2018 to 11-12-2018.
19. Mr.Ciprian Cosmin Stremtan, M/s. Teledyne Technologies, CA 91360, USA, “To give training on operation & maintenance of laser ablation system, with respect to HR-ICPMS.”, from 10-12-2018 to 11-12-2018.
20. Dr.Jean-Paul Vernier, National Institute of Aerospace (NIA), NASA, Hampton, VA 23666, USA, “For balloon experiments under ISRO-NASA collaboration.”, from 14-09-2018 to 14-09-2018.

Theoretical Physics

21. Dr. Sandeep Chatterjee, Dept. Physics AGH University Krakow Poland, “To present a Seminar and Interact with Division Members”, from 02-04-2018 to 06-04-2018,[Seminar : “Heavy quarks as probes of longitudinal structure of the fireball in relativistic heavy ion collisions”].

22. Dr. Mansi Dhuriya, IIT Mumbai, “Visit her Recent Work Discussion ”, from 19-04-2018 to 25-04-2018.
23. Prof. Brajesh K. Mani, Dept. of Physics IIT Delhi Hauz Khas,New Delhi-110016, “Discuss the details of Collaborative project and explore avenues for further collaboration on topics of common interst”, from 23-04-2018 to 28-04-2018.
24. Mr. Ravi Kumar, Dept. of Physics IIT Delhi Hauz Khas,New Delhi-110016, “Discuss the details of project and explore avenues for further collaboration on topics and polices.”, from 23-04-2018 to 28-04-2018.
25. Dr. Dhiraj Kumar Hazra, Paris Centre for Cosmological Physics, Paris, France, “To give a Seminar”, from 13-06-2018 to 16-06-2018,[Seminar : “Decoding cosmic fingerprints: constraining the generation and evolution of primordial fluctuations”].
26. Ms. Disha Bhatia, C-338,TIFR, 1st Homi Bhabha Road Mumbai-400005, “Present her Work at the seminar and pursue collaborative works”, from 25-06-2018 to 29-06-2018,[Seminar : “Photon probes at colliders”].
27. Prof. Sandeep Gautam, Dept. Of Physics IIT Ropar, Nangal Road,Rupnagar, Punjab-140001, “Collaborative Project om the Physics of spin-orbit coupling in optical lattices and explore avenues for other collaborative projects on topics of common interest.”, from 03-06-2018 to 30-06-2018.
28. Mr. Siddharth Dwivedi, Harish-Chandra Research Institute, Allahabad, “Present Work at the Seminar ”, from 02-07-2018 to 06-07-2018,[Seminar : “Pinning the light pseudoscalar in Lepton Specific 2HDM”].
29. Dr. Ketan Patel, IISER Mohali, “Present work at seminar ”, from 04-07-2018 to 06-07-2018,[Seminar : “Clockworking the Yukawa couplings”].
30. Mr. Ajeet Kumar, HP University, Shimla, “visit for a research collaborative ”, from 21-06-2018 to 15-07-2018.
31. Mr. Sabyasachi Chakraborty, TIFR Mumbai-400005, “Present at Seminar on Supersymmetry”, from 26-07-2018 to 01-08-2018,[Seminar : “Non-holomorphic supersymmetry and scalar sequestering”].
32. Dr. Narendra Nath Dutta, Centre of Theoretical Studies, Dept. Of Physics, IIT Kharagpur-721302, “Discuee on the topic of relativistic coupled-cluster theory”, from 15-07-2018 to 14-08-2018.
33. Dr. Mofazzal Azam, Mumbai, “To discuss project on dark-matter and some aspect of QCD.”, from 18-11-2018 to 21-11-2018.
34. Dr. Guruprsad Kadam, Dept. Of Physics, Shivaji University, Kolhapur Maharashtra-416004, “Discussing project on properties of hadronic nateer.”, from 04-12-2018 to 20-12-2018.
35. Dr. Bhaswar Chatterjee, IIT Indore, “Discuss on Magnetic effects on Quark transition”, from 09-12-2018 to 20-12-2018.
36. Dr. Shankha Banerjee, Institute for Particle Physics Phenomenology, Durham University, “Present Work At Seminar”, from 04-01-2019 to 05-01-2019,[Seminar : “Constraining certain Higgs couplings at the HL-LHC and beyond.”].
37. Dr. Arko ROy, Max Planck Institute for the Physics ,Dresden, “Discussing on Project work”, from 21-01-2019 to 25-01-2019.
38. Dr. R. Krishnan, The School of the Good Shepherd,Thiruvananthapuram, “Present At Seminar”, from 21-01-2019 to 24-01-2019,[Seminar : “Fully constrained neutrino mass matrices and how to model them”].
39. Dr. Ranjita Kumari Mohapatra, PDF Dept. of Physics IIT Bombay, Mumbai, “Collaborative Work On Transport Properties of Quark Matter.”, from 18-02-2019 to 28-02-2019.
40. Dr. Siddharth Dwivedi, Indian Association for Cultivation of Science (IACS) Kolkata, “Present At Seminar”, from 29-04-2019 to 03-05-2019,[Seminar : “Reconstructing heavy Higgs boson masses in Leptophilic 2HDM”].

Atomic, Molecular and Optical Physics

41. Dr. Falguni Bhattacharya, Scientist-B, ISR Gandhinagar, “Collaborative Research on Sabarmati Valley and Kutch”, from 10-01-2018 to 10-07-2018.
42. Dr. Sapta rishi dey, Inspire Faculty IIT Gandhinagar, “Collaborative Research in Himalayas”, from 23-01-2018 to 22-04-2018.
43. Biraj Borgohain, SRF, IIT Mumbai, “Collaborative Research Eastern Himalya flood sequences”, from 10-04-2018 to 15-08-2018.
44. Madhavi dabhi, JRF, MSU, Baroda, “Collaborative Research in Kutch”, from 27-06-2018 to 27-12-2019.
45. Anil Devara, JRF, MSU, Baroda, “Training and Collaborative work in Andhra archaelogy”, from 06-08-2018 to 31-07-2019.
46. Atul Kumar Singh, SRF, IISER Kolkata, “Training in luminescence dating”, from 22-08-2018 to 05-09-2019.
47. vinod hegde, SRF, MIT, Bangalore, “collaborative work on artificial phosphors”, from 10-09-2018 to 20-09-2018.
48. Dr. Ajit Singh, PDF, IIT Gandhinagar, “Collaborative Research work on markande river”, from 01-10-2018 to 31-03-2019.
49. Dr. Sapta rishi dey, Inspire Faculty IIT Gandhinagar, “Collaborative Research in Himalayas”, from 18-03-2019 to 18-09-2019.
50. Pawan Kumar, SRF, JNU, Delhi, “Training in luminescence dating”, from 23-07-2018 to 05-08-2018.

Astronomy and Astrophysics

Solar cycle 24: An unusual polar field reversal

It is well known that the polarity of the Sun's magnetic field reverses or flips around the maximum of each 11 year solar cycle. This is commonly known as polar field reversal and plays a key role in deciding the polar field strength at the end of a cycle, which is crucial for the prediction of the upcoming cycle. We investigated solar polar fields during cycle 24, using measurements of solar magnetic fields in the latitude range $55^\circ - 90^\circ$ and $78^\circ - 90^\circ$. Our study showed a prolonged and unusual hemispheric asymmetry in the polar field reversal pattern in solar cycle 24. This study was carried out using medium resolution line-of-sight synoptic magnetograms from the magnetic database of the National Solar Observatory at Kitt Peak (NSO/KP), USA for the period between February 1975 and October 2017, covering solar cycles $21-24$ and high-resolution line-of-sight synoptic magnetograms from the Michaelson Doppler Imager instrument onboard the Solar Heliospheric Observatory. Synoptic magnetograms using radial measurements from the Heliospheric Magnetic Imager instrument onboard the Solar Dynamics Observatory, covering solar cycle 23 and 24, were also used. It was established that the Southern solar hemisphere unambiguously reversed polarity in mid-2013 while the reversal in the field in the Northern solar hemisphere started as early as June 2012, was followed by a sustained period of near-zero field strength lasting until the end of 2014, after which the field began to show a clear rise from its near-zero value. The upper two panels of Figure 1 show, by filled red dots with 1 σ error bars in grey, the signed values of polar field strengths from NSO/KP, in the latitude range $55^\circ - 90^\circ$, in the solar Northern (top panel) and Southern (bottom panel) hemispheres spanning period covering solar cycles $21-24$, each of which is demarcated by vertical dashed lines. A smoothed solid black curve with 1 σ error bars in pink has been drawn through the data points in fig. 1. Also, overplotted by a dashed blue curve are the signed values of polar field strengths from WSO. In order to eliminate yearly geometric projection effects at the poles due to the rotation of the Earth on the measured line-of-sight fields, a 1.58 year (or 20nHz) low pass filter was used to filter WSO polar fields. The time of reversal of polarity in each hemisphere, determined from NSO/KP smoothed curve, is marked by small blue solid lines in each panel. The lower panel of Fig 1. shows the time of completion of polar reversal in the solar north by a small red solid line in cycle 24. The lower two panels of Fig. 1 show only cycle 24, and to avoid clutter and enhance clarity, the error bars have been left out. Overplotted by a solid green curve, in the lower two panels of Fig. 1, is the signed values of polar field strengths from SDO/HMI. In cycle 24, the Southern hemisphere underwent a clean unambiguous reversal in November 2013, while the Northern hemisphere has shown an extended zero-field condition after the first reversal in June 2012. The reversal in the Northern hemisphere was completed only by November 2014.

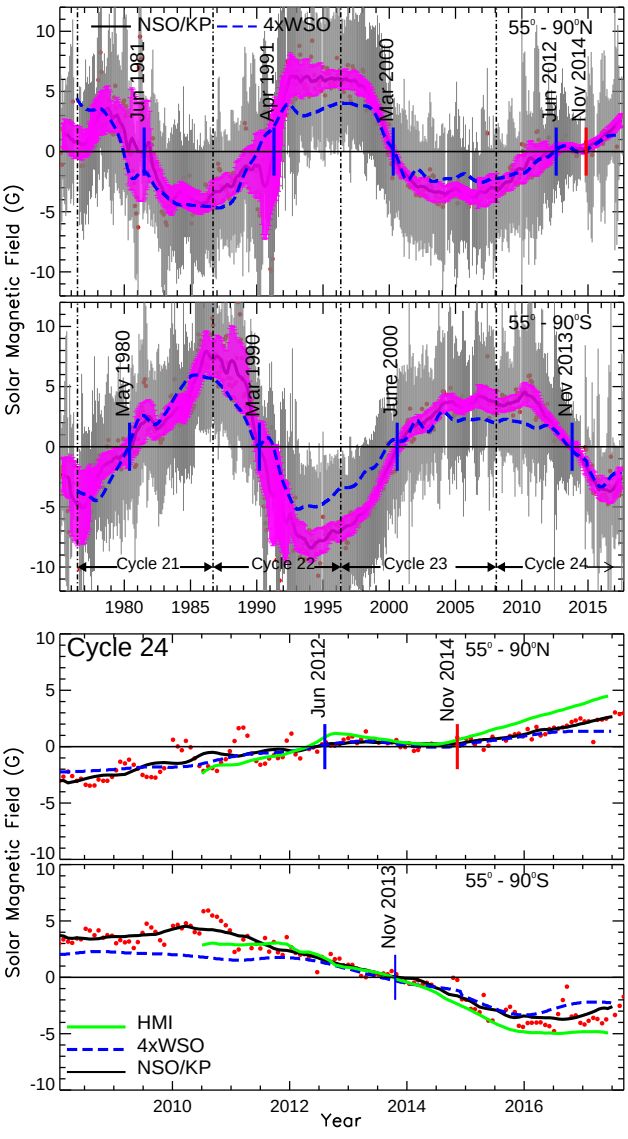


Figure no. 1: This figure shows how in cycle 24, the Southern hemisphere underwent a clean unambiguous reversal in November 2013, while the Northern hemisphere showed an extended zero-field condition after the first reversal in June 2012. The reversal in the Northern hemisphere was finally completed only by November 2014.

While this study compliments a similar study carried out using

microwave brightness measurements which claimed that the field reversal process in cycle 24 was completed by the end of 2015, our results show that the field reversal in cycle 24 was completed earlier i.e. in late 2014. Signatures of this unusual field reversal pattern were also clearly identifiable in the solar wind, using our observations of interplanetary scintillation at 327 MHz (see Fig. 2) which supported our magnetic field observations and confirmed that the field reversal process was completed at the end of 2014.

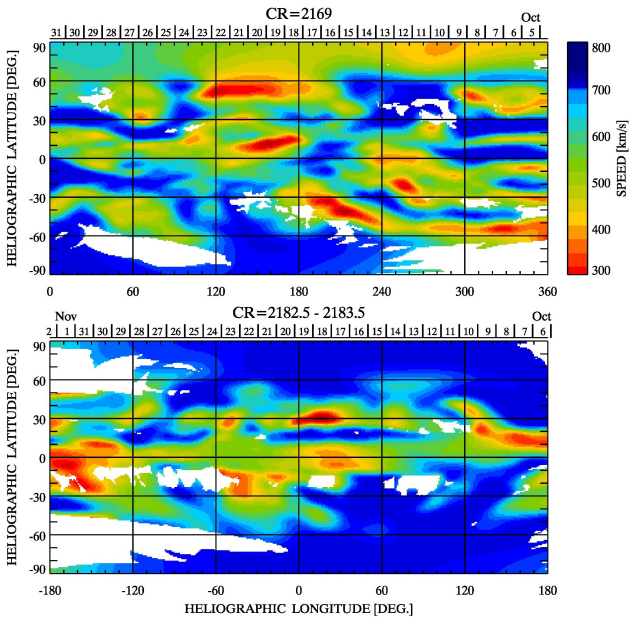


Figure no. 2: Synoptic velocity maps for Carrington rotation 2169 in October 2015 (upper panel) and October 2016 (lower panel). The large polar coronal hole in the Southern hemisphere is apparent but its counterpart in the Northern hemisphere has not formed in as of October 2015 while it is fully developed in October 2016, a year later.

(P. Janardhan)

This work was done in collaboration with ISEE, Japan and NAO, China.

Numerical simulation of coronal spicules

High resolution images from the Hinode mission started indicating that type two spicules are one of the prime candidates responsible for the million degrees solar corona. They are ubiquitous in the solar atmosphere and are believed to be capable of carrying energy from the solar surface to its atmosphere. Type two spicules probably get generated in the lower chromosphere, but understanding how they deposit energy in the corona is still a challenging task. We perform a two dimensional magnetohydrodynamic simulation of type two spicules in the solar corona. The simulation output is then used to produce Extreme Ultraviolet spectral lines. Produced synthetic lines show spectral line red-blue asymmetry as is seen using various space based observations. We also compute the amount of energy and mass spicules can carry from the chromosphere to the corona. We conclude that spicules are capable enough to deposit sufficient amount of energy to the corona to keep it million degree hot.

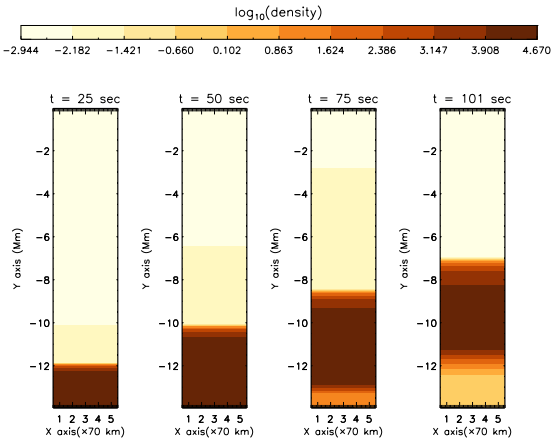


Figure no. 3: Simulation snapshots at different moments showing the propagation of a spicule along the magnetic field structure of the solar corona.

(S. S. Mondal & A. Sarkar)

Triggering of molecular emissions in comet C/2015 V2 (Johnson)

A typical optical spectrum of a comet with well developed coma shows molecular emissions dominated by carbon chain molecules. However, time and again, comets and asteroids show unique characteristics which deviate from their general behavior. Comet C/2015 V2 (Johnson) was observed and found to be one such peculiar case in which molecular gas emissions were triggered at a late stage in its orbit . In general, emission lines start appearing in the spectrum of a comet at around 3 AU. If not for the carbon chain emissions, atleast the CN emission is expected at this distance. However, no emissions were initially seen in this comet inspite of the heliocentric distance being less than 3 AU. The comet was observed on many epochs with a low resolution spectrograph (LISA) mounted on the 1.2 m telescope at Mount Abu Infra-red Observatory during the period from December 2016 to May 2017. In December 2016, the comet was at a heliocentric distance of 2.8 AU. Although the comet showed a fuzzy coma like structure, no emissions were detected. The emissions must have been too low to be detected above the strong dust continuum. Figure 4 shows the spectrum of the comet at two different epochs. As seen from the figure, only continuum is visible at 2.83 AU. The observations of the comet for three consecutive nights on 08-10 December 2016 yielded the same kind of spectra. However, as the comet moved closer to the sun, it started showing stronger emission lines of CN, C_2 and C_3. The production rates of these molecular species were estimated to be of the order of 10^{24} molecules per second and remained roughly constant over the period of observation. As the comet moved towards its perihelion (June 2017), it also moved closer to Earth and therefore, there was increase in its apparent magnitude. Strong CN emissions were detected in the spectrum of the comet in April-May 2017. The coma morphology of this comet was also studied using the Comet Hale-Bopp narrow band filters with the CCD imager on the 1.2-m telescope at Mount Abu IR Observatory. Strong spiral structures were seen in the processed images (Figure 5) of the coma observed using the CN band filter. This suggests a strong affinity of the CN molecules to the dust and the dust jets in the comet's coma.

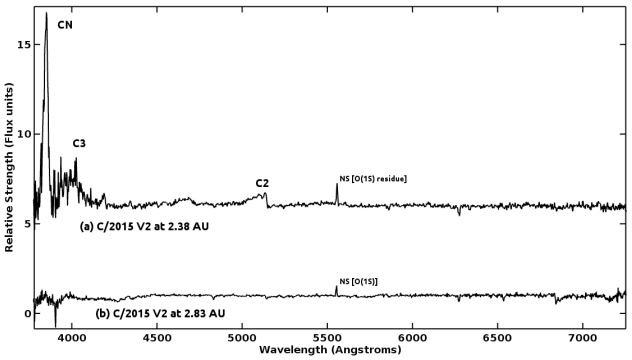


Figure no. 4: Spectra of comet C/2015 V2 on two epochs. The comet does not show any kind of detectable emission features at an initial epoch in December 2016, when the comet was at a heliocentric distance of 2.83 AU.

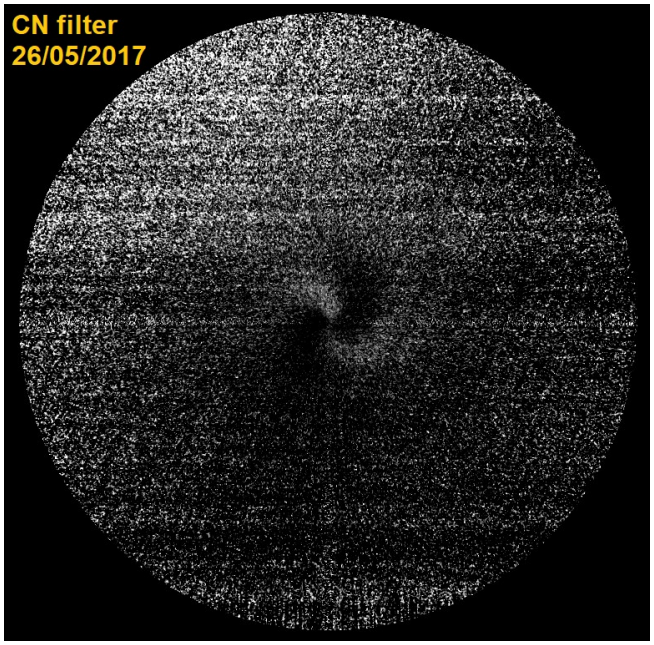


Figure no. 5: Spiral structure seen in processed image of C/2015 V2 observed on 26th May 2017 using the CN filter from the Hale-Bopp comet filter set.

(K. Venkataramani, A. Rai & S. Ganesh)

Ionic emissions in comet C/2016 R2

The comet C/2016 R2 (Pan-STARRS) is an Oort cloud comet which brightened to a visual magnitude of 13 in January 2018. As the comet was approaching its perihelion (May 2018), cometary activity was expected to increase along with strong molecular emissions. With an intention of studying the emission features in the optical spectrum of this comet, observations were carried out using the low resolution spectrograph, LISA, mounted on the 1.2m telescope at Mount Abu Infrared Observatory. The comet was observed on two epochs in January 2018, when it was at a heliocentric distance of 2.8 AU. Our observations and studies revealed that the optical spectrum of this comet is quite unusual as compared to general cometary spectra. The optical spectrum of the comet is shown in Figure 6. Most of the major cometary emissions like C_2, C_3 and CN were absent in comet C/2016 R2. However, the comet spectrum showed very strong emission bands from ionic species like CO^+ and N_2^+. As the CO^+ emissions were extremely strong, the bands were identified by matching the wavelengths of the observed emission peaks with the $\Pi_{1/2}$ and $\Pi_{3/2}$ band head emissions as mentioned in Magnani & A'Hearn (1986, ApJ, 302). However, in order to identify the weaker emissions beyond 5000 Å, cometary lines listed in the catalogues have been used.

The N_2/CO ratio was determined from the spectra and an extremely low depletion factor of 1.6 $\pm$ 0.4 has been estimated. The N_2/CO ratio estimated for this comet is highest ever reported for any comet for which such ratio has been measured. The column densities of CO^+, N_2^+ and were calculated from their emission bands. These values had increased on the second epoch (2018 January 25) as compared to the earlier one (2018 January 13).

The optical spectrum suggests that the cometary ice is dominated by CO (and/or CO_2), N_2 and NH_3. The low depletion factor of N_2/CO ratio in this comet as compared to the solar nebula and the unusual spectrum of the comet are consequences of its distinctive processing at the location of its formation in the early solar nebula.

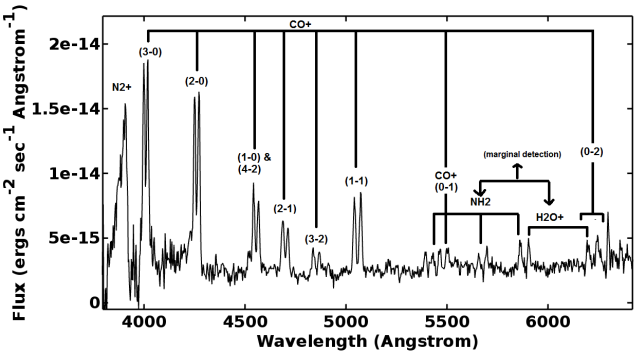


Figure no. 6 : The optical spectrum of comet C/2016 R2 taken on 25th January 2018. All the major emission lines are marked.

(K. Venkataramani, S. Ganesh & K.S. Baliyan)

The study of a system of H II regions toward l = 24°.8, b = 0°.1 at the Galactic bar - Norma arm interface

The physical processes involved in the formation of massive O-type stars ($\geq$ 8 $M_\odot$) and their feedback mechanisms are still under debate. Furthermore, in the Milky Way, there is still a limited detailed multi-wavelength study of large-scale systems ($>$ 25 pc) of several H II regions containing O-type stars, and hence the origin of such extended system of H II regions still remains unexplored. In this connection, we carried out a thorough multi-wavelength investigation of several H II regions located toward l = 24.8 deg, b = 0.1 deg. A system of at least five H II regions including the mid-infrared bubble N36 (hereafter "system N36"; extension $\sim$35 pc) is observationally investigated, and is located at a distance of 6.0 kpc. Figures 7a

and 7b show a spatial view of the system N36 using the *Herschel* 70 μm and *Spitzer* 8.0 μm images, respectively. The images at 8.0 and 70 μm are overlaid with the NVSS radio continuum emission, indicating the locations of the H II regions. The 70 μm image is also overlaid with the ATLASGAL dust continuum clumps at 870 μm. With the distance at 6.0 kpc, the system N36 is found to be situated at the interface of the Galactic bar and the Norma Galactic arm in our Galaxy, where one may expect the collisions of molecular clouds due to the bar potential. Each H II region (dynamical age $\sim$0.4–1.3 Myr) in the system is powered by an O-type star. The system contains 27 ATLASGAL dust clumps at 870 μm. Several clumps are massive ($>$ 10^3 $M_\odot$), and have high bolometric luminosity ($>$ 10^3 $L_\odot$). Using the GRS ^{13}CO line data, in the direction of the system N36, two velocity components are found around 109 and 113 km s^{-1} (see Figure 7c), and are linked in the velocity space. A "Keyhole/intensity-depression" feature in the cloud at 109 km s^{-1} and a "Key/intensity-enhancement" feature in the cloud at 113 km s^{-1} are identified in the system N36 (see Figure 7c). A displacement of $\sim$33.3 pc enables a spatial fit between the Keyhole and Key features (see Figure 7d).

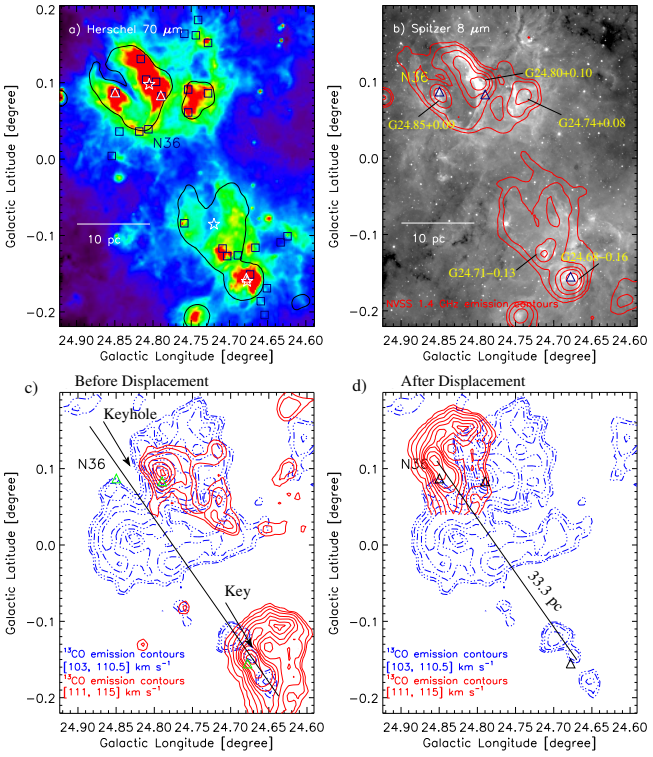


Figure no. 7: a) Overlay of the dust continuum clumps at ATLASGAL 870 μm on a false color *Herschel* 70 μm image. The NVSS 1.4 GHz contour is also shown with a level of 16 mJy/beam. Twenty seven ATLASGAL clumps highlighted with squares (V_{lsr} range $\sim$105–114 km s^{-1}) are found at a distance of 6.0 kpc. Three stars (in white) indicate the positions of the radio recombination line observations. b) Overlay of the NVSS 1.4 GHz emission contours (in red) on the *Spitzer* 8.0 μm image. The NVSS 1.4 GHz continuum contours are shown with the levels of 7.4, 18.6, 74.2, 185.6, and 464.1 mJy/beam. In panels "a" and "b", the positions of the Class II 6.7 GHz methanol masers are shown by triangles (V_{lsr} range $\sim$110–116 km s^{-1}). c) Spatial distribution of the molecular gas associated with clouds at [103, 110.5] and [111, 115] km s^{-1}. d) Same as Figure 7c, but the cloud component at 111–115 km s^{-1} is displaced in the northern direction along a line having the Galactic position angle of 215°.

The morphological analysis of ^{13}CO favours the presence of interacting molecular clouds in the system. Four H II regions and two 6.7 GHz masers are spatially observed at the common areas of the two clouds. The analysis of the *Spitzer* photometric data also traces the noticeable star formation activity in the system. Considering the observational outcomes, the formation of O-type stars (including ongoing star formation) in the system appears to be triggered by the collisions of molecular clouds at the bar-arm interface. This work was done in collaboration with J. S. Dhanya (MNIT, India), D. K. Ojha (TIFR, India), and I. Zinchenko (IAPRAS, Russia).

(L. K. Dewangan)

Investigating inner and large scale physical environments of IRAS 17008-4040

The physical processes involved in the formation of massive OB stars ($\geq$ 8 $M_\odot$) are not well understood. Furthermore, the identification of the earliest stages of massive star formation prior to an ultracompact H II region is extremely challenging task in massive star formation research. To investigate the birth mechanisms of massive stars in a promising massive star-forming site IRAS 17008-4040 (distance $\sim$2.4 kpc), we carried out an extensive analysis of the multi-wavelength data sets including high-resolution near-infrared adaptive-optics images (resolution $\sim$0$''$.1) and radio continuum data (beam sizes $\sim$3$''$–8$''$). In the site IRAS 17008-4040, a previously known O-star candidate without an H II region is identified as an infrared counterpart of the 6.7 GHz methanol maser emission (i.e., IRcmme; see Figure 8a; see a star symbol in yellow color). The 6.7 GHz methanol maser emission has been considered as one of the powerful tools for probing young massive stars. No radio continuum emission at GMRT 1.28 GHz (beam sizes $\sim$3$''$–8$''$) is observed toward IRcmme, confirming its earliest stage in massive star formation. Figure 8b reveals the inner environment of IRcmme using the high-resolution European Southern Observatory (ESO)/Very Large Telescope (VLT) adaptive-optics 3.8 μm image (resolution $\sim$0$''$.1). Based on the adaptive-optics image, the source IRcmme is resolved into two objects (i.e., IRcmme1 and IRcmme2; see Figure 8b) within a scale of $\sim$900 AU that are found to be associated with the Atacama Large Millimeter/submillimeter Array (ALMA) core G345.50M, which was previously traced in the ALMA continuum emission map at 218 GHz (resolution $\sim$0$''$.2).

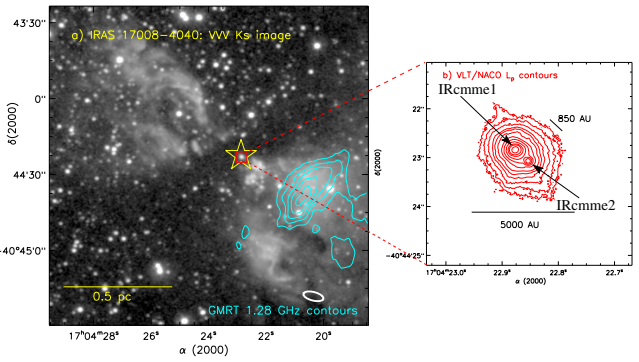


Figure No. 8: a) Overlay of the GMRT 1.28 GHz continuum contours (in cyan; beam size $\sim$5$''$.3 $\times$ 1$''$.7; sensitivity $\sim$0.4 mJy/beam) on the VVV Ks image toward IRAS 17008-4040. The GMRT contours are shown with the levels of 3.5, 6.5, 9.5, 13, 16, 18, 25, 35, 45, and 52 mJy/beam. b) A zoomed-in view of the source "IRcmme" using the ESO-VLT/NACO image at 3.8 μm (resolution $\sim$0$''$.1; see a solid box in Figure 8a).

Considering the separation between IRcmme1 and IRcmme2 (i.e. $\sim$900 AU), the core fragmentation process is likely mechanism for

these sources in the IRcmme system. Furthermore, we find that the source IRcmme1 is a rare accreting massive protostar candidate before the onset of an ultracompact H II region.

This work was done in collaboration with T. Baug (KIAA, China), D. K. Ojha (TIFR, India), and S. K. Ghosh (TIFR, India).

(L. K. Dewangan)

Filamentary structures and star formation activities in the site S234

In recent years, the infrared and sub-millimeter (mm) data have revealed a wealth of bubbles and filamentary structures in star-forming regions, which are often associated with star-forming clumps, clusters of young stellar objects, and massive OB stars ($\geq$ 8 $M_{\odot}$). Understanding the role of filaments in the formation of dense star-forming clumps and the feedback of OB stars in their vicinity are still open research topics in the area of star formation. In this context, to investigate the physical process, we performed an extensive analysis of the multi-wavelength data sets in the direction of the site S234 (distance $\sim$2.8 kpc). The site S234 (IC 417) harbors a nebulous stream (or filamentary structure) and a young cluster "Stock 8". The site S234 is powered by a star HD 35633, with a spectral type of O8 II(f).

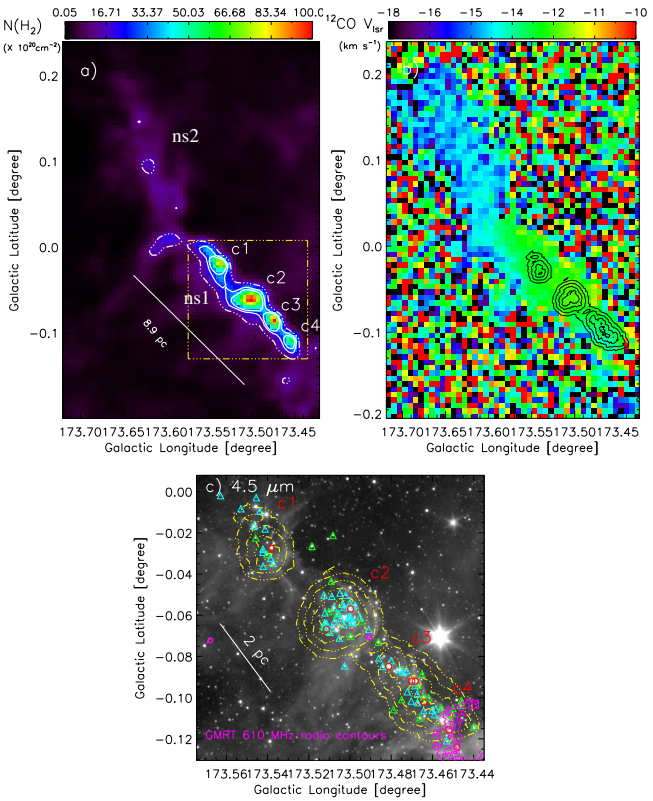


Figure no. 9: a) *Herschel* column density map toward the elongated features in the site S234. The column density contours with the levels of 10^{20} cm^{-2} $\times$ (13.3, 28.3, 38.5) are also drawn in the map. The peaks of four condensations, designated as c1-c4, are also highlighted in the map. b) Velocity-field (moment 1) map of ^{12}CO overlaid with the surface density contours of young stellar objects (in black). c) Overlay of the surface density and GMRT 610 MHz radio continuum emission contours on the *Spitzer* 4.5 μm image (see a dotted-dashed box in Figure 9a).

The earlier studies together indicate that the site S234 contains several OB stars, nebulous stream/filamentary feature, dust shell, and clusters of young stellar objects. However, the molecular velocity structures in these different features have not been investigated yet. Using the molecular line data, the molecular gas associated with the site S234 is traced in the velocity range of [$-$17.75, $-$10] km s^{-1}. In the site S234, two features (i.e. ns1 (length $\sim$8.9 pc; mass $\sim$1154 $M_{\odot}$; dust temperature $\sim$19 K; observed line mass ($M_{\rm line,obs}$) $\sim$130 $M_{\odot}$ pc^{-1}) and ns2 (length $\sim$8.7 pc; mass $\sim$392 $M_{\odot}$; dust temperature $\sim$19 K; $M_{\rm line,obs}$ $\sim$45 $M_{\odot}$ pc^{-1})) are investigated as thermally supercritical filaments, and host several dust clumps (see Figure 9a). The first moment map of 12 CO is presented in Figure 9b, which is also overlaid with the surface density contours of young stellar objects. The first moment map clearly displays the boundary of the filaments ns1 and ns2. Mach number for the filament ns1 is computed to be $\sim$3, indicating that the thermally supercritical filament ns1 is supersonic. Taking into account the turbulence, our analysis reveals $M_{\rm line,vir}$ ($\sim$320 $M_{\odot}$ pc^{-1}) $>$ $M_{\rm line,obs}$ ($\sim$130 $M_{\odot}$ pc^{-1}) for the filament ns1. At least four condensations (M_{clump} $\sim$70–300 $M_{\odot}$) are observed in the filament ns1 (see Figure 9a), and are not associated with the GMRT 610 MHz continuum emission. In Figure 9b, the filament ns2 displays almost no star formation activity, indicating at an early stage of fragmentation. An intense star formation activity is observed in the filament ns1, where both the Class I and Class II young stellar objects are identified (see Figures 9b and 9c). In the filament ns1, the star formation efficiency and the star formation rate are estimated to be $\sim$3.3% and $\sim$40–20 $M_{\odot}$ Myr^{-1} (for 1–2 Myr timescale), respectively. In the site S234, our observational outcomes favour the triggered star formation in the filament ns1. This work was done in collaboration with T. Baug (KIAA, China), D.K. Ojha (TIFR, India), I. Zinchenko (IAPRAS, Russia), and A. Luna (INAOE, México).

(L. K. Dewangan)

The Planck Cold Clump G108.37-01.06: A Site of Complex Interplay between H II Regions, Young Clusters, and Filaments

The Planck Galactic Cold Clumps (PGCCs) are possible representations of the initial conditions and very early stages of star formation. With the objective of understanding better the star and star cluster formation, we probe the molecular cloud associated with PGCC G108.37-01.06 (hereafter PG108.3), which can be traced in a velocity range of -57 to -51 km s^{-1}. The INT Photometric H_{α} Survey images reveal H_{α} emission at various locations around PG108.3, and optical spectroscopy of the bright sources in those zones of H_{α} emission discloses two massive ionizing sources with spectral type O8-O9V and B1V. Using the radio continuum, we estimate ionizing gas parameters and find the dynamical ages of H II regions associated with the massive stars in the range of 0.5-0.75 Myr. Based on the stellar surface density map constructed from the deep near-infrared Canada-France-Hawaii Telescope observations, we find two prominent star clusters in PG108.3; of these, the cluster associated with H II region S148 is moderately massive (240 Msun). A careful inspection of James Clerk Maxwell telescope CO(3-2) molecular data exhibits that the massive cluster is associated with a number of filamentary structures. Several embedded young stellar objects (YSOs) are also identified in PG108.3 along the length and junction of filaments. We find evidence of a velocity gradient along the length of the filaments. Along with kinematics of the filaments and the distribution of ionized, molecular gas and YSOs, we suggest that the

cluster formation is most likely due to the longitudinal collapse of the most massive filament in PG108.3 .

This work has been done in collaboration with Dr. Somnath Dutta (SNBOSE, Kolkata), Dr. Soumen Mondal (SNBOSE, Kolkata) and Dr. Jessy Jose (IISER, Tirupati).

(M. R. Samal)

Understanding Formation of Young, Distributed Low-mass Stars and Clusters in the W4 Cloud Complex

It is well known that most of the stars form in rich clusters. However, recent Spitzer observations have shown that a significant number of stars also form in the distributed mode; their origin is not well understood. In this work, we aim to investigate clustered and distributed modes of star formation in the W4 complex.

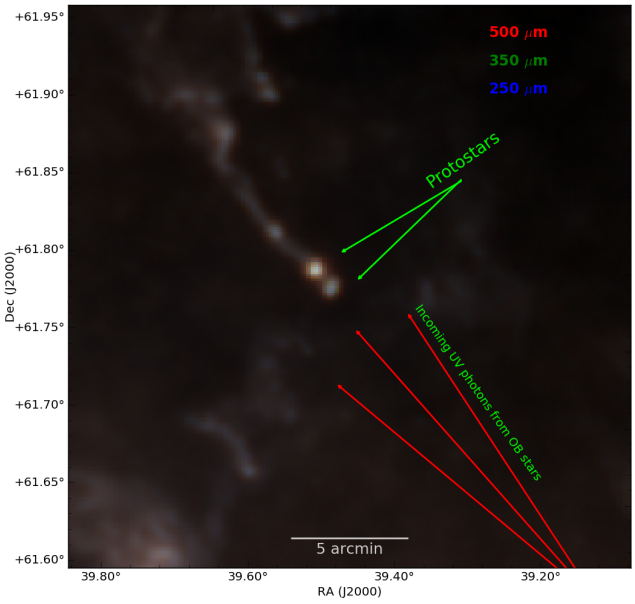


Figure no. 10 : Herschel three color image showing the morphlogy of an elaphant trunk like structure and the location of the newly formed protostars at its tip. The arrows indicate the direction of incoming UV photons from the massive OB stars of the central massive ($\sim$ 2700 $M_{\odot}$) cluster of the complex.

To do so, we identified and characterized the young stellar population associated with the region using homogeneous infrared data sets obtained from the Two Micron All Sky Survey, GLIMPSE, MIPS, and Wide-field Infrared Survey Explorer surveys. We make stellar surface density and minimum spanning tree maps to identify young clusters, and use Spitzer images to identify irradiated structures, such as elephant-trunk-like structures (ETLSs) and pillars in the region. The surface density distribution of the young stellar objects (YSOs) reveals three new clusterings and $\sim$50% distributed protostars in the H II region. The clusters are of low-mass nature but significantly younger than the central cluster IC 1805. We identified $\sim$ 38 ETLSs in the region, a majority of which consist of one or a few stars at their tips. We find that these stars are low-mass ($<$2 Msun) YSOs, located at the outskirts ($>$17 pc) of the cluster IC 1805 and are part of the scattered distributed population. We argued that the star formation in the ETLSs of W4 is going on possibly due to the triggering effect of the expanding W4 bubble. Although high-resolution photometric and spectroscopic data would be required to confirm the scenario, nonetheless, we discuss the implications of this scenario for our understanding of distributed low-mass star formation in cloud complexes as opposed to other mechanisms such as turbulent fragmentation and dynamical ejection.

This work has been done in collaboration with Dr. Neelam Panwar, Prof. A. K. Pandey, Dr. Sourabh Sharma (ARIES, Nanitial) and Prof. H. P. Singh (Delhi University, Delhi).

(M.R. Samal)

SCOPE: SCUBA-2 Continuum Observations of Pre-protostellar Evolution - survey description and compact source catalogue

In the current paradigm, stars form within cold and dense fragments in the clumpy and filamentary molecular clouds. However, the way that filaments form in the cold ISM is still far from being well characterized. Also, the properties of prestellar cores and the way how prestellar cores evolve to form stars are still not fully understood, due to a lack of statistical studies toward a large sample.The Planck team has cataloged 13,188 Planck galactic cold clumps (PGCCs), which are distributed across the whole sky. To obtain a census of dense clumps distributed in widely different environments, to study the roles of filaments in dense core formation, to investigate dust properties, and to detect rare populations of dense clumps. We present the first release of the data and compact-source catalogue for the JCMT Large Program SCUBA-2 Continuum Observations of Pre-protostellar Evolution (SCOPE). SCOPE consists of 850 micron continuum observations of 1235 PGCCs made with the Submillimetre Common-User Bolometer Array 2 on the James Clerk Maxwell Telescope. These data are at an angular resolution of 14.4 arcsec, significantly improving upon the 353 GHz resolution of Planck at 5 arcmin, and allowing for a catalogue of 3528 compact sources in 558 PGCCs. We find that the detected PGCCs have significant sub-structure, with 61 per cent of detected PGCCs having three or more compact sources, with filamentary structure also prevalent within the sample. A detection rate of 45 per cent is found across the survey, which is 95 per cent complete to Planck column densities of $N_{H_2} > 5\times10^{21} cm^{-2}$. By positionally associating the SCOPE compact sources with young stellar objects, the star formation efficiency, as measured by the ratio of luminosity to mass, in nearby clouds is found to be similar to that in the more distant Galactic Plane, with the column density distributions also indistinguishable from each other.

This work has been done in collaboration with Dr. D. J. Eden (Liverpool John Moores University, UK), Dr. Tie Liu (Korea Astronomy and Space Science Institute, Korea), Dr. Kee-Tae Kim (Korea Astronomy and Space Science Institute, Korea), and other SCOPE team members of various international institute/organizations.

(M.R. Samal)

Discovery of two very low mass binary system

The number of very low mass binaries discovered/detected has increased substantially with the advent of large infrared arrays.

Various ground based surveys such as, Sloan Digital Sky Survey (SDSS), Two Micron All Sky Survey (2MASS), together with the space-based surveys such as, Wide-field Infrared Survey Explorer (WISE), have made many successful attempts in such discoveries. Despite the relevant contribution by these surveys in the field of VLM binaries, the number of known pairs formed by mid to late M (or cooler) dwarfs is still small. Because of their small size and low temperature, the low mas stars are intrinsically very faint in nature. As a result, there have been limited studies on the accurate determination of masses, radii, and other physical properties of very low mass stars (VLMSs). Here we report the detection of two very low mass binary pair, LP 1033-31 and LP 877-72 with nearly equal brightness. The very low mass binary pair are identified by direct imaging. Data were obtained with NaCo, the Nasmyth Adaptive Optics System (NAOS) and Near-Infrared Imager and Spectrograph (CONICA) at ESO's Very Large Telescope. We perform the photometry of the components of both the sources and ascertain the separation, relative near-infrared magnitudes and individual spectral classification of its components. The important parameters of these two binary pairs are summarised in Table 1. Figure 11 shows the NaCo K-band image of LP 877 72.

Table 1: System parameters for LP 877 72 and LP 1033-31 by assuming the age of 5 Gyr

Parameter	LP 877 72	LP 1033-31
d [pc]	33.768±0.167	13.8±4.7
Separation [AU]	45.76±0.33	5.5±1.9
Mass (A) [M_{Sun}]	0.18±0.07	0.13±0.07
Mass (B) [M_{Sun}]	0.16±0.07	0.13±0.07
Orbital Period [yr]	530±110	25.4±6.7

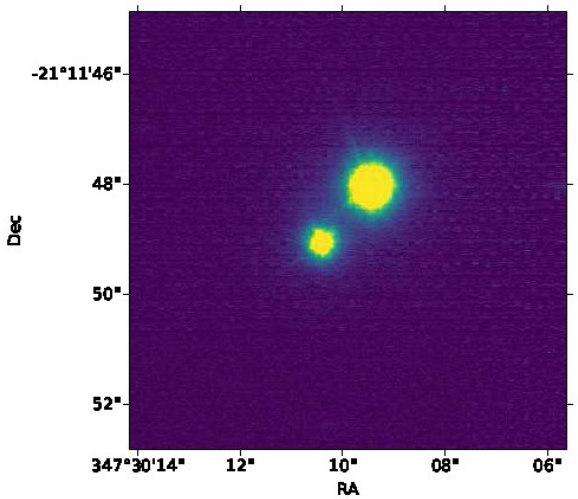


Figure no. 11: NaCo K-band image of LP 877 72. Axis labels denote coordinates in right ascension and declination relative to the centre of the image.

This work has been done in collaboration with Prof. France Allard of ENS Lyon, France and Dr. S. Rajpurohit of Institute for Theoretical physics, Technical University Clausthal, Germany.

(S. Karmakar & A. S. Rajpurohit)

Exploring the atmospheric properties of hot-Jupiters

The observable atmospheric properties of exoplanets are a window into its composition which provides information about its evolution history. Since Hot-jupiters are highly irradiated, they are of major interest to study the effect of irradiation on the atmospheric structure, temperature distribution, internal chemistry, cooling and contraction of the planets. Measurements of time-varying signals, which include transits, secondary eclipses, and phase curves, as well as the spatially resolved imaging and spectroscopy are the tools to study their atmospheric properties. From the theoretical and modelling point of view, more in-depth analysis is required to determine the physical properties of the planets from the calculated composition, thermal structure and circulation mechanism in the atmospheres. We have carried out theoretical study of the atmosphere of exoplanets by calculating the phase fluxes using PHOENIX atmosphere code (Allard et al 2013). We then compared theoretical phase curves with the observed phase curves and the secondary of CoRoT and Kepler planets. We have explored several combinations of the cloud distribution with different assumptions concerning the redistribution of the absorbed stellar flux over the planet's day side. Figure 12 shows such theoretical temperature-pressure (T-P) profile of Kepler-41b computed using PHOENIX model atmosphere.

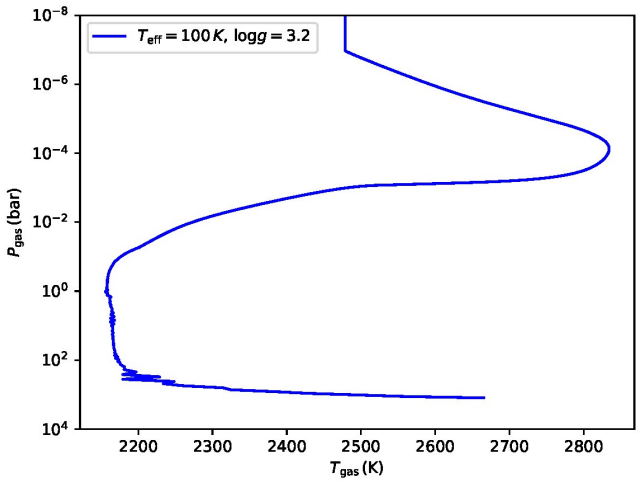


Figure no. 12: Theoretical temperature-pressure (T-P) profile of Kepler-41b computed using PHOENIX model atmosphere.

This work has been done in collaboration with Prof. France Allard of ENS Lyon, France and Dr. S. Rajpurohit of Institute for Theoretical physics, Technical University Clausthal, Germany.

(A. S. Rajpurohit)

The Remarkable Outburst and Post-burst Evolution of PTF14jg

The outbursting source PTF 14jg, which, prior to the onset of its late 2013 eruption, was a faint, unstudied, and virtually uncataloged star. It is located at the position is between two of the sequence of three large H II regions, just east of the "swept-up shell" in W4 and $\sim 1^{\circ}.1$ from the center of the massive cluster IC 1805. The salient features of the PTF 14jg outburst are found as (i) projected location

near the W4 H II region and radial velocity consistent with physical association; (ii) a light curve that underwent an ∼6-7 mag optical (R-band) through mid-infrared (L-band) brightening on a timescale of a few months, peaked and then faded by ∼3 mag, but plateaued still >3.5 mag above quiescence by ∼8 months post-peak, lasting to at least 4 yr after eruption; (iii) strong outflow signatures with velocities reaching 530 km s_{-1}; (iv) a low-gravity and broad (∼100-150 km/s FWHM) optical absorption-line spectrum that systematically changes its spectral type with wavelength; (v) lithium; and (vi) ultraviolet and infrared excess. The rise time and amplitude of the PTF 14jg outburst are roughly consistent with an FU Orionis classification, though it is at an extreme in both parameters relative to other members of the class. The characteristic change in spectral type with wavelength that is a hallmark of the class is present, as is Li I absorption. These signatures allowing us to identified the outburst as exhibiting characteristics of a young star FU Ori event. However, our identification is tentative as the spectral signatures are overall hotter in the early stages, both in the rest velocity (disk) spectrum and the outflowing (wind) spectrum, compared to other FU Ori stars. The burst would be unusually hot, with an absorption spectrum exhibiting high-excitation (∼11,000 to 15,000 K) lines in the optical and no evidence of CO in the near-infrared, in addition to exhibiting an unusual light curve. We thus also considered alternative scenarios, including various forms of novae, nuclear-burning instabilities, massive star events, and mergers, finding them all inferior to the atypically hot FU Ori star classification. The source eventually interpreted as a new category of young star outburst with a larger amplitude and shorter rise time than most FU Ori like events. Figure 13 shows the optical and infrared light curves of PTF14jg.

This work has been done in collaboration with Lynne Hillenbrand and Adam Miller of California Institute of Technology.

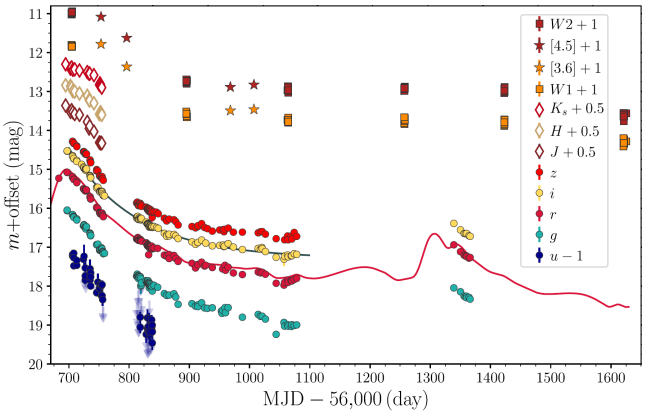


Figure no. 13: Post outburst brightness evolution of PTF14jg in optical and IR filters. The decline over 3 mag in brightness is relatively colorless for the duration of the time series, with color changes of no more than 0.2 mag. The solid red line overlaid on the r-band light curve is a Gaussian-process model fit to the RPTF photometry.

(V. Joshi & D. P. K. Banerjee)

Early formation of carbon monoxide molecules in the supernova SN 2016adj

The formation of small molecules such as carbon monoxide (CO) in Supernova ejecta is a necessary prerequisite for dust formation and indeed, CO is one of the most powerful coolants in the ejecta of Type II Supernovae. Figure 14 shows the composite JHKs image of Cen A, showing the location of the SN2016adj. The outcomes of dust evolution models depend on CO destruction processes. However, detections of first-overtone CO emission in SNe are limited in number. We have studied supernova SN 2016adj in the first two months following discovery. We detected the first-overtone carbon monoxide emission in NIR K band spectrum at ∼58.2 d after discovery, one of the earliest detections of CO in an erupting supernova. We have also modelled the CO emission to derive the CO mass, temperature, and velocity, assuming both pure ^{12}CO and a composition that includes ^{13}CO; the case for the latter is the isotopic analyses of meteoritic grains, which suggest that core-collapse supernovae can synthesize significant amounts of ^{13}C. Figure 15 shows the emission band of CO molecule and best fit models. Our models show that, while the CO data are adequately explained by pure ^{12}CO, they do not preclude the presence of 13CO, to a limit of ^{12}C/^{13}C 3, the first constraint on the ^{12}C/^{13}C ratio determined from near-infrared observations. Our calculations suggested the reddening to the object to be E(B - V) = 0.90 ± 0.09, with the majority arising in the host galaxy. A blackbody fit to the optical and near-IR data shows that the photosphere has a low temperature of ∼3680 K at outburst. SN 2016adj has been proposed to be a Type IIb supernova, which show an initial hydrogen-dominated spectrum but later undergo a transition to a helium-rich Type Ib spectrum. In SN 2016adj, hydrogen lines are prominent initially, but the helium lines do not strengthen as expected. It is possible that this is a peculiar object, or a SN making a rather slow transition from Type IIb to Ib. We have also proposed that an unidentified line at 2.26 μm often seen in the spectrum of SNe arises from the CaI 2.260, 2.262, 2.265 μm transitions routinely seen in the spectra of cool stars.

This work has been done in collaboration with Adam Evans of Keele University, UK and Robert Gehrz of Minnesota Institute for Astrophysics, USA.

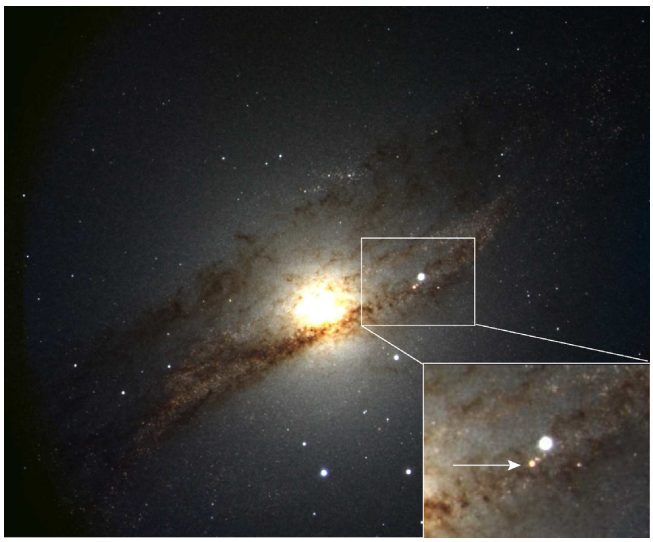


Figure no. 14: A composite JHKs image of Cen A, showing the location of the SN2016adj (arrowed), taken on 2016 Aug 7 (+180.4d) with the Gemini-South telescope. The bright star north-west (NW) of the SN is 2MASSJ13252458-4300485. North is up; East is left.

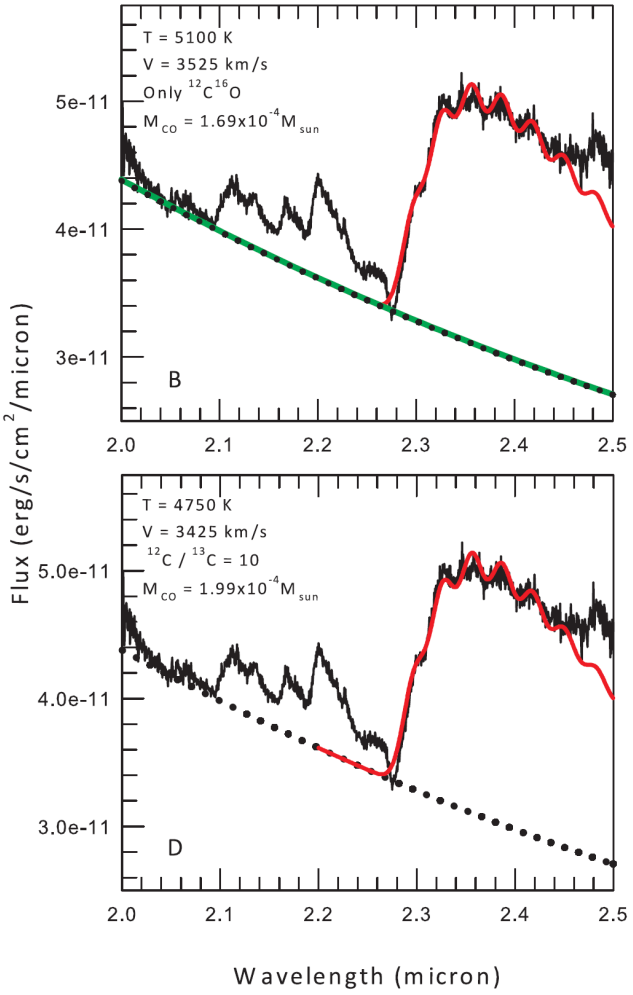


Figure no. 15: K band spectrum of SN 2016adj showing strong emission band of CO molecule. red curves is a model fit for a pure ^{12}CO composition in upper panel and a mixed (^{12}CO + ^{12}CO) composition in lower panel, with the fit parameters indicated within. The black dotted lines show the local continuum that has been adopted using a second-order polynomial of the form fλ = f0 + aλ + bλ^2; this is found to closely match a blackbody continuum at 2550 K, which is shown in green in upper panel.

(V. Joshi, D. P. K. Banerjee, M. Srivastava)

A curious case of the accretion-powered X-ray pulsar GX 1+4

Accretion powered X-ray pulsars constitute a large fraction of the brightest X-ray binaries in our Galaxy. These objects are highly magnetized rotating neutron stars that are powered by mass accretion from their optical companion. Depending on the characteristics of the donor star, mass transfer from the optical companion to the neutron star takes place through different mechanisms such as (i) Roche-lobe overflow (in low-mass X-ray binaries), (ii) capture of stellar wind, and (iii) Be-disc accretion. Irrespective of the accretion mechanisms, the magnetic field of the neutron star has a strong influence on the emission processes that leads towards a characteristic shape of X-ray continuum spectrum and beam geometry. Most of the high-energy emission from the accretion-powered X-ray pulsars originates from the Comptonization of seed photons in the accretion column, formed on the surface of the neutron stars. Therefore, a thorough and detailed investigation of the spectral and temporal characteristics of these objects can provide important information on the fundamental parameters of the neutron star. GX 1+4, one such X-ray binary pulsar, is an interesting accretion powered X-ray pulsar with a spin period of about 2 min. The optical counterpart of GX 1+4 is the bright infrared star V2116 Oph of M6 III spectral type, confirming the system to be a symbiotic binary. The neutron star in this system is thought to accrete from dense stellar wind as the giant companion underfills its Roche lobe. The distance of the binary was estimated in the range of 3-15 kpc.

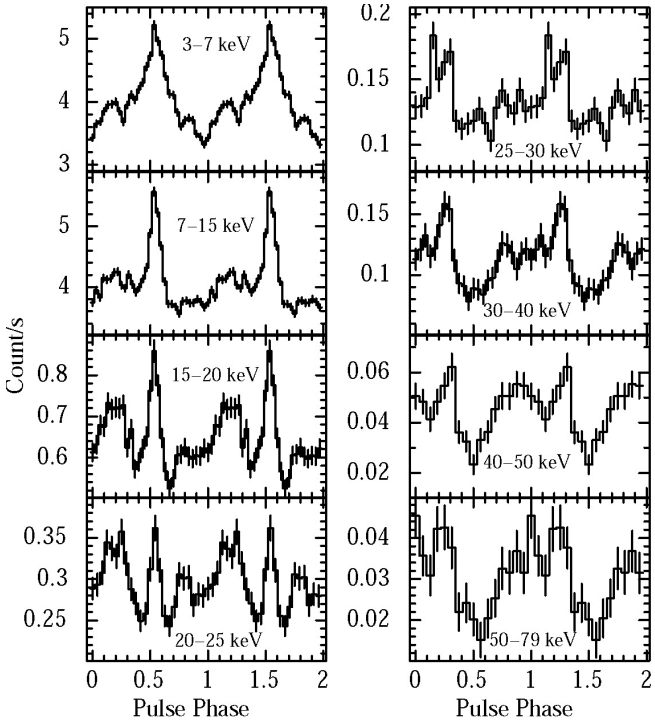


Figure no. 16: Energy-resolved pulse profiles of GX 1+4 obtained from $NuSTAR$ observation in 2015 October. A sharp peak along with plateau like structure can be clearly seen in soft X-ray pulse profiles. Though the profile in $\geq$30 keV is simple, a phase shift of π with respect to the profile observed in 3–7 keV energy range is observed. Two pulses in each panel are shown for clarity.

We have carried out a detailed spectral and timing studies of an accretion powered X-ray pulsar GX 1+4 using a NuSTAR observation in 2015 October during an intermediate-intensity state. The measured spin period of 176.778 s is found to be one of the highest values since its discovery. In contrast to a broad sinusoidal-like pulse profile, a peculiar sharp peak is observed in profiles below $\sim$25 keV. The profiles at higher energies are found to be significantly phase shifted compared to the soft X-ray profiles (Figure 16). Broad-band energy spectra of GX 1+4, obtained from NuSTAR and Swift observations, are described with various continuum models. Among these, a two-component model consisting of a bremsstrahlung and a blackbody component is found to best fit the phase-averaged and phase-resolved spectra. Physical models are also used to investigate the emission mechanism in the pulsar, which allows us to estimate the magnetic field strength to be in $\sim$(5-10) $\times$ 10^{12} G range. Phase-resolved spectroscopy of NuSTAR observation shows a strong blackbody emission component in a narrow pulse phase range. This component is interpreted as the origin of the peculiar peak in the pulse profiles below $\geq$25 keV. The size of emitting region is calculated to be $\sim$400

m. The bremsstrahlung component is found to dominate in hard X-rays and explains the nature of simple profiles at high energies.

This work was done in collaboration with Gaurava K. Jaisawal and Jerome Chenevez of National Space Institute, Technical University of Denmark, Denmark.

(S. Gupta, P. R. Epili & S. Naik)

Spectral and Timing Studies of 2S 1417-624 during a giant outburst

Be/X-ray binaries form the largest subclass of High Mass X-ray Binaries (HMXBs). The orbit of the neutron star in these systems is wide and highly eccentric. The pulsars in these binaries are generally X-ray quiescent. Transient X-ray outbursts, seen in these objects are thought to be due to interaction between the neutron star and the circumstellar disk surrounding the Be star at the periastron passage. We attempted to understand the properties of the neutron star in the Be/X-ray binary system 2S 1417-624 during a giant X-ray outburst. The transient Be/X-ray binary pulsar 2S 1417-624 was discovered in 1978 with SAS-3. During early observations, X-ray pulsations at $\sim$17.5 s were detected in the source light curves. A B-type star located at a distance of 1.4-11.1 kpc, was identified as the optical companion of the pulsar. Using BATSE observations, the binary orbital parameters of the system were derived as orbital period P_{orb}=42.12 d, eccentricity e=0.446, semimajor axis $a_x sini$=188 lt-s, ω=300.3 degree, and time of periastron passage T = JD 2449714.12.

We carried out a systematic and detailed timing and spectral studies of the accretion powered X-ray pulsar 2S 1417-624 during a giant outburst in 2009 by using Rossi X-ray Timing Explorer observations. X-ray pulsations were detected in the light curves obtained from all epochs of observations. The pulsar was found to be spinning-up during the outburst. The pulse profiles were observed to be strongly dependent on photon energy and luminosity. A double-peaked profile at lower luminosity evolved into a triple-peaked profile at the peak of the outburst which is further reverted back to a double-peaked structure during the decay of the outburst (Figure 17). An anticorrelation was also observed between the pulse fraction and the source flux. The 3-70 keV energy spectrum of pulsar was well described with a power law modified with high-energy cut-off model along with an iron fluorescence line at 6.4 keV. Based on the evolution of pulse profile, pulse fraction, and spectral parameters across observed luminosity, we interpret our results in terms of changes in the pulsar beam configuration from sub-critical to super-critical regimes.

This work was done in collaboration with Gaurava K. Jaisawal of National Space Institute, Technical University of Denmark, Denmark.

(S. Gupta, P. R. Epili & S. Naik)

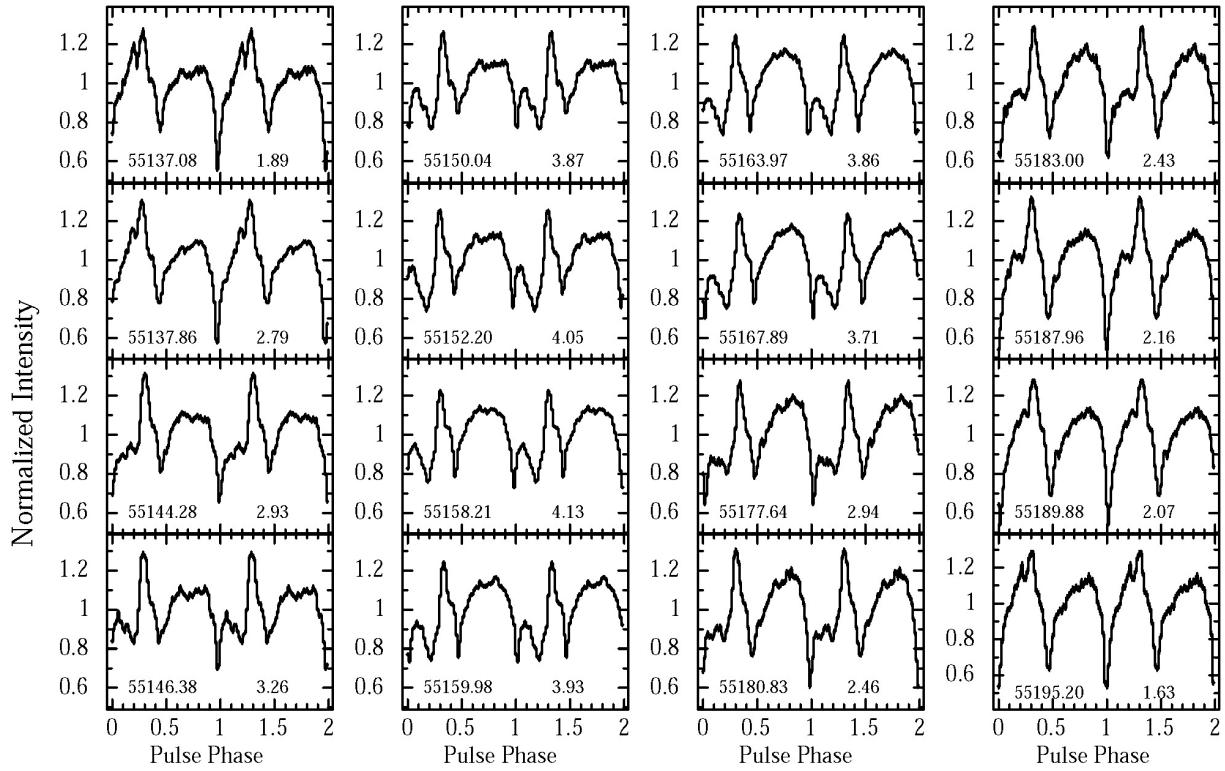


Figure no. 17: Pulse profiles (2-60 keV range) of the pulsar 2S 1417-624 at different phases of the 2009 giant X-ray outburst (from rise to decline). The numbers quoted on the left and right side of each panel indicate the beginning of the corresponding $RXTE$ pointed observation (in MJD) and the flux (in 10^{-9} erg s^{-1} cm^{-2} units), respectively. Two pulses are shown in each panel for clarity.

Cavities, Shocks and a Cold-front around 3C 320

Detection of copious amount of X-ray emission from hot gas in the intracluster medium (ICM) suggests that ∼45% of cores of clusters appear to cool faster than the Hubble time in the local Universe; these are referred to as cool-core clusters. It is expected that the cooling ICM must fall on to the core at a rate up to 1000 $M_\odot$ yr^{-1}, thereby losing its energy in the form of radiation, mostly in the form of X-rays. However, the observed star formation rates in the cores of such clusters are much lower than the cooling rates, leading to the cooling-flow problem. Some kind of heating is, therefore, required to explain the observed low star formation rate in the cores of such clusters. Recent understanding is that the active galactic nucleus (AGN) residing at the core of a cluster releases the required amount of energy through feedback and hence resolves the problem. Such feedback by the AGN is evident in several clusters, in the form of X-ray-deficient regions (cavities or bubbles), as the most discernible features of the interaction between the AGN and the ICM. These cavities are believed to be created as a result of AGN outbursts, by injecting relativistic plasma into the ICM. We investigated the presence of cavities, shocks and cold-fronts in the Fanaroff-Riley II (FR II) radio galaxy 3C 320, located at the centre of a cluster of galaxies at redshift z = 0.342.

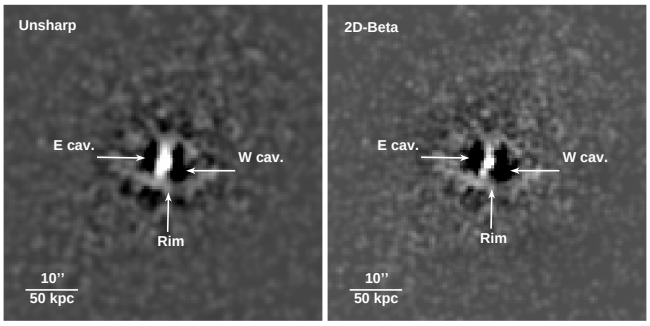


Figure no. 19: 0.5-3 keV residual images of the central $1' \times 1'$ field of 3C 320: *Left panel* shows the residual image generated by unsharped mask imaging technique and *right panel* shows the 2D-β model subtracted residual image.

Analysing a total of 110 ks of Chandra observations of 3C 320, we detected a pair of X-ray cavities at an average distance of ∼38 kpc along the east and west directions, with cavity energy, age and total power equal to 7.7×10^{59} erg, 7×10^{7} yr and 3.5×10^{44} erg s^{-1}, respectively (Figure 19). The cooling luminosity within the cooling radius of ∼100 kpc was found to be $L_{cool} \sim 8.5\times10^{43}$ erg s^{-1}. Comparison of these two estimates (total cavity power and cooling luminosity) implies that the cavity power is sufficiently high to balance radiative loss. A pair of weak shocks has also been detected at distances of 47 and 76 kpc surrounding the radio bubbles.

Using the observed density jumps of 1.8 and 2.1 at the shock locations along the east and west directions, we estimate the Mach numbers to be 1.6 and 1.8, respectively. A sharp surface-brightness edge was also detected at a relatively larger radius (∼80 kpc) along the south direction. The density jump at this surface-brightness edge was estimated to be 1.6 and it is probably due to the presence of a cold front in this cluster. The far-infrared luminosity yielded a star formation rate of 51 $M_\odot$ yr^{-1}, which is a quarter of the cooling rate.

This work was done in collaboration with Nilkanth Vagshette (Maharashtra Udayagiri Mahavidyalaya, Udgir) and M. K. Patil (Swami Ramanand Teerth Marathwada University, Nanded, Maharashtra)

(S. Naik)

Multiwavelength Studies of Active Galactic Nuclei

ctive galactic nuclei (AGNs) exhibit variable and complex spectral energy distribution. The central engine of an AGN, an accreting supermassive black hole (SMBH), is known to radiate in the luminosity range 10^{41-47} erg s^{-1} almost equally over the entire electromagnetic spectrum. In the brightest AGN, the intense radiation emitted from the central engine dominates the light coming from other constituents of the host galaxy such as stars. The huge energy release in these objects is attributed to accretion on to the supermassive black hole. The X-ray continuum emission from these objects is considered to be dominated by the power law model, which is known to be due to the inverse Compton scattering of soft photons, emitted from the accretion disk around the SMBH, in an optically thin and hot electron plasma ($kT_e \sim$ 100 keV). In Seyfert galaxies, radiation emitted from the accretion disc is dominated in the UV band. However, due to large Galactic absorption along the line of sight, the UV radiation peak is hardly detectable. The observed UV/optical emission shows different variabilities on various time-scales from days to years for 10^6–10^9 $M_\odot$ black hole mass range. However, the cause of observed variabilities in UV/optical emission from the accretion disc is not very clear. The observed UV/optical emission variabilities in Seyfert galaxies are thought to be associated with the fluctuation in the mass accretion. However, such interpretation is unable to explain the observed disc variability on short (hours to days) time-scale. This time-scale is very much shorter compared to the expected time-scale of the density fluctuations in the accretion flow. The variations observed in X-ray emission are found to lead the variations in UV/optical band. This is difficult to explain by using the hypothesis that the cause of UV/optical variation is associated with accretion flow fluctuation. Thus, the correlation and variations between the emission in UV/optical and X-ray bands are complex and their intensive exploration is required. Multiwavelength observations of several narrow-line Seyfert galaxies have been carried out by using space-based Indian observatory Astrosat. These observations provide spectral coverages in broad range of the electromagnetic spectrum (from UV to hard X-ray ranges). Simultaneous near-infrared observations of such sources with our 1.2 m telescope at Mnt. Abu also improve the wavelength coverage. Data from these observations can provide important information on the origin of various spectral components in these sources.

(N. Kumari & S. Naik)

Very Long duration X-ray Superflare on an RS CVn type eclipsing binary SZ Psc

The close binaries with convective envelopes are expected to have magnetic activities such as photospheric spots, chromospheric emission, coronal X-ray and flare activities. RS CVn type binaries are usually tidally locked systems consisting of a dwarf star of spectral type F-G and a subgiant companion star. These stars have low-amplitude quasi-sinusoidal light variations owing to the presence of large dark star-spots. The flares produced by stars in RS CVn-type binaries are

usually detected only in the ultraviolet (UV) or X-rays. Luminosity during these UV and X-ray flares is observed to be extremly high. Modelling the dynamic behaviour of UV/X-ray flares allows us to constrain the properties of magnetic loops that cannot be done from analysis of quiescent coronae. Study of such stellar flares in dwarfs, giants and subgiants is, therefore, very important for understanding the stellar coronae.

A very large flare was detected from the eclipsing RS CVn type 3.966 day binary SZ Psc on 15 January 2015. The flare lasted for more than 100 ks and is the longest X-ray flare ever observed from the system. The exponential rise and decay times of the flare were derived to be 2 and 5 hrs, respectively. The peak X-ray luminosity in 0.3-10 keV range, reached to a value of 4.8×10^{33} erg s^{-1}, which is about two orders of magnitude higher than that of the minimum value. Spectral analysis indicates the presence of one temperature corona which represents the flare temperature. The estimated peak temperature of 258 MK, as obtained from X-ray spectral fitting is $\sim$10 times more than the corresponding value at the minimum. The peak stellar abundance was derived to be 0.7 times more than the solar abundance which is about one order more than that of the minimum abundance observed in SZ Psc. The emission measure followed the flare light curve and peaked at a value of 2.53×10^{54} cm^{-3}. The total magnetic field required to produce the observed flare is derived to be 1.5 kG. This large value of magnetic field at the coronal height is assumed to be due to the presence of extended convection zone of the sub-giant and the high orbital velocity.

(S. Karmakar & S. Naik)

Unprecedented flaring in BL Lac S5 0716+71 during 2013-15: Central black hole mass estimated

AGN are intriguingly energetic sources in themselves but when in outburst phase, these provide vital information about their structure and emission processes. With an aim to explore optical variability at diverse timescales in BL Lac source S5 0716+714, an intermediate blazar, it was observed for 46 nights during 2013 January 14 to 2015 June 01 when it underwent two major outbursts. The observations were made using the 1.2 m Mount Abu InfraRed Observatory telescope mounted with a CCD camera. On 29 nights, the source was monitored for more than 2 hr, resulting in 6256 data points in the R band, to check for the intra-nigh variability (INV). Observations in the B, V, and I bands with 159, 214, and 177 data points, respectively, along with daily averaged R-band data are used to address inter-night and long- term variability and the color behavior of S5 0716+71. The study suggests that the source shows significant INV with a duty cycle of more than 31% and night-to-night variations. The average brightness magnitudes in the B, V, R, and I bands were found to be 14.42(0.02), 14.02(0.01), 13.22(0.01), and 13.02(0.03), respectively, while S5 0716+714 was historically brightest with R = 11.68 mag on 2015 January 18, indicating that the source was in a relatively high state during this period. A mild bluer- when-brighter behavior, typical of BL Lacs, supports the shock- in-jet model. We noticed larger amplitudes of variation when the source was relatively brighter. Based on the shortest timescale of variability and causality argument, the upper bound on the size of the emission region is estimated to be 9.32×10^{14} cm, and the mass of the black hole is estimated to be 5.6×10^{8} M$_{\odot}$.

(N. Kaur, K. S. Baliyan, S. Ganesh & S. Chandra)

Detection of strong intra-night optical variability in a radio-loud narrow-line Seyfert 1 galaxy

We report, for the first time, the detection of strong intra-night optical variability (INOV) in a radio-loud narrow-line Seyfert 1 galaxy (RL-NLS1) SDSS J090410+581527. Using *R* band monitoring observations from Mt. Abu telescope we find strong INOV with a change of $\sim$ 0.6 mag in couple of hours and high variability rates of 2 - 3 mag hour^{-1} (see Figure 20). In addition to flux variability this RL-NLS1 also exhibits spectral variability with a mild trend of bluer-when-brighter on days-to-months timescales. Radio observations show an unresolved relatively faint flat-spectrum core-dominated radio emission from AGN. The strong INOV in a flat-spectrum core-dominated RL-NLS1 suggests the existence of beamed relativistic jet. Therefore, our study demonstrates the importance of INOV in inferring the existence of beamed relativistic jets in radio-faint ($S_{1.4\ \mathrm{GHz}} \leq 10$ mJy) RL-NLS1s.

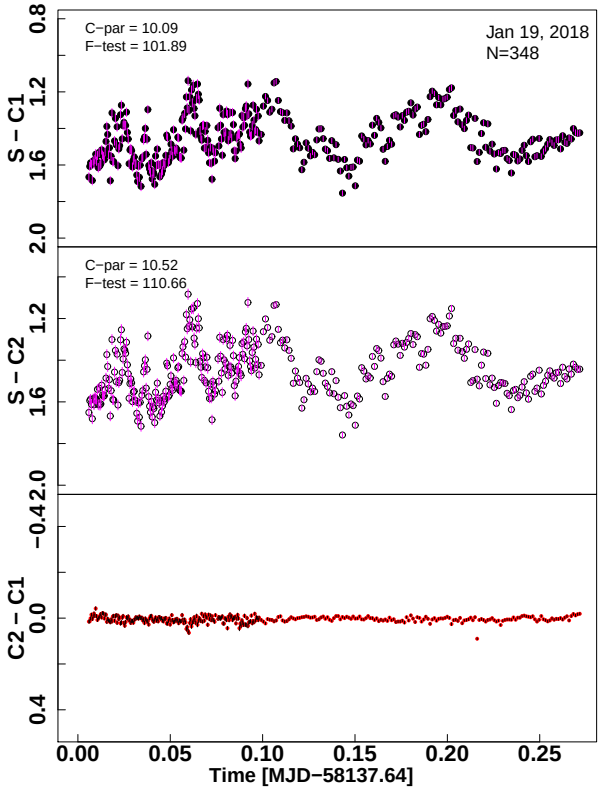


Figure no. 20: *R* band differential light curves of J090410+581527 on 19 January 2018.

(V. Singh, N. Kaur, K.S. Baliyan & S. Ganesh)

Probing cold atomic hydrogen gas in high-redshift AGN

Neutral hydrogen (HI) is a dominant component of the gaseous interstellar medium in galaxies, and can be probed in the vicinities of Active Galactic Nuclei (AGN) via the HI 21 cm absorption technique.

This helps us to discern the distribution and kinematics of the gas relative to the AGN, thus allowing us to understand the AGN-host galaxy co-evolution. Using Giant Metrewave Radio Telescope (GMRT) we recently detected associated HI 21 cm absorption towards AGN TXS 0604+728 at $z = 3.53$ (see Figure 21). This detection confirms that neutral hydrogen can survive under the extreme conditions present in the AGN vicinity. Also, the absorber is at the highest redshift at which HI 21 cm absorption has been detected till date.

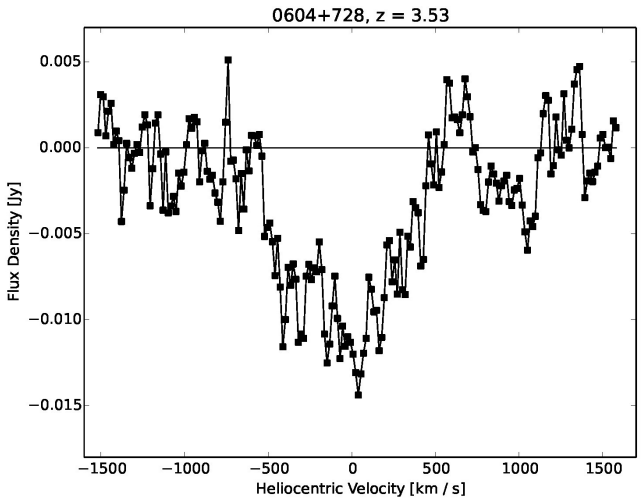


Figure no. 21: Detection of HI 21 cm absorption feature associated with TXS 0604+728, at $z = 3.53$.

This work is done in collaboration with Dr. Yogesh Chandola (IUCAA, Pune).

(J.N.H.S. Aditya & V. Singh)

Probing obscuration around AGN using X-ray spectral studies

The study of obscured AGN is important to reveal the complete census of AGN population and to understand the evolution of galaxies as well as the evolution supermassive black holes (SMBHs).The obscuration in AGN is primarily caused by the putative dusty torus around the accreting SMBH and can be probed with X-ray observations due to it's high penetration depth through the dusty and gaseous osbcuring materials. The existence of heavily obscured AGN ($N_H > 10^{24} cm^{-2}$), also known as compton-thick AGN, is predicted by the XRB synthesis models which explain the X-ray background (XRB) emission peaking at $\sim$ 30 - 40 keV. We probe the obscuration in a sample of AGN using X-ray observations from Chandra, XMM-N, NuSTAR and AstroSat. We find that, in addition to high absorbing column density, the X-ray spectra of obscured AGN exhibit strong reflection component, high equivalent width of Fe K_α line. We also find a tentative evidence that heavily obscured AGN often host radio sources with giga-hertz peaked spectrum.

(A. Kayal & V. Singh)

Search for remnant radio galaxies using deep multiwavelength surveys

Typical morphology of a radio galaxy consists of a radio core, a pair of jets, hotspots at the outer edge of the lobes. The activity of an active galactic nucleus (AGN) can last several tens of million years (Myr). After the cessation of AGN activity, the jets are no longer sustained and core fades away. We can then see the remnant lobes and such radio galaxies are named as remnant radio galaxies. The final phase of a radio galaxy evolution and associated physical processes are very poorly understood. Therefore, we attempt to identify and study remnant radio using deep multi-frequency radio surveys of extragalactic fields. For our study we use radio surveys at 325 MHz, 610 MHz from GMRT and 1.4 GHz from Very Large Array (VLA). Using various selection criteria such as radio sources showing ultra-steep spectrum index, strong radio spectral curvature, radio morphology with no core and jet, we gleaned out a sample of remnant radio galaxy candidates. Preliminary results suggest that these radio galaxies belong to various phases of the final stage of evolution and tend to be found at higher redshifts. This work is done in collaboration with Prof. C.H. Ishwara-Chandra and Prof. Yogesh Wadadekar from NCRA-TIFR Pune.

(S. Dutta & V. Singh)

First light results from 43cm telescope at Mount Abu Infrared Observatory

We have installed the PLANEWAVE CDK17, a 43 cm primary aperture telescope at Gurushikhar Observatory, Mount Abu, India. It is a F/6.8 Corrected Dall-Kirkham Astrograph telescope, which covers a 70 mm field of view (FOV) without any field curvature, off-axis coma, or astigmatism. The primary mirror made up of fused silica glass with Enhanced Aluminium (EA) coating providing $\sim$95 reflectivity. The telescope is mounted on PLANEWAVE ASCENSION 200HR mount, a german equatorial mount, controllable using ASCOM-compatible SiTech control software for PC. The RMS tracking error of telescope during calm conditions is typically 0.14"-0.25". We also attached a finder scope to the telescope. For longer exposures or continuous monitoring of sources, we used the commercially available Iodestar-X2 for telescope auto-guiding. The auto-guiding camera is attached with the finder telescope provides an accuracy upto 1"/sec. We chose ANDOR ikon 2K X 2K CCD (BEX2-DD) to be used as detector as it is highly efficient ($>$90%) in the visible range (400nm - 800nm) . It provides us a wide FOV of $\sim$ 33'X33' with a resolution of 0.7"/pixel. The whole telescope assembly is shown in figure 22. We observed few pre-confirmed explanatory systems in broad "I" band to check the telescope photometric performance. We used the ASTROIMAGEJ (Collins et al 2016) software for photometry data reduction viz. dark, bias and flat corrections, lightcurve (LC) extraction using multi-aperture photometry and fitting the extracted LC. We got the great results with it as we are able to reach upto 18 mag in 30 min exposure time. Along with that we detected the transit shape/depth on already confirmed exoplanetary systems within the 1-sigma errors of the predetermined transit depths. The LC for one of such system observed using 43 cm telescope on 7th February, 2019 is shown in Figure 23 with the best fitted model. The cadence for each datapoint is 124.2 s.



Figure no. 22: The whole telescope assembly of 43cm telescope is shown here. It is kept inside 12ft Astro-Heaven dome. The brown colored small scope attached to main telescope is the finder scope.

(N. J. S. S. V. Prasad, A. Nayak, K. K. Lad, R. Sharma & A. Chakraborty)

PARAS-2 precision radial velocimeter: optical and mechanical design of a fiber-fed high resolution spectrograph under vacuum and temperature control

We are developing a new fiber-fed High-resolution spectrograph, PARAS-2, at resolution (R) = 100,000, which will be kept under vacuum (0.001 to 0.005 mbar) and temperature controlled environment at 25° C $\pm$ 0.001° C. The spectrograph will be attached to the upcoming new PRL 2.5m aperture telescope at Gurushikar, Mount Abu, Rajasthan, India. The spectrograph (PARAS-2) will be operating in the range of 380nm to 690nm wavelength in a single shot using Grism as a Cross Disperser , R4 Echelle (31.6 lines/mm) at blaze angle of 76 degrees, and pupil diameter of 200 mm. The grism material is OHARA S-FSL5Y glass with Apex angle of 13.24 degrees and groove's density of 257.14 lines/mm. We will use a combination of octagonal and circular fibers along with double scrambler and simultaneous calibration for getting down to the RV precision of 50 cm/s or better ($<$ 50cm/s). Minimum 30% time will be reserved for exoplanet work with the spectrograph on the 2.5m telescope when it becomes operational in early 2020. The overall efficiency of the whole spectrograph (Echelle, M1, M2, FM, Grism, Camera lens system, Dewar window) excluding fiber is expected to be 22.5% - 28% and 4% - 8% including optical fiber, telescope and fiber- telescope interface losses. The F/number for camera lens system is 4.8 and transmission of the whole camera lens assembly is expected to be 91%.

To enable efficient coverage of the broad bandwidth of the PARAS 2 spectrograph, we have selected the 6144 $\times$ 6190 pixels from E2V CCD231-C6 as the detector array. This back-thinned CCD has 15 μm square pixels and a custom E2V "astro-broadband" antireflection (AR) coating that provides high quantum efficiency (QE) over most of the operating wavelength region (380nm-690nm) of PARAS 2.

Each optical elements (Echelle, Off-axis parabolas, lens barrel etc.) will be arranged on a very stiff optical bench through their respective support system and the whole assembly will be kept inside a cylindrical vacuum vessel. The vacuum chamber will be kept over an RCC pier, which is dynamically isolated from rest of the facility. The CCD Dewar will be kept outside the vacuum chamber and connected to it through metallic Bellow and It will take care of the deformations due to external pressure .

Temperature variation by 1° C or atmospheric pressure variation by 1 mbar would already produce effects of the order of 100 m/s (Pepe et al. 2002). Therefore, it becomes necessary to house the instrument optics in a very stable temperature and pressure environment. For PARAS-1 (Chakraborty et al. 2014), we have achieved temperature stability (RMS = 0.002°) very close to desired goal by means of enclosing PARAS spectrograph in a closed concentric volume space consisting of two thermally insulated outer (Heating and Cooling) and inner room (Heating only). Similar setup will be used for PARAS-2. For PARAS-2, pt100 sensors of accuracy of 0.001℃ along with MicroK (from ISOTECH) will be used, which makes temperature measurement more accurate.

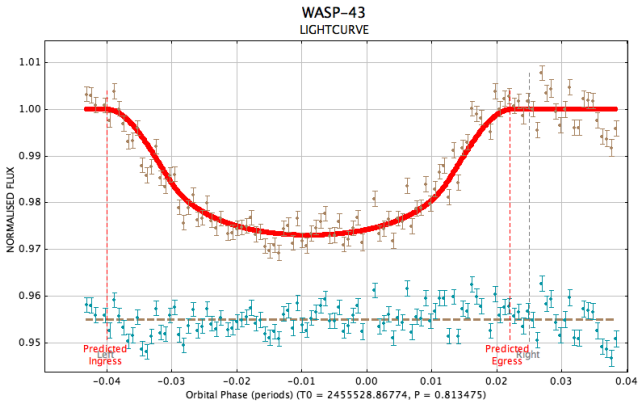


Figure no. 23: The brown colored data points are observed lightcurve from 43 cm telescope, while best fitted model is overplotted in Red. In below panel, teal colored points are the residuals. The typical RMS of the residuals is $\sim$ 1.3 mmag.

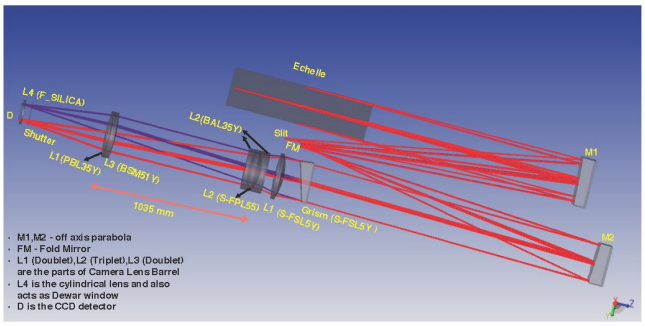


Figure no. 24: 3D Optical layout of the full spectrograph. Material chosen for optical elements is written in parentheses. The Red and Blue colored beams represent the lowest (90) and the highest optical orders (162), respectively.

(A. Chakraborty, K. Kumar, N. J. S. S. V. Prasad & R. Sharma)

Development of MFOSC-P: An Optical Imager-Spectrograph for Mt. Abu 1.2m Telescope

Mt. Abu Faint Object Spectrograph and Camera-Pathfinder (MFOSC-P), under development since mid-2015, has been very successful developed and commissioned on the PRL 1.2m telescope in February 2019. MFOSC-P had been conceptualized as a general-purpose user's instrument to provide imaging and

spectroscopy capabilities in visible waveband (4500-8500 angstroms) for various research programs of A&A division. Based on common collimator and camera design of FOSC series of instrument, the optics has been designed to provide 'seeing limited imaging' in astronomy standard Bessell's B, V, R and I filters. These custom designed optics (lenses, mirrors etc.) was later got fabricated by commercial optics manufacturers. Three plane reflection gratings are used in MFOSC-P to provide resolutions ($\lambda/\Delta\lambda$) of 2000, 1000 and 500 around 6500, 6000 and 6500 angstroms. The mechanical system of the instrument had been designed and successfully evaluated for its structural integrity using finite element analysis. The instrument is equipped with ANDOR 1K X 1K detector which corresponds to 5.2 X 5.2 arc-minute square field of view with seeing limited sampling of 3.3 pixel per arc-second. A calibration unit, with standard spectral lamps coupled to an integrating sphere, is also a part of the instrument. Newport-Oriel make pencil style calibration lamps (Ne and Xe) along with a halogen lamp are being used for spectral calibration purpose. The lamps are mounted onto the ports of the integrating sphere. Two commercial off-the-shelf achromatic lenses and a pupil mask simulates the telescope pupil and f/13 calibration beam to be injected into the instrument's optics. A movable fold mirror mounted on a stepper motor driven linear translational stage is used to direct calibration beam into the instrument. This fold mirror blocks the telescope beam during the spectral calibration of the instrument and is retracted during the science run of the instrument.



Figure no. 25: MFOSC-P Control System.

The automation of the instrument is being provided by various moving components (filter wheel, grating wheel etc.) that are driven by stepper motors. Each of the stepper motor based mechanism is equipped with encoder feedbacks as well as limit sensors. These motion controls along with their limit and encoder feedbacks and switching control of calibration lamps is being provided by an in-house developed control system (Figure-25) based on two commercial PMX series 4-axes stepper motor controllers from M/S ARCUS Technologies. A graphical user's interface (Figure-26) to control these operations is developed in Python PyQT framework. A separate user's interface for the image readout, display and camera control software has been used as a part of ANDOR detector camera system. Figure-27 show the assembly and integration sequence of the instrument in the laboratory. Individual lens elements were first mounted into their respective mounts and barrels and tested for their image quality. The collimator and camera sub systems were then constructed and characterized on the optical test bench for their imaging performance. Once all the sub systems were verified for their designed performance, they were integrated into instrument chassis to complete the instrument.

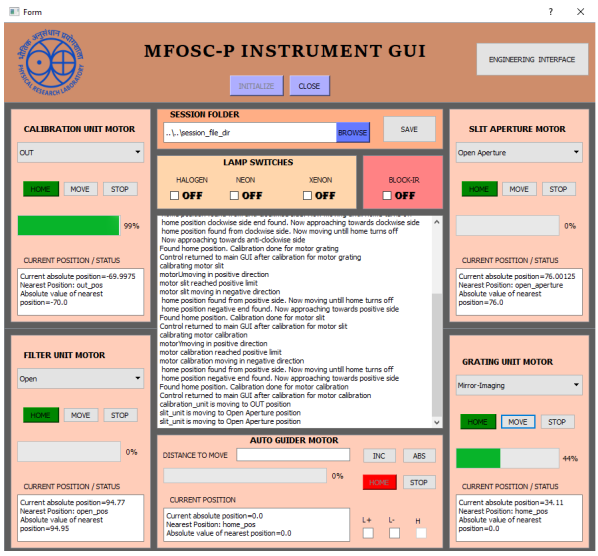


Figure no. 26: MFOSC-P Instrument Control GUI.

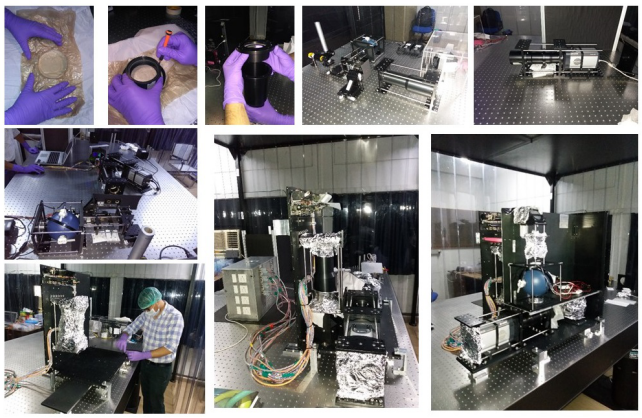


Figure no. 27: Images showing the assembly and integration process of MFOSC-P. Lens mounts, Barrels and other subsystems were constructed and charaterized on an test bench set-up prior to integration into instrument chassis.

The imaging and spectroscopy laboratory performance of MFOSC-P is shown in Figure-28. Intensity distribution over the pixels is shown for 10 microns diameter source (~ 0.44 pixels in size) illuminated with Neon lamp. The full width at half maximum (FWHM) is determined to be 1.16 pixel which is same as designed value. Spectroscopy modes were also verified for their designed performance of resolutions of 2000, 1000 and 500 for centre wavelengths. Figure-28 shows the spectrum of neon lamps for grating of 500 lines pair per mm. The FWHM of emission lines were measure to be ~ 3.25 angstroms thus providing the designed resolutions of 2000. MFOSC-P has been commissioned on PRL 1.2m telescope and saw its first light on February 5^{th} 2019. Figure-29 shows MFOSC-P mounted on the telescope. The spectra of a recurrent nova T CrB obtained using MFOSC-P instrument is shown in Figure-30 for all the three spectroscopy modes of the instrument. A comparison spectrum of the same source from literature (Munari et al. 2016) is also shown for comparison.

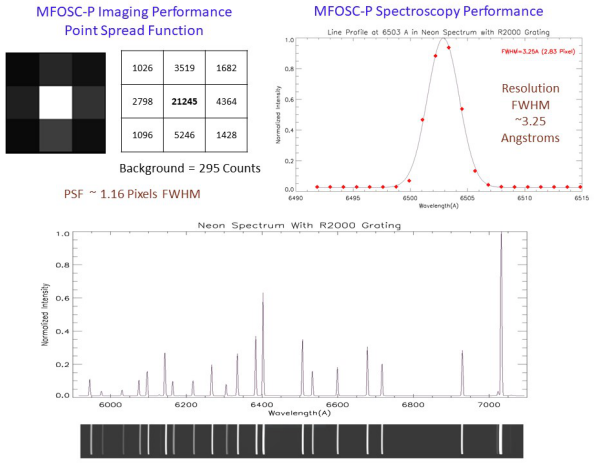


Figure 28: Imaging and Spectroscopy laboratory performance of MFOSC-P. The point spread function FWHM is estimated to be around 1.16 pixels. The spectroscopy resolution for resolution 2000 grating is measured to be ~ 3.25 angstrom at 6503 angstrom wavelength. These measured values are in agreement with the designed specifications.

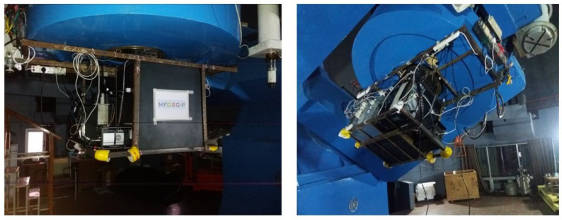


Figure no.29: MFOSC-P mounted on PRL 1.2m telescope.

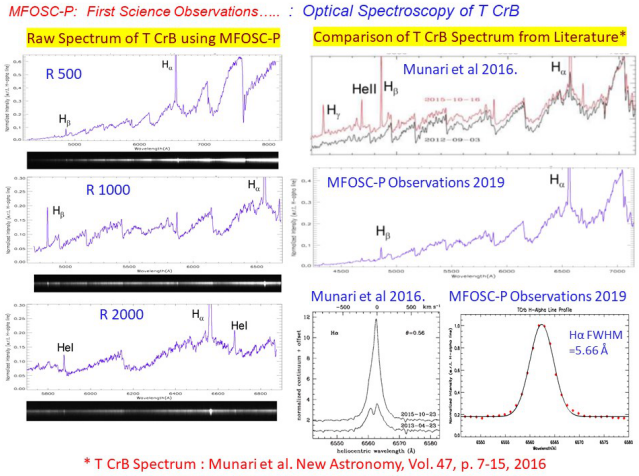


Figure no. 30: Optical Spectroscopy of a recurrent Nova T CrB using MFOSC-P. A spectrum of T CrB from literature (Muanri et al. 2016) is also shown for comparison. Left panel shown raw T CrB spectra in all three of MFOSC-P gratings namely R500, R1000 and R2000.

(M. K. Srivastava, V. Kumar, M.L. Jangra, V. Dixit, A. Patel & S.N. Mathur)

Adaptive Optics (AO) Test Bench Development: Computational Test Bench

Atmospheric turbulence is the major factor in decreasing the resolution of ground-based telescopes in astronomy. Adaptive Optics (AO) is a technique which is usually employed at ground based optical-near infrared telescopes to improve the image quality by measuring and correcting the effects of turbulence. With the upcoming PRL 2.5m telescope, it is highly desirable to have this technique on the telescope. However, a full-fledged AO system is a complex and costly system which requires proper understanding of its various subsystems. AO test-bench setup is a laboratory experimental setup which is currently being designed to evaluate the performance of various elements and sub systems involved. In order to develop a conceptual design of the whole setup, various parameters associated with the system need to be simulated. A computational test bench shall provide a detailed theoretical framework of said AO system including the atmospheric effects.

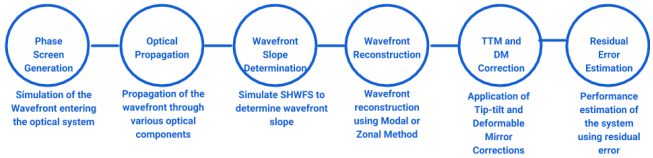


Figure no. 31: An outline of the subsystems of the computation test-bench.

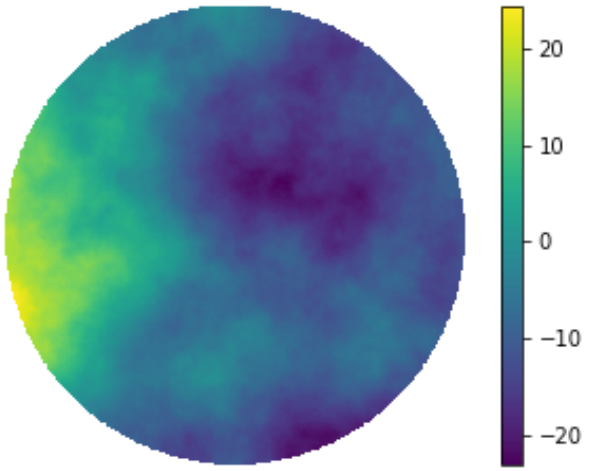


Figure no. 32: A sample Kolmogorov phase screen generated for this work.

This computational model is based on the theoretical framework of Fourier Optics/Fresnel propagation of beams to describe the properties of AO imaging systems. Several effects that are of importance to an astronomical adaptive optics system are being modelled in the computational setup e.g. beam propagation through turbulent media, spatial and temporal variability of phase structures over the pupil, sampling and reconstruction of the pupil phase map, correction applied by deformable mirror and residual error map etc. Figure-32 shows a Kolmogorov phase screen generated in this work which would reasonably simulate the effects of atmospheric turbulence

on the phase of a plane wavefront. These simulations are being used to identify the optimum correction parameters of the system. Figure-33 shows a plot of variation of normalized intensity with respect of D/r_0 value for various Zernike modes corrected. Here D is the diameter of the telescope while r_0 is Fried parameter.

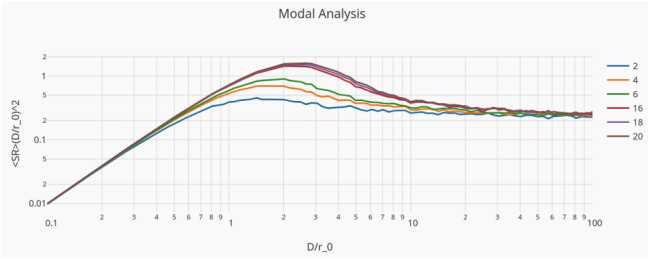


Figure no. 33: Mean Normalized on-axis intensity $< In >= (\mathrm{D}/r_0)^2 <$ SR $>$ Vs. D/r_0. Various colors in the legend show highest Zernike mode corrected.

The theoretical understandings employed in development of this computational simulation model would be validated with the help of hardware test-bench setup for the various error budgets and expected performance. The test bench set up has been designed and the hardware component requirements have been chosen to match the conditions for upcoming PRL 2.5m telescope at Mt. Abu. Based on these requirements various commercially available off-the-shelf options have been identified. Figure-34 shows the layout of the optical components involved in the experiment. The procurement procedure of these components has already been initiated. A hot-air based turbulence generator for simulating atmospheric turbulence is being designed for this experiment and would be fabricated at PRL workshop. The whole hardware setup would be realized in the laboratory by the next year.

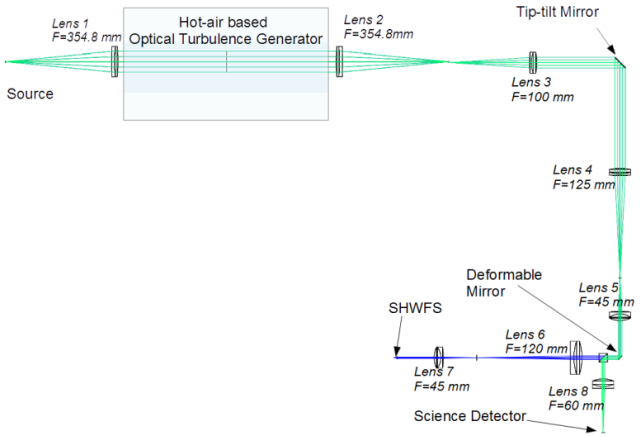


Figure no. 34: A schematics showing the optical train components involved in our setup (Diagram is not in scale).

(V. Dixit and M. K. Srivastava)

Prototype filter wheel development for NISP

Near Infrared Spectrometer and Polarimeter (NISP) is being developed for PRL's upcoming 2.5 m telescope at Mt. Abu. As a part of this instrument development, a prototype filter wheel was designed, fabricated and tested in the laboratory. The crucial design requirement was that these mechanisms should operate at both room temperature and cryo temperature (around 80K). For precise functioning of the instrument, tolerance and alignment play an important role. A good design would be expected to decrease thermal stresses and strains which ensures smooth movement of the parts. Smart stepper motors are being used for motion control. Since these motors cannot be used at cryogenic temperatures and high vacuum conditions, they will be mounted outside the Vacuum Dewar in ambient conditions. Rotary feedthrough would be used to transmit the motion to the filter wheels inside the Vacuum Dewar.

Drive Mechanism: The drive mechanism consists of bevel gear set and Spur gears set. One of spur gears is used as filterwheel. All the bevels, pinion gear and the filter wheel are made of Brass material. Significant backlash is voluntarily introduced in the gear system when setting the distance between the pinion gear and filter wheel rotation axes. This strategy is to reduce the risk of gripping that could occur if the filter wheel does not cool down as fast as its enclosure.

Spring locking system: Precise repeatability of the position of the filter wheel is not always possible due to backlash in the gears. Hence a spring locking system has been devised. It is a simple mechanism where Vee grooves are present in equiangular positions on a pitch circle on the filter wheel surface. Every groove corresponds to a fixed filter position. Spring-ball mechanism is being used to lock the ball in the groove. A spring is used to press the ball against the filter wheel surface on the pitch circle. The ball rolls on the surface between two grooves with minimum friction.

Absolute position encoding: Absolute position readout mechanism of each filter position reduces the filter change time compared to home position method. Magnet and reed switch combinations were used to get a unique number for a filter. Magnet and reed-switch combination is a passive system with a very long life time.

Figure 35 shows the filter wheel assembly, fabricated in PRL Workshop, being tested in the NISP lab.

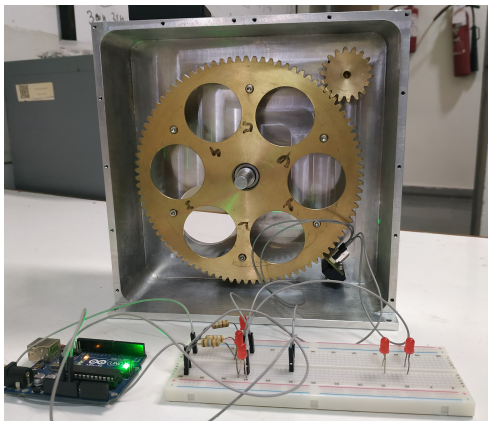


Figure no. 35: Prototype filter wheel assembly being tested in the NISP Lab.

(Prashanth K, A. B. Shah, H. Vaghela, H. Adalja, S. N. Mathur, D. R. Sarkar, A. Singh & NISP team)

Prototype vacuum dewar using Carbon Fibre Reinforced Polymer (CFRP) material

A very crucial part in building a Near Infrared Instrument is to maintain the detector at 77K and optics at around 100K to reduce the thermal noise. Maintaining these low temperatures through out the observation (9-12 hours) requires very good thermal insulation between the detector-lens assembly and the ambient. As Vacuum is the best thermal insulation, we keep all the optics and the detector inside a Vacuum Dewar. CFRP material was chosen to make a prototype vacuum dewar considering the high specific strength. In order to evaluate the suitability of CFRP material for Vacuum dewars a prototype single piece dewar with dimensions (300 mm $\times$ 300 mm $\times$ 320 mm) was made from CFRP at Ahmedabad Textile Industries Research Association(ATIRA), Ahmedabad.



Figure no. 36: Aluminium former for moulding CFRP dewar.

The CFRP dewar was made using TC35-3K Carbon fabric, Lapox ARL-135LV Epoxy Resin and Lapox AH442 epoxy hardener. The challenging task was to make the entire dewar as a single piece. For that an Aluminium 'former' was made as shown in Figure 36. Vacuum Resin infusion process was used to spread the epoxy resin all over the carbon fabric wrapped around the aluminium former. Then the entire system was cured for 4 hours at 150°C with a curing cycle of 10 hours. 150°C with a curing cycle of 10 hours. The dewar (see Figure 37) made using the above process was used for testing the vacuum holding capacity.



Figure no. 37. CFRP dewar.

Test setup was made as shown in Figure 38. Two Aluminium plates with Viton O-ring were used to seal the CFRP dewar. Based on our tests, A vacuum level of 1.2×10^{-3} Torr was achieved in the dewar Aluminium coating on CFRP is being planned to stop the devolatisation and degassing which would further improve the Vacuum level.



Figure no. 38: CFRP dewar undergoing Vacuum test in NISP Lab.

(Prashanth K, H. Adalja, S. N. Mathur & NISP team)

Development of hard X-ray mirrors foils for hard X-ray telescope

A new activity for developing hard X-ray telescope as a potential successor for the AstroSat has been initiated in Astronomy & Astrophysics division. A proposal was submitted to the ISRO in response to the Announcement of Opportunity for future astronomy missions. It was reviewed highly positively by the ADCOS and was recommended to be taken up for study phase of three years. In this context, we have initiated a technology development program for design and fabrication of hard X-ray mirrors. In X-ray waveband, reflection is achieved by grazing angle incidence on the mirror foils coated with high density material. Particularly in hard X-rays ($\sim$>10 keV) multiple alternate layers of high and low density materials on a highly polished substrate are essential to achieve required reflectivity. Such multi-layer coating is required to be done on a substrate formed in appropriate shape to constitute the X-ray mirror foils, which are then assembled in a nested shell configuration to realize the hard X-ray telescope.



Figure no. 39 : Fabrication of the curved glass sheets for X-ray mirror foils using thermal slumping technique before thermal slumping.

We have established a hard X-ray optics laboratory for development of hard X-ray mirror foils consisting of an RF Magnetron sputtering

system (see Figure 41), necessary for the multi-layer coating as well as a thermal slumping sysetm necessary to form thin glass sheets in appropriate curved shape (see Figures 39, 40).

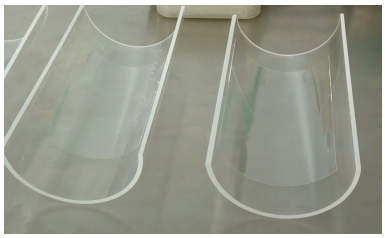


Figure no. 40: Fabrication of the curved glass sheets for X-ray mirror foils using thermal slumping technique after thermal slumping.

In order to obtain appropriately shaped highly polished substrate to realize the nested shell Wolter-I conical approximation X-ray telscope, we have adopted the technique of thermal slumping similar to that used in *NuSTAR* mission. Borosilicate thin flat glass sheets with required surface roughness ($< 1\ nm$ RMS), placed over quartz mandrel of appropriate figure is subjected to specific thermal cycling with programmable ovens. After the thermal cycling process the glass sheets achieve the desired figure which can be then coated with multi-layer to form the mirror foils.

The RF Magnetron sputtering system used for multi-layer coating is equipped with two cathodes, typically one each for a high Z (such as W or Pt) and a low Z (such as Si or B4C). Argon gas supplied into the vacuum chamber ionizes due to the applied bias and these ions gets accelerated towards the target and collides to eject the atoms which finally deposit onto the substrate. The substrates are placed on a rotating platform within the chamber, allowing uniform coating of multiple alternate layers of two materials. Single thin layer depositions of individual targets as well as multi-layer depositions using Tungsten and Silicon targets have been carried out with the system and are characterized. Detailed characterization of the sputtering system using X-ray reflectivity measurement setup to calibrate the obtained thickness with respect to various system parameters is underway.



Figure no. 41: RF Magnetron sputtering system for multi-layer coating for hard X-ray mirror foils.

(Mithun N. P. S., N. Tiwari, B. Mondal, H. Adalja, & S. Vadawale)

Solar Physics

Evidence that abrupt changes in the solar magnetic fields during major flares can drive acoustic oscillations in the solar atmosphere

Solar flares are catastrophic phenomena occurring in the solar atmosphere which release large amount of energy and energetic particles moving with very high speeds. It is believed that magnetic energy stored in the solar active regions is transformed into thermal energy and electromagnetic radiations during the flares. The solar magnetic fields undergo changes during the flares, the signatures of which are seen in the evolution of magnetic field parameters in the solar atmosphere. Occasionally, it is also observed that magnetic fields undergo abrupt changes in some localized regions of the active region, which is basically the imprint of fast re-organization of coronal magnetic fields during the flares. The Lorentz force changes associated with the abrupt changes in the magnetic fields are believed to power the acoustic oscillations in the solar atmosphere.

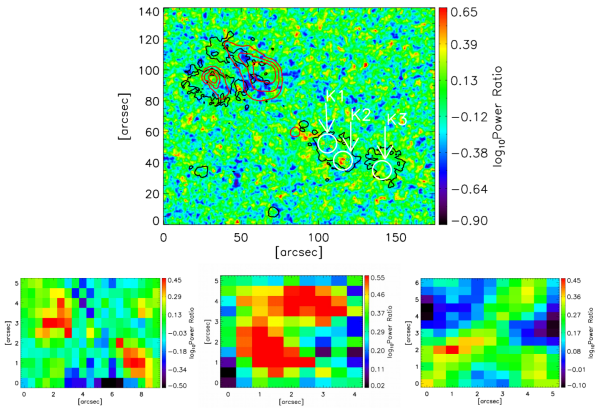


Figure 1.: The top panel shows the ratio of the power spectra of velocity oscillations in the frequency band 2.5-4.0 mHz (p-mode band) in the active region NOAA 11261 estimated before and spanning an M6.0-class flare on August 3, 2011. The red contours show the location of the flare ribbons in the active region whereas the black contours show the outer boundary of the penumbra of the sunspot regions. The locations marked as K1, K2, and K3 are the identified localized regions showing the enhanced acoustic power during the flare. The bottom panels illustrate the blow-up of the kernels K1, K2, and K3, respectively, from LHS to RHS. It is evident from these power maps that acoustic power is enhanced in these locations during the flare. It is also seen that K1, K2, and K3 are away from the flare ribbons.

Here, we present the evidence of enhanced acoustic oscillations in the solar photosphere associated with the abrupt changes in the magnetic fields observed during a major flare (of class M6.0) that occurred in the active region NOAA 11261 on August 3, 2011. For this study, we have used high-resolution photospheric Dopplergrams and magnetograms obtained by the Helioseismic and Magnetic Imager (HMI) solar telescope onboard Solar Dynamics Observatory (SDO) space mission. We have also used the chromospheric H-alpha observations obtained by the Global Oscillation Network Group (GONG) solar telescope for information related to spatial evolution of the flare ribbons in the active region. The power spectra of the acoustic velocity oscillations spanning the flare relative to the pre-flare epoch clearly illustrates enhanced acoustic power within the active region, both in the p-mode band (2.5–4.0 mHz) and high-frequency band (5.0–6.5 mHz) (c.f., Figures 1 and 2), which is associated with abrupt changes in the line-of-sight and vector magnetic fields during the flare (Figures 3 and 4). It is noteworthy mentioning that the aforementioned locations of enhanced acoustic power in the active region are seen to be very much away from the locations of the flare-ribbons and hence these are free from the effects of any contamination in the observed velocity and magnetic field changes during the flare.

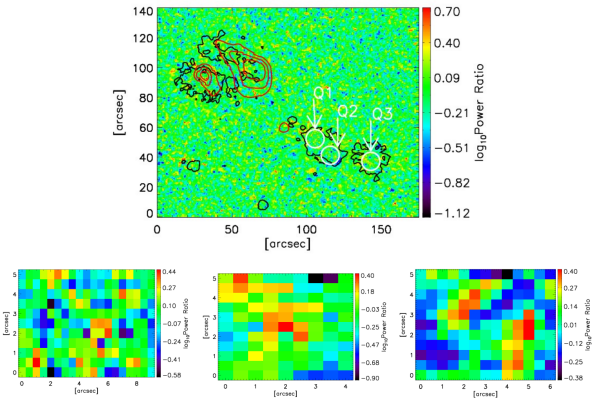


Figure 2.: The top panel shows the ratio of the power spectra of velocity oscillations in the frequency band 5.0-6.5 mHz (high-frequency band) in the active region NOAA 11261 estimated before and spanning an M6.0-class flare on August 3, 2011. The red contours show the location of the flare ribbons in the active region whereas the black contours show the outer boundary of the penumbra of the sunspot regions. The locations marked as Q1, Q2, and Q3 are the identified localized regions showing the enhanced acoustic power during the flare. The bottom panels illustrate the blow-up of the kernels Q1, Q2, and Q3, respectively, from LHS to RHS. It is evident from these power maps that acoustic power is enhanced in these locations during the flare. It is also seen that Q1, Q2, and Q3 are away from the flare ribbons.

These results show that the transient Lorentz forces associated with the abrupt changes in the magnetic fields during the flare could drive the localized oscillations in the active region. These magnetically driven oscillations are important to study in view of the transport of wave energy to the higher solar atmospheric layers.

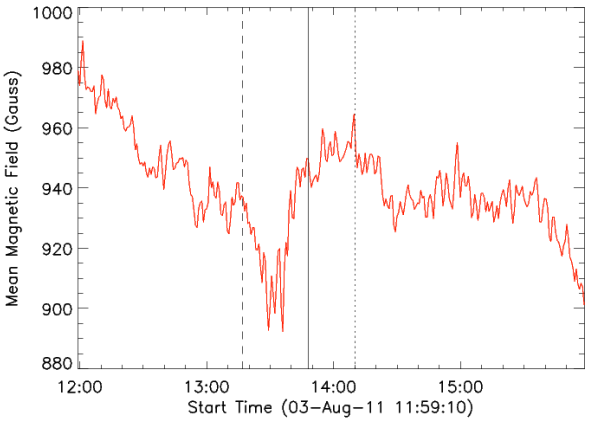


Figure 3.: Temporal evolution of the line-of-sight (LOS) solar magnetic fields in one of the identified locations showing enhancement in power in the active region during the flare. It is clearly seen that the LOS magnetic field in this location observed abrupt changes during the flare.

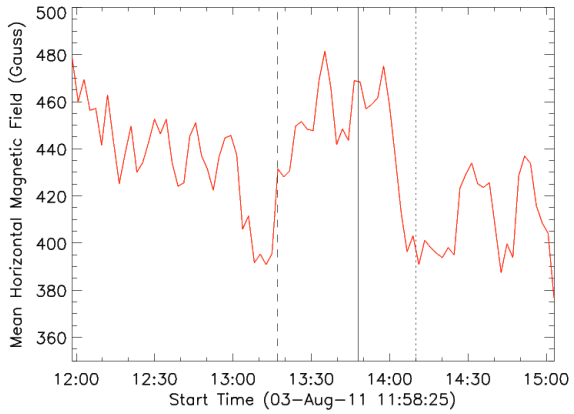


Figure 4.: Temporal evolution of the transverse solar magnetic fields in one of the identified locations showing enhancement in power in the active region during the flare. It is clearly seen that the horizontal magnetic field in this location observed abrupt changes during the flare.

(B. Kumar and H. Kumar)

Multiwavelength analysis and modeling of the largest solar flare in the solar cycle 24 occurring from a δ-sunspot region NOAA 12673

We present a multi-wavelength analysis of the largest solar flare in the solar cycle 24 of class X9.3 which occurred in the sigmoidal active region NOAA 12673 on 2017 September 6 by combining observations of Atmospheric Imaging Assembly and Helioseismic Magnetic Imager instruments on board the *Solar Dynamics Observatory*. On the day of the reported activity, the photospheric structure of the active region displayed a very complex network of δ-sunspots that gave rise to the formation of a coronal sigmoid observed in the hot extreme-ultraviolet (EUV) channels. The flare initiated from the core of the sigmoid and progressed as a single sigmoid-to-arcade event (Figure 5(a)-(c)). Differential emission measure analysis reveals strong heating of plasma at the core of the active region right from the preflare phase, which further intensified and spatially expanded during the event. The identification of a preexisting magnetic null by non-force-free-field (NFFF) modeling of the coronal magnetic fields at the location of early flare brightenings (Figure 5(d)) and remote faint ribbon-like structures during the preflare phase, which were magnetically connected with the core region, provide support for the breakout model of solar eruption. The magnetic extrapolations also reveal flux rope structures before the flare (Figure 5(d)), which are subsequently supported by the observations of the eruption of hot EUV channels. This X-class flare diverged from the standard flare scenario in the evolution of two sets of flare ribbons, which are spatially well separated, providing firm evidence of magnetic reconnections at two coronal heights.

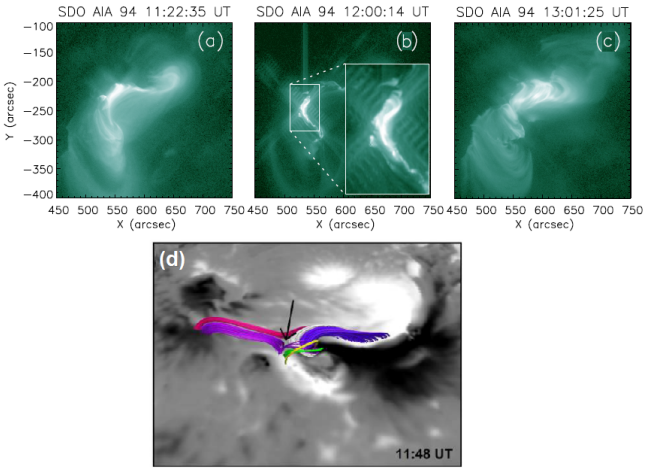


Figure 5.: AIA 94 Å images showing the coronal configuration of the active region NOAA 12673 during the pre-flare phase (panel (a)), impulsive phase of the X9.3 flare (panel (b)), and the late gradual phase (panel (c)). The flare was initiated from the middle of the active region which is shown in the zoomed cutout inside panel (b). Panel (d): NFFF extrapolation results indicating a flux rope (shown by blue lines) associated with a magnetic null point (indicated by the arrow) and two sets of field lines making (shown by the yellow and green lines) an X-type configuration.

This work has been done in collaboration with Astrid M. Veronig (Institute of Physics & Kanzelhöhe Observatory, University of Graz, Austria.)

(P.K.Mitra, B. Joshi, A. Prasad, and R. Bhattacharyya)

Generalisation of the Magnetic Field Configuration of typical and atypical Confined Flares

A typical confined flares cannot be naturally explained with standard flare models. To predict such flares, we need to define their physical characteristics, in particular, their magnetic environment, and identify pairs of reconnected loops. In this article, we study an atypical confined flare of GOES class C5.0 that leads to a long duration event in soft X-rays (SXR) and provide a topological model to understand such exceptional cases. The important multi-wavelength features associated with stages 1 and 2 of the confined event are shown in Figure 6.

We observed the formation of filament F2 from 2014 May 13 to 15 during the continuous flux cancellation in the region underneath the filament. During the formation of flux rope F2, we assume that the loops in the AR should evolve. The expanding loops overlying the filament F2 (shown by the red arrows in Figure 6 (d)) reconnect with the surrounding field as well as with the overlying loops of filament F1 successively in three different phases. The comprehensive analysis of the flare in (E)UV wavelengths and their comparison with modeled coronal magnetic field configuration by an NLFFF technique reveal successive stages of reconnection involving magnetic field lines overlying the two neighboring filaments. The spatial and temporal evolutions of the RHESSI X-ray emission during the rise and maximum phases of the flare provide clear evidence that the magnetic reconnection sequentially proceeded at two adjacent locations within the core region of the flaring environment. The flare is only of C5.0 class, but it is a long duration event. The reason is that it is comprised of three successive stages of reconnection. A non–linear force–free field extrapolation and a magnetic topology analysis allow us to identify the loops involved in the reconnection process and build a reliable scenario for this atypical confined flare. We conclude that the quasi-parallel reconnection leading to two sets of flare loops. The present study thus adds up to a new well-identified case of so-called atypical flares. We also investigated the importance of the curvature of the PIL, that creates a purely 3D topological effect, which in turn allows reconnection between quasi-parallel field lines, and which exists neither in 2D models nor in models of failed eruptions. A comparison with previous extrapolations for typical and atypical confined flares leads us to propose a cartoon for generalizing the concept.

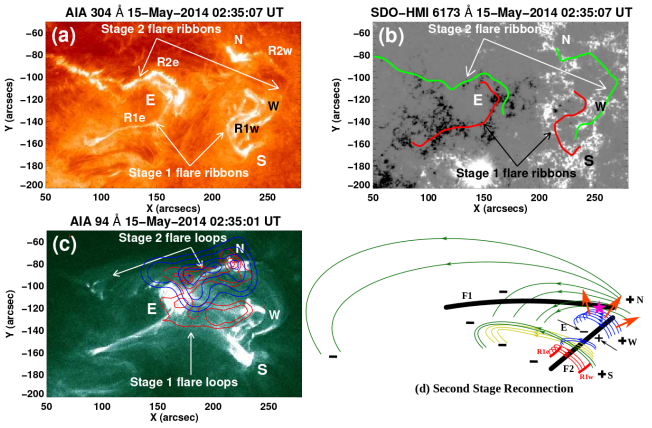


Figure 6.:(a) SDO/AIA 304 Å image showing both the first (R1e and R1w) and second (R2e and R2w) set of flare ribbons formed during the stages 1 and 2 of the event, respectively . (b) SDO/HMI line–of–sight photospheric magnetogram at 02:35:07 UT on 2014 May 15. The over plotted red and green lines show the first and second set of ribbons, respectively. These ribbons are traced from the AIA 304 Å image that is shown in panel (a). (c) SDO/AIA 131 Å image showing the flare loops connecting the flare ribbons. In panel (c) the loops joining the regions E to N are the reconnected loops formed during stage 2 of the flare. (d) Schematic representation of the second stage of the flare event, showing the magnetic topology. Green and blue lines are the pre-reconnected lines, while the red and yellow lines are the post-reconnected lines, respectively. Pink stars show the regions of magnetic reconnection.

This work is done in collaboration with Xiaoshuai Zhu (Max-Planck Institute for Solar System Research, Germany), Brigitte Schmieder (Observatoire de Paris, France), Guillaume Aulanier (Observatoire de Paris, France), Miho Janvier (Institut d'Astrophysique Spatiale, France), Tetsuya Magara (Kyung Hee University, South Korea), Ramesh Chandra (Kumaun University, Nainital), Satoshi Inoue (Nagoya University, Japan)

(N. C. Joshi and B. Joshi)

Investigation of a confined C-class flare close to a regular sunspot

A moderate C1.1 class confined flare occurred outside a regular, isolated sunspot in NOAA AR 11846 on 2013 September 24. Spectro-polarimetric observations from the Tenerife Infrared Polarimeter at the 70 cm German Vacuum Tower Telescope were combined with data from the Helioseismic Magnetic Imager and the Atmospheric Imaging Assembly to identify the processes that triggered the flare. The flare was a result of an erupting filament, connecting the leading sunspot to a diffuse network flux patch of opposite polarity. The extension of the filament, seen in the chromospheric images, can be traced into the leading sunspot's outer penumbra where one observes weak, but discernible, signatures of filamentation in the force-free parameter and current helicity maps derived from spectro-polarimetric data. The moat flow from the sunspot renders a continuous outflow wherein small-scale magnetic fragments stream towards larger patches of pre-existing flux, leading to flux cancellation. These events of flux cancellation drive several pre-cursor events in the chromosphere and transition region, which destabilize the filament. The presence of overlying loops between the positive polarity, leading sunspot and the negative polarity, network flux region, prevent the flare from developing into a CME and render it confined. During the onset of the flare, it was observed that the filament in question had an opposite sign of helicity in comparison to the leading sunspot. However, as the filament reforms at its former location maintaining its previous characteristics, it is unclear if the flare was a mechanism to remove the parasitic helicity.

(R. E. Louis)

Exploring the damping of Alfvén waves along a coronal loop up to 1.4 $R_\odot$

The Alfvén wave energy flux in the corona can be explored using the electron density and velocity amplitude of the wave. The velocity amplitude of Alfvén wave can be obtained from the non-thermal velocity of the spectral line profiles. Previous calculations of the Alfvén wave energy flux with height in active regions and polar coronal holes have provided evidence for the damping of Alfvén waves with height. In this work, we present off-limb Hinode Extreme ultraviolet Imaging Spectrometer (EIS) observations of a long coronal loop reaching up to 1.4 $R_\odot$ (Figure 7). We obtained the electron density (N_e) along the loop using the density sensitive line ratio method (Fe xii $\lambda 186.88/\lambda 195.12$). We found the loop to be almost in hydrostatic equilibrium. We obtained the electron temperature from the emission measure EM-loci method. We found that loop has constant temperature of about 1.37×10^6 K along its length. We obtained the Alfvén wave velocity amplitude (ξ) i.e. non-thermal velocity from the spectral line profiles of Fe xii 195.12 Å. Here, we significantly improved the estimate of non-thermal velocities over previous studies by using the estimated ion (equal to electron) temperature. Estimates of electron densities are also improved after significant updates of the CHIANTI v.8 atomic data.

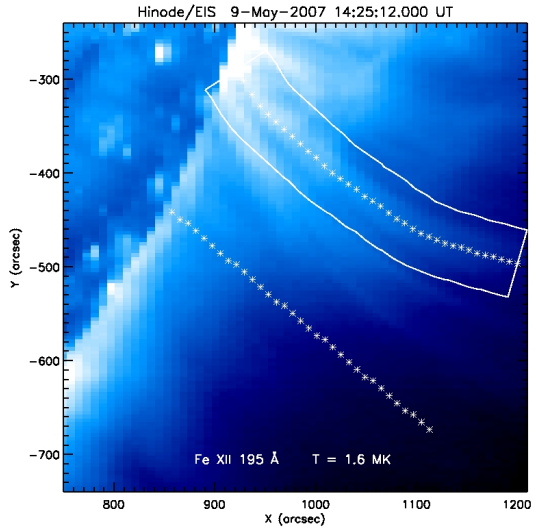


Figure 7.: Intensity maps obtained from Fe xii 195 Å showing the loop traced out to study in detail. The quiet Sun region is also traced out for the purpose of determining the background. The white curved box indicates region chosen along the curved loop.

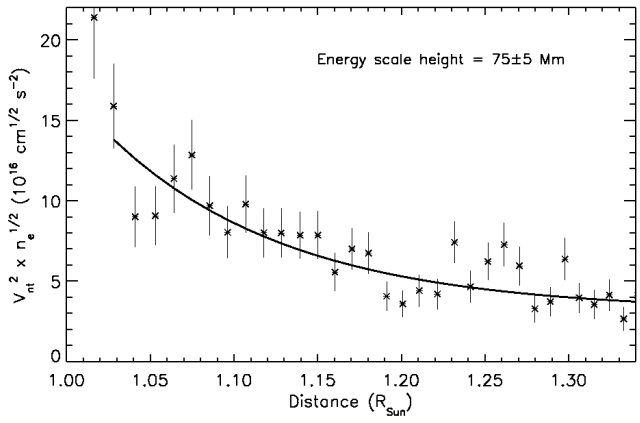


Figure 8.: Proportional Alfvén wave energy flux ($\alpha\ \sqrt{N_e}\xi^2$) obtained along the coronal loop. The energy flux is fitted with exponential function and obtained scale height is also printed.

The total Alfvén wave energy flux along the loop is always proportional to $\sqrt{N_e}\ \xi^2$. We obtained accurate measurements of the Alfvén wave energy flux and its damping along the coronal loop up to distances of 1.4 $R_\odot$ (Figure 8). Alfvén wave energy fluxes are found to be decreasing from $\approx 1.5 \times 10^6$ erg cm^{-2} s^{-1} near the limb to $\approx 0.3 \times 10^6$ erg cm^{-2} s^{-1} at around height of 1.2 $R_\odot$. The obtained Alfvén wave energy flux can contribute significant part of the coronal losses due to radiation along the loop.

This work is being carried out in collaboration with Giulio Del Zanna and Helen Mason of University of Cambridge, UK

(G. Gupta)

Evolution of coronal cavity from quiescent to eruptive phase in association with coronal mass ejection

Coronal mass ejections (CMEs) are one of the most energetic phenomena that occur in the solar atmosphere, which in turn may have severe space-weather impacts on Earth. Therefore, understanding the physical processes behind the initiation and triggering mechanism of CMEs has become the top priority in space-science research. Observing the development of coronal cavities in lower coronal regions can provide intriguing clues to the genesis of CMEs. In this work, we present the evolution of a coronal cavity encompassing its quiescent and eruptive phases in the lower corona.

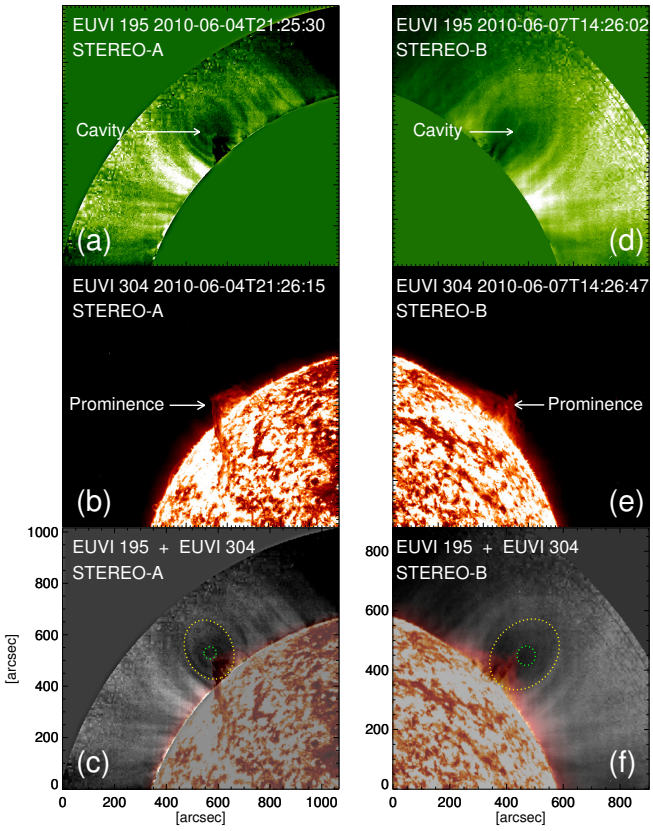


Figure 9.: Observations of the coronal cavity as seen in the 195 Å bandpass of EUVI on STEREO A and B (panels (a) and (d) respectively), the associated prominence structure in 304 Å bandpass (panels (b) and (e)) and a superposition of the 195 Å and 304 Å bandpasses (panels (c) and (f)). The green dotted line denotes the outer boundary of the true cavity. The yellow dotted line depicts the approximate outer boundary of the flux-rope.

Using the multi-vantage point observations from the SDO/AIA, STEREO SECCHI/EUVI and PROBA2/SWAP EUV imagers, we capture the sequence of quasi-static equilibria of the quiescent cavity which exhibited a slow rise and expansion phase during its passage on the solar disc from 2010 May 30 to 2010 June 13 (Figure 9). The cavity finally erupted from the north-west solar limb on 2010 June 13. Combining the observations of SWAP and LASCO C2/C3 we show the evolution of the EUV cavity into the white-light cavity as a three part structure of the associated CME. By applying successive geometrical fits to the cavity morphology we find that the cavity exhibited non self-similar expansion (Figure 10) in the lower corona, below 2.2 $\pm$ 0.2 R_S, which points to the spatial scale for the radius of source surface where the coronal magnetic field lines are believed to become radial.

The kinematic study of the erupting cavity captures both the "impulsive" and "residual" phases of acceleration along with a strong deflection ($\approx 40^{\circ}$ towards the equator) of the cavity at 1.3 R_S. The location of the pre-eruptive filament channel in the vicinity of the northern polar coronal hole indicates that the polar coronal hole has significant influence on the CME kinematics, deflecting the CME towards the heliospheric current-sheet.

The exponent value for the polynomial fit to the height-time profile of the erupting cavity reveals that the impulsive acceleration phase was most likely to be driven by the torus instability. By comparing the decay-index profiles of the cavity system during the different stages of its quiescent and pre-eruptive phases we find that the decay-index value at the cavity centroid height can be used as a good indicator to predict the cavity eruption in the context of torus instability. In short, our study addresses several key questions regarding the CME initiation mechanism that have thereby improved our understanding on the genesis of CMEs.

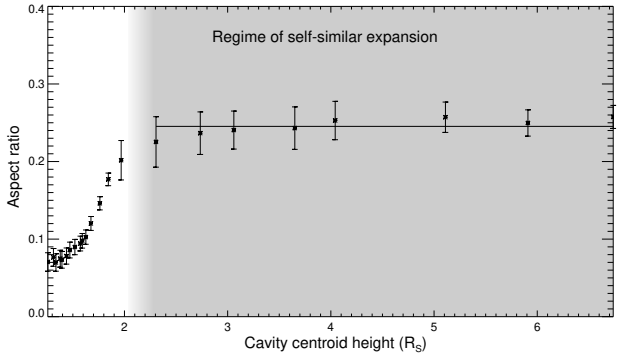


Figure 10.: The evolution of the cavity width to centroid height aspect-ratio

This work was carried out in collaboration with M. Mierla, M. J. West, E. D'Huys of Royal Observatory of Belgium, Belgium.

(R. Sarkar and Nandita Srivastava)

Source region characteristics and interplanetary consequences of a major geo-effective CME from NOAA 12371

We have carried out a multi-wavelength and multi-instrument investigation of a halo coronal mass ejection (CME) from active region NOAA 12371 on 2015 June 21 that led of a major geomagnetic storm of Dst ∼-204 nT. The observations from the Atmospheric Imaging Assembly on board the Solar Dynamics Observatory at hot EUV channel of 94 Å confirm the CME to be associated with a coronal sigmoid that displayed intense emission (T ∼6 MK) from its core before the onset of eruption. Multi-wavelength observations of the source active region suggest tether-cutting reconnections to be the primary triggering mechanism of the flux rope eruption. Interestingly, the flux rope eruption exhibited a two-phase evolution during which the "standard" large-scale flare reconnection manifested in the form of two composite M-class flares. The eruption of the flux rope is followed by the coronagraphic observation of a fast, halo CME with linear speed of 1366 km sec^{-1}. The dynamic radio spectrum in decameter-hectometer frequency range reveals multiple continuum-like enhancement in type II radio emission which imply the interaction of the CME with other preceding slow speed CMEs in the corona within 10–90 $R_{\odot}$.

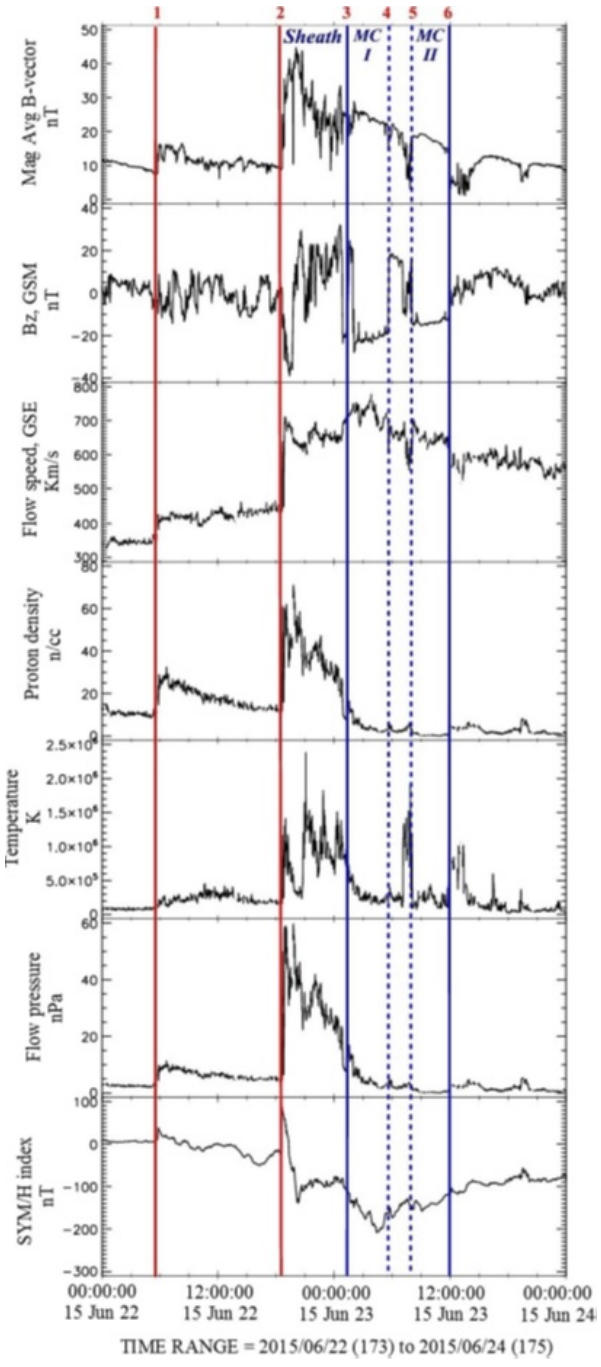


Figure 11.: In-situ observations of interplanetary plasma and magnetic field parameters during 2015 June 22-24. From top to bottom: total magnetic field strength, the z-component of the magnetic field, flow speed, proton density, proton temperature, flow pressure, SYM/H index (i.e., high resolution Dst index). The vertical solid lines (lines 1 and 2) mark the arrival of shocks. We note that the intensity of shock 1 is significantly lower than the shock 2. The shock 2 is associated with the arrival of large halo CME on 2015 June 21. The region between lines 2 and 3 represents sheath of the CME which is followed by the magnetic cloud (MC) structures. The plasma and magnetic parameters exhibit discontinuity during the passage of MC (see the region between vertical dashed lines (lines 4 and 5)) which separates MC into two parts (MC I and MC II).

The scenario of CME-CME interaction in the corona and interplanetary

medium is further confirmed by the height-time plots of CMEs occurring during June 19–21. In-situ measurements of magnetic field and plasma parameters of solar wind at 1 AU exhibit two distinct magnetic clouds, separated by a magnetic hole (Figure 11). Synthesis of near-Sun observations, interplanetary radio emissions, and in-situ measurements at 1 AU reveal complex processes of CME-CME interactions right from the source active region to the corona and interplanetary medium that have played crucial role toward the large enhancement of the geo-effectiveness of the halo CME on 2015 June 21.

This work has been done in collaboration with A. Shanmugaraju (Arul Anandar College,Madurai)

(B. Joshi, M. Syed Ibrahim and D. Chakrabarty)

Observationally constrained analytical model for predicting magnetic field vectors of ICMEs at 1 AU

Coronal mass ejections (CMEs) are powerful expulsions of gigantic clouds containing magnetized plasma that routinely erupt from the Sun and propagate out through the solar system. When such an eruption is directed toward the Earth with high speed and has a southward component of the magnetic field (Bz), an intense magnetic storm occurs upon the impact of the CME on Earth's magnetosphere. The storm can occur when the CME's interplanetary flux rope (FR) and/or the sheath between the FR and the associated shock has southward Bz. Therefore, a prior knowledge of the strength and orientation of the magnetic field embedded in the FR is required in order to forecast the severity of geomagnetic storms caused by CMEs.

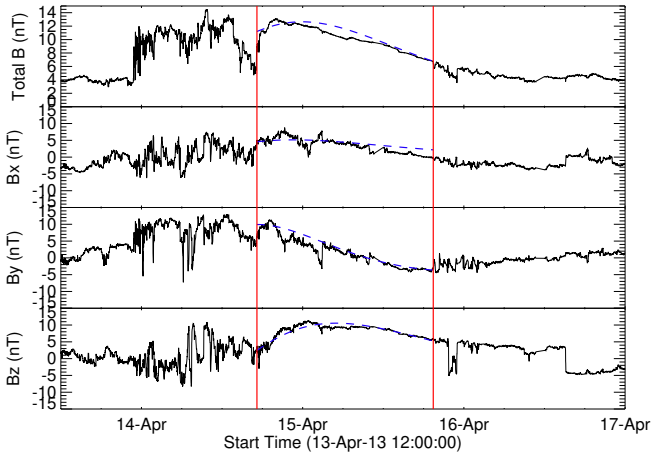


Figure 12.: Magnetic vectors as detected by the WIND space-craft for 14th April ICME event in 2013. The two red vertical lines denote the magnetic cloud boundary. The blue dashed lines denote the predicted magnetic vectors obtained from the model.

We have developed an observationally constrained analytical model to predict the magnetic field vectors of CMEs at 1 AU. The main architecture of this model involves using the near-Sun FR properties obtained from the observational parameters that are evolved through the model in order to predict the magnetic field vectors of ICMEs at 1 AU. As a proof of concept, we present the case study of the 2013 April 11 CME. Using the near-Sun properties of the CME flux rope, we have estimated the magnetic vectors of the ICME as intersected by the spacecraft at 1 AU. The predicted magnetic field profiles of the ICME show good agreement with those observed by the WIND spacecraft (Figure 12). Although our model does not include the prediction of the ICME plasma parameters, as a first order approximation it shows promising results in forecasting of Bz in real time. This could prove to be a simple space-weather forecasting tool compared to the time-consuming and computationally expensive MHD models.

(R. Sarkar and Nandita Srivastava)

Magnetohydrodynamical evolution of a coronal blowout jet

Like solar flares and coronal mass ejections (CMEs), coronal jets are the transients in the solar atmosphere, which are believed to be the manifestation of a fundamental process called magnetic reconnection (MR). The average length and width of a jet are $\approx 1.5 \times 10^5$km and $\approx 1.7 \times 10^4$km, respectively. Additionally, the average velocity of a jet is found to be ≈ 200km s^{-1} and it lasts for a few minutes to several hours. Though the energy released in coronal jets is smaller than that of the flares and CMEs, they play a significant role in governing the dynamics of the solar corona. Based on their evolution mechanism, the jets are classified into two types: standard and blowout. Mostly, the blowout jets develop into CMEs. The work reports one of the blowtype jets on December 5, 2016, in the active region AR12615. The aim is to understand its initial magnetic topology and the eruption mechanism leading to the collimated plasma flow that constitutes the body the jet. In Figure 13, the growth of the blowout jet is depicted.

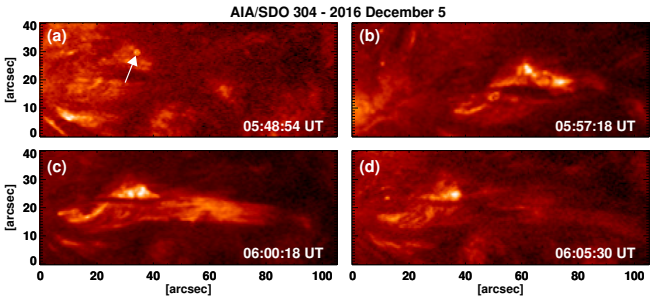


Figure No. 13: The panel-(a) to (d) represent the development of the blowout jet in 304 Å of Atmospheric Imaging Assembly onboard SDO. The white arrow in panel-(a) highlights the bright point which indicates the initiation of MR.

A well developed inverted "Y" or the "lambda" structure—typical to jets— is clearly seen in the panel (c). To understand the dynamical evolution, the photospheric magnetic field is used to construct the coronal magnetic field using a non-force-free-field (NFFF) extrapolation technique. We use the vector magnetic field of AR12615 at 05:48 UT on December 5, 2016, from Helioseismic Magnetic Imager (HMI) onboard Solar Dynamics Observatory (SDO). The physical extents of the computational box are ≈ 220Mm, ≈ 89Mm and ≈ 89Mm in x-, y- and z-axis respectively. A pair of three dimensional (3D) nulls and a flux rope are found in the extrapolated field. The dynamics of the nulls and their surrounding magnetic field lines are explored through the parallelized three-dimensional numerical model EULAG-MHD and is illustrated in Figure 14. The red and blue Magnetic field lines (MFLs) represent the inner and outer spine of the 3D nulls and the yellow MFLs constitute the flux rope. The flow vectors are represented by the green arrows. A

magnified view of the reconnection near the flux rope is shown in the Figure 15. The figure attributes the jet to an eruption of the flux rope and corroborates the empirical models of Moore et al. (2010, 2013) and Sterling et al. (2015), which employ mini-filament eruptions. Importantly, this is the first data-constrained simulation of a coronal jet which highlights the role of complex magnetic topology, including 3D nulls and magnetic flux ropes, in the initiation of the coronal jets.

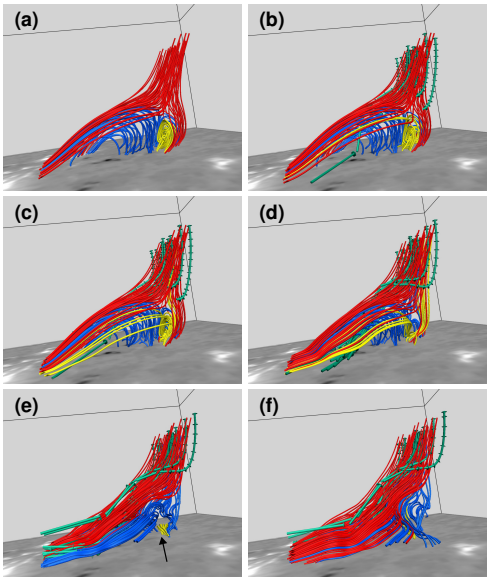


Figure 14.: Evolution of the MFLs near the jet. Gradual alignment of flow vectors with MFLs seen in this evolution points out the escape of confined plasma to the outer atmosphere.

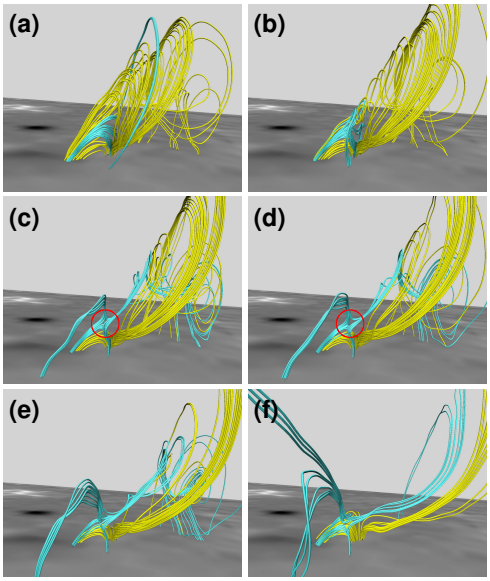


Figure 15.: The detailed evolution of the rope near the jet. The panels show the conversion of less twisted cyan colored MFLs into the rope. The changes in the connectivity of MFLs are the signature of MRs and an X-type null point appears at panel-(c) and (d) (marked by red circles).

(S. S. Nayak and R. Bhattacharyya)

The role of Hall-MHD in magnetic reconnection

The large magnetic Reynolds number $\mathrm{R_M} \approx 10^{12} - 10^{14}$ of the solar corona ensures that the magnetic field lines (MFLs) remain tied with the fluid parcels during their evolution obeying the Alfvén's flux-freezing theorem. In contrast, various eruptive events like solar flares and coronal mass ejections (CMEs), occurring in the corona are believed to be the signatures of magnetic reconnection. For reconnection to take place in the solar corona, a local reduction of magnetic Reynolds number is required to make the plasma locally diffusive. A way to decrease the number is the generation of small length-scales which enhances the magnetic energy dissipation and facilitates reconnection. To focus on the idea, we note, with characteristic scale $\mathrm{L_0}$ = 10^7 m and a coronal temperature T $\approx 10^6$ ^{o}K—the time scale for magnetic dissipation is 10^{14} s, which amounts to almost one million year. In contrast, solar flares typically span a time scale of minutes to hours. With magnetic diffusivity of the corona being 1 m^2/sec, a diffusion time scale of approximately 1 hour corresponds to a length scale $\mathrm{L_0} \approx 60$m and Lundquist number ($\mathrm{R_M}$ calculated with the Alfvén speed) $\mathrm{S} \approx 10^4$. Notably, the dimensionless generalized Ohm's law is

$$\mathbf{E} + \mathbf{v} \times \mathbf{B} = \left(\frac{1}{\mathrm{S}}\right)\mathbf{J} + \left(\frac{\delta_i}{\mathrm{L_0}}\right)\mathbf{J} \times \mathbf{B} - \beta\left(\frac{\delta_i}{\mathrm{L_0}}\right)\nabla \mathbf{P}_e + \left(\frac{\delta_e}{\mathrm{L_0}}\right)^2 \frac{\partial \mathbf{J}}{\partial t} \qquad (1)$$

where v_A is the Alfvén speed; δ_i and δ_e are respectively the ion and electron inertial scale lengths. With typical values like S=10^4, δ_i = 1 m, δ_e = 2 cm, $\mathrm{L_0}$= 60 m and β=0.01 for a flaring event, the Ohm's law takes the following form

$$\mathbf{E} + \mathbf{v} \times \mathbf{B} = (10^{-4})\mathbf{J} + (10^{-2})\mathbf{J} \times \mathbf{B} - (10^{-4})\nabla \mathbf{P}_e + (10^{-4})\frac{\partial \mathbf{J}}{\partial t} \qquad (2)$$

which clearly shows a dominance of the Hall term ($\mathbf{J}\times\mathbf{B}$) before the dissipation kicks in. It is then imperative to include the Hall effect to understand the reconnection physics leading to solar flares.

Generally, the Hall term becomes important in generalized Ohm's law when the thickness Δ of the Sweet-Parker current sheet becomes smaller than the ion skin depth or ion inertial scale length δ_i and greater than electron inertial scale length δ_e, i.e., when $\delta_e < \Delta < \delta_i$. It is further conjectured that an inclusion of the Hall term may speed up the reconnection rate and explain the impulsive nature of the flares. The present effort is directed to develop a Hall-MHD code and benchmark that. For the purpose, we are utilizing the existing EULAG-MHD code already available in-house. For benchmarking, we have initiated a pilot version of the Hall-MHD code by a magnetic field

$$\mathrm{B}_x = tanh(z), \quad \mathrm{B}_y = sech(z), \quad \mathrm{B}_z = 0 \qquad (3)$$

which corresponds to a force-free Harris current sheet and tracked evolution of magnetic field lines. Figure 16 shows the simulation results, where panel (a) and (b) are showing evolution of current, and panel (c) and (d) are showing the evolution of magnetic field lines. The computation is carried out on the Vikram-100, the 100TF computational facility at the Physical Research Laboratory, and have a computational domain of size 64×64×64.

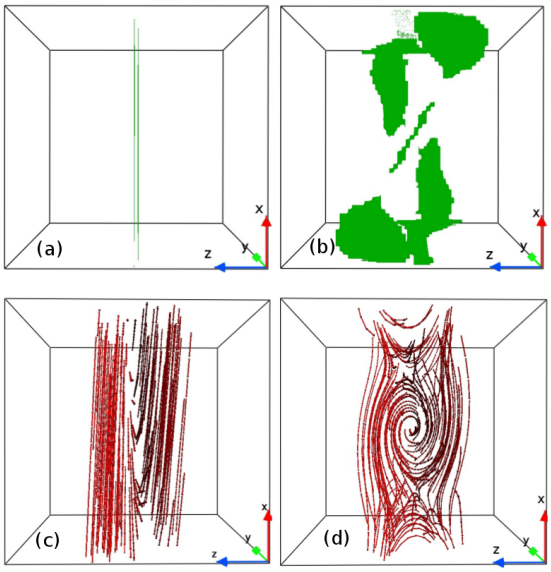


Figure 16.: Evolution of current (a) and (b), Evolution of magnetic field lines (b) and (d), for $t \in \{0, 4000\}$. Important are the formation of magnetic islands (d), and the diffusion of the initial current sheet (a) to (b). The results are in general agreement with the outcomes of contemporary simulations.

(K. Bora and R. Bhattacharyya)

Mass Loss from the Sun via Solar Wind and Coronal Mass Ejections during Solar Cycle 23 and 24

It is well known that Sun loses mass through ubiquitous quasi-steady wind and episodic coronal mass ejections (CMEs). We investigate the mass loss rate via solar wind and CMEs as a function of solar magnetic variability represented in terms of sunspot number and solar X-ray background luminosity. Based on our in-depth study, we find that the solar wind mass loss rate, CME mass loss rate, X-ray background luminosity, and sunspot number during the maximum of solar cycle 24 decreased by 10%, 15%, 20%, and 40% respectively, as compared to the values during the maximum of cycle 23. The observed decrease in CME and solar wind mass loss rate from cycle 23 to 24 is not as large as for the sunspot number. We confirm that there is an increased rate of numerous less massive CMEs from relatively higher latitudes since 2003 to the period of solar cycle 24. Therefore, a strong poor correlation of CME activity with sunspot number exists for solar cycle 24.The solar wind mass loss rate which is an order of magnitude higher than the CME mass loss rate shows no obvious dependency on cyclic variation in sunspot number and solar X-ray background luminosity. The fractional contribution of CMEs to solar wind mass flux is around 5% during solar maximum in the ecliptic and it is much smaller at higher helio latitudes and/or during solar minimum. Our study also suggested that X-ray background luminosity is a better proxy for CME mass loss rate over the solar cycle than the sunspot number. Since it is rather difficult to observe the signatures of stellar CMEs and stellar spots than stellar X-ray flux, we expect that these results could help us understand the mass loss from other solar-type stars (Figure 17).

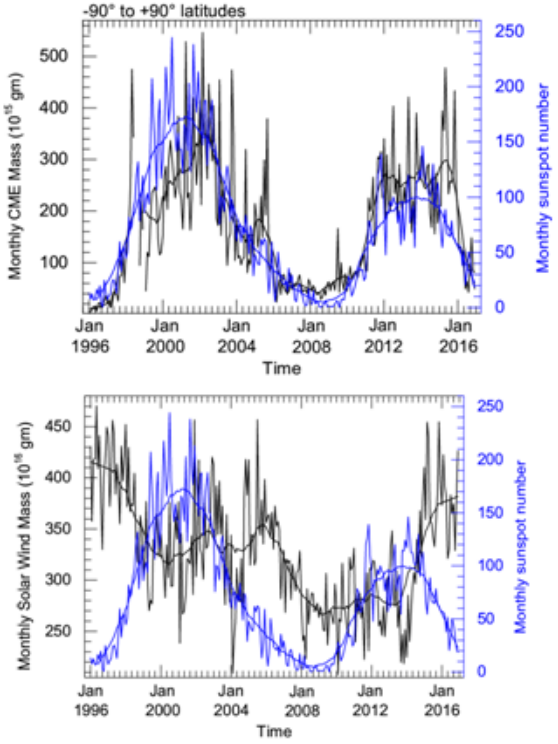


Figure 17.: The variation of rate of mass loss (on the left Y-axis in black) due to CMEs from latitude within -90 to +90 degree (in the top panel of the figure) and due to solar wind (in the bottom panel of the figure) is shown. The monthly sunspot number (on the right Y-axis in blue) with time (on X-axis) during 1996 to 2016 (i.e., solar cycle 23 to 24) is shown. The smoothed values of actual measurements are also overplotted.

This work was carried out in collaboration with Wageesh Mishra, Yuming Wang and Rui Liu of USTC, China and Zavkiddin Mirtoshev of Samarkand University, Uzbekistan

(Nandita Srivastava)

Study of the North-South asymmetry in the rotational profiles of solar corona during the Solar Cycle 24

We have investigated the variability of rotational profiles of solar corona at 94 Å, 193 Å, and 211 Å for the period from 2012 to 2018, covering the maximum and minimum phases of the Solar Cycle 24. Analysis of solar full disk images obtained at the aforementioned wavelengths by the Atmospheric Imaging Assembly (AIA) solar telescope on board Solar Dynamics Observatory (SDO) space mission has been carried out using flux modulation method. Thirty-three strips/bins at equal interval of 5^o extending from 80^o South to 80^o North on the solar disk are selected to extract a time series of extreme ultraviolet (EUV) intensity variations to obtain auto-correlation coefficient. The peak of Gaussian fit to first secondary maxima in the auto-correlogram gives synodic rotation period. We obtain the coronal sidereal rotation rate as a function of latitude. Our analysis of these EUV observations of solar corona reveals the North-South asymmetry and temporal variability of rotation profiles of the solar corona with respect to the solar activity. We observe that the North-South asymmetry in the rotational profiles is quite high during the maximum phase of the solar cycle as compared to the minimum

phase, and this feature is more pronounced in the case of relatively shorter wavelengths (c.f., Figure 18). This investigation is also being extended to the chromospheric and photospheric layers using the observations from Global Oscillation and Network Group (GONG) to study the variations in the North-South asymmetry of the rotational profiles of the Sun at different heights in the solar atmosphere.

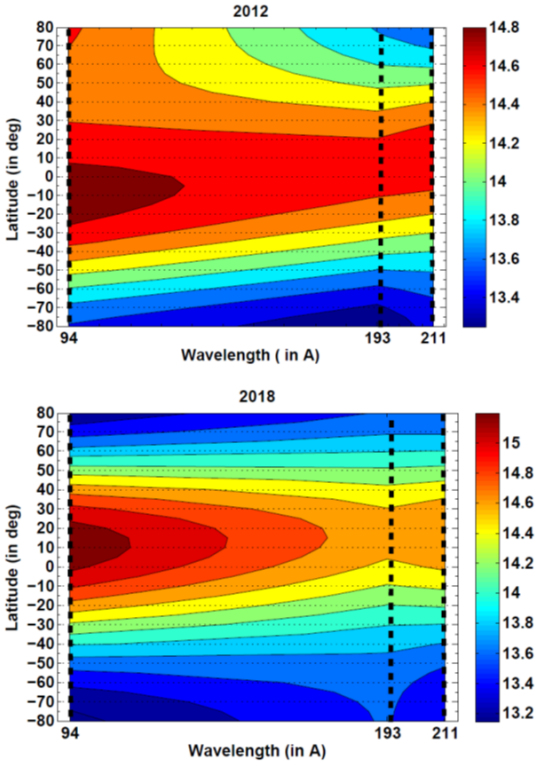


Figure 18.: The panels show the contour plots for the years 2012 (upper panel: solar maximum) and 2018 (lower panel: solar minimum) for the sidereal rotation rates of the solar corona with respect to latitude for different wavelengths and hence heights in the solar atmosphere. It is seen that the North-South asymmetry in the rotational profiles is more pronounced during the phase of maximum activity in the Sun.

This work is being done in collaboration with Jaidev Sharma of CCS University, Meerut and Hari Om Vats of Space Education and Research Foundation, Ahmedabad.

(B. Kumar)

Installation and 'first light' observation of CALLISTO solar radio spectrometer at USO, Udaipur

A new observing facility–Compound Astronomical Low cost Low frequency Instrument for Spectroscopy and Transportable Observatory (CALLISTO)–has been set up at Udaipur Solar observatory for the observation of solar eruptive phenomena (flare and CMEs) in radio wavelengths(Figure 19).The CALLISTO is a solar radio spectrograph which natively operates between 45 and 870 MHz with a frequency resolution of 62.5 KHz. The low frequency radio observations are considered as a valuable tool for real time monitoring of solar origin of the space weather. An indigenously designed and developed Log Periodic Dipole Antenna (LPDA) has been deployed at Udaipur station to collect the solar flux. The radio spectrometer attached to the antenna is a programmable heterodyne receiver developed at ETH Zurich, Switzerland. Radio spectrum at meter and decimeter frequencies, obtained by the CALLISTO, can be used to investigate many important magnetic and plasma processes on the Sun. They provide the first signature of flare shocks (Type II events) and electron beams escaping from the Sun on open magnetic field lines (Type III bursts). In addition, they record unexplained emissions of active regions (Type I noise storms) and long-lasting emission after large flares (Type IV events). The data recorded by CALLISTO at USO is being stored on daily basis at local as well as the central data server located at ETH, Zurich.

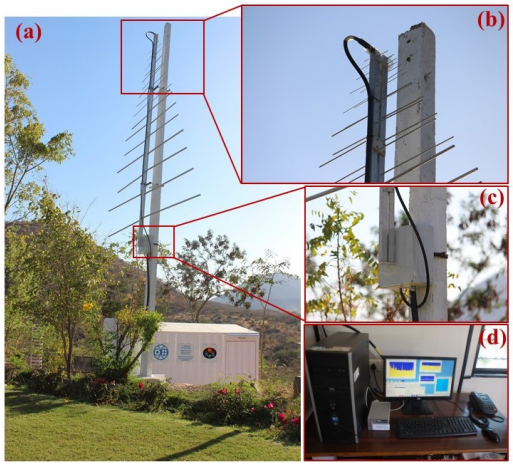


Figure 19.: CALLISTO system at Udaipur Solar Observatory. (a) The wide band (40-870 MHz), Log Periodic Dipole Antenna (LPDA) pointing toward the zenith is deployed to collect the solar radio flux. The antenna has a total of 28 elements. (b) The zoomed images showing short elements of the LPDA which are designed to receive high-frequency radio emission. (c) The low noise amplified (LNA) is housed in the container which is attached to the pole. (d) The CALLISTO spectrograph and a computer is kept inside the portable laboratory container.

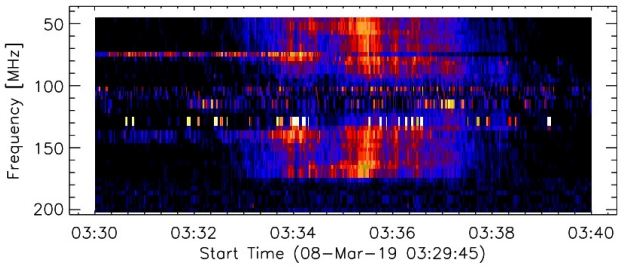


Figure 20.: The 'first light' solar radio burst observed by CALLISTO at Udaipur Solar Observatory. The spectrum shows plasma emission in the frequency range of 50 MHz-180 MHz in association with a GOES C1 flare on March 8, 2019.

In Figure 20, we show the 'first light' solar radio burst observed by CALLISTO at USO, Udaipur. The radio emission was observed in association with a flare of GOES class C1. The radio emission is observed in the frequency range of 50 MHz–180 MHz during 03:33–03:38 UT. We note several vertical drifting structures in radio spectrum which indicate the opening of magnetic field lines and subsequent escaping of electron beams, produced during the magnetic reconnection, into the outer corona.

(B. Joshi, R. Bhattacharyya, K. Upadhyay, and P. K. Mitra)

Planetary Sciences

Planetary Atmosphere and Interplanetary Medium

Modeling of diffuse aurora due to precipitation of $H^+ - H$ and SEP electrons in the nighttime atmosphere of Mars: Monte Carlo simulation and MAVEN observation

The nighttime limb intensity of diffuse auroral emission of CO_2^+ $(B_2\Sigma_u^+ – X^2\Pi_g)$ Ultraviolet Doublet (UVD) is observed in northern hemisphere of Mars during 17-21 December, 2014 from Imaging Ultraviolet Spectrograph (IUVS) instrument onboard Mars Atmosphere and Volatile Evolution (MAVEN). We have used hybrid model and four dimensional yield spectrum approach based on Monte Carlo simulation to calculate the ionization rate, limb intensity, ion and electron densities of diffuse aurora due to precipitation of Solar Energetic Particle (SEP) and proton-hydrogen ($H^+ - H$) fluxes in the nighttime ionosphere of Mars. It is found that the production rates of atmospheric ions (CO_2^+, N_2^+ and O^+) are dominant in the upper ionosphere at about 100-150 km due to impact of $H^+ - H$. The SEP formed auroral ionosphere (CO_2^+, N_2^+ and O^+) in the middle ionosphere between 50 km and 100 km due to precipitation of monoenergetic electrons of energies 25 to100 keV. The simulated limb intensities due to impact of $H^+ - H$ and auroral electrons are compared with IUVS observations. Our model shows that auroral electrons of energy ~100 keV is enough to produce the observed peak limb intensity at about 75 km where MAVEN observed nighttime auroral emissions continuously for 5 days. The densities of upper ionosphere (O_2^+, NO^+, and CO_2^+) due to impact of $H^+ - H$ are smaller by an order of 1-2 than that produced by auroral electrons in the middle ionosphere.

(S. A. Haider and J. Masoom)

Global distribution of column ozone in the Martian atmosphere: Comparison of model and SPICAM observations

We have calculated column ozone density during Martian Year (MY) 28 at different latitudes and Solar Longitude (Ls) in the atmosphere of Mars. The Figures 1 (a-h) represents the annual seasonal variability of zonally averaged column ozone observed by Spectroscopy for the Investigation of the Characteristics of the Atmosphere of Mars (SPICAM) onboard Mars Express (MEX). These observations are compared with the zonally averaged column ozone obtained from Mars Climate Database (MCD) at the same Martian conditions of SPICAM observations. The seasonal change in column ozone is low at low latitudes, but at high latitudes it is chaotic and indicates that atmospheric ozone is highly perturbed. The SPICAM measured maximum and minimum column ozone in northern winter and southern summer respectively at mid-to high latitudes (45°N, 45°S, 70°N and 70°S). The seasonal profiles of column ozone obtained from MCD are in good agreement with the SPICAM observations at these latitudes. At low latitudes (2°N, 2°S, 25°N and 25°S) the observations do not match so well with the MCD model underestimating column ozone by ~20%. The disagreement between observation and model at low latitudes may be associated due to several reasons as given below: (1) The excessive transport of water vapor from Tharsis and Arabia Terrain can reduce column ozone in the model, (2) Modeling biases in water vapor can also explain the underestimation of total ozone at low latitude region, (3) The SPICAM measurements have large error of the order of 1-5 x 10^{15} molecules cm^{-2}.

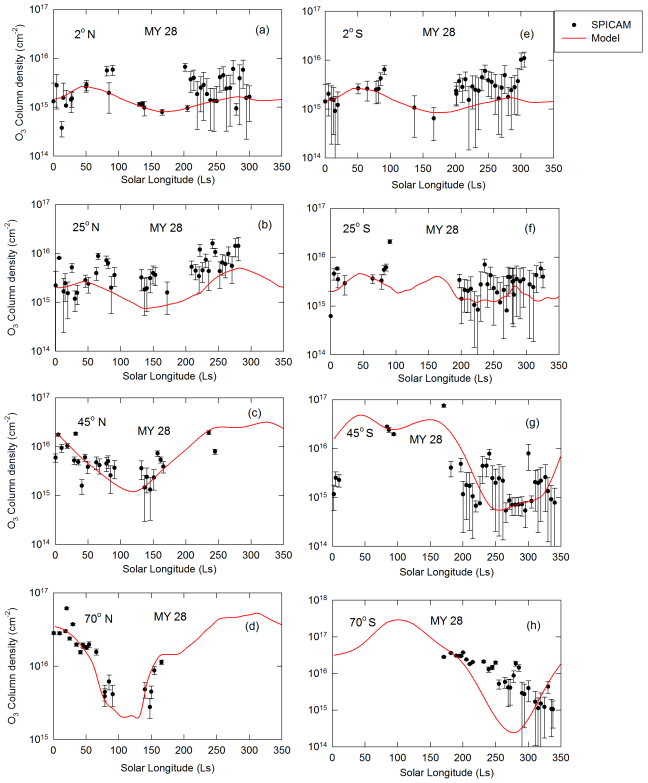


Figure 1 (a-h): The annual seasonal variability of zonally averaged column ozone with error bars as observed by SPICAM in MY 28 at 2°N (a), 25°N (b), 45°N (c), 70°N (d), 2°S (e), 25°S (f), 45°S (g), and 70°S (h). These observations are compared with zonally averaged column ozone obtained from MCD model in MY 28

The estimated column densities of ozone are varying within this error bar at low latitude region and (4) Ozone can also be affected by topography of Mars through the effect of gravity waves. An increase in O_3 column over Hellas basin in SPICAM measurements is attributed to a topographical induced transport of the polar air. At low latitudes (Figures 1a, 1e, 1b and 1f) the two broad peaks have been observed in the column ozone cycle with values $\sim$ 5-8 x 10^{15} cm^{-2} and $\sim$ 1.2 x 10^{16} cm^{-2} at Ls $\sim 50^{\circ}$ and Ls $\sim 250^{\circ}$ respectively. At mid-to high latitudes (Figures 1c, 1g, 1d and 1h) the ozone column densities are maximum in northern winter and minimum in southern summer.

(S. A. Haider, Y. S. Siddhi and J. Masoom)

Effects of dust storms on the electron density profiles in the magnetic anomaly regions of Mars

The Mars Advanced Radar for Subsurface and Ionosphetric Sounding instrument aboard the Mars Express (MEX) observes vertical echoes from the normal ionosphere and oblique echoes from ionization bulges. The peak frequencies of these two kinds of echoes are in general, nearly equal. We have detected oblique echoes whose peak frequencies are much larger than those of the vertical echoes. These echoes were observed on 15, 21, 28 June and 10 July, 2007. All these oblique echoes were observed from a region of strong crustal magnetic fields. After correcting for dispersion effects, the maximum electron density in the first case is found to be 3.75x10^5 cm^{-3} and is observed at an altitude of $\sim$ 88 km. In subsequent cases, a gradual decrease in peak electron density and an increase in altitude are observed. The causative mechanism of these oblique echoes is examined by considering various forces from top and bottom. During the times of the observations, there was no solar flare or meteor in fall. The presence of solar energetic particles also could not be firmly established. We have found that these strong oblique echoes were observed at the initial phase and during the progression of a planet-encircling dust storm in Martian year 28. Similar but weaker features were also observed in other dust storm seasons as well. Figure 2a-d shows ionograms of the four cases of unusually strong oblique echoes. These four cases correspond to MEX orbits 4425, 4447, 4469, and 4513 observed on 15, 21, 28 June and 10 July, 2007 respectively.

This work was carried out in collaboration of N. Venkateswara Rao, NARL, Tirupati

(S. A. Haider, V. Sheel, Y. S. Siddhi, J. Masoom and S. Luhar)

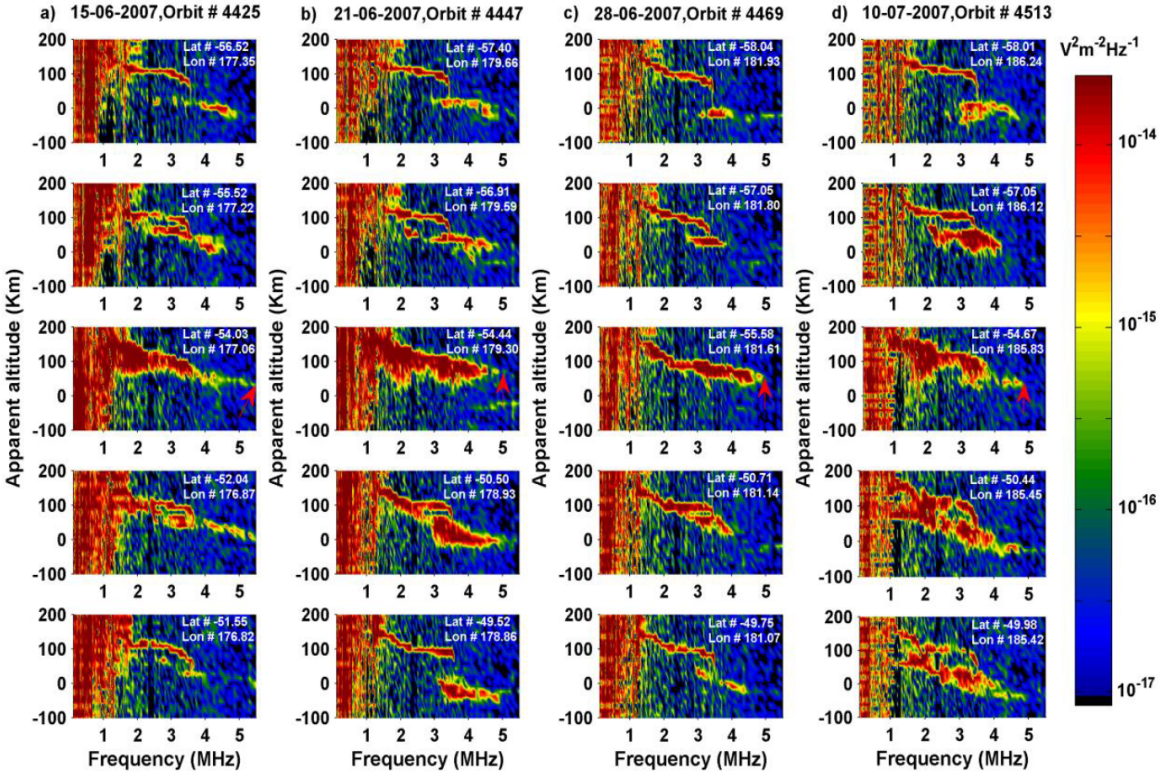


Figure 2 (a-d): A series of five ionograms (a) Orbit # 4425, (b) Orbit # 4447, (c) Orbit # 4469 and (d) Orbit # 4513 on 15 June, 21 June, 28 June and 10 July, 2007 respectively.

Dayglow CO ($a^3\Pi$) Cameron band emission: Model and observations

We have calculated excitation rates, emission rates and limb intensity of CO ($a^3\Pi$) Cameron band in the dayside atmosphere of Mars. The ion and electron densities were estimated under photochemical

equilibrium condition. In this model calculation photoelectron excitation, photodissociation and dissociative recombination processes are used as a production of CO ($a^3\Pi$). The loss of CO ($a^3\Pi$) occurred due to quenching from CO_2, CO and radio decay. The photoelectron production rates are calculated by using Monte Carlo method. Our model suggests that dissociations of CO_2 by photon and photoelectron are the dominant production mechanisms of CO ($a^3\Pi$). Radiative decay is a major loss mechanism of CO($a^3\Pi$). The model results are compared with the observations provided by the SPICAM instrument onboard Mars Express. We have found a good agreement between model and observation carried out for CO ($a^3\Pi$) emission intensity. The effects of solar zenith angles on the production and loss processes are also studied between 0° and 90°. We report that the production rates and intensities are decreasing with increasing solar zenith angles (SZA). This suggests that dayglow emission intensities also depend on the Chapman function directly where electron densities are decreasing with increasing SZA.

(S. A. Haider and J. Ruqaiyah)

Convective vortices on Mars: Meteorological observations and estimates of tangential winds

Convective vortices can lift dust on Mars thereby contributing to the total dust opacity of the atmosphere. Such vortices can be identified in-situ by landers or rovers by the reduced surface pressure when they pass by the instrument. We identify 91 short ($\sim$15 s) pressure drops ($\geq$0.3 Pa) that likely indicate the passage of convective vortices or dust devils in the data measured by the Rover Environmental Monitoring Station (REMS) on board the Mars Science Laboratory (MSL) rover Curiosity during sols 1545 to 1660. Out of the 87 single peak vortices which we utilize in the present study, 35 have pressure drop $>$ 1.0 Pa, with the largest pressure drop being 4.0 Pa. The diurnal distribution of the pressure drops shows a distinct rise in vortex activity around noon hours between 12:00 and 13:00 Local Mean Solar Time (LMST). Of the vortices detected, a few also show a simultaneous drop in ultraviolet intensity, which signifies obscuration of sunlight by dust laden in the atmosphere. To estimate the tangential winds of the detected vortices, we use Burgers model and Rennó model. The wind velocities are well below the Martian dust lifting threshold, indicating that either the vortices passed far from the measuring instrument or that dust lifting may not have occured by tangential winds alone.

(S. Uttam, V. Sheel and D. Singh)

Variability of lower ionosphere of Mars due to water vapour and dust

The structure of the lower ionosphere of Mars can vary with location and time as a result of variability in solar forcing, atmospheric dynamics and neutral composition. We have studied this variability of the ionosphere due to the seasonal variability of the neutrals (especially water vapour) and dust. The PRL ion model (developed over the last decade) has been used, with inputs of neutral and dust density from the LMD general circulation model for MY 27, to simulate the lower ionosphere for different latitudes and seasons. In MY 27, dust optical depth varied from 0.1 to 0.5. In these dust scenarios, the role of water vapour and odd Ox becomes important in order to determine the seasonal variation in the ion densities. The lower order hydrated hydronium ions ($H_3O^+, H_3O^+H_2O$) do not show much variation in the low altitudes despite the variation in dust and water vapour whereas in the high altitudes loss due to water vapour introduces seasonal variations. Higher order hydrated hydronium ions ($H_3O^+(H_2O)_2$ and $H_3O^+(H_2O)_3$) are positively correlated with the water vapour present in the atmosphere as they increase during summer and decrease in winter. Presence of dust decreases the density of hydronium ions due to their loss through ion-dust attachment, as found earlier by Haider et al (2010) and Sheel and Haider (2016). Odd oxygen plays an important role in determining the densities of CO_4^- and $CO_3^-H_2O$. The ion CO_4^- seems to be dependent on the amount of ozone and atomic oxygen present in the atmosphere. Odd oxygen is anti-correlated with water vapour in Martian atmosphere which thus establishes a correlation of ion density with water vapour. The seasonal variability of ions in the D layer of the ionosphere is large over the high latitudes and is comparatively weak in the low latitude regions. The study has improved our understanding of the lower ionosphere in terms of its response to the seasonal variation of water vapour and dust.

(V. Sheel and A. Modak)

First Observation of Transport of Solar Wind Protons Scattered From Magnetic Anomalies into the Near Lunar Wake: Observations by SARA/Chandrayaan-1

We report the first observational evidence for the transport of the solar wind protons scattered from the lunar magnetic anomaly (LMA) into the near wake region from SWIM/Sub-keV Atom Reflecting Analyzer (SARA) aboard Chandrayaan-1. These protons with high angular spread are observed in the near wake region for specific orientations of interplanetary magnetic field. The typical energy range is 600-1,000 eV, which is either smaller or comparable to that of solar wind. Using our back-tracing model, the source region of these protons is found to be the large Lunar Magnetic Anomaly (LMA) at South Pole-Aitken basin on the day side, suggesting that these are solar wind protons forward-scattered from LMA at the South Pole-Aitken. The flux of these protons is $\sim 5 \times 10^{-4}$ of the solar wind proton flux, which is comparable to the proton population in near wake due to other known processes. Such protons can significantly affect the electromagnetic environment in near wake region.

This work was done in collaboration with scientists from SPL-VSSC, Trivandrum; Institute of Space Physics, Sweden; and University of Bern, Switzerland.

(A. Bhardwaj)

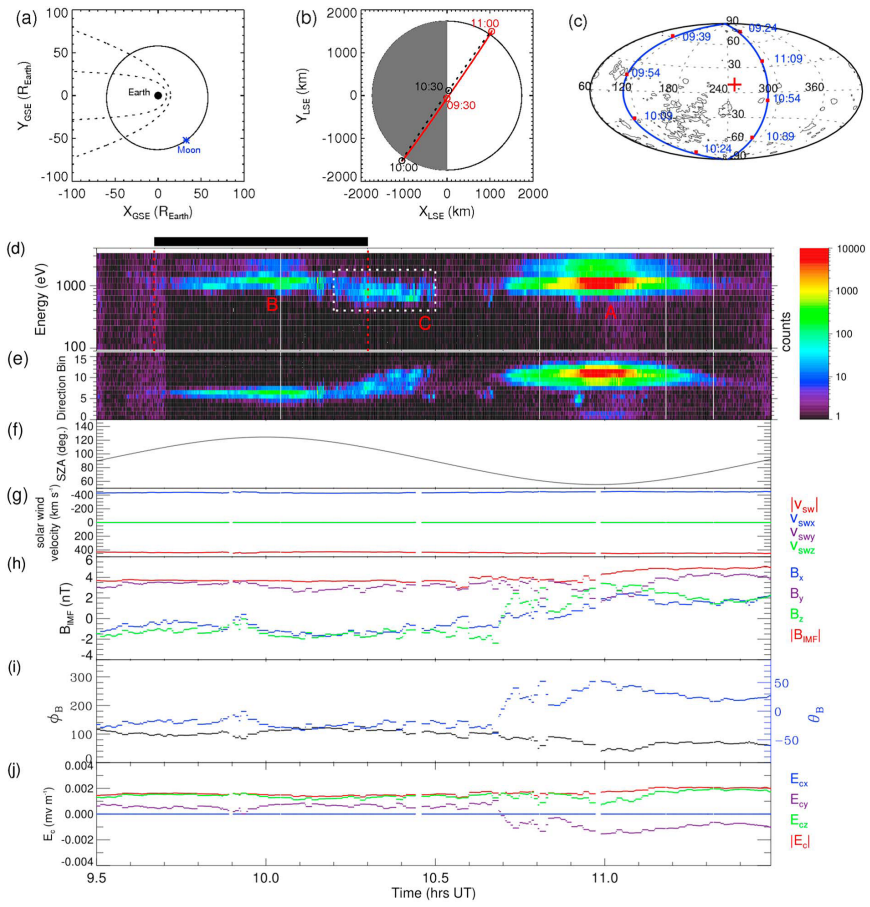


Figure 3: (a) Orbit of the Moon around the Earth for April 2009 projected on the x-y plane of the Geocentric Solar Ecliptic (GSE) coordinates. GSE has its origin on the Earth center, the x axis is toward the Sun, z axis toward the ecliptic north, and the y axis completes the right-handed coordinate system. Estimated boundaries of Earth's magnetosphere and bow shock are shown. Position of the Moon on 20 April 2009 is indicated by the asterisk symbol (blue color). (b) Orbit of Chandrayaan-1 around the Moon during the orbit 1977 on 20 April 2009 ($\sim$ 09:30 UT to 11:30 UT), projected on the x-y plane of lunar-centered solar ecliptic (LSE) coordinates as viewed from +zLSE. The red solid curve indicates the part of orbit with zLSE $>$0, and black dotted curve is with zLSE $<$ 0. The position of Chandrayaan-1 at four time instants are also indicated. (c) Chandrayaan-1 orbit 1977 in the hammer projection of lunar map. The black contours represent the magnetic field magnitude (2 nT at an altitude of 30 km) of the anomalies based on Purucker and Nicholas (2010). The projection is roughly centered at the subsolar point, which is indicated by the symbol "+" in red color. (d) Energy-time spectrogram from SWIM observations for the orbit 1977 of Chandrayaan-1. The horizontal axis shows time in hours universal time. The black-filled box on the top indicates the time interval when Solar Wind Monitor (SWIM) made observations in lunar wake ($\sim$09:42 to $\sim$10:18 UT). A pair of dotted vertical lines in red color mark the wake entry and exit timings for Chandrayaan-1. Different population of ions observed by SWIM in this orbit are indicated as A, B, and C. The white colored rectangle is used to highlight the population C observed during the day-night terminator crossing and extending into the wake. (e) Direction-time spectrogram from the SWIM observations for the same orbit. The vertical axis shows the 16 direction bins in which ions are observed by SWIM. Direction bin 0 refers to close to nadir, and direction bin 15 refers to close to zenith. (f) Solar zenith angle. (g) Solar wind velocity: magnitude (Vsw) and the components (Vx , Vy, and Vz). (h) Interplanetary magnetic field magnitude (BIMF) as well as the components Bx , By, and Bz. (i) The azimuth (ΦB) and elevation (ΘB) angles of BIMF. (j) Convective electric field (Ec) of the solar wind: the magnitude Ec and the components Ex , Ey, and Ez. The solar wind parameters shown in the panels (g)–(j) are in aberrated LSE coordinates.

Short-term Variation in the Dawn–Dusk Asymmetry of the Jovian Radiation Belt Obtained from GMRT and Hisaki EXCEED Observations

In order to reveal variations of days to weeks in the brightness distribution of Jovian Synchrotron Radiation (JSR), we made simultaneous radio and ultraviolet observations using the Giant Metrewave Radio Telescope (GMRT) and the Hisaki EXtreme ultraviolet spectrosCope for ExosphEric Dynamics (EXCEED). It is known from visible and ultraviolet observations that Io plasma torus (IPT) has dawn–dusk asymmetry, and that this asymmetry is believed to be due to the dawn-dusk electric field. Continuous ultraviolet observation by Hisaki telescope reveals that dawn–dusk asymmetry of IPT changes in days to weeks, therefore, if this global electric field around Io's orbit (5.9 Jovian radii) could penetrate the radiation belt region ($<$2 Jovian radii), the variations in brightness distribution of JSR and IPT are expected to be correlated. The GMRT observations were made from 2013 December 31 to 2014 January 16 at 610 MHz and 2016 March 14–June 23 at 1390 MHz, while Hisaki continuously monitored IPT. The statistical analysis indicates that JSR and IPT do not have a significant correlation. Although these results do not support the hypothesis, we cannot rule out the possibility that the dawn-dusk electric field was masked by some other process, including the conductivity variation and/or the time-variable longitudinal asymmetry of JSR.

This work is done in collaboration with scientists from Japan working at ISAS-JAXA, Tohoku University, NIICT, University of Tokyo, and Tokyo Institute of Technology.

(A. Bhardwaj)

MAVEN Observations of the Response of Martian Ionosphere to the Interplanetary Coronal Mass Ejections of March 2015

The Mars Atmosphere and Volatile EvolutioN (MAVEN) spacecraft provides an opportunity to observe the response of the Martian upper atmosphere to the passage of interplanetary coronal mass ejections. We study the response of Martian ionosphere to two successive solar disturbances during 3 and 4 March and 8 and 9 March 2015 using the observations from Neutral Gas and Ion Mass Spectrometer and Langmuir Probe and Waves aboard MAVEN. During these events, the ionospheric boundary was significantly lowered. During 3 March the ionopause is seen to be at a lower altitude, compared to that during 8 March. The higher ionopause seen on 8 March could be due to the sustained effect of heating and inflation by the 3 March interplanetary coronal mass ejection event or due to the heating by the enhanced particle precipitation. The comparison of the O^+/O_2^+ ratio indicates that there is a preferential decrease of O_2^+ and a relative enhancement in O^+, probably due to increased dissociative recombination and charge exchange as a result of the higher solar wind densities during the 3 March event.

(A. Bhardwaj)

Transport properties of complex plasma having a dust size distribution

The blackout phenomenon is a notable example of ambient modification due to rocket exhaust; in this case the large electron generation due to thermionic emission blocks the electromagnetic (EM) signal on account of its heavy attenuation and causes communications blackout. It was also proposed later that the insertion of high work function (dielectric) fine dust may modulate the local plasma features and restore the signal communication. In order to evaluate the transport features of the complex plasma, it is essential to have a notion on the charged particles consequence on the plasma. Taking up this problem, the transport properties of the complex plasma, comprising of size distributed dust, kept under influence of the external electric field, have been investigated. Accounting for the openness nature of the complex plasma, the kinetics has been developed on the basis of number and energy balance of the plasma constituents along with the dust charge balance. Implementing the uniform potential theory for the dust size distribution, the kinetic formulation has been used to configure the steady-state complex plasma composition, and hence the transport features. A substantial departure of the plasma equilibrium from dust free case is observed in the presence of size distributed dust; the altered density, temperature and collision frequency of the electrons are the significant parameters, determining plasma transport. Electromagnetic opacity is predicted in the presence of an external electric field (steady/ alternating) due to Ohmic heating in case of dark plasma, while enhanced transparency is noticed for the field-free case. Furthermore, the propagation features of an EM RF wave have been specified in terms of complex dielectric constant and refractive index of the complex plasma; the wave propagation and attenuation are found to be a significant function of the dust size distribution and amplitude.

(S. K. Mishra)

Amplification of weak ultra-short pulses in Plasma via Resonant BRA scheme

Multiple technological infrastructures have been planned and under operation in developing controlled ultrashort sub femto second pulses. These secondary sources are anticipated to produce weak (pJ) ultra-short (fs) broad spectrum pulses in soft X-ray regime; the tentative achievable intensity of these secondary pulses is very weak and for practical significance need to be amplified. In this report, we briefly examine the possibility to utilize the resonant Backward Raman amplification (BRA) as an efficient mechanism in plasma to amplify such weak pulses. Utilizing the slowly varying envelope approximation (SVEA) based analytical expressions for the resonant three wave interaction along with viable physics constraint, a parameter space configuring the laser/ plasma features required to achieve significant pulse amplification and compression, has been derived; these expressions has further been used to determine the analytical expressions for optimum intensity and compressions of the pulses. A specific parametric configuration for resonant BRA operation in short wavelength regime has been identified and validated using particle in cell (PIC) simulation results. For the suitable choice of the system parameters, seed pulse can be intensified by $\sim$four orders of magnitude but the pulse compression is little difficult, specifically if the pulse is in attosecond regime and in this case one need to operate pump at orders of magnitude higher intensities. Nonetheless, based on the understanding via present analysis, it may be concluded that the resonant BRAmp's operating in XUV regime may efficiently be utilized to amplify and compress the weak ultra-short pulses to Exawatt cm^{-2} and sub fs time scale.

(S. K. Mishra)

Lightning on Mars

Lightning is a transient electrical discharge, which can occur in clouds of planetary atmosphere, volcanic clouds, dust storms or snow storms. In case of Mars, lightning is likely to occur within dust devils or storms near surface. We have carried out modelling work related to Schumann Resonance (SR) on Mars, through which lightning can be studied. We have solved the Maxwellian equations of electromagnetic waves, which oscillate within the cavity formed in the lower atmosphere of Mars between 0 and 70 km.

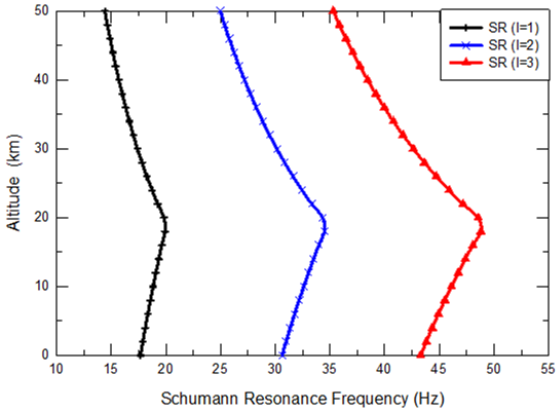


Figure 4: Altitude profiles of Schumann Resonance frequency in the nighttime ionosphere of Mars in MY 25 during high dust storm (s=1.7) at low-latitude region (25-35°S).

The electrical conductivity and SR frequencies are calculated in the lower ionosphere of Mars, in the presence of a major dust storm that occurred in Martian Year (MY) 25 at low latitude region (25-35°S). It is found that the atmospheric conductivity is reduced by one to two orders of magnitude in the presence of a dust storm. It represents a small dust layer at about 25-30 km altitudes, where the lightning can occur. We also found that the SR frequencies peak at ∼18 km with values 19.9, 34.5 and 48.8 Hz for the modes l = 1, 2 and 3, respectively, in the non-homogeneous medium, as shown in Figure 4. Our results indicate that practical or measurable values of SR are dependent on the altitudes.

(S. A. Haider, J. P. Pabari, J. Masoom and S. Y. Shah)

Orbital Altitude Dust at Mars

Orbital altitude dust, basically Interplanetary Dust Particles (IDPs) are in question recently regarding their origination, distribution and flux at Mars. We have carried out modelling of IDPs at Mars and estimated the flux. The results are depicted in Figure 5.

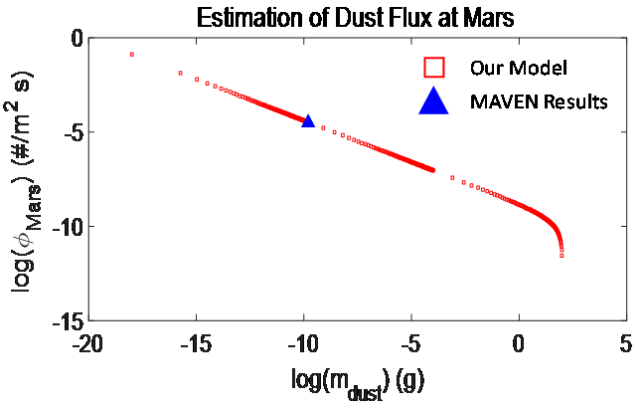


Figure 5: Logarithmic plot of estimated dust flux at Mars versus the dust mass. MAVEN results are shown with blue triangle.

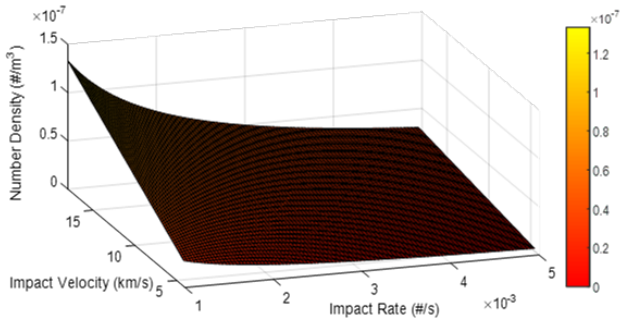


Figure 6: Expected countable particle density as a function of dust impact rate and possible particle velocity.

Our results are in agreement with MAVEN indirect observation of dust particles, as shown in Figure 5. Further, we have also estimated dust density at Mars and results are shown in Figure 6. Most probable dust particle density at Mars could be of the order of 10^{-7} #/m^3. Our IDP model at Mars is a practical model, as it is constrained using observed parameters.

(J. P. Pabari, S. A. Haider, B. M. Pandya, R. K. Singh, A. Kumar, D. K. Patel and A. Bogavelly)

Micrometeorite Impact on Lunar Surface

Dust particles exist everywhere in the interplanetary space and evolve dynamically after their origination from sources like asteroid belt, Kuiper belt, comets or space debris left during the formation of solar system. Due to impact of hypervelocity dust particles on lunar surface, ejecta come out in the lunar environment. In some cases, the ejecta velocity could be larger than escape velocity and the particles may escape from Moon. Further, escaping ejecta may carry water ice (volatiles) when incoming projectile hits the surface in polar region, where water ice is expected to be present. We have initiated modelling and estimation of volatile (water ice) escape due to hypervelocity dust impact on Moon. We have also proposed an instrument to study micrometeorite impact on lunar mission for future ISRO-JAXA mission. Figure 7 illustrates the scenario on lunar surface due to the bombardment of micrometeorites.

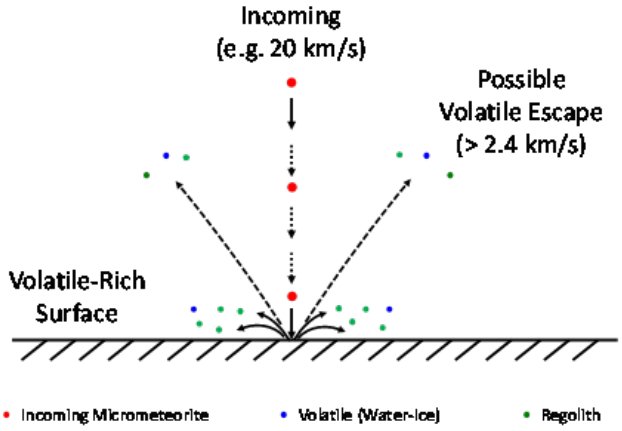


Figure 7: Micrometeorite impact on lunar surface possible volatile escape along with dust.

(J. P. Pabari, S. Nambiar, V. Shah and A. Bhardwaj)

Temporal Perturbations in Mars' upper atmosphere due to a strong solar flare event of September, 2017

It is well-established that the solar radiation is responsible for various photochemical processes in the upper atmosphere of Mars, such as photodissociation and/or photoionization, that triggers the entire ion chemistry thus determining the structure and composition of its various regions. Solar flare ionizes and heats the upper atmosphere of Mars. Similar to all other planetary atmospheres, Mars also responds to the enhanced x-ray and UV fluxes produced during flares that

significantly enhance the plasma number densities thereby resulting in a substantial change in the structure and composition of its topside ionosphere. Significant enhancements of the orders of 200% or more in the number densities during flares have been reported from earlier observations. In Sept. 2017, a strong solar flare of magnitude X8.2 erupted from the Sun which impacted Mars on 10 Sept. 2017. NASA's MAVEN spacecraft provided a unique opportunity to observe the response of Mars' upper atmosphere to this flare event. We have made an attempt to study the temporal variation in the structure of Martian upper atmosphere caused due to this solar flare using data from Langmuir Probe and Waves (LPW) experiment onboard MAVEN spacecraft. The electron density and electron temperature data obtained from LPW have been analysed for both pre-flare and post-flare periods. Three different instances of flare occurences on 2^{nd}, 10^{th} and 17^{th} Septemeber, 2017 were considered for this study. Preliminary analysis show significant enhancement in electron densities in lower ionosphere and depletions in upper ionosphere of Mars with ionopause like structure were observed in all cases as shown in figure 8. However, electron temperatures did not show much temporal variability. The ionosphere seems to be relaxed in around a day after the perturbation. Further, a systematic study of the variation in the electron density over a period of time before and after the flare for all three instances show a significant temporal variation in the upper atmospheric structure of Mars caused either due to only these events or could be a combined effect of other processes which needs further study. Details of these analysis and results will be discussed.

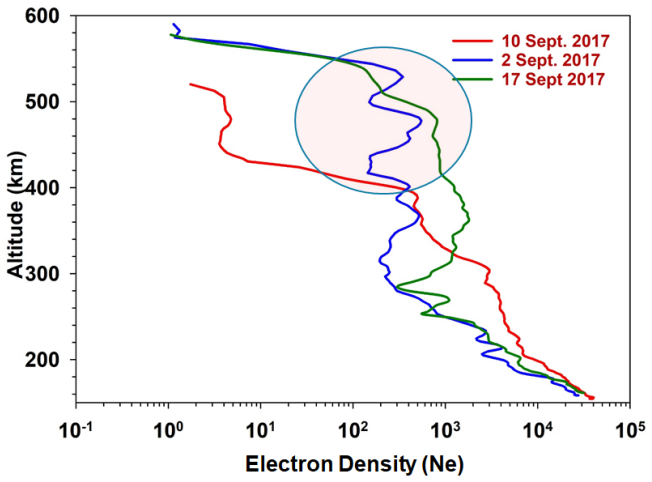


Figure 8: Comparison of variation in the electron density for all three instances of flare. An ionopause like structure in upper atmosphere of Mars is clearly seen.

(K. D. Prasad, A. J. Desai, Chandan Kumar, V. Sheel and S. A. Haider)

Implications of Fast Diffusion of CO for Astrochemical Models

The mobility of lighter species on the surface of interstellar dust grains plays a crucial role in the formation of simple through complex molecules. Recent laboratory experiments found the diffusion barrier for CO on the amorphous water ices to be 158 $\pm$ 12 K, which is significantly lower compared to the presently used values in the astrochemical models. With a gas-grain network, the effect of different diffusion rates of CO in the formation of various molecules was studied. Three physical conditions are used to study cold core and warm-up regions. Five different models are run for each physical conditions; two with coverage dependent barrier energies for diffusion and desorption, two with currently used barriers, and one with a diffusion barrier of 158 $\pm$12 K. Two different ratios (0.3 and 0.5) between diffusion and desorption barrier is utilized. Solid CO abundance for the model with the fastest diffusion rate yields only 0.1 % of water ice for cold clouds and $\sim$ 8.5 % for slow and fast warm-up models. It is found that the observed solid CO for dense clouds can only be explained with the higher diffusion barrier. Solid carbon dioxide is overproduced by a factor of two for cold core model with the fastest diffusion of CO and significantly under-produced with all the other models. No noticeable improvement in abundance is seen for the molecules which can be formed due to the efficient surface diffusion of CO on the grain surface.

(K. Acharyya)

Remote Sensing and Data Analysis

Degana crater, Mars: Insights from it fluvial, glacial and volcanic activities

Mars preserved substantial evidence for the ancient fluvial activities in the form of valley networks, channels associated with either alluvial fans or delta deposits. Despite these, there have been no report of unambiguous fluvial sedimentary deposits or alluvial fans within a volcanic dome on Mars.

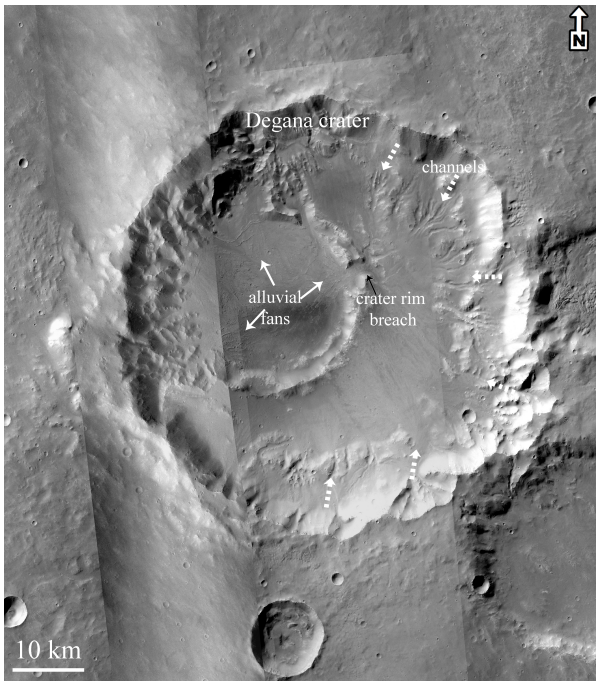


Figure 9: Degana crater with alluvial fans on its floor and channels present all around the rim

Alluvial fans are fluvial landforms formed by the deposition of loose material transported by flowing water. Their observation is crucial to substantiate evidence for flowing liquid water over the Martian surface. However, the most important in this is not only finding the fluvial deposits, it is solving the quest for the source of water. This study provides a comprehensive evidence for fluvial activities within a crater named Degana which formed over the volcanic dome in the highland region of Mars. Degana crater is a ∼52 Km diameter situated in the southern hemisphere and south of Eos chaos. The presence of smaller crater within Degana give raise to diverse fan deposits. This study also substantiates Hesperian/Amazonian fluvial activities over the Martian surface. The presence of Olivine and Low Calcium pyroxene confirms the dome comprised of volcanic material. The moraine ridges on the pole facing wall superimposing fan deposits suggest the glacial activity likely occurred after fluvial activity. The tentative discharge rate from the eastern side fan is ∼84 m^3/s. We infer that the snow/ice precipitation over the dome and within the Degana could be the source for the channel and fan formation. Taken altogether, this study substantiates that Degana crater witnessed volcanic, fluvial and glacial activities in different epochs over this region of Mars.

(Harish and Vijayan S)

Global distribution and characteristics of domical crater on the Moon

Several studies on the Moon are carried out to understand the plutonic intrusions of mafic magma within anorthisitic lunar crust. Sometimes such intrusions within craters are reported to have a role in forming the floor fractured craters (FFCs). Within FFC, the most interesting type of crater is the one with the presence of convex-up upliftment on their floor, called domical craters.

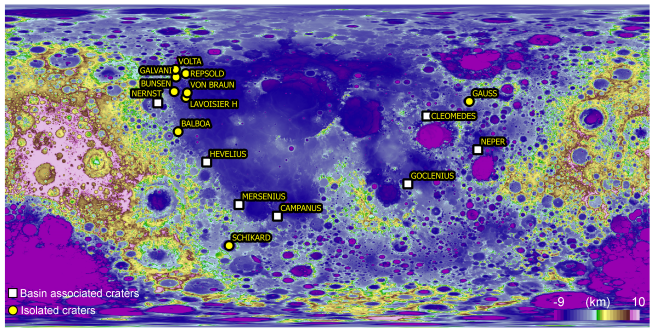


Figure 10: Distribution of domical craters on the Moon, classified based on their association with or without adjacent impact basins.

A global survey of such craters on the moon revealed they are only 16 in numbers and predominantly present around the mare region. We have studied the intrusions in these domical craters in a comprehensive manner from mineralogical, morphological, topographic and chronological perspectives. The detailed mineralogical analysis revealed the diversity of minerals including Mg-Spinel and Pure Anorthosite (PAN) along with orthopyroxene/ clinopyroxene and pyroclastic glass present on the floor, central peak and along the floor fractures. This lead to infer the regional stratigraphy in addition to diverse composition. The morphology of the craters unravelled formation of fractures, not accounted for previously. An enigmatic observation was extension of fractures beyond the rim of the craters, which reveals that they are regionally controlled and not constrained to the crater floor fractures. The topographic study of domical uplift within the craters suggested that the domes never covered the central peak and their extent varies with diameter. The chronological analysis suggested that domical formation peaked during Imbrium epoch and spreads from Pre-Nectarian to Eratosthenian epoch. We provide a favourable model for formation of these craters within different regions of Moon i.e., their association with respect to basins and crustal thickness along with a detailed model of magma ascent within their floors. Thus, this comprehensive study of domical craters helped us to reassess the fracture formation and their unique presence on the moon.

(Nandita Kumari, Harish and Vijayan S)

Alkaline rocks of the Moon: Recent Discoveries and Implications for Formation

It is commonly believed since Apollo era to the very recent time that the Moon is bone dry and constituted with significantly lower abundance of volatile elements than that of the Earth. Discoveries of volatiles and their retention in deep inside the lunar interior has changed this vision. Further, high abundance of volatile alkali element sodium (3-7 wt.% Na_2O) is observed by Chandrayaan-1's X-ray Spectrometer (C1XS) at the nearside of the southern highland. The modal mineralogy and the bulk composition by C1XS from the same region indicate that the rock type is alkaline and is classified as nepheline troctolite.

The C1XS coverage on 4^{th}, 6^{th}, and 8^{th} July 2009 includes Tycho crater and the adjoining areas, which underwent $>$ B3 class flares. The studied area is located along the discrete C1XS tracks from -20° to -70° latitude and from 28° to -30° longitude at the southern nearside highland of the Moon. The northernmost part of the C1XS coverage of 6^{th} and 8^{th} July 2009 coincides with the mare – highland boundary. The remaining study areas are mainly composed of the highland rocks dominated by large impact craters. Significantly high Na in the four out of the seven C1XS footprints have been observed covering a large area on the southern nearside. In this study we have focused on the individual C1XS footprints of approximately 50x50 square km size to find out the ground source of sodium by tallying the lunar crustal thickness map of the Gravity Recovery and Interior Laboratory (GRAIL) and observing locations of the large craters and the mare-highland boundaries. The chemical compositions derived from C1XS observation are the result of averaged C1XS spectrum that was obtained for statistically significant values of 250x250 square km area. We have found that the enhancement of the Na-signal is rather localized and corresponds to the deep craters (25 - 40 km) and/or at the mare - highland boundary regions. The crustal thickness values have been extracted from GRAIL. All the three C1XS tracks belong to unique geological settings. The C1XS track on 4^{th} July sampled a heavily cratered region (relatively old) with an increasing crustal thickness towards north. The C1XS track on 6^{th} July is dominated by crater Tycho and its ejecta. The crustal thickness at Tycho's floor is in the range of 25-35 km whereas that at the rim is in the range of 35-45 km. The crustal thickness decreases towards north.

In order to find the link between mineralogy and Na content

distribution, we have used a topographically and photometrically corrected Moon Mineralogy Mapper (M^3) spectral reflectance mosaic map of 20 pixels per degree resolution and computed the band I (absorption band around 1 μm) and band II (absorption band around 2 μm) spectral parameters. We computed the Integrated Band Depth (IBD) for band I and band II from the M^3-smoothed reflectance spectra after removing the continuum using the convex hull of the spectrum. In the IBD mosaic, we have assigned red and green channels to IBDs of band I and band II that indicates the presence of mafic minerals (pyroxenes and/or olivine). The blue channel of the IBD mosaic has been assigned to 1.5 μm wavelength, which is an approximate indicator of mafic-free minerals. This study shows presence of mafic minerals at the rim of the crater Tycho. Distinct gabbroic lithologies in Tycho crater and other localities at the western hemisphere of the lunar near-side indicates its regional occurrence and a more complex evolution of the lunar crust than previously understood.

Petrogenesis of these Na-rich rocks is decoded using the field relations and the compositional trends of the highland rocks to define the syn-crystallization assemblages and to calculate the parent melt composition. GRAIL crustal thickness from our studied region indicates that these alkali-rich rocks occur at 25-45 km depth. Parent melt of the highland rocks / minerals is derived at the onset of plagioclase crystallization. The parent melt has higher alkali (0.6-0.7 % more Na_2O) and simultaneously lower silica than the other traditional models. The parent melt composition is further calculated back by mass-balance of selected mineral phases and their corresponding modal abundances. The mass balance calculations indicate that an intermediate to felsic melt composition of the last $\sim$ 30% of LMO yielded floating plagioclase and silica along with sinking heavier mafic phases including ilmenite. The latter formed troctolites (occasionally nepheline-bearing) at 25 – 40 km depth. The reconstructed LMO composition and its crystallization sequence are considerably different from the earlier formulated ones and closer to that of the bulk silicate Earth.

The giant impact hypothesis is the most commonly acceptable one to-date to explain the origin of the Moon. This is mainly due to the satisfactorily explanation of the angular momentum of the Earth-Moon system, the small lunar core and the formation of a global-scale magma ocean. However, similarities in several isotopic characteristics between the Earth and the Moon along with the volatile enrichment in deeper mantle of the Moon puts a serious constraint on the giant impact origin hypothesis. One potential implication is that the Moon formed in a much cooler regime than predicted and with high volatile content similar to that of the Earth. Global exploration from the upcoming Chandrayaan-2 mission will aim to produce Na abundance map of the surface of the Moon along with in-situ analysis at the nearside of the southern highland.

This work has been done in collaboration with S. Narendranath, URSC, Bangalore; and D. Dhingra, IIT Kanpur.

(A. B. Sarbadhikari, M. Bhatt, G. Arora and A. Bhardwaj)

Geological characterization of Chandrayaan-2 landing site in the southern high latitudes of the Moon

Chandrayaan-2 mission will be the third giant leap by the Indian Space Research Organisation (ISRO) in their continued planetary exploration program. This mission will be realized in three phases that includes orbiting, landing and roving. Successful implementation of the Chandrayaan-2 lander (named 'Vikram') and rover shall be attributed as the first-ever touchdown on the surface of lunar highlands at southern high latitudes. In this work, we use the remote sensing datasets collected during the last two decades to characterize and map the proposed landing site of Chandrayaan-2 mission. The landing site is located in the southern nearside highlands within an area between 70 and 72° S and 22° and 24° E. We find that the topography of the landing region is generally flat and it is largely confined by craters of various diameters ($\sim$9-34 km). The majority of the landing region is characterized by slopes $<$15° and the estimated crater retention age is $\sim$3.7 Ga. The landing region is found to be dominated by craters (diameter: $\sim$2.28 m to $\sim$1.13 km) consistent with morphologies varying from very fresh to degraded, although it is noted that the ellipse center is apparently devoid of deep craters. A spectral reflectance study shows weak absorption features at 1μm and 2μm, which are suggestive of a low-calcium pyroxene component. Additionally, the estimated average elemental abundances are Mg: 5.4 wt.%, Ca: 9.97 wt.%, Fe: 4.2wt.%, and Ti: 0.3wt.%, respectively. Together, the spectral results indicate that the surface composition (Mg#75) is different from typical FAN (ferroan anorthosite), whereas it corresponds to FAN materials mixed with Mg-suite rocks. We explain this lithological association by suggesting that there might be a possible mixing of ejecta from the SPA basin, where the impact excavated the lower crustal and/or upper mantle materials, ensuing in hybridisation of highland regolith. Collectively, the results from this study indicate a complex geological history of the landing site and provide a framework for in-situ investigations at the geologically interesting locations in and around the landing site.

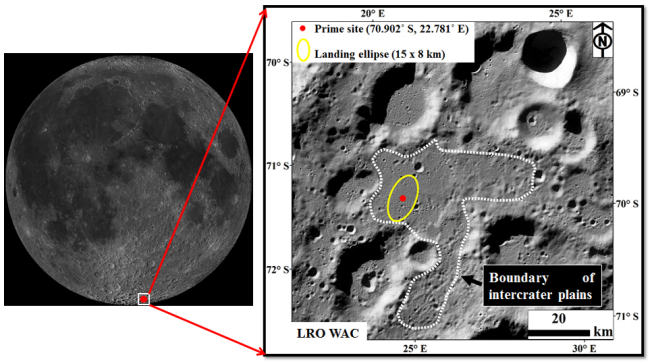


Figure 11: Lunar Reconnaissance Orbiter (LRO) Wide Angle Camera (WAC) mosaic showing the location of prime site of landing (red circle) and the landing ellipse (yellow solid line) within the heavily cratered portion of the southern polar region, also known as the intercrater plains (boundary is shown by white dashed lines).

(R. K. Sinha, V. Sivaprahasam, M. Bhatt, H. Nandal, Nandita Kumari, N. Srivastava, I. Varatharajan, D. Ray and A. Bhardwaj)

Geomorphic evidence of lobate deposits in gullies on Mars – global survey using HiRISE images

Gullies on Mars, represent steep slope drainage systems comprising an alcove, a channel and a depositional apron. Lobate deposits

similar to those found in terrestrial debris-flow gullies have been observed in martian gullies, consequently researchers suggested that water-bearing debris-flows likely formed martian gullies. However, since there are only few sites on Mars where the evidence of lobate deposits is preserved, and recent observations have revealed present-day modifications in martian gullies that result in features akin to water-bearing debris-flows, sublimation of seasonal CO_2-frost has been suggested to drive gully formation. Hence, water has been suggested to never have been involved in gully formation, thereby raising a question whether lobate deposits are from wet (water-bearing) or dry (CO_2-frost) flows.

In this study, we have conducted geomorphic investigation utilizing the High Resolution Imaging Science Experiment (HiRISE) images of the gullies formed inside the craters emplaced between 30°-75° latitudes in both the northern and southern hemispheres. We focused on morphologic identification of overlapping lobate deposits in gullies. Our study led to the identification of 20 new craters (14 in south and 6 in north) on Mars that have unambiguous evidence of multiple overlapping lobes. Additionally, we found evidence of scoured channels with levee deposits, significant cross-cutting and overprinting relationships within channels, and tongue-shaped deposits preserved within these craters. The estimated ages of some of these craters suggest recent (within ∼5-10 Ma) formation of lobate deposits in gullies. Based on the terrestrial examples analogous to Mars (in Ladakh), we propose that episodic melting of snow accumulated within the sheltered alcoves is the probable source of fluid (e.g. water) ultimately triggering the debris-flow within gullies. In summary, our study suggest that possibly water played some role in the formation of Martian lobate deposits and gullies vis-a-vis the present-day dry (CO_2-frost) processes may not hold explaining the formation and evolution of entire string of gullies on Mars.

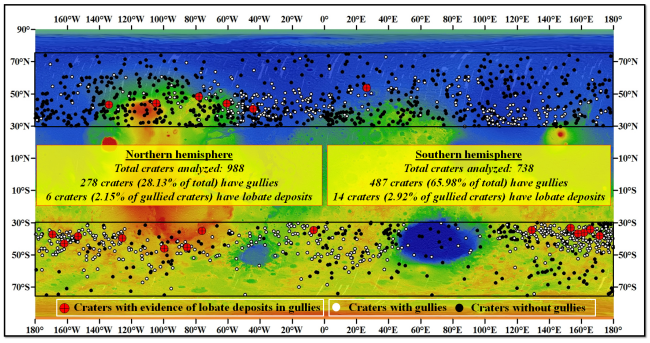


Figure 12: Mars Reconnaisance Orbiter (MRO) High Resolution Imaging Science Experiment (HiRISE) image based global distribution of gullies and lobate deposits inside the craters emplaced between 30°-75° latitudes in both the northern and southern hemispheres of Mars.

(R. K. Sinha and D. Ray)

Geological characterization of an albedo feature 'Nodus Alcyonius' on Mars: New insights on its origin and evolution

Nearly one third of Mars surface area is covered with albedo features. Despite that, till date, albedo features reported on Mars have been only studied for temporal estimation of brightening and darkening (i.e. change in albedo) of the surface using the images acquired during the Mariner, Viking, Mars Global Surveyor, and Mars Express missions. Thereof, our understanding regarding the morphology, topography and subsurface of such features is significantly limited, resulting in a very immature conjecture on the origin and evolution of albedo features. In this study, using datasets from multiple missions, we conduct first detailed geological characterization of an albedo feature named 'Nodus Alcyonius' (also called as 'Thoth') (centered at 32.5° N, 95.5° E). Topographic contours lines (100 m) from Mars Orbiter Laser Altimeter (MOLA; ∼463 m/pixel) onboard Mars Global Surveyor (MGS) reveal that the darkening originated under the influence of steep troughs evident in the slope map and Mars Reconnaissance Orbiter (MRO) Context camera (CTX; ∼6 m/pixel) images. Geomorphic investigation of the dark region using the CTX and High Resolution Imaging Science Experiment (HiRISE; ∼0.25 m/pixel) images unveil presence of cones, plateaus, ridges, fresh layered ejecta craters, gullies and several flow features. Preliminary investigation using MRO Shallow Radar (SHARAD) data shows that there is an absence of any apparent dielectric discontinuity in the subsurface. Surface reflectivity is between -15 dB to -12 dB, which suggests that the surface is slightly rough and material density is high. A widespread infilling, followed by significant erosion and removal of materials from the dark region is apparent through geomorphic evidence of infilled and inverted craters. Together, a rich plethora of geomorphic attributes is concealed within this dark region that stipulates the need for investigation of other dark regions elsewhere and for their eventual inclusion into the geological history of Mars.

(R. K. Sinha and R. R. Bharti)

Recent Volcanism and Tectonism in the Grimaldi Basin on the Moon

The Grimaldi Basin, centered at 5.2°S 68.6°W, is a highly degraded, Pre-Nectarian double-ring impact structure with outer ring diameter of 410 km.

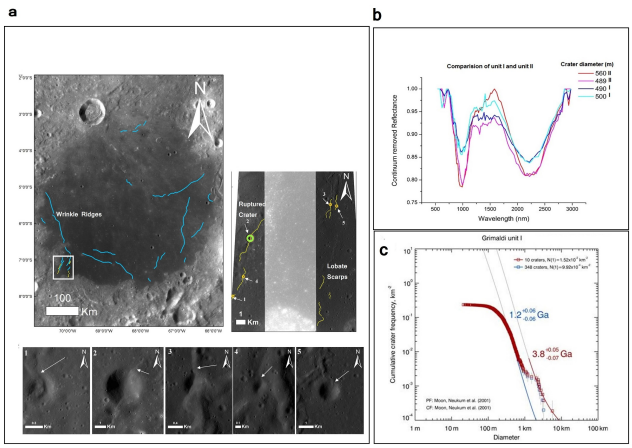


Figure 13: (a) Examples of small fresh craters ruptured by thrust faults using LROC WAC & NAC data. (b) Reflectance spectra showing presence of high Ca-pyroxene in the Grimaldi basalt. (c) A CSFD plot of the Grimaldi mare basalt showing resurfacing in Copernican period.

The basin is located between the Oceanus Procellarum and the Orientale Basin. Very high to moderate resolution images from LROC (Lunar Reconnaissance Orbiter Camera) NACs (Narrow Angle Cameras, 0.5 m/pixel)) and WACs (Wide Angle Cameras, 100 m/pixel) respectively, have been used to observe the morphological relationships between small impact craters and the tectonic features to decipher the evolutionary state of the basin. Several cross-cutting of small Copernican craters by lobate scarps in the Grimaldi basin have been noticed. The M^3 (Moon Mineral Mapper) data from Chandrayaan-1 mission has been used to derive the mineral composition of the region through spectral reflectance curves and Integrated Band Depths (IBD). The mineralogy results suggest that the basin is filled with two distinct basaltic units which are composed of high Ca-pyroxene with varying amount of Fe-content. The estimated model age of these two units have been found to be 3.8 Ga and 3.4 Ga. A small Copernican aged unit has also been found in the lower central part of the basin. On the basis of all of these evidences it has been inferred that the basin was experiencing volcanic and tectonic activities during the Copernican period. Thus, late stage volcanism has a greater spatial span on the Moon than understood earlier. KREEP may not be essential for producing the magma during the Copernican time.

(T. Singh and N. Srivastava)

Resource potential and planning for exploration of the Hebrus Valles, Mars

Mars is the only planetary body, which could be host to primitive lifeforms and also has the potential to host a human base in the near future.

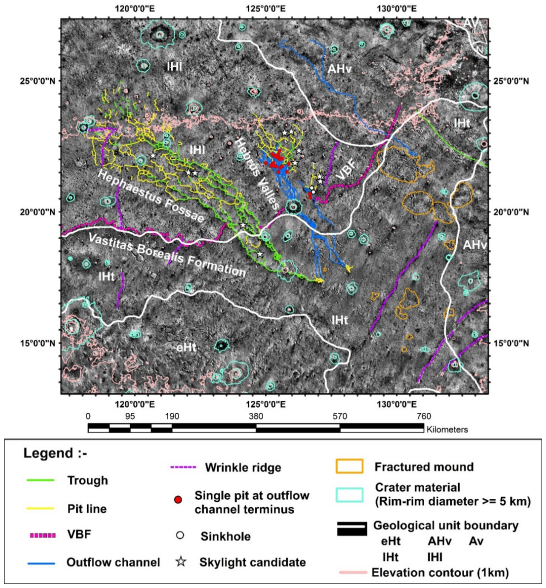


Figure 14: Geological context map of the HVHF region prepared on a background of THEMIS daytime-IR image mosaic. The geological units in this region are - Late Hesperian lowland unit (lHl), Amazonian and Hesperian volcanic unit (AHv), Late Hesperian transition unit (lHt), Early Hesperian transition unit (eHt), and Amazonian volcanic unit (Av). VBF refers to the Vastitas Borealis Formation.

Towards fulfilling these objectives, several remote sensing missions and rover based missions have been sent to Mars till date. Still, confirmation of existing or extinct life on this planet in any form has not been achieved and possibly human missions at selected sites in the future is key to address this problem. Here, we have used remote sensing data from MRO (Mars Reconnaissance Orbiter; NASA), MGS (Mars Global Surveyor; NASA), Mars Odyssey (NASA), and MEX (Mars Express; ESA) to work out exploration strategy for one such area known as Hebrus Valles, which is a potential site for human exploration to the surface of Mars. A geological context map of the Hebrus Valles and Hephaestus Fossae region has been prepared and a candidate landing site has been proposed in the Hebrus Valles region. Suitable rover paths have been worked out from the proposed landing site for harnessing the science and resource potential of the region. The proposed landing site is located in the equatorial region at (20°40' N, 126°23' E) and due to its proximity with the Potential Subsurface Access Candidates (PSACs) in the region such as sinkholes and skylights and also other resources such as crater ejecta, silicate material, and fluvial channel, is appropriate for exploration of the region.

The work has been carried out in collaboration with JJT University, Rajasthan.

(N. Srivastava)

Geological study of a floor-fractured crater in Central Eastern Arabia Terra: Possible evidences for early igneous processes on Mars

The highly cratered plain of Arabia Terra is one of the oldest provinces of Mars, located at the highland-lowland boundary. We document a previously unreported crater (diameter: ∼85 km; 27.95° N, 28.12° E) in the central eastern region of Arabia Terra that has preserved the morphological evidence of cones and ridges in the central portion of the crater floor (Fig. 15).

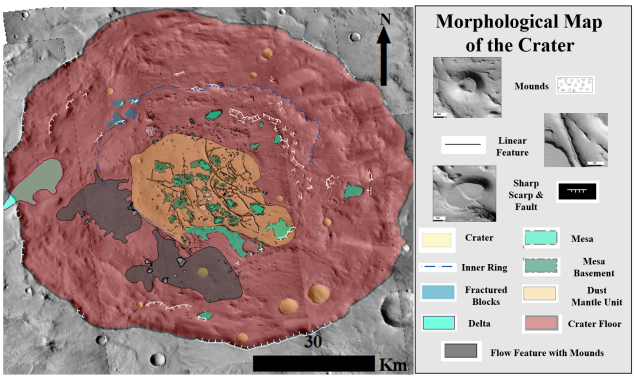


Figure 15: MRO CTX image based morphological map (1:25,000) showing the features mapped within the studied crater. The map signifies the rich assemblage of mounds and linear features, interpreted as cones and dykes in the central portion of the crater.

Such a finding raises a fundamental question "whether the observed morphological features are related to impact cratering or provide an evidence of a regional-scale intrusive activity". In that context, a detailed investigation is carried out by using the different remote sensing datasets viz. MOLA (∼463 m/pixel), THEMIS visible band (∼ 18 m/pixel), CTX (∼6 m/pixel) and HiRISE (∼0.25 m/pixel). To see

the landscape (3D) view, DTM of the crater is generated by draping THEMIS visible band image over the MOLA DTM, which reveals evidence for significant erosion of the crater rim and exhumation from the central portion of the crater floor. Morphological investigation of the central portion using CTX and HiRISE images reveals evidence of various types of mounds (conical, crater at its summit and flat top), mesas, ridges (linear and curvilinear), and plateaus. We interpret that these morphological features have possibly originated from intrusive processes and later exhumed on the crater floor by subsequent erosional processes (viz. aeolian and fluvial). Furthermore, similar morphological features were evident in regions outside the study crater as well, which iterates that the igneous activity perhaps extended regionally. Hence, it is critical to evaluate the origin vis-à-vis the triggering mechanism, i.e. the processes that lead to extensive formation of the aforementioned geomorphological features over a large region of Mars. Together, from our study, we bring to the notice a previously undocumented region within the Arabia Terra that has preserved evidence of the ancient (Noachian epoch) intrusive processes on Mars.

(A. Goswami, R. K. Sinha and A. B. Sarbadhikari)

Elemental mapping of lava flow structures in Mare Serenitatis

Serenitatis basin on the lunar eastern nearside is mapped extensively in order to find spectral differences among basalt units in the near-infrared range and their corresponding model ages.

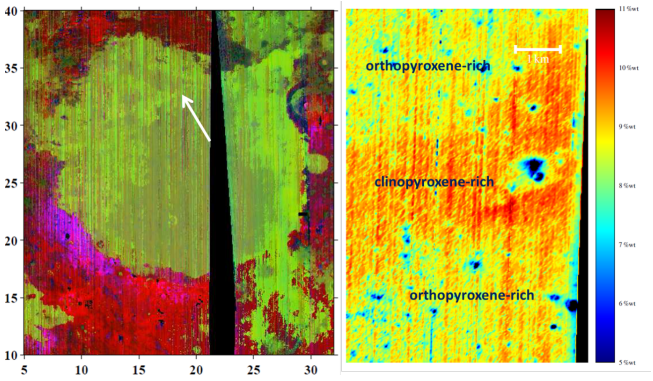


Figure 16: The M3 band center mosaic (left). Red colour assigned to band I center, green to band II center and blue to FWHM of band II. Arrow shows the area enlarged in right. The lava flow structure shows enrichment in Ca. Black denotes missing data.

The detection of lunar lava flows based on local morphology highly depends on the available high-resolution images. Lunar lava flows are shown to be as thick as 200 m in several previous studies from nearside western mare regions but not reported in Mare Serenitatis situated at near eastern side. We applied a digital terrain model (DTM) refinement method to Lunar Reconnaissance Orbiter (LRO) Narrow Angle Camera (NAC) images and constructed 2 m resolution DTM. We derived band center mosaic and elemental abundance maps of Mare Serenitatis using the Moon Mineralogy Mapper (M^3) on-board Chandrayaan-1. We identified two major basalt units from band center mosaic which can be further divided into sub spectral units based on the band I and band II centers and the full width at half maximum (FWHM) value of band II (fig. 16, left). The spectral units show variations in pyroxene compositions indicating lava flows from different eruption events. The boundary shown by arrow in fig. 16 shows a lobate, flow like shape. The lava flow structure has been examined in detail using 2 m resolution DTM. We found that this structure occurs on a boundary between basalts consisting of low-Ca and high-Ca lithologies. The total thickness of the lava flow is about 100 m, which is composed of two or more layers based on our DTM.

This work has been done in collaboration with Dr. A. Grumpe, Dr. C. Wöhler, TU Dortmund, and Dr. U. Mall from Max Planck Institute for Solar System Research, Germany.

(M. Bhatt)

Global mapping of lunar refractory elements

The nearly global coverage of the lunar surface in the visible to near-infrared (VIS-NIR) wavelength range using the Moon Mineralogy Mapper (M^3) onboard Chandrayaan-1 have been used for estimating Fe, Ti, Ca and Mg. The spatial resolution of global elemental maps is 20 pixels per degree which corresponds to about 1.5 km at equatorial region. The proposed algorithm relies on empirical relationships between the derived M^3 spectral parameters and a global elemental estimation derived using remotely sensed gamma ray spectrometer (GRS) data as a reference. The spectral parameters computed in VIS-NIR wavelength range are a sensitive indicator of chemical composition due to the Fe^{2+} transition at the crystallographic sites of different minerals and dependent on surface maturity caused by space weathering effects. Hence, the successful estimation of refectory elements in the VIS-NIR range depends on the choice of spectral parameters that can decouple maturity from lunar soil composition.

We developed empirical multivariate regression models to estimate the abundances of the refractory elements Fe, Mg and Ca on the Moon, by defining a set of spectral parameters that minimizes the sensitivity to maturity. For this purpose, the classical approach of multivariate linear regression (MLR) and the machine learning technique of support vector regression (SVR) have been employed, where the input for both regression techniques is kept exactly the same. Lunar Prospector GRS (LP GRS) and Kaguya GRS (KGRS) global elemental abundance maps have been considered as ground truth information for the regression. We validate the newly developed algorithms at the Apollo and Luna landing sites by comparing the estimated abundances of Fe, Ca, and Mg with laboratory-based measurements. For this purpose, we applied the MLR and SVR models to M^3 mosaics at full resolution of the sample-return missions Apollo 11, 12, 14-17 and Luna 16, 20, and 24 landing sites as shown in Fig. 17. The element-wise RMS deviations between sample-based and estimated abundances are also included in the plots. It should be noted that the returned samples cover Mg and Ca contents in a relatively narrow value range when compared to the broad range available for the Fe content.

We applied the maturity-independent MLR and SVR models to the site specific and global M^3 observations. The derived results have been compared with the previous works. We found that the newly proposed approach do not show dependencies on immature soil even for regions with high optical maturity indices. All the global maps clearly reflect the compositional differences between maria and highlands. Additionally, the compositional variations among different mare regions and mare-highland boundary regions are

clearly distinguishable. We found that the Fe, Mg, and Ca estimates derived by MLR and SVR models considering LP GRS as a reference are comparable in all regions except at the pyroclastic deposits of Sulpicius Gallus, Mare Vaporum, and the northwestern parts of Oceanus Procellarum. In these regions, the MLR-based maps show enrichments of Fe and Mg and depletions of Ca. These anomalies are not apparent in the maps constructed with the SVR model, which indicates that they probably correspond to extrapolation artifacts of the MLR model due to the fact that the combinations of spectral parameters encountered in the pyroclastic deposits do not occur on larger spatial scales resolved by the GRS data used for calibration. We found that the SVR model better constrains the elemental abundances in such "unusual" areas with spectral properties that were "unknown" while adapting the regression models. The improved global maps of refractory elements will serve as important tools to investigate the lunar geologic evolution.

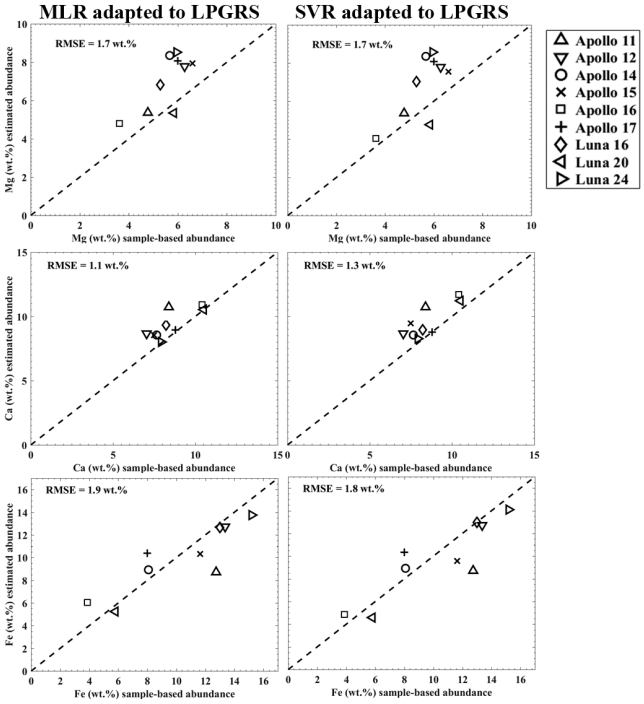


Figure 17: Estimated vs. sample-based elemental abundances for the Apollo and Luna landing sites, obtained by the MLR and SVR models. The LP GRS elemental maps of Fe, Ca, and Mg have been used here as a reference.

This work has been done in collaboration with Dr. C. Wöhler, TU Dortmund, Germany

(M. Bhatt)

Spectral characterization of lunar swirls

Lunar swirls are curvilinear albedo markings of tens of kilometres associated with magnetic anomaly regions but not associated with distinct topography. These features are associated with the magnetic crustal anomalies but in some cases extend outside the anomaly region. The formation of swirls is not yet fully understood. A commonly accepted mechanism for the origin of swirls is magnetic shielding of the surface from the solar wind, reducing the effects of space-weathering. We carried out detailed spectral characterization of six swirls situated at Mare and highland regions and found that the spectral trends between on-swirl and off-swirl material cannot always be explained by reduced space-weathering alone. We computed compaction index map based on empirical relation of on-swirl and off-swirl spectra. We propose that the combination of soil compaction and magnetic shielding is able to explain all observed on-swirl vs. off-swirl spectral trends. Our results support the hypothesis of swirl formation by interaction between the uppermost regolith layer and cometary gas.

Further, based on the compaction map we extracted reflectance spectra from fresh crater locations associated with very high and very low compaction indices. We found that the crater formed on the highly compacted area removed the compaction effect significantly and the spectral trends at such locations are comparable to fresh crater locations from surroundings. We found that the compaction effect is high for the regions with least crater and a fresh impact on compacted area weakens the compaction. We plan to conduct a systematic spectral analysis of swirls in order to find their find relative age and corresponding spectral properties that will lead towards better understanding of origin of swirls.

This work has been done in collaboration with Dr. C. Wöhler, TU Dortmund, Germany.

(M. Bhatt, N. Srivastava and A. Bhardwaj)

Loss tangent and dielectric constant measurement of subsurface material near Mangala Fossa region on Mars

SHAllow RADar (SHARAD) observations of subsurface reflections across the Mangala region reveal a low loss tangent subsurface material; such subsurface reflections are prominent around the margins of Mangala Fossa and within an unnamed crater (17.27°S, 151.35 W). The subsurface reflections support an interpretation that crater infilling occurred in more than two events with multiple successive lava flows. Based on the sounding radar data analysis, the loss tangent and dielectric constant are estimated to exhibit in the range $\sim$(0.007–0.011) and (5.0–5.5) respectively – a value significantly lower than earlier estimates of lava flows in the adjacent Tharsis region. These low dielectric values may indicate that dry, moderate density sedimentary rock or pyroclastic ash comprise the geologic units. Because of the proximity to morphological evidence of cryospheric eruptions in the Mangala region, the presence of high porosity material containing a small fraction of trapped ice may not be ruled out.

This work has been done in collaboration with Dr. Isaac Smith, Planetary Science Institute, Colorado, USA.

(R. R. Bharti and S. K. Mishra)

Infrared luminescence dating of Spituk Lake sediments in the Indus River Valley, Ladakh, India

We present infrared stimulated luminescence (IRSL) ages of Spituk Lake deposits in Ladakh, India. The IRSL ages for seven samples

from the Spituk section range from 105 to 170 ka, and suggest that deposition in the Spituk area began at ∼170 ka after damming of the Indus River. These ages are substantially older than ∼50,000 years BP reported previously by Phartiyal et al (2005). The uppermost unit in this section marks a change in climate and fluvial activity and the IRSL ages suggest that lake existed for another ∼70 ka, and later disappeared due to breaching of the dam at ∼100 ka.

Background and Objectives: The major tectonic features in the Higher Himalaya comprise the Indus Tsangpo Suture Zone, the Shyok Suture Zone and the Karakoram Fault. Many sedimentary deposits are preserved in the form of terraces, fans, lake and moraines, and represent archives of paleoclimatic changes during the late Quaternary. The Indus River flows along NW-SE tending Karakoram Fault and along the Indus Tsangpo Suture Zone which marks the boundary between the Asian and the Indian continental plates. The present work aims at infrared stimulated luminescence dating of Spituk Lake deposits to decipher the timing of formation of the Spituk Lake in Ladakh. The Spituk section is the best preserved >50 m high Quaternary section which represents deposits of fluvial, glacial and lacustrine environments.

Materials and Methods: The feasibility of infrared stimulated (IRSL) luminescence dating of 63-150 μm quartz-rich grains was investigated in 7 samples collected from Spituk, Ladakh. Although HF etching was performed during chemical processing of the samples, all aliquots exhibited significant IR and post-IRIR signals. Hence, a modified SAR protocol was to estimate the infrared stimulated luminescence (IR_{60}) equivalent doses following the procedures outlined in Buylaert et al. (2012). The same preheat conditions were applied prior to the measurement of the natural and regenerative dose as well as the test dose. The first IR stimulation was carried out at 60°C for 200 s, followed by the second stimulation at 290°C. External dose rates for the samples were calculated from the activity concentrations of decay chains ^{238}U, ^{232}Th and ^{40}K measured using high resolution gamma spectrometry (HPGe).

Results and Discussion: The lower units in the Spituk section were observed to be fine sandy, whereas the middle layer has a thick clay representing a lacustrine environment. The uppermost layers contain gritty sand and coarse sand layers, suggesting a fluvial environment. The IRSL luminescence ages for the seven samples from the Spituk section range from 105 to 170 ka. The IRSL age at the bottom of the Spituk section is ∼170 ka, and suggests that deposition in the Spituk area began at ∼170 ka after damming of the Indus River. These ages are substantially older than ∼50,000 years BP reported previously by Phartiyal et al (2005). The uppermost unit in this section marks a change in climate and fluvial activity and the IRSL ages suggest that lake existed for another ∼70 ka, and later disappeared due to breaching of the dam at ∼100 ka in marine isotope stage (MIS) 5.

(D. K. Panda, D. Banerjee and A. D. Shukla)

Effect of local topography on lunar surface thermophysical behavior

Understanding of the global thermo physical behavior and its implications on heat loss from lunar interior is necesary to estimate the net heat flow and thereby the evolution history of the Moon. The thermal behaviour within the uppermost (top few metres) regolith layers is more complex due to their complex geometric, thermal and radiative properties. Furthermore, regional scale topography also significantly influences the heat exchange within the uppermost layer of the lunar surface. Therefore, a comprehensive understanding is needed to estimate the global lunar heat flow. In order to understand these aspects, a comprehensive three dimensional finite element thermal model of the Moon has been developed and validated the details of which were already reported earlier. The diurnal, annual and latitudinal variability of lunar surface and subsurface temperatures have been derived from the model and compared with available literature. Subsurface temperature differences obtained from these simulations have exhibited a significant variability as a function of stratigraphy, composition and latitude. Further, we have made an attempt to understand the role of local topography on the surface and subsurface thermophysical behaviour in the vicinity. Topographic data from LOLA (Lunar Orbiter Laser Altimeter) instrument onboard LRO has been used in conjunction with the model and the surface and subsurface temperatures were derived. Simulations were carried out for few important sites on the Moon that includes Apollo 17 landing site. Qualitative results show that the significant effect of local topography on the surface and subsurface temperatures and their diurnal variation. Quantitative analysis is underway.

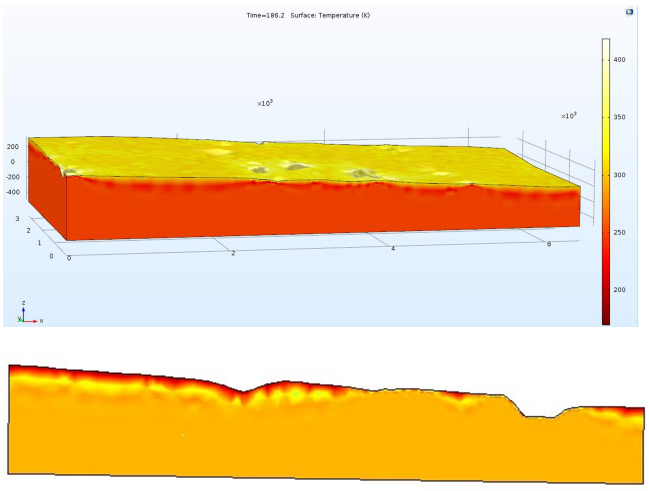


Figure 18: A 3D and cross-section views of the effect of local topography on the surface and subsurface temperatures for Apollo 17 Landing site

(K. Durga Prasad, P. K. Reddy)

Surface erosion due to lunar soft landing - A theoretical evaluation in view of Chandrayaan-2 Vikram Landing

An in-depth understanding of the surface damage and its implications due to spacecraft soft landing on the Moon is important from both scientific as well as engineering perspectives. Such an understanding helps to plan an optimum descent trajectory that minimizes the extent of disturbance to the lunar soil. The information about the extent of damage will also be helpful in interpreting the data obtained from experiments carried on the lunar surface in vicinity of the lander. As lunar lander approaches the surface, the exhaust plume impinges on the surface causing dust and debris to disperse in the flow field and modifying the surface underneath. We have made an attempt to numerically investigate this disturbance caused to the lunar surface

during soft landing and its effect on the lander subsystems and surroundings. This work gains significance in view of the upcoming landing of Chandrayaan-2 Vikram Lander. A numerical model based on the laws of motion and conservation laws of momentum and energy, encompassing the plume thermodynamics and plume-soil interaction, was used to analyze the landing scenario. Plume dynamics parameters obtained from DSMC (Discrete Simulation Monte Carlo) simulations for the plume-soil interaction (carried out by LPSC, Valiamala team) were utilized to estimate the surface damage. The variability of eject velocity of dust, eject mass flux rate, ejecta amount, damage to the lander subsystems etc. has been studied. The kinematics of the ejected particles was obtained and the consequent damage to the surroundings was evaluated. The effect of lander hovering time and hovering altitude on the extent of disturbance is also evaluated. Initial results show that the blown out dust due to landing may have less impact on the lander sub-systems and operations of the lander. Fig. 19 shows a schematic of the prediction of overall damage that is likely to happen underneath the Vikram lander. We expect that a total of ∼7-10 kg of mass would be ejected during the landing which could disturb a surface upto 4 m^2 thereby removing surficial layer of ∼1.5 mm to 2 mm in the vicinity. Some of the results are shown in figure 20.

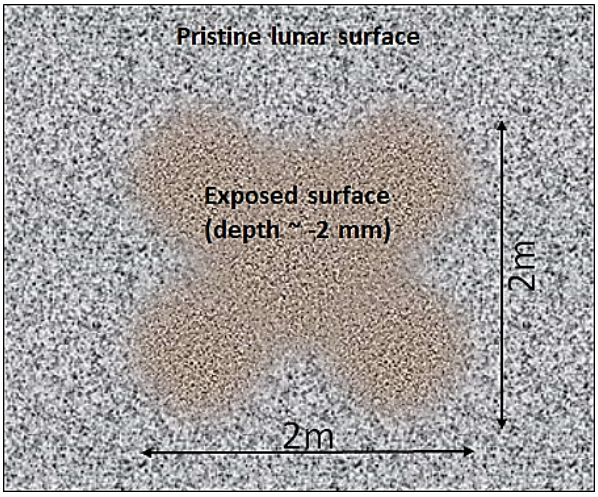


Figure 19: An artistic view of the kind of damage pattern expected during hovering and vertical landing

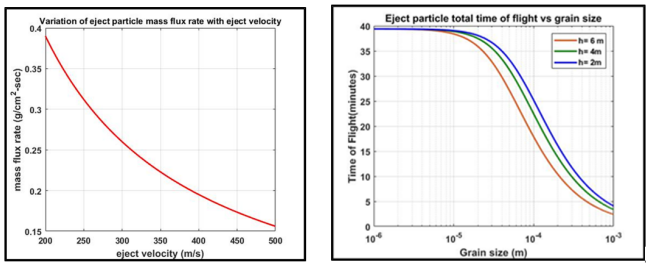


Figure 20: Plots showing eject particle velocities (for 11 μm dia.) from DSMC and eject particle kinematics respectively

(S. K. Mishra, K. Durga Prasad, A. Bhardwaj, Pranavnath, D. Agarwal)

Meteorite Study

The thermal evolution of meteorite parent body estimated from Insoluble Organic Matter

The insoluble fraction of carbonaceous chondrites is composed of macromolecular matter that is commonly referred to as "kerogen-like" material and it is this material that is refer to as Insoluble Organic Matter (IOM). Carbonaceous chondrites (CCs) contain a wide range of carbon abundances varying from 0.1 to 5 weight % of carbon, which is present in both organic and inorganic form. Spectroscopic analyses of CCs have revealed a major insoluble organic component consisting of >60-70 % of the total organic carbon. In various studies these IOMs were separated using two different methods, one which involved a series of HF-HCl treatment and other with a less labor intensive process using a mixture of Cesium Fluoride, Dioxane and Carbon disulfide. These IOMs were then analyzed using K edge Carbon X-ray Absorption Near Edge Structure (C-XANES) spectroscopy to derive a thermo-kinetic expression from the data obtained. Followed by Raman spectrometer analyses to complement the observed temperature affects.

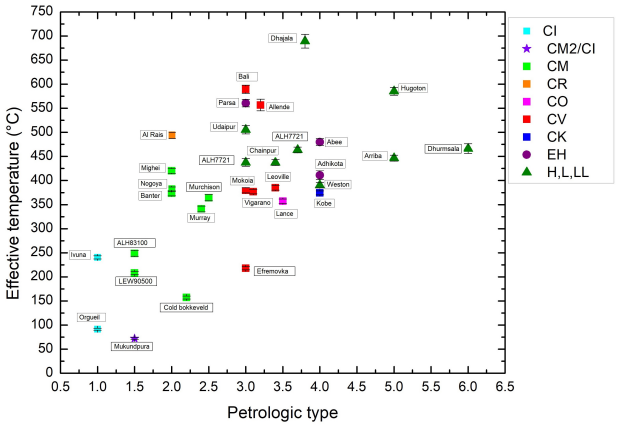


Figure 21: Effective temperatures calculated from Xanes spectra for IOMs separated from various types of meteorites encompassing different petrographic grades.

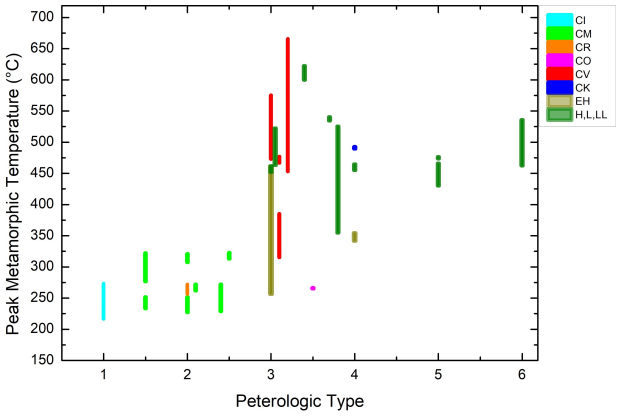


Figure 22: Range in peak metamorphic temperatures calculated from Raman spectra for IOMs separated from various types of meteorites encompassing different petrographic grades.

A total of 35 different samples (20 Carbonaceous, 1 Ordinary, 2 enstatites, 2 Martian) of IOM spanning multiple groups and petrological types (1-6) were analyzed. The intensity of 1s-σ^* excitation (at 291.63 eV) obtained from the C-XANES analysis of the samples is used to estimate the effective temperature(T_{EFF}) integrated over time by using the thermo-kinetic expression previously derived along with the Arrhenius equation. This T_{EFF} is used as a measure of parent body metamorphism which can determine the conditions in which these meteorite bodies initially formed. Similarly, peak metamorphic temperatures that the organics have observed, has been derived from Raman D and G bands. Mukkundpura meteorite, which was the primary subject of project, indicates the temperature observed to be close to CI meteorites-especially Orgueil, rest follow the petrographic trend, as shown in the figure.

(K. K. Marhas, S. Natrajan and V. Goyal)

Sputtering of presolar grains via galactic cosmic rays in interstellar medium

Presolar grains that condense in cooling circumstellar disk envelops of stars are ejected into Interstellar Medium(ISM) during events like mass loss or death of stellar objects. Spectroscopically they are observed as carbides, nitrides, oxides and silicates.

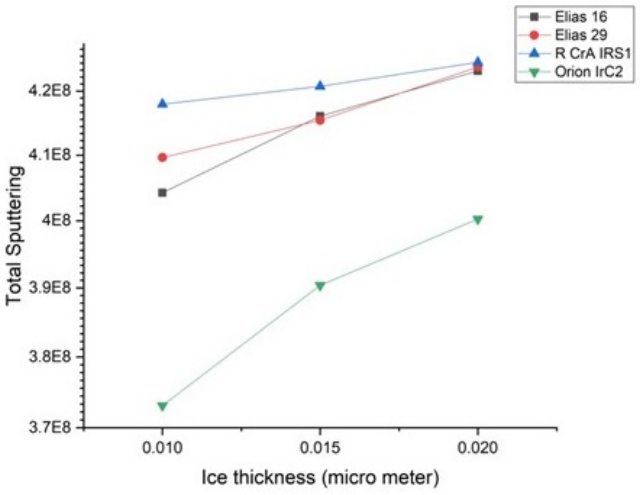


Figure 23: Plot shows sputtering due to Galactic Cosmic Rays (GCRs) in terms of total number of atoms sputtered for a micron sized SiC grain varying with the ice-mantle thickness over the grain-core. Four different molecular cloud regions (Elias 16, Elias 20, R CrA IRS1, Orion IrC2) have been shown for comparison.

The grains travelling in low density and temperature region allows molecules to be adsorbed on the grain, eventually forming an ice mantle on the grain. The composition of ice in a molecular cloud varies with the local conditions depending on various factors like shock waves, the collision of grains, absorption of photons etc. The sputtering of grains in the interstellar medium also occurs due to galactic cosmic rays(GCRs). GCRs are mainly composed of hydrogen (90%) and helium with a small portion of heavy metals. The sputtering depends upon the surface binding energy of the elements present in the ice mantle and the core. In the present study, sputtering rate of presolar Silicon Carbide (SiC) grains, of different sizes and different thickness of ice-mantle, in ISM due to GCRs have been calculated for their experimentally deducted lifetime ($\sim$1Gyr). Relative velocities of GCRs with respect to grains as they condense and evolve at different temperatures, environment, as well as various density and composition of ISM (quiescent, low mass young stellar objects (YSO), intermediate mass YSO, high mass-YSO weak processing), were considered using an ion target simulator SDTrimSP (freeware). It was believed that the mantle acts as a protective layer for the core of the grain however, as the GCR travels through the mantle, it loses some energy and the 10 MeV to 1GeV energy per nucleon level, the sputtering yield increases with decrease in the energy to GCRs. Therefore, having an ice mantle actually accelerates the destruction of core whose absolute value is very low. It would require a total of around 3 x10^{10} of C, O, Fe GCRs (which constitute less than 1% of total number of GCRs) to completely destroy the ice mantle over 1Gyr.

(K. K. Marhas, A. Garg and V. Goyal)

Noble gas and nitrogen in two eucrites Vissannapeta and Piplia Kalan

The eucrite meteorites, Vissannapeta (Fall 13 Dec. 1997; Andhra Pradesh) and Piplia Kalan (Fall 30 Oct. 1994; Rajasthan) are studied with the objective of finding cosmic ray exposure age, and understanding the signature of trapped gases. Neon is cosmogenic in both the eucrites. The cosmic ray exposure ages estimated from noble gases are 23.8 ± 6.1 Ma and 28.4 ± 8.1 Ma for Vissannapeta and Piplia Kalan, respectively. Isotopically light nitrogen is observed in Vissannapeta, while heavy nitrogen is present in Piplia Kalan. This demonstrates that the distinct nitrogen components are present in the eucrites. This has implications for the eucrite parent body evolution. The trapped ^{14}N/^{36}Ar in both the eucrites are 10^6 and clearly distinct from other solar system reservoirs. The HED meteorites contain extraneous components along with an evolved component of indigenous Vesta. Elemental ratios of the trapped Ar, Kr and Xe together with N in eucrites indicate their distinct sources in the Vesta. From the elemental ratios of Ar, Kr and Xe, it is found that the gases in Vissannapeta are influenced by the solar wind implantation. Therefore, regolithic exposure is expected in Vissannapeta. Indiscernible amount of iodine-derived Xe and bromine-derived Kr implies a case of depletion of halogens in the eucrites. Devoid of ^{129}Xe, a decay product of radiogenic ^{129}I implies heterogeneous distribution of ^{129}I during the early stages of the solar system formation. The gas retention ages of both the eucrites are short, which is attributed to the He loss. Short ^{40}Ar ages support the gas loss during a thermal event in the history of eucrites.

(R. R. Mahajan, A. B. Sarbadhikari, M.S. Sisodia)

Noble gases and nitrogen in Raghunathpura (IIAB) and Nyaung (IIIAB) iron meteorites

Noble gases and nitrogen isotopic studies of iron meteorites help in understanding the interplanetary journey of the meteoroid, as well as provide clues to the formation and evolution history of the parent body. Noble gases in iron meteorites are mostly dominated by in situ produced components (cosmogenic, radiogenic and fission components), but indigenous trapped components, either of Q (a

primordial noble gas of solar nebular origin) or occasionally HL (a trapped noble gas of interstellar origin) composition are observed. Noble gases and nitrogen were measured in two adjacent samples each from two iron meteorites - Raghunathpura (IIAB) and Nyaung (IIIAB) (both are falls). Light noble gases in both meteorites are of pure cosmogenic origin.

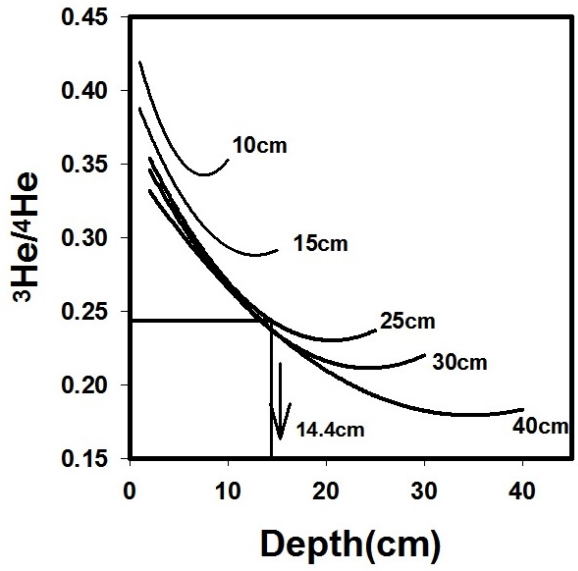


Figure 24: Cosmogenic ratio (^{3}He/^{4}He) produced at various depths using production systematic in objects with composition of Raghunathpura iron and radii 10, 15, 25, 30 and 40 cm were plotted.

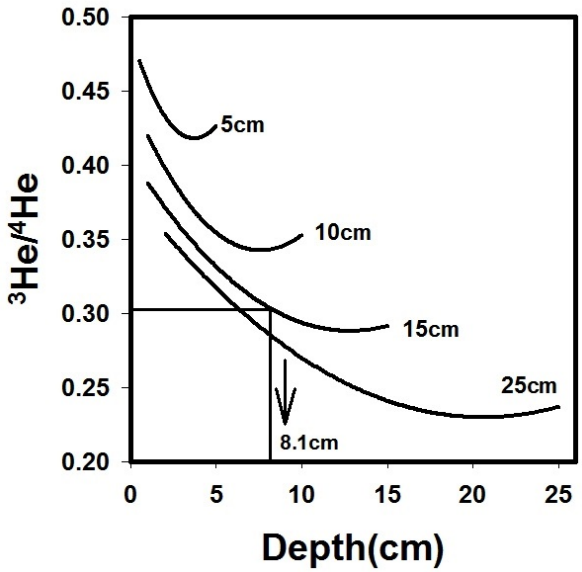


Figure 25: Cosmogenic ratio (^{3}He/^{4}He) produced at various depths using production systematic in objects with composition of Nyaung iron and radii 5, 10, 15 and 25 cm were plotted.

Cosmogenic He, Ne and Ar production in iron meteorites are mostly dependent on the major elements Fe, Ni, while cosmogenic Ne production is also very sensitive to the abundance of minor elements S and P. Using (^{3}He/^{4}He) ratio and the production systematic of Ammon et al. 2009, we estimate the sample depth and meteoroid size for Nyaung (∼8 cm depth in ∼15 cm radius object) and Raghunathpura (∼14 cm depth in ∼25 cm object). We derive cosmic ray exposure ages of 1710±256 Ma (for Nyaung, the highest reported for IIIAB group till date) and 225±34 Ma (for Raghunathpura), respectively. Variable amounts of trapped Kr and Xe have been found in both meteorites. The Q like elemental ratio (^{84}Kr/^{132}Xe) suggests that the trapped component is of indigenous origin, and most likely hosted in the heterogeneously distributed micro-inclusions of troilite/schreibersite. Both meteorites show light nitrogen, and need at least two N components, to explain the observed N systematics. Variable amounts of trapped noble gases and presence of more than one N component suggests that the magmatic process that has formed the parent body of these meteorites has not been completely homogenized or completely degassed all the phases.

(S.V.S. Murty, S.Ghosh and D. Ray)

Shock excursion of core of a differentiated Asteroid (IIAB iron)-Evidences of multiple impacts

Iron meteorites represent the core of a differentiated asteroid. Amongst iron groups, magmatic irons are thought to be originated from core of planetary embryo. The study of iron meteorites, thereof, leads to understand the mineralogy of the deep interior of the Earth and other differentiated asteroids. Without iron meteorites, our chance to probe the deep interior of differentiated bodies like Earth is, therefore, next to nil.

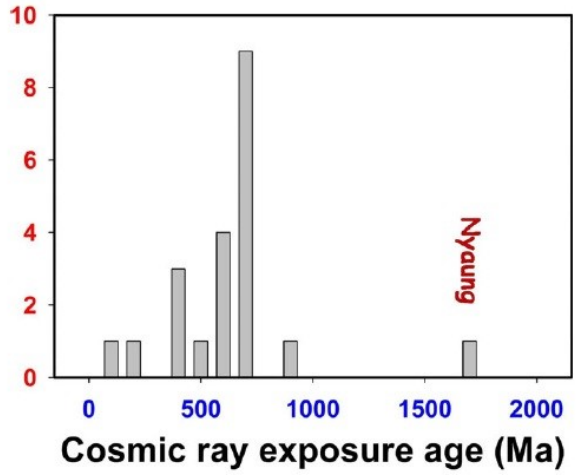


Figure 26: Histogram showing the Cosmic Ray Exposure Age (CREA) of IIAB irons.

Asteroidal cores experienced continuous collisions in the parent body. The shocks produced during the impacts are likely to be manifested through development of different microstructures and variability of chemical composition. We examine here magmatic iron - Agoudal (a find 2000 in Morocco) belonging to IIAB group and attempt to find the evidences of shock in order to understand the thermal and shock history. Our study suggests that an initial event of pre-crystallisation, mild deformation within IIAB parent body ignited

kamacite precipitation through massive transformation mechanism (α_m) followed by formation of a set of primary macro-scale 'Transform twins'. The parent body once got solidified was subjected to several successive impacts of low shock (<110 kb) magnitude resulting development of multiple shock-induced twins (Neumann bands) on microscopic to submicroscopic scale. Post-shock low temperature mild reheating ($\sim$400°C) is envisaged from kamacite polygonisation, imperfect recrystallisation of kamacite with subgrain boundaries and partial annealing of Neumann bands with pinch-swell, boudinage and kink band textures.

This work is done in collaboration with H. Chennaoui, University of Casablanca, Morocco.

(D. Ray)

Origin and evolution of primordial planetary crust: clues from lunar anorthositic meteorite

The origin of primordial lunar crust is important to understand the early evolution of terrestrial planets in the Solar system. The anorthositic crust ($\sim$34-43 km thick) is a major component of lunar primary crust ($\sim$80%). The current paradigm favoured two alternative hypotheses, majority of researchers believe in plagioclase floatation hypothesis, while serial magmatism remains within the minority view to explain the origin of the lunar highland crust. The lunar feldsphatic meteorites always offer a global representation of lunar crust (randomly sample) as compared to small fraction sampling from near side during Apollo and Luna missions. Analyses of meteorites suggest that ferroan anorthosite crust may not necessarily product of global magma ocean, rather complex magmatic processes are equally important to explain the chemical diversity in the crust. The pristine lunar anorthositic meteorite - Dhofar 081 is studied to evaluate the petrogenesis of lunar crust. The relict igneous texture includes subhedral prismatic low-Ca pyroxene shows inter-tonguing relationship with anhedral anorthitic plagioclase suggesting eutectic crystallization of parent magma. This leads to explain the formation of the protolith of Dhofar 081 by serial magmatism, a process not consistent with the popular global magma ocean model. The new geochemical data and synthesis of literature data suggest that low Ca-low Fe orthopyroxene is in equilibrium with high Ca-low Fe clinopyroxene, and application of pyroxene thermo-barometry estimates the pressure and temperature of crystallization of its parent magma as $\sim$8 kbar and 1050°C respectively. The parent magma of the Dhofar 081 envisaged a low-SiO_2 (40-47 wt%) melt was generated during partial melting of the lunar chondritic precursor (at a pressure of 8 kbar with corresponding depth 144 km). This study is also well timed as ISRO's upcoming Chandrayaan-2 mission is expected to be landed and probed on the feldspathic-rich highland region of southerly Moon and is aimed to provide new results on the early evolution and origin of the lunar crust.

(D. Ray)

Glimpse of aqueous alteration in Mukundpura (CM2) chondrite.

The CM types of meteorites represent one of the most primitive meteorite groups and are the fragments of primitive asteroids. CM types are also very important to understand the role of extra-terrestrial water in the early solar system. CM type meteorite mostly consists of aqueously altered fine grain matrix, CAI inclusion with fine grained phyllosilicates, chondrule (with fine grain rim), phyllosilicates, sulphides, carbonates and AOA (amoeboid olivine Assemblage).

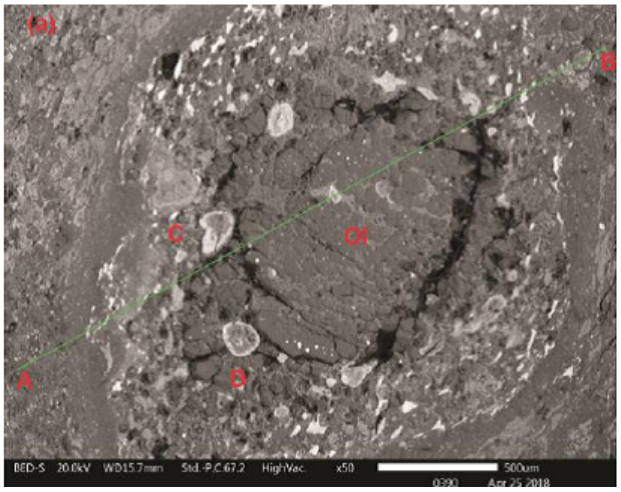


Figure 27: Line scan across the chondrule has been carried using EPMA.

The recently fall Mukundpura meteorite has been classified as CM2 chondrite. Three polished thick-section of Mukundpura has been scanned under the JEOL SEM with an operating voltage of 20 kV and 500 pA at a working distance of 16mm. For chemical composition, these samples are being analysed by Electron-Microprobe Analyzer (EPMA), Cameca SX100 with an operating voltage of 15 keV, 15nA and beam diameter of 2 μm. For the chemical composition and geochemical studies, the elemental analysis for Na, Mg, Si, Al, P, K, Ca, Ti, Fe, Mn, Cr, Ni, S and Cl were carried out. Counting time for the major element were kept at 20 seconds while for the Na, K and Cl it was kept about 10 seconds.

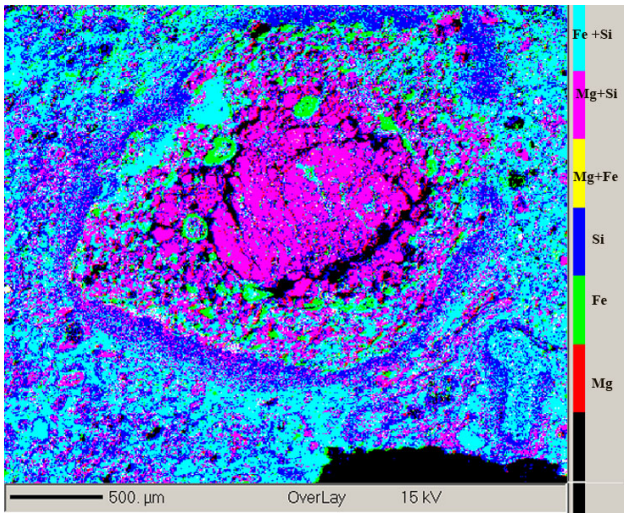


Figure 28: X-ray map of Fe, Mg, Si of the chondrule.

From the EPMA chemical composition and BSE image it was observed that almost all the chondrules are altered and the chondrules are surrounded by very thin accretionary rim ($\sim$20-50 μm). EPMA line

scan across the chondrule and surrounding rim shows differential elemental enrichment and depletions, e.g. hydrous accretionary rim sector is characterised by variable Fe-enrichment (FeO ∼18- 44 wt %). The mesostasis phase inside the chondrules are observed to be Fe-rich (FeO ∼24-30 wt %) and very low Al (2-7 %). Ternary plot in figure 29 shows the change of composition from one end to the other end of the chondrul due to the interaction of fluid with the chondrul. The matrix of Mukundpura is mainly dominated by mineral clasts and poorly characterised phases (phyllosilicates and different polymorphs of serpentine). It has also observed that phosphate phases and calcite also common in Mukundpura meteorite.

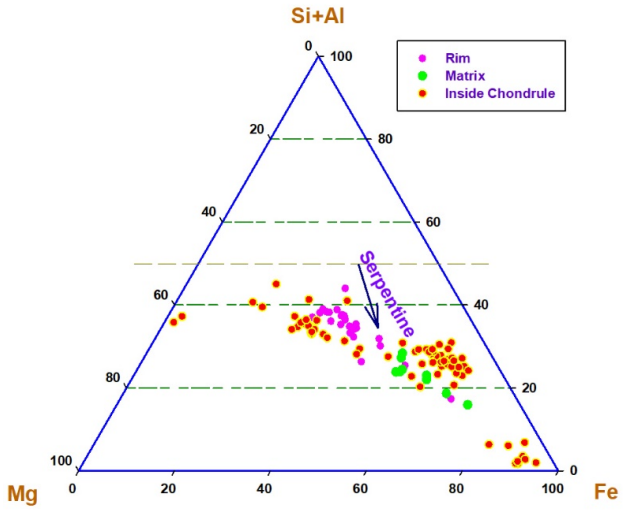


Figure 29: Ternary plot of the chemical composition measure using EPMA to show the variation of composition from end-end of the chondrule

This studies shows that Mukundpura is a CAI (Calcium Aluminium Inclusion)- poor, clast-rich Carbonaceous chondrite. The high extent of aqueous alteration might have promoted dissolution of the pre-existing CAI, chondrules and matrices. The formation of phosphate phase may be due to the reaction of fluid with the Fe-Ni metal/ phosphide phase with CAI. Presence of calcite further provides evidence of secondary aqueous alteration.

(D. K Panda, D. Ray and A. D. Shukla)

Colour Cathodoluminesence study and Astromineralogy of carbonaceous chondrite

The primitive records of the solar system are provided by studying the pristine carbonaceous chondrites. Mukundpura carbonaceous chondrite (CM2) fell on June 6, 2017 (5:15 IST) in Mukundpura village near Jaipur, Rajasthan, India. Colour Cathodoluminesence (CL) imaging along with chemical studies of forsteritic olivine was performed in order to understand defects in crystal structure along with the inhomogeneities in the distribution of activator elements and investigate the role of aqueous alteration. Mukundpura chondrite appears as various clast and matrix-rich (a variety of phyllosilicate, Mg-serpentine, Fe-cronstedtite, tochilinite) CM2 type, however a few relict chondrules with fine grained accretionary rim are likely to be survived despite the pervasive alteration. Forsteritic ($Fo_{98.74-99.66}$) and fayalitic (Fa_{50}) olivines both occur as isolated grains within matrix, however, fayalitic olivines are CL-negative. Instead, highly forsteritic olivines are CL sensitive and show typical blue CL emission at core and red to dark red luminescent at margin. The CL colour variation is mostly intrinsic and likely attributed to structural defects. However, patchy, heterogeneous and complex CL zoning are also common. Additionally, altered forsteritic olivines appear dull red CL luminescent. The innermost, unaltered core of forsterite is CaO (0.63 - 0.74 wt %), Al_2O_3 (0.32 – 0.46 wt %) and TiO_2 (0.06 – 0.12 wt %) rich as compared to margin, which show differential enrichment in FeO (1.34 – 1.50 wt %), Cr_2O_3 (0.51 – 0.55 wt %) and MnO (0.24 – 0.28 wt %). Emission of blue CL luminescent corresponds to rapid cooling and crystallisation, while the migration of diffusible elements can be linked with hydrothermal alterations occurred within the asteroidal parent body.

This study, therefore, suggests that Colour CL imaging is unique, powerful tool to assess the growth structures like colour zonation (insensitive to optical microscope), crystal-chemical properties and to elucidate the unusual minor element distribution manifested by complex CL textures to unravel asteroidal parent body process. This novel technique deserves application in detection of forsterite in protoplanetary and planetary nebula or even cosmic dust and may aid in mineralogical investigations for the future planetary missions.

(S. Baliyan and D. Ray)

Optimisation of laser parameters with reduced spot sizes for trace element analysis

Laser Ablation technique has been intensely used for the in-situ trace element determination in meteorite samples at very low detection limits and with minimal sample preparation. We have obtained optimal laser parameters like laser fluence, repetition rate, gas flows, iteration count and shot count for available spot sizes from 4-200 micron. The results have been verified by measuring the concentrations in NIST and USGS standards and the results matched with the certified values. External calibration has been done using ablation of the NIST 612 glass standard, in conjunction with internal standardisation (Si as the internal standard) since it allows calibration using a standard that is not matrix-matched with the sample. For data acquisition in the desired units, we have made use of Trace Elements_IS Data Reduction scheme (DRS) of Iolite software, which was judiciously applied to simultaneous data analysis of various mineral phases like pyroxene, maskelynite, and olivine in the Martian meteorite Tissint.

We have been able to tune till 10-micron and the experiments for 4-micron sizes are ongoing which will further help us to analyse the smallest phases or melt inclusions. Figure 30 shows trace element concentrations in pyroxene of the Martian meteorite Tissint at 20-micron spot size. The laser parameters used are: Laser energy-50 %, Repetition rate-20, MFC1(He)-0.7 LPM, MFC2(He)- 0.3 LPM, Shot count-50 and Iteration count-1. Similar results have been obtained for olivine and maskelynite also. Analyses for further smaller spot sizes will provide more improved results on finer mineral phases.

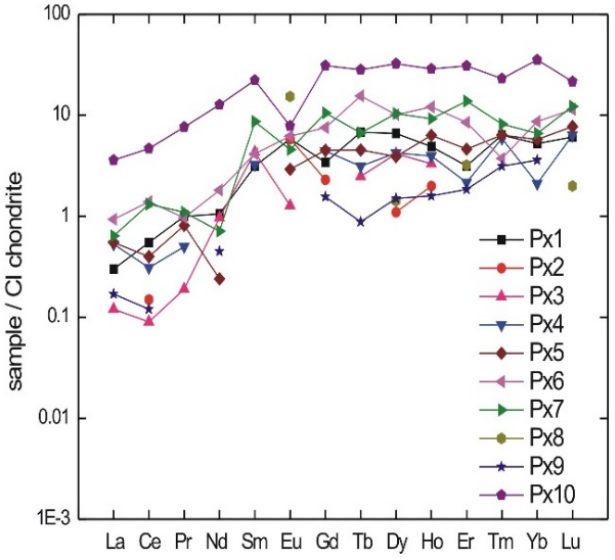


Figure 30: Rare earth element abundances in Martian meteorite Tissint with 20-micron spot size.

(G. Arora, Y. Srivastava and A. B. Sarbadhikari)

Instrumentation for Planetary Mission
Alpha Particle X-ray Spectrometer onboard Chandrayaan-2 rover

Alpha Particle X-ray Spectrometer (APXS) is one of the two scientific payloads on Chandrayaan-2 rover.

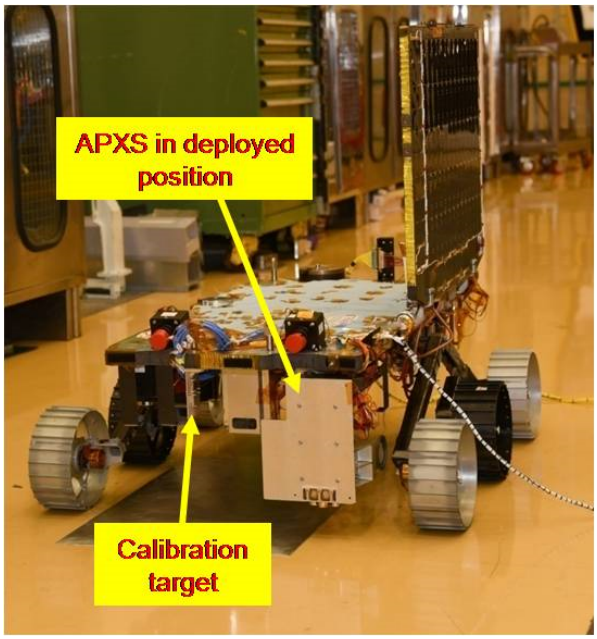


Figure 31: Photographic view of Flight Model of the APXS payload integrated with Ch-2 Rover.

Primary scientific objective of APXS is to determine the elemental composition of the lunar surface in the regions surrounding the landing site. This will be achieved by employing the technique of X-ray fluorescence spectroscopy using in-situ excitation source in the form of an alpha source having both X-ray and alpha particle emissions. These radiations excite the elemental characteristic X-rays by the processes of particle induced X-ray emission (PIXE) and X-ray fluorescence spectroscopy (XRF). The characteristic X-rays are detected by the 'state-of-the-art' X-ray detector known as Silicon Drift Detector (SDD), which provides high energy resolution as well as high efficiency in the energy range of 1 to 25 keV. This enables APXS to detect all major rock forming elements like Na, Mg, Al, Si, Ca, Ti, Fe etc. and some trace elements such as Sr, Y, Zr which are found in the lunar surface. The Flight Model (FM) of the APXS payload has been completed and tested for various instrument parameters. The developed APXS instrument provides energy resolution of $\sim$140 eV at 5.9 keV for the detector operating temperature of $\sim$ -35°C. Subsequently, the interface tests of FM version of the payload with Chandrayaan-2 Rover subsystems has been completed as shown in figure 31. The APXS payload has been tested with Rover at various stages for last one year and the performance is normal. The actual radio-active source Cm-244 with 30 mCi activity has been integrated with APXS during phase-2 of thermo-vac which was specially planned for APXS experiment. During this phase, the APXS is operated as planned on the moon. The calibration plate spectrum is acquired during the stowed condition and the aluminium target spectrum is acquired in the deployed condition. The calibration plate spectrum is as shown in figure 32, showing clearly identified spectral lines from the metal targets. This measurement is repeated after the rover movement inside the thermo-vac. The calibration target spectrum will be acquired as when required on moon surface and will be used for the APXS energy calibration. The data processing and pipeline software for the APXS instrument namely APXS Data Analysis Software (APXSDAS) has been developed. The adequacy of APXSDAS has been reviewed and subsequently this software has been tested at Indian Space Science Data Center (ISSDC) Bylalu. A quick look software for the first cut verification of the data from APXS instrument has been developed and a sample window is as shown in figure 33.

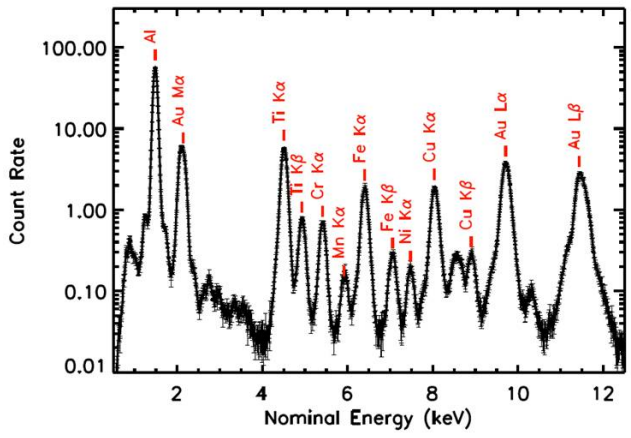


Figure 32: The XRF spectrum obtained from the calibration target plate using actual Cm-244 radio-active alpha source along the Rover.

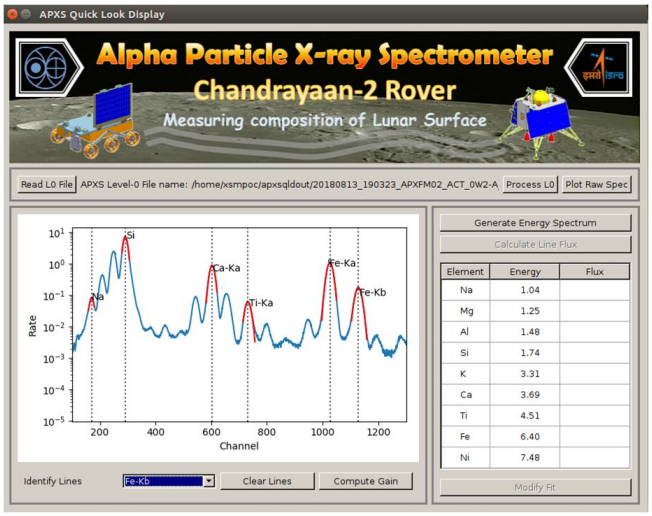


Figure 33: APXS quick look software window.

(M. Shanmugam, S. V. Vadawale, A. Patel, N. P. S. Mithun, Hitesh Kumar, S. K. Goyal, T. Ladiya, N. K. Tiwari, N. Singh, S. Kumar and D. K. Painkra)

Solar X-ray Monitor (XSM) onboard Chandrayaan-2 Orbiter

Solar X-ray Monitor (abbreviated as XSM) is one of the scientific instruments on-board Chandrayaan-2 orbiter. XSM along with another instrument CLASS (Chandra's Large Area Soft x-ray Spectrometer) comprise the remote X-ray fluorescence spectroscopy experiment of Chandrayaan-2 mission with an objective to determine the elemental composition of the lunar surface on a global scale. XSM instrument will accurately measure the Solar X-rays in the energy range of 1-15 keV using state-of-the-art Silicon Drift Detector (SDD). The Flight Model (FM) of the XSM payload has been designed, realized and characterized for various instrument parameters.

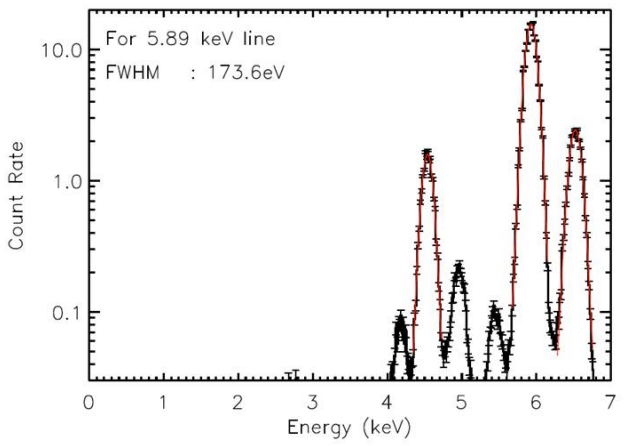


Figure 34: Spectral response of XSM payload integrated with Ch-2 spacecraft using calibration source 55Fe.

XSM provides energy resolution of ∼180 eV at 5.9 keV with high time cadence of one second. Solar X-ray spectra observed with XSM will also contribute to the study of Solar Corona. Flight Model of XSM is realized after verification of performance of the qualification model during various environmental tests. Further, the flight model of the instrument has undergone extensive test and evaluation. Subsequently, the interface tests of FM version of the payload with Chandrayaan-2 Orbiter subsystems has been completed. The XSM payload has been tested with spacecraft at various stages for last one year and the performance is normal as shown in figure 34. It is well known that in X-ray spectrometers, the peak energy channel varies with the incident rate and the energy resolution (FWHM) is expected to degrade beyond a limit of count rate. In order to verify performance of XSM as function of incident rate, experiment was carried out at X-ray beam line BL-16 of Indus-2 synchrotron facility at RRCAT, Indore. Data was acquired with XSM by varying the incident rate using slits in the beam line. Monochromatic line at 5.0 keV is fitted with a Gaussian to obtain peak channel and FWHM as a function of incident rate as shown in figure 35. It is to be noted that upto an incident rate of 1E5 counts/s the variation in peak channel is less than ∼2 % and FWHM variation is within 4 %. Beyond that rate, both peak channel and FWHM begins to vary drastically. This shows that the spectral performance of XSM is not affected significantly up to incident count rates of 1E5 counts/s, as required. The data processing and pipeline software for the XSM instrument namely XSM Data Analysis Software (XSMDAS) has been developed. The adequacy of XSMDAS has been reviewed and subsequently this software has been tested at Indian Space Science Data Center (ISSDC) Bylalu. A quick look software for the first cut verification of the data from XSM instrument has been developed and a sample window is as shown in figure 36.

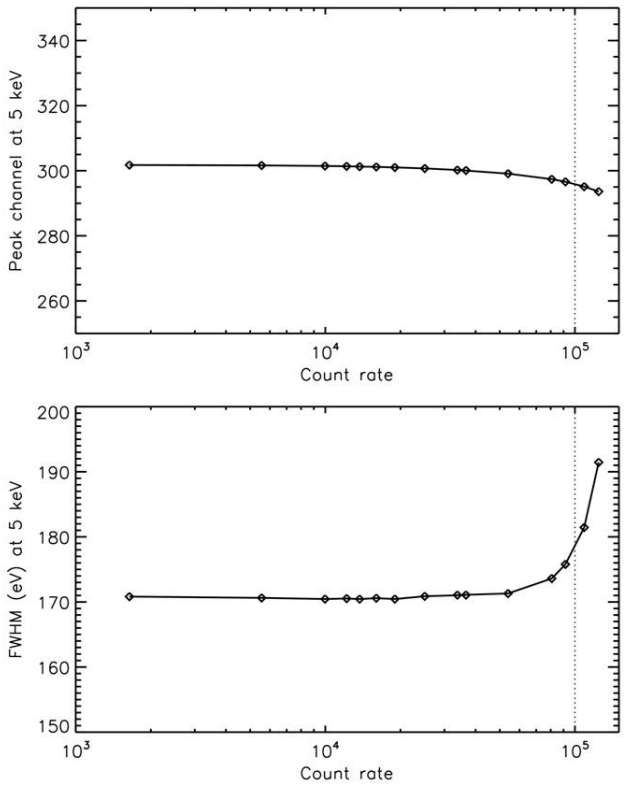


Figure 35: High count rate performance measurements of the XSM payload using monochromatic beam line.

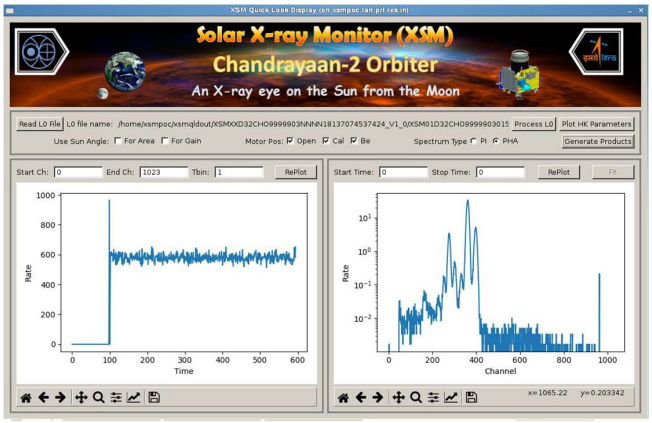


Figure 36: XSM quick look software window.

(M. Shanmugam, S. V. Vadawale, A. Patel, N. P. S. Mithun, Hitesh Kumar, S. K. Goyal, T. Ladiya, N. Kumar Tiwari, N. Singh, Sushil Kumar and D. K. Painkra)

MODEX Detector and Electronics

To study interplanetary dust at Mars, a Mars Orbit Dust Experiment (MODEX) is proposed for future Mars orbiter.

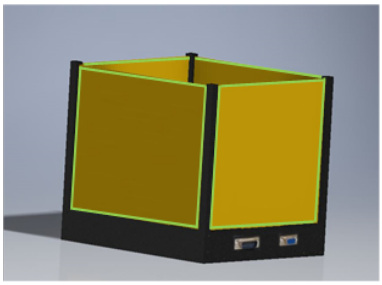


Figure 37: A dust detector under fabrication in workshop.

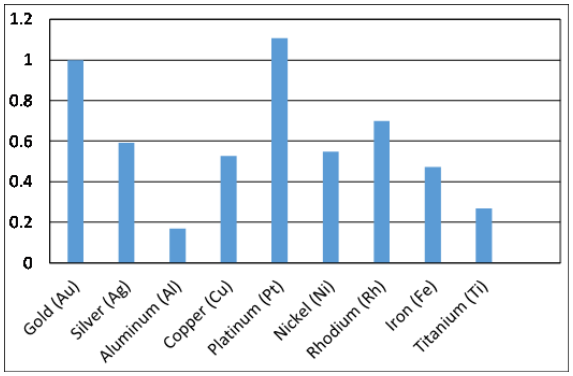


Figure 38: Yield comparison of various target materials with respect to that of gold (Pabari et al., PSS, 2018).

The additional objective is to measure interplanetary dust particle (IDP) during cruise phase between Earth and Mars. Hypervelocity dust impact on detector target creates charge carriers, which can provide the information about the incoming dust particles. Figure 37 shows an updated version of dust detector which is under fabrication in PRL workshop. The dust detector target is usually made from gold material. We have applied the impact plasma theory first time for designing the detector and carried out the optimization. Due to the dust impact on different target materials, different yields are produced. We have compared performance of various materials with respect to that of gold as shown in Figure 38. One can observe from Figure 39 that platinum is better than gold, however, practically it is difficult to make foils from the platinum. Hence, gold is suggested as the detector target for impact ionization dust detector. Further, a small crater is formed on detector target due to dust impact. We have computed its value for incoming IDPs and results are depicted in Figure 39, which can help decide the detector target thickness. A laboratory model of the detector has been made and its detection electronics is developed using COTS components. Further, MODEX electronics has been in development and its detailed block diagram is shown in Figure 40. Similarly, a power scheme of MODEX is also designed. Further work is underway.

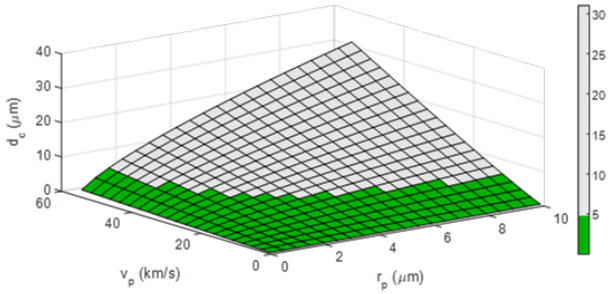


Figure 39: Crater diameter due to dust impact on gold surface of the detector as a function of incoming particle radius and particle speed. Green zone indicates the particles found in nature, i.e., smaller particles travel with larger speeds and larger particles travel with lesser speeds (Pabari et al., PSS, 2018).

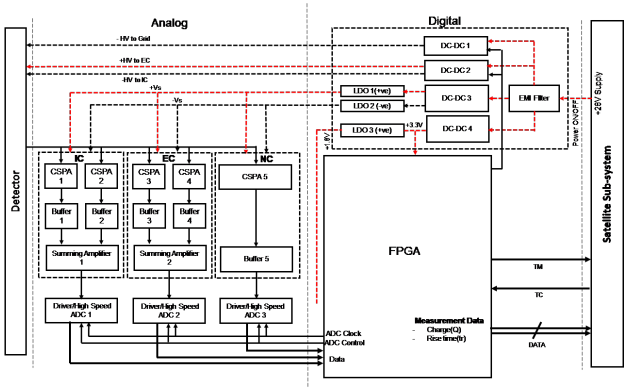


Figure 40: MODEX electronics.

(J. P. Pabari, S. Nambiar, D. Patel, S. Jitarwal, K. Acharyya, A. Bhardwaj, S. A. Haider, V. Sheel, B. M. Pandya, R. Mahajan and Team)

Laboratory Testing of MODEX

Extensive testing of the dust detector using a pulse laser has been carried out. During the hypervelocity particle impact on the dust detector the particle-target interaction times (∼10ns) is comparable with duration of pulsed laser. Hence, a ns pulse laser is used to mimic the impact which is created by a hypervelocity dust particle.

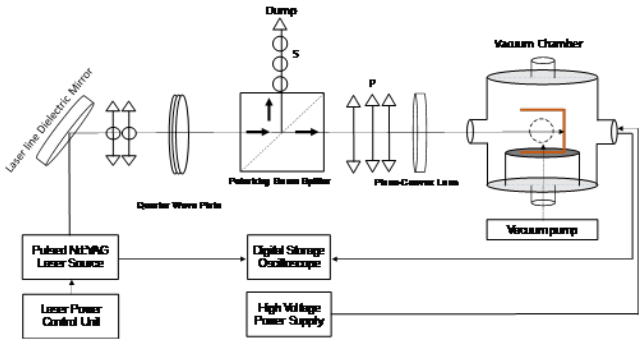


Figure 41: Optical set up of dust detector testing using Nd:YAG pulse laser with 1064 nm wavelength.

The optical set up for the experiment is shown in Figure 41, where a Nd: YAG pulse laser is fired on target plate of the dust detector inside a vacuum chamber. The electrons and ions generated by the material ablation are captured using biased electrodes of the dust detector. The responses are processed in the processing electronics, which is also kept inside the vacuum chamber. The outputs from dust detector and trigger pulse of the laser are displayed on an oscilloscope. Overall testing set up is depicted in Figure 42 and typical results are shown in Figure 43. Approximate equivalence of pulse laser with the dust particle parameters has been shown.

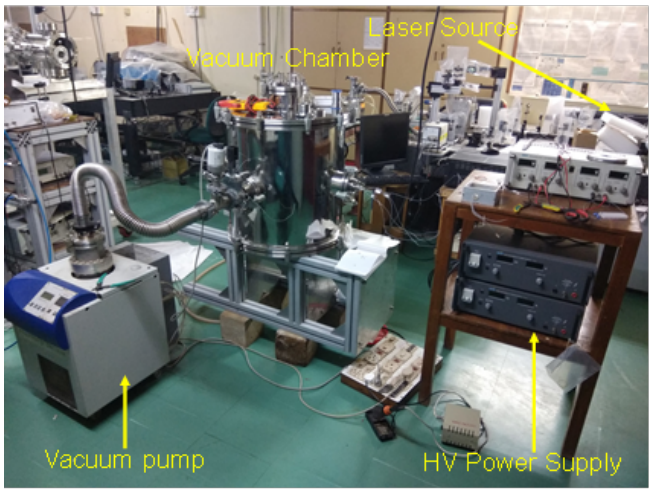


Figure 42: Snapshot of pulse laser testing set up.

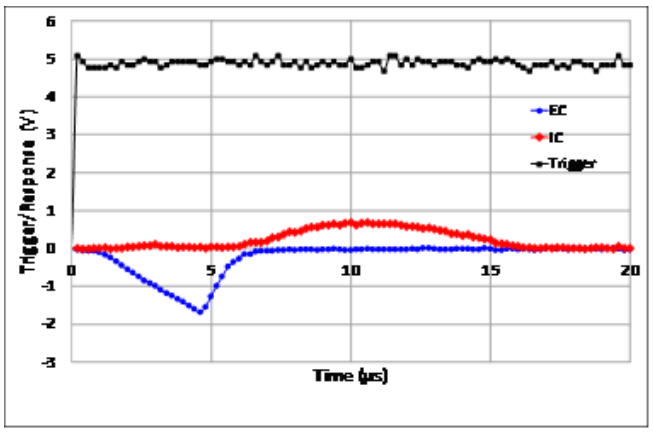


Figure 43: MODEX testing results, showing simultaneous extraction of electron channel (negative pulse, blue) and ion channel (positive pulse, red) signals (Pabari et al., PSS, 2018).

(J. P. Pabari, D. Patel, S. Nambiar, S. Jitarwal, R. Singh, R. Mahajan, A. Kumar, K. Acharyya, A. Bhardwaj, S. A. Haider, V. Sheel, B. M. Pandya and Team)

Venus Orbit Dust Experiment (VODEX)

The Interplanetary Dust Particles (IDPs) are expected to be coming from asteroid belt and bigger ($>$ 0.5 μm) partilces travel inward, toward the Sun. The IDP flux is known at Earth, however, it has not been measured at Venus, expect a few spot measurements at larger distances from Venus. The IDPs are ablated in the atmosphere when they enter Venus and contribute metal ions in the atmosphere, giving enhancement in the conductivity profile. A Venus Orbit Dust Experiment (VODEX) is proposed for future Venus orbiter to study flux and distribution of high altitude dust at and around Venus and also between Earth and Venus. The detector is similar to MODEX given above. A laboratory model has been designed, developed and tested using a pulse laser.

(J. P. Pabari, D. Patel, S. Nambiar, S. Jitarwal, K. Acharyya, R. Mahajan, R. Singh, A. Bhardwaj, S. A. Haider, V. Sheel, B. M. Pandya, A. Kumar and Team)

Lightning Instrument for VEnus (LIVE)

Lightning is a transient electrical discharge occurring in planetary atmosphere, which generates optical signal, electromagnetic waves in ELF-VLF/Radio range as well as acoustic waves. Lightning on Earth is caused due to convective motion of atmospheric ions and the electrification of colliding precipitation. In addition, the lightning can also be produced in dust/snow storms and volcanic clouds. There are sulphuric acid clouds on Venus from ∼47 to 65 km altitudes, where lightning is expected to occur. Some past observations exist, suggesting lightning activity in night side of Venus. The flash rate, strength, cloud model etc are yet to be fully understood on Venus. A Lightning Instrument for Venus (LIVE) for future orbiter is

proposed to study the lightning on Venus in ELF-VLF/Radio frequency range. A laboratory model has of LIVE has been developed and demonstrated working successfully for natural lightning on Earth. Figure 44 depicts the instrument model, Figure 45 shows snapshot of one of the natural lightning events, captured using an optical camera, Figure 46 depicts lightning signal captured by the instrument on 17^{th} August 2018 at PRL Thaltej campus, while Figure 47 shows time-frequency analysis of the signal. Further work is underway.



Figure 44: Laboratory model of LIVE kept on terrace of PRL Thaltej campus.



Figure 45: Snapshot of one of the lightning events, captured using an optical camera on 2^{nd} July 2018.

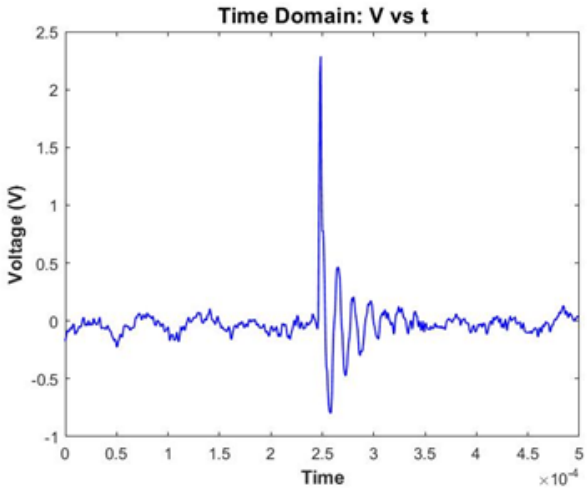


Figure 46: Captured lightning signal which occurred on 17^{th} August 2018 at PRL Thaltej campus in Ahmedabad.

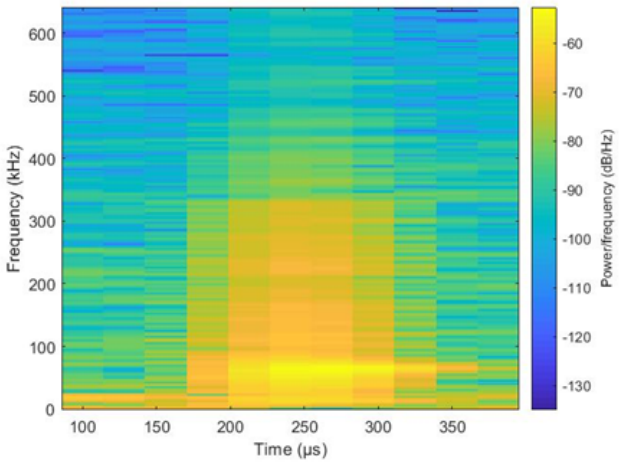


Figure 47: Time-frequency analysis of the captured lightning signal, showing lightning transient in time domain and lightning frequency components in frequency domain.

(J. P. Pabari, S. Jitarwal, D. Kumar, S. Nambiar, D. Patel, K. Acharyya, A. Bhardwaj, V. Sheel and Team)

Pre-flight activities and Characterisation of ChaSTE through laboratory based thermophysical measurements

A payload called “Chandra’s Surface Thermophysical Experiment (ChaSTE)” for Chandrayaan-2 Lander (Vikram) is being developed jointly by PRL, Ahmedabad and SPL/VSSC, Trivandrum. In addition to the other responsibilities, the front-end electronics card of the payload is designed and developed at PRL. The qualification and flight models of the same have been realised and delivered to SPL/VSSC for integration and further activity. The FE electronics card and the integrated electronics box of ChaSTE are shown in figure 48. The entire payload is now integrated with the Chandrayaan-2, Vikram lander and currently undergoing various qualification tests. PRL team is involved in all these activities currently being carried out at URSC, Bangalore. The results of ChaSTE measurements during Integrated and Assembled Mode Tests with the Lander are satisfactory. On the other hand, it has been reported earlier that a calibration and characterization facility has been setup in our SIMPEX (Simulations for Planetary Exploration) Lab at PRL for ChaSTE payload which was developed for Chandrayaan-2 Lander. The aim of this setup was to cater to the needs of calibration and characterization aspects of ChaSTE at various stages. Using this setup, we have carried out laboratory experiments for characterising the ChaSTE payload which is an important aspect of interpreting the post-flight data from ChaSTE. The experimental setup has been used to derive the thermal diffusivity of a various soil samples of known bulk density. The setup is shown in figure 49. Initially, the electronics was calibrated using a Reference Calibrator. The sample was kept in a cylindrical sample holder which was illuminated with a halogen lamp that served as a simulator for solar insolation. RTD sensors, PT1000 in this case, were inserted at varying depths into the sample cup to give a vertical profile of temperature gradient as in the case of ChaSTE experiment. These RTD sensors were interfaced to the front end electronics card of

ChaSTE which consists of signal conditioning, RTD excitation circuitry, multiplexing and digitization of analog data. The temperature data obtained at different depths (z) from the top layer of sample was monitored and continuously logged using a microcontroller based processing card developed at PRL. Experiment was continued till equilibrium condition of temperature is achieved by the bottom most sensor. One such plot for 2 sensors at equilibrium is shown in figure 49. Using this time varying temperature data, the thermal diffusivity of the soil sample is derived through amplitude decay method. The experiment was repeated multiple times to correct for the systematic errors in the measurements. The thermal diffusivity of the same soil sample is also measured using a standard reference system. It was found that the results from ChaSTE like setup are in good agreement with that of those measured using a standard reference system.

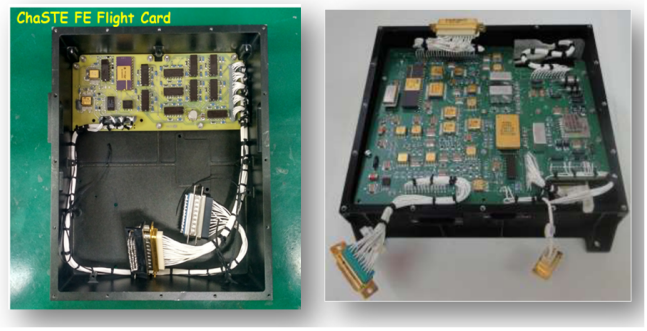


Figure 48: Flight Model Front-End electronics and integrated electronics box of ChaSTE

Table 1: Comparison of Thermal diffusivity of a Sample obtained from ChaSTE with that from a standard measurement system

Measurement System	Thermal Diffusivity (m^2/s)	Average Thermal Diffusivity (m^2/s)
Standard Measurement System	1.63×10^{-7} 1.67×10^{-7} 1.69×10^{-7} 1.66×10^{-7}	1.663×10^{-7}
ChaSTE	1.66×10^{-7} 1.63×10^{-7}	1.645×10^{-7}

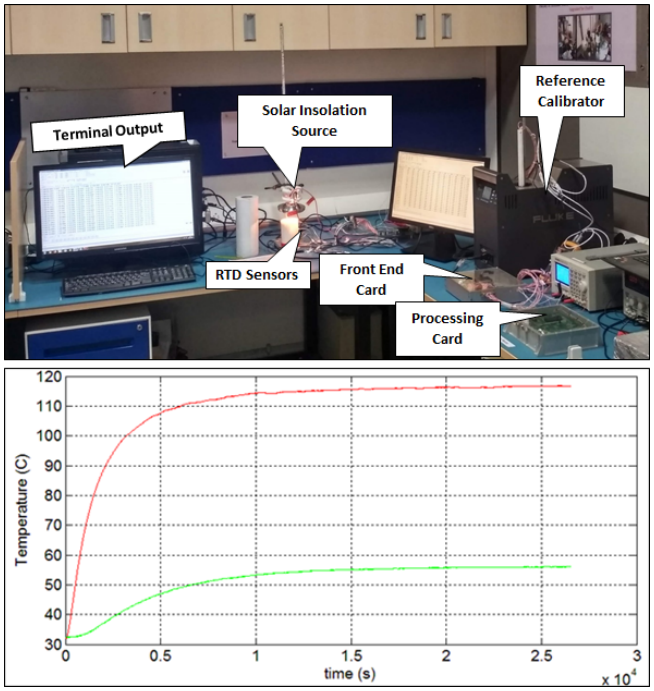


Figure 49: Experimental setup for ChaSTE Characterisation and time dependent temperature profile of one soil sample

(K. Durga Prasad, Chandan Kumar, S. Mishra, P. K. S. Reddy, Janmejay Kumar, T. Ladiya, A. Bhardwaj and ChaSTE Team)

A 3D model study to understand the role of probe material on the performance ChaSTE experiment

ChaSTE ('Chandra's' Surface Thermophysical Experiment) experiment is being flown on Chandrayaan-2 lander for obtaining an insight into the thermophysical behaviour of the surficial lunar layer of the Moon at a high latitude region for the first time. Experimental details of this experiment have been reported earlier. ChaSTE experiment deploys a thermal probe that contains a series of temperature sensors which are made to be in contact with the soil to obtain surface/subsurface thermal profile. When ChaSTE probe is deployed into the surface of the moon, the four wire RTD sensors assembled onto the probe starts measuring the vertical temperature profile as a function of time. The top few centimetres of lunar regolith is porous with very low thermal conductivity while the thermal conductivity of the probe material is an order of magnitude higher than that of the surrounding soil. Thus, the probe shunts more heat into the subsurface than that of the surrounding soil itself and could perturb the thermal measurements carried out from ChaSTE. In order to derive accurate temperature values from ChaSTE measurements, the effect of probe and sensor material on the temperature measurements needs to be properly assessed and corrected for. Therefore, we have developed a three dimensional finite element model to derive appropriate correction coefficients that may be applied to the post-landing data. The exact CAD model of the probe along with sensors is realised A 1 m x 1 m lunar regolith is modelled in such a way that the imported probe is inserted in the soil. With material properties assigned and a semi-sinusoidal function of solar heat flux as the boundary conditions, the simulation was carried out for few lunar days. The vertical temperature profile is also obtained simultaneously at a far off distance (where the effect of probe material on surrounding soil is negligible) from the probe and compared to the values obtained for the one close to the sensing

element of sensor. Correction ratios were obtained for each of the sensors to arrive at realistic temperature values from the experiment.

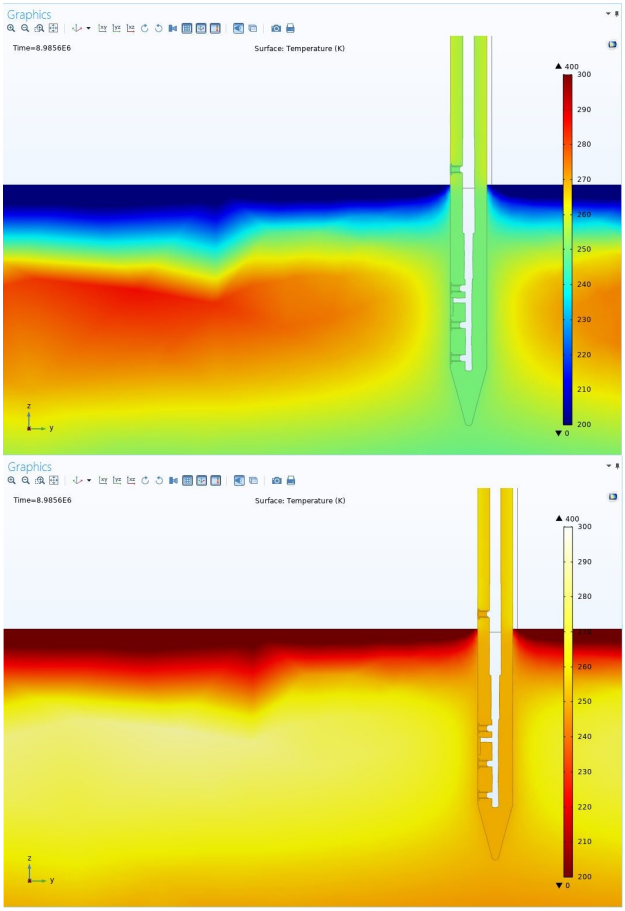


Figure 50: The cross section of probe and soil during night and daytime. The disturbed temperature profile due to the presence of the probe can be seen near the probe.

(K. Durga Prasad, Chandan Kumar, S. Mishra, P. K. S. Reddy, Janmejay Kumar, T. Ladiya, A. Bhardwaj and ChaSTE Team)

Front-End development of Langmuir Probe for (LPEX) on-board MOM-2

We are developing a Langmuir Probe and Electric Field experiment for Indian Mars Orbiter Mission-2 which was already reported earlier.

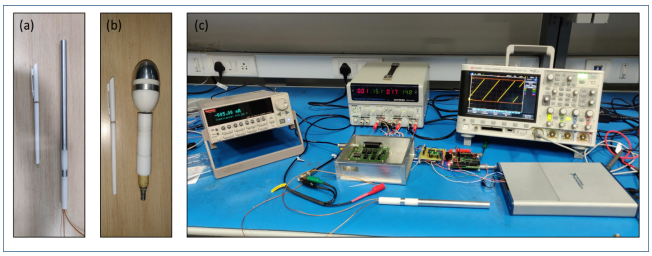


Figure 51: (a) The designed Cylindrical sensor (b) The designed Hemispherical sensor (c) The complete electrometer with Auto-Gain switching and sweep bias generator

LPEX experiment aims at in situ investigation of electron density, electron temperature and electric field in the vicinity along the spacecraft path at different regimes of upper atmosphere of Mars. LPEX consists of two independent instruments, a Langmuir probe (LP) and Electric field (EF) experiment. Development of Langmuir probe involves several challenges viz. probe with miniaturized pre-amplifier, precision current and voltage monitoring, sweep and bias generation, isolation, filter design and signal processing etc. The engineering model of the instrument is currently under development. Precision electrometer and sweep bias electronics have been developed and tested. The designed electrometer is capable of sensing currents ranging from $\sim$0.1nA – 0.01μA with a resolution of $\sim$0.08 nA. The design incorporates automatic gain switching for various ranges of ambient electron densities. The response time for the electrometer is around 33ms. The sweep bias electronics is fully programmable and was developed for a range of -20V to +20V in step sizes of 10mV. For evaluation purposes, two different type of sensors, cylindrical and spherical, are developed for characterisation and proper science goal derivation. The processing and power system design of the Langmuir probe is currently under progress. Figure 51 shows the prototype sensors and their DVM electronics and their evaluation.

(K. Durga Prasad, Chandan Kumar, S. K. Mishra, P. K. S. Reddy, Janmejay Kumar, V. Sheel, S. A. Haider and A. Bhardwaj)

Development of Front End Electronics for Electric Field Experiment for MOM-2

The irregularities in plasma densities in the ionosphere of Mars gives rise to electrostatic electric field in that region. Understanding of electric field level and its variability with time and space will help understand the plasma dynamics of Martian ionosphere.

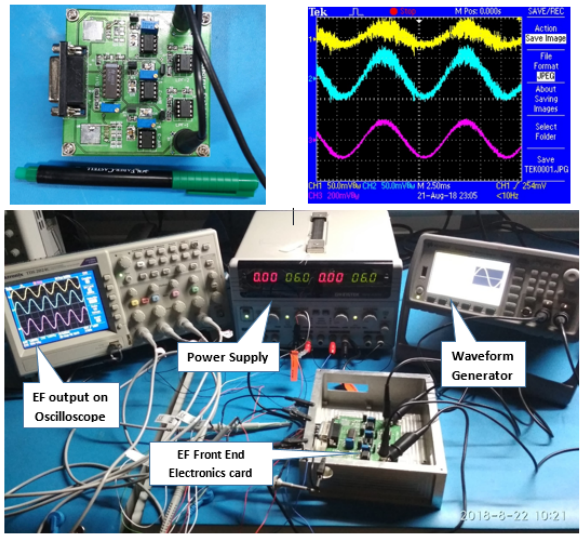


Figure 52: PCB, Test results and complete test setup for Electric Field Measurement

Electric field detection of plasma waves serves as an indicator for understanding the bow shock processes, magneto sheath and magneto tail boundaries. Electric field measurements using Double Probe technique are very popular and have been used on several missions. One of the instrument of LPEX experiment being developed

for Indian Mars Orbiter Mission-2 is the Electric field (EF) instrument. A lab verification model of front end electronics of this EF instrument has been designed and tested. It consists of a voltage sense unit to differentiate the voltage levels captured by the two probes and a gain stage followed by a filter bank. We have evaluated two schemes - one having difference amplifier as voltage sense unit with single OpAmp, manual switched filter banks and the other having a programmable gain instrumentation amplifier as voltage sense unit with Discrete Filters for each band. The first scheme trades off performance over space and power while the second scheme trades of space and power over performance. The filter banks consisted of following frequency ranges- one low pass Filter with cut off at 1KHz, three band pass filter 1-5 kHz, 5-10 kHZ, 10-50 kHz. One of the populated cards, result and the complete test setup is shown in figure 52.

(K. Durga Prasad, Chandan Kumar, S. K. Mishra, P. K. S. Reddy, Janmejay Kumar, V. Sheel, S. A. Haider and A. Bhardwaj)

Design and development of deployment mechanism for LPEX payload for MOM-2

A Langmuir probe and electric field experiment (LPEX) is being developed to be flown on Indain Mars Orbiter Mission-2. LPEX consists of a Langmuir probe sensor and two electric field sensors each mounted ona boom of lenth $\sim$1.5 m. All the three booms would be in stowed condition during flight and needs to be deployed once MOM-2 reaches the designated orbit. Therefore, a deployment mechanism optimised in mass and power is being developed and tested.

The mechanism system consists of sensors which is on 1 m or 1.5 m Carbon Fiber Reinforced Polymer (CFRP) boom. In this mechanism two torsional springs have been used. The deployment is accomplished by releasing the stored energy by the springs. Initially during launch, boom will be stowed with the help of a Frangibolt and will be deployed into desired orbit using a ground command. The design is highly optimised in mass and requires a very low power, only for frangibolt operation. A lab verification model of the mechanism has been developed and demonstrated. We have also carried out a preliminary structural analysis of the designed mechanism.

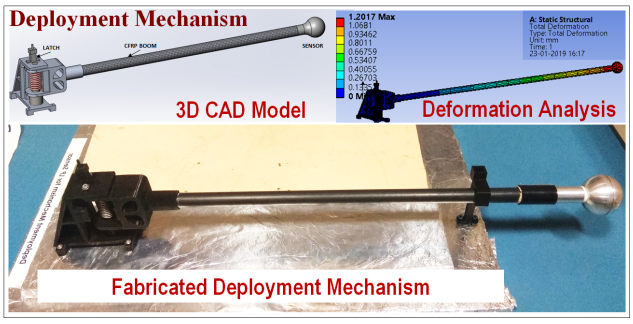


Figure 53: The designed CAD, structural analysis and actual model of the mechanism

(Janmejay Kumar, P. K. S. Reddy and K. Durga Prasad)

Langmuir Probe Characteristics for low density space plasma conditions through finite element simulations

Planetary ionospheres are characterised by complex plasma distribution and dynamics. Depending on the altitude, the plasma densities can vary from few electrons/ions per cm^3 to $\sim$10^6 electrons/ions per cm^3 which are nominally termed as low density plasmas. Such a low density space plasma encountered in the planetary ionospheres are primarily measured using the Langmuir probe technique. A Langmuir probe consists of a sensor which is a metallic conductor exposed to space plasma whose characteristics needs to be assessed apriori. For this purpose, we have made an attempt to simulate this conductive spherical Langmuir probe in low density plasma and examined its performance as a function of various parameters viz. material properties, diameter, voltage biasing etc. through finite element simulations. Low density plasma measurements pose extreme challenge in simulating as their densities can go below 10 electrons/ions per cm^3.

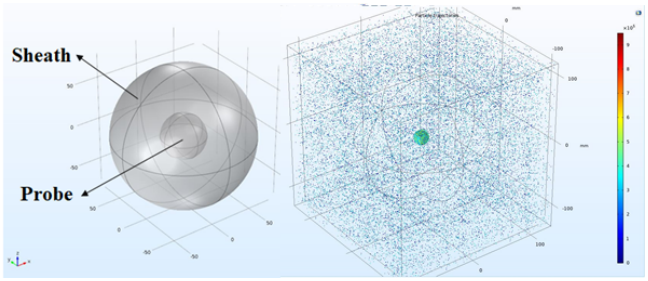


Figure 54: Configuration of the simulation and the Simulated Particle cloud around a spherical probe for a particular condition

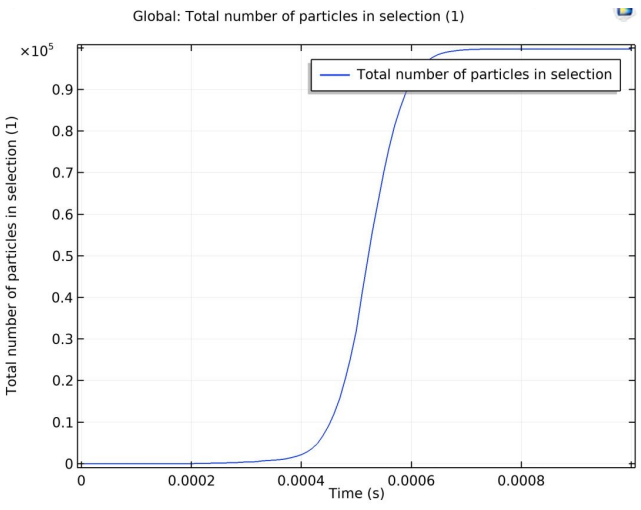


Figure 55: A plot showing the total number of particles falling onto the probe as a function of time (for a particular condition)

Further, the sensor dimensions are constrained by the minimum detectable current and the sheath dimension. Using the Charge Particle Tracing theory, we have tried to generate a volume consisting of positive and negative charges with some electron/ion density. There is a provision to manipulate the particle velocities as well, which have

been used to evaluate the particle trajectories. Particle trajectory affects the current collection properties of the probe when operating in Orbital Motion Limited (OML) current collection regime. A spherical probe of 1 cm radius is modelled with a concentric sheath boundary inside a cube of side 25 cm as shown in the figure 54. Particles are released as a cloud surrounding the probe and a known voltage function is swept on the probe surface with respect to the sheath boundary which is at ground potential. The particles falling onto the probe as a function of time are plotted as shown in figure 55. However due to large computational time the sweep period is limited to one millisecond as of now. Effort is underway to improve the simulations further.

(P. K. S. Reddy, K. Durga Prasad, S. K. Mishra and Chandan Kumar)

Design and Development of an Anemometer Prototype for Planetary Exploration

Wind velocity is an important in situ meteorology measurement on planetary bodies like Mars and Venus. Direct measurement of winds was feasible only occasionally on the planets and vertical profiles were obtained through entry probes using interferometric tracking from Earth This has been successfully done for Venus, Jupiter and Titan.

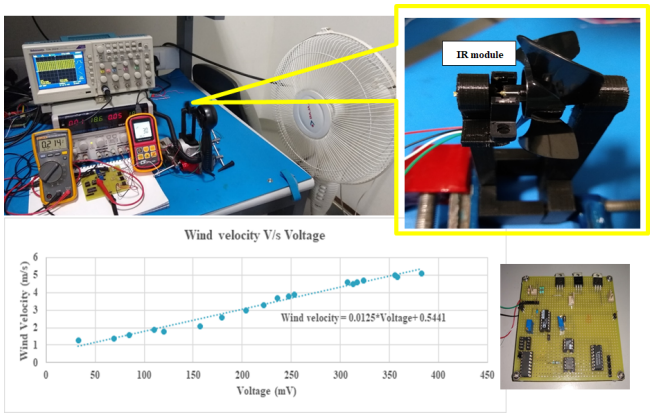


Figure 56: Test setup and results of anemometer prototype developed at PRL

Acoustic technique can also be exploited for in situ wind velocity measurements on planetary bodies. Anemometers are simple yet effective way to measure wind velocity especially in planetary environment. Unlike for terrestrial applications, such a design should be rugged where reliability and performance are most important factors. An effort is being made to develop an anemometer for planetary wind velocity measurements to be flown on a future mission. The development of an anemometer for planetary exploration, especially Venus, involves the design of a vane and sensor capable of measuring velocities in the range from 10m/s up to 300m/s. We have developed a proto-type of the front-end for such a system and evaluated its performance. The front-end consists of a special sensor arrangement that translates the motion of the vane to frequency followed by a signal conditioning electronics along with various other power modules and biasing electronics. The sensor combined with front-end electronics produces output in the form of pluses whose frequency is proportional to the wind velocity. This frequency is then converted to voltage and further digitized using a 12-bit ADC. Industrial grade components of qualified parts were identified and used in the development of the prototype. The developed prototype of the anemometer, its testing and test results are shown in figure 56.

(T. Ladiya, K. Durga Prasad, Chandan Kumar and P. K. S. Reddy)

RPA Sensor and front-end development for future planetary missions

A retarding potential analyser (RPA) experiment is being developed as a joint payload of PRL, Ahmedabad and IIST, Trivandrum for the both upcoming Mars and Venus missions of India. PRL is a lead team in Science while IIST will develop the instrument. At PRL, we are also developing the experiment in parallel with a different design as a backup which be flown on any future mission. The instrument being developed uses multi-layer grids biased at different Potentials. The instrument is capable of detecting both ions and electrons. Electrons are detected when the outermost grid is biased at negative potential while the grid is positively biased for acquiring electrons. The plasma particles pass through the different grids based on their charge and fall on a collector plate. The particles hitting the collector results in generation of a current. This current with respect to the applied bias results in a characteristic curve. One of the important aspect of this instrument is the precise design and fabrication of the sensor. Based on the CAD model which was reported earlier, the sensor for RPA has been fabricated and assembled. The front-end electronics to be used with the sensor is also designed and integration with the sensor is currently under progress.



Figure 57: The fabricated parts of RPA sensor

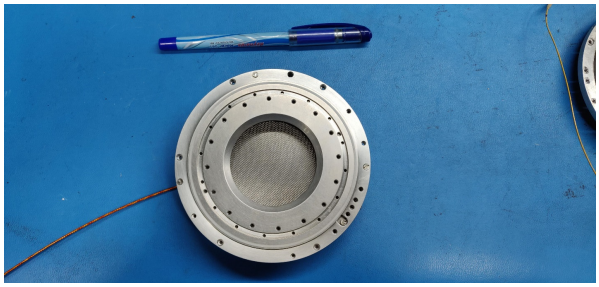


Figure 58: The Assembled RPA sensor with SS Mesh

(Chandan Kumar, K. Durga Prasad, S. K. Mishra, Janmejay Kumar, P. K. S. Reddy, V. Sheel, S. A. Haider, A. Bhardwaj and H. Vaghela)

Supra Thermal & Energetic Particle Spectrometer (STEPS) - Subsystem of ASPEX payload

Aditya Solar wind Particle EXperiment (ASPEX) is one of the seven scientific experiments onboard the Aditya - L1 mission (the forthcoming Indian solar mission), to be placed in a halo orbit around the L1 Lagrangian point of the Sun-Earth system, at a distance of 1.5 million km from the Earth. ASPEX will carry out the in-situ, multi-directional measurements of the slow and fast solar wind, supra-thermal particles and solar energetic particles in the energy range of 100 eV to 20 MeV/n with its two sub-systems namely Solar Wind Ion Spectrometer (SWIS) and Supra Thermal & Energetic Particle Spectrometer (STEPS). SWIS measures the angular and energy distribution of solar wind ions in the energy range of 100 eV to 20 keV and STEPS measures the energy spectrum of high energetic particles from six directions covering the energy range of 20 keV/n to 20 MeV/n. The scientific objective of the STEPS is to investigate the origin of the suprathermal particles and their relationship with the primary solar wind constituents.

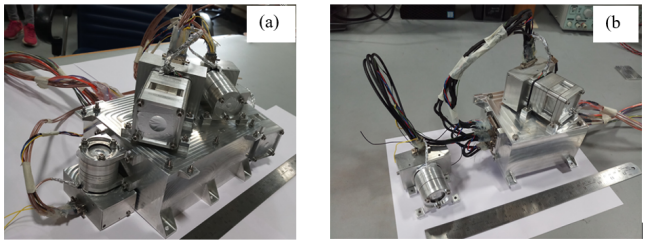


Figure 59: (a) STEPS-1 engineering model, (b) STEPS-2 engineering model

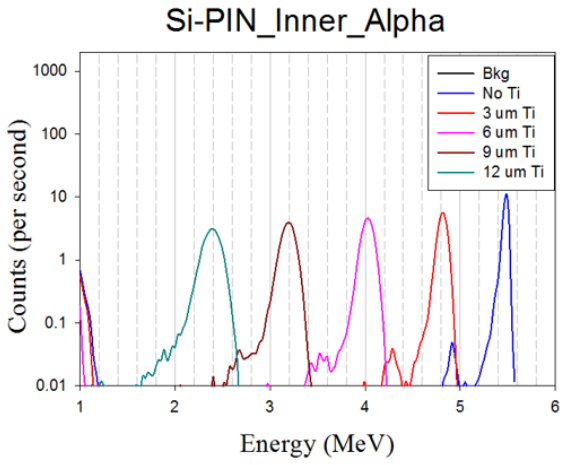


Figure 60: STEPS-2 dual window detector test results using high-energy alpha source (Ealpha = 5.4 MeV)

The STEPS subsystem has been configured into two packages: STEPS-1 and STEPS-2. STEPS-1 has four detector units for four different directional measurements (1) Sun Radial, (2) Intermediate to Sun radial and Parker Spiral, (3) Parker Spiral and (4) Northward direction. STEPS-2 has two detector units for two directional measurements (1) Earthward direction and (2) Southward direction. Figure 59 shows the engineering models of the STEPS-1 & STEPS-2.

STEPS-2 has been subjected to high energy particle tests. Figure 60 shows the detection of 5.4 MeV alpha particles and attenuated energy using several Titanium foils. Dual window Si-PIN detector and single window Si-PIN detector both have been tested using Pelletron facility of TIFR-Mumbai for the high-energy proton detection in the ΔE-E mode. Figure 61 shows the results of dual window detector using high-energy proton beam in ΔE mode. The engineering model is ready for STEPS. Thermal & structural analysis have been completed. The realization of the qualified model (QM) & flight model (FM) is going on.

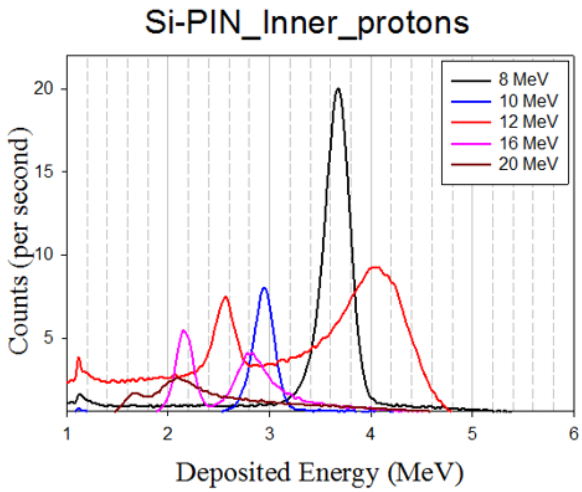


Figure 61: STEPS-2 dual window detector test results using high-energy protons (8 MeV – 20 MeV) at TIFR Pelletron facility

(S. K. Goyal, M. Shanmugam, A. R. Patel, N. K. Tiwari, T. Ladiya, A. Sarada, S. V. Vadawale, P. Janardhan, D. Chakrabarty, A. Sarkar, A. Auknoor, P. Sharma and Team)

Design & development of position sensitive Hard X - ray detector using Scintillator and SiPM

Position sensitive spectroscopic detectors operating in the hard X-ray energy range have a wide array of applications in high-energy astrophysics, planetary explorations, industrial measurements, security and medical imaging. Though the specific requirements of detector characteristics for each of these applications may differ, common requirements include good spectral and spatial resolution, compactness and high detection efficiency.

Scintillation detectors read by conventional photo-multipliers (PMTs) are widely used in space-based observations as veto detectors for background rejection as well as high – energy X-ray spectroscopic detectors. However, large size of PMTs limits the spatial resolution of such detectors and their applications in high – energy astrophysics. With the use of SiPMs, instead of conventional PMTs for readout of scintillation detectors, it is possible to sample the scintillation photon distribution with smaller pixel sizes (e.g. $\sim$3 mm x 3 mm) and thereby achieve the spatial resolution of the order of mm while having energy resolution similar or slightly worse in comparison to semiconductor detectors, making them suitable for astrophysical

applications. Moreover, low operating voltages and insensitivity to the external magnetic fields of SiPMs are added advantages of such compact detector systems for space-based observatories.

In our experiment, we have carried out the development of the position sensitive detector (2D) using new generation scintillator and SiPM. Figure 62 shows the hybrid packaged $CeBr_3$ scintillation crystal packaged in an aluminum housing. A quartz window is provided on the readout side. The total size of the hybrid packaging is 33 mm x 33 mm x 9 mm with weight of 30 gm. The surface area of the crystal is 25 mm x 25 mm with thickness of 5 mm. The $CeBr_3$ crystals have been procured from M/s Scionix, Netherlands.

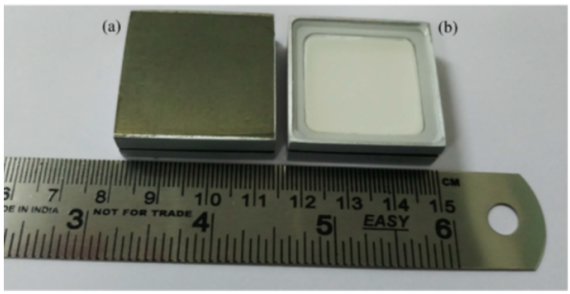


Figure 62: $CeBr_3$ crystal. (a) Top view, (b) Rear view

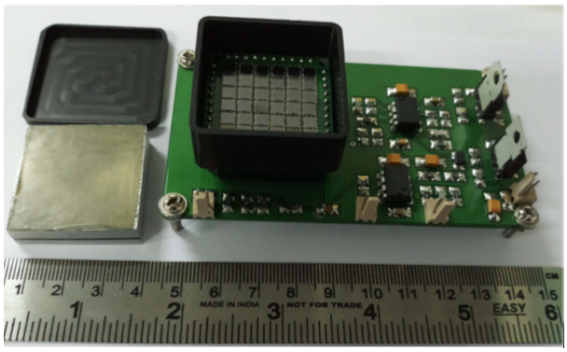


Figure 63: $CeBr_3$ scintillator detector with SiPM array (6x6) interfaced with the CSPA and shaping amplifier.

Figure 63 shows experimental setup for the $CeBr_3$ scintillation crystal, readout by the 6x6 SiPM array along with the FEE board consisting of CSPA, shaping amplifier and voltage regulator circuit. The experiment is carried out in a light tight black Delrin box. This detector module has been tested at $\sim$25°C operating temperature using different X-ray sources: ^{241}Am, ^{109}Cd and ^{57}Co. The energy spectrum shown in Fig. 64 is for the biasing voltage of 26.5 V_{dc}. The pulse peaking time of the shaping amplifier is 0.3 μs. The lower energy threshold obtained is $\sim$10 keV and full width at half maximum (FWHM) at 59.5 keV is $\sim$13 keV.

We have also carried out experiment with X-ray source placed at different positions of the detector. Using the three-axis stage, the position of the source was varied by 1 mm in x and y directions and data was acquired. After carrying out the MPFIT of the acquired data, the reconstructed positions for two cases are shown in Fig. 65, where the beam is placed 1 mm apart.

The project "position sensitive hard X-ray detector using scintillator and silicon photomultiplier (SiPM)" is under development as part of Technology Development Program (TDP) of PRL.

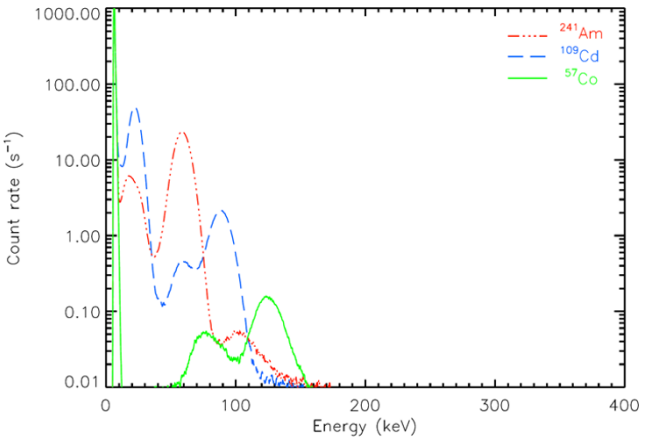


Figure 64: Spectra obtained with $CeBr_3$ scintillator and MicroC series SiPM array for three laboratory radioactive sources.

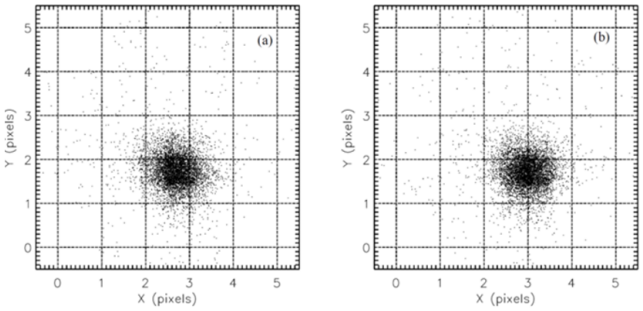


Figure 65: Scatter plot for reconstructed positions in two cases where X-ray beams are positioned at 1 mm apart on the $CeBr_3$ detector module.

(S. K. Goyal, S. Vadawale, Mithun N. P. S., N. K. Tiwari, A. Auknoor, P. Sharma and V. R. Patel)

Energetic Ion Spectrometer (EIS) for Mars Orbiter Mission (MOM-2)

Energetic particles of the solar and interplanetary origin continuously bombard the Martian ionosphere and can play an important role in the atmospheric loss processes at a shorter time scale. These particles can change the state of the Martian ionosphere significantly. In order to evaluate and quantify the changes in the Martian ionosphere due to the arrival of energetic particles generated close to the Sun during flare or due to the passage of interplanetary coronal mass ejection (ICME) and co-rotating interaction region (CIR), it is important to identify the arrival of these energetic particles at the Martian orbit relatively accurately. By measuring the alpha (H^{++}) - proton (He^{++}) ratio in the Solar Energetic Particles (SEP), the precise time of arrival of these particles at the

Martian orbit will be known. Further, measurements of the proton and alpha fluxes at the Martian orbit will also help to understand the energetic particle environment around the Martian orbit.

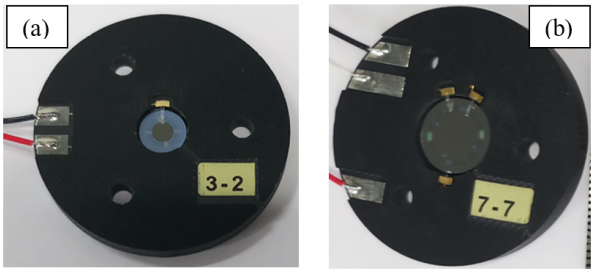


Figure 66: (a) 20 micron thick Si-PIN detector, (b) 1.5 mm thick Si-PIN detector

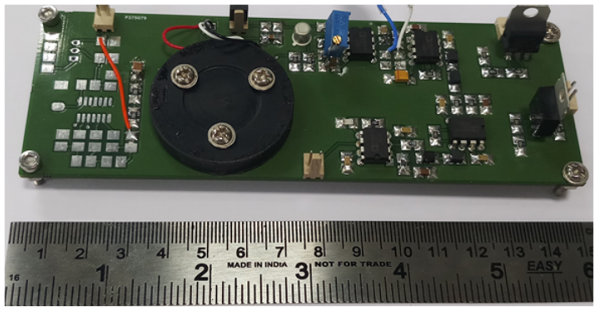


Figure 67: FEE PCB for 1.5 mm SiPIN detector

Keeping these objectives in mind, the Energetic Ion Spectrometer (EIS) is planned for future Indian Mars Orbiter Mission. The prime objective of the EIS is to make the in-situ measurements of the high-energy charged particles (H^+ and He^{++}) in the energy range of 20 keV/n to 20 MeV/n from the Martian orbit. EIS uses customized Si-PIN detectors in the ΔE-E configuration mode for the energy measurement and identification of the H^+ and He^{++} particles. It uses a stack of 20 μm thick and 1.5 mm thick Si-PIN detectors (Figure 66) to cover the entire energy range. Third detector is placed behind the 1.5 mm Si-PIN detector to work in the flag mode. This detector and the Anti-Coincidence Shield (ACS) are designed using plastic scintillator and Silicon Photomultiplier (SiPM) readout. Figure 66 shows the SiPIN detectors of thicknesses: 20 microns and 1.5 mm. The diameter of each of the detectors is 37 mm.

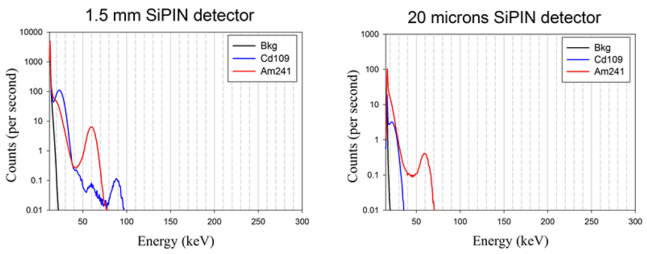


Figure 68: Preliminary results from SiPIN detectors using 241Am and 109Cd radioactive sources.

Front End Electronics (FEE) for both the detectors consists of two independent chains of charge sensitive preamplifiers, shaping amplifiers and discriminators circuits. Figure 67 shows the PCB designed and tested for 1.5 mm thick Si-PIN detector. Preliminary results acquired for both types of detectors are shown in Figure 68. It can be see that lower energy threshold achieved for both the detectors is $<$ 20 keV, as required for the EIS having energy range of 20 keV to 20 MeV/n. Stack of these detectors will be tested using high energy proton beam at TIFR Pelletron facility Mumbai in near future. The design of the engineering model is under process.

(S. K. Goyal, D. Chakrabarty, S. V. Vadawale, A. Sarda, A. Auknoor, N. K. Tiwari and P. Sharma)

Neutral & Ion Mass Spectrometer (NIMS)

Neutral and ion mass spectrometer is being developed as a new initiate for the in-situ measurements of neutral and ion species for future planetary missions. This has been proposed for the Venus Orbiter, the first Indian mission to Venus. The scientific objective of the instrument is to measure the composition, structure, variability and thermal state of the Venus atmosphere and its dynamics. The mass spectrometer will operate in the dual mode, separately for both neutrals and ions. The instrument will be operated from helium to mass 200 amu.

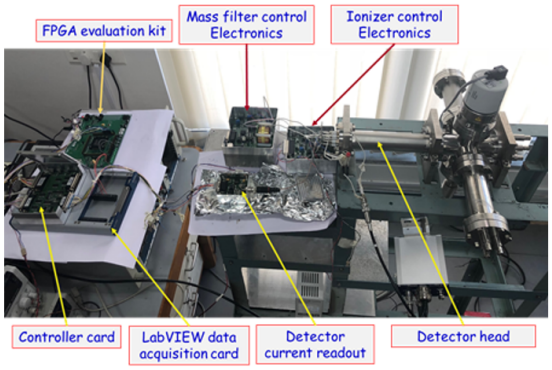


Figure 69: Hardware photograph of the quadrupole mass spectrometer.

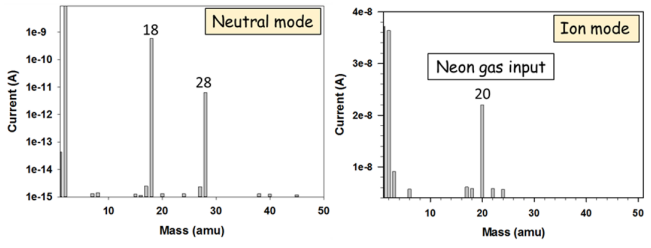


Figure 70: Preliminary results from the Quadrupole mass spectrometer for both neutral mode and ion mode.

The basic instrument consists of an ionizer, which converts neutral species into positive ions, quadruple filter for scanning of the charged particle as per their m/q ratio and CEM detector. The required electronics for all three parts: Ionizer, quadrupole filter and detector

current readout has been developed and tested with the commercially available SRS make detector head. Figure 69 shows the setup photograph. The detector current has been acquired using precise current to voltage converter circuit and then digitized using 16 bits ADC. LabVIEW based software has been developed for the data acquisition and control of the mass spectrometer. The testing has been carried out for both neutral mode and ion mode. In case of neutral mode, ionizer is used for ionizing the neutral species while in case of ion mode, ionizer has been kept off. The results shown in Fig. 70 are the preliminary results with in-house designed electronics, which require further correction factors in the acquired data as well as baking of the system. Engineering model design for the quadrupole based mass spectrometer is under progress.

(S. K. Goyal, R. R. Mahajan, A. Auknoor, P. Sharma, V. Sheel, S. A. Haider and A. Bhardwaj)

Characteristic study low Background $CeBr_3$ for gamma ray spectrometer in the future planetary mission.

Previously we have presented the development of gamma ray spectrometer using a 3"x3" Cerium doped Lanthanum Bromide ($LaBr_3$:Ce) and 1"x 1" scintillation detector, which includes the shaping amplifier, processing electronics including the ADC for digitization and a FPGA for processing the digital signal (Panda et. al. 2016, 2017).



Figure 71: 2"x3" $CeBr_3$ couple with PMT & voltage divider

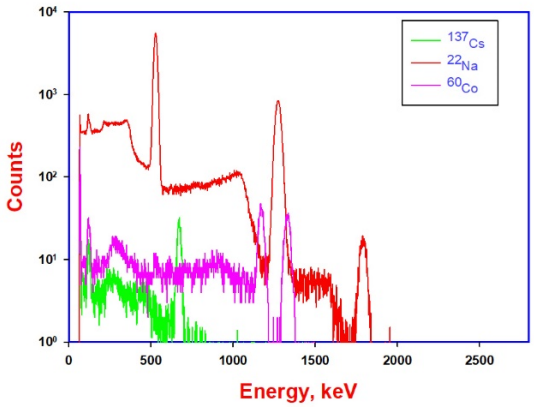


Figure 72: Background measurements of $CeBr_3$

It has been observed that due to high intrinsic activity $LaBr_3$:Ce could not be used for the estimation of concentration of K, U and Th, whereas $CeBr_3$ has a very low internal activity as compared to $LaBr_3$:Ce. Because of lower intrinsic activity, $CeBr_3$ could be used to estimate concentration of K and U. But concentration of Th could not be estimated due to the low thickness of the detector. Therefore, a higher thickness detector was needed to study the feasibility of $CeBr_3$ for planetary application. With the advancement in technique larger volume with low background CeBr3 detector has been made. In this study we have used a 2" x 3" $CeBr_3$ from Scionix coupled with a 2" PMT (Photo-multiplier) and voltage divider is show in figure 71.

The performance of the detector is carried out by supply a biasing voltage of -700V to the PMT through Canbera 3106D High voltage module and the pre-amplifier (test module) output is feed to a Ortec shaping amplifier (model no 672). The amplified signal is then digitized through the ortech 8K MCA (multi-channel Analyzer). For a stable background the background measurement has carried out for $\sim$52 hrs integration as shown in figure 72. From the background measurement it has been observed that the intrinsic background at K (peak at 1461 keV), U (peak at 1764 keV) and Th are 0.03 cps (peak at 2615 keV), 0.02 cps, and 003 cps respectively. The response of $CeBr_3$ with radioactive sources has been shown in figure 73. With the commercial setup an energy resolution of $\sim$ 4.1 % at 662 at 662 keV (^{137}Cs). The future work will be focused on to interface the low background $CeBr_3$ (2"x3") with the in-house developed gamma ray spectrometer processing electronics and measurement of rock/soil to estimate the concentration of K, U and Th.

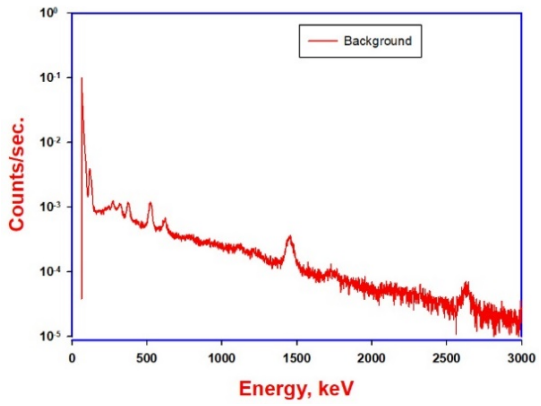


Figure 73: Response of radioactive sources from $CeBr_3$.

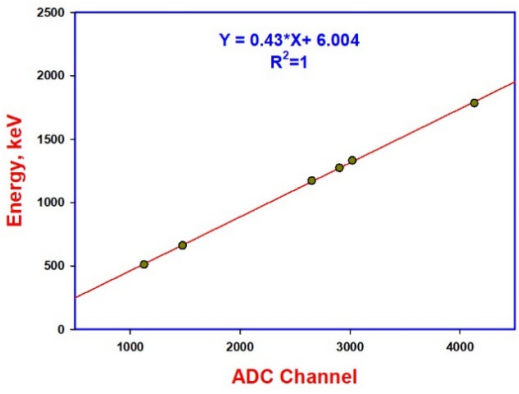


Figure 74: Calibration of $CeBr_3$.

(D. K. Panda and D. Banerjee)

Space and Atmospheric Sciences

Influence of atmospheric dynamics and meteorology on aerosols over urban region

Investigations on the influence of variations in relative humidity, mixed-layer height, and mesoscale vertical velocity on column and surface aerosol characteristics over urban regions are quite rare. A comprehensive investigation was conducted over Ahmedabad, an urban location in western India. In a campaign, columnar and surface aerosol characteristics were measured and compared to relative humidity, mixed-layer height, and mesoscale vertical velocity to examine their influence on urban aerosol characteristics. The 500-nm aerosol optical depth was $\sim$0.8 between 24 and 26 December while on a cleaner day such as 7 December the aerosol optical depth was 0.1. Aerosol optical depths based on Moderate Resolution Imaging Spectroradiometer (MODIS) level-2 and level-3 data, and on in situ Sun photometer measurements, showed good agreement. The scattering coefficient (β_{sca}) and absorption coefficient (β_{abs}) increased by a factor of 5-10 on 26 December compared to 7 December (a normal day). This latter date was characterized by a clear atmosphere, a lower mixed-layer height ($\approx$1650 m), positive vertical velocity and higher aerosol scale height ($>$3 km), while 26 December was marked with hazy and smoky conditions, a larger mixed-layer height ($\approx$2500m), negative vertical velocity and smaller aerosol scale height ($\approx$1 km). These atmospheric conditions lead to lower and higher values of surface and columnar aerosol concentrations on 7 and 26 December, respectively (Figure 1).

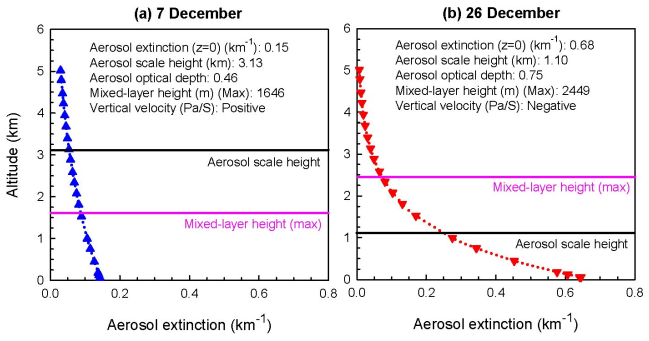


Figure 1. Aerosol characteristics and atmospheric parameters on 7 (a) and 26 December 2006 (b) respectively. Parameters shown include the aerosol extinction at the surface (β_{ext} (z=0)), aerosol scale height (km), aerosol optical depth, maximum values of the mixed-layer height (m), and vertical velocity (Pa s^{-1}). These days were selected because they represent the lowest (7 December) and highest (26 December) surface aerosol amounts.

A measure of spectral aerosol absorption, α'abs$>$2, indicating the dominance of carbonaceous aerosols from biomass/biofuel emissions (open biomass burning), is rather surprising as fossil-fuel emissions that produce strongly light absorbing carbonaceous particles usually dominate urban regions. The single-scattering albedo on both days is 0.56 and 0.67 respectively, while monthly mean hemispheric backscatter fraction b and asymmetry parameter g values are 0.16 and 0.53 respectively. Higher b and lower g values on 7 December, and lower b and higher g values on 26 December, provide the relative scale of variation in the amount of sub-micron aerosols that dominate on a normal/clear day vis-à-vis a smoky/perturbed day. Lower single-scattering albedo indicates the dominance of absorbing aerosols above Ahmedabad, and higher b and lower g values suggest the abundance of fine mode particles in aerosol size distribution. The in-depth results serve as representative inputs to modelling the column and surface characteristics, and the resultant radiative forcing of urban aerosols influenced by variations in relative humidity, mixed-layer height, and mesoscale vertical velocity.

This work was done in collaboration with Dr. Sumita Kedia, Centre for Development of Advanced Computing, Pune.

(S. Ramachandran and T. A. Rajesh)

Importance of 100 nm aerosols, and aerosol mixing state over an urban region

A quantitative approach to characterize the aerosol mixing state over an urban location is presented. In order to achieve the objective a measurement setup was designed to quantify the size selected refractory black carbon mixing state. The measurement setup comprised state-of-the-art instruments, namely, a differential mobility analyzer (DMA) and a single particle soot photometer (SP2). Aerosols of size 70, 100, 200, 300, 400 and 500 nm were selected using DMA and further size selected refractory black carbon (rBC) mass concentration, and mixing state quantification was done using SP2. Strong correlation exists between rBC mass concentrations and particle number concentrations suggesting the possible source for the rBC is roadways traffic activity near the measurement location. Refractory BC mass concentrations mostly peaked at 200 nm due to higher particle number concentrations (Figure 2). A unique observation was made during the measurement period where refractory externally mixed and internally core-shell mixed black carbon aerosol population decrease with the increase in particle size while the trend reversed for the nonrefractory aerosol. The mixing state information shows that particle at lower size (70 nm) are mostly externally mixed refractory black carbon (78.7%), whereas particle at higher size (500 nm) are nonrefractory (74.2%). Further,

particle at lower sizes are more (7.5%) internally core-shell mixed BC particles whereas higher size particles are less (2.9%) internally core-shell mixed. Particle population near 100 nm has relatively equal number of refractory and nonrefractory particles but the populations differ below and above 100 nm. Particles below 100 nm show different mixing trend compared to higher size ($\geq$ 100 nm) particles. These results are important and highlight that particles near 100 nm size could be a barrier for equilibrium mixing of refractory and nonrefractory aerosol populations. The aerosol population below and above 100 nm will have different implication over the aerosol optical and hygroscopic properties and hence the climate effects.

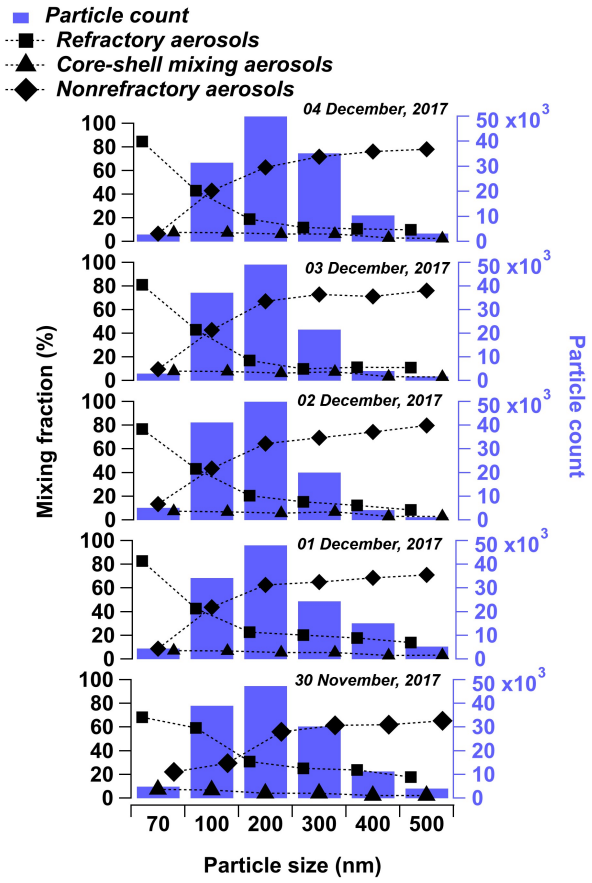


Figure 2. Size resolved percentage fraction of refractory, nonrefractory and core-shell mixing particles observed during the measurement period over the urban Ahmedabad.

(B. Sarangi, S. Ramachandran, T. A. Rajesh and Vishnu K. Dhaker)

Heterogeneity in black carbon emission sources

Black carbon (BC) aerosol is produced by the incomplete combustion of fossil fuels (coal, petrol, diesel), and biomass burning (wood, forest wildfires, shrubs, dry leaves, agricultural crop residue, waste material, dung cakes, etc.). It plays an important role in global warming, modulates the large-scale circulation patterns, alters cloud albedo, affects crop yields, and human health. BC sources exhibit large heterogeneity over the globe, with the anthropogenic (vehicular and industrial) emissions dominating in the urban regions, and the biomass burning in rural and remote areas. The study examines real-time simultaneous BC mass concentration measurements made using multi-wavelength Aethalometer at an urban location (Physical Research Laboratory, Ahmedabad) and a rural location (Sardar Patel University, Anand) during postmonsoon (Oct - Nov 2018), and winter (Dec 2018 - Feb 2019) seasons. The study has been conducted exclusively during this period as BC mass concentrations are observed to be higher. Aethalometer based source apportionment model using the measured aerosol absorption coefficients at different wavelengths is used to estimate the contribution of fossil fuel (BC_{ff}) and biomass (wood, BC_{wb}) burning sources to the total BC mass concentrations. The average BC mass concentrations over Ahmedabad (9.7 $\pm$ 3.7 μg m^{-3}) and Anand (10.3 $\pm$ 3.3 μg m^{-3}) are found to be comparable during the study period (Figure 3a), while BC_{ff} (78%) dominates over Ahmedabad due to the significant anthropogenic activities, whereas over Anand contributions of BC_{wb} (54%) dominates in total BC due to the significant emissions from biomass burning sources (Figure 3b). The study highlights the observed heterogeneity in black carbon emission sources over urban and rural locations with comparable total BC mass concentrations.

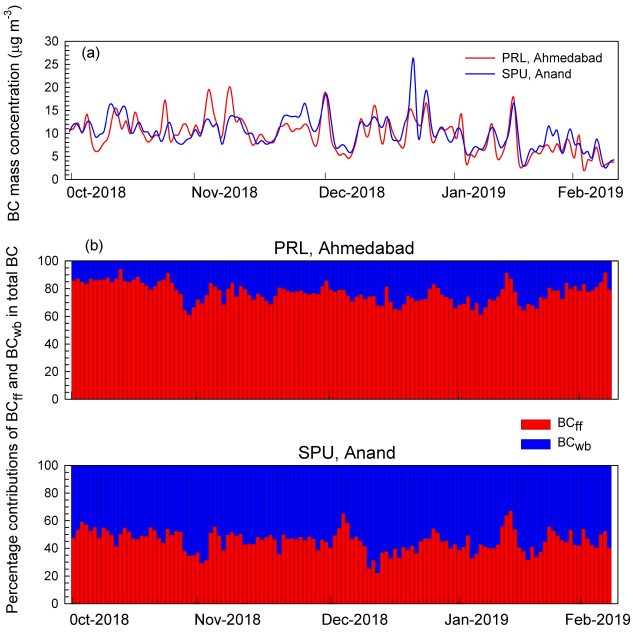


Figure 3. (a) Daily variation of black carbon (BC) mass concentration over Ahmedabad (urban) and Anand (rural) during Oct 2018 - Feb 2019. (b) Percentage contributions from fossil fuel (BC_{ff}) and wood burning (BC_{wb}) in total black carbon mass concentrations.

(T. A. Rajesh, Vishnu K. Dhaker, S. Ramachandran and Atul Manke)

Surface and column single scattering albedo: Radiative implications

Single scattering albedo (SSA) is the ratio of scattering to extinction coefficient of aerosols, and is a combination of their absorption and scattering properties. It is very crucial in the estimation of

aerosol radiative forcing and even a small error in its estimation can flip the sign of aerosol radiative forcing particularly over bright surfaces. Extensive measurements of aerosol scattering and absorption coefficients were made over distinct environments (Ahmedabad, urban and Gurushikhar, a high altitude remote) in western India to derive the near surface SSA. In addition, the column SSA retrieved from the satellite-borne Ozone Monitoring Instrument (OMI) sensor over the same locations are utilized to estimate the aerosol radiative forcing. The surface SSA is lower than the columnar SSA as most of the black carbon (absorbing in nature) are concentrated near the surface, hence, the aerosol absorption coefficients near the surface will be higher when compared to the column. The atmosphere forcing estimated using column SSA is a factor of 3 lower than surface SSA over Ahmedabad (Figure 4). The significant differences in forcing arise due to the differences in the SSA as AOD remains same in both the methods. The SSA shows a rare diurnal variability over Gurushikhar when compared to Ahmedabad. The surface SSA is higher over Gurushikhar than Ahmedabad due to the dominance of absorbing aerosols over Ahmedabad from the anthropogenic emissions. Over Gurushikhar, the surface SSA is lower than column SSA despite being a high altitude remote site. However, when compared to Ahmedabad surface and column SSA are higher over Gurushikhar, though the differences between surface and column SSA are lower over Gurushikhar. The top of the atmosphere forcing is always negative due to the dominance of scattering aerosols (higher SSA) (Figure 4). Radiative forcing values are comparable over Gurushikhar because of the small differences observed in surface and column SSA.

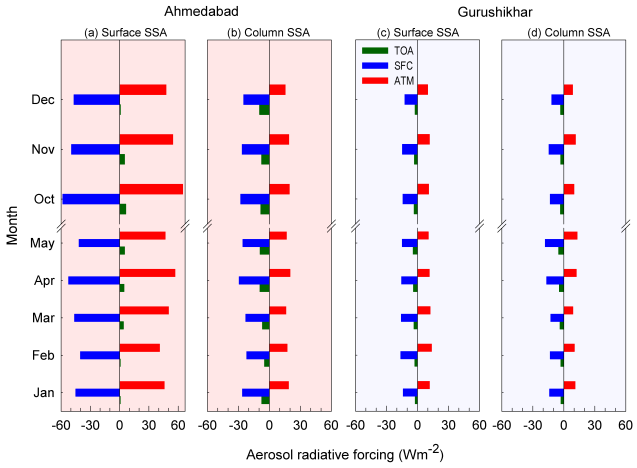


Figure 4. Clear sky aerosol radiative forcing (ARF) (Wm^{-2}) at the TOA (top of the atmosphere), SFC (surface) and ATM (atmosphere) estimated using surface and columnar single scattering albedo (SSA) over Ahmedabad and Gurushikhar.

(T. A. Rajesh and S. Ramachandran)

Evaluation of black carbon measuring techniques

Black carbon (BC) aerosol play an important role in the Earth-atmosphere system by warming the atmosphere due to strong absorption of incoming solar radiation. The measurement of BC is complicated due to the lack of methodology which is uniquely sensitive to BC. In the present study, the BC mass concentration is estimated in three ways: (1) measurement of refractory black carbon (rBC) component of individual particles by laser-induced incandescence method using a single particle soot photometer (SP2), (2) conversion of light absorption measured with an aethalometer to give equivalent black carbon (EBC), and (3) thermal desorption of elemental carbon (EC) with semi continuous EC-OC analyser to give elemental carbon (EC). The intercomparison exercise has been carried during December 2018 over urban Ahmedabad, which is a source region. EBC and EC are always found to be higher by a factor of 4.2 and 1.5 respectively than rBC (Figure 5). The overall diurnal pattern of rBC, EC, and EBC are similar, however, EBC and EC are biased higher relative to rBC. The overestimation of EBC and EC measurements are due to the influence of the measurement techniques rather than BC aerosols.

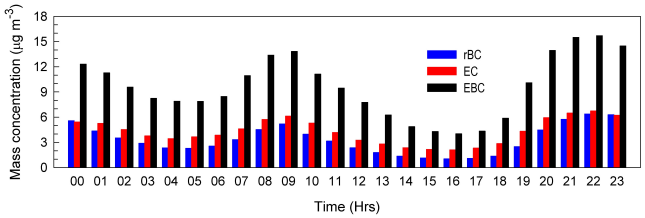


Figure 5. The temporal variation of refractory black carbon (rBC) from SP2, elemental carbon (EC) from EC-OC analyser, and equivalent black carbon (EBC) from aethalometer during December 2018 over an urban site (Ahmedabad).

(T. A. Rajesh, Vishnu K. Dhaker, S. Ramachandran and Malaidevan P.)

Temporal variability of the atmospheric particulate matter concentration

Atmospheric particulate matter (PM) is a complex heterogeneous mixture, whose size distribution and chemical composition exhibit large temporal and spatial variation. PM is classified and defined by its aerodynamic diameter, and the most widely measured particles are PM10 (coarse particle) and PM2.5 (fine particle), which refers to particles with aerodynamic diameter less than or equal to 10 or 2.5 μm, respectively. PM concentrations depend on meteorological conditions, emissions sources and atmospheric chemistry, and it has important health (respiratory and cardiovascular disease) and environmental impacts (visibility degradation, global climate change, radiative effects, etc.). PM particles originate from diverse sources and exhibit different physico-chemical properties. The PM2.5/PM10 ratio can provide information relating to the particle origin, and its production mechanism. PM concentrations measured using environmental dust monitor EDM180 over Ahmedabad during winter 2018-2019 show typical diurnal variation (Figure 6a) and overall, fine particles (PM2.5) make up 66% of PM10 in Ahmedabad which reveals the dominance of fine particle in the atmosphere. The PM2.5 to PM10 ratio is found to be 0.61 during winter. The ratio increases in the nocturnal period due to the sedimentation of the coarse particle (PM10) caused by temperature inversion (Figure 6b). Thus, these ratios can be used to better understand the atmospheric processes.

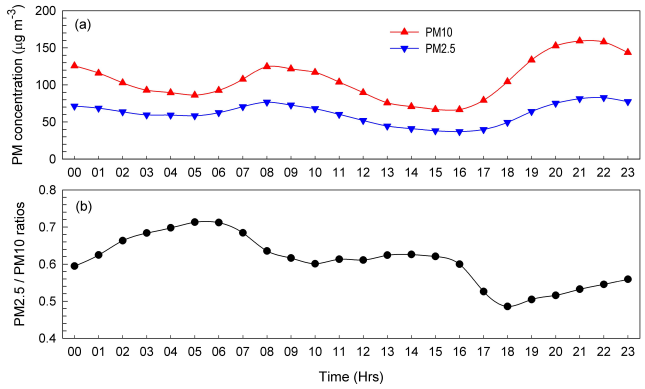


Figure 6. Diurnal variation of (a) particulate matter (PM) concentration, and (b) PM2.5/PM10 ratio over Ahmedabad (urban) during winter season (Oct 2018 – Feb 2019).

(T. A. Rajesh, Vishnu K. Dhaker and S. Ramachandran)

Cloud detection using image processing technique

Clouds play a major role in Earth's climate. They influence the Earth-atmosphere system by interacting with the incoming solar radiation and outgoing terrestrial radiation, and affect the columnar retrievals of atmospheric parameters. A study has been initiated and accomplished to quantify the sky condition for cloud detection using image processing technique. The in-house developed system comprises hardware (high resolution vandal proof fish-eye IP camera) and software (data acquisition, image processing and cloud detection algorithm) units. The acquired sky images undergo intensity and area, and piecewise analysis through a MATLAB code developed for the detection of clouds in the visible spectra. The system has been implemented for the cloud detection in real-time to examine and classify the sky conditions as clear sky, partially cloudy, and cloudy.

(Malaidevan P., T. A. Rajesh and S. Ramachandran)

Photochemistry and dynamics over Doon Valley of the Himalayan Foothills

Elevated ozone concentrations are observed every spring over the northern Indian region, however, studies investigating the influences of photochemistry and dynamics in the valleys of the central Himalaya are limited. In this direction, we combined observations (in situ and satellite-based) with model results (CAMS: Copernicus Atmosphere Monitoring Service) to study the O_3 variations at Dehradun (77.99°E, 30.27°N, 600 m amsl) in the Doon valley during April-July 2018. Entrainment through boundary layer dynamics is found to significantly enhance noontime O_3 in Doon valley, besides the photochemical production. CAMS model successfully reproduced the observed day-to-day variability in ozone at Dehradun (r = 0.86), however absolute ozone levels were typically overestimated. Positive relationship between modelled O_3 and CO (r = 0.65) together with O_3/CO slope of 0.16 are attributed to influences of biomass-burning. Model based calculations, supported by observations, show that O_3 was enhanced by 10-65% due to biomass burning over this region.

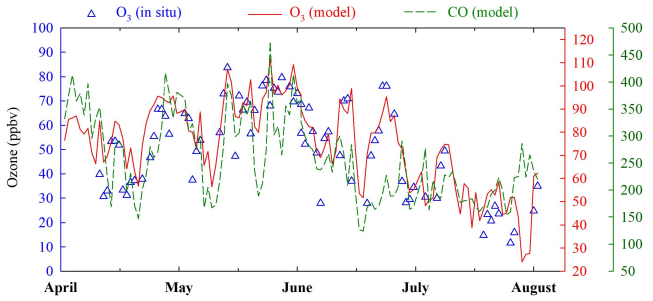


Figure 7. Ozone and carbon monoxide mixing ratio variations from April 2018 to July 2018 at Dehradun.

This work is done in collaboration with I. Girach, P. Nair, K. V. Subrahmanyam of Space Physics Laboratory, Trivandrum, K. Sharma, and N. Sharma of Graphic Era, Dehradun, J. Singh, N. Singh of ARIES Nainital, J. Flemming, A. Inness of ECMWF, UK.

(Narendra Ojha)

Measurements of volatile organic compounds (VOCs) at New Delhi: Source identification and atmospheric processes

Atmospheric VOCs are short-lived compounds which play indirect but very important role in the climate change. Atmospheric VOCs are oxidized by hydroxyl (OH) radical and in the presence of sunlight react with NO_x ($NO+NO_2$) to produce secondary oxidants (peroxy radicals, O_3, etc.) and secondary organic aerosol (SOA). Therefore, VOCs also affect the air quality, oxidation capacity of the troposphere.

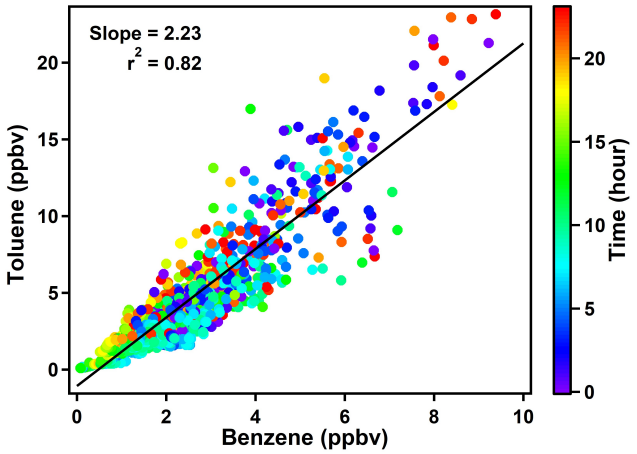


Figure 8. the average △T/△B slope of 2.23 ppbv/ppbv suggests that the vehicular exhaust is the dominant source of aromatic VOCs during the study period in Delhi.

The Indo-Gangetic Plain (IGP) is one of the most polluted regions in Asia where measurements based studies of VOCs are very limited.

VOCs were measured using a Proton Transfer Reaction-Time of Flight-Mass Spectrometer (PTR-TOF-MS) at Delhi (IGP) during winter season (January-February, 2018). In the winter season, Delhi faces severe problems such as poor air quality, fog and low visibility. One of the objectives of this study is to estimate the contribution of pollutants from different sources such as vehicular exhaust, biomass burning, industrial and biogenic emissions. We have used the mixing ratios of isoprene, benzene and acetonitrile as tracers for biogenic, vehicular and biomass burning sources, respectively. The episodic enhancements of acetonitrile concentration (>10 ppbv) are due to transport from crop residue burning in the surrounding areas of Delhi. The toluene/benzene (ΔT/ΔB) slope has been used to identify the source and estimate the photochemical age of air. Typically, the ΔT/ΔB slope values of 1-4 ppbv/ppbv characterize fresh vehicular emissions. As shown in Figure 8, the average ΔT/ΔB slope of 2.23 ppbv/ppbv suggests that the vehicular exhaust is the dominant source of aromatic VOCs during the study period in Delhi.

(Nidhi Tripathi and L. K. Sahu)

Role of local meteorology on ambient particulate and gaseous species at an urban site of western India

Dependencies of ambient concentrations of PM2.5, PM10, CO and O_3 on meteorology in Udaipur of India were studied based on the measurements from April 2011 to March 2012. PM2.5 and CO were highest in winter due to lower PBL depth and calm winds while PM10 and O_3 were highest in the pre-monsoon season due to convective activities. In lower wind regimes (<2 km hr^{-1}), highest values of both PM2.5 and CO indicate the accumulation of anthropogenic pollutants while lower levels in higher wind regimes indicate the impact of dispersion. A positive slope of Δ PM10/ΔWS = 4.4 μg m^{-3}/km hr^{-1} indicates predominance of natural sources of coarser particles. Higher concentrations of PM2.5 and CO with correlation coefficient (r = 0.42 and 0.52) under high RH and low temperature during winter season indicate the strong temperature inversion. A negative correlation between PM10 and RH during monsoon indicates the role of rainfall in wetting the soil reducing its aerosolization and particle washout. Rainfall was significant for PM10 ($\sim$53% reduction) than those observed for PM2.5 and CO. Overall, this study suggests the strong influence of meteorology in the variation of air pollutants.

(Ravi Yadav, L. K. Sahu and Nidhi Tripathi)

Influences of local meteorology and convection on carbon monoxide distribution over Chennai

The influences of local meteorology and convective activities on the vertical distribution of CO over Chennai in southern India are investigated by analyzing the Measurements of Ozone aboard Airbus In-service Aircraft (MOZAIC) observations during the years 2012-13. The seasonal variation of CO in the free troposphere is observed to be different and less pronounced than that in the planetary boundary layer. The near surface mixing ratio of CO showed a highest (190$\pm$68 ppbv) during winter, while enhanced values (117$\pm$11 ppbv) in the free troposphere were observed during post-monsoon. The mixing ratios were lowest throughout the troposphere during the monsoon. In the PBL, the mixing ratios of CO showed a decline with increase in wind speed and were highest (>200 ppbv) under stagnant conditions (1-2 ms^{-1}) during winter. The higher CO in the lower free troposphere during pre-monsoon period is attributed to the stronger biomass burning emissions. In the middle-upper troposphere, higher levels of CO during post-monsoon is due to enhanced vertical mixing of regional emissions associated with weaker wind shears and frequent convective activities (Figure 9). Overall the contrasting effects of stronger CO emissions in winter/pre-monsoon, while efficient vertical mixing in monsoon/post-monsoon govern the observed seasonality of CO. The Model for Ozone And Related Chemical Tracers version -4 (MOZART-4) provides a reasonable representation of the convection effect on CO mixing ratio. This study highlights a need to conduct more observations especially aircraft-borne instruments to understand the effects of regional-scale emissions and dynamics in the middle-upper tropospheric chemistry over South Asia.

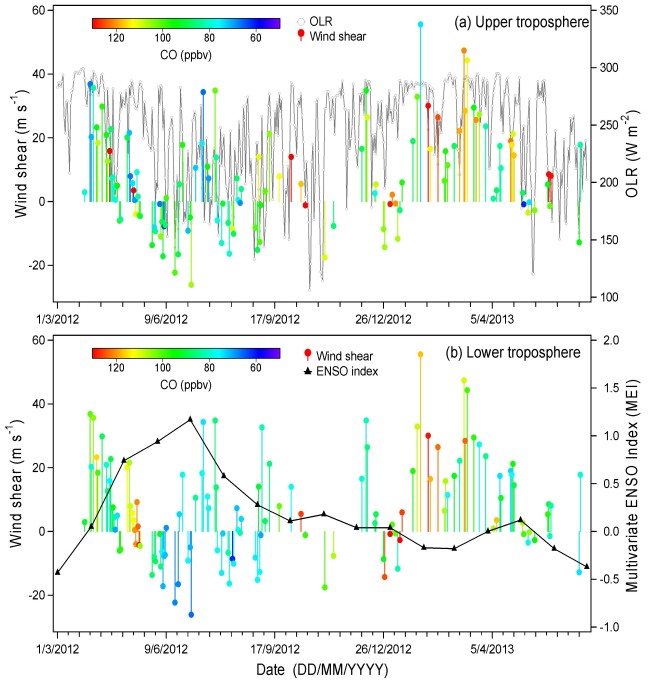


Figure 9. Variation of the MOZAIC flights derived wind shear (average wind speed at 10-12 km-average wind speed at 0-2 km) color-coded with CO mixing ratio in the upper and lower troposhere over Chennai along with OLR and Multivariate ENSO index (MEI).

(L. K. Sahu, Nidhi Tripathi, Varun Sheel and N. Ojha)

The level, variation features and emission sources of ambient non-methane volatile organic compounds (NMVOCs) at an urban site of western India

This is the first study to characterize the variation and emission of C_2-C_5 non-methane volatile organic compounds (NMVOCs) in a semi-urban site of western India. Anthropogenic NMVOCs show clear seasonal dependence with highest in winter and lowest in monsoon season. Biogenic NMVOCs like isoprene show highest

mixing ratios in the pre-monsoon season. The diurnal variation of NMVOC species can be described by elevated values from night till morning and lower values in the afternoon hours. The elevated levels of NMVOCs during night and early morning hours were caused mainly by weaker winds, lower mixing depth and reduced chemical loss. The correlations between NMVOCs, CO and NO_x indicate the dominant role of various local emission sources. Use and leakage of liquefied petroleum gas (LPG) contributed to the elevated levels of propane and butanes. Mixing ratios of ethylene, propylene, CO, NO_x, etc. show predominant emissions from combustion of fuels in automobiles and industries. The Positive Matrix Factorization (PMF) source apportionments were performed for the major emission sectors. Emissions from industry-related sources contributed to about 40% of the NMVOCs while from vehicle exhaust account for about 20% of the total NMVOCs. And the rest 40% were attributed to emissions from biogenic sources, LPG, gasoline evaporation and biomass burning. This study provides a good reference for framing environmental policies to improve the air quality in western region of India.

(Ravi Yadav, L. K. Sahu and Nidhi Tripathi)

High levels of methane at Ahmedabad

The urban areas emit large amounts of methane (CH_4) to the atmosphere from landfills, wastewater treatment facilities, waste dump and consumption and infrastructure of natural gas. Simultaneous measurements of CH_4, CO_2 and CO are being made at PRL since November 2013 using a highly sensitive laser-based cavity ring down spectrometer. These measurements have been analyzed to understand the emission characteristics of CH_4 and its seasonal and diurnal characteristics. Elevated CH_4 levels have been observed mostly during the winter and spring seasons (Fig. 10).

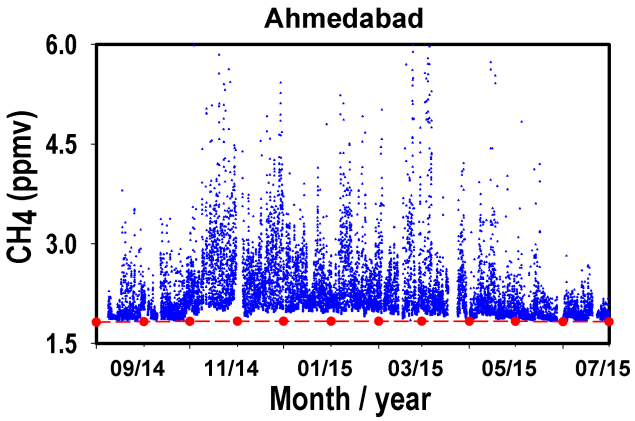


Figure 10. Methane time series observed at Ahmedabad for the period of August 2014 to July 2015. The red dots and red line show global monthly average CH4 from NOAA for the same period.

The red line shows global monthly average CH_4 from NOAA for the same period for a comparison. These high levels suggests strong and persistent emission sources of CH_4 in this city. Furthermore, the CH_4:CO_2 and CH_4:CO correlations indicate the combustion-related and fugitive anthropogenic sources as the major emission sources of CH_4 in Ahmedabad. The CH_4:CO_2 ratio combined with the CO_2 emissions from EDGARv4.2 FT2010 is used to compute the total CH_4 emission in the study region, which comes to about 58 $\pm$ 16 Gg for the year 2014, which is $\sim$45% higher than the EDGARv4.2 FT2010 inventory estimates. This difference could be due to the errors in the spatial allocation of diffuse emissions to inventory grid cells as well as the existence of local CH_4 sources that were not considered in emission inventories. Further, the observed CH_4 mixing ratios are used to evaluate the performance of two state-of-the-art global chemistry-transport models (ACTM and LMDzINCA). Both the models under-predict the diurnal and seasonal variations of CH_4 observed at Ahmedabad. The ACTM shows larger biases compared to the LMDzINCA model, which has a better horizontal resolution. Although this study suggests substantial CH_4 emission in Ahmedabad and attributes it to combustion-related and fugitive sources, it is not possible to further distinguish the individual source types due to the limited measurements of tracers available.

This work is done in collaboration with scientists from Japan and France.

(S. Venkataramani and Shyam Lal)

In-situ Measurements of Microphysical & Optical properties of Cirrus Clouds during BATAL Campaign

Clouds significantly impact Earth's radiation budget and hence its climate. Radiative effects of clouds depend on their macrophysical (altitude, coverage and thickness) and microphysical properties (number concentration, size and shape-distributions of cloud droplets/ice-crystals). However, the microphysical representation of clouds, especially the extremely cold and thin cirrus clouds in the global climate model is poor owing to the uncertainties involved in the size distribution and number concentration of ice-crystals having size less than 100μm. The mechanisms involved in their formation, maintenance and decay are also not well understood. Under the framework of Balloon measurement campaigns of Asian Tropopause Aerosol Layer (BATAL), size distribution of cloud droplets and ice-crystals inside cloud layers were measured over TIFR Balloon Facility at Hyderabad in India during August 2017 by using an optical particle counter called Boulder Counter. Boulder counter can count particles at six different size bins (5, 10, 25, 40, 50 and 100μm) at a flow rate of 28.3 litres per minute. Simultaneous measurements from Boulder counter and a backscatter sonde called COBALD reveal the presence of multi-layered clouds with a 2 km thick cirrus cloud layer located at extremely cold conditions (-860 C) of tropopause. The top of this cloud layer is found to cross the cold point tropopause (at 17.8 km). Majority of ice-crystals in this cloud have sizes between 5 and 10μm. However, a small concentration of particles with sizes between 25 and 40μm are also present near the bottom of the cloud exhibiting the effect of aggregation and subsequent sedimentation.

This work is done in collaboration with Dr. Jean-Paul Vernier, Dr. T. Duncan Fairlie, B. G. Doddridge of NASA Langley Research Center, USA, Shri B. Suneel Kumar of TIFR Balloon Facility, Hyderabad and Dr. M. V. Ratnam of NARL, Gadanki

(Amit Kumar Pandit and Harish Gadhavi)

Impacts of dust-ice-cloud interaction on precipitation variability.

Mineral dust significantly perturbs hydrological and energy cycles of Earth's climate by modifying cloud microphysics and radiation budget. Although recent studies suggest a positive radiative feedback of mineral dust on precipitation variability during the Indian Summer Monsoon (ISM), the various mechanisms and feedback processes remain poorly understood. We investigated dust-induced changes in ice-cloud microphysics and precipitation over the ISM region, using an integrated set of 11-year multi-satellite observations and reanalysis datasets. To examine the dust-cloud-precipitation interaction and its meteorological dependency, we segregated the satellite-observed parameters into two groups with the likelihood that: (1) dust interacts with ice cloud (DII); (2) dust does not interact with ice clouds (DNI), using distance between aerosol and cloud layer from CALIPSO lidar. We have found that elevated dust frequency is associated with significantly increased small ice particle concentrations in clouds observed at warmer temperatures due to heterogeneous nucleation in the thin ice-cloud regimes. On the other hand, the role of dust-induced cloud invigoration in thick ice-cloud regimes is likely responsible for the further development of ice-clouds in the DII case. Additionally, the positive Ice Water Path (IWP) susceptibility is greater in strong updraft regime with more humid conditions via more effective ice nuclei production (Figure 11 top-panel).

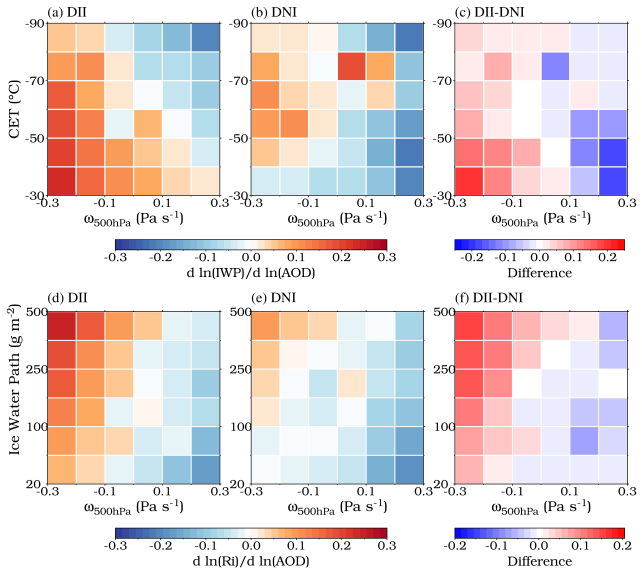


Figure no.11: (top) Frequency distribution of response of ice liquid water path to aerosol optical depth (AOD) as a function of vertical velocity and cloud effective temperature. (Bottom) Frequency distribution of precipitation response to AOD as a function Ice water path and vertical velocity. Strong updraft regime (negative omega) produces stronger response to Ice Water Path and Precipitation in case of DII (dust interacting with ice-cloud).

The positive IWP susceptibility further results in a positive response of precipitation intensity to aerosol optical depth (AOD) in an updraft regime (Figure 11 bottom panel). This "microphysical-dynamical interaction" will lead to a negative feedback, which mitigates (buffers) the aerosol effects due to enhanced wet scavenging. These observational-derived process-level understandings of dust-induced modification of clouds and precipitation variability underscore the importance of incorporating regime dependent dust-ice cloud-precipitation interactions into numerical models for more accurate climate simulations.

This work is done in collaboration with Takuro Michibata of Kyushu University, Japan and Ritesh Gautam of Environmental Defense Fund, USA.

(Piyushkumar Patel and Harish Gadhavi)

Anomalous Behavior of Vertical Wavenumber Spectra Over a Tropical Station of India

The vertical wavenumber (VWN) spectra of height profiles of winds over a tropical station of Gadanki (13.5°N, 79.2°E; obtained using Indian Mesosphere Stratosphere Troposphere radar) show distinct nature of VWN spectra, which do not match with the so-called universal wavenumber spectra. The universal wavenumber spectra have three distinct regions: unsaturated (having log-log slope of 2), saturated (having log-log slope of -3), and turbulence region (having log-log slope of -5/3). In present work, we report the presence of positive slope at the higher end of the VWN spectra indicating the presence of unsaturated gravity waves, a kind of which is not reported so far. Many negative slopes of the order of $\sim$ -6, $\sim$ -9, and $\sim$ -12 are noticed at the end of the spectra beyond the turbulence region of the wavenumber spectra.

This work has been done in collaboration with Dr. R. Ram Kumar of National Atmospheric Research Laboratory, Gadanki, India

(Priyanka Ghosh and Som Sharma)

A comprehensive statistical study of cloud base height using ceilometer over western India

A comprehensive statistical analysis of the cloud base height (CBH) measured by ground-based Vaisala ceilometer (CL31) has been performed to study different layers of the cloud in the lower troposphere up to 7.5 km height over Ahmedabad, western India during 2014 and 2015. The total observations ($\sim$69%) of cloud by using ceilometer show annual cloud occurrence frequency of around 64%. Seasonal variation of CBH and cloud occurrence frequency reveal that the maximum/minimum cloud cover is found during southwest (SW) Indian summer monsoon/pre-monsoon season. Three CBHs (CBH1, CBH2, and CBH3) are presented in monsoon period due to high cloud occurrence, and two CBHs (CBH1 and CBH2) are observed in other seasons due to low cloud occurrence by ceilometer over the observational site. The CBH1 ($\sim$100-2000 m) and CBH2 (500-3000 m) are observed during SW monsoon and summer season, respectively. The CBH3 is occurred usually in SW monsoon season. Moreover, the cloud cover during the day and night time shows that the occurrence of cloud is more frequent in daytime than night-time during pre-monsoon and post-monsoon season. The statistical analysis of cloud with ground-based observations is also performed in this study that may be useful for the development/improvement of regional weather and climate models to reduce the uncertainty in the prediction.

(Som Sharma)

Influence of tropical-extratropical interactions on the dynamics of extreme rainfall event: A case study from Indian region

A diagnostic investigation of an extreme rainfall episode that occurred over the central and north Indian region is carried out in this study using data from a suite of observations from space-borne instruments and the reanalysis datasets. This event is unique in the sense that the organized tropical and extratropical forcing stimulated the intense rainfall on 01 Jan 2012. The WindSat (multi-frequency polarimetric microwave radiometer) observations indicate the source of the moisture flux coming from the adjoining tropical Ocean. The dynamical and thermo-dynamical contributions are evaluated based on the atmospheric instability analysis using the Atmospheric Infrared Sounder (AIRS) and reanalysis datasets by computing various stability indices such as total totals (TT) index, Potential Vorticity (PV), static stability and the Convective Available Potential Energy (CAPE). High TT index values ($>$ 40 K) are observed both in satellite and reanalysis data indicating thermodynamic instability. PV intrusion to low latitudes is also observed with extreme rainfall occurrence ahead of the PV tongue. The vertical structure of PV intrusion shows remarkable features with enhanced upward motions ahead of the intrusion representing the dynamical instability. The reduced static stability, increased CAPE and upper-level cyclonic anomalies together with enhanced moisture in the lower troposphere coming from the adjoining tropical Indian Ocean regulate the amplitude and region of occurrence of the extreme rainfall. Therefore, this study identifies the significant implications of tropical and extra-tropical influences that generate the thermodynamical and dynamical instabilities for the occurrence of the extreme rainfall event over the Central and Northern parts of India.

This work has been done in collaboration with D. V. Phanikumar and M. Naja of Aryabhatta Research Institute of Observational Sciences (ARIES), Nainital, India; G. Basha and M. V. Ratnam of National Atmospheric Research Laboratory (NARL), Gadanki, India; T. B. M. J. Ouarda of INRS-ETE, National Institute of Scientific Research, Quebec City, Canada; K. Kishore Kumar of Space Physics laboratory, VSSC, Trivandrum, India.

(Kondapalli Niranjan Kumar and Som Sharma)

Characteristics of high-frequency gravity waves generated during pre-monsoon season over a tropical location: A case study

Mesoscale convection weather events, associated with deep cumulonimbus clouds transport moisture, energy and momentum to upper troposphere and lower stratosphere (UTLS), affect the energetics and general circulation of the middle atmosphere. Therefore, it is necessary to understand the atmospheric dynamics during pre-monsoon periods (when strong mesoscale convective events occur) for improving the parameterization of model physics. The present study investigates the characteristics of high-frequency gravity waves (GWs) generated over Gadanki (13.5° N, 79.2° E), India during one such severe convection event in the pre–monsoon period. For this purpose, the Mesosphere Stratosphere Troposphere (MST) radar at Gadanki was operated continuously for the period of $\sim$10 h during 27-28 May 2015. A wide spectrum of high frequency GWs with different generation mechanisms are found during this convective event whose vertical propagation characteristics fulfill the non-hydrostatic GW dispersion relation. The temperature and wind data of ERA (ECMWF Re-Analysis)-interim reanalysis and GPS radiosonde, launched at Gadanki, are also analyzed for ten days around the event day to determine the background atmospheric thermodynamical conditions. Strong up- and down-drafts are observed in the altitude range of $\sim$3.6-20 km (radar limited top height); presence of which even up to $\sim$20 km height is quite rare. The WRF (Weather Research and Forecasting) model simulated relative humidity on 27-28 May 2015 clearly depicts the mid-tropospheric moisture intrusion. Presence of moisture is also observed at the higher heights $\sim$17-18 km which could be due to strong low level convergence leading to high divergence value of deep cumulonimbus clouds in UTLS region. Furthermore, this is supported by the Doppler Weather Radar (DWR) and simulated reflectivity of WRF model reaching the tropopause height of $\sim$18 km. The altitude profiles of phase of some oscillations during convection period depict that the sources of these waves are near $\sim$20 km which is first of its kind outcome and it is corroborated with high resolution WRF model simulations.

This research has been done in collaboration with National Atmospheric Research Laboratory, Gadanki, India.

(Priyanka Ghosh and Som Sharma)

Vertical Coupling from the Lower Atmosphere to the Ionosphere: Observations Inferred From Indian MST Radar, GPS Radiosonde, Ionosonde, Magnetometer, OLR, and SABER/TIMED Instrument Over Gadanki

Simultaneous wind observations from Mesosphere Stratosphere Troposphere (MST) radar collectively with Global Positioning System (GPS) radiosonde over Gadanki, covering altitude range of 3.6-20 km (January-December 2009; 365 days), divulge the propagation of lower atmospheric waves up to the ionosphere. It is combined with temperature data (20-110 km) observed from Sounding of the Atmosphere using the Broadband Emission Radiometry (SABER) instrument onboard Thermosphere Ionosphere Mesosphere Energetics and Dynamics (TIMED) satellite, ionosonde observations, and daily Outgoing Longwave Radiation (OLR) data acquired from the National Ocean and Atmospheric Administration (NOAA; centered around Gadanki [13.5°N, 79.2°E]) for the same time period. Long-period oscillations with periodicities of $\sim$64, $\sim$32, and $\sim$21 days are witnessed along with the well-known oscillations of $\sim$16, $\sim$6.4, and $\sim$5.3 days. Most of the long-period oscillations are dominantly perceived during the summer months (April-June 2009), which can even exist up to September. These long-period oscillations are found to propagate from lower tropospheric heights up to ionospheric heights with large vertical wavelengths ($\sim$300-400 km, in some cases) near transition zones of atmospheric layers (e.g., tropopause, stratopause, and mesopause). Signatures of vertical coupling of atmosphere through large vertical wavelengths (indicating possible intraseasonal connections) is observed in the equatorial electrojet current and the peak plasma frequencies of ionospheric layers (E and F regions). Noticeable reduction of the wave oscillations in spatial scale with upsurge in spatial damping is visible in the tropical stratosphere and mesosphere, which can be attributed to stratospheric ozone. *This work has been done in collaboration with Dr. A. K. Patra and Dr. R. Ramkumar of National Atmospheric Research Laboratory, Gadanki, India.*

(Priyanka Ghosh and Som Sharma)

Variability of the quarterdiurnal tide in the low latitude mesosphere and lower thermosphere

The characteristic features of the quarterdiurnal tide (QDT) in the mesosphere and lower thermosphere (MLT) are investigated using meteor radar observations from three low latitude southern hemispheric stations, Sao Joao do Cariri (7.4°S, 36.5°W), Cachoeira Paulista (22.7°S, 45°W) and Santa Maria (29.7°S, 53.7°W) in 2005 (Figure 12). The QDT shows consistent appearance with a weak enhancement during late summer and fall interval. The QDT amplitudes are found to be much smaller (< 3 ms^{-1}) than the longer period tidal components most of the times of the year, consistent with the previous investigations carried out from various locations over the globe. The vertical wavelength is found to reach up to 80 km in the MLT maximizing in winter, although most of the times it remains within 20 km. Therefore, based on the observed characteristics of the QDT, it is surmised that both the migrating and nonmigrating components are involved in the manifestation of the QDT at present locations.

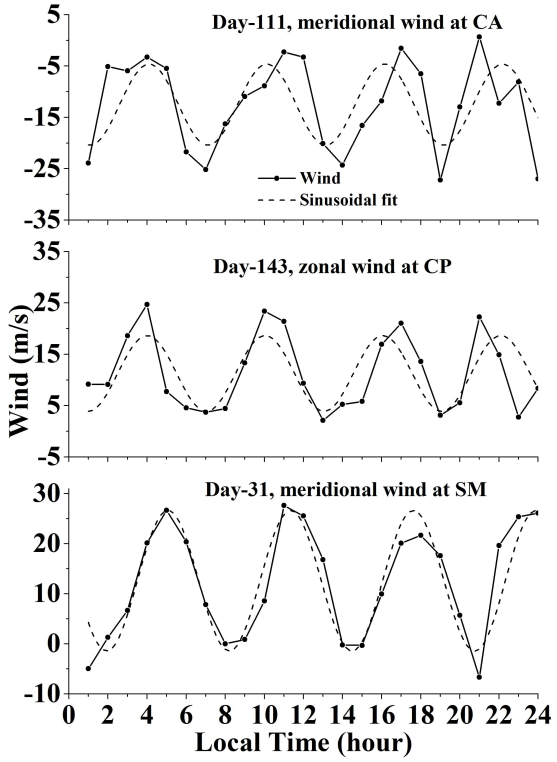


Figure 12. Typical residual winds at 90 km on removing the diurnal and semidiurnal components shows prominent 6-h wave at (a) CA in the meridional wind on Day-111, (b) CP in the zonal wind on Day-143 and (c) SM in the meridional wind on Day-31.

This work is carried out in collaboration with P. P. Batista, National Institute for Space Research, São Paulo, Brazil, R. A. Buriti, Federal University of Campina Grande, Paraiba, Brazil, and N. J. Schuch, Southern Regional Space Research Center, Santa Maria, Brazil.

Tidal response to a major sudden stratospheric warming at low latitude middle atmosphere

Investigation of the middle atmospheric tidal response to the September 2002 sudden stratospheric warming (SSW) is carried out from a Southern hemispheric extra-tropical location Cachoeira Paulista (22.7°S, 45°W) using meteor radar observations and reanalysis database (Figure 13). Significant diurnal and semidiurnal tidal amplitudes are found in the mesosphere and lower thermosphere (MLT) a few days prior to the warming onset consistent with the high latitude observations. In the troposphere and stratosphere (TS) the tidal amplitudes attain higher value during the main phase of the warming which decrease subsequently. The simultaneous enhancement of the tidal amplitudes in the TS and diminution in the MLT may imply strong dissipation of the upward propagating tides during the SSW at present location. An evident signature of the tide-planetary wave coupling due to nonlinear interactions is found. A preferential modulation of the tidal amplitudes by long/short period planetary waves are observed in the MLT/TS. The migrating diurnal tide (DW1) and nonmigrating semidiurnal tide (SW1) at 10 hPa pressure level show considerable variability during the warming episode.

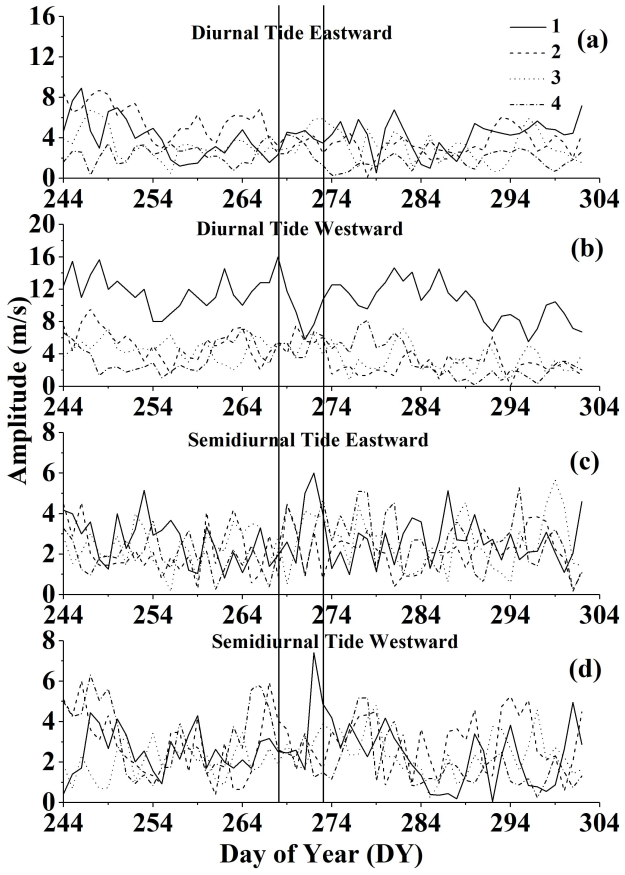


Figure 13. Amplitudes of the wavenumbers 1, 2, 3 and 4 estimated from the meridional wind at 10 hPa at present site using MERRA dataset for the (a) eastward diurnal tide, (b) westward diurnal tide, (c) eastward semidiurnal tide and (d) westward semidiurnal tide. The warming interval is shown by two vertical lines.

(A. Guharay)

This work is carried out in collaboration with P. P. Batista, National Institute for Space Research, São Paulo, Brazil, R. A. Buriti, Federal University of Campina Grande, Paraiba, Brazil, and N. J. Schuch, Southern Regional Space Research Center, Santa Maria, Brazil.

(A. Guharay)

Long-term variations in OH(6-2) and O_2(0-1) nightglow emission intensities and temperatures

The near infrared imaging spectrograph (NIRIS) is being operated to measure the OH(6-2) and O_2(0-1) nightglow emission intensities and temperatures from Mount Abu since January 2013. This long-term NIRIS observation show the responses of the mesospheric nightglow emissions and temperatures to solar radiation. This observation is being investigated using complimentary satellite based observation of different nightglow emissions that emanate from mesosphere lower thermosphere (MLT) region. Initial investigations using satellite based observations indicate that the influence of solar radiation on the emissions at lower altitudes is weaker than the ones higher above. OH and O_2 nightglow emission observations show significant annual and semi-annual oscillations in both intensity and temperature. These aspects of the solar and dynamical influences into the MLT region are being investigated in detail.

(Ravindra P. Singh and Duggirala Pallamraju)

Automation and Data Analysis for PRL Airglow Infrared Spectrograph (PAIRS)

To investigate the solar influences and atmospheric dynamics into the Earth's Mesosphere Lower thermosphere (MLT) region a new infrared spectrograph has been developed. The short wave infrared (SWIR) region is a promising yet, least explored region for the MLT research. The spectrograph will measure OH nightglow emission intensities and corresponding rotational temperatures using OH(3-1) emission band and named as PRL Airglow Infrared Spectrograph (PAIRS).

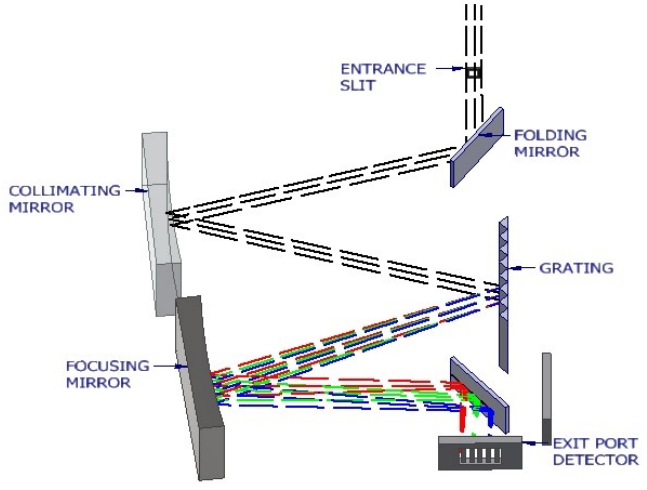


Figure 14. Optical layout of the PRL Airglow Infrared spectrograph (PAIRS).

It is planned to commission PAIRS at optical aeronomy observatory at Gurushikhar and will be operated in an automated mode. The software to run the instrument in a pre-defined mode of settings has been developed (Figure 14) that will provide the nocturnal spectra in FITS format. Data analysis method is also developed for the derivation of nightglow emission intensities and rotational temperatures from the OH(3-1) nightglow spectra obtained from PAIRS.

(Ravindra P. Singh, Duggirala Pallamraju, Shashank Urmalia, and Pradip S. Suryawanshi)

Development of the CCD based Photometer for Mesospheric Temperatures (CPMT):

For the investigation of the Mesosphere Lower thermosphere (MLT) region a new multi-wavelength nightglow photometer is being developed (Figure 15). This photometer will provide near simultaneous measurements of OH(6-2) Meinel and O_2(0-1) atmospheric band nightglow emission intensities and corresponding rotational temperatures and named as CCD based Photometer for Mesospheric Temperatures (CPMT).

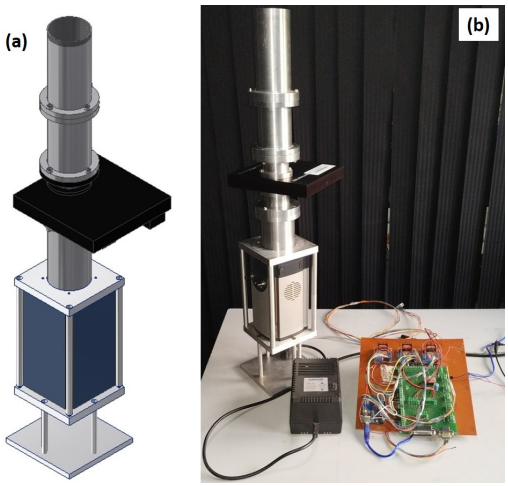


Figure 15. (a) Mechanical drawing and (b) final assemble of CPMT.

CPMT is a narrow field of view ($\sim 5^{\circ}$) nightglow photometer in which narrow bandwidth interference filters of FWHM $\sim$0.4 nm have been used. It will measure nightglow emission intensities at 840.0, 846.5, 866.0, 868.0 and 857.0 nm wavelengths from which the corresponding rotational temperatures will be derived. The mechanical and optical design of CPMT has been completed. Prevention of temperature fluctuations and maintenance of a set temperature of the interference filters is achieved with the use of Peltier elements around the filter wheel assembly. The filter wheel can accommodate five filters at a time. A near infrared sensitive CCD has been used in CPMT. A LabVIEW based software has been developed for the automation of the CPMT that is used to control the filter wheel and CCD parameters in a pre-defined mode of operation. CPMT is a field proven instrument that will be commissioned at optical aeronomy observatory at Gurushikhar and will be operated in automated mode routinely. The data obtained from CPMT will be compared with the collocated

NIRIS data, once the data analysis methods are developed and frozen, CPMT is planned to be commissioned at different strategic locations.

(Ravindra P. Singh, Duggirala Pallamraju, Pankaj K. Kushwaha, Shashank Urmalia, and Pradip S. Suryawanshi)

New approach to derive neutral gravity waves in the daytime through radio method

The neutral waves play a major role in the dynamics of the Earth's upper atmosphere. As these waves propagate in the medium they perturb the densities and temperatures of both the neutrals and plasmas. Conventionally, variations/fluctuations in the intensities of naturally occurring airglow emissions in optical wavelengths have been investigated to obtain neutral gravity wave information. Airglow emissions carry information on the wave dynamical behaviour that exists at the altitudes of their origin. However, here, we present a radio technique, digisonde, by which one can obtain the information on neutral dynamics that are not constrained by clear sky conditions as in the case of conventional measurements by optical techniques. The data from the Digisonde operating from PRL's Thaltej Campus have been used to obtain this information.

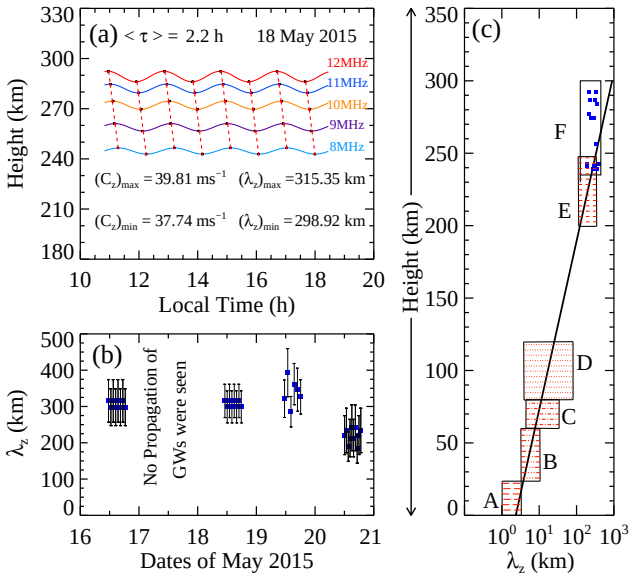


Figure 16. (a) Variations in the heights of isoelectron density contours corresponding to transmission frequencies of 8, 9, 10, 11, and 12 MHz on 18 May 2015 for the GW period of 2.2 h are shown. Clear downward phase movement can be seen. The maximum and minimum phase propagation speeds and the corresponding vertical scale sizes of the GW as obtained are also indicated. (b) The vertical scale sizes obtained for the duration of 16 - 21 May 2015. (c) Distribution of GW vertical scale sizes with altitude as seen from different measurements (adapted and augmented from Figure 10 of Oliver et al., 1997). Boxes A-D as reported by Yamanaka & Fukao (1994), box E is from Oliver et al. (1997), and box F represents the results obtained through the current method.

Information on phase offset in the variations of height of isoelectron density contours have been used to derive gravity wave propagation characteristics. According to Hines (1960) gravity wave theory, downward phase propagation is a characteristic signature of upward propagating waves. Investigations have been carried out whenever both the requirements, namely there exists a phase offset in the height variations of isoelectron density contours at different transmission frequencies and they show the presence of a common time period (which confirms that these perturbations are due to the same source). The vertical phase speed (C_z = Δh/Δt) of the gravity wave has been calculated by using the measured values of the difference in heights (Δh) of the isoelectron density variations and the phase offset times (Δt) with height of the gravity wave. Thus, the vertical scale sizes (λ_z) of the gravity wave can be estimated as: $C_z \times \tau$, τ being the common time period of the gravity wave.

Figure 16 (a) shows the estimation of modulations in the heights corresponding to the isoelectron density for a gravity wave period of 2.2 h on 18 May 2015. The distribution of vertical scale sizes for the duration 16-20 May 2015 obtained by such analyses can be seen in figure 16 (b). Earlier reported values of vertical scale sizes are shown in boxes A-E (Yamanaka and Fukao, 1994; Oliver et al., 1997) in figure 16 (c). Box F represents the values that resulted from the present analysis, and can be seen to agree well with the theoretical estimate (solid black line) of vertical scale sizes as a function of altitude. To the best of our knowledge, such measurements of vertical scale sizes of gravity waves corresponding to an altitude of $\sim$ 270 km has hitherto been not reported.

By virtue of being a radio technique, this approach of deriving gravity wave propagation characteristics can be used in all-weather conditions and is capable of filling in the much needed gap, especially during monsoons and cloudy sky conditions.

(Subir Mandal, Duggirala Pallamraju, Deepak Karan, Ravindra P. Singh and Pradip Suryawanshi)

Derivation of daytime vertical E×B plasma drifts using optical dayglow measurements

It is well-known that the ionospheric equatorial zonal electric fields of Earth play a key role in the generation and development of all the large-scale coupled equatorial and low latitude phenomena as they govern the plasma neutral coupling proccess. Thus, the knowledge of equatorial electric fields is essential for comprehensive investigations on the equatorial and low latitude upper atmospheric processes.

Measurements of vertical drifts of plasma above the magnetic equator give direct information on the electric fields. Conventionally, the Incoherent Scatter Radar at Jicamarca in American longitudes, the MST Radar at Gadanki in Indian longitudes and the Equatorial Atmospheric Radar (EAR) over the Indonesian sector are used to obtain this information. Other than these, satellite based ion-drifts have yielded some measurements. In this work, a novel and an unconventional approach using optical technique is presented to measure the daytime equatorial vertical drifts. In order to do that, diurnal pattern of the ground-based daytime optical airglow emissions at OI 557.7, 630.0, and 777.4 nm wavelengths obtained from Hyderabad (78.4°E, 17.5°N; 8.9°N MLAT) have been carefully looked into. This pattern is observed to be symmetric with respect to local noon on some days and asymmetric on some others. The extent of asymmetric nature has been characterized by our earlier work with a parameter called the Asymmetricity in Time (AT). AT is estimated as the product of the difference in times between the peak emissions and local noon and the ratio of intensities at the peak and local noon. The AT values show similar variation with

the integrated Equatorial Electrojet (EEJ) strength. However, there exist a linear relationship between the EEJ strengths and the vertical drifts. With these considerations, the AT values obtained from the dayglow measurements have been used to infer the vertical drifts by comparing them with the EEJ values. Figure 17a shows the variations in the derived vertical drifts and F10.7 cm solar flux, which indicates that the variations in the derived drifts are not due to the solar flux variations. Figure 17b shows the derived drift values which match well with the model estimates and other measurements (references indicated in the figure). This method of deriving vertical drifts can be used to carry out both, the day-to-day and large time scale estimates of vertical drifts, which will help in the advancement of comprehensive understanding of equatorial electrodynamics. Such method opens up a new and independent technique to derive the equatorial vertical drifts on a day-to-day basis.

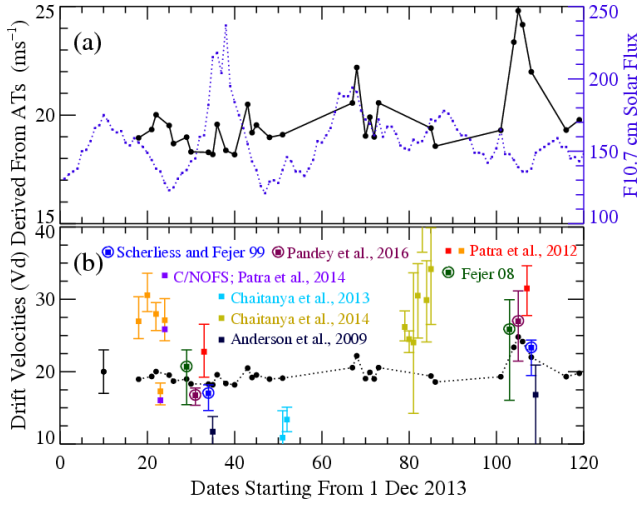


Figure 17. (a) Variations of the vertical drifts derived from the present optical method (wherein AT values are used as inputs) and solar flux (b) Comparison between the derived vertical drifts with the model estimated values, and measurements from published literature.

(Deepak K. Karan and Duggirala Pallamraju)

Mid and Low-latitude dayglow and compositional variation

Daytime oxygen airglow intensity variability provides us with a means of remote investigations of the upper atmospheric behaviour. The dayglow emissions typically show a diurnal pattern with a peak at around noontime, especially during geomagnetic quiet conditions. The photochemical and empirical models show that the emissions vary as a function of solar zenith angle and solar flux. Thus, both, larger solar flux magnitudes and smaller solar zenith angles, contribute to a larger dayglow brightness as the yield of excited oxygen atoms is expected to be greater in those conditions. However, seasonal dayglow emission variability obtained from measurements at low-latitudes (Hyderabad, India; 17°N, 80°E; 8.7°N Mag. Lat.) and mid-latitudes (Boston, USA; 42.2°N, 71°W; 48.3°N Mag. Lat.) show different behaviour with regard to solar flux variation. While the low-latitude emission variability is dependent on solar flux variations, the variability over mid-latitudes is not. This discrepancy is understood to be due to the relative effects of solar flux and the naturally varying compositional variability that are operative differently at different latitudes. Seasonal compositional variation due to transport processes is attributed to be the cause for the observed discrepancy which is also confirmed by independent satellite measurements.

This work is done in collaboration with T. Vijaya Lakshmi, JNTUH and S. Chakrabarti, UML, USA.

(Duggirala Pallamraju and Deepak K. Karan)

Interhemispheric Meridional Circulation During Sudden Stratospheric Warming

Sudden stratospheric warming (SSW) is mostly a northern high-latitude phenomenon. Our earlier dayglow work from Hyderabad showed that there were enhancements in the oxygen emission intensities whenever the SSW events occurred. Based on this and other supporting satellite measurements, setting up of circulation and meridional wind in the MLT region during SSW events was postulated. In the present work, we show based on global empirical models that such a wind circulation does indeed exist. The present investigation uses wind observations from two ground-based specular meteor radars over northern high- and mid-latitudes and global winds from a high altitude meteorological analysis system to characterize global mesospheric circulation anomalies for major SSW events that occurred during 2010 and 2013. During these events the radar observations and the reanalysis winds exhibited strong southward winds over the two northern mid- and high-latitude stations. Using space-time filtering of the high altitude meteorological analyses, to remove background winds and dominant migrating and non-migrating tidal components, we show that these southward wind anomalies are part of a larger global scale circulation pattern extending from the Northern to some parts of Southern Hemisphere in the MLT altitudes. From selective filtering of various waves, it is observed that planetary waves play a key role in driving this circulation. These results also clearly show the influence on low-latitude ionospheric electrodynamics by the SSW-induced changes in circulation at high-latitudes. This independent approach confirms the setting up of meridional wind circulation during SSW postulated by the earlier dayglow work.

This work is done in collaboration with Fazlul I. Laskar, J. Chau, P. Hoffmann at IAP, Germany, and J. P. McCormack at NRL, USA.

(Duggirala Pallamraju and Ravindra P. Singh)

Diffusion coefficient during NLC

The Andenes specular meteor radar shows meteor-trail diffusion rates increasing on an average by ∼20 % at times and locations where noctilucent clouds (NLCs) were seen to be present in the lidar observations. This high-latitude effect has been attributed to be predominantly due to thermal tides. This conclusion has been arrived at by the analysis of data from three stations, at high-, mid-, and low-latitudes, for the years 2012 to 2016. Comparison of diffusion rates at these locations shows that thermal tides correlate strongly with the presence of NLCs. These data also show that the connection

between meteor trail diffusion and thermal tides occur at all altitudes in the mesosphere while the NLC influence exists only at high-latitudes and at around peak of NLC layer.

This work is done in collaboration with Fazlul I. Laskar, IAP, Germany.

(Duggirala Pallamraju)

Evidence for significant impact of disturbance dynamo on equatorial ionosphere

The role played by disturbance dynamo electric field (DDEF) disturbances on equatorial ionosphere is identified based on 16 years of hourly variations of equatorial electrojet (EEJ) strength over the Indian sector.

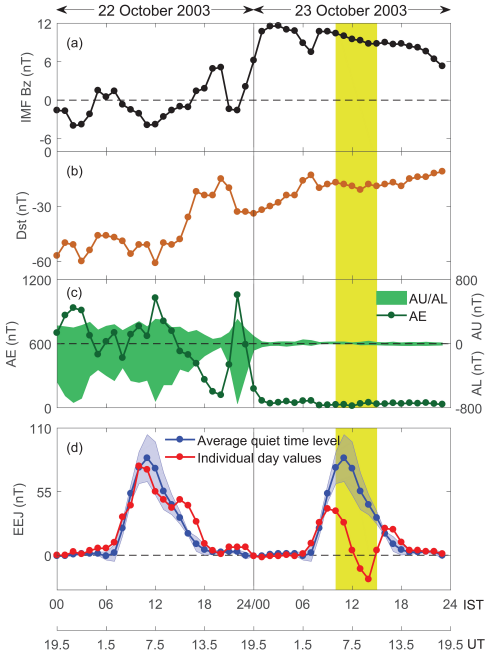


Figure 18.From the top to bottom are (a) variations in the z component of interplanetary magnetic field (IMF Bz), (b) disturbance storm time (Dst) index, (c) eastward (AU), westward (AL) and auroral electrojet (AE) indices, and (d) strength of equatorial electrojet (EEJ) along with average quiet time EEJ values of the month with standard deviations (blue-coloured shaded area) for the event day (23 October 2003) when disturbance dynamo effects are observed (marked by the yellow rectangular box) as well as on a day prior to it (22 October 2003).

It is found that, in three extreme cases (one case is presented in Figure 18), the reduction in EEJ strength from quiet time average values of the respective month is more than twice the standard deviations for at least 3 hr. Interestingly, the equatorial electric field perturbations associated with disturbance dynamo are found to be as large as -0.7 $\pm$ 0.2 to -1.2 $\pm$ 0.3 mV/m around noon hours. These values are significantly larger than the DDEF perturbations over equatorial latitudes expected from the earlier models. A possible contribution from semidiurnal-tides is suggested to augment the additional reduction in the electric field.

(Kuldeep Pandey, D. Chakrabarty, and R. Sekar)

Evidence for deep ($\sim$3.5° magnetic latitude) ingression of the mid-latitude MSTID

Based on OI 630 nm airglow imaging observation from a low latitude station, Gadanki (13.5°N, 79.2°E; 6.6° MLAT) on 12 January 2016, an observational evidence (Figure 19) of medium scale traveling ionospheric disturbances (MSTIDs) reaching to magnetic latitude as low as $\sim$3.5° over the Indian sector is provided for the first time. Imaging observations from Allahabad, a station close to the equatorial ionization anomaly (EIA) crest, confirmed that the noted MSTID event was of mid-latitude origin and propagated to low latitudes. In addition, a quasi-periodic southward moving wave (QPSMW) signature was also observed during pre-midnight hours on this night. In addition to the above features, a small scale southward moving wave signature also noted during this night. Though the direction of propagation of this feature is similar to the QPSMWs, their characteristics are different. Global GPS- TEC maps suggest that weak and asymmetric EIA crest on this night provided favourable background condition for the deep ingression of the mid-latitude MSTID to very low latitudes. In the course of propagation through the midnight pressure budge, the MSTID and QPSMW structure disappeared. Therefore, the present investigation shows that the mid latitude MSTIDs can influence the F-region plasma processes even over very low latitudes under favourable background conditions.

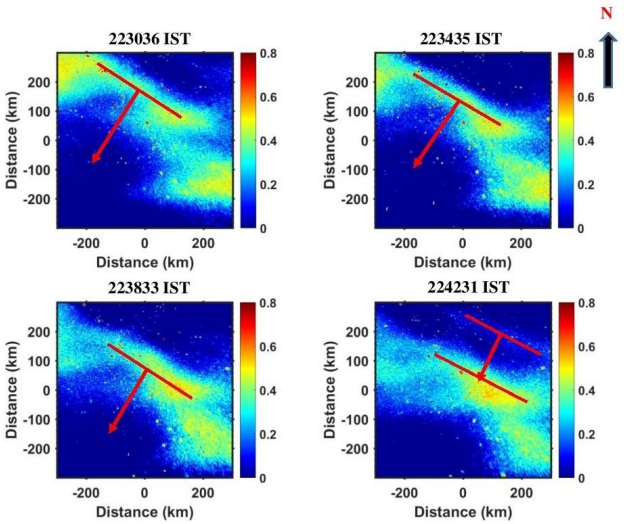


Figure 19. Consecutive OI 630.0 nm nightglow images obtained from Gadanki (0, 0 point) that capture the North-West to South-East aligned phase fronts with South-Westward moving wave signature from 22:30 IST to 22:42 IST. In these images, phase fronts are marked by the red line and the phase propagation is represented by the red arrow.

This work is done in collaboration with T. K. Ramkumar from National Atmospheric Research Laboratory, Gadanki, India, A. Taori from Regional Remote Sensing Centre-(Central), Nagpur, India and N. Parihar from Equatorial Geophysical Research Laboratory, Indian Institute of Geomagnetism, India.

(M. Sivakandan, D. Chakrabarty and A. Guharay)

Imaging observations of nearly field-aligned plasma depletion structures over Hanle with mid-latitude origin

Observations made using an airglow imager from Hanle (32.7°N,

78.9°E; dip lat. ∼24.1°; Height: ∼4200 m above the mean sea level) reveal nearly field-aligned plasma depletion structures. The plasma depletion structures drift westward with phase speed of 76.9±14 m/s and thus, different from medium scale traveling ionospheric disturbances (MSTID) structures Global Navigation Satellite System (GNSS) total electron content (TEC) measurements from Hanle also show depletion in the TEC at the same time. Interestingly, radar observations from Gadanki show absence of low latitude plasma depletion structures. This strongly indicates that the nearly field-aligned structures observed over Hanle have mid-latitude origin.

This work is carried out in collaboration with S. Mondal, S. Sarkhel and M. V. Sunil Krishna from the Indian Institute of Technology, Roorkee, P. Pavan Chaitanya and A. K. Patra from National Atmospheric Research Laboratory, Gadanki, A. K. Upadhayaya from the National Physical Laboratory, Delhi and R. K. Choudhary and T. K. Pant from the Space Physics Laboratory, VSSC, Tiruvananthapuram.

(M. Sivakandan, and D. Chakrabarty)

Observational evidence of the influence of geomagnetic storm on the low latitude MLT region

Using the observations from the ground-based all sky airglow imager at Gadanki (13.5°N; 79.2°E), Meteor radar observations from Tirupati and space borne Sounding of the Atmosphere using Broadband Emission Radiometry (SABER) satellite data, the dynamical and chemical changes in the low latitude mesosphere lower thermosphere (MLT) region during 17 March 2015 severe geomagnetic storm are brought out. Our analysis shows that characteristically different chemical and dynamical changes occurred on this night vis-à-vis the other nights. These changes are brought out based on in-depth analyses.

This work is carried out in collaboration with T. K. Ramkumar from the National Atmospheric Research Laboratory, Gadanki.

(M. Sivakandan, D. Chakrabarty and A. Guharay)

Dawn-dusk asymmetry in the ring current and role of IMF By

The ring current is found to be asymmetric during the main phase of the geomagnetic storm and a dawn-dusk asymmetry is observed. This dawn-dusk asymmetry is caused by the partial ring current (PRC) which is closed via region 2 field-aligned currents (R2 FACs) through the auroral ionosphere. We investigated the magnetic local time (MLT) variations in the H-component at 27 ground magnetic stations (09-45° magnetic latitude) with respect to the mean H variation calculated by averaging these stations for three cases of geomagnetic storms, with different solar wind background conditions. Significant dawn-dusk asymmetries were observed during the main phase of the geomagnetic storms showing the relative importance of PRC. The investigation brings up, for the first time, the additional importance of IMF By using AMPERE data in addition to the known importance of southward IMF Bz and solar wind dynamic pressure in determining the MLT dependence of dawn-dusk asymmetry.

(Sandeep Kumar and D. Chakrabarty)

Study of temporal and spectral characteristics of the X-ray emission from solar flares

Temporal and spectral characteristics of X-ray emission from 60 flares of intensity ≥C class observed by the Solar X-ray Spectrometer (SOXS) during 2003-2011 are presented. We analyze the X-ray emission observed in four and three energy bands by the Si and Cadmium-Zinc-Telluride (CZT) detectors, respectively. The number of peaks in the intensity profile of the flares varies between 1 and 3. We find moderate correlation (R ≃0.2) between the rise time and the peak flux of the first peak of the flare irrespective of energy band, which is indicative of its energy-independent nature. Moreover, the magnetic field complexity of the flaring region is found to be highly anti-correlated (R = 0.61) with the rise time of the flares while positively correlated (R = 0.28) with the peak flux of the flare. The time delay between the peak of the X-ray emission in a given energy band and that in 25-30 keV decreases with increasing energy, suggesting conduction cooling is dominant in the lower energies. Analysis of 340 spectra from 14 flares reveals that the peak of differential emission measure (DEM) evolution is delayed by 60-360 s relative to that of the temperature, and this time delay is inversely proportional to the peak flux of the flare. We conclude that temporal and intensity characteristics of flares are dependent on energy as well as the magnetic field configuration of the active region. *This work has been done in collaboration with Dept. of Physics, Kadi Sarva Vishwavidyalaya, Gandhinagar.*

(Som Sharma)

Anomalous variations of VLF sub-ionospheric signal and Mesospheric Ozone prior to 2015 Gorkha Nepal Earthquake

The subject of pre-earthquake ionospheric signatures has always been contentious and debatable. Some of the previous reports have documented unforeseen and unusual variations in some of the atmospheric and ionospheric parameters well before an earthquake. Here, we analyze the ionospheric response from the Indian Subcontinent to Nepal Gorkha Earthquakes occurred between April and May 2015, which were the most powerful and disastrous natural calamities in past ∼80 years over the Himalayan region left ∼9000 causalities and more than ∼20000 people injured with the property damage of the order of several billion dollars. In view of severe earthquakes occurrences, their prior information on the shorter time scales are warranted for mitigation of associated disasters. Here, we report for the first time, a case which shows a strong link in anomalous variations between VLF sub-ionospheric signal and mesospheric ozone prior to both April 25, 2015 (Mw = 7.8) earthquake and its biggest aftershock on May 12, 2015 (Mw = 7.3). Observations show an unusual variation in VLF signals amplitude /shift in terminator time (TT) strongly linked with positive (negative) mesospheric ozone anomaly in D-region altitudes prior to the Gorkha Nepal earthquakes. It is surmised that simultaneous continuous observations of both VLF waves and mesospheric ozone can be considered as an important tool to identify the prior earthquake signatures in the vicinity of the extremely earthquake-prone zone such as Himalayan region. In this context, the current report opens up a new dimension in lithosphere-atmosphere-ionosphere coupling during the earthquake preparation processes itself.

This work has been done in collaboration with Aryabhatta Research Institute of Observational Sciences (ARIES), Nainital, India.

(Kondapalli Niranjan Kumar and Som Sharma)

Geosciences

Geochemical Provenance of Vindhyan Sediments

The Vindhyan Basin of western India is a part of the largest Proterozoic sedimentary basin of the Indian subcontinent. Deposited in a largely shallow marine environment, the sedimentary sequence of the basin, known as the Vindhyan Supergroup, is believed to hold clues to our understanding of the evolution of life and climate during the Proterozoic. In spite of multiple important paleobiological discoveries from these rocks, our knowledge about the development of the basin and responsible regional tectonics had remained rudimentary. We propose a model for the evolutionary history of the Vindhyan Basin based on quantitative provenance analysis through geochemical and isotopic compositions of siliciclastic sediments. According to our model, the basin opened up in a foreland setting during an event that was contemporaneous with the amalgamation of the supercontinent Columbia. In the Lower Vindhyans, most of the sediments were derived from the basement gneisses (BGC-I & II) and a younger differentiated magmatic arc, whereas the $>$1.7 Ga rocks of the Aravalli and Delhi supergroups formed the source area for the Upper Vindhyans. In comparison to their counterparts in the eastern sector in the Son Valley, the Semri and Kaimur groups of the western sector had a relatively younger provenance; whereas, the Rewa and Bhander groups of both the sectors appear to have shared geochemically similar provenances. Unlike its counterpart in the eastern sector, the provenance of the sediments in the western sector had remained constant across the supposedly 400 million years break in sedimentation between the Lower and the Upper Vindhyans. However, a change in the provenance is observed during the transition from the Kaimur to Rewa group in the western sector which we infer to be a break in the deposition.

(A.D. Shukla and J.S.Ray)

Geochemistry of carbonate formations of the Chhattisgarh Supergroup

The Chhattisgarh Supergroup is one of the major Proterozoic marine sedimentary sequences of India. It consists of largely undeformed and unmetamorphosed siliciclastic, volcaniclastic, and carbonate formations deposited in two sub-basins, Hirri and Bharadwar, separated by an Archean greenstone belt. In spite of its apparent importance for Mesoproterozoic oceanic records, very few geochemical studies have been carried in the basin. Here, we present results of our high resolution geochemical and C-O-Sr isotopic studies in two carbonate formations of the supergroup: the Charmuria and the Chandi. We observe elevated $\delta\ ^{13}$C values increasing from 2.6‰to 3.6‰in these formations, which is consistent with the globally reported late Mesoproterozoic values. Such consistently positive $\delta\ ^{13}$C values are attributed to increased organic carbon burial in the basin margins during the deposition of these carbonates. Based on the principles of $\delta\ ^{13}$C isotope stratigraphy, we suggest a depositional age between 1.0 and 1.2 Ga for these carbonates which form the upper part of the supergroup. The lowest ^{87}Sr/^{86}Sr ratios obtained from the Charmuria and Chandi formations, 0.70723 and 0.70816, respectively, are more radiogenic than the contemporaneous seawater, suggesting that the Sr isotopic system of the formations are altered. Based on the similarity in the $\delta\ ^{13}$C values, we stratigraphically correlate the carbonate formations of the Raipur Group in both the Hirri and Bharadwar sub-basins. We compile the available $\delta\ ^{13}$C and ^{87}Sr/^{86}Sr records from all the Proterozoic sedimentary successions of India and compare it with the global datasets. We find that while the Indian basins possess records of the Bitter Springs and Shuram $\delta\ ^{13}$C anomalies, they lack evidence for the other major global events of the Proterozoic.

(B.G.George and J.S.Ray)

Timings of formation and obduction of Andaman Ophiolite

The Andaman ophiolite forms part of the ophiolite chain that encircles the northern and eastern boundaries of the Indian plate. Unlike its northern counterparts it occurs on an accretionary prism, located at the convergent margin of Indian and Burma plates. It not only forms the basement of the accretionary complex but also occurs as thrust sheets on outer-arc sediments. The timing of formation and emplacement of this ophiolite had remained sketchy. Here we present results of our effort to date these events by ^{147}Sm - ^{143}Nd and ^{40}Ar - ^{39}Ar methods and understand their implications for the evolution of the Andaman subduction zone. Our geochemical data suggest that the ophiolite had formed in a supra subduction zone setting. The whole-rock ^{147}Sm - ^{143}Nd isochron age for nine samples from crustal and mantle sections suggests a formation age of 98$\pm$8 (2σ)Ma, which is consistent with the existing age data and with the age of the ocean crust beneath the volcanic arc, located $\sim$100 km to the east. The ^{40}Ar - ^{39}Ar apparent age spectra for four samples from the faulted margin of the east coast of the south and middle Andaman Islands, though disturbed, yield plateaus for low temperature steps ($< 900^{o}$C) having concordant ages with an average of 0.9$\pm$0.3 (2σ) Ma, the timing of argon resetting. This timing points to a mega thrusting event responsible for obduction of the entire eastern belt ophiolite onto the accretionary prism. Based on our results and lithostratigraphy of sediments on the Andaman Ridge we propose a tectonic evolutionary model for the prism that involves twofold ophiolite obduction, one at $\sim$ 60 Ma and the other at $\sim$ 0.9 Ma.

(J.S. Ray)

Revelation of hydrometeorological processes affecting precipitation in different climatic zones of Indian sub-continent

The South West (SW) redundant monsoon (Jun-Sep), North East (NE) winter monsoon (Oct-Dec), Western Disturbance (WD) (Jan-Apr) and local recycling are the four major rain forming systems, governing water availability in Indian Sub-continent, which covers only $\sim 3.2\%$ of the global land area but accommodates $\sim 23.2\%$ of the global population. Major knowledge gap in hydrometeorology concerns regions of prominent local recycling, effect of large wetlands in NE India, extent of evaporation from falling raindrop in arid regions, latitudinal extent of NE monsoon, etc. Daily precipitation was sampled from Ahmedabad, Jorhat, Jammu and Hyderabad (inset of Fig.1b), in different climatic zones to understand the subtle hydrometeorological processes from their oxygen and hydrogen isotopic signatures. All the four stations exhibit positive values of δ^{18}O associated with high or low d-excess (Fig. 1b), suggest either a very low condensation temperature and thus, higher fractionation or extensive evaporation from falling raindrops.

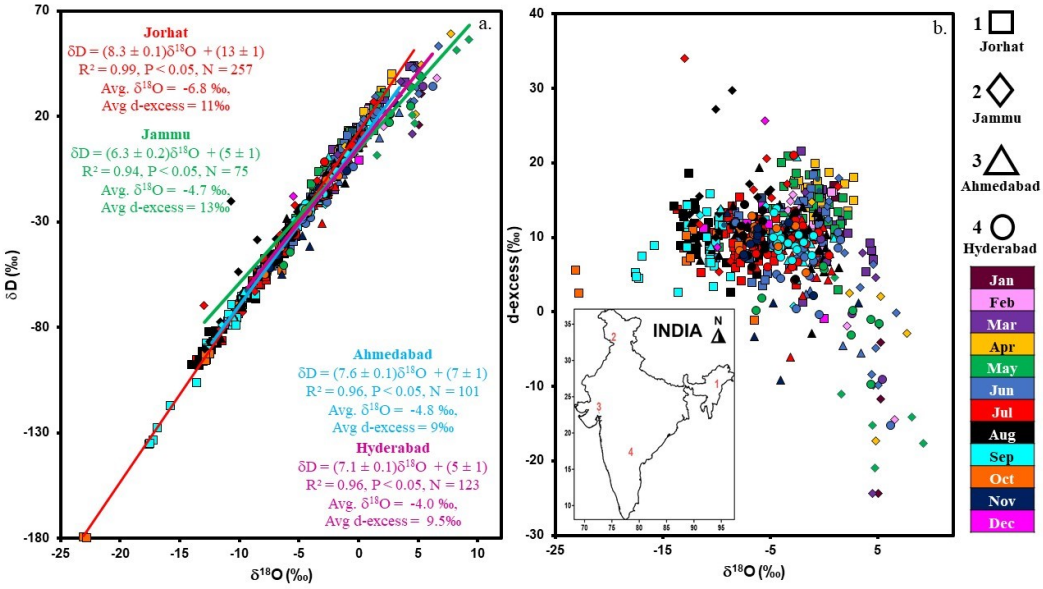


Figure no 1: . (a) LMWL and average isotopic composition of daily precipitation at four stations in India; (b) δ^{18}O - d-excess plot for all four stations, with inset showing the geographical location. Shape of marker represents station and its colour represents the month.

The salient features and inferences drawn from them are:(a) The slopes of all Local Meteoric Water Lines (LMWL) except Jorhat (8.3$\pm$0.1 ‰) shows varied degree of evaporation (Fig. 1a) through falling raindrop. The higher value of intercept (13$\pm$1 ‰) than GMWL (Global Meteoric Water Line) at Jorhat suggests contribution from significant local recycling from wetlands and rivers. (b) The LMWL slope for Jammu (6.3$\pm$0.2 ‰) and Hyderabad (7.1$\pm$0.1 ‰) is lesser than the most arid station of Ahmedabad (7.6$\pm$0.2 ‰). This is because rainfall intensity (mm/day) at Ahmedabad is higher compared to other two places, which receive scanty rainfall during non-monsoon period and facilitate evaporation from falling rain. The high d-excess (Fig. 1(b)) at Jammu during SW monsoon indicates contribution of moisture picked up by winds flowing over the Indo-Gangetic plains. Contrary to expectation, isotopic signature of WD is absent at Jammu. (c) About 74$\%$ of rain with δ^{18}O less than annual amount weighted average (-4.8 ‰) occurs in Aug-Sep at Ahmedabad. The average δ^{18}O (-6 ‰) is lighter and d-excess (-9.5 ‰) is higher during Aug-Sep indicating increased continental recycling, facilitated by increased water availability due to rainfall of Jun-Jul. (d) Lower δ^{18}O (-6.3 ‰) during NE monsoon period compared to SW monsoon (-3.8 ‰) at Hyderabad (17.37^{0}N) suggests change in moisture source from the Arabian Sea to the Bay of Bengal and influence of NE monsoon.

(H. Oza, V.R. Padhya, A. Ganguly & R.D. Deshpande)

Isotope extremes in precipitationinsights into atmospheric processes

There are numerous studies showing increasing trend in temperature, rainfall, cyclone frequency, intensity and spatial coverage of droughts and sea surface temperatures. However, understanding about the hydro-meteorological processes underlying these observations is far from complete. Oxygen and hydrogen isotopic composition of precipitation provide useful information about contemporary hydro-meteorological processes governing the precipitation, and hence the water availability in a region. Thus, based on δ^{18}O and d-excess (=δ D $-$ 8$\times\delta^{18}$O) in precipitation samples various meteorological phenomena and weather extremes, such as strong convection, heavy rain, evaporation from falling raindrop, unusual rainout history, significant contribution of continentally recycled moisture can be identified. With these objectives, the oxygen and hydrogen isotopic composition of 369 daily precipitation samples from Ahmedabad in semiarid western India, collected over a period of 12 years has been examined. Of these 369 samples, 40 rain samples had exceptionally different isotopic composition (20$<$ d-excess$<$ 0). The atmospheric processes underlying these observed isotope extremes have been studied. The high d-excess ($>$ 20 ‰) indicates locally derived vapor source and high amount of rainfall with d-excess ($>$ 20 ‰) further indicates rain events associated with strong convection

and rapid upward movement of warm and moist air from local moist sources during thunderstorm. On the other hand, there are rain events with very low d-excess values (< 0 ‰) which are associated with both low and high rainfall. Rain events with low d-excess and high amount of rainfall can be ascribed to major rain event from a cloud parcel with significant rainout history. In addition, rain events with low d-excess and low rainfall could be related to significant evaporation from falling raindrop in a minor rain event. It was observed that precipitation events with extremely low and high d-excess in 2013 and 2014, with seemingly similar physical manifestations of heavy rain and floods, were in fact related to two different meteorological processes viz. (i) major rain event from cloud parcel with significant rainout history and (ii) strong convection derived local moisture during thunderstorm. This fact could be discerned using oxygen and hydrogen isotopic composition in precipitation and proved using backward wind trajectory analysis. Many of the low and high d-excess events are also associated with similar hydrometeorological processes but with lesser intensity. Therefore, such events did not result in extreme rainfall and flood but, could be identified based on their isotopic composition. This study suggests that isotopic composition of precipitation can also be used as an indicator and early warning system for unusual meteorological processes which do not result in extreme rainfall.

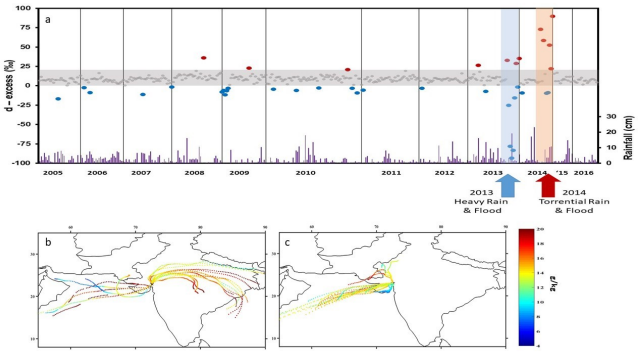


Figure no 2: (a) 12 years of annual time series of d-excess and daily rainfall. Highlighted in blue and red are two rain events in 2013 and 14, resulting in heavy floods caused by two different meteorological processes, as identified by d-excess; (b) and (c) are ensembles of 78 h back trajectories initiated at 1.5 km above ground level (agl), starting at 6 hourly intervals during 24 hours for each daily rain event at Ahmedabad, for low d-excess events and high d-excess events, respectively. Colour code indicates specific humidity in g/kg

(H. Oza, V.R. Padhya, A. Ganguly & R.D. Deshpande)

Effect of Narmada Canal on groundwater scenario in North Gujarat

Narmada main canal, spreading from Narmada district in the south to Banaskantha district in the north is one of the large irrigation canal networks in the world, which is set up to recharge the overexploited aquifer of northern Gujarat and is supplying water to north Gujarat and Kachchh region for agricultural purposes. Due to scanty rainfall and lack of perennial rivers the north Gujarat and Kachchh experience severe water scarcity and groundwater depletion. Over 4 meters fall in groundwater level has been observed in most parts of northern Gujarat during the last one decade. However, the use of groundwater has declined after commencement of water flow in Narmada canal and consequent increase in availability of surface water. The irrigation return flow from canal fed irrigation is also expected to augment the groundwater recharge and ameliorate groundwater depletion scenario. With a view to understand effect of Narmada Canal on groundwater, the groundwater level data for 1996 (before Narmada Canal) and 2015 (after Narmada Canal became operational) were studied. The percentage rainfall departure and groundwater level change from pre-monsoon to post-monsoon season as recorded for observation wells has been compiled. The study suggests that the groundwater withdrawal in wells near the Narmada canal corresponds to rainfall in the area before the practical commencement of canal. The contribution of rainfall to groundwater recharge during 1996 is more as compared to 2015, which are rainfall deficit and rainfall excess years respectively, as evident from the Fig. 3. However, after the commencement of canal, the change in groundwater level during pre and post monsoon periods has increased significantly (during 2015) by up to $\sim$ 14 m, indicating an enhanced groundwater recharge due to impact of canal water availability (Fig. 3). This preliminary information based on two selected years, 1996 and 2015, (one each in pre-canal and post-canal) needs to be substantiated with data from other locations along the Narmada Canal. It is necessary to isotopically characterise the groundwater in the vicinity of Narmada Canal and the canal water itself to understand the interaction between groundwater and canal water.

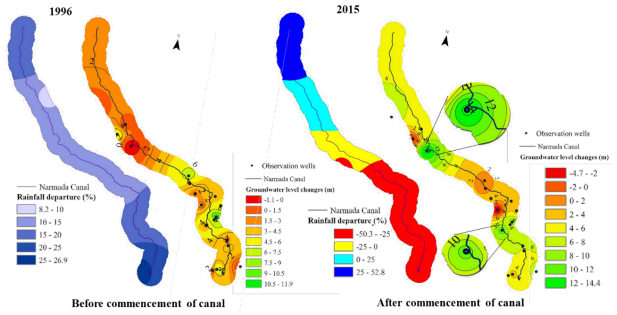


Figure no 3: The spatial variation of percentage rainfall departures and change in groundwater level in wells during pre and post monsoon periods in the study area in 1996 (before commencement of canal) and 2015 (after commencement of canal). The elevated changes in groundwater level during 2015 are shown in insets.

(M.C. Raicy, A. Pandey & R.D. Deshpande)

An innovative approach to estimate ground level vapour isotopic composition through liquid condensation and non-linear regression

Oxygen and hydrogen isotopic composition form a powerful tool to trace origin, movement and mixing of atmospheric water vapour and understanding contemporary hydrometeorological processes affecting spatio-temporal distribution of water in different hydro-climatic regions. Isotopic composition of ambient water vapour is one of the most important input parameters for isotope mass balance and isotope enabled atmospheric circulation models. Currently, laser-based absorption spectrometers exist but are costly and often lack portability whereas Satellite based measurements are prone to large error.

Therefore, a novel, simple and cost-effective method for collecting ambient water vapor for estimating its isotopic composition has been developed. This method involves liquid condensation of ambient water vapour on an ice-cooled (0°C) metallic surface under the supersaturated environment which involves kinetic fractionation due to diffusion of isotopic water molecules through supersaturated boundary layer at the metallic surface. The condensate obtained is found to be isotopically more depleted compared to true isotopic composition of vapor collected by complete cryogenic trapping. In this study we have developed a non-linear regression equation to obtain true vapor isotopic composition using the condensate values. The difference between true and predicted values is calculated and the standard deviations for this are be 1.83 ‰for δ^{18}O and 10 ‰for δD based on the 254 vapor samples collected both by conical condensation. This exercise was repeated with 96 samples from National Institute of Hydrology (NIH), Roorkee and 296 samples from National Geophysical Research Institute (NGRI), Hyderabad and the standard deviations were 2.86 ‰and 2.61 ‰respectively for δ^{18}O which is far superior than the best satellite based methods (10 ‰δ^{18}O precision). The difference between isotopic composition estimated using non-linear regression and the true values are ascribed to uncertainties in estimating: 1. The condensation temperature being greater than 0°C owing to latent heat of condensation; 2. Diffusivity coefficient at condensation temperature; 3. Presence of an isotopic gradient near the surface which further hinders the flow of heavier isotopologues; 4. Possible backflow in the micron thick boundary layer. In spite of these known limitations, the innovative approach proposed by us provides isotopic composition more accurately than that obtained from satellite-based observations. Further, this innovative approach can be employed in any location, independent of climatic condition and with minimum laboratory resources. This approach will provide a big boost to monitoring isotopic composition of vapour, particularly in remote areas of deserts, mountains, forests where infrastructure is available for conducting such experiments.

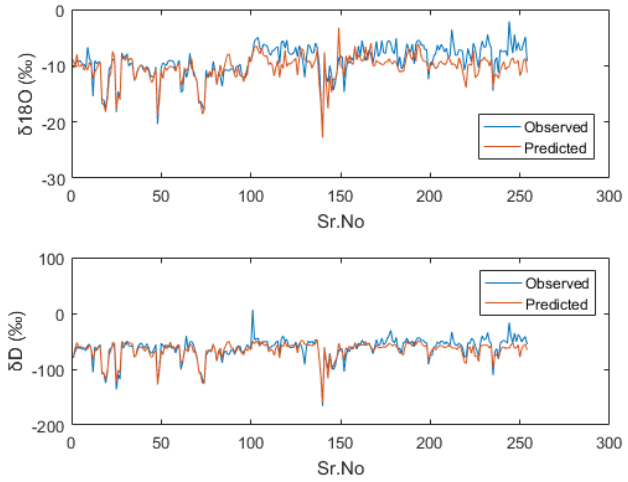


Figure no 4: The predicted Δ^{18}O and δ^{18}O values are plotted and compared against the observed experimental values

(A. Ganguly, V.R. Padhya & R.D. Deshpande)

Zn-Fe/ H_2 - Fe graphite preparation line

Radiocarbon activity of ancient and modern carbon sample having small size ($\sim$ 1mg C) can be measured in an Accelerator Mass Spectrometer (AMS).These measurements require carbon to be converted into graphite which is further used as a target to generate carbon beam in AMS. Two methods of graphite preparations viz. H_2 - Fe method and Zn-Fe method are currently adopted by most of the radiocarbon dating laboratories. To understand intricacies and optimum conditions of the procedures we have successfully executed both the reactions in the in-house developed radiochemical lines. Although the Zn-Fe based method is slower than H_2 - Fe method it does not require use of hydrogen gas and cooling traps and hence unattended safe reactions are warranted. A glass vacuum system to handle five samples at a time has been developed in our lab and is currently being used for routine sample processing following Zn-Fe method. The reactions have high graphite yield (90-100 $\%$) for $\sim$ 200-300 microgram carbon samples. The same setup without any modification can be used to execute H_2 - Fe method as well.

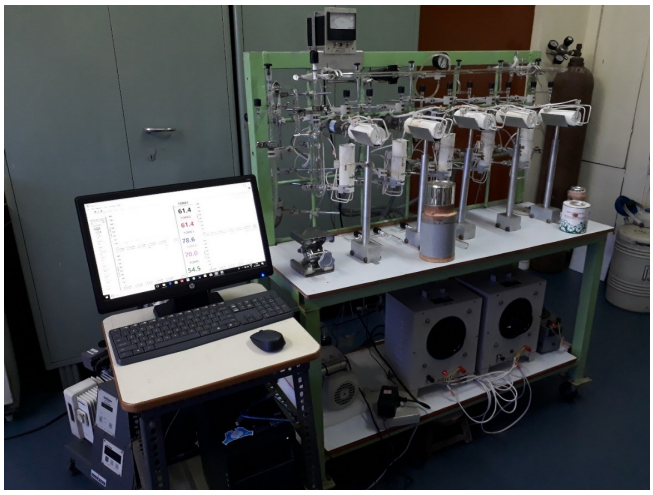


Figure no 5: Graphite preparation line for Zn-Fe/H_2-Fe method.

(M. Shah, P. Kiran Kumar, P. Nayak & M.G. Yadava)

Water Isotope Analyser

Conventional mass spectrometers use magnetic and electric fields to identify mass to charge ratio. The method requires water vapour to be collected cryogenically and later equilibration of the sample with external standard gas reservoir. These are time consuming and also restrict sampling frequency ($\sim$ 0.5 to 1 hr per sample). Therefore, for isotope ratio measurement of water in vapour form, laser based mass spectrometers are presently the preferred method. A machine procured from ABB Los Gatos Research that follows Off-axis Integrated Cavity output laser spectroscopy (OA - ICOS) method was installed in May 2017. A laser cavity is filled directly with ambient air and ring down time for various characteristic ro-vibrational levels of water molecules are estimated and used to find out concentrations of isotopes of oxygen and hydrogen. Continuous high time resolution

(100s) measurements of isotopic composition of water vapour in ambient air from Ahmedabad using the machine is shown in (Fig. 6). We observe that during transition of seasons around Sept-Oct in 2018 CE, mixing ratio has a decreasing trend from $\sim$ 30,000 ppm to $\sim$ 15,000 ppm. Average δ^{18}O values during wet period are close to -9 ‰with variable values between -6 ‰and -15 ‰during dry period in Oct. δD shows similar type of variability, with average value during wet period remaining around -65 ‰and between -60 ‰to -100 ‰during dry period in Oct. In addition, a persistent diurnal variability is observed throughout the observational period.

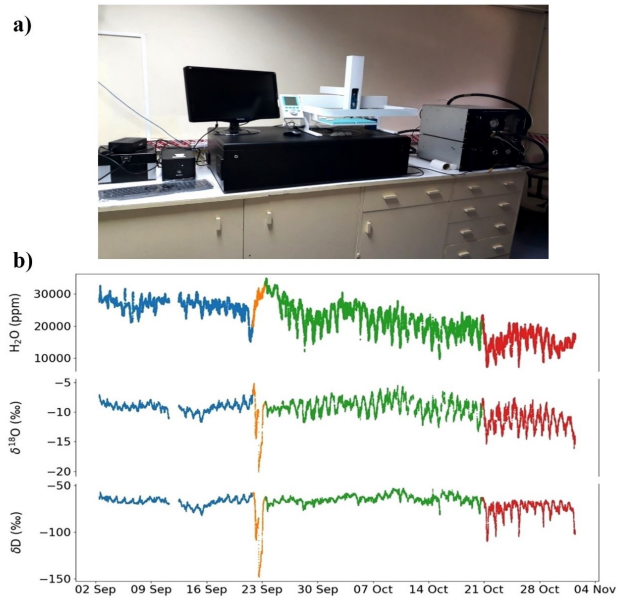


Figure no 6: a) Water isotope Analyser with necessary peripherals shown in the photo in the panel above. b) Variations in δD, δ^{18}O and water content in the air mass, around PRL main campus at Ahmedabad, directly injected in the water isotope analyser is shown in the plot. A short spell of rain event that occurred on 22-Sept-2018 is seen as depletes levels in the isotopic signals. Diurnal variability seems to be effect of day time enhanced evaporation from the open land surface.

(P. Nayak, P. Kiran Kumar & M.G.Yadava)

Measurement of trace elements in seawater using SeaFAST-HR-ICP-MS

Trace metals in seawater play an important role in regulating the oceanic primary production by acting as enzymes in several metabolic processes like carbon fixation, N^2 fixation, Silica uptake etc., and hence influence the biological pump (export of carbon from the surface ocean to sea floor through primary production). Insufficient concentration of these essential micro-nutrients will limit phytoplankton growth in ocean. Hence, their biogeochemical cycling has direct implications to the carbon cycle, climate change, ocean ecosystems, in addition to environmental contamination.These essential metals exist in seawater at a very low concentration (sub-nanomolar to picomolar), and are prone to contamination during sampling and analysis.The method protocol for determining such low level concentrations of trace metals (Fe, Zn, Mn, Ni, Cu, Co) was established using Seafast-HR-ICP-MS. SeaFAST is a sample introduction system attached to the HR-ICP-MS to remove the salt matrix of the seawater samples online by retaining trace metals on an ion exchange resin and successive elution of the retained species.

In this process, samples were pre-concentrated to $\sim$75 times to get the sufficient signal. Nobias-PA1 resin, which is a combination of Iminodiacetate and EDTA that enhances the pH range of the trace metals, was used to pre-concentrate the samples. Calibration was performed using low trace metal seawater matrix and confirmation was done by measuring various international seawater reference standards as well as commercially available standards and by standard addition method. In addition, measured Zn concentrations were compared with the data obtained using another independent analytical method on Flow injection system and found agrees within 10%. Typical depth profiles of Fe, Zn, Mn, Ni, Cu and Co in the Andaman Sea obtained by using this method is given in Fig. 7.

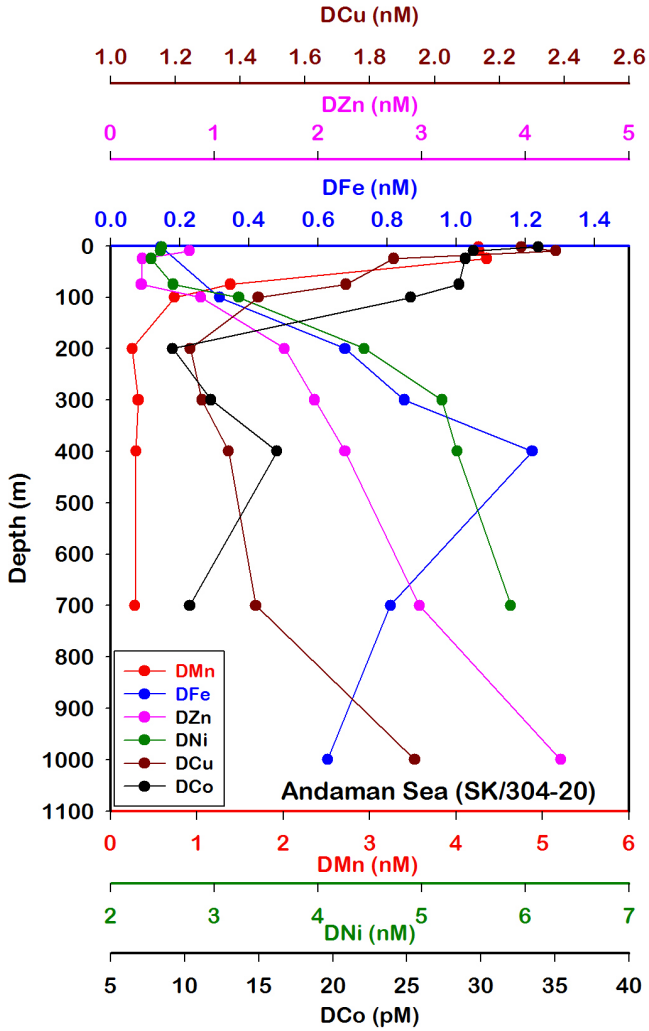


Figure no 7: Profiles of Fe, Zn, Mn, Ni, Cu and Co in sea waters of Anadaman Sea.

(V. Chinni, A.K. Sudheer, M. Gaddam & R. Bhushan)

Pervasive climatic events of Meghalayan Age from southern Saurashtra mudflats, Gujarat, India

A recent subdivision in the Holocene period proposed by International Commission on Stratigraphy (ICS) demarcated last 4.2 ka as Meghalayan Age based on a speleothem of Mawmluh Cave situated in Meghalaya of Indian subcontinent.

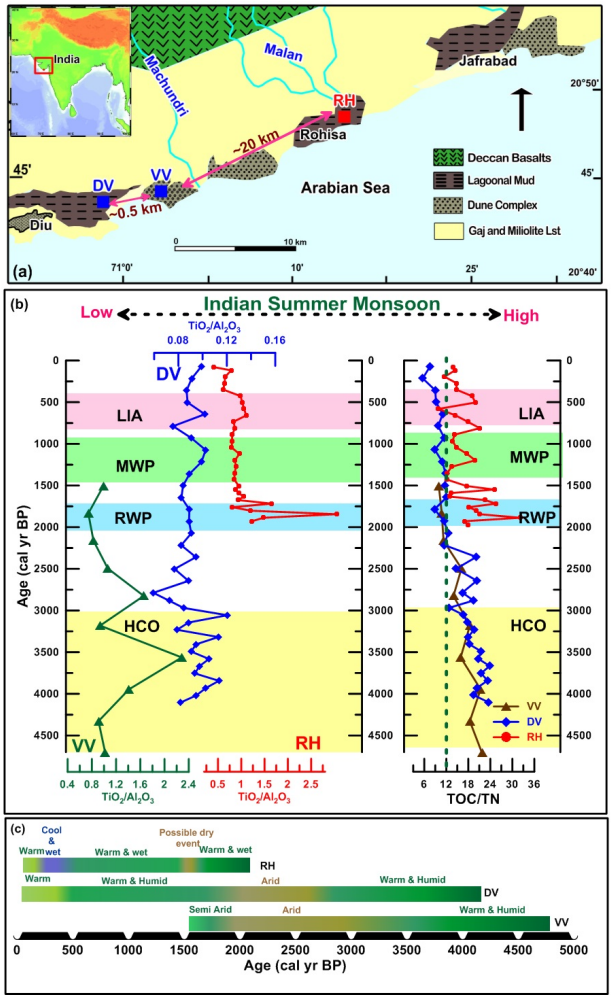


Figure no 8: (a) Map showing surrounding geology of Rohisa (RH), Diu (DV) and Vasoj (VV) mudflats. (b) Downcore variation of TiO_2/Al_2O_3 (weathering proxy) and TOC/TN for VV, DV and RH (c) Climate reconstruction for RH, DV and VV locations.

The present study aimed to decipher the climatic events and response of Indian Summer Monsoon (ISM) during Meghalayan Age from Southern Saurashtra region. The region is unique, as it presently receives detrital flux due to activation of seasonal rivers during monsoon. Two sediment cores from active mudflat of southern Saurashtra (Diu: DV and Rohisa: RH) and a relict mudflat section (Vasoj: VV) were investigated for geochemical proxies chronologically supported by radiocarbon dates. The VV section demonstrated warm and wet climate caused by ISM strengthening during 4710 - 2825 cal yr BP and 1835 - 1500 ka corresponding to globally known Holocene Climate Optimum (HCO), and similar observation was inferred from DV sediment core. Both VV and DV demonstrated that the ISM strengthened period was interrupted by an arid event. During last two millennia, the Roman Warming Period (RWP) and Medieval Warming Period (MWP) has been identified as warm and wet climate caused by ISM strengthening from both DV and RH sediment core. A short dry climate interspersed between RWP and MWP has been observed in RH which corresponds to globally known DACP event with weak ISM (Fig. 8). The LIA observed in DV and RH have indicated cool and wet climate suggesting weak ISM with enhanced winter precipitation caused by westerlies. On comparing VV, DV and RH it can suggested that the ISM has fluctuated significantly since the onset of Meghalayan Age with noticeable climate perturbations during ~4 ka, RWP and MWP interrupted by dry climatic events in the region. The present study demonstrates that the southern Saurashtra mudflats have responded in unison with the global climatic event as a function of changing ISM.

(U. Banerji and R. Bhushan)

Correlation between the Arabian Sea and high latitude climate oscillations for the past 50 ka

Paleoclimatic proxy records have documented concurrence in climatic vacillation between low latitude monsoonal climate variability and rapid temperature fluctuations of high-latitudes recorded as the Dansgaard-Oeschger (DO) and Heinrich events during late Quaternary period.

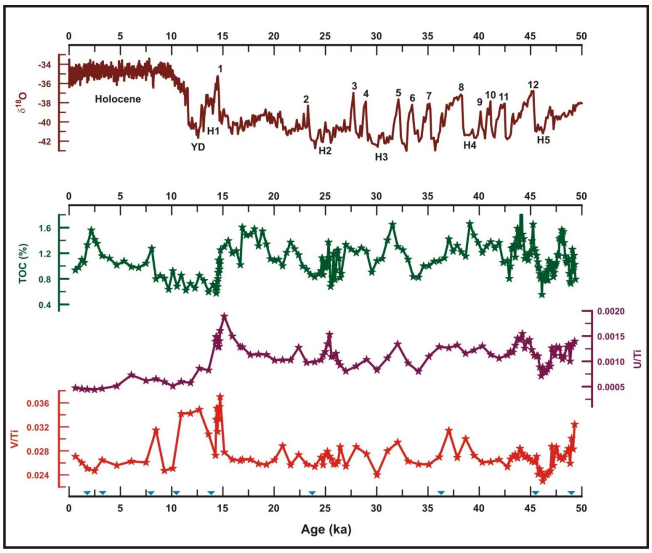


Figure no 9: Comparison of productivity index organic carbon (OC) and redox sensitive proxies (U/Ti and V/Ti ratios) from the northern Arabian Sea with GSIP2 $\delta^{18}O$ ice core record. Numbers above indicate Greenland interstadial numbers, YD and H represents Younger Dryas and Heinrich events. AMS ^{14}C dates are represented by the blue inverted arrows.

Multi-proxy geochemical approach on a radiocarbon dated sediment core was used to assess the strength of this teleconnection and to decipher signatures of the major climate events from the northern Arabian Sea sedimentary records. The sediment core from the northern Arabian Sea (SK - 324/08) being in proximity of the oxygen minimum zone (OMZ) region provides a crucial platform to delineate the seasonal monsoon influence on overhead productivity and its

impacts on prevalence of OMZ in millennia timescales. Enrichment in redox sensitive elements along with high OC in the sediment core reflected strong SW monsoon induced biological productivity and intensified OMZ correlated with interstadial events in the latitute region. In contrast, stadial events are characterized by low OC and redox sensitive elements indicating a period of reduced SW monsoon and weak OMZ associated with high latitude cooling intervals. The study underlines that the high latitude DO and Heinrich events are also a significant component of low latitude monsoonal climate variability during the past 50 ka due to a common forcing factor such as solar forcing.

(K.R. Chandana, R. Khichi, & R. Bhushan)

Changes in the coastal sediment deposition in the eastern Arabian Sea regulated by productivity and provenance

An important component of paleoceanographic and paleoclimatic investigation is to decipher the changes in source of organic matter in sediments deposited with time during the past. The bulk biogenic fraction of sediment comprises mainly opaline silica (SiO_2), and carbon both in organic (C_{org}) and inorganic (principally $CaCO_3$) forms collectively known as surface productivity. Marine sediments preserve these deposited biogenic fractions and provides information about the past productivity changes. Along with C/N, δ^{13}C has been extensively used to decipher the source of organic matter as C-3 and C-4 plants have distinctly different values for both δ^{13}C and C/N. Basically, bulk organic δ^{13}C and C/N should reflect the relative contributions of organic matter from varied sources.

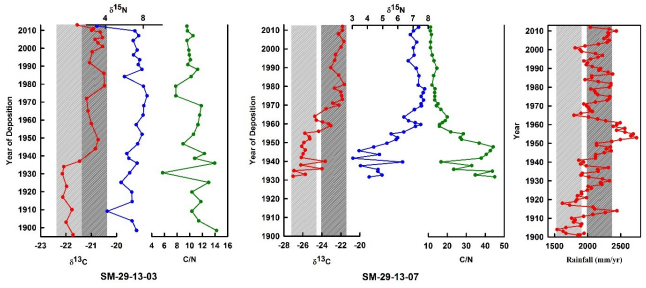


Figure no 10: Carbon and Nitrogen isotopic signature in the south-eastern Arabian Sea Sediment cores.

The δ^{13}C values for SM/29/13/03 located in the eastern Arabian Sea shelf vary between -20.5 and -22.5/textperthousand with an average value of -21.3 $\pm$ 0.61 ‰(n=27), while values of -21.6 and -27‰for δ^{13}C has been observed for SM/29/13/07 with average of -23.8$\pm$1.74 ‰(n=37). The δ^{15}N values show a spread between 3 and 8 ‰for both the sediment cores. The δ^{13}C values for the sediment core SM/29/13/03 located in the eastern Arabian Sea shelf indicate source of organic matter mainly derived from marine phytoplankton, thereby suggesting overhead productivity as the major controlling factor for the C_{org}. This has implications to the changing precipitation and summer monsoon (Fig. 10). Whereas, the sediment core SM/29/13/07 has high C_{org} between 1930 to 1950, depleted δ^{13}C (nearly - 28 to - 26 ‰) and low δ^{15}N (3 to 5 ‰) indicating terrestrially derived C_{org} as source of the sediments, which is further corroborated with C/N $>$ 12. Post 1960, the C_{org} deposited at the core location SM/29/13/07 is a function of overhead productivity as demonstrated by enriched δ^{13}C and δ^{15}N values, which corresponded well with C/N $<$ 12. Thus, it can be suggested that the core location for SM/29/13/07 received C_{org} from both terrestrial and marine source till 1950, while post 1950 most of the C_{org} has been deposited as a result of in situ productivity. Enhanced δ^{13}C and δ^{15}N values in the sediment core with signatures of marine organic matter signifies enhanced rainfall conditions. This study has implications to high resolution paleoclimatic records beyond the instrumental data where such rainfall data doesn't exist.

(C. Shah, N. Khonde & R. Bhushan)

Monsoonal events from Radiocarbon records of the Andaman corals

Radiocarbon of the dissolve inorganic carbon (DIC) in surface seawater changes as a result of air-sea CO_2 exchange and water mixing. Temporal and spatial variation of radiocarbon concentration provide important information about ocean dynamics. Corals record the radiocarbon variation of DIC (seawater) in their calcareous skeleton.

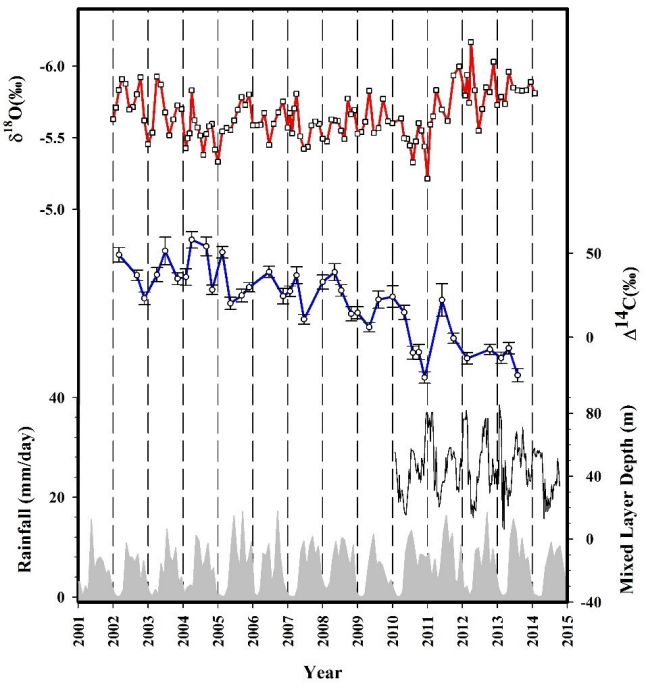


Figure no 11: δ^{18}O (red line) and Δ^{14}C (blue line) values of Andaman (Chidiyatapu) coral along with mixed layer depth (black line) and rainfall (grey area) of the region.

The annual bands of massive corals growing at rates of more than 10 mm per year can provide a continuous and high resolution proxy records. Such high resolution radiocarbon records can be studied to understand air-sea CO_2 exchange, ocean circulation, mixing and upwelling like processes. In this study, a 25 cm long coral core from Andaman Island was analysed for its radiocarbon concentration. The Δ^{14}C record of coral from Andaman Islands between 2003 -

2014, shows an overall decreasing trend of around - 5.4 ‰per year. The radiocarbon measurement shows highly depleted value around December month of 2010. This depleted Δ^{14}C value coincides with an enriched value of coral oxygen isotopic value suggesting cooler sea surface condition. Enhanced deepening of the mixed layer depth during winter monsoon in the Andaman region can lead to such enrichment and depletion of δ^{18}O and Δ^{14}C respectively. This suggests that these coral proxy records can be used to study enhanced monsoon events of the past in the Andaman region.

(H. Raj, R. Bhushan & R.A. Jani)

Signature of 1998 El Nino event in Lakshadweep corals

Massive scleractinian corals growing in shallow seawater, secrete calcareous exoskeleton with annual growth bands. A set of a high and low density bands generally grows every year, thus growth band counting can be used to determine the chronology of coral proxy records. Coral being sensitive organisms are susceptible to changes in sea surface condition. During bleaching events, corals experience stressed conditions in its growth and prolong stress condition can lead to death of corals. The coral growth rate is indicative of condition in which they are growing. Here, we have compared growth rate of corals growing in the Lakshadweep Islands, and its relation with the sea surface condition in the Lakshadweep region. A coral core sampled from a live coral (Porites) at Kadmat Island (11°15'N, 72°46'E) was analysed for its growth rate, using bandwidth and stable isotope of the skeleton. Growth rate of two corals each from Bangaram Island (Ahmad et al 2010) and Kavaratti Island (Sagar et al 2016) were also calculated. The common period for the above analysed coral was between 1985 - 1999. For this period these Lakshadweep corals show lowest annual growth rate in the year 1998 (Fig. 12).

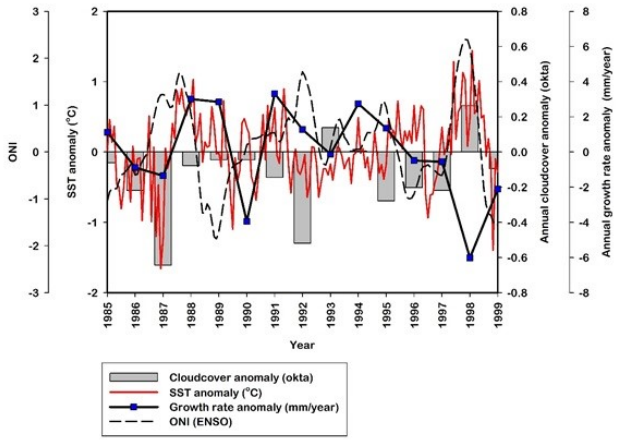


Figure no 12: Annual growth rate anomaly (blue square) of Lakshadweep corals with sea surface temperature anomaly (red line), cloudcover anomaly (grey bars) and Ocean Nino Index (black dashed line).

This was year of extreme ENSO (El Nino) event and experienced wide spread bleaching of coral reef. During this year, the Lakshadweep region experienced high sea surface temperatures and increased cloudiness, both together causing stressed condition for coral to grow. This suggests that warming water along with increase in cloudiness can adversely affect the corals in the region.

(H. Raj, R. Bhushan & S. Kumar)

Paleo-temperature reconstruction using stable isotopic composition of Lakshadweep corals

Corals, a colourful invertebrate marine animal, have often been used as archive of past climatic records. These corals generally grow in shallow seawater, as many of them live in symbiosis with zooxanthellae, which requires sunlight for carrying out photosynthesis. While growing in surface ocean these animals keep on secreting calcareous skeleton, recording signatures of the sea surface conditions in its isotopic and geochemical composition. The proxy records from corals going beyond (older than) instrumental records are very crucial in understanding the changing sea surface conditions with changing climate. Reconstructing past Sea Surface Temperature (SST) is an important aspect for studying various oceanic and coupled ocean-atmospheric processes. The SST reconstruction requires a paleo-temperature equation to calculate the past SST using proxy records. Previous studies on corals have shown that their stable oxygen isotope composition shows inverse correlation with sea surface temperature and is a good proxy for SST. In view of this, a coral (*Porites*) core from Kadmat Island, Lakshadweep, India (LK-15-KD-1) was analysed for its stable isotopic composition. The proxy record span between 1997 to 2014. The average stable oxygen isotopic composition (δ^{18}O) and stable carbon isotopic composition (δ^{13}C ‰) of the coral for this time period was - 5.2±0.2 ‰and - 1.5±0.4 ‰respectively (Fig. 13).

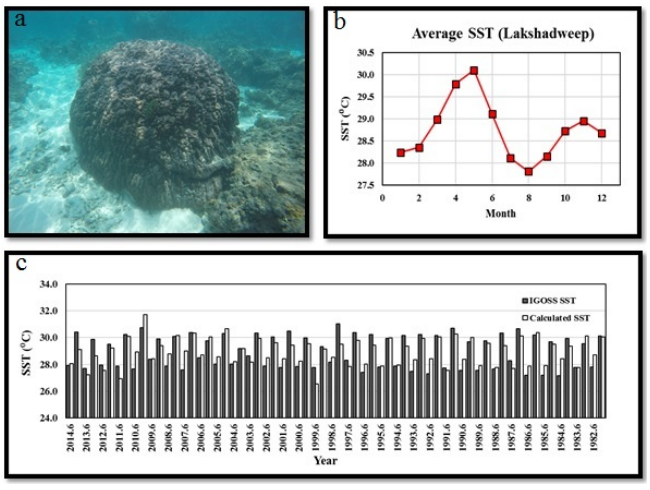


Figure no 13: (a) A massive coral; (b) Average sea surface temperature (SST) of Lakshadweep region; (c) Observed and calculated sea surface temperature based on δ^{18}O values of Kadmat coral.

Surface seawater in Lakshadweep is warmest around in the month May of the year and decreases to minimum around August due to monsoon winds induced sub surface water mixing (Fig. 13). Thus, minima and maxima of coral δ^{18}O values were assigned time of May

and August month for every year. Using the coral δ^{18}O values of May and August month and the observed sea surface temperature values (IGOSS SST; 72.5°E, 11.5°N), following relationship was obtained, $[SST = -3.6\,(\delta_c - \delta_w) + 8.8]$ Where, *SST* is sea surface temperature, (δ_c) and (δ_w) is stable oxygen isotopic composition of coral and sea water respectively. Here, (δ_w) value was assumed to be 0.28 for May and 0.412 for August month (Chakraborty and Ramesh, 1997). This paleo-temperature equation was used to calculate the sea surface temperature for May and August month and was compared with observed SST values. The difference between observed and calculated SST was in the range of -1.4°C to 1.5°C, which is better than previously reported value for this region. Therefore, the derived equation might be a better representative for paleo-temperature reconstruction in Lakshadweep region.

(H. Raj, R. Bhushan & S. Kumar)

Status of larger symbiont bearing benthic foraminiferal assemblages in the shelf sediments of Andaman and Nicobar Islands

The Andaman and Nicobar archipelago is one among the important active seismic zone in the northern Indian Ocean. The Island is well known for its pristine environment and mega biodiversity. The coral reefs are one among the important diversity in marine environment of this archipelago. The coral reefs harbour thousands of different group of flora and fauna, among them the symbiont bearing larger benthic foraminifera is one important member. This group is a main contributor of the carbonate production in the coral reef environment and it is a significant tool for monitoring coral reefs (to assess the condition and health status of coral reef). Very little is known about the distribution, diversity and its ecology of larger symbiont bearing benthic foraminifera in the diverse coral reefs of Andaman and Nicobar Islands.

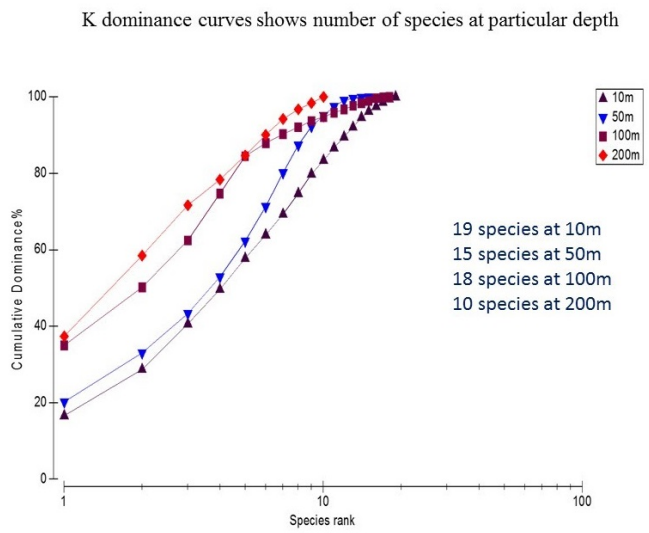


Figure no 14: K-Dominance curves for variation in number of species to respective depth.

To document the distribution and diversity of this group, ∼ 25 shelf sediments were studied. A total of 30 species were identified from different water depths (10, 50, 100 and 200 m) at 5 geographical locations North Andaman, Middle Andaman, South Andaman, Little Andaman and Car Nicobar of this archipelago (Fig. 14). The study has identified 4 different dominant group of community for respective depth ranges and found decreasing species diversity with increasing water depth. In addition, the Shannon-Wiener Diversity Index (H) ranged from 0.47 to 2.27, Margalef Species Richness Index (D) from 0.21 to 2.14 and the Pielou's Equitability index (J) from 0.37 to 0.98. These index values suggest that the coral reef ecosystem of Andaman and Nicobar Island consists of good diversity of larger symbiont bearing foraminifera.

(M. Muruganantham and R. Bhushan)

Estimates of paleo deep-water ventilation ages for the Indian Ocean using foraminifera

Global ocean circulation has undergone major changes during glacial and interglacial periods, as revealed by radiocarbon ages of benthic foraminifera extracted from sediment cores of Atlantic and Pacific Ocean. The deep waters thus show changes in ventilation age shift from interglacial to glacial periods. Equatorial Indian Ocean, located far from deep water formation regions is expected to provide better estimates of deep water circulation changes as a function of ventilation age during glacial and interglacial periods. Sediment cores from the Indian Ocean are being investigated to decipher the rate of thermohaline circulation during quaternary period based on radiocarbon dates of select species of fossilized planktonic and benthic foraminifera. The deep waters in this region are ventilated by Modified North Atlantic deep water (MNADW).

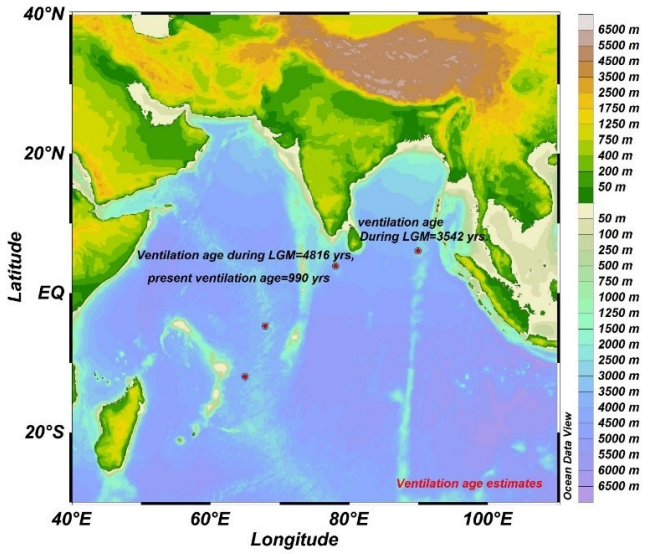


Figure no 15: Sampling location (red dots) and preliminary ventilation ages of deep waters in the equatorial Indian Ocean.

Radiocarbon dates of planktonic (monospecific species) and benthic foraminiferal (mixed benthic species) shell using PRL AURiS at two locations of equatorial Indian Ocean demonstrate that ventilation age

during last glaciation was higher compared to the present ventilation age (Fig. 15). Detail analyses at various depth of sediment core at multiple locations is in the process. The estimation of paleo ventilation ages can provide clues to some debatable topics such as slowdown/cessation of thermohaline circulation during Last Glacial Maxima (LGM), changes in the CO_2 sequestration in the ocean as a function of rate of change of deep ocean ventilation.

(N. Bharti and R. Bhushan)

Dissolved aluminium cycling in the Bay of Bengal and subtropical gyre region of the Indian Ocean

Dissolved aluminium (dAl) concentrations have been determined on 13 full vertical water column profiles, sampled along the GEOTRACES – India transect, GI–01 (Fig. 16A), to understand biogeochemical controls on dAl distribution in the Bay of Bengal and subtropical gyre region of the Indian Ocean. The meridional section (station GI-01/2 to GI-01/8, Fig. 16A) in the BoB, in general, showed a decreasing dAl concentrations trend from northern to southern BoB in the surface mixed layer (Fig. 16B). The impact of huge supply of suspended lithogenic sediments to the Bay of Bengal waters (BoB), from the Ganga–Brahmaputra river system, Indian peninsular rivers and resuspended terrigenous sediments from the continental shelf and slope, on dAl distribution is seen as an overall increase in the dAl concentrations throughout the water column towards the northern BoB. Considering the steady state balance between the dAl input from the lithogenic sediment flux in the upper water column and first-order scavenging removal of dAl, the fractional solubility of Al from the lithogenic sediments in the BoB surface waters is estimated to be in the range of 1.2 – 4.7 %. dAl enrichment in the upper water column ($<$ 500 m) at the northern end of the Indian Subtropical Gyre (GI-01/11 and 12, Fig. 16B) results from the deposition and partial dissolution of Australian dust and advection of, relatively, dAl-rich Indonesian Through flow waters. Sediment resuspension from the Central Indian Ridge and ventilation of dAl-rich bottom water ($>$ 3500 m) across the Ninety East Ridge from Western Australian Basin is observed to control the dAl distribution in the deeper ($>$ 2000 m) waters of the Central Indian Ocean Basin.

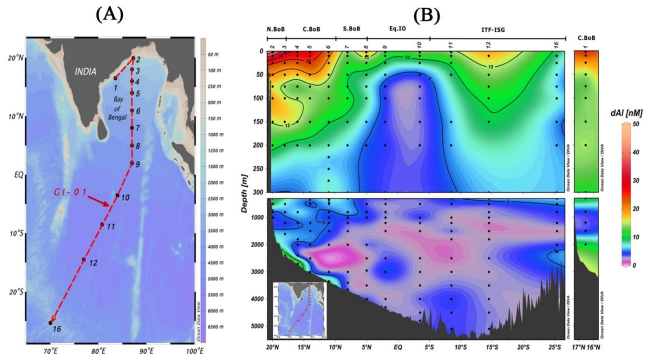


Figure no 16: (A) Sampling locations for the GI-01 cruise. (B) Distribution of dissolved aluminium along the GI-01 cruise transect.

(N.D. Singh, V. Chinni & S.K. Singh)

Paleo-monsoonal variability in the central Arabian sea

The Arabian sea is one of the most productive region in the world. Seasonal reversing of monsoon winds induces coastal upwelling in the Arabian sea which brings nutrient rich water to the surface and thereby increasing productivity. Monsoonal winds are governed by land-sea thermal contrast caused by variation in solar radiation, which shifts position of Inter Tropical Convergence Zone(ITCZ). Productivity in north-western Arabian Sea is mainly driven by southwest monsoonal wind whereas eastern Arabian sea becomes productive during northeast monsoonal wind upwelling. To reconstruct variational in paleo monsoon, multi-proxy approach was used for a sediment core from the central Arabian sea. The chronologically of the core SK-312/16 was established by Accelerator Mass Spectrometer(AMS) radiocarbon dating on mixed planktonic foraminifera ($>$ 250μm). High sedimentation rate was observed from 13ka-present and no significant change in sedimentation rate was observed during Last Glacial Maximum(LGM) (Fig. 17). During LGM, decreased productivity in the north-western Arabian sea and increased productivity in the eastern Arabian sea was reported. LGM did not experience significant change in productivity in the central Arabian Sea. Gradual increase in Productivity during early Holocene period with sudden decrease in productivity during transition period of early to mid-Holocene was observed, which corresponds to well documented 8.2ka cooling event. In mid- Holocene, decrease in productivity extended till 7.4ka and further increased up to 5.7ka with decline in late Holocene (Fig.17). Since 40ka, the overall southwest monsoon enhanced in Holocene period, with millennium scale variation. Correlation of productivity variation and Δ TSI suggest solar activity as one of the major driving force regulating southwest monsoon intensity during Holocene.

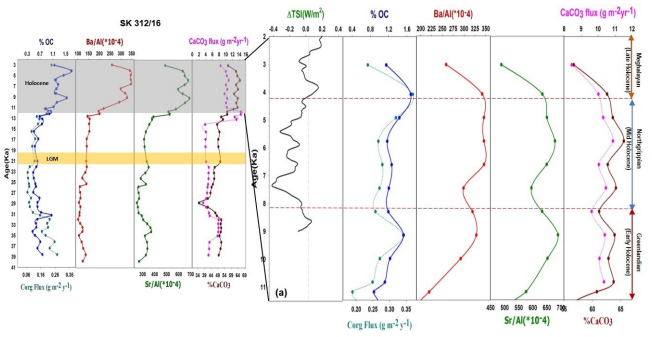


Figure no 17: Correlation of OC, Ba/Al, Sr/Al and $CaCO_3$ of SK312/16 sediment core with ΔTSI (Steinhilber et. al., 2012).

(R. Nambiar, A.K. Sudheer, H. Raj & R. Bhushan)

Bottom water redox condition in the Arabian sea during past 40ka

Ocean circulation plays an important role in global transport and redistribution of heat, salt, carbon, oxygen and nutrients which thereby regulates climate and support marine life. Ocean circulation has modulated as a function of climate change during the past. These changes in ocean circulation influence redox condition at sediment water interface. Trace element sensitive to redox changes serve as a

good proxy to understand oxygenation condition of water at sediment water interface and helps in reconstruction of deep water circulation changes with climate change. The Arabian sea is northernmost part of the Indian ocean where all deep water masses terminate. The deep waters below 2kms gets ventilated in the Indian ocean as Deep Western Boundary Current (DWBC), a mixture of North Atlantic deep water (NADW) and Antarctic bottom water (AABW) which gets mixed at Antarctic circumpolar current. The water mass between 2 to 3.8km has larger proportion of NADW known as Upper Circumpolar Deep Water, and below 3.8km is known as Lower Circumpolar Deep Water with higher proportion of AABW. Sediment core from the Arabian Sea SK-312/16 chronologically constrained by AMS radiocarbon dating was investigated to understand changes in deep water circulation during the past. Multielement proxies indicate suboxic condition during Greenland Warmer Interstadial events and oxic condition during Last Glacial Maximum (LGM) (Fig.18). This suggests that proportion of NADW increased during Interstadial events resulting in suboxic condition as dissolved oxygen concentration of NADW decreases enroute North Atlantic to Pacific Ocean by the remineralization of sinking organic material. During LGM, reduced proportion of NADW led to enhanced oxic conditions due to AABW at sediment water interface.

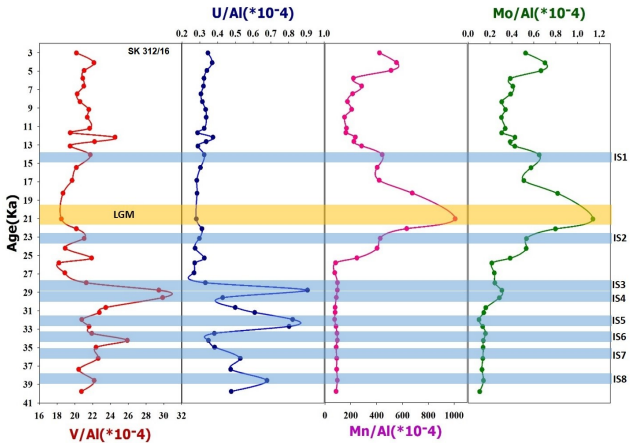


Figure no 18: Down core variation of V, U, Mn and Mo normalised by Al in Arabian sea sediment core (water depth = 4350m) [Yellow shade: oxic condition; Blue shade: suboxic condition; LGM: Last Glacial Maximum; IS: Interstadial warming event]

(R. Nambiar, A.K. Sudheer & R. Bhushan)

Characteristics and atmospheric aging of fine aerosol over Ahmedabad using HR-ToF-AMS: Source apportionment of organic aerosol

An unprecedented increase in submicron particles concentrations over urban regions is a serious threat to both air quality and climate. Organic aerosol (OA), although a dominant fraction of submicron aerosol, are the least understood component due to their numerous sources, complex composition, tedious formation mechanism, and complicated atmospheric evolution. Chemical characteristics, sources, and atmospheric aging of NR-PM_1 with the major emphasis on OA were investigated during post monsoon (PoM) season of 2017 using high-resolution time-of-flight aerosol mass spectrometer (HR-ToF-AMS) over Ahmedabad, a big urban city located in the semi-arid region of western India. All the components of NR-PM_1 [i.e., organic aerosol (OA),SO_4^{2-},NO_3^-), $NH_4^+$and Cl^-] showed a strong diurnal variation with the overall dominance of OA (58%) in NR-PM_1, and the OA composition was found to be a mixture of fresh and aged species. Oxygen to carbon (O/C) elemental ratio varied from 0.04 to 0.91 whereas, hydrogen to carbon (H/C) elemental ratio varied from 1.34 to 2.26. A strong diurnal variation in O/C caused a large variability in organic matter to organic carbon (OM/OC) ratio (ranging from 1.2 to 2.3) during the study period, which suggests that a constant conversion factor for OM estimation (from OC) can be a source of large uncertainty in their load assessment over the study region. Furthermore, the observed slope (-0.78$\pm$0.01) of Van Krevelen (VK) diagram suggests that plausible major functional groups of ambient oxidized OA could be the mixture of alcohols and carboxylic groups. Three distinct sources of OA including low volatility oxygenated organic aerosol (LV-OOA) and semi-volatile OOA (SV-OOA), and primary OA (POA) were identified via positive matrix factorization (PMF) analysis of HR-ToF-AMS data. Overall, OA mass was dominated by POA (42%), followed by LV-OOA (33%) and SV-OOA (25%) (Fig. 19). Diurnal variations in PMF factors suggest that secondary OA (SOA) formation was high during early morning and afternoon hours whereas, primary OA (POA) was most abundant during traffic rush hours. Observations also suggest that the high OA loading events were dominated by POA during the whole study period. Such studies are important in understanding the characteristics of OA components over big urban cities of semi-arid tropical regions.

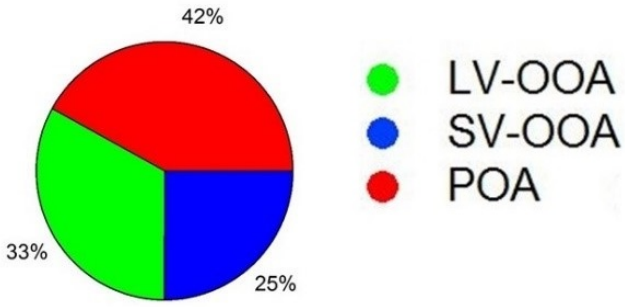


Figure no 19: Average composition of organic aerosol during post monsoon season over Ahmedabad.

(A.P Singh and N. Rastogi)

Characteristics of submicron particles due to big firecrackers burning event

Firecrackers burning on different occasions all over the world is a short-term big source of fine particles and their precursors in the air.This study presents the real-time changes in concentrations, composition and characteristics of non-refractory particulate matter smaller than 1μm aerodynamic diameter (NR-PM_1), and black carbon (BC) during the Diwali festival, when a huge amount of firecrackers are burnt in India. Online measurements (1 min integration time) of organics, SO_4^{2-}, NO_3^-, NH_4^+, and Cl^- were performed using high-resolution time-of-flight aerosol mass spectrometer (HR-ToF-AMS), and that of BC with seven wavelength aethalometer over Ahmedabad. A sharp increase (3 to 23 times higher) in the concentrations of all the measured species was

observed on the evening of the Diwali that persisted overnight due to a combination of primary emissions and secondary formation of aerosol. Organics were the dominant contributor (∼85 %) followed by SO_4^{2-} (∼13 %), Cl^-(∼4 %), NO_3^-(∼4 %) and NH_4^+(∼2 %) to NR-PM_1 on the Diwali night. Further, variations in H/C and O/C ratios before, during and after the Diwali suggest fresh emissions of primary organics on the Diwali night, and highly oxidized secondary organic formation on the next day. Aerosol neutralization ratio (ANR, defined as the molar ratio of NH_4^+ to sum of SO_4^{2-}, NO_3^- and Cl^-, an indicative of aerosol acidity, reduced to as low as 0.1 on the Diwali night, which has implications to short-term acute atmospheric air pollution.

(A.P. Singh, R.V. Satish & N. Rastogi)

Use of Brown Carbon Spectra as a tool to understand their broader composition and characteristics: A Novel Approach

This study proposes a novel approach on the use of brown carbon (BrC) absorption spectra as a tool to understand their broader composition and characteristics. It is well documented that BrC may consist of a variety of organic chromophores with variable concentrations and different absorbing characteristics. Absorption coefficient (b_{abs}) spectra of water-extracts or methanol-extracts of aerosol over a wavelength range (300 to 600 nm) represent the bulk optical property of water-soluble or methanol-soluble (assumed to be total) BrC, respectively. If the BrC composition is uniform from sample to sample, then the ratio of b_{abs} spectra for different samples shall be uniform (constant) as function of wavelength. The magnitude of this constant would suggest the relative abundance of BrC chromophores in different samples. However, if the BrC composition is not uniform from sample to sample then one would expect variable ratio at different wavelengths depending upon the change in composition and concentrations of different chromophores. Further, the same concept can be applied to water-extracts and methanol-extracts of the same sample. The ratio of b_{abs} spectra for water-extract to methanol-extract can be used to quantify the relative contribution of water-soluble and water-insoluble chromophores to the total BrC as a function of wavelength in a given sample. As a case study to validate the proposed approach, day/night pair of $PM_{2.5}$ samples collected from Patiala (30.33°N, 76.4°E) during paddy-residue burning were used. Majority of the BrC from paddy-residue burning were found to be water-insoluble, which showed an increasing trend with increasing wavelength. During burning period, night time b_{abs} at 450 nm were found to associated with higher water-soluble organic nitrogen to water-soluble organic carbon ratio, suggesting the presence of nitrogenous BrC from paddy-residue burning. The proposed method may be very useful for BrC studies over the globe.

Logistic support for the sample collection was provided by Dr. Atinderpal Singh and Prof. Darshan Singh (Punjabi University, Patiala).

(R.V. Satish and N. Rastogi)

Chemical composition and oxidative potential of aerosol over the marine atmospheric boundary layer of the Arabian Sea

Atmospheric deposition is among the major source of nutrients to the open ocean. Trace metals in aerosol are not only important micro-nutrients for regulating primary productivity, but also can be associated with negative effects. One of their negative effects can be the generation of high levels of reactive oxygen species (ROS) in surface ocean waters. When the level of ROS exceeds the defense mechanisms, oxidative stress is generated which can pose a threat to cells by causing damage to bio-molecules such as DNA, lipids and nucleic acids. Some redox active particulate matter (PM) species (such as trace metals and organics) are shown to have capability of generating ROS (known as their oxidative potential, OP) in the atmosphere, human body and plants. The OP studies are lacking over the Indian sub-continent, and missing over the marine environments worldwide. To fill this gap, a total of 22 PM_{10} (aerodynamic diameter less than or equal to 10μm) samples were collected on tissuquartz filters using high volume air sampler (flow rate:1.13 $m^3 min^{-1}$) during April over the Arabian Sea. These samples were analyzed for wide range of chemical species. The OP was analyzed using Dithiothreitol (DTT) assay. There was a clear contrast in non-sea-salt (nss) fraction of chemical species in samples collected along different legs of the cruise. Initial 10 samples collected along first leg of the cruise showed insignificant sea-salts contribution to K^+, Ca^{2+} and SO_4^{2-} (average nss- K^+: 93 %,nss-Ca: 97 % and nss-SO_4^{2-}:98 %); whereas, sea-salts contribution was noticeable during the second leg of the cruise (nss-K^+: 63 % nss-Ca:91 % and nss-SO_4^{2-}: 87 %). PM_{10} composition data was classified in two parts based on the averaged 72-hour air mass back trajectories using the Global Data Assimilation System (GDAS, 1°, global, 2006–present) meteorological data set as input in the HYbrid Single-Particle Lagrangian Integrated Trajectory (HYSPLIT) model. First part (initial 10 samples) was named as Class-A, which is found to be associated with the air masses travelled from Indian continent (PM_{10} range: 61 to 119μg m^{-3}), whereas the second part (Class-B) received the air masses from open ocean as well as the Arabian continent (PM_{10} range: 81 to 184μg m^{-3}). The OP values of Class-A samples were found to be similar to those observed over Mount Abu during spring season (April). Interestingly, elemental carbon (EC, emitted from the combustion of biomass and/or fossil fuel), is found to be positively correlated with mass normalized OP for samples under Class-A (Fig. 20).

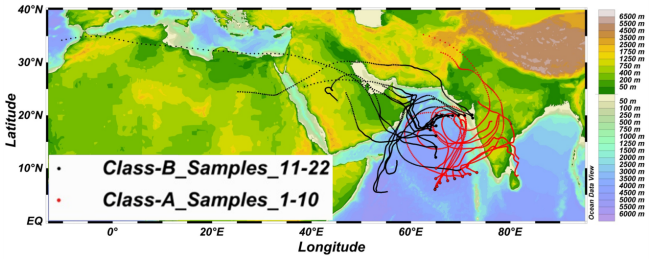


Figure no 20: Seven days air mass back trajectories ending 1000 m above at sampling locations. Red and black lines represent samples under Class-A and Class-B, respectively.

On the contrary, no relationship between these species was observed for the samples under Class-B, where aerosol composition is expected to be dominated by mineral dust. This work has implication in better understanding air sea exchange of species and surface ocean biogeochemistry.

Ship cruise was led by Dr. Arvind Singh, GSDN, PRL

(A. Patel and N. Rastogi)

Carbon biogeochemistry of two contrasting tropical estuarine ecosystems

Comprehensive understanding and quantification of different aspects of carbon (C) biogeochemical cycle of estuaries are essential to decipher regional and global change. The post-monsoon C biogeochemistry of two contrasting estuarine systems (Hooghly-anthropogenically influenced and Sundarbans - mangrove dominated) located in the deltaic region of Ganges, India were investigated. It was found that the salinity of well oxygenated estuaries of the Sundarbans (DO:91 - 104%) varied over a narrow range (12.74 - 16.69) relative to the Hooghly (0.04 - 10.37).

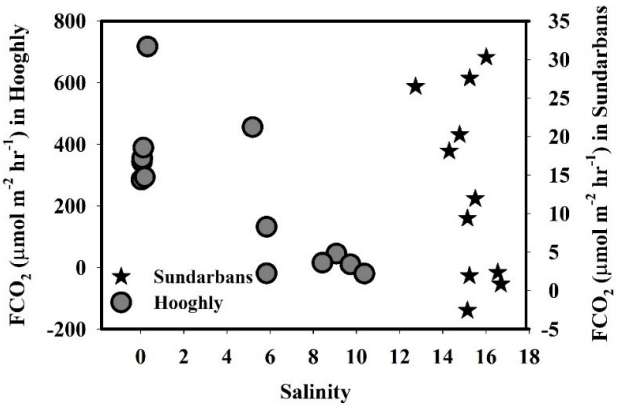


Figure no 21: The flux of CO_2 in the Hooghly-Sundarbans system during post-monsoon.

A mixing model suggested a combination of processes including freshwater intrusion, carbonate precipitation, and carbonate dissolution to be major factor controlling dissolved inorganic carbon (DIC) dynamics in the freshwater regime of the Hooghly, whereas phytoplankton productivity and CO_2 outgassing dominated in the mixing regime.

In the Sundarbans, removal of DIC (via CO_2 outgassing, phytoplankton uptake, and export to adjoining continental shelf region) dominated over its addition through mineralization of mangrove derived organic C. The concentration of dissolved organic carbon (DOC) in the Hooghly was $\sim$40 % higher than in the Sundarbans, which was largely due to cumulative effect of anthropogenic inputs, DOC-POC interconversion, and groundwater contribution rather than freshwater mediated input. The average pCO_2in the Hooghly was higher by $\sim$1291μatm compared to the Sundarbans with surface runoff and organic matter degradation by respiration as dominant factors controlling pCO_2 in the Hooghly and Sundarbans, respectively. The entire Hooghly-Sundarbans system acted as a source of CO_2 to the regional atmosphere with $\sim$17 times higher emission from the Hooghly compared to the Sundarbans. Taken together, the cycling of C in estuaries having different levels of anthropogenic influences was evidently different with significantly higher CO_2 emission from the anthropogenically influenced estuary than the mangrove-dominated ones.

(M. K. Dutta and S. Kumar)

Gross nitrogen transformation rates in semi-arid tropical soils: implications for nitrogen cycling under changing climate

Dryland ecosystems, home to over 2.1 billion people, are degrading at alarming rates due to both human-induced and natural causes. Phenomena such as sea-level rise and prolonged droughts, consequences of climate change, are the human-induced causes which can reduce productivity of dryland ecosystems leading to their desertification. These changes can also affect the cycling of elements required to maintain the photosynthetic activity of plants. Mineral nitrogen in soils is one such element which is produced as an intermediate of biologically mediated processes and is required for photosynthesis. During this study, we measured gross rates of nitrogen transformations responsible for generation, consumption, and retention of mineral nitrogen in semi-arid soils of different land-types, to address the controls on nitrogen transformation processes in semi-arid tropical climate. With the above mentioned aim, soils were collected from five land-types including two in salt flat and one each in grassland, wetland, and an agricultural field from Kutch, Gujarat, which falls in north-western arid region of the India. Soils with high salinity-high moisture-low vegetation (salt flat) showed significant decline in gross production of nitrogen (mineralization rate: 0.21$\pm$0.10 mg Nkg^{-1}d^{-1}; nitrification rate: 0.27$\pm$0.17 mg Nkg^{-1} d^{-1}) compared to soils with low salinity-low moisture-high vegetation (grassland, wetland, and agricultural soils) (mineralization rate: 2.47$\pm$ 1.74 mg Nkg^{-1}d^{-1}; nitrification rate: 1.43$\pm$1.30 mg Nkg^{-1} d^{-1}).Results of this study indicated cumulative negative effect of high salinity, high moisture, and lack of vegetation on nitrogen transformation rates. Backward stepwise regression analysis of the results indicated salinity to be the most important factor controlling nitrogen transformation rates during the study. It appears that soils of the regions undergoing frequent seawater exposure or excessive evaporation experience slowdown of nitrogen cycling leading to limited nutrient production and consumption. Due to climate change, the areal extent of coastal drylands undergoing such decline in rates of nutrient production is likely to increase leading to loss in productivity and eventual desertification.

(N. Sharma and S. Kumar)

Hydrological and ecological variations in the Lower Himalayas during late MIS 3

Being one of the most complex systems, the Indian Summer Monsoon (ISM) dominantly controls the hydrology and ecology, and hence the human life, in the Indian sub-continent. In the past, the ISM has varied with respect to global glacial and interglacial periods.It is well known that ISM was relatively intense during MIS 3 (60 to 25 ka) with globally reported extreme warm and cold events.In this context, during this ongoing study, we have attempted to understand changes in ecological and hydroclimatic conditions by analysing total organic carbon (TOC) and nitrogen (TN) content along with their isotopic compositions (δ^{13}C and δ^{15}N) in a sedimentary lake succession (Pipalkoti) from Lower Himalayas. Variations in δ^{13}C and δ^{15}N values of organic matter reflect changes in lake processes, productivity, vegetation type, and runoff conditions in the catchment area. The data obtained during this study suggested the possibility of gradual decline in intensity of ISM and lake level from 45 to 40 ka

as documented by increasing δ^{13}C and TN percentage along with decreasing TOC percentage and TOC/TN ratios. Increase in TOC/TN ratios with decrease in δ^{13}C and δ^{15}N suggested warm and humid climate (intense ISM) and increase in lake level from 40 to 30 ka. High TOC/TN ratios and low δ^{13}C values suggested relatively high contribution of land derived organic matter in the lake. In addition, there are two peaks in the data that shows the cooling events at 39 and 30 ka which are connected to the cold Heinrich event (H4 and H3).

(A. Rahman and S. Kumar)

Cosmogenic radioactivity in the Mukundpura (CM2) carbonaceous chondrite

The Mukundpura chondrite is the new carbonaceous meteorite fall near Jaipur, Rajasthan, India on June 6, 2017 at 5:15 IST. Based on geochemistry and petrology, the meteorite is characterized and classified as carbonaceous chondrite (CM2). Several meteorite fragments were collected from GSI (∼100 gm) for non-destructive analysis of cosmogenic radionuclides which were counted in fixed geometry sample container using ultra low back ground hyper pure germanium (HPGE) planar co-axial detector. We could detect and analyse ^{22}Na,^{54}Mn, and ^{26}Al. The preliminary results show that ^{54}Mn, ^{22}Na and ^{26}Al isotopes to be 39±5 (dpm/kg), 45±5 (dpm/kg) and 38±7 (dpm/kg) respectively. The estimated activities of the cosmogenic nuclides are consistent with earlier observed activities in various meteorites. The ^{22}Na activity found to be lower than the Sutter's Mill CM2 which fell on April 2012 at peak activity of solar cycle 24. The Mukundpura fall took place declining phase of the current solar cycle 24. The effect of solar activity is well demonstrated by the cosmogenic nuclides specifically which are having lower half life. Most significantly the ^{22}Na/^{26}Al ratio which is influenced by the galactic cosmic rays and solar activities and is independent of irradiation history in the interstellar space. This is further supported by the low activity of ^{54}Mn in Mukundpura in comparison to Sutter's Mill indicate that its production is controlled by solar cosmic rays which is get modulated due to interaction of galactic cosmic rays.The observed activities of long lived ^{26}Al found to be quite higher then Sutter's Mill ($<$ 23 dpm/kg)[4] hints that the Mukundpura meteorite might be having older cosmic ray exposure ages. Here it is to be noted that the neutron capture reaction produced nuclide ^{60}Co is absent or not measurable. This might be due to the small size of its parent body in the space, where thermalization of neutrons could not take place. This radionuclide which is produced during thermalization of neutron suggests for a small preatmospheric size of this meteorite parent body. Our preliminary results are consistent with their production rate by the solar and galactic cosmic ray interactions.

(A.D. Shukla)

Factors governing the pattern of glacier advances since the Last Glacial Maxima in the transitional climate zone of the Southern Zanskar Ranges, NW Himalaya

To understand the relics of glacier advances and retreats in the transitional climatic zone of the Southern Zanskar Range, NW Himalaya we studied five glaciated valleys.

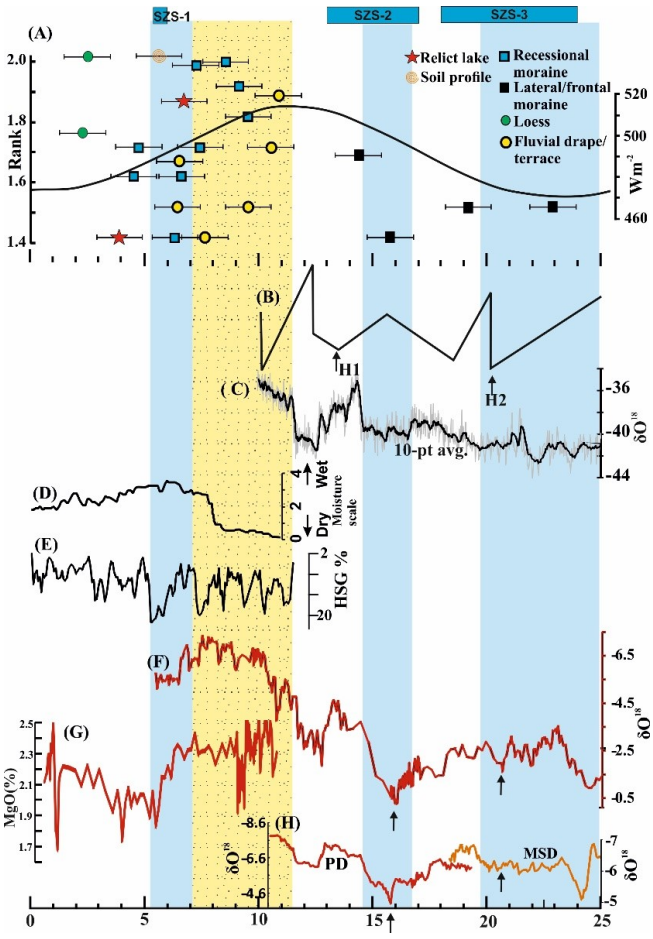


Figure no 22: The distribution of optical and radiocarbon ages obtained on lateral and recessional moraines, relict lake, loessic silt, palaeosol, and outwash gravel terraces/sand drapes. Three OSL ages 3.8±0.5, 2.5±0.2, and 4.9±0.4 ka are from Sharma et al. (2018). The black solid line curve is the insolation data (Berger and Loutre, 1991) for the northern hemisphere at 30°N. The glacial advance (SZS-3- ∼24e18 ka), represented by lateral/frontal moraines, corresponds to the insolation minima; whereas the recessional moraines and outwash terraces correspond with the insolation maxima. (B) The millennial scale cooling cycles culminating into the Heinrich events-2 (H2) and (H1) are shown by a line diagram (Bond et al., 1993) which is traced using the δ^{18}18 data from GRIP ice core (Andersen et al., 2005) shown in (C). The lateral/frontal moraines of SZS-3 and SZS-2 (late glacial- ∼17-13 ka) correspond to millennial scale cooling culminating in H2 and H1 respectively. (D) The moisture contribution by the westerlies plotted from lake records of arid central Asia (Chen et al., 2008) shows a monotonous increase after ∼8 ka. The period is represented by recessional moraines, relict lake, loess and palaeosol deposits. The SZS-1 (∼6 ka) could not sustain inspite of the enhanced moisture from the westerlies and therefore it seems that the millennial scale cooling event was critical for the advance. (E) The Haematite Stained.

Specifically, objective was to in response to the temporal changes in the Indian Summer Monsoon (ISM) and mid-latitude westerlies. Based on landform stratigraphy and optical chronology four glacier advances were identified and named from the oldest to youngest as the Southern Zanskar Glacier Stage-4 (SZS-4) to SZS-1. The SZS-4 remains undated, and is conjectured to the Marine Isotope Stage-4 (MIS-4) based on the existing chronology of the stratigraphically equivalent moraines/trimlines in the region. The optical chronology obtained on 21 samples enabled us to restrict the SZS-3 to 22.8±1.9 - 19.1±1.9 ka. The period corresponds to the Last Glacial Maxima (LGM). The SZS-2 is dated to 15.7±1.3-14.3±1.3 ka (late Glacial period). The youngest SZS-1 is assigned to ∼ 6 ka (mid-Holocene) based on the chronology of the recessional moraines (4.9±0.4-4.5±0.3 ka). The

pulsating deglaciation associated with each advance since the LGM is represented by the recessional moraines and outwash gravel terraces. The older gravel terrace is dated between 10.8±0.9 and 6.5±0.5 ka and is attributed to SZS-2 deglaciation. The same is also manifested by the deposition of sandy facies in a relict lake sequence (6.7±0.6 ka) and development of palaeosol (5.6±0.5 ka). We suggested that the glacial advances were triggered by the millennial scale cooling events during the periods of strengthened westerlies and thus, suggest a synoptic scale coupling with the Northern Atlantic. The deglaciation is suggested to occur during the warmer ISM dominated phases. The late Holocene climatic instability that followed the recession of SZS-1 is manifested by the development of rhythmites (3.8±0.5 ka), loess (2.5±0.2 ka), and palaeosol (2189±296 cal yr BP).

This work is carried out in collaboration with Shubhra Sharma from IISER, Mohali.

(A.D. Shukla)

Understanding Evolution of the Great Rann of Kutch during the Quaternary period

The Great Rann of Kachchh provide unique opportunity to understand the land and sea interaction. Occurrence of fluvial sand rich Bets (elevated surfaces with in the Rann) indicate the contribution of rivers probably derived from the combined Indus and Nara Rivers, which extended southwards towards the present Indus delta with some of its waters escaping into the Arabian Sea via the Kori Creek. It is also indicate presence of some river that was transporting sediment from the Himalaya hinterland was flowing through the eastern Nara-Hakra into the Great Rann of Kachchh. In order to reconstruct the history of sedimentation pattern and hence the processes responsible for filling the rain, three sediment cores up to 40 m deep are raised from the western and eastern Great Rann including in the vicinity of the dried Nara river bed. Preliminary sediment logical obviations indicate that the majority of the sediment are dominated by fine micaceous sand implying that the sediment provenance was from the Himalayan region with subordinate clayey silt, which seems to be contributed from the Arabian sea through Kori Creek. We are working on the chronology and geochemistry in order to get an insight into the temporal changes in sediment provenance and causes responsible for the variability. Towards this work on the sediment cores that were raised from the Great Rann is under progress.

This work is done in the collaboration with Banasthali Vidyapith.

(A.D. Shukla)

Nature of rootless cone distribution at aureole of Olympus Mons, Mars

The shield volcano, Olympus Mons is one of the largest volcanoes in the Solar System, is suspected as a site of latest volcanic activity on Mars and various theories have been suggested for the origin of deposit surrounding the main dome.To enhance our knowledge with regard to the origin of deposits and the region condition an attempt has been made to study the distribution and variation in size of aureole cones by using high resolution CTX and HiRISE images along with topographic information. The analysis of large cone fields may provide new line of evidence to understand relationship between climate, volcanism and hydrothermal systems on Mars. For this purpose we have chosen the north region of Olympus Mons known as aureole deposit (Lat: 30°N to 36°N, Long: 133°W to 140°W). The volcano consists of main dome with calderas at the top. The aureole deposit is widespread from the bottom of dome and makes groove terrain that can be easily differentiate. The entire region is believed to contain water and lava in past. In fact, the presence of lava floods and water ice has been proposed on the surface of Mars. The source of water or lava floods is not clear yet, but it generated relatively young smooth surface (probably mid to late Amazonian period) on Mars by resurfacing process. The smooth plain is characterised by some of the distinct targets, one of them is large cone fields. In the current study, we identified and analysed cone structure on the north of Olympus Mons aureole. The cone fields are easily distinguished due to their bright steep slope and high elevation. Similar cone structures are present in Iceland on Earth. The Iceland cones resemble the cones which are observed on Mars. By taking these cones as a reference, we can identify the cone group on Mars. The cones form due to the explosive interaction between lava and water which may be in the form of liquid or solid. The identified cones depict a large variety of morphologies and sizes.

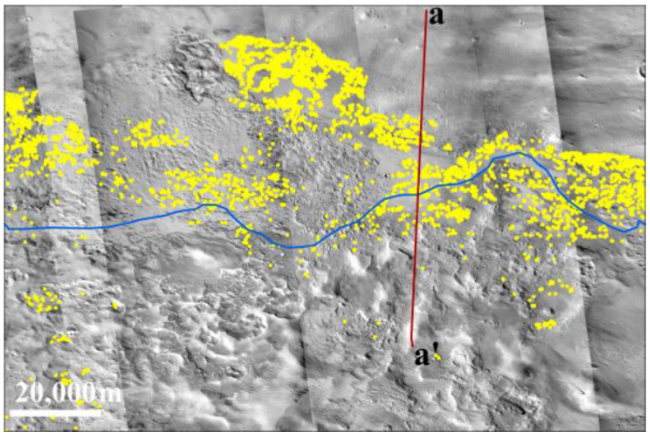


Figure no 23: In associated yellow dots indicates location of cones in CTX and HiRISE. Maroon (a- a'): is a counting line for cone, perpendicular to the basin. Blue line: primary flow line.

Our aim was to analyse the distribution patter, size and morphology of cones and understand possible formation mechanism for the observed features. For detail distribution pattern analysis we counted number of cones along the line (a-a', Fig.23), parallel to flow line (blue line in Fig.23) and divided the region into 1.7 km^2 boxes.

The cones of aureole follows unique distribution pattern: large number of cones is concentrated on the flanks of the flow channel (Fig. 24) and parallel to the flow direction. The cones concentrated at the flank are dominantly of small in size (300m, (Fig. 24C) are confined in the centre part of the valley in aureole. Similar phenomena is seen in case of Athabasca valley, where double cones and lotus cones are confined at the central part of the channel in low elevated area. The large spectrum of variation in cones depends upon the availability of resources (water and/or lava) during the time of formation. In case of Asthabasca Valley, the thick lava flow in the central part channel and large amount of water/ ice in the pore

space are thought to be one of the reason for large double cones and lotus cones. We are assuming similar mechanism could be the reason for larger cone size in our study region. Furthermore, DEM from HiRISE stereo pairs will be generated to study detail cone morphology and measurement of slope, height of cones.

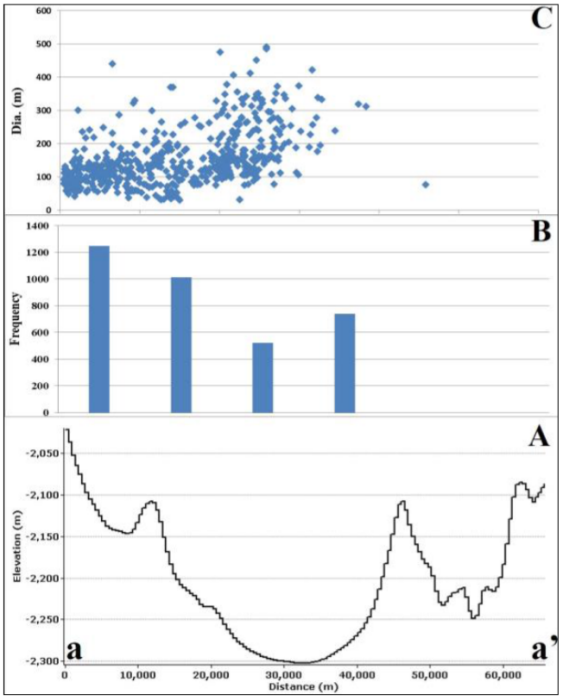


Figure no 24: (A) Elevation graph of basin perpendicular to the primary flow (a- a') (B) Distribution graph of cone perpendicular to the flow direction. Large number of cone group is clustered at the flank of the basin. The topographic information taken from MOLA MEGDR (NASA/Cal-Tech/ASU). (C) Distribution of cones according to its crater size.

(R. Parekh and A.D. Shukla)

Controls on δ^{18}O, δD and δ^{18}O-salinity relationship in the northern Indian Ocean

Oxygen isotopic composition (δ^{18}O) and salinity (S) of the surface ocean are useful tracers for studying imprints of physical processes in the modern ocean, while δ^{18}O - S relation is important to estimate paleo-salinity. Effects of Precipitation (P), Runoff (R) and Evaporation (E) (i.e., P+R – E budget) on δ^{18}O, δD (hydrogen isotopic composition), S and their relations (δ^{18}O-δD and δ^{18}O-S) in the surface ocean are relatively well understood but understanding of such relations (e.g., δ^{18}O-S) in subsurface ocean waters remains elusive. Based on a new dataset of 352 water samples, which includes vertical profiles of δ^{18}O estimates, we have attempted to understand the effect of surface boundary currents and lateral mixing of different water masses on the δ^{18}O - S and δ D-δ^{18}O relation in the northern Indian Ocean. The δ^{18}O-S relation for deeper water samples with lower slope and higher intercept compared to the mixed zone characterizes the presence of Persian Gulf Water mass at 200 – 500 m depth in the Andaman Sea.

(P. Kiran Kumar, A. Singh & R. Ramesh)

Determination of Rare Earth Elements (REEs) in seawater using SeaFAST-HR-ICP-MS

Investigation of relative changes in rare earth elements (REEs) concentration in seawater is a potential tool to understand oceanic processes and trace metal inputs. The Northern Indian Ocean is one of the least explored oceanic region with unique hydrographic setting in terms of REE distribution. Quantification and demonstration of various factors impacting the distribution of seawater REEs in various oceanic reservoirs are essential to understand their oceanic cycling. Towards this, measurement protocol for concentrations of REEs was established using Seafast-HR-ICP-MS, a new instrument facility in Geosciences Division. SeaFAST is a sample preparation system to remove the salt matrix of the seawater samples and pre-concentrate, by retaining trace metals on an ion exchange resin and successive elution of the retained species, and subsequently introduce to HR-ICP-MS. Nobias-PA1 resin, which is a combination of Iminodiacetate and EDTA was used to pre-concentrate the samples. Calibration was performed using low trace metal seawater to match the metal retaining characteristics of pre-concentration resin column. Confirmation of calibration was done by measuring NASS-6 (international seawater reference standard) and found agreeing within 10% for all the measured elements. Typical depth profiles of 14 REEs and Yitrium in the Bay of Bengal obtained by using this method is given in Fig. 25.

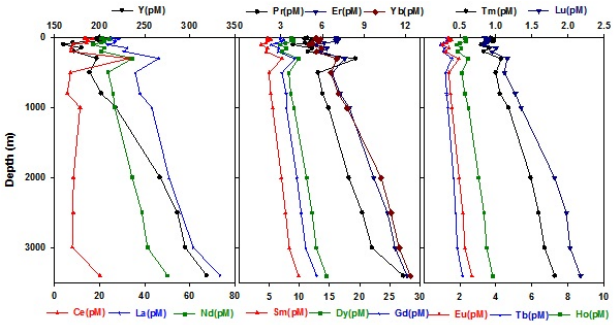


Figure no 25: Typical depth profiles of 14 REEs and Yitrium in the Bay of Bengal

(A.K. Sudheer and M. Gaddam)

Radium isotope distribution in the Indian Ocean

^{226}Ra($t_{1/2}$=1600 y) and ^{228}Ra ($t_{1/2}$=5.75 y) are naturally occurring radium isotopes which have been used as tracers for estuarine, coastal and open ocean mixing processes. Ra isotopes were measured from 67 seawater profiles from surface to 400 m depth from the Bay of Bengal, Arabian Sea and the Indian Ocean between 21°N to 27°S during Indian GEOTRACES and SIBER cruises conducted between 2011 and 2016. The ^{228}Ra activity and ^{228}Ra/^{226}Ra activity ratio decreased from surface to 400 m depth while the trend for ^{226}Ra activity is the opposite. However, a few stations recorded sub-surface depth maxima for ^{228}Ra in the Bay of Bengal. Surface activity of ^{228}Ra in the Arabian Sea, Bay of Bengal, Andaman Sea and the Indian Ocean varied from 1.78±0.57 to 11.29±0.34 dpm 100L^{-1}; 9.44 ±0.41 to 24.11±0.60 dpm 100L^{-1}; 23.83±0.44 dpm 100L^{-1} to 36.72±0.52 dpm 100L^{-1} and 2.20±0.31 to 15.40±0.62

dpm 100L^{-1}, respectively. Similarly, the surface ^{228}Ra/^{226}Ra activity ratios for these basins varied from 0.22±0.04 to 1.70±0.06; 1.18±0.04 to 2.77±0.09; 2.91±0.06 to 2.99±0.10 and 0.34±0.05 to 1.55±0.07, respectively.

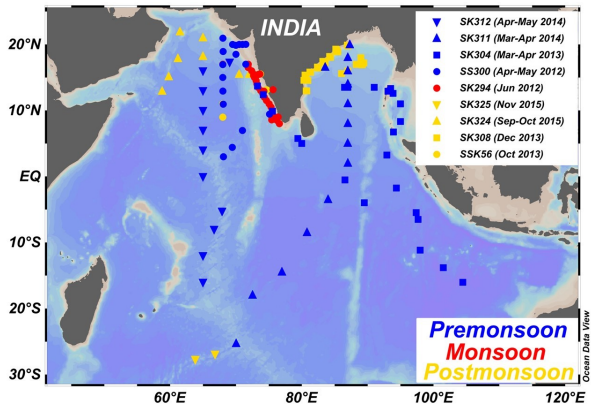


Figure no 26: Location of sampling stations for radium isotopes of GEOTRACES and SIBER cruises.

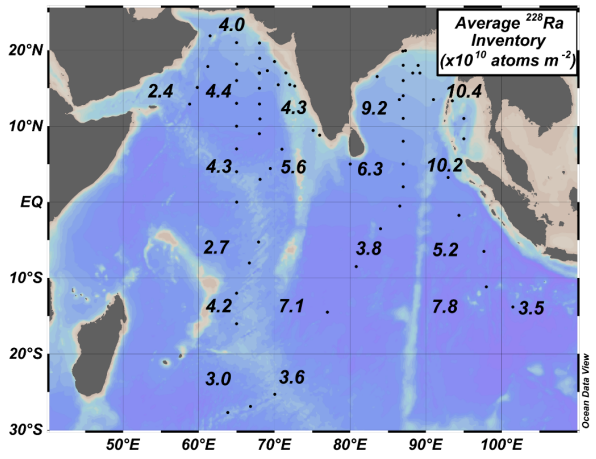


Figure no 27: Inventory of ^{228}Ra (x 10^{10} atoms m^{-2}) in the upper 400 m of the Arabian Sea, Bay of Bengal and the Indian Ocean based on data from Indian GEOTRACES and SIBER cruises. Each dot represents a station with at least 4 ^{228}Ra measurements in the upper 400 m. All stations within each 10° X 10° box are averaged to produce a bin average, shown as a number in each box.

The vertical eddy diffusivities, K_z, (without advection) derived for the southern Indian Ocean are higher by a factor of 3-30 than the ones similarly obtained for the Bay of Bengal, Arabian Sea and Andaman Sea. This may be attributed to the gyres prevailing in the southern Indian Ocean for most of the year. ^{228}Ra inventories computed for the Bay of Bengal are high when compared to those in the Arabian Sea. Hydrothermal vent regions in the Indian Ocean are showing higher ^{228}Ra inventories than those from the adjacent locations.

(R. Rengarajan and S. Subha Anand)

Observationally - constrained attribution of labile iron in aerosols to combustion sources

Atmospheric deposition of iron (Fe) to the ocean has been suggested to modulate primary ocean productivity and thus indirectly affect the climate. However, there are large uncertainties regarding the relative importance of different sources of Fe and effects of atmospheric processing on the bioavailability of the delivered Fe. Here, four atmospheric models and a number of field measurements were used to investigate the effects of atmospheric processing on Fe solubility and contribution of different sources of Fe to labile Fe in atmospheric aerosols. A model result suggests that combustion aerosols substantially contribute to labile Fe loading (>90 %) at high solubility (>10 %) in sum of combustion and dust aerosols sampled in the Northern Hemisphere (NH). The larger contribution of combustion aerosols correspond to stronger degrees of atmospheric transformation measured at higher solubility in the North Atlantic. As the dust is transported to the west in tropical Atlantic, low solubility with no trend is captured by three models. Moreover, the higher solubility in fine particles can be reproduced by mixing with combustion aerosols in two models. These results clearly indicate that high solubility can be attributed to Fe released from pyrogenetic iron oxides. Thus, assessments of atmospheric fluxes of labile Fe to the open ocean should include Fe-containing aerosols emanating from combustion sources.

This work was done as a Member of UN/GESAMP-Working Group #38 on "Atmospheric input of chemicals to the ocean".

(M.M. Sarin)

Theoretical Physics

$\mathrm{B} \to \mathrm{K}_2^*(1430)\ell^+\ell^-$ distributions in Standard Model and beyond at large recoil

The rare decay $\mathrm{B} \to \mathrm{K}_2^*(1430)\ell^+\ell^-$ is studied within and beyond the standard model by exploiting the symmetries of the form-factors that emerge when the final state meson carries a large fraction of the available energy. In this limit, optimised observables are found to be less sensitive to hadronic contributions and are therefore clean. The mode is found to have a large branching fraction within the standard model and is thus expected to be a good study candidate at the current and future experiments. Detailed predictions are provided for the optimised observables within the standard model as well as in the scenarios that seem to be favoured by other $b \to s\ell^+\ell^-$ data.

This Work Done in collaboration with D.Das from University of Delhi, India and G. Kumar from Tata Institute of Fundamental research, Mumbai, India

(B. Kindra, and N. Mahajan)

Factorization in the rare decay $\mathrm{B}^+ \to \mu^+\mu^-\mu^+\nu_\mu$

LHCb collaboration has provided the first upper limit on the branching fraction of the rare decay mode $\mathrm{B}^+ \to \mu^+\mu^-\mu^+\nu_\mu$. The upper limit is in conflict with an approximate theoretical estimate. This mode is studied employing proper QCD techniques and factorization is examined in detail. The form-factors, employing a dipole behaviour are found to yield branching ratio compatible with the experimental limits. The form-factors are computed at the leading order in QCD factorization, employing dispersion relations and are found to have good asymptotic behaviour though there is need to go beyond the tree level to improve the accuracy and stability.

This Work Done in collaboration with A. Bharucha from Aix-Marseille University, CPT, Marseille France.

(B. Kindra and N. Mahajan)

Soft pions and asymptotic dynamics

The soft theorems, where one or more external particles have soft (zero) momentum, have been recently shown to be intimately related to the asymptotic dynamics and an infinite set of Ward identities. This is extended to the case of pions, pseudo-scalar particles, and the asymptotic dynamics and soft charges are found to be related to physical quantities via relations like Goldberger-Treiman result. This paves way for understanding analogues of gravitational and electromagnetic memory for systems involving soft (pseudo-)scalars.

(N. Mahajan)

Exploring dark matter, neutrino mass and $\mathrm{R}_{\mathrm{K}^{(*)},\phi}$ anomalies in $\mathrm{L}_\mu - \mathrm{L}_\tau$ mode

In a new variant of $\mathrm{L}_\mu - \mathrm{L}_\tau$ model with a scalar inert doublet and a scalar leptoquark, Majorana dark matter is studied. The dark matter relic abundance and cross-section of scattering off nucleons is evaluated and compared with experimental limits to constrain the parameter space. This parameter space is further constrained by comparison with the data from B-decays and it is shown that neutrino masses of right order can be generated.

Work At University of Hyderabad S. Singrala and R. Mohanta.

(S. Sahoo)

Probing new physics in semileptonic Λ_b decays

Taking a cue from the recent hints of deviations from the standard model expectations, both in the charged current as well as neutral current B-decays, a model independent analysis of $b \to c\ell\nu_\ell$ is performed and the parameter space is tightly constrained employing the available experimental information on decays mediated by this quark level process. The constrained parameters are used to study the processes $\Lambda_b \to (\lambda_c, p)\ell\nu_\ell$, including forward-backward asymmetry and polarization asymmetries as well as impact on lepton flavour universality.

This Work is done in Collaboration with A. Ray and R. Mohanta from University of Hyderabad.

(S. Sahoo)

Collider signature of V_2 Leptoquark with $b \to s$ flavour observables

The role of V_2 leptoquark is carefully studied with respect to flavour observables and the recent tensions in the data, both in the $b \to c$

charged current as well as in $b \to s$ neutral current processes, in particular the component having electric charge 4/3. It is found that a considerable portion of the parameter space consistent with flavour data gets excluded once the collider constraints are taken into account.

This Work is done in Collaboration with Dr. A, Biswas And Dr. A. K.Swain from IACS Kolkata.

(A. Shaw)

Reconciling dark matter, $\mathrm{R}_{\mathrm{K}^{(*)}}$ anomalies and $(g-2)_\mu$ in an $\mathrm{L}_\mu - \mathrm{L}_\tau$ scenario

A unified and anomaly free scenario with an additional $\mathrm{U}(1)_{\mathrm{L}_\mu - \mathrm{L}_\tau}$ gauge symmetry is proposed that simultaneously solves $\mathrm{R}_{\mathrm{K}^{(*)}}$ and muon $(g-2)_\mu$ discrepancies and at the same time provides a viable dark matter candidate. The model requires the introduction of an additional scalar doublet, a real singlet and and a coloured fermion having vectorial interactions under the additional $\mathrm{U}(1)$. Low mass dark matter ($<$ 60 GeV) regime is still allowed within this scenario and the model is compatible with $\mathrm{B} \to \mathrm{X}_s\gamma$ data and is capable of explaining neutrino masses and mixings if three right handed neutrinos are added.

This Work is done in Collaboration with A. Biswas from IACS kolkata.

(A. Shaw)

Looking for $\mathrm{B} \to \mathrm{X}_s\ell^+\ell^-$ in non-minimal Universal Extra Dimensional model

Non-vanishing boundary localised terms significantly modify the mass spectrum and various interactions among the Kaluza-Klein excited states of 5-Dimensional Universal Extra Dimensional scenario. In this scenario the contributions of Kaluza-Klein excitations of gauge bosons and third generation quarks for the decay process $\mathrm{B} \to \mathrm{X}_s\ell^+\ell^-$ incorporating next-to-leading order QCD corrections are computed and branching ratio as well as Forward Backward asymmetry are obtained. Also considering the constraints from other $b \to s$ observables and electroweak precision data, lower limit on the inverse of the radius of compactification R^{-1} as high as $\geq$760 Ge are obtained.

(A. Shaw)

Bosonic quantum Hall states in single-layer two-dimensional optical lattices

Quantum Hall (QH) states of two-dimensional (2D) single-layer optical lattices are examined using the Bose-Hubbard model (BHM) in the presence of an artificial gauge field. We study the QH states of both the homogeneous and inhomogeneous systems. For the homogeneous case, we use cluster Gutzwiller mean-field (CGMF) theory with cluster sizes ranging from 2*2 to 5*5. We then consider the inhomogeneous case, which is relevant to experimental realization. In this case, we use CGMF and exact diagonalization (ED). The ED studies are using lattice sizes ranging from 3*3 to 4*12. Our results show that the geometries of the QH states are sensitive to the magnetic flux α and cluster sizes. For homogeneous systems, among various combinations of $\frac{1}{5} \leq \alpha \leq \frac{1}{2}$ and filling factor ν, only the QH state of α = $\frac{1}{4}$ with ν= $\frac{1}{2}$, 1, $\frac{3}{2}$, and 2 occur as ground states. For other combinations, the competing superfluid (SF) state is the ground state and QH state is metastable. For BHM with envelope potential, all the QH states observed in homogeneous systems exist for box potentials, but none exist for the harmonic potential. The QH states also persist for very shallow Gaussian envelope potential. As a possible experimental signature, we study the two-point correlations of the QH and SF states.

(R. Bai, S. Bandyopadhyay, S. Pal, K. Suthar and D. Angom)

Condensates in double-well potential with synthetic gauge potentials and vortex seeding

We demonstrate an enhancement in the vortex generation when artificial gauge potential is introduced to condensates confined in a double well potential. This is due to the lower energy required to create a vortex in the low condensate density region within the barrier. Furthermore, we study the transport of vortices between the two wells, and show that the traverse time for vortices is longer for the lower height of the well. We also show that the critical value of synthetic magnetic field to inject vortices into the bulk of the condensate is lower in the double-well potential compared to the harmonic confining potential.

This Work done in collaboration with Dr. Arko Roy from Max-Planck-Institute für Physic komplexer System, Dresden, Germany. And Prof. P.Muruganandam from Department of Physics, Bharathidasan University, India.

(R. Bai, and D. Angom)

A New Sensitivity Goal for Neutrinoless Double Beta Decay Experiments

We study the implications of the Dark-LMA solution to the solar neutrino problem for neutrinoless double beta decay ($0\nu\beta\beta$). We show that while the predictions for the effective mass governing $o\nu\beta\beta$ remains unchanged for the inverted mass scheme, that for normal ordering becomes higher for the Dark-LMA parameter space and moves into the “desert region” between the two. This sets a new goal for sensitivity reach for the next generation experiments if no signal is found for the inverted ordering by the future search programmes.

(K.N. Vishnudath and S. Goswami)

Electroweak Vacuum metastability in a natural minimal Type-III Seesaw Model

We study the minimal type-III seesaw model in which we extend the SM by adding two SU (2) L triplet fermions with zero hypercharge to explain the origin of the non-zero neutrino masses and mixing. We show that the naturalness conditions and the limits from lepton flavor violating decays provide very stringent bounds on the model along with the constraints on the stability/met stability of the electroweak vacuum. We perform a detailed analysis of the model parameter space including all the constraints for both normal as well as inverted hierarchies of the light neutrino masses. We find that most of the region that are allowed by lepton flavor violating decay and naturalness fall in the met stable region.

(K.N. Vishnudath and S. Goswami)

Enhancing the hierarchy and octant sensitivity of ESSνSB in conjunction with T2K, NOνA and ICAL@INO

The main aim of the ESSνSB proposal is the discovery of the lepton CP phase $\delta_{\rm CP}$ with a high significance (5σ for 50% values of $\delta_{\rm CP}$) by utilizing the physics at the second oscillation maxima of the I $P_{\mu e}$ channel. In this work, we concentrate on the hierarchy and octant sensitivity of the ESSνSB experiment. We show that combining the ESSνSB experiment with the atmospheric neutrino data from the proposed India-based Neutrino Observatory(INO) experiment can result in an increased sensitivity to mass hierarchy. In addition, we also combine the results from the ongoing experiments T2K and NOνA assuming their full runtime and present the combined sensitivity of ESSνSB + INO + T2K + NOνA. We show that while by itself ESSνSB can have up to 3σ hierarchy sensitivity, the combination of all the experiments can give up to 5σ sensitivity depending on the true hierarchy-octant combination. The octant sensitivity of ESSνSB is low by itself. However the combined sensitivity of all the above experiments can give up to 3σ sensitivity depending on the choice of true hierarchy, octant. We discuss the various degeneracies and the synergies that lead to the enhanced sensitivity when combining different experimental data.

(K. Chakraborty, S. Goswami and C. Gupta)

Exploring Partial μ-τ Reflection Symmetry at DUNE and Hyper - Kamiokande

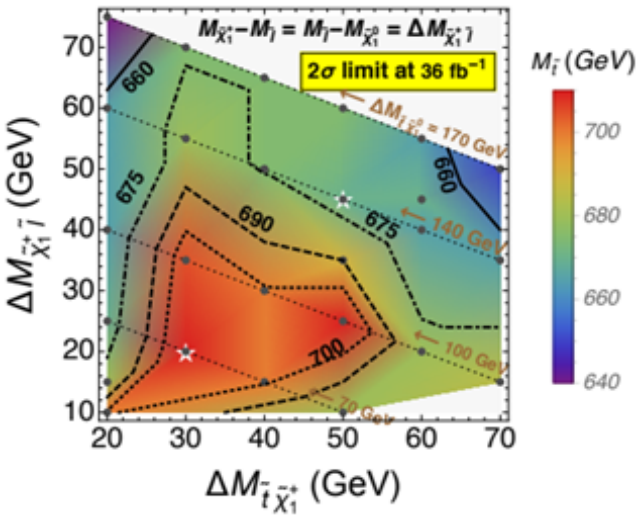
The origin, consequences and testability of a hypothesis of 'partial μ-τ' reflection symmetry were studied. This symmetry predicts $|U_{\mu i}| = |U_{\tau i}|$ $(i = 1, 2, 3)$ for a single column of the leptonic mixing matrix U. Depending on whether this symmetry holds for the first or second column of U different correlations between θ_{23} and $\delta_{\rm CP}$ can be obtained. This symmetry can be obtained using discrete flavour symmetries. In particular, all the subgroups of SU(3) with 3-dimensional irreducible representation which are classified as class C or D can lead to partial μ-τ reflection symmetry. We show how the predictions of this symmetry compare with the allowed area in the $\sin^2\theta_{23} - \delta_{\rm CP}$ plane as obtained from the global analysis of neutrino oscillation data. Furthermore, we study the possibility of testing these symmetries at the proposed DUNE and Hyper-Kamiokande (HK) experiments (T2HK, T2HKK), by incorporating the correlations between θ_{23} and $\delta_{\rm CP}$ predicted by the symmetries. We find that when simulated data of DUNE and HK is fitted with the symmetry predictions, the $\theta_{23} - \delta_{\rm CP}$ parameter space gets largely restricted near the CP conserving values of $\delta_{\rm CP}$.

Finally, we illustrate the capability of these experiments to distinguish between the two cases leading to partial $\mu - \tau$ symmetry namely $|U_{\mu 1}| = |U_{\tau 1}|$ and $|U_{\mu 2}| = |U_{\tau 2}|$.

(K. Chakraborty, K. N. Deepthi, A. Joshipura and S. Goswami)

Constraining slepton and chargino through compressed top squark search

In a continuation of a previous study where usefulness of different kinematic variables sensitive to the compressed mass region were proposed a search strategy to discriminate a well-motivate new physics signal where top squark undergoes a four-body decay due to its extremely narrow mass difference with the lightest supersymmetric particle (LSP). In this work, we investigate the merit extending the search by introducing additional states, chargino and slepton (sneutrino) having masses in between the top squark and the LSP. Enhanced production and lack of branching suppression are capable of providing a strong limit on chargino and slepton/sneutrino mass along with top squark mass. We perform a detailed collider analysis using simplified SUSY spectrum and found that with the present LHC data stop mass can be excluded up to 710 GeV right away for LSP mass of 640 GeV for a particular mass gap between different states (Fig:1).



Reach of 13 TeV LHC with 36fb$-$1 data for different values of different mass gaps between top squark, chargino and the neutralino. The horizontal axis is responsible for the b-jet pT , while the vertical axis controls the lepton phase space. The white space in top right corner is not analyzed as in this region the top squark - neutralino mass difference goes beyond the top-corridor. The bottom right white space is numerical artifact due to computational constraints.

(P. Konar)

Electrical conductivity and Hall conductivity of hot and dense hadron gas in a magnetic field: a relaxation time approach

We estimate the electrical conductivity and the Hall conductivity of hot and dense hadrons gas using the relaxation time approximation of the Boltzmann transport equation in the presence of electromagnetic field. We have investigated the temperature and the baryon chemical potential dependence of these transport coefficients in presence of magnetic field. The explicit calculation is performed within the ambit of the hadrons resonance gas model. We find that the electrical conductivity decreases in the presence of magnetic field. The Hall conductivity on the other hand shows a non monotonic behavior with respect to the dependence on magnetic field. We argue that for a pair plasma (particle-anti particle plasma) with vanishing chemical potential, Hall conductivity vanishes. Only for non vanishing baryon chemical potential, the Hall conductivity has non zero value. We also estimate the electrical conductivity and the Hall conductivity as a function of the center of mass energy along the freeze out curve as may be relevant for relativistic heavy ion collision experiments.

Work done in collaboration with Dr. Ranjita K Mohapatra from IIT Bombay, Mumbai.

(A. Das and H. Mishra)

Transport coefficients of hadronic matter in a van der Walls hadron resonance gas model

We estimate the transport coefficients like shear and bulk viscosities of hot hadronic matter in van der Waals hadron resonance gas (VDW HRG) model in the relaxation time approximation. We also have compared these results with excluded volume hadron resonance (EV HRG) calculations. η/s decreases as the temperature of the hadronic system increases at a fixed baryon chemical potential. The specific shear viscosity, the ratio of shear viscosity to entropy density, in VDW HRG is always less than that of EV HRG case due to the large entropy density in VDW HRG compared to EV HRG case. At a fixed chemical potential, the specific bulk viscosity, in VDW HRG is also less than that of EV HRG case. We also have estimated these transport coefficients along the freezeout curve. There is an increase in chemical freezeout temperature in VDW HRG case determined from the universal condition energy per nucleon energy per nucleon V. We have calculated the variation of attraction parameter along the freezeout curve keeping the freezeout parameters same as in ideal HRG and the repulsion parameter fixed. We observe a nontrivial variation of attraction parameter along the freezeout curve where it increases in the meson dominated region and decreases in the baryon dominated region along the chemical freezeout curve. The specific shear viscosity and the specific specific bulk viscosity in EV HRG is always large than that VDW HRG along the freezeout curve.

Work done in collaboration with Ranjita K Mohapatra, Basanta Nandi and Sadhana Dash from IIT Bombay, Mumbai.

(H. Mishra)

Heavy quark diffusion in a Polyakov loop plasma

We calculate the transport coefficients, drag and momentum diffusion, of a heavy quark in a thermalised plasma of light quarks in the background of Polyakov loop. Quark thermal mass and the gluon Debye mass are calculated in a non-trivial Polyakov loop background. The constituent quark masses and the Polyakov loop is estimated within a Polyakov loop quark meson (PQM) model. We have studied the temperature and momentum dependence of heavy quark drag and diffusion coefficients. It is observed that the temperature dependence of the drag coefficient is almost constant which may play a key role to understand heavy quark observables at RHIC and LHC energies.

Work done in collaboration with Santosh Das from IIT Goa.

(H. Mishra, B. Singh and A. Abhishek)

Spin Polarization and Chiral Condensation in 2+1 flavor Nambu-Jona-Lasinio model at finite temperature and baryon chemical potential

We investigate the ferromagnetic (spin polarization) condensation in (2+1) flavor Nambu Jona-Lasinio(NJL) model with non-zero current quark masses at finite temperature and density which may be relevant in the context of neutron stars. The spin polarization condensation arises due to a tensor type interaction which may be generated due to non-perturbative effects In Quantum Chromodynamics(QCD). In this investigation we have shown the interplay between chiral condensate and spin polarization condensation for different values of tensor coupling. Spin polarization in the case of 2+1 flavor is different from two flavor case because of additional condensate associated with flavor generator. We find a non-zero value of the two spin condensates in the chirally restored phase. Beyond a certain temperature the spin polarization condensates vanish for rather large quark chemical potentials. The spin condensates affect the chiral phase transition, quark masses, and the quark dispersion relation. The spin polarization condensate appears only in the chiral restored phase for light quarks. For large enough tensor couplings, it is observed that the spin polarization condensate acts as a catalyst for chiral symmetry restoration. Thermodynamic behavior of the two spin condensates are found to be different and they affect the quark masses differently.

Work done in collaboration with Dr. Ranjita K Mohapatra from IIT Bombay, Mumbai.

(A. Das , A. Abhishek and H. Mishra)

Probing vorticity in heavy ion collision with dilepton production

We study the effect of vortices present in heavy ion collisions (HICs) on the temperature Evolution of hot quark-gluon plasma in the presence of spin-vortices coupling. The initial global rotation entails a nontrivial dependence of the longitudinal flow velocity on the transverse coordinates and also develops a transverse velocity component that depends upon longitudinal coordinate. Both of these velocities lead to a 2+1 dimensional expansion of the fireball. It is observed that with the finite vorticity and spin-polarization fireball cools faster in comparison with the case without vorticity. Furthermore, we also discuss the consequence of this on thermal dilepton production.

(H. Mishra, B. Singh and J. Bhatt)

Impact of Magnetic field on neutron star properties

We derive an equation of state for magnetized charge neutral nuclear matter relevant for neutron star structure. The calculations are performed within an effective chiral model based on generalization of sigma model with nonlinear self interactions of the sigma mesons along with vector mesons and a rho and sigma meson cross-coupling term. The effective chiral model is extended by introducing the contributions of strong magnetic field on the charged particles of the model. The contributions arising from the effects of magnetic field on the Dirac sea of charged baryons are also included. The resulting equation of state for the magnetized dense matter is used to investigate the neutron star properties, like, mass-radius relation and tidal deformability. The dimensionless tidal deformability of 1.4 solar mass NS is found to be consistent with recent observation of GW170817. The maximum mass of neutron star in presence of strong magnetic field is consistent with the observational constraints on mass of neutron star from PSR J0348 - 0432 and the radius at 1.4 solar mass of the neutron star is within the empirical bounds.

Work done in collaboration with Tuhin Mallik, Tarun K Jha and Debashree Sen from BITS Pilani, Goa campus.

(H. Mishra)

Quantum oscillations of the Stoner susceptibility: theory

Oscillatory effects in magnetic susceptibility of free electrons in a strong magnetic field is well known phenomenon and is well captured by Lifshitz-Kosevich formula. In a recent paper we point out similar oscillatory effects in Stoner susceptibility which makes the system to oscillate between paramagnetic phase and ferromagnetic phase alternatively as a function of external magnetic field.

This Work is done in Collaboration with A. Kumar and R. Sharma from Dept. of Physics, HP University, Shimla, Hp.

(N. Singh)

Resistivity of a 2d quantum critical metal

We calculate resistivity in the paramagnetic phase just above the Curie temperature in a 2d ferromagnetic metal. The required dynamical susceptibility in the formalism of resistivity is calculated within the Random Phase Approximation (RPA). The mechanism of resistivity is magnetic scattering in which s-band electrons are scattered off the magnetic spin fluctuations of d'band electrons. We use the s-d Hamiltonian formalism. We find that near the quantum critical point the resistivity in 2d scales with temperature exponent of 4/3. Our RPA result agrees with the Self Consistence Renormalization (SCR) theory result.

(This Work is done in Collaboration with K, Kumari and R. Sharma from Dept. of Physics, HP University, Shimla, Hp)

(N. Singh)

Atomic, Molecular and Optical Physics

High-power, high repetition-rate, ultrafast fibre laser based source of DUV radiation at 266 nm

We report on a compact, high-power, high repetition-rate, ultrafast source of deep ultraviolet (DUV) radiation. Using a Yb-fibre laser at 1064 nm producing 260 fs output pulses at a 78 MHz repetition rate and usingtwo stage single-pass frequency-doubling, we have generated ultrafast DUV radiation at 266 nm. The fibre laser is first frequency-doubled into green at 532 nm using a LBO crystal with output power as high as 2.4 W and with a conversion efficiency of $\sim$ 50%. Further, the generated green is frequency-doubled in BBO crystal generating DUV radiation with an output power as high as 616 mW corresponding with near-IR to DUV conversion efficiency of $\sim$ 12.8%.

(A. Srinivasa Rao, N. Apurv Chaitanya, and G. K. Samanta)

Simultaneous generation of high-power, ultrafast 1D and 2D Airy beams and their frequency-doubling characteristics

We report on a simple experimental scheme based on a pair of cylindrical lenses (convex and concave) of the same focal length and common optical elements, producing high power optical beams in 1D and/or 2D Airy intensity profiles with laser polarization as the control parameter. Using an ultrafast Yb-fiber laser at 1064 nm of average power of 5 W in a Gaussian spatial profile and pulse width of $\sim$180 fs, we have generated 1D and 2D Airy beams at an efficiency of 80% and 70%, respectively, and a pulse width of $\sim$188 and $\sim$190 fs, respectively. We have measured the transverse deflection rate of 1D and 2D beams to be $\sim 5.0\times\ 10^{-5}\frac{1}{mm}$ and $\sim 2.0\times\ 10^{-5}\frac{1}{mm}$ respectively. Simply rotating the polarization state of the 1D cubic phase modulated beam in the experiment, we can produce 1D and 2D Airy beams on demand. Using a 5 mm long bismuth borate ($Bi\ B_3O_6$), we have also studied frequency-doubling characteristics of both 1D and 2D Airy beams. Like the 2D Airy beam, the 1D Airy beam also produces a frequency-doubled 1D Airy and an additional 1D spatial cubic structure. Like the Gaussian beams, we have observed the focusing dependence of conversion efficiency for both 1D and 2D Airy beams, producing green 1D and 2D Airy beams of output powers in excess of 110 and 150 mW for 3.4 and 2.8 W of fundamental power, respectively.

(Raghwinder S. Grewal, Anirban Ghosh, and G. K. Samanta)

Orbital angular momentum exchange in a picosecond optical parametric oscillator

We report on the orbital angular momentum (OAM) exchange among the interacting beams in an ultrafast optical parametric oscillator (OPO). The singly-resonant OPO is synchronously pumped by a picosecond vortex beam from a frequency-doubled Yb-fiber laser at 532 nm in the green. We demonstrate successful transfer of the pump OAM mode to the non-resonant idler beam tunable across 1109–1209 nm, with OAM as high as l_p =3. Controlling the cavity loss and spatial overlap between the resonant signal and the pump beam in the nonlinear crystal, we have generated signal and idler OAM mode combinations, (l_s, l_i) of (0,2) and (1,1), and (0,3) and (1,2) for pump OAM mode l_p=2 and 3, respectively. Using a pump power of 1 W, we have generated idler OAM mode of orders, l_i=1, 2, and 3, with maximum output powers of 202, 113, and 57 mW, respectively. To the best of our knowledge, this is the first report on controlled generation of OAM modes from an ultrafast OPO. *This work was done in collaboration with Majid Ebrahim-Zadeh and his group from the Institute of Photonic Sciences, Barcelona.*

(Varun Sharma and G. K. Samanta)

On-axis intensity modulation-free, segmented, zero-order Bessel beams with tunable ranges

We propose and experimentally demonstrate a novel experimental scheme to generate high on-axis peak intensity, segmented, smooth, zero-order quasi-Bessel beams with tunable ranges. Illuminating the axicon with hollow Gaussian beams (HGBs) of different orders, we have generated Bessel beams of varying ranges at different positions away from the axicon. The presence of a dark core at the center of the HGBs removes the effect of imperfection in the axicon tip. As a result, the entire power of the input beam is transformed into a zero-order Bessel beam without any on-axis intensity modulation. We observe the decrease in range and increase in on-axis peak intensity of the zero-order Bessel beam with the order of HGBs. Controlling the superposition of the HGBs of different orders to the axicon, we have demonstrated the increase in the range of the Bessel beam. The current technique can also produce Bessel beams of different intensity distributions, including single-peak or multiple-peak Bessel beams. Using single-pass second-harmonic generation in nonlinear crystals of different lengths, we have further verified the increase of on-axis peak intensity of the Bessel beam with the order of the HGBs and the increase in the range of the Bessel beam due to the superposed HGBs.

(A. Srinivasa Rao and G. K. Samanta)

High-power, continuous-wave, tunable mid-IR, higher-order vortex beam optical parametric oscillator

We report on a novel experimental scheme to generate continuous-wave (cw), high-power, and higher-order optical vortices tunable across a mid-IR wavelength range. Using a cw, two-crystal, singly resonant optical parametric oscillator (T-SRO) and pumping one of the crystals with a Gaussian beam and the other crystal with optical vortices of orders l_p=1–6, we have directly transferred the vortices at near-IR to the mid-IR wavelength range. The idler vortices of orders l_i=1–6 are tunable across 2276–3576 nm with a maximum output power of 6.8 W at an order of l_i=1 for the pump power of 25 W, corresponding to a near-IR vortex to mid-IR vortex conversion efficiency as high as 27.2%. Unlike the SROs generating optical vortices restricted to lower orders ($\leq$ 2) due to the elevated operation threshold of SROs with higher-order pump vortices, here the coherent energy coupling between the resonant signals of two crystals of T-SRO facilitates the transfer of pump vortex of any order to the idler wavelength without a stringent operation threshold condition. The generic experimental scheme can be used in any wavelength range across the electromagnetic spectrum and in all timescales, from cw to ultrafast regimes.

(A. Aadhi, Varun Sharma, and G. K. Samanta)

Nonlinear frequency doubling characteristics of asymmetric vortices of tunable, broad orbital angular momentum spectrum

We report on a simple experimental scheme to generate and control the orbital angular momentum (OAM) spectrum of the asymmetric vortex beams in a nonlinear frequency conversion process. Using a spiral phase plate (SPP) and adjusting the transverse shift of the SPP with respect to the incident Gaussian beam axis, we have transformed the symmetric (intensity distribution) optical vortex of order l into an asymmetric vortex beam of measured broad spectrum of OAM modes of orders l, $l-1$, $l-2$, ..., 0 (Gaussian mode). While the position of the SPP determines the distribution of the OAM modes, we have also observed that the modal distribution of the vortex beam changes with the shift of the SPP of all orders and finally results in a Gaussian beam (l = 0). Using single-pass frequency doubling of the asymmetric vortices, we have transferred the pump OAM spectra, l, $l-1$, $l-2$, ..., 0, into the broad spectra of higher order OAM modes, 2l, $2l-1$, $2l-2$, ..., 0 at green wavelength, owing to OAM conservation in nonlinear processes. We also observed an increase in single-pass conversion efficiency with the increase in asymmetry of the pump vortices producing a higher power vortex beam of mixed OAM modes at a new wavelength than that of the pure OAM mode.

(SabirUl Alam, A. Srinivasa Rao, Anirban Ghosh, Pravin Vaity, and G. K. Samanta)

Systematic study of violet stimulated luminescence (VSL) from quartz for extending dating limits of quartz.

The work explores the possibility of using Violet stimulated luminescence (VSL) for extending the dating limits of quartz. There were several studies reporting, that VSL can be used for extending the dating limits as it is able to probe the deep traps, which are expected to be higher in number and thus expected to saturate later in time. In this work, first the protocol suggested by others research works was employed for estimating equivalent doses for old samples. However, it was found that the proposed protocol doesn't provide the desired results due to significant sensitivity change by Violet light and no specific procedures was suggested to correct such sensitivity changes. Further, analysis of the results suggest that improper analysis protocols were employed for suggesting the high dose values. Thus, in order to establish VSL a systematic study was needed in order to suggest the appropriate methodology for dating using VSL. Towards this we conducted experiments related to characterization of VSL signal from quartz and effect of VSL on the traps centers in quartz. Experiments were conducted to optimize the experimental parameters suitable for luminescence studies using VSL. Further, multiple methodological protocols- additive and regenerative, were employed for estimating equivalent dose for old samples. Finally, the suitable protocol was identified and optimized for routine applications. Using the optimized method, we could estimate a dose of about $\sim$600 Gy from quartz. The dose is about 3 times more than the limit of quartz using routine protocol. We expect that the suggested protocol can give further higher dose for suitable samples.

(N. Chauhan, H. M. Rajapara)

Sensitivity Changes in Single Grains of Quartz During the measurement of Natural OSL: Implications for the reliability of OSL ages

Single Aliquot Regeneration (SAR) protocol is routinely used to estimate palaeodose for sediment samples. However, it was observed that significant changes in the OSL sensitivity occur during the read out of natural OSL and SAR protocol does not take into account these changes. It was suggested that if not corrected, this change of sensitivity would lead to substantive systematic offsets in ages based on conventional SAR protocol. To circumvent the issue of sensitivity change, a natural correction factor based SAR (NCF-SAR) protocol and a correction procedure was suggested by Singhvi et al., (2011) with an implicit but a reasonable assumption that the sensitivity of 110° C TL peak of quartz correlates with the OSL sensitivity. Use of this correction resulted in reduced over-dispersion of paleodoses and helped resolve cases where natural signal was way above the regenerated signal.

As a logical extension of this work, sensitivity changes in the OSL from single grains of quartz were examined, during the read out of their natural OSL and their import on the accuracy and reliability of single grains based SAR ages. Toward this over 200 single grains each for 9 samples of diverse depositional environments were analysed and the NCF of each grain was estimated. NCF varied from 0.7 to 20 with $\sim$ 50% in the range of 0.7-1.3. The results indicated that, i) the brighter grains (photon counts $>$ 1000 cs^{-1}) had NCF closer to 1, though significant outliers did exist, ii) the distribution of NCF was positively skewed with significant number of values greater than one, iii) the averaged single grain NCF values and the measured single aliquot NCF values were different, suggesting that in the case of single aliquots, sensitivity changes of dull grains also contribute, significantly.

(N. Chauhan, A. K. Singhvi)

Tunable optical nonlinearity of Au-TiO2 nanocomposites

TiO_2 is at the focus of material science because of its unique electrical, chemical and optical properties which has vast applications in biosensors, photocatalysis, photovoltaic, optoelectronics and energy storage devices. The performance of TiO_2 in these applications can be improved with the modification of surface of TiO_2 by doping noble metals like Au and Ag. The present work is focused on the correlation studies of Fermi energy level and optical nonlinearity of Au-TiO_2 nanocomposites. The Fermi energy and optical nonlinearity are found to be proportionally related with respect to the concentration of Au. The observed shift in Fermi level with increasing concentration of Au is due to charge transfer between TiO_2 and Au in the presence of ultraviolet light irradiation during the formation of Au-TiO_2 nanocomposites. The estimated third order optical nonlinearity was found to increase from 3.80×10^{-6} to 9.69×10^{-6} esu with increase in Au concentrations from 0 to 1.0×10^{-2} M. This observed increment in nonlinearity is due to the enhancement of local electric field created by excitation of surface plasmon resonance that affects the Fermi energy level or work function.

This work was done in collaboration with Ajay Taneja of Department of Chemistry, Dr. B. R. Ambedkar University, Agra, India, and T. Mohanty of School of Physical Sciences, Jawaharlal Nehru University, New Delhi, 11006, India.

(Avesh Kumar and R. P. Singh)

Holocene megafloods and its consequence on the valley landscape, Eastern Himalayan Syntaxis

Downstream of the Tsangpo gorge, huge slack water deposits have shaped the Siang valley of Eastern Himalaya, suggesting rapid deposition of sediments derived from the gorge by ancient floods due to dam outbursting in Tibet. Luminescence ages of paleoflood deposits from the Siang River (downstream reach of Yarlung-Tsangpo River in the Eastern Himalaya) allow identification of two flood events about ca. 6.6 ka and ca. 3.2 ka ago. Combining the flood chronology with hydrological modeling suggest that despite relatively large discharge (minimum 0.38 -1.31 $\times$ 106 $m^3 sec^{-1}$) in megaflood events, no evidence of bedrock incision in the Siang River is observed. Instead, the Siang valley acts as a potential depositional site. The measured detrital zircon fission track ages from the deposits of 6.6 kamegafloods along the valley indicate high bedrock erosion in the upstream Tsangpo gorge, as inferred from increased percentage of young detrital thermochronological ages ($>$ 2 Ma) population. We provide a model for the evolution of Siang valley through the reconstruction of paleoflood hydrology with detrital thermochronology at different stages throughout the Holocene. This model sheds light on intense erosional and depositional potential of the extreme geomorphic process on landscape by removing more material from the upstream regions and depositing quickly in the downstream valley. The study gives an important new source of information for understanding the risk of flood hazards, which is vital for safe town-planning and construction of engineering structures along the Siang River.

This work is done in collaboration with BirajBorgohainand George Mathew from IIT Mumbai.

(N. Chauhan, A. K. Singhvi)

Photoemission and thermoluminescence characteristics of Dy^{+3} -doped zincsodium bismuth borate glasses

This is continuation of the work initiated last year to explore the luminescence properties of amorphous phosphors for estimating high radiation doses using luminescence. The work suggests linear luminescence response of amorphous materials upto 3000 Gy doses which is much higher than the limit of conventionally used phosphors. The work involves preparation and characterization of Dy^{+3} -doped PbO free alkali-heavy-metal-borate glasses for luminescent applications. The amorphous nature of the glasses and the presence of various structural groups like BiO6, BO3 and BO4 were confirmed through XRD and FTIR measurements. The Oscillator strength of Dy^{+3} absorption transitions as well as the bond formed with the O^{-2} ion in the glass network were determined using the absorption spectra. Radiative parameters extracted from Judd-Ofelt theory proved the degree of suitability of prepared glasses for lasing applications. The photoluminescence spectra exhibited the emission characteristics of Dy^{+3} ions and used to calculate the branching ratio, stimulated emission cross-section and radiative lifetime. Metastable lifetimes of Dy^{+3} ions were obtained through exponential fitting of respective decay profiles. The luminescence quenching phenomena was reasoned using Inokuti-Hirayama (IeH) model. The optical gain and quantum efficiency values clearly suggested Dy^{+3} doping at 0.3 mol% was optimum for 587nm lasing action. Further, CIE chromaticity plot indicated the possible applications in solid state lighting devices. The thermoluminescence glow curves of 0.3 mol% Dy^{+3} -doped glasses were considered for gamma irradiation and kinetic parameters of the same were evaluated using Computerized Glow Curve Deconvolution (CGCD) technique. The dose response was found to be linear upto 3 kGy.

This work is done in collaboration with Vinod Hegde and Sudha Kamath Department of Physics, Manipal Institute of Technology, Manipal. Bangalore.

(N. Chauhan)

Investigation of propagation dynamics of truncated vector vortex beams

We experimentally investigate the propagation dynamics of truncated vector vortex beams generated using a Sagnac interferometer. Upon focusing, the truncated vector vortex beam is found to regain its original intensity structure within the Rayleigh range. In order to explain such behavior, the propagation dynamics of a truncated vector vortex beam is simulated by decomposing it into the sum of integral charge beams with associated complex weights. We also show that the polarization of the truncated composite vector vortex beam is preserved all along the propagation axis. The experimental observations are consistent with theoretical predictions based on previous literature and are in good agreement with our simulation results. The results hold importance as vector vortex modes are eigenmodes of the optical fiber.

This work was done in collaboration with P. Srinivas and B. Srinivasan of Department of Electrical Engineering, IIT Madras, Chennai, India.

(P. Chithrabhanu, N. Lal, and R. P. Singh)

Transition from two-photon absorption to saturable absorption in gold patterned ruby thin film

Ruby has potential applications in the field of nonlinear optics. Various nonlinear effects such as slowing down of light, non-degenerate two wave mixing, spectral hole burning has been experimentally as well as theoretically studied in Ruby. Among these applications, slowing down of light has emerged as a promising application due to its usefulness in quantum memory. Therefore, nonlinear behavior of gold micro disks patterned Ruby film has been investigated via Z-scan technique. Open Z-scan was performed for Ruby and Ruby/gold thin film using 532 nm Laser source. Two-photon absorption (TPA) and Saturable absorption (SA) have been observed in pure Ruby and Ruby/gold thin film respectively. The values for nonlinear absorption coefficient (β) for Ruby/gold was two orders of magnitude higher than that of Ruby. Further, TPA and SA were confirmed by open Z-scan on these films using 633 nm Laser source.

This work was done in collaboration with Satchi Kumari and Shompa Kumari of Centre for Applied Physics, Central University of Jharkhand, Ranchi, India.

(Avesh Kumar, Vijay Kumar, and R. P. Singh)

Survival of Extremotolerant Bacteria from the Mukundpuara Meteorite Impact Crater

Carbonaceous meteorites provide clues with regard to prebiotic chemistry and the origin of life. Geological Survey of India recorded a carbonaceous chondrite meteorite fall in Mukundpura, India, on June 6, 2017. We conducted a study to investigate the microbial community that survived the meteorite impact. 16S rRNA metagenomic sequencing indicates the presence of Actinobacteria, Proteobacteria, and Acidobacteriain meteorite impact soil. Comparative phylogenetic analysis revealed an intriguing abundance of class Bacilli in the impact soil. Bacillus thermocopriae IR-1, a moderately thermotolerant organism, was isolated from a rock, impacted by the Mukundpura meteorite. We investigated the resilience of B. thermocopriae IR-1 to environmental stresses and impact shock in a Reddy shock tube. B. thermocopriaeIR-1 survived (28.82% survival) the effect of shock waves at a peak shock pressure of 300 kPa, temperature 400 K, and Mach number of 1.47. This investigation presents the first report on the effect of impact shock on B. thermocopriae IR-1. The study is also the first report on studying the microbial diversity and isolation of bacteria from impact crater soil immediately after meteorite impact event.

This work was carried out in collaboration with Modern College, Pune and Jet Propulsion Laboratory, USA.

(E Shivakarthik, J K Meka, K K Rahul, S Vijayan, B Sivaraman)

VUV photoabsorption of Hydroxylamine: A Prebiotic Molecule of Astrobiological Interest

The aim of the experiments was to synthesize complex molecules that are either precursors of organic molecules or intermediates of bacterial metabolism. Prebiotic molecules have astrobiological significance can be considered as precursors of complex organic compounds like amino acids and prebiotic material. N-bearing molecules are necessary precursors of such prebiotic material and among them hydroxylamine (NH_2 OH) appears to be one of the best candidates. As a first step towards obtaining complex molecules we carried out experiments to synthesize and record the very first Vacuum UltraViolet (VUV) photoabsorption spectra of hydroxyl amine (NH_2OH). To-date the photoabsorption features of NH_2OH in the solid phase are not known. Both experimental and theoretical have shown that in its protonated form hydroxylamine can react in the gas phase with acetic and propanoic acids to yield protonated glycine (the simplest non-chiral amino-acid) and protonated alanine (the second simplest and chiral amino-acid). Hydroxylamine is also one of the first intermediate formed in Biological nitrogen fixation by a reaction between NH_3 and O_2 catalyzed by ammonia monooxygenase enzyme. Hence, Hydroxylamine is an important biomolecule with Astrobiological implications. The photoabsorption features of NH_2OH in the solid ice phase are still not known. Hence, the present study is presumably the first report on the photoabsorption spectra of Hydroxylamine at 3K. This study has significant implications in NH_2OH synthesis on the surface of dust grains in the interstellar and circumstellar medium and can have an enormous impact on astrobiology, Earth biochemistry, and the origin of life.

This work was carried out in collaboration with National Synchrotron Radiation Research Center - Taiwan, The Modern College - Pune, University of Kent – UK, RRCAT – India, IISER – Mohali and University of Hawaii, USA.

(K K Rahul, B Sivaraman)

Reversible Phase Change Observed in 1-hexyne Astrochemical Ices

Icy dust grains in the InterStellar Medium (ISM) are very well known to be the tiny chemical factories that are responsible for the synthesis of variety of complex molecules, both organic and inorganic, that are observed to-date and those awaiting identification. Perhaps, due to advent of space telescopes the molecular icy mantles on dust grains are also studied at InfraRed (IR) wavelengths and are compared with the laboratory based spectra. Existing spectral repository of simple molecules suggest that the morphology of astrochemical ices can be either amorphous or crystalline. In fact, IR spectroscopy of astrochemical ices are quite sensitive to the changes in morphology.

Laboratory ice analogues of simple and complex molecules, that are made by recreating the pressure and temperature conditions of the ISM, probed using IR spectroscopy has clearly shown the existence of amorphous phase when molecules are deposited at very low temperature, say 10 K, and then a phase change to crystalline ice to occur by warming the ice to higher temperatures. Indeed, warming the ice to temperatures above the crystalline phase results in the sublimation of the molecular ice as it is kept at ultra-high vacuum condition. However, recently a reversible phase change in ethanethiol astrochemical ices was observed where the ice subjected to temperature cycle was observed to switch morphology from amorphous to crystalline then back to amorphous. Following the first report on reversible phase change, Hudson reported similar change to occur in the ethanol ices too suggesting there may exist

more such molecules that undergo the reversible phase change. In our recent experiments using 1-hexyne [HCC$(CH_2)3CH_3$] we observed similar reversible phase change to occur.

(J Meka, K K Rahul, B Sivaraman)

Impact Induced Shock Processing of Complex Astromolecules

The chemical modification of astrochemical materials has been studied principally due to processing induced by UV photolysis, radiation of charge particles etc. However, impacts shock could be also an efficient energy source for driving interesting chemistry. A wide variety of impact craters has been observed on the Solar System bodies showing evidence for impact activity over in the past, producing various geophysical phenomenon. Besides those geophysical phenomena, it is widely suggested that impact shock may induce chemical synthesis. Shock waves can create sudden intense pressure and temperature, which can affect chemical pathways.

Laboratory analogue of impact processes are mostly producedby hypervelocity impact experiments. Such experimental techniques are quite useful for analysis of cratering mechanism, dynamics of ejecta and other physical phenomenon. However, laboratory analysis of chemical aspects of impact event is restricted. We present experimental technique for impact shock chemistry utilizing shock tube in laboratory. Shock tubes are extensively used to generate shock waves in the laboratory for studying various phenomenon like interaction of shock-heated gases with materials, with applications for space vehicle re-entry, combustion and chemical kinetics and investigating gas phase reactions at high temperatures. Our experimental technique will provide a mechanism for shock synthesis of complex astromolecule at realistic impact condition.

This work was carried out in collaboration with IISc, Bangalore.

(V S Surendra, J K Meka, U Deva, K K Rahul, E Shivakarthik, B Sivaraman)

Highly Charged Ions as Prospective Ultra High-precision Atomic Clocks

By carrying out rigorous investigations, the Ni^{12+}, Cu^{13+}, Pd^{12+}, and $Ag^{+}13+$ highly charged ions (HCIs) were proposed for making very accurate optical clocks with the fractional uncertainties below 10^{-19} level. These HCIs have simple atomic energy levels, clock transitions with quality factors larger than 10^{15} , and optical magnetic-dipole (M1) transitions that can be used for laser cooling and detecting quantum jumps on the clock transitions by the shelving method. To demonstrate the projected fractional uncertainties, we estimated orders of magnitude of the Zeeman, Stark, blackbody radiation, and electric quadrupole shifts of the clock transitions by performing calculations of the relevant atomic properties in the above HCIs. Similar investigations were also undertaken in the ground-state fine-structure transitions of boron-like S^{11+}-K^{14+} and gallium-like Nb^{10+}-Ru^{13+} ions, but it is found that these HCIs have lower quality factors than the aforementioned HCIs for making the atomic clocks.

These works were done in collaboration with Dr. Yan-mei Yu of Beijing National Laboratory for Condensed Matter Physics, Institute of Physics, Chinese Academy of Sciences, Beijing 100190, China.

(B. K. Sahoo)

Relativistic Normal Coupled-Cluster Theory for Atoms

Previous calculations on electric dipole moments (EDMs) of diamagnetic atoms due to parity and time-reversal violating (P,T-odd) interactions, which are essential ingredients for probing new physics beyond the standard model of particle interactions, using relativistic coupled-cluster (RCC) methods differed substantially from the other available theoretical results. It was, there- fore, necessary to perform an independent test of the validity of these results. In view of this, the normal coupled-cluster method was developed to calculate the EDMs of atoms by simultaneously incorporating the electrostatic and P,T-odd interactions in order to overcome the shortcomings of the ordinary RCC method. This new relativistic method has been applied to 199Hg, which currently has a lower EDM limit than that of any other system. The results of our RNCC and self-consistent RCC calculations of the EDM of this atom are found to be close. The discrepancies between these two results on the one hand and those of previous calculations on the other were elucidated. Furthermore, the electric dipole polarizability of this atom, which has computational similarities with the EDM, was evaluated and found to be in very good agreement with its measured value.

This work was done in collaboration with Prof. B. P. Das of Department of Physics and International Education and Research Center of Science, Tokyo Institute of Technology, 2-12-1 Ookayama Meguro-ku, Tokyo 152-8550, Japan.

(B. K. Sahoo)

High Precision Calculations of Electric Dipole Polarizabilities of Xe and Cd Atoms

We have performed rigorous calculations of the ground-state polarizability of Xe and Cd atoms using a self-consistent relativistic coupled-cluster (RCC) method and the relativistic normal coupled-cluster (RNCC) method. The discrepancies between the results from these two methods are found to be very small, thereby implying high accuracies of these results. The Cd result has also been independently verified by employing a finite-field procedure in the RCC theory frameworks. The Cd atom results are, however, differ substantially from the available experimental value while the calculated values of Xe atom are well within the experimental error bars. On the basis of these analyses, we suggest to carry out new measurement of dipole polarizability of the Cd atom to affirm its actual value.

These works were done in collaboration with Yan-mei Yu of Beijing National Laboratory for Condensed Matter Physics, Institute of Physics, Chinese Academy of Sciences, Beijing 100190, China, and A. Sakurai and B. P. Das of Department of Physics and International Education and Research Center of Science, Tokyo Institute of Technology, 2-12-1 Ookayama Meguro- ku, Tokyo 152-8550, Japan.

(B. K. Sahoo)

Higher-component quadrupole polarizabilities

For the first time, derivations for the higher tensor components of the quadrupole polarizabilities were given and using these formulas, higher component quadrupole polarizabilities of the metastable states of the Cr^+ , Sr^+ , and Ba^+ alkaline-earth-metal ions were estimated. The scalar quadrupole polarizabilities of the ground and metastable states of these ions were also evaluated to compare our results with the previously available theoretical and experimental results. Reasonably good agreement between our calculations with the previous values of scalar quadrupole polarizabilities demonstrated correctness of wave functions of the above ions. Our reported quadrupole polarizabilities will be useful to estimate the uncertainties due to the gradient of the electric fields in the clock frequencies of the above alkaline-earth-metal ions when the accuracies of these frequency measurements attain a precision level below 10^{-19} .

This work was carried out in collaboration with S. Singh, M. Kaur and B. Arora of Department of Physics, Guru Nanak Dev University, Punjab, India.

(B. K. Sahoo)

Dynamics of resonant energy transfer in one-dimensional chain of Rydberg atoms

We had studied resonant energy transfer in a one-dimensional chain of two to five atoms by analyzing time-dependent probabilities as function of their interatomic distances. The dynamics of the system were first investigated by including the nearest-neighbour interactions and then accounting for all next-neighbour interactions. We found that inclusion of nearest-neighbour interactions in the Hamiltonian for three atoms chain exhibits periodicity during the energy transfer dynamics; however, this behavior displayed aperiodicity with the all-neighbour interactions. It showed for the equidistant chains of four and five atoms the peaks are always irregular but regular peaks are retrieved when the inner atoms are placed closer than the atoms at both the ends. In this arrangement, the energy transfer swings between the atoms at both ends with very low probability of finding an atom at the center. This phenomenon resembles with quantum notion of Newtons cradle. We also found out the maximum distance up to which energy could be transferred within the typical lifetimes of the Rydberg states.

This work was carried out in collaboration with M. Kaur, P. Kaur and B. Arora of Department of Physics, Guru Nanak Dev University, Punjab, India.

(B. K. Sahoo)

High-Precision Multiphoton Ionization of Accelerated Laser-Ablated Species

We demonstrated that the pulsed-time structure and high-peak ion intensity provided by the laser-ablation process can be directly combined with the high resolution, high efficiency, and low background offered by collinear resonance ionization spectroscopy. This simple, versatile, and powerful method can offer new and unique opportunities for high-precision studies of atomic and molecular structures, impacting fundamental and applied physics re- search. We showed that even for ion beams possessing a relatively large energy spread, high-resolution hyperfine-structure measurements can be achieved by correcting the observed line shapes with the time-of-flight information of the resonantly ionized ions. This approach offers exceptional advantages for performing precision measurements on beams with large energy spreads and allows measurements of atomic parameters of previously inaccessible electronic states. The potential of this experimental method in multidisciplinary research was illustrated by performing, for the first time, hyperfine-structure measurements of selected states in the naturally occurring isotopes of indium, 113,115 In. Relativistic coupled-cluster calculations were performed to highlight the importance of our findings in the development of state-of-the- art atomic many-body methods, nuclear structure, and fundamental-physics studies.

This work was carried out in collaboration with R.F. Garcia Ruiz, A.R. Vernon, C.L. Binnersley, M. Bissell, J. Billowes, K.T. Flanagan and C.M. Ricketts of School of Physics and Astronomy, The University of Manchester, Manchester M13 9PL, United Kingdom; T.E. Cocolios, W. Gins, R.P. de Groote, G. Neyens, and X. F. Yang of KU Leuven, Instituutvoor Kern- en Stralingsfysica, B-3001 Leuven, Belgium; and K.D.A. Wendt of Institutfu¨rPhysik, Johannes Gutenberg-Universit¨at Mainz, D-55128 Mainz, Germany.

(B. K. Sahoo)

Generalized binomial state: Nonclassical features observed through various witnesses and a quantifier of nonclassicality

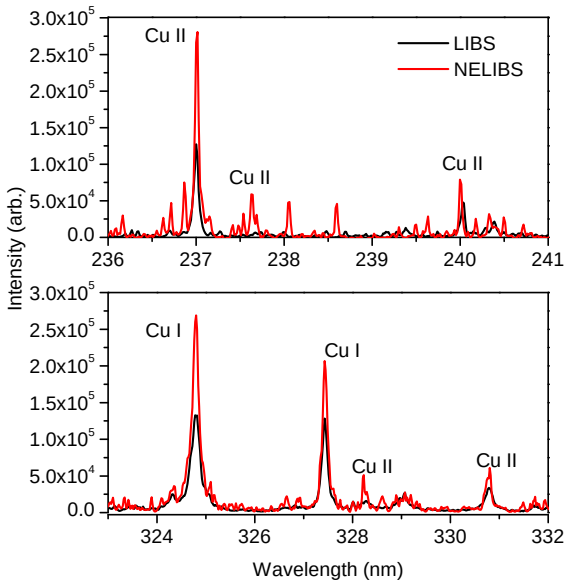
Experimental realization of various quantum states of interest has become possible in the recent past due to the rapid developments in the field of quantum state engineering. Nonclassical properties of such states have led to various exciting applications, specifically in the area of quantum information processing. We have studied lower- and higher-order nonclassical features of such an engineered quantum state (a generalized binomial state). Our study has revealed that the state is highly nonclassical. Specifically, higher-order nonclassical properties of this state are reported using a set of witnesses, like higher-order antibunching, higher-order sub-Poissonian photon statistics, higher-order squeezing (both Hong–Mandel type and Hillery type). A set of other witnesses for lower- and higher-order nonclassicality (e.g., Vogel's criterion and Agarwal's A parameter) have also been explored. Further, an analytic expression for the Wigner function of the generalized binomial state is obtained which is used to witness nonclassicality and to quantify the amount of nonclassicality present in the system by computing the nonclassical volume (volume of the negative part of the Wigner function). Optical tomogram of the generalized binomial state is also computed for various conditions as the Wigner function cannot be measured directly in an experiment in general, but can be obtained from the optical tomogram with the help of Radon transform.

This work was done in collaboration with K. Mandal, N. Alam, A. Verma and A. Pathak from Jaypee Institute of Information Technology, Noida.

(J. Banerji)

Aluminum nanoparticles enhanced Laser Induced Breakdown Spectroscopy of copper sample

Role of Aluminum(Al) nanoparticles on enhancement of emission spectra in Laser Induced Breakdown Spectroscopy has been investigated using the Nd: YAG laser of 532 nm wavelength and 7 ns pulse duration, various concentrations of Al-nanoparticles deposited on Cu-substrate and AndorEchelle Spectrometer. Solutions of different Al-NPs concentrations viz., 0.1, 0.2 and 0.8 mg/ml were made by dispersing 1 mg of Al NPs in 10, 5 and 1.25 ml of acetone and 0.4 $\frac{mg}{ml}$ solution by dispersing 2 mg of Al NPs in 5 ml of acetone.For each concentration of Al nanoparticles deposited on Cu substrate, the experiment was performed at different gate delays to understand the signal enchantment mechanism. The 2-3 times enhancement in emission spectra of Cu sample has been observed. A comparison of LIBS and Al-NPs LIBS spectrum is shown in figure in which enhancement by NPs is clearly seen.



Comparison between LIBS and NELIBS for different wavelength ranges for the given acquisition settings and laser fluence = 11.2 J/cm^2

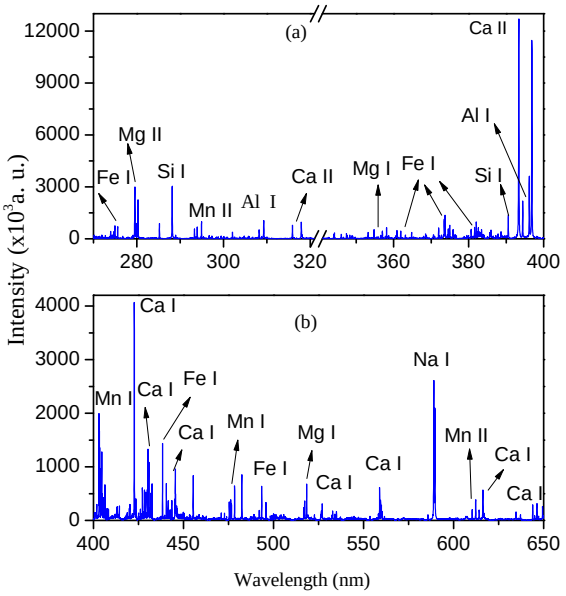
(Swetapuspa Soumyashree, Nageswara Rao E., Prashant Kumar, Pooja Chandravanshi, Madhusudhan P, Rajesh K. Kushawaha, S. B. Banerjee, K.P. Subramanian)

Elemental composition estimation of rock samples employing synthetic spectrum method and LIBS:

In the present study, the synthetic generated spectrum method has been utilized to estimate the accurate elemental concentrations of the atomic emissions of Al, Ca, Fe, Mg, Mn, Na, Si and Ti of basalt rock sample using a nonlinear fitting routine. In this algorithm the self-absorption of emissions has considered for the calculation of number density and stark width of different elemental species in the plasma. Our results of elemental compositions by synthetic generated spectrum are matched well with the reference value obtained from the X-ray fluorescence (XRF) spectroscopy.

Figure 2: Experimental LIBS spectra of basalt rock sample with spectral window (a) 270-400 nm, (b) 400-650 nm at gate delay 2500 ns, gate width 2000 ns averaged over 500 laser shots at 180 mJ energy

Time resolved spectra have been recorded to observe the spectral signatures and especially signal to background ratio at different gate delays. Simulated emission profile based on local thermodynamic equilibrium (LTE) model at different concentrations was generated for two minor elements of phosphors (P) and potassium (K) present in the sample. These simulated line profiles were then compared with the experimental value to understand the non-appearance of some elements in the LIBS spectrum.



Experimental LIBS spectra of basalt rock sample with spectral window (a) 270-400 nm, (b) 400-650 nm at gate delay 2500 ns, gate width 2000 ns averaged over 500 laser shots at 180 mJ energy

(NageswaraRao E., Swetapuspa Soumyashree, Prashant Kumar, Pooja Chandravanshi, Madhusudhan P, Rajesh K. Kushawaha, S. B. Banerjee, K.P. Subramanian)

Publications

Publications in Journals

Astronomy and Astrophysics

1. Bisoi. S. K., Sawant H.S., Janardhan P., Yan Y., Chen L., Awasthi. A.K., Srivastava S. and Gao, G., 2018, *"Decimetric emission 500" away from a flaring site: possible scenarios from GMRT solar radio observations"*, Astrophyical Journal, v. 862, p. 65-79.
2. Janardhan, P., Fujiki, K., Ingale, M., Bisoi, S. K., and Rout, D., 2018, *"Solar Polar Fields During Cycle 24: An Unusual Polar Field Reversal"*, Astronomy & Astrophysics, v. 618, p. A148.
3. Gupta, G. R., Sarkar, A. and Tripathi, D., 2018, *"Observation and Modeling of Chromospheric Evaporation in a Coronal Loop Related to Active Region Transient Brightening"*, The Astrophysical Journal, v. 857, Issue 2, p. 137.
4. Bisht, D., Yadav, R. K. S., Ganesh, S., Durgapal, A. K., Rangwal, G., Fynbo, J. P. U., 2019, *"Mass function and dynamical study of the open clusters Berkeley 24 and Czernik 27 using ground based imaging and Gaia astrometry"*, Monthly Notices of the Royal Astronomical Society, v. 482, Issue, p.1471-1484.
5. Dey, L., Valtonen, M. J., Gopakumar, A., et al. 78 authors including Baliyan, K.S., Kaur, N., Ganesh, S., 2018, *"Authenticating the Presence of a Relativistic Massive Black Hole Binary in OJ 287 Using Its General Relativity Centenary Flare: Improved Orbital Parameters"*, The Astrophysical Journal, v. 866, p. 11-30.
6. Kaur, N., and Baliyan, K. S., 2018, *"CTA 102 in exceptionally high state during 2016-2017"*, Astronomy & Astrophysics, v. 617, p. A59-70.
7. Goyal, A., Stawarz, Ł., Zola, S., et al. 72 authors including Baliyan, K.S., and Kaur. N., 2018, *"Stochastic Modeling of Multiwavelength Variability of the Classical BL Lac Object OJ 287 on Timescales Ranging from Decades to Hours"*, The Astrophysical Journal, v. 863, p. 175-184.
8. Kaur, N., Baliyan, K. S., Chandra, S., Sameer, and Ganesh, S., 2018, *"Optical variability in IBL S5 0716+714 during the 2013-2015 Outbursts"*, The Astronomical Journal, v. 156, p. 36-50.
9. Dewangan, L. K., Baug, T., Ojha, D. K., Ghosh, S. K.,, 2018, *"Investigating inner and large scale physical environments of IRAS 17008-4040 and IRAS 17009-4042 toward l = 345.5 deg, b = 0.3 deg"*, The Astrophysical Journal, v. 869, p. 30.
10. Dewangan, L. K., Dhanya, J. S., Ojha, D. K., Zinchenko, I.,, 2018, *"The study of a system of H II regions toward l = 24.8 deg, b = 0.1 deg at the Galactic bar-Norma arm interface"*, The Astrophysical Journal, v. 866, p. 20.
11. Dewangan, L. K., Baug, T., Ojha, D. K., Zinchenko, I., Luna, A., 2018, *"Filamentary structures and star formation activities in the sites S234, V582, and IRAS 05231+3512"*, The Astrophysical Journal, v. 864, p. 54.
12. Dewangan, L. K., Ojha, D. K., Zinchenko, I., Baug, T., 2018, *"Cloud-cloud collision induced star formation in IRAS 18223-1243"*, The Astrophysical Journal, v. 861, p. 19.
13. Dutta, S., Mondal, S., Samal, M. R., Jose, J., 2018, 2018, *"The Planck Cold Clump G108.37-01.06: A Site of Complex Interplay between H II Regions, Young Clusters, and Filaments"*, The Astrophysical Journal, v. 864, p. 154.
14. Panwar, N., Samal, M. R., Pandey, A. K., Singh, H. P., Sharma, S.,, 2019, *"Understanding Formation of Young, Distributed Low-mass Stars and Clusters in the W4 Cloud Complex"*, The Astronomical Journal, v. 157, p. 112.
15. Eden, D. J., et al. including Samal, M. R., 2019, *"SCOPE: SCUBA-2 Continuum Observations of Pre-protostellar Evolution - survey description and compact source catalogue"*, Monthly Notices of the Royal Astronomical Society, v. 485, p. 2895.
16. Rajpurohit, A. S., Allard, F., Rajpurohit, S., Sharma, R., Teixeira, G. D. C., Mousis, O., Kamlesh, R., 2018, *"Exploring the stellar properties of M dwarfs with high-resolution spectroscopy from the optical to the near-infrared"*, Astronomy & Astrophysics, v. 620, p. 8.
17. Hillenbrand, L., Miller, A., Carpenter, J., Kasliwal, M., Isaacson, H., Tang, S., Joshi, V., Banerjee, D. P. K., and Cutri, R., 2019, *"PTF14jg: The Remarkable Outburst and Post-burst Evolution of a Previously Anonymous Galactic Star"*, The Astrophysical Journal, v. 874, p. 82.
18. Hsiao, E. Y.; Phillips, M. M.; Marion, G. H.; Kirshner, R. P.; ... Banerjee, D. P. K. et al.,, 2019, *"Carnegie Supernova Project-II: The Near-infrared Spectroscopy Program"*, Pub. of the Astron. Soc. of the Pacific, v. 131, p. 014002.
19. Rho, J., Geballe, T. R., Banerjee, D. P. K., Dessart, L., Evans, A., and Joshi, V,, 2018, *"Near-infrared Spectroscopy of Supernova 2017eaw in 2017: Carbon Monoxide and Dust Formation in a Type II-P Supernova"*, The Astrophysical Journal Letters, v. 864, p. 20.
20. Gehrz, R. D.; Evans, A.; Woodward, C. E.; Helton, L. A.; Banerjee, D. P. K.; Srivastava, M. K.; Ashok, N. M.; Joshi, V.

et al., 2018, *"The Temporal Development of Dust Formation and Destruction in Nova Sagittarii 2015#2 (V5668 SGR): A Panchromatic Study"*, The Astrophysical Journal, v. 858, p. 78.

21. Banerjee, D. P. K.; Joshi, V.; Evans, A.; Srivastava, Mudit; Ashok, N. M.; Gehrz, R. D.; Connelley, M. S.; Geballe, T. R.; Spyromilio, J.; Rho, J.; Roy, R.,, 2018, *"Early formation of carbon monoxide in the Centaurus A supernova SN 2016adj"*, Monthly Notices of the Royal Astronomical Society, v. 481, p. 806.
22. Banerjee, D. P. K.; Hsiao, E. Y.; Diamond, T.; Galbany, L.; Morrell, N.; Minniti, D.; Kuncarayakti, H.; Mattila, S.; Harmanen, J.,, 2018, *"Unraveling the Infrared Transient VVV-WIT-06: The Case for the Origin as a Classical Nova"*, The Astrophysical Journal, v. 867, p. 99.
23. Ghosh, S.; Mondal, S.; Das, Ramkrishna; B., D. P. K.; Ashok, N. M.; Hambsch, F.; and Dutta, S.,, 2018, *"Phase-dependent Photometric and Spectroscopic Characterization of the MASTER-Net Optical Transient J212444.87+321738.3: An Oxygen-rich Mira"*, The Astronomical Journal, v. 155, p. 216.
24. Mathew, B.; Manoj, P.; Narang, M.; Banerjee, D. P. K.; Nayak, P.; Muneer, S.; Vig, S.; Pramod Kumar, S.; Paul, K. T.; Maheswar, G., 2018, *"Excitation Mechanism of O I Lines in Herbig Ae/Be Star"*, The Astrophysical Journal, v. 857, p. 30.
25. Jaisawal, G. K., Naik, Sachindra, Gupta, S., Chenevez, J., and Epili, P. E.,, 2018, *"A curious case of the accretion-powered X-ray pulsar GX 1+4"*, Monthly Notices of the Royal Astronomical Society, v. 478, p. 448-459.
26. Gupta, S., Naik, Sachindra, Jaisawal, G. K., and Epili, P.,, 2018, *"Spectral and timing studies of 2S 1417-624 during a giant outburst"*, Monthly Notices of the Royal Astronomical Society, v. 479, p. 5612-5619.
27. Vagshette, N. D., Naik, S., and Patil, M. K.,, 2019, *"Cavities, shocks and a cold front around 3C 320"*, Monthly Notices of the Royal Astronomical Society, v. 485, p. 1981-1989.
28. Singh V., and Chand H., 2018, *"Investigating kpc-scale radio emission properties of narrow-line Seyfert 1 galaxies'"*, Monthly Notices of the Royal Astronomical Society, v. 480, p. 1796-1818.
29. Chand, V., Chattopadhyay, T., Oganesyan, G., Rao, A. R., Vadawale, S. V., Bhattacharya, D., Bhalerao, V. B., and Misra, K., 2018, *"AstroSat-CZTI Detection of Variable Prompt Emission Polarization in GRB 171010A"*, The Astrophysical Journal, v. 874, p. 70.
30. Pahari, M., Bhattacharyya, S., Rao, A. R., Bhattacharya, D., Vadawale, S. V., Dewangan, G. C., McHardy, I. M., Gandhi, P., Corbel, S., Schulz, N. S., and A., Diego,, 2018, *"AstroSat and Chandra View of the High Soft State of 4U 1630–47 (4U 1630–472): Evidence of the Disk Wind and a Rapidly Spinning Black Hole"*, The Astrophysical Journal, v. 867, p. 86.
31. Basu, A., Joshi, B. C., Bhattacharya, D., Rao, A. R., Naidu, A., Krishnakumar, M. A., Arumugsamy, P., Vadawale, S. V., Manoharan, P. K., Dewangan, G. C., Vibhute, A., Mithun, N. P. S., and Sharma, V., 2018, *"Timing offset calibration of CZTI instrument aboard ASTROSAT"*, Astronomy & Astrophysics, v. 617, p. 6.
32. Chand, V., Chattopadhyay, T., Iyyani, S., Basak, R., Aarthy, E., Rao, A. R., Vadawale, S. V., Bhattacharya, D., and Bhalerao, V. B., 2018, *"Violation of Synchrotron Line of Death by the Highly Polarized GRB 160802A"*, The Astrophysical Journal, v. 862, p. 154.
33. Banerjee, D. P. K., Hsiao, E. Y., Diamond, T., Galbany, L., Morrell, N., Minniti, D., Kuncarayakti, H., Mattila, S., Harmanen, J, 2018, *"Unraveling the Infrared Transient VVV-WIT-06: The Case for the Origin as a Classical Nova"*, Monthly Notices of the Royal Astronomical Society, v. 867, p. 99-104.
34. Pavlenko, Ya. V., Evans, A., Banerjee, D. P. K., Southworth, J., Shahbandeh, M., Davis, S., 2018, *"Infrared spectroscopy of the merger candidate KIC 9832227"*, Astronomy & Astrophysics, v. 615, p. 120-123.

Solar Physics

35. Joshi, N.C., Zhu, X., Schmieder, B., Aulanier, G., Janvier, M., Joshi, B., Magara, T., Chandra, R., and Inoue, S.,, 2019, *"Generalization of the Magnetic Field Configuration of Typical and Atypical Confined Flares"*, ApJ, v. 871, 165, pp. 17.
36. Sindhuja, G., Srivastava, N., Veronig, A. M., Pötzi, W.,, 2019, *"Study of reconnection rates and light curves in solar flares from low and mid chromosphere"*, MNRAS., v. 482, p. 3744-3756.
37. Mitra, P. K., Joshi, B., Prasad, A., Veronig, A. M., Bhattacharyya, R.,, 2018, *"Successive Flux Rope Eruptions from δ-sunspots Region of NOAA 12673 and Associated X-class Eruptive Flares on 2017 September 6"*, ApJ, v. 869, 69, pp. 19.
38. Ranganathan, M., Sankarasubramanian, K., Bayanna, A. R., Mathew, S. K.,, 2018, *"Lenslet Array and Fabry–Pérot based Hyperspectral Imaging"*, ApJ, v. 867, 77, pp. 7.
39. Sivaram, C., Arun, K., Prasad, A.,, 2018, *"Extremal charged black holes, dark matter and dark energy"*, Ap&SS, v. 363, 202, pp. 3.
40. Pal, S., Nandy, D., Srivastava, N., Gopalswamy, N., Panda, S.,, 2018, *"Dependence of Coronal Mass Ejection Properties on Their Solar Source Active Region Characteristics and Associated Flare Reconnection Flux"*, ApJ, v. 865, 4, pp. 11.
41. Chandra, R., Chen, P. F., Joshi, R., Joshi, B., Schmieder, B.,, 2018, *"Observations of Two Successive EUV Waves and Their Mode Conversion"*, ApJ, v. 863, 101, pp. 9.
42. Joshi, B., Ibrahim, M. S., Shanmugaraju, A., Chakrabarty, D.,, 2018, *"A Major Geoeffective CME from NOAA 12371: Initiation, CME-CME Interactions, and Interplanetary Consequences"*, Sol. Phys., v. 293, 107, pp. 20.
43. Prasad, A., Bhattacharyya, R., Hu, Q., Kumar, S., Nayak, S. S.,, 2018, *"A Magnetohydrodynamic Simulation of Magnetic Null-point Reconnections in NOAA AR 12192, Initiated with an Extrapolated Non-force-free Field"*, ApJ, v. 860, 96, pp. 16.
44. Zhang, J., Blanco-Cano, X., Nitta, N., Srivastava, N., Mandrini, C. H.,, 2018, *"Earth-affecting Solar Transients : Editorial"*, Sol. Phys., v. 293, 80, pp. 6.

Planetary Sciences

45. A. Niyogi, J. K. Pati, M. K. Panigrahi, D. Panda, M. Chakarvorty and G. Parthasarathy, 2018, *"Raman, Infrared and Chemical Characterization of Fly Ash-Generated spherules to better Constrain their Material Applications"*, Journal of Applied Spectroscopy, 85, No. 5, p. 856-863.

46. Haider, S. A., Y.S. Siddhi, J. Masoom and S. Bougher, 2019, *"Effect of dust storm and GCR impact on the production rate of O3+ in MY28 and MY29: Modeling and SPICAM observation"*, JGR, v. 124, p. 2271-2282.

47. Haider, S.A., J. P. Pabari, J. Masoom, and Y. S. Siddhi, 2019, *"Schumann resonance frequency and conductivity in the nighttime ionosphere of Mars: A source for lightning"*, Adv. Space Res., v. 63, p. 2260-2266.

48. H. Kita, H. Misawa, A. Bhardwaj, F. Tsuchiya, G. Murakami, C. Tao, T. Kimura, K. Yoshioka, A. Yamazaki, Y. Kasaba, I. Yoshikawa, M. Fujimoto, 2019, *"Short-term variation 1 in the dawn-dusk asymmetry of the Jovian radiation belt obtained from GMRT and Hisaki EXCEED observations"*, Astrophysical Journal Letters, v. 872, L24 (5pp).

49. Kinsuk Acharyya and E. Herbst, 2018, *"Hot Cores in Magellanic Clouds"*, ApJ, v. 859, p. 859:51 (20pp).

50. M B Dhanya, Anil Bhardwaj, Abhinaw Alok, Yoshifumi Futaana, Stas Barabash, Martin Wieser, Mats Holmström, and Peter Wurz, 2018, *"First observation of transport of solar wind protons scattered from magnetic anomalies into the near lunar wake: Observations by SARA/Chandrayaan-1"*, Geophysical Research Letters, v. 45, p. 8826-8833.

51. Murty, S.V.S., Ghosh, S. and Ray, D., 2018, *"Noble gases and nitrogen in Raghunathpura (IIAB) and Nyaung (IIIAB) iron meteorites"*, Meteoritics and Planetary Science, v. 54, p. 90-103.

52. Pabari, J. P., S.A. Haider, B.M. Pandya, R.K. Singh, A. Kumar, D. K. Patel, and A., 2018, *"Orbital altitude dust at Mars, its implication and a prototype for its detection"*, Planet and Space Sci, v. 161, p. 68-75.

53. R. K. Mishra and K. K. Marhas, 2018, *"Meteoritic evidences of a late superflare as a source of 7Be in the early Solar System"*, Nature Astronomy, v. 3, p. 498-505.

54. R. R. Mahajan, A. Basu Sarbadhikari, M.S. Sisodia, 2019, *"Noble gas, nitrogen composition and cosmic ray exposure history of two eucrites Vissannapeta, Piplia Kalan and one howardite Lohawat"*, Planetary and Space Science, v. 165, p. 23-30.

55. Goyal, S. K., Kumar, P., Janardhan, P., Vadawale, S. V., Sarkar, A., Shanmugam, M., Subramanian, K. P., Bapat, B., Chakrabarty, D., Adhyaru, P. R., Patel, A. R., Banerjee, S. B., Shah, M. S., Tiwari, N. K., Adalja, H. L., Ladiya, T., Dadhania, M. B., Sarda, A., Hait, A. K., Chauhan, M., and Bhavsar, R. R., 2018, *"Aditya Solarwind Particle EXperiment (ASPEX) onboard the Aditya-L1 mission"*, Planetary and Space Science, v. 163, p. 42-55.

56. S. K. Mishra and Shikha Misra, 2019, *"Transport properties of complex plasma having a dust size distribution"*, Physics of Plasmas, v. 26, p. 023702.

57. S. K. Goyal, A. P. Naik, N. P. S. Mithun, S. V. Vadawale, N. Nagrani, S. Madhvi, N. K. Tiwari, T. Ladiya, A. R. Patel, H. K. Adalja, T. Chattopadhyay, M. Shanmugam, A. Auknoor, P. Sharma, V. R. Patel, 2019, *"Development of position sensitive detector module using scintillator and Si photomultiplier for hard x-ray imaging and spectroscopy"*, Journal of Astronomical Telescopes, Instruments, and Systems, v. 5(1), p. 016001.

58. Singh, T., Kshirsagar, P., Das, A., Yadav, K., Mallik, S., Mascarenhas-Pereira, M.B.L., Thomas, T., Mamatha, S.S., Lokabharathi, P.A., Khadge, N., Nagender Nath, B., Dhakephalker, P., Iyer, S.D., Ray, D., Valsangkar, A.B., Garg, A., Babu, C., Waghole, R., Waghmare S., Rajwade, J., Paknikar, K., 2018, *"Implications of microbial thiosulfate utilization in red clay sediments of the Central Indian Basin - The Martian Analogy"*, Geochemistry, Geophysics, Geosystems, v. 20, p. 708-729.

59. Smitha V. Thampi, C. Krishnaprasad, Anil Bhardwaj, Yuni Lee, R. K. Choudhary, and T. K. Pant, 2018, *"MAVEN-NGIMS observations of the response of Martian ionosphere to the interplanetary coronal mass ejections of March 2015"*, Journal of Geophysical Research, v. 123, p. 6917–6929.

60. Venkateswara Rao N., V. Leelavathi, P. Mohanamanasa, S.A. Haider and S.V.B. Rao, 2019, *"Enhanced ionization in magnetic anomaly regions of the Martian lower ionosphere associated with dust storms"*, JGR, V. 124, P. 3007-3020.

61. Vrinda Mukundan and Anil Bhardwaj, 2018, *"A Model for Negative Ion Chemistry in Titan's Ionosphere"*, Astrophysical Journal, V. 856, P. 168 (11pp).

Space and Atmospheric Sciences

62. Singh, R. P., and Pallamraju, D., 2018, *"Results on mesospheric temperature inversions observed in OH and O2 rotational temperatures from Mount Abu (24.6° N, 72.8° E), India"*, J. Geophys. Res., v. 123, p. 8823 - 8834.

63. Karan, D. K., and Pallamraju, D., 2018, *"Effect of geomagnetic storms on the daytime low-latitude thermospheric wave dynamics"*, J. Atmos. Sol.-Terr. Phys., v. 170, p. 35-47.

64. Chandra, H., 2019, *"Personal News"*, Curr. Sci., v. 116, p.5.

65. Ghosh, P., Ramkumar, T. K., and Sharma, S., 2018, *"Anomalous Behavior of Vertical Wavenumber Spectra Over a Tropical Station of India"*, Geophys. Res. Lett., v. 45, p. 12,553-12,559.

66. Choithani, V., Jain, R., Awasthi, A. K., Singh, G., Chaudhari, S., and Sharma, S. K., 2018, *"Study of temporal and spectral characteristics of the X-ray emission from solar flares"*, Res. Astro. Astrophys., v. 18 (No.10), p. 121 (16pp).

67. Ghosh, P., Ramkumar, T. K., Patra, A. K., Sharma, S., and Pavan Chaitanya, P., 2019, *"Vertical Coupling From the Lower Atmosphere to the Ionosphere: Observations Inferred From Indian MST Radar, GPS Radiosonde, Ionosonde, Magnetometer, OLR (NOAA), and SABER/TIMED Instrument Over Gadanki"*, J. Geophys. Res. Space Phys., v. 124, p. 489-503.

68. Kumar, K. N., Phanikumar, D. V., Sharma, S., Basha, G., Naja, M., Ouarda, T. B. M. J., Ratnam, M. V., and Kumar, K. K., 2019, *"Influence of tropical-extratropical interactions on the dynamics of extreme rainfall event: A case study from Indian region"*, Dynamics of Atmospheres and Oceans, v. 85, p. 28-40.

69. Phanikumar, D. V., Maurya, A. K., Kumar, K. N., Venkatesham, K., Singh, R., Sharma, S., and Naja, M., 2018, *"Anomalous variations of VLF sub-ionospheric signal and Mesospheric Ozone prior to 2015 Gorkha Nepal Earthquake"*, Scientific Reports, v. 8, p. 1-9.

70. Vaishnav, R., Sharma, S., Shukla, K. K., Kumar, P., and Lal, S., 2019, *"A comprehensive statistical study of cloud base height using ceilometer over western India"*, Advances in Space Res., v. 63, p. 1708-1718.

71. Bhardwaj, P., Naja, M., Rupakheti, M., Panday, A. K., Kumar, R., Mahata, K., Lal, S., Chandola, H. C., and Lawrence, M. G., 2018, *"Variations in surface ozone and carbon monoxide in the Kathmandu Valley and surrounding broader regions during SusKat-ABC field campaign: Role of local and regional sources"*, Atmos. Chem. Phys., v. 18, p. 11949-11971.

72. Ramachandran, S., Rajesh, T. A., and Kedia, S., 2019, *"Influence of relative humidity, mixed-layer height, and mesoscale vertical-velocity variations on column and surface aerosol characteristics over an urban region"*, Boundary Layer Meteorol., v. 170, p. 161-181.

73. Sarangi, B., Ramachandran, S., Rajesh, T. A., and Dhaker, V. K., 2019, *"Black carbon linked aerosol hygroscopic growth: Size and mixing state are crucial"*, Atmos. Environ., v. 200, p. 110-118.

74. Rajesh, T. A., and Ramachandran, S., 2018, *"Black carbon aerosols over urban and high altitude remote regions: Characteristics and Radiative implications"*, Atmos. Environ., v. 194, p. 110-122.

75. Bhaskar, B. V., Rajesh Kumar, R. M., Muthuchelian, K., and Ramachandran, S.,, 2018, *"Spatial, temporal and source study of black carbon in the atmospheric aerosols over different altitude regions in Southern India"*, J. Atmos. Solar-Terr. Phys., v. 179, p. 416-424.

76. Sharma, A., Ojha, N., Pozzer, A., Beig, G., and Gunthe, S. S., 2019, *"Revisiting the crop yield loss in India attributable to ozone"*, Atmos. Environ., v. 1, p.100008.

77. Shukla, K. K., Phanikumar, D. V., Newsom, R. K., Ojha, N., Niranjan Kumar, K., Singh, N., Sharma, S., Kotamarthi, V. R., and Kumar, K. K., 2019, *"Investigations of vertical wind variations at a mountain top in the Himalaya using Doppler Lidar observations and model simulations"*, J. Atmos. Sol. Terr. Phys., v. 183, p.76-85.

78. Yadav, R., Sahu, L. K., Beig, G., Tripathi, N., Maji, S., and Jaaffrey, S. N. A., 2019, *"The role of local meteorology on ambient particulate and gaseous species at an urban site of western India"*, Urban Climate, v. 28, p.1-10.

79. Sinha, P. R., Nagendra, N., Manchanda, R. K., Ojha, D. K., Suneel Kumar, B., Koli, S. K., Trivedi, D. B., Lodha, R. K., Sahu, L. K., and Sreenivasan, S., 2019, *"Development of balloon-borne Impactor payload for profiling free tropospheric aerosol"*, Aerosol Sci. and Tech., v. 53, p. 231-243.

80. Sahu, L. K., Tripathi, N., Sheel, V., Kajino, M., Deushi, M., Yadav, R., and Nedelec, P., 2018, *"Impact of the tropical cyclone "Nilam" on the vertical distribution of carbon monoxide over Chennai on the Indian peninsula"*, Quarterly J. Royal Meteorol. Soc., v. 144, p. 1091-1105.

81. Singh, V., Khaiwal, R., Sahu, L., and Sokhi, R., 2018, *"Trends of atmospheric black carbon concentration over the United Kingdom"*, Atmos. Environ., v. 178, p. 148-157.

82. Vernier, J-P., Fairlie, T. D., Deshler, T., Venkat Ratnam, M., Gadhavi, H., Kumar, S. Natarajan, M. Pandit, A. K., Akhil Raj, S. T., Kumar, A.H., Jayaraman, A., Singh, A. K., Rastogi, N., Sinha, P. R., Kumar, S., Tiwari, S., Wegner, T., Baker, N., Vignelles, D., Stenchikov, G., Shevchenko, I., Smith, J., Bedka, K., Kesarkar, A., Singh, V., Bhate, J., Ravikiran, V., Rao, M. D., Ravindrababu, S., Patel, A., Vernier, H., Wienhold, F. G., Liu, H., Knepp, T., Thomason, L., Crawford, J., Ziemba, L., Moore, J., Crumeyrolle, S., Williamson, M., Berthet, G., Jégou, F., and Renard, J. B., 2018, *"BATAL: The Balloon measurement campaigns of the Asian Tropopause Aerosol Layer"*, Bull. Amer. Meteorol. Soc., v. 99, p. 955-973.

83. Mani, S., Chakrabarty, D., Ramkumar, T., Guharay, A., Taori, A., and Parihar, N., 2019, *"Evidence for deep ingression of the mid-latitude MSTID into as low as 3.5° magnetic latitude"*, J. Geophys. Res. Space Phys., v. 124, p. 749-764.

84. Pandey, K., Chakrabarty, D., and Sekar, R., 2018, *"Critical evaluation of the impact of disturbance dynamo on equatorial ionosphere during daytime"*, J. Geophys. Res. Space Phys., v. 123, p. 9762-9774.

85. Bagiya, M. S., Thampi, S. V., Hui, D., Sunil, A. S., Chakrabarty, D., and Choudhary, R. K., 2018, *"Signatures of the solar transient disturbances over the low latitude ionosphere during 6 to 8 September 2017"*, J. Geophys. Res. Space Phys., v. 123, p. 7598-7608.

86. Joshi, B., Ibrahim, M. S., Shanmugaraju, A., and Chakrabarty, D., 2018, *"A major geoeffective CME from NOAA 12371: Initiation, CME-CME interactions, and interplanetary consequences"*, Sol. Phys., v. 293:107, p. 20.

87. Rout, D., Chakrabarty, D., Sarkhel, S., Sekar, R., Fejer, B. G., Reeves, G. D., Aponte, N., Sulzer, M., Mathews, J. D., Kerr, R. B., and Noto, J., 2018, *"The ionospheric impact of an ICME driven sheath region over Indian and American sectors in the absence of a typical geomagnetic storm"*, J. Geophys. Res. Space Phys., v. 123, p. 4298-4308.

88. Guharay A., and Batista, P. P., 2019, *"On the variability of tides during a major stratospheric sudden warming in September 2002 at Southern hemispheric extra-tropical latitude"*, Adv. Space Res., v. 63, p. 2337-2344.

89. Guharay, A., Batista, P. P., Buriti, R. A., and Schuch, N. J., 2018, *"On the variability of the quarter-diurnal tide in the MLT over Brazilian low-latitude stations"*, Earth, Planets and Space., v. 70, p. 140.

Geosciences

90. Anand, S. S., Rengarajan, R., and Sarma, V. V. S. S., 2018, *"^{234}Th based carbon export flux along the Indian GEOTRACES GI02 section in the Arabian Sea and the Indian Ocean"*, Global Biogeochem Cy., v. 32, p. 417-436.

91. Anand, S. S., Rengarajan, R., Sarma, V. V. S. S., Sudheer, A. K., Bhushan, R., and Singh, S. K., 2017, *"Spatial variability of upper ocean POC export in the Bay of Bengal and the Indian ocean determined using particle-reactive ^{234}Th."*, J Geophys Res-Oceans., v. 122, p. 3753–3770.

92. Anand, S.S., Rengarajan, R., Shenoy, D., Gauns, M., and Naqvi, S. W. A., 2018, *"POC export fluxes in the Arabian Sea and the Bay of Bengal: A simultaneous $^{234}Th/^{238}U$ and $^{210}Po/^{210}Pb$ study"*, Mar. Chem., v. 198, p. 70–87.

93. Balaji, D., Bhushan, R., and Chamyal, L. S., 2018, *"Variations of the Somali upwelling since 18.5 ka BP and its relationship with southwest monsoon rainfall"*, Climate of the Past, v. 14, p. 1331-1343.

94. Band, S., Yadava, M. G., Lone, M. A., Shen, C. C., Sree, K., and Ramesh, R., 2018, *"High-resolution mid-Holocene Indian Summer Monsoon recorded in a stalagmite from the Kotumsar Cave, Central India"*, Quat. Int., v. 479, p. 19-24.

95. Banerjee, Y., Ghosh, P., Bhushan, R. and Rahul, P., 2018, *"Strong sea forcing and warmer winter during solar minima ∼2765 yr BP recorded in the growth bands of Crassostrea sp. from the confluence of river Ganges, Eastern India"*, Quat. Int., v. 479, p. 48-57.

96. Bhushan, R., Bikkina, S., Chatterjee, J., Singh, S. P., Goswami,V., Thomas, L. C., and Sudheer, A.K., 2018, *"Evidence for enhanced chlorophyll-a levels in the Bay of Bengal during early north-east monsoon"*, J. Oceanogr. Mar. Sci., v. 9, p. 15-23.

97. Bhushan, R., Sati, S. P., Rana, N., Shukla, A. D., Majumdar, A. S., and Juyal, N., 2018, *"High-resolution millennial and centennial scale Holocene monsoon variability in the Higher Central Himalayas"*, Palaeogeogr. Palaeoclimatol. Palaeoecol., v. 489, p. 95-104.

98. Bhushan, R., Yadava, M, G., Shah, M. S., and Raj, H., 2018, *"Performance of 1 MV AMS Facility (AURIS) at PRL, Ahmedabad. Nuclear Instruments of Methods in Physics Research: Section B – Beam Interactions with Materials and Atoms"*, Nucl. Instr. Meth. Phys. Res., v. 439, p. 76-79.

99. Bhushan, R., Yadava, M. G., Shah, M. S., Banerji, U. S., Raj, H., Shah, C., and Dabhi, A. J., 2019, *"First results from PRL Accelerator Mass Spectrometer"*, Curr. Sci., v. 116, p. 361-363..

100. Chandana, K. R., Upasana, B.and Bhushan, R., 2018, *"Review of Indian Summer Monsoon (ISM) Reconstruction since LGM from the Northern Indian Ocean"*, Earth Science India, v. 11, p. 71-84.

101. Chinni, V., Singh, S. K., Bhushan, R., Rengarajan, R., and Sarma, V. V. V. S., 2018, *"Spatial variability in dissolved iron concentrations in the marginal and open waters of the Indian Ocean"*, Mar Chem., v. 208, p. 11-28.

102. Dutta, M. K., Kumar, S., Mukherjee, R., Sanyal, P., and Mukhopadhyay, S. K., 2018, *"The post-monsoon carbon biogeochemistry of the Hooghly–Sundarbans estuarine system under different levels of anthropogenic impacts"*, Biogeosciences, v. 16, p. 289-307.

103. George, B. G., Ray, J. S., and Kumar, S., 2018, *"Geochemistry of carbonate formations of the Chattisgarh Supergroup, central India: implications for Mesoproterozoic global events"*, Can. J. Earth Sci., v. 56, p. 335-346.

104. George, B. G., Ray, J. S., Shukla, A. D., Awasthi, N., Chatterjee, A., and Laskar, A. H., 2018, *"Stratigraphy and geochemistry of the Balwan Limestone, Vindhyan Supergroup, India: Evidence for Bitter Spring $\delta\ ^{13}C$ anomaly"*, Precambrian Res., v. 313, p. 18-30.

105. Jeelani, G., Deshpande, R. D., Galkowski, M., and Rozanski, K., 2018, *"Isotopic composition of daily precipitation along the southern foothills of the Himalayasimpact of marine and continental sources of atmospheric moisture"*, Atmos. Chem. Phys., v. 18, p. 8789-8805.

106. Jeelani, G., Deshpande, R. D., Shah, R. A., and Hassan, W., 2017, *"Influence of southwest monsoons in the Kashmir Valley, western Himalayas"*, Isot Environ Healt Studies, v. 53, p. 400-412.

107. Kaushal, N., Breitenbach, S. F. M., Lechleitner, F. A., Sinha, A., Tewari, V. C., Ahmad, S. M., Berkelhammer, M., Band, S., Yadava, M., Ramesh, R., and Henderson, G.M., 2018, *"The Indian Summer Monsoon from a Speleothem $\delta^{18}O$ Perspective-A Review"*, Quaternary Res., v. 1, pp. 29.

108. Kumar, P. K., Singh, A., and Ramesh, R., 2018, *"Controls on $\delta\ ^{18}O$, δD and $\delta\ ^{18}O$ – Salinity relationship in the northern Indian Ocean"*, Mar. Chem., v. 207, p. 55-62.

109. Kumar, S., Bhavya, P. S., Ramesh, R., Gupta, G. V. M., Chiriboga, F., Singh, A., Karunasagar, I., Rai, A., Rehnstam-Holm, Edler, L., and Godhe, A., 2018, *"Nitrogen uptake potential under different temperature-salinity conditions: Implications for nitrogen cycling under climate change scenarios"*, Mar. Envi. Res., v. 141, p. 196-204.

110. Mehrotra, N., Shah, S. K., Basavaiah, N., Laskar, A. H., and Yadava, M. G., 2019, *"Resonance of the '4.2ka event' and terminations of global civilizations during the Holocene, in the palaeoclimate records around PT Tso Lake, Eastern Himalaya"*, Quatern. Int., v. 507, p. 206-216.

111. Park, Ji-Hyung, Nayna, O.K., Begum, M.S., Chea, E., Hartmann, J., Keil, R.G., Kumar, S., Lu, X., Ran, L., Richey, J. E., Sarma, V. V. S. S., Tareq, S., Xuan, D. T., and Yu, R., 2018, *"Anthropogenic perturbations to carbon fluxes in Asian river systems-Concepts, emerging trends, and research challenges"*, Biogeosciences, v. 15, p. 3049-3069.

112. Patel, A., and Rastogi, N., 2018, *"Seasonal variability in chemical composition and oxidative potential of ambient aerosol over a high altitude site in western India"*, Sci. Total Environ., v. 644, p. 1268-1276.

113. Rastogi, N., Singh, A., and Satish, R. V., 2019, *"Characteristics of submicron particles coming from a big firecrackers burning event: Implications to atmospheric pollution"*, Atmos. Pollut. Res., v. 10, p. 629-634.

114. Sarkar, S., Kumar, T. N., Ray, D., Bhattacharya, S., Shukla, A. D., Moitra, H., Dagar, A., Chauhan, P., Sen, K., Das, S., 2018, *"Mineralogy and spectroscopy (VIS near infrared and micro-Raman) of chromite from Nidar ophiolite complex, SE Ladakh, India: Implications for future planetary exploration"*, Planet. Space Sci., v. 165, pp. 1-9.

115. Satish, R. V., and Rastogi, N., 2019, *"On the use of brown carbon spectra as a tool to understand their broader composition and characteristics: A case study from crop-residue burning samples"*, ACS Omega, v. 4, p. 1847-1853.

116. Shah, C., Sudheer, A. K., and Bhushan, R.,, 2018, *"Distribution of dissolved organic carbon in the Bay of Bengal: Influence of sediment discharge, fresh water flux, and productivity"*, Mar. Chem., v. 4, p. 91-101.

117. Sharma, S., and Shukla, A. D., 2018, *"Factors governing the pattern of glacier advances since the Last Glacial Maxima in the transitional climate zone of the Southern Zanskar Ranges, NW Himalaya"*, Quaternary Sci. Rev., v. 01, p. 223-240.

118. Shukla, A. D., George, B. G., and Ray, J. S.,, 2019, *"Evolution of the Proterozoic Vindhyan Basin, Rajasthan, India: insights from geochemical provenance of siliciclastic sediments"*, Int. Geol. Rev., v., p..

119. Sinha, N., Gandhi, N., Chakraborty, S., Krishnan, R., Yadava, M. G., and Ramesh, R., 2018, *"Abrupt climate change at ∼2800 Yr BP evidenced by high-resolution oxygen isotopic record of a Stalagmite from peninsular India"*, The Holocene, v. 28, p. 1720-1730.

120. Myriokefalitakis, S., Ito, Akinori, Kanakidou, Maria, Nenes, Athanasios, Krol, Maarten C., Mahowald, Natalie M., Scanza, Rachel A., Hamilton, Douglas S., Johnson, Matthew S., Meskhidze, Nicholas, Kok, Jasper F., Guieu, Cecile, Baker, Alex R., Jickells, Timothy D., Sarin, M. M., Bikkina, S, Shelley, Rachel, Bowie, Andrew, Perron, Morgane M. G. and Duce, Robert A., 2018, *"Reviews and syntheses: the GESAMP atmospheric iron deposition model intercomparison study"*, Biogeosciences, v. 15, pp. 6659-6684.

121. Vernier, J. P., Fairlie, T. D., Deshler, T., Venkat Ratnam, M., Gadhavi, H., Kumar, S., Natarajan, M., Pandit, A. K., Akhil Raj, S.T., Kumar, A. H., Jayaraman, A., Singh, A. K., Rastogi, N., Sinha, P. R., Kumar, S., Tiwari, S., Wegner, T., Baker, N., Vignelles, D., Stenchikov, G., Shevchenko, I., Smith, J., Bedka, K., Kesarkar, A., Singh, V., Bhate, J., Ravikiran, V., Rao, M. D., Ravindrababu, S., Patel, A., Vernier, H., Wienhold, F. G., Liu, H., Knepp, T., Thomason, L., Crawford, J., Ziemba, L., and Moore, J., Crume., 2018, *"BATAL: The Balloon measurement campaigns of the Asian Tropopause Aerosol Layer"*, B. AM. Meterol Soc., v. 99, p. 955-973.

Theoretical Physics

122. Kindra, B., and Mahajan, N.,, 2018, *"Predictions of angular observables for* $\bar{\mathrm{B}}_s \to \mathrm{K}^* \ell\ell$ *and* $\bar{\mathrm{B}} \to \rho\ell\ell$ *in the standard model"*, Phys. Rev. D, v. 98, p. 094012-1 – 094012-17.

123. Ray, A., Sahoo, S., and Mohanta,R.,, 2019, *"Probing new physics in semileptonic* Λ_b *decays"*, Phys. Rev. D, v.99, p. 015015-1 – 015015-22.

124. Bai, R., Bandyopadhyay, S., Pal, S., Suthar, K., and Angom, D.,, 2018, *"Bosonic quantum Hall states in single-layer two-dimensional optical lattices"*, Phys. Rev. A, v.98, p 023606 (1-11).

125. Bai, R., Roy, A., Angom, D., and Muruganandam, P.,, 2018, *"Condensates in double-well potential with synthetic gauge potentials and vortex seeding"*, Physics Letters A, v.382, p.2376-2381.

126. Navinder Singh., and L. Rani.,, 2019, *"Novel Effect of Electron Spin Resonance on Electrical Resistivity"*, Journal of Magnetism and Magnetic materials, v.474, p.501-504.

127. Kumar, A., Sharma, R., and Navinder Singh.,, 2019, *"Quantum oscillations in Stoner susceptibility: A theory"*, Magnetism and Magnetic materials, v.487, p.165302-xx.

128. Atrey, A., Bhatt, J. R., and Mishra, A.,, 2018, *"Viscous self interacting dark matter and cosmic acceleration"*, Journal of Cosmology and Astroparticle Physics, v.2018, p.1-13.

129. Azam, M., Bhatt, J. R., and Sami, M.,, 2018, *"Many-body aspects of gravity in compact stars"*, Physica Scripta, v.93, p.1-xx.

130. Singh, B., Thakur, L., and Mishra H.,, 2018, *"Heavy quark complex potential in a strongly magnetized hot QGP medium"*, Physical Review D, V. 97, p.1-17.

131. Chakraborty, K., Deepthi, K, N., Goswami, S., Joshipura, A, S., Nath, Nath.,, 2018, *"Exploring partial* μ-τ *reflection symmetry at DUNE and Hyper-Kamiokande"*, Phys. Rev. D 98, v.98, p.1-11.

132. Deepthi, K, N., Goswami, S., Nath, N.,, 2018, *"Challenges posed by non-standard neutrino interactions in the determination of* δ_{CP} *at DUNE"*, Nuclear Physics B, v.936, p.91-105.

133. Srivastava, K., Chaturvedi, O. S. K., and Thakur, L.,, 2018, *"Heavy quarkonia in a potential model: binding energy, decay width, and survival probability"*, Eur. Phys. J. C 78, v.79, p.77-80.

134. Jana, S., Chakravarty, G, K., and Mohanty, S.,, 2018, *"Constraints on Born-Infeld gravity from the speed of gravitational waves after GW170817 and GRB 170817A"*, Phys.Rev. D97, v.91, p.1-5.

135. Lambiase, G., Mohanty, S., and Stabile, An.,, 2018, *"PeV IceCube signals and Dark Matter relic abundance in modified cosmologies"*, Eur.Phys.J C78 (2018) no.4, 350, v.79, p.1-11.

136. Mohanty, S., Anand, S., Chaubal, P., Mazumdar, A., and Parashari, P.,, 2018, *"*$\sigma 8$ *Discrepancy and its solutions"*, Journal of Astrophysics and Astronomy, v.39, p.1-14.

137. Chauhan, B., and Mohanty, S.,, 2018, *"Signature of light sterile neutrinos at IceCube"*, Phys.Rev. D98 (2018) no.8, 083021, v.97, p.1-14.

138. Mohanty, S., and Sadhukhan, S.,, 2019, *"Explanation of IceCube spectrum with* $\nu \to 3\nu$ *neutrino splitting in a* ν*2HDM model"*, JHEP 1810 (2018) 111, v.111, p.1-19.

139. Anand, S., Chaubal, P., Mazumdar, A., Mohanty, S., and Parashari, P.,, 2018, *"Bounds on Neutrino Mass in Viscous Cosmology"*, JCAP 1805 (2018) no.05, 031, v.2018, p.1-19.

140. Chakrabortty, J., Maji, R., Patra, S, K., Srivastava, T., and Mohanty, S.,, 2018, *"Roadmap of left-right models based on GUTs"*, Phys.Rev. D97, v.97, p.1-80.

141. Chakraborty, K., Deepthi, K, N., Goswami, S.,, 2018, *"Spotlighting the sensitivities of Hyper-Kamiokande, DUNE and ESS*ν*SB"*, Nuclear Physics B, v.937, p.303–332.

142. Chakraborty, K., Deepthi, K, n., Goswami, S., Joshipura, A, S., and Nath, N.,, 2018, *"Exploring partial* μ*-T reflection symmetry at DUNE and Hyper-Kamiokande"*, Phys. Rev. D 98, V. 98, Iss. 7, p.1-11.

143. Dasgupta, A., Jain, R, K., and Rangarajan, R.,, 2018, *"Effective chemical potential in spontaneous baryogenesis"*, Phys.Rev. D98, V.98, p.1-16.

144. Kindra, B., and Mahajan, N.,, 2018, *"Predictions of angular observables for* $\bar{\mathrm{B}}_s \to \mathrm{K}*ll$ *and* $\bar{\mathrm{B}} \to \rho ll$ *in the standard model"*, Phys.Rev. D98 (2018) no.9, v.98, p.1-16.

145. Joshipura, A, S., and Patel, K.,, 2018, *"Pseudo-Dirac neutrinos from flavour dependent CP symmetry"*, JHEP 1807 (2018) 137, V.10, p.1-17.

146. Chauhan, B., Kindra, B., and Narang, A.,, 2018, *"Discrepancies events using leptoquarks"*, Phys. Rev. D 97, v.97, p.1-17.

147. Kumar, A., Jamal, M, Y., Chandra, V., and Bhatt, J, R.,, 2018, *"Collective excitations of a hot anisotropic QCD medium with the Bhatnagar-Gross-Krook collisional kernel within an effective description"*, Phys. Rev. D 97, v.97, p.1-16.

148. Abhishek, A., and Mishra, H.,, 2019, *""Chiral symmetry breaking, color superconductivity, and the equation of state for magnetized strange quark matter""*, Phys. Rev. D 99, 054016, V.99, p. 1-27.

149. Ghosh, S., Serna, F, E., Abhishek, A., Krein, G., and Mishra, H.,, 2019, *""Transport responses from rate of decay and scattering processes in the Nambu–Jona-Lasinio model""*, Phys. Rev. D 99, 014004, v.99, p. 1-9.

150. Bhatt, J, R., Das, A., and Mishra, H.,, 2019, *""Thermoelectric effect and Seebeck coefficient for hot and dense hadronic matter""*, Phys. Rev. D 99, 014015, v.99, p.1-11.

151. Kadam, G, P., Pawar, S., and Mishra, H.,, 2018, *""Estimating transport coefficients of interacting pion gas with K-matrix cross sections""*, Journal of Physics G: Nuclear and Particle Physics, v.96, p.1-21.

152. Singha, p., Abhishek, A., Kadam, G, P., Ghosh, S., and Mishra, H.,, 2018, *""Calculations of shear, bulk viscosities and electrical conductivity in the Polyakov- quark–meson model""*, Journal of Physics G: Nuclear and Particle Physics, v.46, p.1-21.

153. Kadam, G, P., Mishra, H., and Thakur, L.,, 2018, *""Electrical and thermal conductivities of hot and dense hadronic matter""*, Phys. Rev. D 98,114001, v.98, p.1-11.

154. Abhishek, A., Mishra, H., and Ghosh, S.,, 2018, *""Transport coefficients in the Polyakov quark meson coupling model: A relaxation time approximation""*, Phys. Rev. D 97, 014005, v.97, p.1-22.

155. Das, A., Malik, T., and Nayak, A, C.,, 2019, *""Confronting nuclear equation of state in the presence of dark matter using GW170817 observation in relativistic mean field theory approach""*, Phys. Rev. D 99, 043016, v.99, p. 1-17.

156. Das, A., Dave, S, S., Ganguly, O., and Srivastava, A, M.,, 2019, *""Pulsars as Weber gravitational wave detectors""*, Physics Letters B, v.791, p. 167-171.

Library & Information Services

157. Alam, M. N, Sen, B. K. and Shukla, A., 2018, *"Space Science Literature in India 1970-2014"*, ICSI Journal of Library and Information Science, v.1(1), p.33-46.

Atomic, Molecular and Optical Physics

158. A. Srinivasa Rao, N. Apurv Chaitanya and G. K. Samanta, 2019, *"High-power, high repetition-rate, ultrafast fibre laser based source of DUV radiation at 266 nm"*, OSA Continuum, v.2, p.99-106.

159. Raghwinder S. Grewal, Anirban Ghosh, and G. K. Samanta, 2018, *"Simultaneous generation of high-power, ultrafast 1D and 2D Airy beams and their frequency-doubling characteristics"*, Optics Letters, v. 43, p. 3957-3960.

160. Varun Sharma, S. Chaitanya Kumar, G. K. Samanta, and M. Ebrahim-Zadeh, 2018, *"Orbital angular momentum exchange in a picosecond optical parametric oscillator"*, Optics Letters, v. 43, p. 3606-3609.

161. A. Srinivasa Rao, and G. K. Samanta, 2018, *"On-axis intensity modulation-free, segmented, zero-order Bessel beams with tunable ranges"*, Optics Letters, v. 43, p. 3029-3032.

162. A. Aadhi, Varun Sharma, and G. K. Samanta, 2018, *"High-power, continuous-wave, tunable mid-IR, higher-order vortex beam optical parametric oscillator"*, Optics Letters, v. 43, p. 2312-2315.

163. Sabir Ul Alam, A. Srinivasa Rao, Anirban Ghosh, Pravin Vaity, and G. K. Samanta, 2018, *"Nonlinear frequency doubling characteristics of asymmetric vortices of tunable, broad orbital angular momentum spectrum"*, Applied Physics Letters, v. 112, p.171102.

164. Yu., Yan-mei and Sahoo, B. K., 2018, *"Selected highly charged ions as prospective candidates for optical clocks with quality factors larger than 10^{15}"*, Phys. Rev. A, v. 97, p. 041403(R) (1-5).

165. Sahoo, B. K. and Das, B. P., 2018, *"Relativistic Normal Coupled-Cluster Theory for Accurate Determination of Electric Dipole Moments of Atoms: First Application to the ^{199}Hg Atom"*, Phys. Rev. Letts, v. 120, p. 203001 (1-6).

166. Sakurai, A., Sahoo, B. K., and Das, B. P., 2018, *"Electric dipole polarizability of ^{129}Xe using the relativistic coupled-cluster and the normal coupled-cluster methods"*, Phys. Rev. A, v. 97, p. 062510.

167. Singh, S., Kaur, M., Arora, B., and Sahoo, B. K.,, 2018, *"Higher-component quadrupole polarizabilities: Estimations for the clock states of the alkaline-earth-metal ions"*, Phys. Rev. A, v. 98, p. 013406 (1-9).

168. Sahoo, B. K., and Yu, Yan-mei, 2018, *"Dipole polarizability calculation of the Cd atom: Inconsistency with experiment"*, Phys. Rev. A, v. 98, p. 012513 (1-9).

169. Kaur, M., Kaur, P., Sahoo, B. K., and Arora, B., 2018, *"Dynamics of resonant energy transfer in one-dimensional chain of Rydberg atoms"*, Eur. Phys. J. D, v. 72, p. 150 (1-8).

170. Garcia Ruiz, R. F., Vernon, A. R., Binnersley, C. L., Sahoo, B. K., Billowes, J., Cocolios, T. E.,Gins, W., de Groote, R. P., Flanagan, K. T., Koszorus, A., Lynch, K. M., Neyens, G., Ricketts, C., Wilkins, S. G., and Yang, X. F., 2018, *"Multi-photon ionization of accelerated laser-ablated ions: Exploring physics over a wide range of energy scales"*, Phys. Rev. X, v. 8, p. 041005 (1-18).

171. Yu., Yan-mei and Sahoo, B. K., 2019, *"Investigating ground-state fine-structure properties to explore suitability of boronlike S^{11+} Ru^{13+} ions as possible atomic clocks"*, Phys. Rev. A, v. 99, p. 022513 (1-12).

172. Hegde, V., Chauhan, N., Kumar, V., Viswanath, C. S. D., Mahato, K. K. and Kamath, S. D., 2019, *"Effects of high dose gamma irradiation on the optical properties of Eu^{3+} doped zinc sodium bismuth borate glasses for red LEDs"*, Journal of Luminescence, v. 207, p. 288-300.

173. Lokesha, H. S., Chauhan, N., Nagabhushana, K. R. and Singh, F., 2018, *"Dosimetric properties of ZrO2 and ZrO2:Sm^{3+} exposed to beta rays"*, Ceramics International, v. 44, p. 18871.

174. Hegde, V., Chauhan, N., Petwal, V. C., Pal Verma, V., Dwivedi, J., Mahato, K. K. and Kamath, S. D., 2019, *"Effects of 7.5 MeV electron beam irradiation on optical properties of Eu^{3+}-doped zinc sodium bismuth borate glasses"*, Nuclear Instruments and Methods in Physics Research Section B: Beam Interactions with Materials and Atoms, v. 446, p. 5-9.

175. Morthekai, P., Biswas, R. H. and Singhvi, A. K., 2019, *"Charge transport in band-tail states of irradiated alkali feldspar I: Super-Arrhenius kinetics"*, Physica B: Condensed Matter, v. 561, p. 103-110.

176. Hegde, V., Chauhan, N., Viswanath, C. S. D., Kumar, V., Mahato, K. K. and Kamath, S. D.,, 2019, *"Photoemission and thermoluminescence characteristics of Dy^{3+}-doped zinc sodium bismuth borate glasses"*, Solid State Sciences, v. 89, p. 130-138.

177. N. M. Fazil, V. S. Prasannaa, K. V. P. Latha, M. Abe, and B. P. Das, 2018, *"Electron correlation trends in the permanent electric dipole moments of alkaline-earth-metal mono hydrides,"*, Phys. Rev. A, v. 98, p. 032511.

178. A. Sunaga, V. S. Prasannaa, M. Abe, M. Hada, and B. P. Das, 2018, *"Enhancement factors of parity- and time-reversal-violating effects for monofluorides"*, Phys. Rev. A, v. 98, p. 042511.

179. A. Sunaga, V. S. Prasannaa, M. Abe, M. Hada, and B. P. Das, 2019, *"Ultracold mercury–alkali-metal molecules for electron-electric-dipole-moment searches"*, Phys. Rev. A, v. 99, p. 040501.

180. N. M. Fazil, V. S. Prasannaa, K. V. P. Latha, M. Abe, and B. P. Das, 2019, *"RaH as a potential candidate for electron electric-dipole-moment searches,"*, Phys. Rev. A, v. 99, p. 052502.

181. Kumari, S., Kumar, A., Kumar, V., Singh, R. P., 2019, *"Transition from Two-photon Absorption to Saturable Absorption in Gold Patterned Ruby Thin Film"*, Optik, v. 182, p. 186-193.

182. Kumar, A., Singh, R. P., Mohanty, T., Taneja, A., 2019, *"Tunable optical nonlinearity of Au-TiO2 nanocomposites"*, Photonics and Nanostructures - Fundamentals and Applications, v. 33, p. 1-9.

183. Srinivas, P., Chithrabhanu, P., Niji lLal, Singh, R. P., Srinivasan, B., 2018, *"Investigation of propagation dynamics of truncated vector vortex beams"*, Optics Letters, v. 43, p. 2579-2582.

184. R Thombre, E Shivakarthik, B Sivaraman, P A Vaishampayan, A Seuylemezian, J K Meka, S Vijayan, P PKulkarni, T Pataskar, B S Patil., 2019, *"Survival of extremotolerant bacteria from the Mukundpura meteorite impact crater"*, Astrobiology, v. 19, p. 6.

185. S Pavithraa, J –I Lo, B – M Cheng, B N Raja Selhar, N J Mason and B Sivaraman, 2019, *"Identification of a unique VUV photoabsorption band of carbonic aid for its identification in radiation and thermally processed water-carbondioxideices"*, Spectrochimica Acta: Part – A, v. 215, p. 130-132.

186. Aditi Krishna Dave, Marie-Agnes Courty, Kathryn E. Fitzsimmons, Ashok Kumar Singhvi, 2019, *"Revisiting the contemporaneity of a mighty river and the Harappans: Archaeological, stratigraphic and chronometric constraints"*, Quaternary Geochronology, v. 49, p. 230-235.

187. James T. Tellera, Roderick A. McGinn, Haresh M. Rajapara, Anil D. Shukla, Ashok K. Singhvi, 2018, *"Optically stimulated luminescence ages from the Lake Agassiz basin in Manitoba"*, Quaternary Research, v. 89, p. 478-493.

188. Robert James Wasson, Vikrant Jain, Ajay Katuri, Siddhartha Lahiri, Surya Parkash, Ashok kumar Singhvi, Navarun Varma, Priya Bansal and C. Joon Chuah, 2019, *"Riverine Flood Hazard: Part B. Disaster Risk Reduction in India"*, Proceedings Indian National Science Academy, v. 85, p. 1.

Publications

Publications in Proceedings of Conference/ Symposia/ Workshops

Astronomy and Astrophysics

1. Janardhan, P., Fujiki, K., Ingale, M., Bisoi, S. K., and Ananthakrishnan, S., 2018, *"Long term trends in solar photospheric fields and solar wind turbulence levels: Implications to the near-Earth space"*, Proc. of the IAU Symposium,, v. 340, p. 121-124.

2. Valtonen, M. J., Dey, L., Hudec, R., Zola, S., Gopakumar, A., Mikkola, S., Ciprini, S., Matsumoto, K., Sadakane, K., Kidger, M., Gazeas, K., Nilsson, K., Berdyugin, A., Piirola, V., Jermak, H., Baliyan, K. S., Reichart, D. E., Caton, D. B., Haque, S. and, 2018, *"High accuracy measurement of gravitational wave back-reaction in the OJ287 black hole binary"*, Proc. of IAU Symposium 338, v. 13, p. 29-36.

3. Venkataramani, K., and Ganesh, S., 2018, *"Results from two unusual comets C/2016 R2 (Pan-STARRS) and C/2015 V2 (Johnson)"*, European Planetary Science Congress 12, EPSC2018-1207.

4. Venkataramani, K., Ganesh, S., Joshi, U., 2018, *"The Compositional Behavior of the Jupiter Family Comets"*, 42nd COSPAR Scientific Assembly, B1.1-55-18.

5. Bisht, D., Ganesh, S., Baliyan, K. S., Yadav, R. S., Durgapal, A., 2018, *"Study of II Galactic quadrant of Milky Way Galaxy using open clusters"*, Bulletin de la Societe Royale des Sciences de Liege, v. 87 p. 229-233.

6. Ganesh, S., Venkataramani, K., Baliyan, K. S., Joshi, U. C., 2018, *"Solar system astronomy with the 3.6-m DOT and the 4-m ILMT"*, Bulletin de la Societe Royale des Sciences de Liege, v. 87, p. 125-131.

7. Joshi, U. C., Ganesh, S., Baliyan, K. S., 2018, *"Polarimetry - Scope on the 3.6-m Devasthal Optical Telescope"*, Bulletin de la Societe Royale des Sciences de Liege, v. 87, p. 117-120.

8. Naik, S.,, 2018, *"Optical/Infrared properties of Be stars in X-ray Binary systems"*, Bulletin de la Société Royale des Sciences de Liège, v. 87, p. 167-175.

9. Singh, V., Chand, H., Ishwara-Chandra, C.H., and Kharb, P.,, 2018, *"Kpc-scale radio-jets in narrow-line Seyfert 1 galaxies"*, Proceedings of Science, v. 328, p. 29.

10. Srivastava, M.K., Jangra, M., Dixit, V., Munjal, B.S., Arora, H., and Mavani, T., 2018, *"Design and development of Mt. Abu faint object spectrograph and camera-pathfinder (MFOSC-P) for PRL 1.2m Mt. Abu telescope, India"*, Proceedings of the SPIE, v. 107024I.

Solar Physics

11. Sarkar, R., Srivastava, N., Dhara, S. K.,, 2018, *"On the Dynamics of the Largest Active Region of the Solar Cycle 24"*, Space Weather of the Heliosphere: Processes and Forecasts, Proceedings of the IAU, IAU symopsium, v. 335, p. 32-35.

12. Srivastava, N., Mirtoshev, Z., Mishra, W.,, 2018, *"Geomagnetic Consequences of Interacting CMEs of June 13-14, 2012"*, Space Weather of the Heliosphere: Processes and Forecasts, Proceedings of the IAU, IAU symposium, v. 335, p. 65-68.

13. Singh, J., Priyal, M., Sindhuja, G., Ravindra, B.,, 2018, *"Variations in Ca-K line profiles and Ca-K line features as a function of latitude and solar cycle during the 20th century"*, Long-Term Datasets for the Understanding of Solar and Stellar Magnetic Cycles Proceedings of the IAU, IAU symposium, v. 340, p. 23-26.

14. Kumar, B.,, 2018, *"Solar-Cycle variation in the photospheric mean velocity flows: GONG observations"*, Long-Term Datasets for the Understanding of Solar and Stellar Magnetic Cycles Proceedings of the IAU, IAU symposium, v. 340, p. 59-60.

15. Prasad, A., Bhattacharyya, R., Hu, Q., Nayak, S. S., Kumar, S.,, 2018, *"Study of magnetic field topology of active region 12192 using an extrapolated non-force-free magnetic field"*, Long-Term Datasets for the Understanding of Solar and Stellar Magnetic Cycles Proceedings of the IAU, IAU symposium, v. 340, p. 81-82.

16. Dave, K., Mishra, W., Srivastava, N., Jadhav, R. M.,, 2018, *"Study of Interplanetary and Geomagnetic Response of Filament Associated CMEs"*, Long-Term Datasets for the Understanding of Solar and Stellar Magnetic Cycles, Proceedings of the IAU, IAU symposium, v. 340, p. 83-84.

17. Bhatt, M., Srivastava, N., Jadhav, R.,, 2018, *"Study of Stealth CMEs and associated ICMEs"*, Long-Term Datasets for the Understanding of Solar and Stellar Magnetic Cycles, Proceedings of the IAU, IAU symposium, v. 340, p. 89-90.

18. Mishra, W., Srivastava, N., Mirtoshev, Z., Wang, Y.,, 2018, *"Solar cycle variation of coronal mass ejections contribution to solar wind mass flux"*, Long-Term Datasets for the Understanding of Solar and Stellar Magnetic Cycles, Proceedings of the IAU, IAU symposium
    340, 175-176, v. 340, p. 175-176.

19. Nayak, S. S., Bhattacharyya, R., Prasad, A., Hu, Q.,, 2018, *"Magnetic field topology from non-force free extrapolation and magnetohydrodynamic simulation of its eventual dynamics"*, Long-Term Datasets for the Understanding of Solar and Stellar

Magnetic Cycles, Proceedings of the IAU, IAU symposium, v. 340, p. 183-184.

20. Sarkar, R., Srivastava, N.,, 2018, *"Geometric and magnetic properties of coronal flux ropes associated with CMEs leading to geomagnetic storms"*, Long-Term Datasets for the Understanding of Solar and Stellar Magnetic Cycles, Proceedings of the IAU, IAU symposium 340, 191-192, v. 340, p. 191-192.

Planetary Sciences

21. A. Basu Sarbadhikari, 2018, *"Implications for formations of alkali-rich rocks of the Moon"*, New Views of the Moon 2 - Asia. Aizu, Japan, Abstract # 6022.
22. A. Basu Sarbadhikari, J. Ghosh and S. Narendranath, 2018, *"Alkali-rich rocks at and near tycho crater of the Moon"*, 49th Lunar and Planetary Science Conference. Houston Texas, Abstract # 1980.
23. A. Garg, V. Goyal and K. K. Marhas, 2019, *"Sputtering of presolar grains via galactic cosmic rays in interstellar medium"*, 49th Lunar and Planetary Science Conference. Houston Texas, Abstract # 1980.
24. J. Ghosh, G. Arora and A. Basu Sarbadhikari, 2018, *"Lunar Magnetic Field Anomaly - Global Distribution and Possible Origin"*, 49th Lunar and Planetary Science Conference. Houston Texas, Abstract # 1972..
25. R. K. Mishra and K. K. Marhas, 2018, *"Evidence of fossil record of 7Be in a CAI: Implications for the early Solar system"*, Goldschmidt 2018, Boston., ..
26. R. K. Sinha, S. Vijayan, M. Bhatt, H Nandal, N. Kumari, N. Srivastava, I. Varatharajan, D. Ray, C. Wohler, A. Bhardwaj, 2019, *"Geological insights into Chandrayaan-2 landing site in the southern high latitudes of the Moon"*, 50th Lunar and Planetary Science Conference (LPSC) 18-22 March 2019 in the Woodlands, Texas., Abstract#1493.
27. S. Baliyan, D. Ray, 2019, *"Colour Cathodoluminiscence study of forsteritic olivine in Mukundpura (CM2) meteorite"*, 50th Lunar and Planetary Science Conference (LPSC) 18-22 March 2019 in the Woodlands, Texas., Abstract #1603.
28. S. Ghosh, M. Miyahara, K. Tiwari, D. Ray and E. Ohtani, 2018, *"Formation of Al-bearing Bridgmanite in a Katol meteorite"*, AGU Fall Meeting, Washington D.C., Dec 10-14, 2018., Abstract ID 431975.
29. S. Rajpriye, S. Baliyan, D. Ray, T.K. Goswami, 2019, *"Chondrule morphology, mineralogy, thermal metamorphism and shock excursion of Mahadevpur chondrite (H4/5)"*, 50th Lunar and Planetary Science Conference (LPSC) 18-22 March 2019 in the Woodlands, Texas., LPI Contrib. No. 2132 (#1371).

Space and Atmospheric Sciences

30. L. Chutia, N. Ojha, I. Girach, B. Pathak, 2018, *"Distribution of volatile organic compounds over Indian subcontinent during winter: WRF-Chem simulations versus observations"*, Proceedings of Indian Aerosol Science and Technology Association (IASTA), v. 252, p.191-195..
31. Patel P. N., Machibata T., Gautam R., and Gadhavi H., 2018, *"Impacts of dust-ice-cloud interactions on precipitation variability"*, Biennial conference of Indian Aerosol Science and Technology Association 2018, IIT Delhi, v.723, p.719..

Geosciences

32. Subha Anand, S., and Rengarajan, R.,, 2018, *"Simultaneous Determination of $^{234}Th/^{238}U$ and $^{210}Po/^{210}Pb$ Disequilibria in a Hydrothermal Vent Region along the Southwest Indian Ridge System"*, Goldschmidt Conference, Boston, 12-17 August, 2019., pp. 2206..

Theoretical Physics

33. Konar. P, Sharma. P, and Swain , A. K, 2018, *"CP Sensitive Observable Exploring Tau Lepton Pairs from Higgs at the LHC"*, v.203 p. 547-550.
34. Bhardwaj, A. , Konar, P ., and Swain A. K., 2018, *"Towards Efficient Reconstruction of Semi-invisible Events from Higgs at the LHC"*, v.203 pp. 547-550.
35. Konar, P., Mondal, T., and Swain, A.K, 2018, *"Exploring Compressed Top Squark Region with Kinematic Variables"*, v.203 p. 539-542.

Library & Information Services

36. Nishtha, A., 2018, *"Research Data Management in India: A Pilot Study"*, EPJ Web of Conferences Proceedings, v.186, 03002, pp.1-10.

Atomic, Molecular and Optical Physics

37. V. Sharma, S. C. Kumar, A. Aadhi, H. Ye, G. K. Samanta, and M. Ebrahim-Zadeh, 2018, *"Vector vortex beam generation from a doubly-resonant nanosecond optical parametric oscillator"*, Laser Science, JW4A. 50.
38. M. V. Jabir, A. Anwar, and G. K. Samanta, 2018, *"Enhancing the number of bi-photon orbital angular momentum modes using asymmetric vortex beam"*, Laser Science, JTu2A. 56.
39. A. S. Rao, and G. K. Samanta, 2018, *"High Peak Intensity and Tunable Range Bessel Beams Generation and Characterization"*, Laser Science, JTu2A. 16.
40. V. Sharma, G. K. Samanta, R. P. Singh, S. C. Kumar, and M. Ebrahim-Zadeh, 2018, *"Continuous-wave, singly-resonant optical parametric oscillator source of vortex beams tunable in the ultraviolet"*, Frontiers in Optics, JW3A. 41.
41. A. Aadhi, V. Sharma, and G. K. Samanta, 2018, *"Generation of high power, higher order, continuous-wave optical vortices tunable in the mid-IR wavelength ranges"*, CLEO: Science and Innovations, STh3F. 6.
42. V. Sharma, S. C. Kumar, G. K. Samanta, M. Ebrahim-Zadeh, 2018, *"Tunable vortex beam, singly-resonant ultrafast optical parametric oscillator"*, CLEO: QELS Fundamental Science, FTh3E. 5.
43. V. Sharma, S. C. Kumar, A. Aadhi, H. Ye, G. K. Samanta, and M. Ebrahim-Zadeh,, 2018, *"Generation of vector vortex beam from doubly-resonant nanosecond optical parametric oscillator"*, CLEO: QELS Fundamental Science, FTh3E. 8.

44. R. S. Grewal, A. Ghosh, and G. K. Samanta, 2018, *"Simultaneous generation of 1D and 2D Airy beams and their frequency doubling characteristics"*, CLEO: QELS Fundamental Science, JTu2A. 142.

45. Sahoo, B. K. and Das, B. P., 2018, *"The role of relativistic many-body theory in probing new physics beyond the standard model via the electric dipole moments of diamagnetic atom"*, J. Phys.: Conf. Series, v. 1041, p. 012014 (1-14).

46. Pachav, S., Lal, N., Viswanathan, N. K., Singh, R. P., Srinivasan, B., 2018, *"Investigation of polarization structure of vector vortex beams upon scattering"*, OSI - International Symposium on Optics (OSI-ISO 2018), 19 - 22 September 2018, IIT Kanpur., p. 252-253.

47. Kumar, V. and Singh, R. P., 2018, *"Polarization correlations in vector speckle field"*, PHOTONICS-2018, International Conference on Fiber Optics and Photonics, 12th – 15th December 2018, IIT Delhi., TP005.

48. Reddy, S. G. and Singh, R. P., 2018, *"Bessel-Gauss coherence functions and their realization using speckles"*, PHOTONICS-2018, International Conference on Fiber Optics and Photonics, 12th – 15th December 2018, IIT Delhi., TP008.

49. Lal, N., Biswas, A., Anwar, Ali, Banerji, A., Singh, R. P., 2018, *"Photon correlation properties of heralded twisted single photons"*, PHOTONICS-2018, International Conference on Fiber Optics and Photonics, 12th – 15th December 2018, IIT Delhi., TP083,.

Publications

Books Edited / Review Articles / Other Publications

Books Edited

1. S. Ramachandran, 2018, *"Atmospheric Aerosols: Characteristics and Radiative Effects"*, CRC Press, Taylor and Francis Group, USA,294 pages, ISBN:9781498750738 (Book)
2. Zhang, J., Blanco-Cano, X., Nitta, N., Srivastava, N., Mandrini, C.H.,2018, *"Earth-affecting Solar Transients"*, Springer NetherlandsISBN : 978-94-024-1569-8
3. A. Andreev, L. Zsolt, and S. K. Mishra2019, *"Relativistic Laser Plasma Atto-Physics. In: Progress in Photon Science"*, Springer Series in Chemical Physics, Vol. 119. Springer, Cham.
4. Grumpe, A., WÖhler, C., Rommel, D., Bhatt, M., Mall, U.2018, *"Elemental and topographic mapping of lava flow structures in Mare Serenitatis on the Moon, Planetary Remote Sensing and Mapping"*, CRC Press,ISBN 9781138584150-CAT# K376961
5. Deshpande, R. D.,2018, *"'Isotope Tracer Applications in Groundwater HydrologyA Review of Indian Scenario'"*, In: Mukherjee A. (eds), Groundwater of South AsiaSpringer Hydrogeology. Springer, Singapore, doi.org/10.1007/978-981-10-3889-1_14.
6. Jeelani, G., Shah, R. A., Deshpande, R. D.,2018, *"'Assessment of Groundwater in Karst System of Kashmir Himalayas, India'"*, In: Mukherjee A. (eds), Groundwater of South AsiaSpringer Hydrogeology. Springer, Singapore, doi.org/10.1007/978-981-10-3889-1_6.
7. Deshpande, R. D.,2019, *"'Isotope Hydrology'"*, Water Futures of India - Status of Science and Technology.P.P. Mujumdar and V.M. Tiwari (Eds), Indian National Science Academy, IISc Press, Bangaluru, p. 117-144.
8. Bhowmik, H. S., Naresh, S., Bhattu, D., Rastogi, N., Prevot, A. S. H., and Tripathi, S. N.,2018, *"'Seasonal variation of carbonaceous and waster-soluble inorganic constituents of $PM_{2.5}$ aerosols over a megacity '"*, IASTA-Bulletin, New Delhiv. 23, p. 326-329, ISSN 0971 4510.
9. Patel, A., and Rastogi, N.,2018, *"'Reactive oxygen species generation capability of ambient aerosol over the Arabian Sea'"*, IASTA-Bulletin, New Delhiv. 23, p. 703-705, ISSN 0971 4510.
10. Rastogi, N., Satish, R. V., Tripathi, S. N., and Ganguly, D.,2018, *"'Diurnal variability in characteristics of water-soluble brown carbon through online measurements over New Delhi'"*, IASTA-Bulletin, New Delhiv. 23, p. 712-715, ISSN 0971 4510
11. Singh, A., Satish, R.V., and Rastogi, N.,2018, *"Evolution and characteristics of organic aerosol in the urban atmosphere through highly time resolved measurements"*, IASTA-Bulletin, New Delhiv. 23, p. 700-702, ISSN 0971 4510
12. Shah, M. S., Bhushan, R., Saxena, A., and Prajapati, N. D.,2018, *"'A proposed automated instrument to analyse coral reef sample (Spectral luminescence scanner)'"*, IEEEpp 1-5, doi: 10.1109/ICICICT1.2017.8342721, ISBN: 978-1-5090-6106-8.
13. Shah, M. S., Sudheer, A. K., Singh, S., Vaghela, H., and Vaidya, H. H.,2018, *"'A proposed automated instrument for separation of Rare Earth Elements & Strontium by ion exchange chromatography'"*, IEEEpp. 1-5, doi: 10.1109/ICICICT1.2017.8342723,ISBN: 978-1-5090-6106-8.
14. Verma, P. K., Sah, D., Satish, R. V., Rastogi, N., Kumari, K. M., and Lakhani, A.,2018, *"'Atmospheric gas and particulate phase distribution of parent polycyclic aromatic hydrocarbons and their nitro-derivative and their variation with NOx'"*, IASTA-Bulletin, New Delhiv. 23, p.156-160, ISSN 0971 4510.
15. S. Ramachandran,2018, *"Aerosols and Climate Change: Present Understanding, Challenges, and Future Outlook"*, in Land-Atmospheric Research Applications in South and Southeast Asia,edited by K.P. Vadrevu, T. Ohara, and J. Chris Springer, Chapter 17, 341-378.

Review Articles

1. Caprini, J. Fischer, G. Abbas, B. Ananthanarayan2018, *"Perturbative Expansions in QCD Improved by Conformal Mappings of the Borel Plane"*, "Perturbation Theory: Advances in Research and Applications, Nova Science Publishers", v.v.1, p. 211-254
2. Ray, J.S., 2018, *"Rengaswamy Ramesh (1956-2018)"*, Current Science , v.v. 114, p. 2199-2200.
3. Ray, J.S., 2018, *"Barren Island: the only active volcano of India"*, RDWU Bulletin of Science , v.v. II, p. 17-23

Papers Presented in National/ International Conferences

National Conferences

Oral Presentations: 56

Poster Presentations: 28

1. D. Pallamraju, D. Chakrabarty, A. Mishra, S. Thampi, T. P. Das, C. Vineeth, T. K. Pant, R. K. Choudhary, S. Sarkhel, S. Narendranath, and A. Bhardwaj., "ISRO's Aeronomy Satellite mission – DISHA (Disturbed and quiet time Ionosphere-thermosphere System at High Altitudes)", 20^{th} National Space Science Symposium,Pune, 29-31 January 2019
2. Duggirala Pallamraju, Deepak. K. Karan, Fazlul I. Laskar, T. Vijaya Lakshmi, and M. Anji Reddy, "On the influence of solar flux and compositional variations on atomic oxygen dayglow emission rates", 20^{th} National Space Science Symposium,Pune, 29-31 January 2019
3. Deepak K. Karan and Duggirala Pallamraju, "Estimation of Daytime F-region Vertical (E x B) Drift Velocities from Neutral Optical Oxygen Dayglow Measurements", 20^{th} National Space Science Symposium,Pune, 29-31 January 2019
4. Subir Mandal, Duggirala Pallamraju, Deepak K. Karan, Ravindra P. Singh, Pradip Suryawanshi, and Sovan Saha, "Gravity Wave Characteristics Over Low-latitude Upper Atmospheric Region Obtained by Radio Technique", 20^{th} National Space Science Symposium,Pune, 29-31 January 2019
5. S. Ramachandran, "Stratospheric sulfur injections: Benefits and Risks", National Roundtable Discussion on Geoengineering and India: Science and Policy", Indian Institute of Science, Bengaluru, 26 July 2018
6. S. Ramachandran, "Aerosols and Climate", Space Applications Centre, Ahmedabad, 7 August 2018
7. S. Ramachandran, "Ozone: Past, Present and Future", Space Applications Centre, Ahmedabad, 14 September 2018
8. S. Ramachandran, "Ozone", Gujarat Science City, Ahmedabad, 16 September 2018
9. S. Ramachandran, "Aerosol Characterization: Challenges", Indian Institute of Technology, Delhi, 26-28 November 2018
10. Diptiranjan Rout, D. Chakrabarty and R. Sekar, "Impact of ICME and CIR driven storm on low latitude ionospheric electric field", 20^{th} National Space Science Symposium held at Savitribai Phule Pune University, 29-31 January 2019
11. Kuldeep Pandey, D. Chakrabarty and R. Sekar, "Effects of disturbance dynamo electric field on equatorial ionosphere during daytime", 20^{th} National Space Science Symposium held at Savitribai Phule Pune University, 29-31 January 2019
12. Sandeep Kumar and D. Chakrabarty, "A comparative study on daw-dusk asymmetry of the ring current during CME and CIR driven geomagnetic storms", 20^{th} National Space Science Symposium held at Savitribai Phule Pune University, Pune, 29-31 January
13. Ankit Kumar, D. Chakrabarty, Anil Yadav, and G. K. Seemala, "On the post-sunset responses of OI 630.0 nm nightglow intensity over the EIA crest region under various space weather conditions", 20^{th} National Space Science Symposium held at Savitribai Phule Pune University, India, 29-31 January
14. Tripathi, N., and Sahu, L.K., "Anthropogenic, biogenic and secondary sources of atmospheric volatile organic compounds (VOCs) in Delhi", National Space Science Symposium (NSSS), Pune, Maharashtra, India, 29-31 January 2019
15. Sahu, L. K., and Tripathi, N., "Atmospheric biogenic volatile organic compounds (BVOCs) over India and surrounding oceans", National Space Science Symposium (NSSS), Pune, Maharashtra, India, 29-31 January 2019
16. Ravi Yadav, Sahu L. K., Beig G., Tripathi N., and Jaaffrey S.N.A., "Features of ambient particulate matters (PMs) and carbon monoxide (CO) at an urban atmosphere in India: Impact of meteorology and long-range transport", National Space Science Symposium (NSSS), Pune, Maharashtra, India, 29-31 January 2019
17. Som Sharma, Priyanka Ghosh and Kamran Ansari, "Investigation on Stratospheric Sudden Warming (SSW): An evidence of interaction between planetary wave and stratospheric circulation over Indian Region", 20^{th} National Space Science Symposium (NSSS-2019), Pune, India, 29-31 January 2019
18. Vaidehi Joshi, Som Sharma and Nisha Patel, "Climatology of the Middle Atmospheric Ozone over the mid-latitudes in Northern and the Southern Hemispheres", 20^{th} National Space Science Symposium (NSSS-2019), Pune, India, 29-31 January 2019
19. Nisha Patel, Som Sharma, and Vaidehi Joshi, "Long Term Changes and Trends in the Middle Atmosphere over Northern and Southern Hemispheres and over the Equatorial Region", 20^{th} National Space Science Symposium (NSSS-2019), Pune, India, 29-31 January 2019
20. Kamran Ansari, Som Sharma and Priyanka Ghosh, "Middle Atmospheric Temperature Climatology over Indian Region

using SABER on board Timed Observations", 20^{th} National Space Science Symposium (NSSS-2019), Pune, India, 29-31 January 2019

21. Kindra, B., "Study of $b \to d$ semileptonic decays", University of Hyderabad, Hyderabad, 07/15/2018
22. Singh, R. P. and D. Pallamraju, "Mesospheric temperature inversions observed in OH and O2 rotational temperatures and it's possible causes", National Space Science Symposium, Savitribai Phule Pune University, Pune, 29-31 January 2019
23. Ojha, N., Girach, I. A., Saha, S., Sharma, S. K., and Singh, N., "Spatio-temporal distribution of tropospheric ozone over South Asia: Model results versus observations", National Space Science Symposium (NSSS), Pune, 29-31 January 2019
24. Girach, I. A., Tripathi, N., Ojha, N., Nair, P. R., and Sahu, L. K., "Trace gases in the marine boundary layer of the Arabian Sea and Indian Ocean during winter", National Space Science Symposium (NSSS), Pune, 29-31 January 2019
25. Sahoo, S, "Exploring lepton no universality in $b \to c\ell\nu - \ell$ decay modes in the light of recent experimental", FCP 2018 University of Hyderabad, Hyderabad, 07/14/2018
26. Sahoo, S, "Testing lepton non universality in $b \to c\ell\nu - \ell$ decay modes", XXIII DAE-BRNS High Energy Physics Symposium, IIT Madras, 12/10/2018
27. Chutia, L., Ojha, N., Kumar, M., Kumar, A., Girach, I. A., Pathak, B., and Bhuyan, P. K., "Regional scale modeling of secondary organic aerosols using WRF-Chem during winter", National Space Science Symposium (NSSS), 29-31 January 2019
28. Sahoo, S, "Investigation of dark matter, neutrino mass and flavor anomalies in L_μ - L_τ model", International Meeting on High Energy Physics, IOP Bhubaneswar, 17 January, 2019
29. Singh, J., Singh, N., and Ojha, N., "Effect of spatial resolution on the simulated meteorology over the central Himalaya", National Space Science Symposium (NSSS), 29-31 January 2019
30. Kindra, B, "Predictions of angular observables of $\bar{\mathrm{B}} \to \rho\ell\ell$ and $\bar{\mathrm{B}}_s \to \mathrm{K}^*\ell\ell$ in standard model", XXIII DAE-BRNS High Energy Physics Symposium, IIT Madras, 12/10/2018
31. Chutia, L., Ojha, N., Girach, I., Pathak, B., "Distribution of volatile organic compounds over Indian subcontinent during winter: WRF-Chem simulations versus observations", Indian Aerosol Science and Technology Association (IASTA), IIT Delhi, 26-28 November
32. Kindra, B, "Predictions of angular observables of $\bar{\mathrm{B}} \to \rho\ell\ell$ and $\bar{\mathrm{B}}_s \to \mathrm{K}^*\ell\ell$ in standard model", Belle Analysis Workshop, IISER Mohali, 03/01/2019
33. Sahoo, S, "Vector-like dark matter and flavor anomalies with leptoquarks", XXIII DAE-BRNS High Energy Physics Symposium, IIT Madras, 12/10/2018
34. Shukla, K., Ojha, N., and Khare, M., "Air quality simulations over Delhi using WRF-Chem: Influences of local emissions and dynamics", Indian Aerosol Science and Technology Association (IASTA), IIT Delhi, 26-28 November 2018
35. Sahoo, S, "Impact of leptoquarks on flavor anomalies", International Meeting on High Energy Physics, IOP Bhubaneswar, 01/17/2019
36. S. S. Nayak, "Investigation of the magnetohydrodynamic evolution of a solar coronal jet", Young Astronomers' Meet, September 24−28, 2018
37. N. C. Joshi, "An eruptive circular ribbon flare triggered by the low coronal breakout", Advances in Physics from Small to Large Scales (APSLS-2019), March 14−16, 2019
38. N. C. Joshi, "Successive stages of magnetic reconnection associated with the flux rope eruption in a multiple-ribbon solar eruptive flare", 33^{rd} National Symposium on Plasma Science & Technology, December 4−7, 2018
39. A. Raja Bayanna, "Fizeau-mask interferometry of solar features using the Multi-Application Solar Telescope at Udaipur Solar Observatory", 37^{th} Meeting of Astronomical Society of India, February 18−22, 2019
40. M. Syed Ibrahim, "Major X-class flare, halo coronal mass ejection and geomagnetic storm driven by the eruption of magnetic flux rope from active region NOAA 12673", Advances in Plasma Science and Technology (APST-18), October 24−26 , 2018
41. P. K. Mitra, "Evolution of solar magnetic fields and Large-scale reconnection events in extremely complex solar active region NOAA 12673", 37^{th} Meeting of Astronomical Society of India, February 18−22, 2019
42. P. K. Mitra, "Evolution of solar magnetic fields and Large-scale reconnection events in extremely complex solar active region NOAA 12673", 33^{rd} National Symposium on Plasma Science & Technology, December 4−7, 2018
43. K. Bora, "The role of Hall-MHD in magnetic reconnection on the Sun", 33^{rd} National Symposium on Plasma Science & Technology, December 4−7, 2018
44. B. Kumar, "On the magnetic-jerk driven acoustic oscillations in the solar atmosphere observed during major solar flares", 20^{th} National Space Science Symposium, January 29−31, 2019
45. M. Bhatt, "M3-based global maps of lunar refractory elements", 20th National Space Science Symposium, 29.1.2019 to 31.1.2019
46. M. Bhatt, "Lunar Swirls: Linkage between Space weathering, regolith compaction, and formation mechanism", 20th National Space Science Symposium, 29.1.2019 to 31.1.2019
47. K. K. Marhas, "Nano-SIMS: a unique imaging tool using secondary ion emission and recent results from Planetary science", Indian Institute of Technology, Chennai, 09/03/2019
48. Sinha, R.K., "Study of layered deposits in the East Melas Chasma, Mars using MCC, HiRISE, THEMIS and MOLA data", National Symposium on Advancements in Geospatial Technology for Societal Benefits 2018, December 05-07, 2018
49. Sinha, R.K., "Role of recent water flow and debris-flow activity in gullies: New evidences from two northern mid-latitude craters on Mars", National Symposium on Advancements in Geospatial Technology for Societal Benefits 2018, December 05-07, 2018
50. Sinha, R.K. and Dwijesh Ray, "Geomorphic evidence of debris-flow deposits in Martian gullies: Implications for involvement of liquid water in their formation", Young Astronomers Meet (YAM) 2018, September 24-28
51. Patel, A., Rastogi, N., Singh, A., and Singh, D.,, "Reactive Oxygen Species Generation Capacity of Ambient Fine Aerosol

over the Indo-Gangetic Plain: Effect of Intense Biomass Burning", National Space Science Symposium - 2019, January 29 -31, 2019.

52. Rastogi, N., and Satish, R. V.,, "Effect of Biomass Burning Emissions on the Characteristics of Water-soluble and Water-insoluble Brown Carbon", National Space Science Symposium-2019, January 29-31, 2019
53. D. Ray, "Towards mitigating disputes on microbial imaging techniques in astrobiological investigations", 20th National Space Science Symposium held at Pune, Jan 29-31, 2019
54. Chandan Kumar, "Role of materials and interface contacts on the performance of planetary thermal probes", COMSOL conference, August 2018
55. K. Durga Prasad, "CubeSats aided Wireless Sensor Networks for exploration of Mars and Venus", URSI APRASC-2019,New Delhi, 9-15 March., 2019
56. K. Durga Prasad, "Temporal Perturbations in Mars' upper atmosphere due to a strong solar flare event of September", URSI APRASC-2019, New Delhi, 9-15 March., 2019
57. N. Srivastava, "Lunar Sample Return Missions: Next Logical step for planetary exploration", NSSS 2019 at S.P. University Pune, 29-31 January 2019 at
58. P. Jha, P. Das, D. Ray, "The study of ferruginous concretions from Nutangram, Bankura, West Bengal, India", Biogeochemical Cycles and Climate Change, Department of Environment science and engineering, IIT(ISM) Dhanbad, 08/2018
59. P. Jha, R. Jha, P. Das, D. Ray, "Mineralogical and Spectral characterization of Iron oxides concretions present in the Biharia, Shankargarh, Prayagraj, India: Implications for formation of Martian hematite spherules", National Seminar on Sedimentary researches by Indian association of Sedimentologist, Dr Harisingh Gour Sagar University, 01/2019
60. P. Jha, R. Jha, P. Das, D. Ray, "The study of Iron oxides concretions from Jurassic Sandstone, Kutch, Gujarat, India", Recent Studies on the Geology of Kachchh Basin, KSKV Kutch University, Bhuj, Gujarat, 12/2018
61. R. Jha, P. Jha, P. Das, D. Ray, "Characterization of experimentally precipitated iron compounds using Eh-pH variations, Pourbaix diagrams and SEM images: implications for formation of hematite spherules in earth and mars terrestrial environment", . 55 th Annual Convention on Indian Geophysical Union: Changing Water Cycle & Water Resources, Rabindranath Tagore University, Bhopal, 12/2018
62. R. Jha, P. Jha, P. Das, D. Ray, "Oxidation process of Iron sulphate to form iron oxides minerals in experimental conditions: Implications for formations of hematite spherules in earth and mars terrestrial environment", Seminar cum Workshop on Recent Advances in the Earth, CAS in Geology, Kumaun University, Nainital (Uttarakhand), 03/2019
63. R. Jha, P. Jha, P. Das, D. Ray, "Understanding the redox processes involvement in precipitation of Iron in Martian bedrock", Biogeochemical Cycles and Climate Change, Department of Environment science and engineering, IIT(ISM) Dhanbad, 08/2018
64. R. Sharma, "Detection and Mapping of Skylights on the flank of Elysium Mons, Mars", National Space Science Symposium (NSSS), S.P. University Pune, 29-31 Jan 2019
65. Sinha R. K., "Pre-Chandrayaan-2 understanding of lunar morphology, topography, mineralogy, and chronology at the Vikram Landing site", National Space Science Symposium (NSSS) at S.P. University Pune., 29-31 January 2019
66. S. Ghosh and D. Ray, "Thermal and shock history of Kheri Mahem, the largest L5 chondrite shower in India", National Space Science Symposium held at Pune, Jan 29-31, 2019.
67. S. Natrajan, V. Goyal and K. K. Marhas, "The thermal evolution of meteorite parent body estimated from Insoluble Organic Matter", National Space Science Symposium , Pune, 29-31 Jan 2019
68. T. Singh, "Geomorphology and mineralogy of Grimaldi basin on the Moon", National Space Science Symposium (NSSS) at S.P. University Pune., 29-31 Jan 2019
69. V. Goyal and K. K. Marhas, "Inclusion of Volatiles within first forming solids and late irradiation scenario", National Space Science Symposium (NSSS) at S.P. University Pune., 29-31 Jan 2019
70. Satish, R. V., and Rastogi, N.,, "Quantification of polar organic marker compounds from biomass burning emissions over the Indo-Gangetic Plain", National Space Science Symposium-2019, January 29-31, 2019
71. Singh, D., and Rastogi, N.,, "Change in characteristics of fine organic aerosol with atmospheric evolution: Insights from aerosol mass spectrometry", National Space Science Symposium-2019, January 29-31, 2019
72. Swetapuspa Soumyashree, "Nanoparticle enhanced LIBS of Cu target using pulsed Nd: YAG laser as excitation source", 22nd National Conference on Atomic and Molecular Physics, Indian Institute of Technology Kanpur, 25th March 2019 – 28th March 2019
73. NageswaraRao E., "Estimation of elemental concentration using plasma emission spectroscopy employing synthetic spectrum method", 22nd National Conference on Atomic and Molecular Physics, Indian Institute of Technology Kanpur, 25th March 2019 – 28th March 2019
74. J. K. Meka, "Reversible phase changes in astrochemical ices", 22nd National Conference on Atomic and Molecular Physics, Indian Institute of Technology Kanpur, 25th March 2019 – 28th March 2019
75. Surendra Vikram Singh, "Radiation Induced Chemistry on Icy surfaces: Case study of Carbon-Boron Mixture", 36th Annual Meeting of Astronomical Society of India held at Osmania University, Hyderabad, India, 5-9 February 2018
76. Rahul Kumar Kushwaha, "Ozone on Callisto", National Symposium on Space Science (NSSS) at Pune University, IUCAA, NCRA, Pune., 29th – 31st Jan 2019
77. Rahul Kumar Kushwaha, "Evidence for Layered Ice in the Solar System Bodies", National Symposium on Space Science (NSSS) at Pune University, IUCAA, NCRA, Pune., 29th – 31st Jan 2019
78. Rahul Kumar Kushwaha, "IR attenuation due to phase changes observed in astrochemical propargyl ether ices", 22nd National Conference on Atomic and Molecular Physics (NCAMP) at IIT – Kanpur, 25th – 28th March 2019
79. Srinivasa Prasannaa V, "The search for the electric dipole moment of the electron using molecules.", Young Physicists' Meet-2019, held in PRL, Ahmedabad, 18th to 20th,March 2019

80. Srinivasa Prasannaa V, “The Search for the Electric Dipole Moment of the Electron (eEDM) in Mercury Halides Using the Relativistic Coupled Cluster Theory”, 22nd National Conference on Atomic and Molecular Physics (NCAMP), held at IIT Kanpur, 25th to 28th March, 2019

81. Srinivasa Prasannaa V, “Relativistic Coupled Cluster Studies of the Electric Dipole Moment of the Electron in YbOH.”, Workshop on Recent Trends in Electronic Structure of Atoms and Molecules’, held in Tokyo Institute of Technology, 11th January, 2019

82. Jinee Gogoi, Som Sharma and Kalyan Bhuyan, “Effects of Sudden Stratospheric Warming over India”, symposium on “Advances in Remote Sensing & GIS Applications”, NESAC, Indian Society of Remote Sensing (ISRS) and Indian Society of Geomagnetics (ISG) at North Eastern Space Applications Centre (NESAC), Shillong, India, 10-11 May, 2018

83. Nisha Patel, Som Sharma, Vaidehi Joshi and Jinee Gogoi, “Long-term Changes and Trends in the Middle Atmospheric Temperatures over the Northern and Southern Hemispheres”, symposium on “Advances in Remote Sensing & GIS Applications”, NESAC, Indian Society of Remote Sensing (ISRS) and Indian Society of Geomagnetics (ISG) at North Eastern Space Applications Centre (NESAC), Shillong, India, 10-11 May, 2018

84. Vaidehi Joshi, Nisha Patel and Som Sharma, “Temperature and Ozone Time Series and Climatological Differences in the Middle Atmosphere of the Earth over sub-tropical Region”, symposium on “Advances in Remote Sensing & GIS Applications”, NESAC, Indian Society of Remote Sensing (ISRS) and Indian Society of Geomagnetics (ISG) at North Eastern Space Applications Centre (NESAC), Shillong, India, 10-11 May, 2018.

International Conferences

Oral Presentations: 42

Poster Presentations: 28

1. Fazlul I. Laskar, Gunter Stober, John McCormack, Duggirala Pallamraju, Peter Hoffmann, and Jorge L. Chau, “Interhemispheric Meridional Circulation During Sudden Stratospheric Warmings”, The 07^{th} IAGA/ICMA/SCOSTEP Workshop on Vertical Coupling in the Atmosphere-Ionosphere System will take place at the Helmholtz Centre Potsdam, GFZ, 2-6 July 2018

2. Duggirala Pallamraju, Deepak Karan, Fazlul I. Laskar, T. Vijaya Lakshmi, M. Anji Reddy, and Supriya Chakrabarti, “On the inter-dependency of variations of solar flux and composition on thermospheric dayglow emissions at different latitudes”, 15^{th} International Symposium on Equatorial Aeronomy (ISEA-15), 22-26 October 2018

3. Subir Mandal, Duggirala Pallamraju, and Deepak Kumar Karan, “Gravity wave characteristics over low-latitude upper atmospheric region obtained by radio technique”, 15^{th} International Symposium on Equatorial Aeronomy (ISEA-15), 22-26 October 2018

4. Fazlul I. Laskar, Gunter Stober, John McCormack, Duggirala Pallamraju, Jorge L. Chau, and Peter Hoffmann, “Meridional Circulation in the Whole Atmosphere during Sudden Stratospheric Warmings”, 15^{th} International Symposium on Equatorial Aeronomy (ISEA-15), 22-26 October 2018

5. Deepak K Karan and Duggirala Pallamraju, “Existence of small scale longitudinal variations in the low-latitude upper atmospheric wave dynamics”, 15^{th} International Symposium on Equatorial Aeronomy (ISEA-15), 22-26 October 2018

6. Deepak K Karan and Duggirala Pallamraju, “Estimation of daytime F-region vertical E x B drift velocities from optical neutral dayglow measurements”, 15^{th} International Symposium on Equatorial Aeronomy (ISEA-15), 22-26 October 2018

7. Deepak K Karan and Duggirala Pallamraju, “Variations of daytime thermospheric gravity waves over long time scales”, 15^{th} International Symposium on Equatorial Aeronomy (ISEA-15), 22-26 October 2018

8. Deepak K Karan and Duggirala Pallamraju, “Effect of geomagnetic storms on the daytime low-latitude thermospheric wave dynamics as inferred from large field-of-view dayglow measurements”, 15^{th} International Symposium on Equatorial Aeronomy (ISEA-15), 22-26 October 2018

9. Sharma, K., Ojha, N., Girach, I. A., Sharma, N., Nair, P. R. and Singh, N., “Ozone pollution in the Doon valley of the central Himalaya: Observations and model results, International conference on atmospheric chemistry and physics in highly polluted environments”, The 2019 CIAAS Meeting, Indian Institute of Technology Delhi, New Delhi, India, 22-24 March 2019

10. Ojha, N., Girach, I. A., Saha, S., Sharma, S. K. and Singh, N., “Tropospheric ozone over South Asia: Climatology and long-term trend”, URSI AP-RASC 2019, New Delhi, India, 09-15 March 2019

11. Sharma, S. K., Patel, N., Ojha, N., Joshi, V. and Saha, S., “Satellite and modelling based investigations of the middle atmospheric temperature climatology over the equatorial regions”, URSI AP-RASC 2019, New Delhi, India, 09-15 March 2019

12. Shukla, K., Ojha, N., Cai, X. and Khare, M., “Air quality simulations over Delhi using WRF-Chem: Effects of local pollution and regional-scale transport”, AGU Fall Meeting 2018, Washington, D. C., USA, 10-14 December 2018

13. Som Sharma, Shyam Lal, Harish Chandra, and Sourita Saha, “Lidar and Satellite Observed Temperature Trends and its Association with Ozone over a Sub-tropical Location”, European Geosciences Union (EGU) General Assembly 2018, Vienna, Austria, 8-13 April 2018

14. Tripathi, N., and Sahu, L.K., “First PTR-TOF-MS based measurement of volatile organic compounds (VOCs) in New Delhi: Implication to regional atmospheric chemistry and climate during winter-summer transitions”, Stratosphere-troposphere Processes And their Role in Climate (SPARC) General Assembly, Kyoto, Japan, 1-5 October 2018

15. Vats, P., Ganguly D., Sinha V., and Sahu L. K., “Simulation of secondary organic aerosols over the Indian region using a global climate model with extensive interactive atmospheric chemistry”, EGU General Assembly, Vienna, Austria, 8-13 April 2018

16. Singh, R. P. and D. Pallamraju, “Mesospheric temperature inversions observed in OH and O2 rotational temperatures from Mount Abu (24.6oN, 72.8oE), India”, 15^{th} International Symposium on Equatorial Aeronomy (ISEA-15), 22-26 October 2018

17. Amitava Guharay, “Investigation of the quarter-diurnal tide in the MLT over low-latitude stations”, 15^{th} International symposium on equatorial aeronomy (ISEA-15), Physical Research Laboratory, Ahmedabad, 22-26 October 2018

18. S. K. Goyal, P. Kumar, D. Chakrabarty, P. Janardhan, S. Vadawale, M. Shanmugam, A. Sarkar, P. R. Adhyaru, A. R. Patel, M. S. Shah, Neeraj K. Tiwari, H. Adalja, A. Sarda, T. Ladiya, S. B. Banerjee, K. P. Subramanian, B. Bapat, M. Chauhan, A. K. Hait, and R. R. Bhavsar, “Investigation of anisotropy of solar wind and energetic particles using ASPEX measurements on-board Aditya-L1”, 42^{nd} COSPAR Assembly in Pasadena, California, USA, 14-22 July 2018

19. S. K. Goyal, D. Chakrabarty, S. A. Haider, S. Vadawale, A. Sarda, A. Auknoor, P. Sharma, A. K. Hait and N. Kumar Tiwari, “High energy particle environment in the Martian orbit: proposed measurements using Energetic Ion Spectrometer”, 42^{nd} COSPAR Assembly in Pasadena, California, USA, 14-22 July 2018

20. Diptiranjan Rout, D. Chakrabarty and R. Sekar, “Extreme impacts over low latitude ionosphere during a space weather event”, 15^{th} International Symposium on Equatorial Aeronomy (ISEA-15) held at Physical Research Laboratory, India, 22-26 October 2018

21. Kuldeep Pandey, D. Chakrabarty and R. Sekar, “Significantly Large Impact of Disturbance Dynamo on Equatorial Ionosphere: Case Studies”, 15^{th} Annual meeting of Asia Oceania Geosciences Society (AOGS) held at Honolulu, Hawaii (USA), 3-8 June 2018

22. Kuldeep Pandey, R. Sekar, B. G. Anandarao, S. P. Gupta, and D. Chakrabarty, “On the Occurrence of Afternoon Counter Electrojet Over Indian Longitudes During June Solstice in Solar Minimum”, 15^{th} Annual meeting of Asia Oceania Geosciences Society (AOGS) held at Honolulu, Hawaii (USA), 3-8 June 2018

23. Kuldeep Pandey, R. Sekar, B. G. Anandarao, S. P. Gupta, and D. Chakrabarty, “Afternoon counter electrojet over Indian longitudes during June solstice in solar minimum”, 15^{th} International Symposium on Equatorial Aeronomy (ISEA-15) held at Physical Research Laboratory, 22-26 October 2018

24. Kuldeep Pandey, D. Chakrabarty and R. Sekar, “Effect of disturbance dynamo on equatorial ionosphere during daytime”, 15^{th} International Symposium on Equatorial Aeronomy (ISEA-15) held at Physical Research Laboratory, India, 22-26 October 2018

25. Sandeep Kumar, B. Veenadhari, D. Chakrabarty, and S. Tulasi Ram, “On the dawn-dusk asymmetry in the ring current during geomagnetic storms: Case studies”, 15^{th} International Symposium on Equatorial Aeronomy at PRL, Ahmedabad, 22-26 October 2018

26. M. Sivakandan, D. Chakrabarty, T. K. Ramkumar, A. Guharay, R. Sekar and N. Parihar, “Evidence for the presence of MSTID and Quasi-Periodic Southward Moving Waves over 6° Magnetic latitude”, 15^{th} International Symposium on Equatorial Aeronomy (ISEA-15) held at Physical Research Laboratory, India, 22-26 October 2018

27. M. Sivakandan, A. Taori, and T.K. Ramkumar, “The Predominant Occurrence Altitudes of Middle Atmospheric Temperature Inversions and Mesopause Over the low Latitude Indian Sector”, SPARC General Assembly, in Kyoto, Japan, 1-5 October 2018

28. M. Sivakandan, T.K. Ramkumar, A. Taori, Venkateswara Rao, and K. Niranjan, “Long-term variation of OH peak emission altitude and volume emission rate over Indian low latitudes”, SPARC General Assembly, in Kyoto, Japan, 1-5 October 2018

29. S. Venkataramani, “First observations of light non-methane hydrocarbons (NMHCs) over an high altitude site in Southern India”, 14^{th} iCACGP Quadrennial Symposium & 15th IGAC Science Conference Takamatsu, Kagawa, Japan, 25-29 September 2018

30. S. Venkataramani, “IGAC-MANGO (Monsoon Asia and Oceania Networking Group)”, Takamatsu, Kagawa, Japan to discuss the scientific programmes specific to Asian region, 29-30 September 2018

31. N. C. Joshi, “Investigation of Magnetic Field Configuration of typical and atypical Confined Flares”, Exploring the Universe: Near Earth Space Science to Extra-galactic Astronomy (EXUNIV2018), November 14−17, 2018

32. P. K. Mitra, “Multi-wavelength analysis and modeling of successive flux rope eruption from solar active region NOAA 12673 and associated X-class flares on 2017 September 6”, Exploring the Universe: Near Earth Space Science to Extra-galactic Astronomy (EXUNIV2018), November 14−17, 2018

33. Nandita Srivastava, “Interplanetary and geomagnetic signatures of stealth CMEs”, ISSI workshop, Bern, Switzerland, April 16−20, 2018

34. Nandita Srivastava, “Evolution of coronal cavities leading to CMEs”, ISEST workshop, Hvar, Croatia, September 24−28, 2018

35. Nandita Srivastava, “Key Solar Inputs for PreSTo: NSP (SCOSTEP)”, ISSI-BJ Forum meeting, Beijing, China, November 14, 2018.

36. S. S. Nayak, “Non-force-free-field initiated magnetohydrodynamic simulation of the coronal jet and the C-class flare at the active region 12615”, Model Coupling and Data Driven Simulations of Solar Eruptions, August 13−16, 2018

37. K. K. Marhas, “The observed planetary architecture in the solar system and the evolution of the early solar system”, UK-India Frontiers of Science” (FoS) meeting, organised by the Royal Society (UK) and the Department of Science and Technology of India (DST), 05/ 2018

38. K. K. Marhas, “Infrastructure of Solar System”, International conference on exoplanets, 07/02/ 2019 to 09/02/2019

39. S. K. Goyal, “STEPS: an instrument to understand the anisotropy of the high-energy particles in the interplanetary medium”, AOGS, June 03- June 08, 2018

40. A. Basu Sarbadhikari, “Implications for formations of alkali-rich rocks of the Moon”, New Views of the Moon 2 - Asia. Aizu, Japan, 2018

41. Bhattu, D., Slowik, J. G., Canonaco, F., El Haddad, I., Tiwari, S.B., Kumar, P., Tiwari, S., Satish, R. V., Rastogi, N., Srivastava, A. K., Bisht, A. K., Tiwari, S., Ganguly, D., Tripathi,

S. N., Baltensperger, U., and Prévôt, A.S.H.,, "Long-term Characterization and Source Apportionment of Carbonaceous Aerosols over Five Sites in Northern India", 10th International Aerosol Conference (IAC) 2018, September 2-7, 2018

42. Kumar, V., Bhattu, D., Tong, Y., Pospisilova, V., Stefenelli, G., Bertrand, A., Cassotto, R., Satish, R. V., Vats, P., Baltensperger, U., Ganguly, D., Rastogi, N., Tripathi, S.N., Prévôt, A.S.H., and Slowik, J. G.,, "Investigation of Organic Aerosol in Delhi, India, using an Extractive Electrospray Ionization Time-of-Flight Mass Spectrometer (EESI-LTOF)", 10th International Aerosol Conference (IAC) 2018, September 2-7, 2018

43. Patel, A., Satish, R. V., Singh, A., Singh, D., and Rastogi, N.,, "Oxidative Potential of Ambient Fine Aerosol during Intense Biomass Burning over the Indo-Gangetic Plain-India", 10th International Aerosol Conference (IAC), September 2-7, 2018

44. Rastogi, N., Agnihotri, R., Salwani, R., Patel, A., Satish, R. V., and Suresh Babu. S.,, "Chemical and Isotopic Characteristics of Ambient Aerosols over the Bay of Bengal: Impact of Continental Outflow", 15th annual conference of Asia Oceania Geosciences Society (AOGS), June 3-8, 2018

45. D. Ray, "The Mukundpura (CM2) chondrite; A new carbonaceous meteorite fall in India", 81st Annual Meeting of the Meteoritical Society in Moscow, Russia, July 22-27, 2018

46. K. K. Marhas and D. Ray, "Corundum within silicate/graphite inclusions in Iron meteorite", 81st Annual Meeting of the Meteoritical Society, Moscow, July 22-27, 2018

47. R. K. Mishra and K. K. Marhas, "Fossil record of 7Be and 10Be in a CAI: implications for the origin and early evolution of our solar system", 81st Annual Meeting of the Meteoritical Society, Moscow, July 22-27, 2018

48. Rajiv . R. Bharti, "Characterizing the Martian subsurface using SHAllow RADar (SHARAD)", 2019 URSI Asia-Pacific Radio Science Conference (AP-RASC 2019), 09–15 March 2019

49. S. K. Mishra and A. Andreev, "Reflection of chirped pulse from an overdense plasma", 2018 International Conference Laser Optics (ICLO), IEEE, 2018

50. S. K. Mishra and A. Andreev, "Ultrashort pulse amplification/ compression via BRA Scheme", XXI International Conference on Ultrafast Phenomena, Hamburg, Germany, July 15 – 20, 2018

51. S. K. Mishra, "Photoelectron sheath on lunar sunlit regolith and fine particle levitation", 2019 URSI Asia-Pacific Radio Science Conference (AP-RASC 2019), 09–15 March 2019

52. Rastogi, N., Singh, A., and Satish, R. V.,, "Change in Submicron Particle Composition and Characteristics Due to Large Amount of Firecrackers Burning", 15th annual conference of Asia Oceania Geosciences Society (AOGS), June 3-8, 2018

53. Satish, R. V., Rastogi, N., Singh, N., and Singh, A.,, "Change in Brown Carbon Characteristics during Paddy-Residue Burning over the Indo-Gangetic Plain", European Geosciences Union (EGU) General Assembly 2018, April 8–13, 2018

54. Singh, A., Satish, R. V., and Rastogi, N.,, "10th International Aerosol Conference (IAC) 2018", Composition and Characteristics of NR-PM1 Using HR-TOF-AMS over a Big Urban City of Western India, September 2-7, 2018

55. Tripathi, S. N., Bhattu, D., Thamban, N. M., Lalchandani, V., Mishra, S., Kumar, P., Tiwari, S., Tripathi, N., Sahu, L. K., Tiwari, S. B., Satish, R. V., Rastogi, N., Srivastava, A. K., Bisht, D. S., Tiwari, S., Sutaria, R., Mohan, M., Ganguly, D., Ghosh, S., Vats, P., Tobler, A., Kumar, V., Rai, P., Pospisilova, V., and Stefenelli, G.,, "Chemical Characterization and Source Apportionment of PM2.5 Aerosols in the Capital City "New Delhi" of India", 10th International Aerosol Conference (IAC) 2018, September 2-7, 2018

56. Verma, P. K., Sah, D., Satish, R. V., Rastogi, N., Maharaj Kumari, K., Lakhani, K.,, "Atmospheric Concentration of Polycyclic Aromatic Hydrocarbons (PAHs) and Nitro-PAHs, Their Temperature Dependence and Gas to Particle Partitioning at a Traffic site in Agra", 10th International Aerosol Conference (IAC) 2018, September 2-7, 2018

57. Surendra Vikram Singh, "Radiation Induced Chemistry on Icy Satellites: New experimental facilities at PRL Ahmedabad", Exploring the Universe: Near Earth Space Science to Extragalactic Astronomy (EXPUNIV2018), 14-17 November 2018.

58. Rahul Kumar Kushwaha, "Ozone on Callisto", Asian International Symposium on Atomic and Molecular Physics (AISAMP) IIT – B and TIFR Mumbai, 3rd – 8th Dec 2018

59. Srinivasa Prasannaa V, "Ultracold Mercury Alkali Molecules for Electron Electric Dipole Moment Searches", 13th Asian International Seminar on Atomic and Molecular Physics (AISAMP), organized in IIT Mumbai and TIFR, 3rd to 8th December , 2018

60. Srinivasa Prasannaa V, "Accurate relativistic calculations of molecular properties relevant to the search for new physics beyond the Standard Model", International Conference on Quantum and Atom Optics-2018 (ICQAO), organized in IIT Patna, 16th to 18th December , 2018

61. Priyanka Ghosh, T. K. Ramkumar, V Yessubabu and Som Sharma, "Convection Generated High-Frequency Gravity Waves: Comparison between MST Radar Observations & WRF Simulation", SPARC General Assembly 2018, Kyoto, Japan, 1-5 October, 2018

62. Priyanka Ghosh, T. K. Ramkumar, A. K. Patra, Pavan Chaitanya and Som Sharma, "Vertical Coupling from the Lower Atmosphere to the Ionosphere: Observations Inferred from Indian MST Radar, GPS Radiosonde, Ionosonde and SABER/TIMED Instrument over Gadanki", SPARC General Assembly 2018, Kyoto, Japan, 1-5 October, 2018

63. Som Sharma, Harish Chandra, and Shyam Lal, "Earth's Middle Atmospheric and Ionospheric Changes over Western India: Long Term Scenario", 15^{th} International Symposium on the Equatorial Aeronomy (ISEA-15), Physical Research Laboratory, Ahmedabad, India, 22-26 October, 2018

64. Priyanka Ghosh and Som Sharma, "Investigation of vertical wavenumber spectra from the lower atmosphere to the ionosphere over tropical and subtropical regions", 15^{th} International Symposium on the Equatorial Aeronomy (ISEA-15), Physical Research Laboratory, Ahmedabad, India, 22-26 October, 2018

65. Jinee Gogoi, Som Sharma and Kalyan Bhuyan, "Ionospheric response to Sudden Stratospheric Warming episodes of 2007 and 2009 over Western region of India", 15^{th} International Symposium on the Equatorial Aeronomy (ISEA-15), Physical Research Laboratory, Ahmedabad, India, 22-26 October, 2018

66. Jinee Gogoi, Som Sharma and Kalyan Bhuyan, “Ionospheric response to Sudden Stratospheric Warming episodes of 2007 and 2009 over Western region of India”, 15^{th} International Symposium on the Equatorial Aeronomy (ISEA-15), Physical Research Laboratory, Ahmedabad, India, 22-26 October, 2018
67. Som Sharma, N. Patel, N. Ojha, V. Joshi and S. Saha, “Satellite and Ground Based Investigations of the Middle Atmospheric Temperature Climatology over the Equatorial Regions”, URSI AP-RASC-2019, New Delhi, India, 09-15 March, 2019
68. P. Janardhan, Susanta Kumar Bisoi, “Solar polar fields during cycle 24: An unusual polar field reversal”, URSI, Asia Pacific Radio Science Conference 2019 (APRASC 2019), , 9-15, March 2019
69. P. Janardhan, Susanta Kumar Bisoi, “High resolution imaging of coronal Type III bursts: First MUSER solar radio observations”, URSI, Asia Pacific Radio Science Conference 2019 (APRASC 2019), , 9-15, March 2019
70. P. Janardhan, Susanta Kumar Bisoi, “A decimetric emission source 500” away from a flaring site: Possible scenarios from GMRT solar radio observations”, URSI, Asia Pacific Radio Science Conference 2019 (APRASC 2019), , 9-15, March 2019

Various Events, and Outreach Activities at PRL

Young Astronomers Meet September 2018

The 15^{th} YAM, a student conference at the national level, was held at PRL from 24 - 28 September 2018. There were students from across the length and breadth of the country. A wide spectrum of topics were covered in this conference ranging from Astronomical Instrumentation, Sun and Planetary Science, Exoplanets, Stellar Astrophysics, Extra-galactic Astrophysics and IGM, Galactic Physics and ISM, Cosmology, General Relativity and Gravitational Waves and High Energy Astrophysics. From the healthy exchange of new research ideas and trends among the participants it is seen that the meeting was very successful.



Participants of YAM 2018.

Students Conference on Optical Physics (SCOP) 2018

The SCOP-2018 was conducted at PRL during 4-6 October 2018. The conference was attended by 70 students from all over the country who presented their works as both oral and poster presentations. Shri. A. S. Kiran Kumar (Chairman, PRL council) inaugurated the conference and delivered a plenary talk. SCOP-18 was enriched with an increased number of invited talks intended towards an enhanced academic benefit for the participants. Fifteen invited talks by young scientists were hosted from different institutes all over the country on topics across a wide spectrum of optics – ranging from physical optics to quantum optics. The conference hosted extensive poster sessions in which student researchers exchanged their ideas among peers and experts through rigorous interaction.



Inaugural event of SCOP 2018.

The 15^{th} International Symposium on Equatorial Aeronomy (ISEA-15)



Inaugural event of ISEA 15, October 2018.

The 15^{th} International Symposium on Equatorial Aeronomy (ISEA-15) was held at PRL during October 22 – 26, 2018. ISEAs are held to bring together global scientists involved in research on various aspects of low- and equatorial latitudinal regions of the upper atmosphere (altitude of 80 km and above the earth's surface) which includes the

regions of the mesosphere, the thermosphere, and the ionosphere. The 3rd ISEA meeting was held in 1969 at PRL under the leadership of Prof. Vikram Sarabhai, the founder of PRL. This 15th ISEA meeting was a kick-off of the Birth Centenary celebrations of Prof. Vikram Sarabhai at PRL. This time, it brought together around 180 scientists from 22 countries involved in research of both fundamental and applications aspects. There was sizeable participation from young scientists (under 30 years).

Udaipur Solar Observatory Foundation Day - 20 September 2018

The Foundation Day 2018 of the Udaipur Solar Observatory was organized on 20 September 2018 to commemorate the rich history and growth of the Observatory which was established in 1975 on Lake Fateshsagar under the arduous effort of Prof. Arvind Bhatnagar and his team, providing rich insight into the dynamic solar chromosphere and its associated phenomena.

The event was held at USO in the afternoon with an inaugural address by Prof. Anil Bhardwaj, Director PRL, who emphasized the important role played by USO in several crucial aspects of Solar Physics, including Space Weather and Sun-Earth coupling. Prof. Ashok Ambastha, Honorary Scientist USO-PRL, gave a talk on the "The first 25 years of USO from its inception". Prof. Nandita Srivastava, Deputy Head USO-PRL, then spoke on the current activities and future research programmes at the Observatory. The special lecture of the day was delivered by the guest of honour Prof. Amita Das, Senior Professor Institute for Plasma Research Gandhinagar, on The Enigma of Magnetic Fields. The Foundation Day gathering also included several PRL personnel, as well as faculty and students from local colleges and Universities.



Celebration of Foundation Day of USO, Udaipur.

The 84th Anniversary General Meeting of Indian National Science Academy (INSA-AGM)

The 84th Anniversary General Meeting of Indian National Science Academy (INSA-AGM) was hosted by Physical Research Laboratory (PRL) during December 26-28, 2018. This prestigious event was co-hosted by Institute for Plasma Research (IPR) and Indian Institute of Technology, Gandhinagar (IIT-Gn), and two half-day sessions were organized at IPR and IIT-Gn on 27 December, 2018. The anniversary meeting was attended by around 200 delegates including INSA Fellows, other eminent scientists of the country from various disciplines, young scientist awardees, teacher awardees, newly inducted fellows.

This meeting was also graced by Shri A. S. Kiran Kumar (Chairman, PRL council of Management), other dignitaries from ISRO that includes Dr. B. N. Suresh (Vikram Sarabhai Distinguished Professor at ISRO-HQ), Shri P. Kunhikrishnan (Director, URSC), Dr. P. Diwakar (Director, EDPO, ISRO-HQ) as well as directors of a number of prominent research institutions of India. In view of the upcoming Birth Centenary Celebrations of Prof. Vikram Sarabhai, the founder of PRL and the Father of India's Space Programme, a special symposium entitled "Vikram Sarabhai Space Science Symposium (VS4): Innovations from Space Program" was planned as one of the seven symposia. Other six symposia were based on themes such as "Sustainable Energy and Chemical Engineering Platforms", "Drug Discovery and Drug Development: The Indian Narrative", "Ethics in Science and Education", "Water Futures", "AIScaling Up Artificial Intelligence in India", "Food Security and Genomics". In addition to symposia on these societally relevant and nationally important themes, there were two special award lectures, namely, "Meghnad Saha Medal Lecture" on Navigating Complexity by Common Sense and "Aryabhatta Medal Lecture" on Need for Integration of Ayurveda with Modern Biology and Medicine. The INSA AGM was a huge success in terms of the richness of scientific deliberations and the exemplary standards of planning and execution that went into arranging this meeting.

The 10th Structured Training Programme (STP) of the ISRO-STP

The 10th Structured Training Programme (STP) of the ISRO-STP Calendar for the year 2018-19 was successfully conducted at Physical Research Laboratory(PRL), Ahmedabad during 4-8 February, 2019.



Delegations of STP 2019.

The theme for this ISRO-STP was "Recent Advances in Scientific Research in the Earth, Planetary and Space Sciences using Ground and Space-based data: Global Perspectives". A total of 40 scientists and engineers from 17 different centres of DOS/ISRO participated in the ISRO-STP 2019. Further, new JRF's and UN-CSSTEAP students at PRL were also invited to attend lectures. In the inaugural

address Dr. Anil Bhardwaj, Director PRL welcomed all the participants and highlighted the importance and themes of the ISRO-STP 2019. About 22 distinguished scientists from ISRO centers, other reputed institutions and universities of India were invited to deliver talks in different sessions covering various themes of the program. These talks were organized during 10 different sessions, chaired by the eminent scientists of PRL. Noteworthy events comprising of first PRL–IAPT Dr. Vikram Sarabhai Lecture by Dr. Anil Bhardwaj, Director, PRL and Special Colloquium by Dr. Shailesh Nayak, Director, NIAS were also organized along with ISRO-STP 2019 at PRL. The Project work was an important component of the ISRO-STP program. All participants, in a group of 6-7, very enthusiastically completed their project work on eight different topics mentored by the scientists of PRL as project mentors with different fields of expertise. On 8th February, the ISRO-STP 2019 concluded after evaluation session, feedback session, distribution of certificate and memento to all participants by the director PRL. The contributions of students (JRF/SRF), postdoctoral fellow and PRL staff members were important in the success of the ISRO-STP 2019. ISRO-STP 2019 organizing team comprising, Dr. Som Kumar Sharma (Chair), Dr. Lokesh Kumar Sahu, Dr. Neeraj Srivastava, Dr. Arvind Singh and Dr. Vishal Joshi worked coherently with the Chair, PPEG, Dr. R D Deshpande for a successful ISRO-STP, 2019 at PRL.

Activities on the promotion of Basic Sciences

PRL – IAPT Dr. VIKRAM SARABHAI Lecture

The first 'PRL – IAPT (Indian Association for Physics Teachers) Dr. VIKRAM SARABHAI LECTURE' was been arranged at on 07 February 2019 at PRL Ahmedabad. The lecture was delivered by Dr, Anil Bhardwaj, Director, PRL on a topic ' Indian Planetary missions'. The lecture was attended by the participants of structured training programme, students, teachers, IAPT members and PRL fraternity.

This lecture will be published in annual Physics magazine 'Pragaami Tarang', being brought out regularly for the last ten years by the IAPT Regional Council RC-7, Gujarat.



First PRL – IAPT (Indian Association for Physics Teachers) Dr. VIKRAM SARABHAI LECTURE at PRL, Ahmedabad.

Celebration of World Space Week - 8-9 October 2018

In its responsibility towards popularization of Science, PRL has always been on the front foot. About 900 students participated in the World Space Week celebrations at PRL during 8th and 9th October. On 09 October 2018, World Space Week celebration was organized at the Udaipur Solar Observatory (USO) campus.



Celebration of World Space Week at PRL Ahmedabad, 8-9 October 2018.



Celebration of World Space Week at USO, Udaipur, 9 October 2018.

For this event, meritorious students of classes VIII to XII and their science teachers were invited from five state government owned schools located in the Udaipur city and the neighboring rural areas. This programme began with a lecture in Hindi language highlighting the importance of World Space Week, the beginning of space science programme in our country on global scale, the journey of its progress and the current programme and applications. This was followed by a lecture in Hindi on the Sun covering the solar structure, solar activity and the space weather. The participants inquisitively attended the lectures and showed keen interest in space science. Later on, the participants were explained the structure and working of solar telescopes along with the real time images of the Sun and the presence of dark absorption lines in the solar spectrum. This was followed by the visit to the GONG telescope site at USO, where the participants got the opportunity to visualize the online images of the Sun in photospheric Doppler velocity, chromospheric Hydrogen-alpha and the photospheric magnetic map of the solar disk. The participants also visited the recently installed e-Callisto radio telescope site inside the USO campus. In the end, the participants were explained the working and usage of the "astro-kit" which comprised of Sun-dial, Direction-finder, locating stars in the sky, and their identification. The outreach team distributed necessary material to the participants for making astro-kit at home for creating interest in their mind towards astronomy. All the participants were delighted to gain knowledge about space science, the Sun and the stars, and the space science programme in our country. USO arranged suitable transport for the pick-up and drop-off of the students/teachers from their respective schools apart from providing lunch during these celebrations.

National Science Day (NSD) 2019 celebrations

National Science Day (NSD) in India is celebrated on 28 February each year to mark the discovery of the Raman Effect. The major focus of the NSD celebration is to widely spread the message about the importance of science in the daily life of people. As a result, this event is celebrated all over the country in schools, colleges, universities and other academic, scientific, technical, medical and research institutions. PRL celebrated NSD on 02 March, 2019 by conducting various competitive events among the students selected through a screening test conducted on 20th January, 2019. Five students were awarded the Aruna Lal fellowship selected through personal interview. Unlike previous years, this year screening test in online mode along with the offline mode was initiated with the aim to facilitate the students to appear from their school without travelling to exam centres, sometimes situated at a far distance. In total, 152 students were selected to participate in various events organized in PRL. **Additionally, to popularize girl child education PRL invited 151 girl students from schools across Gujarat to visit PRL.** Centre toppers of the 14 exam centres were also awarded prizes. In addition, 12 for poster/model competition were also given to the students who presented their models/posters on the topics i) Sequences and series in nature, ii) IOT-your idea of improving human life.



Celebration of National Science Day, 2 March 2019.

Science Express

To mark birth centenary of Dr. Vikram A. Sarabhai, the father of the Indian space programme, National Science Day 2019 team at PRL has planned to organize science exhibition/demonstrations at different places of Gujarat and Rajasthan in co-ordination with local schools/community science centres. The motive is to reach out to the general public and students and share the excitements of science.

Around 30 volunteers from PRL, primarily PhD students, spending their time in a very special way demonstrating 20 odd experiments and interacting scientifically with numerous students, kids and common people. These experiments are setup by different divisions of PRL to demonstrate different aspects of science, such as, anti-gravity, roller coaster, light guiding, optical cloaking, light polarization, super conductor, liquid nitrogen, light box, radio meter, aspects of theoretical physics, thermohaline circulation model, experiments demonstrating the Lenz's law and Bernoulli's laws, twinkling effect, imaging in telescope, pulser model, shock tube, payload description of solar X-ray monitor, alpha particle X-ray spectrometer on Chandrayaan–II, hands-on with astrokit and astronomical activities, sky spectra poster, sun photometer and Gale crater model, Mars.

On 22 January 2019, the third stop of the Science-Express was arranged in Ravindra Nath Tagore School and College, Kapasan, a remote place, one and half hours of drive from Udaipur towards Chittorgarh, Rajasthan. An exhibition showcasing different scientific activities ongoing at PRL along with popular lectures by Prof. S. Mohanty and Dr. K. Acharyya, were organised. These were well received by more than 1000 students attending it. On 23rd January, the Science-Express reached the Govt. Senior Secondary School, Badgaon, a remote corner of Udaipur. About 600 students attended

the exhibition, starting from early morning. They were extremely excited to learn from this scientific exposure at their doorstep. The Express ignited curiosity in minds of all the children.



Glimpse of Science Express at Dhrol, Gujarat.

Science Express team has so far presented their demonstration in Dhrol-Jamnagar, Rajkot, Udaipur, Kapasan, Bhavnagar, Una. Science Express has received an overwhelming response from the students, teachers and common people with an estimated footfall of more than 7000. To do so, around 30 volunteers traveled more than 2000 KM for 45 hours. This effort can be summarized by 1230 working hours of volunteered contribution in demonstration and talk, toward this cause excluding the travel and stay period.

VOICE 2019 (Vikram Sarabhai cOmpetitIon for Concept-Essay Writing VOICE – 2019)

The VOICE 2019 (Vikram Sarabhai cOmpetitIon for Concept-Essay Writing VOICE – 2019) was a pan-India level essay competition organized for the school children in two categories. Category-I for 8-10 standard students, the theme of the essay was “Home at a distant planet.” Category-II for 11-12 standard students, the topic was “Design innovative experiments for space station.” PRL had received about 1000 essays from 24 states and union territories, with more than 50 % participation from the girl students. After three rounds of evaluation, 30 students from the category I and 20 students from category II, were invited for presentation at PRL which covered 14 different states. Cash prize and certificate was awarded for 1st, 2nd, and 3rd position along with special mention prizes in each category.

Vikram Sarabhai Innovation Competition (VISION) 2019

Vikram Sarabhai Innovation Competition (VISION) 2019 is a national level competition organized by PRL to commemorate the birth centenary year of Dr. Vikram Sarabhai. The concept of VISION-2019 is to promote experimentation in the physical sciences among the science and engineering college students. Project proposals were invited from B.Tech./B.Sc./M.Sc. etc. students which could be executed within 6 months in their colleges. The project grants up to Rs. Three Lacs (Rs. 300000/-) is to be given to the shortlisted proposals. First, Second and Third prizes of Rs. Three Lacs, Two Lacs and One Lac are also to be given to winner teams, on the successful completion of the projects.

The competition opened in February 2019 and total 121 proposals were received in the VISION-2019 program from all over India including several IITs, IISERs, NISERs, NITs, Central and State Universities, government and private engineering colleges etc. 7 proposals were rejected due to improper format/incomplete information etc.

Rest 114 proposal were comprehensively reviewed through a multiple level screening process. 25 (out of 114) proposals were then selected and were reviewed by the domain experts (both within and outside PRL). 29 PRL faculties from all the research divisions and 9 external reviewers (from IISc, NCRA-TIFR, VSSC-ISRO, National Institute of Hydrology-Roorkee, IIT-Kanpur, IIT-Gandhinagar, Ahmedabad University, NPRL-CSIR) reviewed the selected 25 proposals as domain experts. Each of the 25 proposals was reviewed by two experts independently and review reports were provided. The above selected 25 proposal, along with their domain expert’s reports, were further reviewed and deliberated by 11 members Screening Committee consisting 6 PRL and 5 external (from IIT Gandhinagar, IPR, SAC-ISRO) members. The screening committee recommended 11 proposals to be invited at PRL for in-person presentations. 11 VISION proposal teams will be invited for their proposal presentation in May 2019.

The 11 teams invited teams will be from IIT-BHU, IISERs (Kolkata and Tirupati), NITs (Tiruchirappalli and Durgapur), NISER-Bhubaneshwar, Osmania University, two private universities (Thapar University Patiala and GD Goenka University Gurgaon) and Rajalakshmi Engineering College, Chennai. The teams are currently working on the projects in their college and would be called again to PRL for final round of the competition by the end of the year 2019.

NSD celebrations at Udaipur Solar Observatory, Udaipur:

National science day was celebrated at Udaipur on 25 March 2019. On the occasion, the PRL-jointly with the Vidya Bhawan Society, Udaipur-organized a stimulating public lecture by Dr. Anil Bhardwaj, Director PRL at Vidya Bhawan School in Udaipur. The lecture, entitled “Indian Planetary Missions” highlighted the achievements and discoveries by Indian space missions and was highly appreciated by the audience which mainly comprised of students. After the lecture, some science experiments were demonstrated to the school students by the PhD students and post-doctoral fellows of the Udaipur Solar Observatory, PRL along with the members of the science express team of PRL. The total number of audiences was well over 500. In addition, a press meet was organized where Dr. Bhardwaj interacted with the media. There was an active participation from the students from different academic institutions of Vidya Bhawan Society, who also showcased their knowledge and interest in space sciences by presenting posters. The best ten posters were rewarded by Dr. Bhardwaj. The program also comprised an open session of scientists with the audience where interactions were focused on diverse aspects of science ranging from its societal to everyday impact.



Celebration of National Science Day, 2 March 2019.

Celebration of International Day of Women and Girls in Science on February 11, 2019

On the occasion of the International Day of Women and Girls in Science, an all-women team of USO visited Heritage Girls School, an all-girls residential school, about 20 km from Udaipur City. The program included talks on "The International Day of Women and Girls in Science" by Prof. Nandita Srivastava, "Introduction to Our Star: the Sun" by Ms. Sangeeta Nayak, "Women's contribution to Science and Technology Development" by Ms.Bireddy Ramya, "How to become a Scientist: career opportunities for research" by Ms. Kamlesh Bora. A poster was presented by Ms. Anisha Kulhari on few women scientists as well as facts and statistics of the participation of women in Science. Presentations were also made by school children on two topics– Efforts to Enhance the Contribution of Women in Science (Class XI & XII), and Space Exploration Benefits our world (Class IX and X). The best presentation from each category was awarded.



Glimpse of Science Express at Dhrol, Gujarat.

Outreach Activity: Visits to the island observatory and GONG instrument site

In the year 2018-2019, the Outreach Committee of USO organized several visits of groups of students, mainly from Colleges. These student groups visited the Multi-Application Solar Telescope (MAST) located on the island in the Fatehsagar lake and also visited the Global oscillation Network Group (GONG) site and the e-CALLISTO facility in the office campus. The visits were organised on the basis of the requests received from various colleges in India. These include MSc students from Ganpat University, Ganpat Vidyanagar, Marwadi University, Rajkot, Gujarat, Tolani College of Arts & Science, Adipur, Kachchh, Gujarat and B.N. College, Udaipur. Like previous years, the selected winners of Astronomy Competition held for school students by Aryabhat Foundation, Bhopal, were sent to USO on an educational trip in May 2018. Students from St. Anthony's School, Udaipur and participants of UN CSSTEAP Space Science school also visited the island observatory and other solar observing facilities in USO. In total, USO team reached out to approximately 200 students/visitors in the year 2018-2019 during their visit to the observatory.

Apart from the visits organised at the observatory, the outreach team also stepped out and planned visits at different venues to reach out to a wider student community. In this context following efforts made by the USO outreach team are worth mentioning.

Outreach Activity: Visits to the IR observatory, Mt. Abu

Ten students & three faculty members of PTS College of Science, Surat visited the 1.2 m Infrared Telescope on 14th February 2019. They got familiar with the various scientific observations carried out at observatory. They were also explained about the working of various instruments, data recording & control systems of the telescope.

PRL Student chapter

PRL student chapter was formed on 15 June 2015. Currently the chapter has 40 PhD student members from different divisions of PRL. Although the PRL student chapter started with the vision of popularizing optics and photonics among the school and college students through hands on experiments, however, with time the chapter has expanded its scientific portfolio by incorporating hands on experiments from other branches of science. So far the PRL student chapter have devised more than 50 hands on basic experiments to explain many phenomena in our daily life. The major activists of the student chapter during 2018-2019 are as follows.

Visiting remote school

As part of PRL outreach activities the National Science Day celebration team 2019 started Science Express event with the motivation to reach the rural students across Gujarat and Rajasthan to demonstrate scientific activities of PRL through various exhibits and encourage young generation towards science. The idea of this event is conceived from the outreach activities of PRL student chapter to access remote places. As a result, the student chapter members (current strength of the chapter is 40) have contributed whole heartedly in this event to visit six places, Dhrol, Rajkot,

Bhavnagar, Una in Gujarat, and Kapasan, Udaipur in Rajasthan. The Science Express has received an overwhelming response from the students, teachers and common people with an estimated footfall of around 6000. We have restricted the age group of the students in the range of class six and above. During the six days of event in those six places, science express team has so far travelled for around 39 hours covering more than 1800 km, demonstrated more than 20 experiments simultaneously over 40 hours and also arranged 2 hours of popular lecture accommodating 800 students.

Demonstration during NSD and open house activity of PRL

Like previous years, our student chapter members as part of Science Express event demonstrated their hands-on experiments to the students participated in the National Science Day (NSD) activities organized by PRL on 2nd March 2019.

Swachhta Pakhwada Celebration 2019

Swachhta Pakhwada-2019 was celebrated during 01.02.2019 to 15.02.2019 at PRL. The theme of this year's campaign was "Plastic Free Campus" and the event saw several innovative programmes to create awareness for a clean and healthy workspace and residences. To begin with, a mass pledge was taken by PRL employees to contribute to the Swachh Bharat Campaign, arrangements for e-pledge were also made, in which about 100 people participated. A lecture on "Weeding out of records" was delivered by Shri Sangeet Mishra, Sr. Admin. Officer, SAC, Ahmedabad. Keeping in view this year's theme, a competition was announced for giving innovative ideas/models on the theme "Alternative to Plastic PET Water bottles". Also, a drawing competition on the Theme "No Plastic & No Tobacco" was conducted at Thaltej campus for the Children of PRL Employees and CISF Employees. In addition, cleanliness campaign along with plantation of saplings was carried out in Navrangpura & Vikram Nagar PRL residential colonies. Residents of both the colonies along with students from Navrangpura Hostel had participated in large numbers for sloganeering, plantations etc. A similar campaign was also carried out at PRL Thaltej Campus. During the fortnight-long campaign, an Awareness lecture on "No Plastic and No Tobacco" was delivered by Dr. Samir Dani to the Contract workers of PRL. Dr. Dani apprised them of the health hazards of using Tobacco based products and expenses involved in treatments of ailments caused due to Tobacco use. The workers pledged not to use any form of tobacco. A Medical Camp was organised at Ramdev Nagar slum Area in Ahmedabad by the Medical Team at PRL. The main focus was on hygiene and women health. A large number of slum dwellers especially women took part in the Camp. A Medical Kit consisting of First-Aid material was distributed among the slum dwellers for their daily use. Solar LED system was commissioned by Director, PRL, as a step towards using green and renewable energy. The programme concluded with a formal prize distribution ceremony to the children who participated in the drawing competition.

Vigilance Awareness Week 2018

The 'Vigilance Awareness Week' was observed in Physical Research Laboratory, Ahmedabad from October 29 to November 3, 2018 and the Pledge has been administered to staff members of PRL on 29th October 2018.

The banner and various pamphlets with regard to Vigilance Awareness were displayed at prime location of Physical Research Laboratory, Ahmedabad. An essay writing competition on "Eradicate Corruption-Build a New India" as a part of vigilance awareness week was also organized on 1st November, 2018 at PRL, Ahmedabad and an awareness lecture was arranged on 2nd November, 2018. The lecture was delivered by Mr. Jaypal Singh Rathore, IPS, Deputy Commissioner of Police, Zone-I, Ahmedabad.

Celebration of International Yoga Day at PRL

The International Day of Yoga, a "Yoga" Session in Physical Research Laboratory, was organised at PRL Main Campus, Udaipur Campus and Mount Abu Campus on 21st June, 2019 at 07:00 Hrs. There were about 100 participants in the session and all had participated Yoga enthusiastically. A Trained Yoga Instructor was invited for yoga session. The session was attended by the Registrar, Mr. Chavali V R G Deekshitulu who encouraged and motivated all staff members and Research Scholars to actively participate and practice Yoga on regular basis in our day-to-day life and brightened the event with his presence.

Internal Complaints Committee

Since inception in 2010, the PRL Internal Complaints Committee has been meeting at regular intervals to discuss and plan activities as well as strategies to make sure that the workplace is women friendly. The Committee has organized several awareness seminars and talks on gender sensitization for PRL employees. The ICC at PRL makes sure that the policy is communicated to all PRL women employees and display details of the dedicated officers on all its notice boards. A web page on Internal Complaints Committee has been also set up on the PRL website. ICC members are also deputed to attend workshops on prevention of sexual harassment of women at workplace from time to time. During 2018-19 following activities were undertaken:

- On 21 September 2018, ICC members had an interactive session with women employees of USO and Mt Abu Campus
- On 30 November 2018 an informal interactive session was arranged to familiarize the new women entrants about the sexual harassment at workplace. In addition, two talks were delivered – one on gender sensitization by Dr. Indu Capoor and one on nutrition and wellness by Dr. Arti Kodani.
- On 8th March 2019, International Women's Day was celebrated with great enthusiasm. Dr Anil Bhardwaj, Director PRL had an interactive session with all women employees of PRL. He welcomed suggestions to improve the work environment for women employees. This was followed by IWD celebration with entire PRL community comprising of a cultural programme, a welcome speech by Mr. Deekshitulu, Registrar, PRL and a very inspiring

talk by Ms Ruzan Khambatta, a social entrepreneur, Founder, Force Empowerment Foundation. The Director in his speech emphasized on the importance of giving equal opportunity without any bias.

- Three women staff members (Ms Sneha Nair, Ms Jaldhi Mehta and Ms Ishita Shah) were nominated to participate in the IWD celebration held during 8-9 March 2019 organized by one of the ISRO units – ISRO Propulsion Complex (IPRC), Mahendragiri. They found the experience of meeting, interacting and sharing of views with 134 ISRO women employees very enriching.

In addition to these, Prof Srubabati Goswami and Ms Pauline Joseph attended the workshop on Prevention of sexual harassment at workplace organized by NAHRD at Mussoorie during 30 April – 1 May 2019. For the period April, 2018 to March, 2019, no complaints on sexual harassment have been received by the ICC.

Celebration of Ambedkar Jayanti at PRL

The 128^{th} Birth Anniversary of Dr.Babasaheb Bhimrao Ambedkar was celebrated in Physical Research Laboratory on 14th April, 2019. The programme commenced with lighting of lamp and offering floral tributes to Babasaheb's photograph. Dr. Anil Bhardwaj, the Director, PRL recalled the significant contributions of Babasaheb towards shaping up of today's India. He opined that unless life of people in villages and remotest parts of our Country are improved, the real vision of our forefathers may not see reality. The changes in our social set up towards equality and education would be the real tribute to the views of Bharat Ratna Dr.Babasaheb Ambedkar.

Sh. Chavali V R G Deekshitulu, Registrar, PRL and Professor Dr. Angom Dilipkumar Singh, Liasion Officer PRL participated in the event. Beside, a few faculty members and officers of PRL participated enthusiastically.

Status of Scheduled Caste/ Scheduled Tribe Personnel as on 31/03/2019

Centre/ Unit	Total Strength of Employees 2018-19	Strength of SC Employees	Strength of ST Employees	Strength of OBC Employees
PRL	256	7	1	20

Status of Differently Abled persons as on 31/03/2019

Centre/ Unit	Total Strength of Employees	Strength of Differently Abled Persons	Classification of employees with Disabilities			
			Deaf and Dumb	Blind	Partially Blind	Orthopedically Handicapped
PRL	256	5	1	0	0	4



Glimpses of various events and activities by PRL.

Capacity Building Programmes

RESPOND Programme

Physical Research Laboratory (PRL) administers the Indian Space Research Organization (ISRO) RESPOND programme to provide funding to academia in India for conducting research and development activities related to Space Sciences, particularly in the fields of Astronomy and Astrophysics, the Physics of Earth's atmosphere/ionosphere, Solar Physics, Space Weather, and Space Plasma Physics. The main aim of the RESPOND programme is to encourage quality research in areas of relevance to the Indian space programme.

RESPOND programme at PRL mainly supports space sciences research in university, college and national institutes. The main deliverables of the RESPOND programme at PRL have been publication of research papers in international and national refereed journals, training of manpower and PhD theses. The proposers also seek funding for augmenting computational facilities; occasionally the RESPOND grant is also utilized to set up a new laboratory facility for research at the university or the host institute.

During 2018-2019, PRL received about 17 proposals for possible funding through RESPOND programme, out of which 5 have been approved, 10 are at different stages of review and recommendation process. Two proposals were redirected to other ISRO centres for review and few were not selected. The total number of ongoing projects in 2019 is 17. Some of these new proposals are aimed at scientific investigations based on observations of ISRO's astronomy satellite, i.e. ASTROSAT. A few proposals in the upcoming field of Astrochemistry have also been received. Many projects aimed at providing theoretical modeling support to various problems in Space physics, Astrophysics and Earth Sciences have been received at PRL. The recipients of project funding through RESPOND, mainly include researchers from Universities/Colleges, national research institutes, and also from IITs. In September 2018, 8 research topics were submitted by PRL scientists to the RESPOND basket programme in response to a call by ISRO. The RESPOND basket proposals comprise a set of most urgent and immediate research areas for the academia to select and prepare detailed proposals on priority basis.

UN Course on Space and Atmospheric Science

A nine-month Post-Graduate Diploma Course in Space and Atmospheric Science is conducted every alternate year at Physical Research Laboratory (PRL), Ahmedabad under the auspices of Center for Space Science and Technology Education in Asia and the Pacific (CSSTEAP). CSSTEAP has headquarters in Dehradun and is affiliated to the United Nations. So far 11 courses have been conducted and 123 participants from around 20 countries in the Asia-Pacific region have benefited. In suitable cases this course leads to an M.Tech. degree on fulfillment of the requirements of the Andhra University.

Official Language promotion at PRL

Activities on the Promotion of Official Language

- Hindi Technical Seminar organized on 02 May 2018
- An online competition was organized by PRL on behalf of TOLIC on May 24, 2018
- OLIC meeting on June 26, 2018
- Hindi Workshop organized on June 26, 2018
- On the occasion of World Space Week scientific lecture was organized for school children
- Hindi Essay Competition was organized on 01.11.2018 during Vigilance Awareness Week
- On the occasion of World Hindi Day Hindi Essay Competition and talk on medical issues were organized
- Release of Hindi Patrika 'Vikram' July 2018 and January 2019 Issues.
- Participation of members of PRL Hindi section in the Hindi Technical Seminar held in Space Applications Center on 26.07.2018.
- In the 72nd half-yearly meeting held in National Design Institute, Ahmedabad, on 16.08.2018 Chairperson and members of Hindi section were present. The TOLIC prizes were also given for the online competition "Shabd Se Kavita Tak". Hindi Pakhwada was organized during 14-28 September in which Hindi Essay, Hindi Bhasha Gyan, Dainik Prashnottari, Sulekh, Hindi typing, Word Quiz, Hamara Karya, Swarachit Kavita Path etc. competitions were organized.
- PRL OLIC meeting was held at Udaipur Solar Observatory on 21.09.2018.
- Hindi Workshop organized on 21.09.2018
- Scientific lectures in Hindi organized on 8-9 October during World Space Week
- Hindi Essay Competition organized during Vigilance Awareness Week.
- Smt, Rumkee Dutta, Sr. Translator got First prize for best presentation in the official language session during the Inter-Center Hindi Technical Seminar held in NRSC Hyderabad on 15 November.
- Participation of PRL staff members in various TOLIC level competitions.
- Participation of member of Hindi section in Orientation competition held in Chandigarh on 7 December and got prize in typing competition.
- OLIC meeting was conducted on 17.12.2018 at Mt. Abu and Udaipur.
- Hindi Workshop organized on 21.12.2018
- Parangat training of two members completed.
- Hindi Essay Competition and Health Related Lectures on World Hindi Day.
- TOLIC meeting held on 25.01.2019 attended by HOD, PRL
- Hindi Patrika Vikram released on 26.01.2019
- Translation of question papers for scholarship exams of National Science Day.
- Translation of question paper for recruitment of Scientific Assistant
- Participation of three members in the Hindi workshop organized by SAC, ISRO, Ahmedabad on 14 March,2019
- OLIC meeting was conducted on 26.03.2019 at Udaipur.
- Hindi Workshop organized on 28.03.2019
- "Modeling of South Asian atmosphere during winter", a talk given by Dr. N. Ojha, Hindi Technical Seminar, 2019-04-05

Facilities and Services

Computational Services Group

The Computational Services Group (CSG) is responsible for providing services/facilities like Networking (Internet, Local Area Network, Wifi, SPACENET), High performance Computing, E-mail, Web, DNS, Proxy, VPN, Centralized Printing, DHCP, Video Conference, software development and maintenance. Following services/facilities are added/upgraded/provided during the year 2018-2019.

[A] Web Site/Web Application:

1. Newly Developed Main PRL Website

Computer Centre has designed a new website of Physical Research Laboratory both in Hindi and English.

Following are the new features of website: The website is designed using latest Content Management System (CMS) – Drupal The website has Responsive Design i.e. easy to navigate on devices like smartphones There is no impact on the division web pages managed by respective divisions. Still they all are covered under responsive design Ease in the management of the website. Link of PRL uploaded movies from Amazon Web Service (AWS) Cloud. The site has also following New Captions: - Projects/Programs - Latest Happenings - What's New - Vikram Patrika - PRL News – The Spectrum - PRL's Facebook and Twitter page link



Figure 1: New PRL web site

2. Online Examination Software for National Science Day

Software has been developed to conduct online examination over Internet for National Science Day organized by PRL. Total 196 students from 32 school appeared for online examination mode on 20/January/2019. To provide support during online examination, Two Help Line numbers for the schools has been provided.

3. Online Quiz Competition Software – Hindi Pakhwada

Software has been developed to conduct competitions like Daily Quiz, Hindi Gyan, and Hindi Typing online over PRL Intranet during Hindi Pakhwada.

[B] Internet and Intranet

1. Upgradation of Disaster Recovery Site and Virtual Infrastructure

Since 2014, all the IT services/servers were running on the Virtual server environment and consolidated all the services to just three servers. Which provides key benefits like; (1) Server Consolidation (2) Easy and hassle free Management and Deployment which increases Reliability and Availability (3) Immediate and fast Redundancy, Backup and Recovery (4) Facilitates Better Disaster Recovery (5) Easier Migration to Private Cloud services and many more.



Figure 2: Disaster Recovery Site of IT Services (Thaltej Campus)

Apart from this, to comply with Cyber Crisis Management Plan(CCMP) of DOS/ISRO, PRL's Disaster Recovery (DR) site was established using available resources at Thaltej campus in 2017, as a fail-safe backup mechanism to mitigate any catastrophic disastrous event at the Main/Navrangpura campus Site (Primary Site). Entire DR Site and Uplink network connectivity is supported by uninterruptible power supply backup facility with minimum capacity of 32 KW (N+1) with frame size minimum 48KW modular fail-safe UPS. It is further backed up by 160KVA DG set to handle longer duration power failure incidents/events for uninterrupted DR site replication operations.

Many new services and virtual servers were added to facilitate PRL

scientific community, which has increased our CPU, Memory and storage requirements. So the virtual infrastructure has been upgraded to newer machines that have 24 cores CPU, 512GB Memory, and 100TB storage capacity. The infrastructure has been upgraded at both the sites to maintain the technical compatibility.

2. Upgradation of Network Switches

To improve the Intranet connectivity services, edge network switches has been replaced at various location in PRL. To provide failsafe redundancy, the core switch and distribution switch has also been installed and configured. The new switches have various new security features like Loop Avoidance, DHCP Snooping.

3. Live streaming setup over Intranet, Intranet and PRL's Facebook Page

A setup has been established to perform live streaming of various events organized in K R Ramanathan Auditorium for viewers over Internet, Intranet. The setup also provides live feed to PRL's Facebook page.

Library and Information Services

Library and Information Services plays an important role in catering to the information needs of the PRL researchers and staffs, these information services are being provided in all the campuses of PRL. To name a few important ones, documents (books, journals, CDs) lending services, Online Access (intranet and through remote access) to Institutional Repository, E- journals, Theses, E-books, Archives, Technical Reports etc. Library also provides the Newspaper Clipping Service, Inter library loan facility, Plagiarism Check facility through Ithenticate tool, Reprographic facility, Information display through Digital Notice Board, Book procurement for research scholars and Current Awareness Service, Discovery service etc. The updates and additions to the library during the year 2018-19 are mentioned below:

Statistics

In the year 2018-19, there has been an addition of 256 Scientific, 22 General and 83 Hindi books and 42 CDs/DVDs to the collections of three libraries in Main, Thaltej and USO campuses. 5334 visitors visited the library during the year and the document circulation saw an issue and return of 1438 and 1443 respectively. The Library provides Inter Library Loan (ILL) service for its users and to other Institutes as well, 101 ILL requests were fulfilled by PRL and 24 articles were sought from other institutes. Students availed book grant book purchase facility through the Library and 33 book grant requests were processed this year. The reprographic service of the library is high in demand where the library facilitated 43758 photocopies in-house along with 112841 photocopies from outside agency. 346 e-books are available and 194 journals are subscribed out of which 185 are online.

Library Webpage

PRL Library continues to have access to full-text databases like AGU Digital Library, GSA Archive, PROLA, Science Archive, SPIE and IEEE Digital Library. The Library homepage gives access to the digital content subscribed by PRL as well as the open access content. The PRL library also subscribes to 'Discovery Tool' which searches a topic through all the journals simultaneously with filters like full-text and peer reviewed.

Plagiarism Check Facility

Library is responsible for carrying out the similarity check for students using the Ithenticate tool. They avail this facility before submitting the thesis; users also get their content checked for originality for the research papers they submit to various journals.

Digital Notice Board

It is maintained by the library to disseminate information about PRL activities like division seminars, colloquia, public talks, images of events like Republic Day celebration, Women's Day celebration, etc. In addition, list of recent publications of PRL scientists, new books added to the library collection are also displayed in three campuses simultaneously through the LAN. Mt. Abu campus will be linked soon.

Institutional Repository

The Institutional repository maintained by the Library consists of journal articles published by the PRL authors from 1990 to present and is also linked through the Library homepage. About 4300 articles by PRL authors are now part of this repository. All the PRL theses from 1952 onwards (414) are now available full text for PRL users. All the Technical Notes since 1977, published by PRL have been digitized (110) and are available full text for PRL users. Currently, Library is carrying out the digitization of the photographs archive. Scanning of the photographs of 250 albums is completed. Giving the captions and metadata for each photograph for easy retrieval is in process using the digital library software - Greenstone Digital Library (GSDL).

Library Outreach

Library organized a book exhibition in Thaltej campus in March' 2019 so as to facilitate the researchers and students to suggest books for Thaltej library and also to procure books using their academic allowance. More than 120 books were recommended for addition to the library collection.



Figure 3: Books Exhibition at Thaltej Campus

Workshop

ASPEX PAYLOAD FABRICATION (ADITYA L1 MISSION)

Manufacturing of mechanical component of engineering model of ASPEX payload has been carried out completely in house. ASPEX payload of ADITYA L1 mission consist of mainly two sub systems namely SWIS and STEPS. ASPEX payload is having total 7 different packages namely, THA1, THA2, HV, PE, STEPS1, STEPS2A and STEPS 2B. More than 291 new components fabricated with tight assembly tolerances. During the testing of engineering model of the payloads many components have been revised and fabricated to facilitate end to end testing of the payload.

- Langmuir probe

- CFRP Dewar for NISP

- Other Fabrication supports for various lab test setups.

Sr. No	Package	Verities of Components	Total Mechanical Components
1	THA1	25	79
2	THA2	10	24
3	HV	9	13
4	PE	10	20
5	STEPS1	34	107
6	STEPS2A & 2B	19	48
Total		107	291

Figure no.4: Table for Total Components Manufactured for ASPEX Payload



HV PE

Figure no.5: Package for HV and PE



THA1 & THA2 COMPONENTS

Figure no.6: THA1 & THA2 Components



STEPS

Figure no.7: Package for STEPS

Aluminum Profile Based Housing for Vacuum Chamber and Electron Gun

Building Aluminum profile based housing of vacuum chamber and electron gun and it would help in performing spectrometer based experiments. These System is mounted on Aluminum profile structure with 200cm length, 107cm width and height to base structure 80cm. The structure is optimized to house vacuum chamber including customized SS based support and an adjustable for support of Electron Gun. All the profile has been used with minimum wastage and optimized usage. A frame for installing Swagelok valves, a housing for all in one desktop have been built. An aluminum design was made for coupling the foot master castor wheels to 90 mm x 90 mm profile. A power distribution board has also been included on the frame in such way that makes the structure professional.

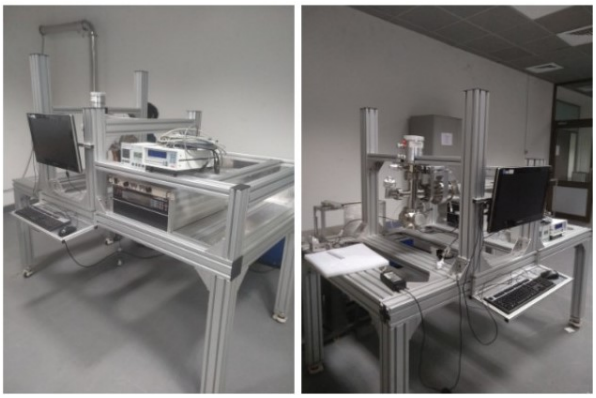


Figure no.8: Aluminum Profile Based Housing for Vacuum Chamber and Electron Gun

Development of New Velocity Map Imaging Spectrometer

For studying the ultrafast molecular physics using femtolaser and charged particle imaging spectrometer, a new Velocity Map Imaging(VMI) spectrometer has been built in PRL. In VMI, the 3D Newton sphere (3D Velocity vectors) mapped on to the 2D detector. This spectrometer can be used for both the electrons and ions. This spectrometer has 11 plates for kinetic energy dispersion control which also help for velocity mapping of high kinetic energy of charged particles.Our multi-plates VMI spectrometer will be suitable for mapping the higher kinetic energy (up to 500 eV) electrons.The design and fabrication of Velocity Map Imaging spectrometer has been performed in PRL's workshop. The photograph of setup and spectrometer plates is shown in figure 9.

Scientific objectives:

- Mapping of velocity of electrons and ions for understanding the molecular fragmentation dynamics.

- This spectrometer will be used in combination of femtolaser for ultra fast science. Based on this spectrometer, the ultra fast processes can be probed based on measured electron/ion velocity map information.

- Perform the electrons/ions imaging experiments and explore the processes in atomic and molecular system.

Schematic diagram of this spectrometer is shown in below.

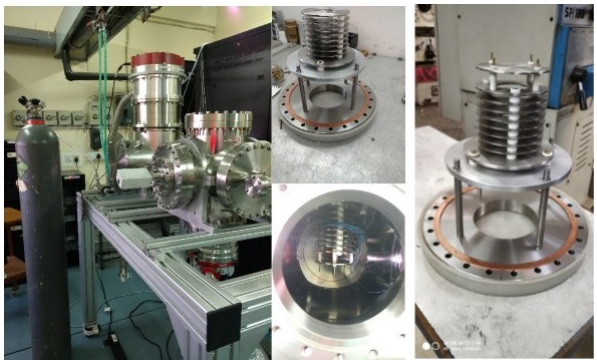


Figure no. 9: New Velocity Map Imaging Spectrometer

The actual Vacuum chambers, Power Supply for Detector & Spectrometer Plates, MCP detector, Turbo Molecular Pumps & Dry Scroll Pumps, Vacuum Gauges and All Mechanical Mounts/Al. Sections are supplied by the FOURVAC Technologies, Pune.Actual dimensions of all the instruments were measured and some of the dimensions were taken from the Drawings supplied by the vendor. Then based on these, the vacuum chambers, Aluminum sections etc. were designed in Solid works and assemble to gather such that center of both the vacuum chambers are in line.And accordingly mounting plates were designed for front vacuum chamber and mounting studs also designed for the back side Vacuum Chamber. After placing the Mounting Plates and Mounting Studs on the Al. Section Table and also placing off both the Vacuum chambers on to it, the model was checked for the centering.

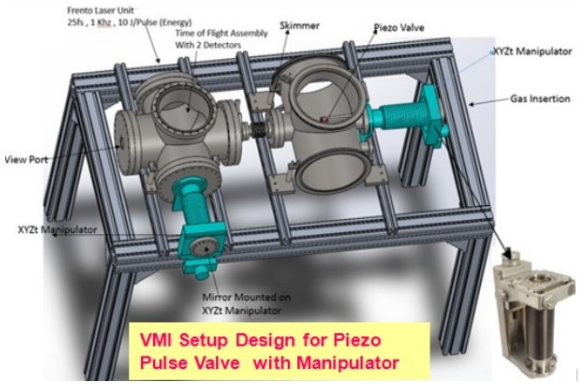


Figure no. 10: VMI Setup Design for Piezo Pulse Valve with Manipulator

The Instrument named as Manipulator with CF 35 Mounting Flange was assembled to one Set up of Configuration and accordingly Vacuum Pumps are mounted on the SS Studs.Another Set-Up of the Mounting of both Vacuum Chambers are also Designed and accordingly new set of Mounting Studs with clamps are completed going as shown in figure 7. As shown in figures, A Laser is penetrating from Femto Laser Unit 25 fs, 1 KHz, 10 mJ/Pulse (Energy)from the left side of the chamber. Opposite side on Femto Unit, a Mirror is mounted on to the XYZt Manipulator. A Laser is propagating on the surface of the Mirror and focused on the Centre of the Vacuum Chamber.

From the side of another XYZt Manipulator, a Gas is injected through Piezo Pulse Valve. And injected in to the Skimmer which converts diffuse gas in to the beam.

Rain water Sampler

The Design and Fabrication of Automated Rain Water Sample Collection is completed to collect High Frequency Precipitation for Hydrology Application. When the Rain is starting at that point of time, These system senses and start the collection of Rain Water. Based on Intensity of Rain & Flow of Rain, These Instrument automatically calculate & sequentially store the Empty Vials of Total 90 in nos. and each of 30 ml capacity. Electronics will take care for, how much Rain water collection is required? When to move forward or Backward for filling the sample bottles, Position Accuracy, Intimation to end user via. SMS for collection of full bottles or Reloading of Empty Bottles, Rotational movement as well Reciprocate movements of the Bottles & Rain water tube, How Remotely you can control and update the status of the instrument etc. You can connect the system with Mobile Communication for updating the status of the system. When all Bottles filled with Rain water, It is in Memory of Hardware that these Bottles are full and accordingly the instrument will work.

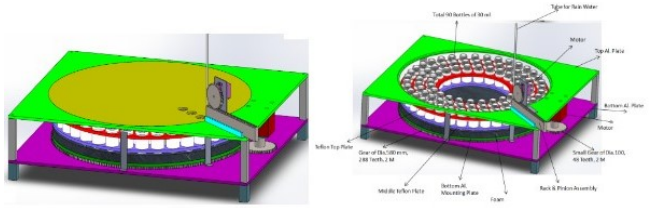


Figure no. 11: Design of Rain Water Sampler

Preliminary the System is checked for Position Accuracy by means of Mechanical & Electronics configuration & Accuracy. To be able to collect the rainwater samples at desired high frequency, mechanical design of an automated rainwater sampler has been developed to match electronics and power design as per the scientific requirements of isotope hydrology programme of PRL.A total 2700 ml of rainwater samples can be collected in total 90 vials, each of 30 ml capacity, at a programmable interval ranging.



Figure no. 12: Rain Water Sampler

All 90 vials are set on Al. disk of Dia. 572 mm such that on inside PCD there are 24 vials then on to next row of PCD there are 30 vials and on to exterior PCD there are 36 vials. Two nos. of Teflon Plates of Dia.572 mm x 10 mm thick with total 90 nos. of holes on each are fitted on to Aluminum plate of same diameter and whole assembly mounted on Gear of Dia. 580 mm, having total Tooth of 288 nos. with 2 modules. A foam is placed in between middle Teflon plate and bottom Al. plate for avoiding any kind of overflow of rain water collection which absorb on to it. Another Small Gear of Dia.100 mm, having a total tooth of 48 nos. with 2 modules which is the main driving gear and fitted with Motor. A Rack & Pinion Mechanism is designed and placed on to the one corner of Top Plate for the purpose of filling of Rain Water. Whenever Rain is started at the same time the rack is in position to the inside row of one of vial such that rain water tube is in center of one vial. After completion of Rain Water filling in first raw, a Rack is in position to the middle raw and same process is continue Up till all 90 vials are to be filled. For exact alignment of rotation of all plates in one plane, Roller Bearings are provided with housing for both the motors shafting. Two nos. of Sensors are provided for the feedback of position accuracy and home position identification for each & Every bottle. A potentiometer is coupled with the shafting of Motor which gives exact feedback of rotation which helps in maintaining the position accuracy of each 90 vials.

Fabrication of a narrow band, narrow field-of-view photometer with Mirror Scanning Arrangement

It was shown earlier that by limiting the spectral bandwidth and field-of-view of a night-glow photometer, it is possible to enhance the signal-to-noise ratio (SNR) significantly so that it's capability to detect small variations in the intensity associated with space weather impact and plasma irregularity events over low latitudes can be picked up unambiguously.

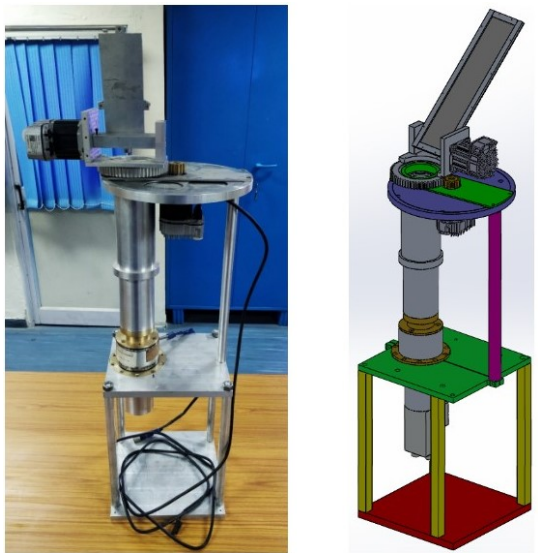


Figure no. 13: Design and Fabrication of Narrow Band-Narrow Field of View Photometer with Mirror Scanning Arrangement

In view of this, a number of portable night-glow photometers were designed and fabricated in PRL in which spectral bandwidth was 0.3 nm and FOV was 3o. However, these portable photometers were not equipped with mirror scanning arrangement so that different parts of the sky could be scanned in quick succession. In the present design, servo motors that can be controlled precisely are used for this mirror scanning system. In addition, the mechanical design of the photometer has been changed completely to bring in more stability

and to facilitate complete automation. The plans are on to introduce filter wheels in this design. Once completed, this miniaturized photometer will be self-sufficient and can be operated remotely.The Mechanical Design and Fabrication of system was completely made in PRL Workshop.

Mechanical Design of Controller Box for MFOSC-P

We have designed two controller boxes, for assembly of the components required for controlling the MFOSC-P instrument. The boxes are designed using Auto Cad software. The hardware is developed fully in house, with the help of PRL workshop. Entire mounting of the components, connectors preparation, wire harnessing and its characterization was done in the PRL laboratory.

Both the boxes have provision for 2 controllers, 8 motor drivers, power supplies, relay PCB, D-type connectors and lamp socket connections.

Controller box version-0:

Its dimensions are: 386 x 206 x 336 (mm). In this design all the 8 drivers are mounted on 2 sides of an acrylic sheet which in turn is fixed with the back plate of the box. Both controllers are also mounted on the back wall, which are insulated from aluminum via acrylic plate. The base plate holds the major power supplies of the system. Encapsulated power modules and switch & sockets are placed on each of the 2 sides of the box. The D type connectors for linking the instrument with controller are provided on the outer side of the rear wall. The relay PCB is supported by the top plate. Slots for AC supply and communicating with software are provided on one the side walls.



Figure no. 14: Controller Box for MFOSC-P Version-1

Controller box version-1:

Its dimensions are: 386 x 210 x 447 (mm). It is a modified form of version-0. The purpose was to provide more space for easy access to components while debugging or monitoring the instrument. The mounting orientation of drivers and controllers has been changed, it is more modular so that each component acts as a standalone unit and can be dealt with individually. Additional D type connectors have been used to provide a better path for wire routing.Apart from these two controllers boxes we have also designed and developed a separate power supply box, to provide isolation between AC and DC signal, and to avoid interference of AC with USB communication



Figure no. 15: Controller Box for MFOSC-P Version-2

CMAP (CCD based Multi-wavelength air-glow photometer) flanged version & Barrel and Lens housing for CDAP (CCD based day time air-glow photometer).

In CCD based Multi-wave Length Air-glow Photometer, Three-cylinder arrangement enclosing optical lenses, the cylinders have flanged joints, Cylinders are of 60mm diameter and lengths of 120,100 and 90mm.

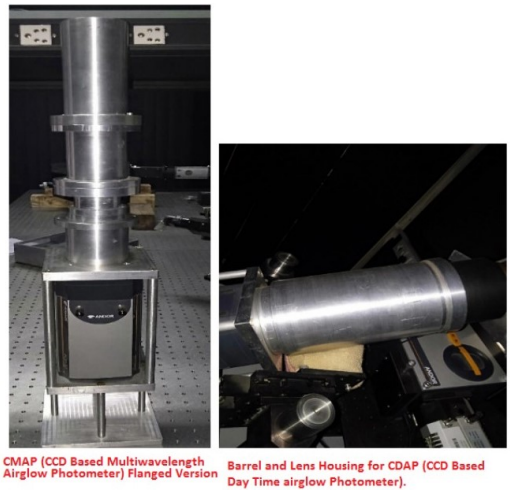


Figure no. 16: CCD Based Multi-wave Length Air-glow Photometer and CCD Based Day Time Air-glow Photometer

Brass housing with lock rings is used for placing lenses. This instrument is used to measure night glow, via focusing images on CCD camera. This instrument is in testing phase. Barrel & Lens Housing for CCD based Day Time Air-glow Photometer is a barrel of size, Dia.=105 mm and height 210mm, the barrel has threads from top to 70mm length, bottom of the barrel is a Dia. of size 75mm having external threads which get attached to CCD stand. PVC lens housing having external threads and having top of cotton fiber encloses the optical lens. The lens inside the barrel is adjusted to get focal point on CCD chip, for day glow Measurement.

Prototype filter wheel development for Near Infrared Spectro Polarimeter (NISP).

Near Infrared Spectro Polarimeter (NISP) is being developed for PRL 2.5m telescope at Mt. Abu. As a part of this instrument development, a prototype filter wheel was designed, fabricated and tested in the laboratory.

The crucial design requirement was that these mechanisms should operate at both room temperature and Cryogenic temperature (around 80K). For precise functioning of the instrument, tolerance and alignment play an important role. A good design would be expected to decrease thermal stresses and strains which ensures smooth movement of the parts. Smart stepper motors are being used for motion control. Since these motors cannot be used at cryogenic temperatures and high vacuum conditions, they will be mounted outside the Vacuum Dewar in ambient conditions. Rotary feed through would be used to transmit the motion to the filter wheels inside the Vacuum Dewar.

Drive Mechanism:

The drive mechanism consists of bevel gear set (4 Nos.) and Spur gears set (2 Big Gears & 2 Small Gears). One of spur gears is used as filter wheel. All the bevels, pinion gear and the filter wheel are made of Brass material. Significant backlash is voluntarily introduced in the gear system when setting the distance between the pinion gear and filter wheel rotation axes. This strategy is to reduce the risk of gripping that could occur if the filter wheel does not cool down as fast as its enclosure.

Spring locking system:

Precise repeatability of the position of the filter wheel is not always possible due to backlash in the gears. It is a simple mechanism where “Vee” grooves are present in equiangular positions on a pitch circle on the filter wheel surface. Every groove corresponds to a fixed filter position. Spring-ball mechanism is being used to lock the ball in the groove. A spring is used to press the ball against the filter wheel surface on the pitch circle. The ball rolls on the surface between two grooves with minimum friction.

Absolute Position:

Absolute position readout mechanism of each filter position improves the filter change time compared to home position method. Magnets and reed-switches combinations were used to get a unique number for a filter. Magnet and reed-switch combination is a passive system with a very high life time. Figure-17 shows the filter wheel assembly manufactured in PRL Workshop and being tested at NISP laboratory.

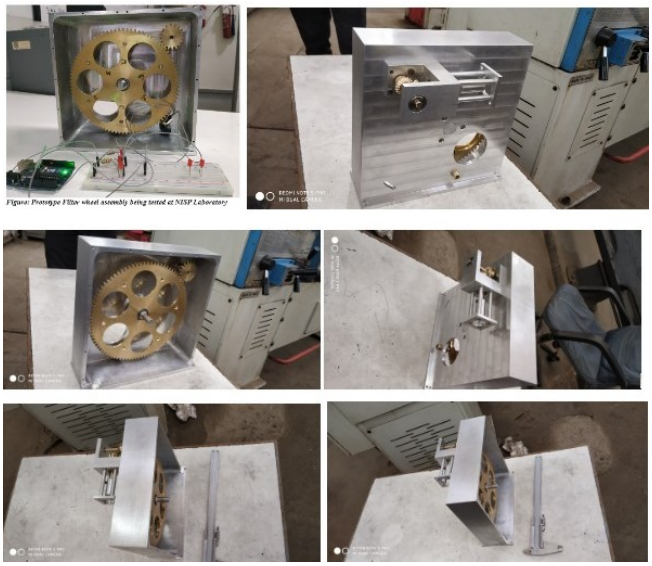


Figure no.:17 Prototype Filter Wheel Development for Near Infrared Spectro Polarimeter (NISP)

Honorary Fellows & Faculty

Honorary Fellows

A. Hewish

J. E. Blamont

K. Kasturirangan

P. J. Crutzen

Honorary Faculty

A. K. Singhvi
FNA, FASc, FNASc, FTWAS
DST-SERB-Year of Science Chair Professor

A. S. Joshipura
FNA, FASc, FNASc
J.C. Bose & Raja Rammanna Fellow

J. N. Goswami
FNA, FASc, FNASc, FTWAS
J.C. Bose Fellow

S. A. Haider
Honorary Scientist - A

M. M. Sarin
FNA, FASc, FNASc
DST-SERB-Distinguished Fellowship.

R. Sridharan
FASc, FNASc, NASI Senior Scientist

Shyam Lal
FNA, FASc, FNASc
J.C. Bose Fellow & INSA Sr. Scientist

S.D. Rindani
FNASc & J.C.Bose Fellow

PRL Faculty

Sr. No.	Name	Designation	Specialization	Academic Qualification	Division
1	Acharyya K.	Reader	Astrochemistry	Ph.D. (2008)	PSDN
2	Adalja H. L.	Scientist/Engineer-SD	Mechanical Engineering	M.Tech. (2009)	A&A
3	Adhyaru P. R.	Engineer-SF	Development of Electronic Sub Systems For Spectrometry	B.E. (1991)	GSDN
4	Agrawal R. L.	Scientist/Engineer-SD	Mechanical Engineering	B.Tech. (2013)	CMDV
5	Banerjee D.	Professor	Thermoluminescence and Planetary Physics	Ph.D. (1997)	PSDN
6	Banerjee S. B.	Scientist-SF	Experimental Molecular Physics	Ph.D. (2012)	AMOPH
7	Basu Sarbadhikari A.	Scientist-SE	Planetary Geochemistry	Ph.D. (2007)	PSDN
8	Bayanna A. R.	Scientist-SE	Optical Instrumentation & Solar Physics	Ph.D. (2015)	USO
9	Bhardwaj A.	Director	Planetary & Space Science	Ph.D. (1992)	ADMDIR
10	Bharti R. R.	Scientist/Engineer-SD	Computer Science	M.Sc. (2003)	PSDN
11	Bhatt J. R.	Professor	Astrophysics	Ph.D. (1992)	THEPH
12	Bhatt M. U.	Scientist-SD	Planetary Remote Sensing	Ph.D. (2012)	PSDN
13	Bhattacharyya R.	Asso. Professor	Plasma Physics	Ph.D. (2006)	USO
14	Bhavsar K. J.	Engineer-SE	Electrical Systems	B.E. (1995)	CMDV
15	Bhushan R.	Scientist-SG	Oceanography and Paleoclimatology	Ph.D. (2009)	GSDN
16	Bireddy R.	Scientist/Engineer-SD	Embedd Systems	M.Tech. (2019)	USO
17	Chakrabarty A.	Professor	Extra-Solar Planets, Star Formation & Instrumentation	Ph.D. (1999)	A&A
18	Chakraborty D.	Asso. Professor	Space Weather	Ph.D. (2008)	SPASC
19	Chauhan N.	Scientist-SD	Luminescence Dating and Luminescence Dosimetry	Ph.D. (2012)	AMOPH
20	Dani S. V.	Medical Officer-SF	Medicine	MBBS (1993)	DISSR
21	Deshpande R. D.	Scientist-SG	Application of Environmental Tracers In Hydrology	Ph.D. (2007)	GSDN
22	Dewangan L. K.	Scientist-SD	Astrophysics	Ph.D. (2011)	A&A
23	Dixit V.	Scientist/Engineer-SD	Scientific Computing	M.Tech. (2017)	A&A
24	Doshi S. H.	Technical Officer-D	Electronics	Dip. In Electronics & Radio Eng (1982)	A&A
25	Durga Prasad Karanam	Reader	Planetary Surface Science & Instrumentation	Ph.D. (2018)	PSDN
26	Gadhavi H. S.	Asso. Professor	Atmospheric Physics	Ph.D. (2006)	SPASC
27	Ganesh S.	Scientist-SF	Milky Way, Comets, Agn, Astronomical Polarimetry	Ph.D. (2010)	A&A
28	Goswami S.	Senior Professor	High Energy Physics	Ph.D. (1998)	THEPH
29	Goyal S. K.	Scientist/Engineer-SE	Electronics & Communication	M.Tech. (2019)	PSDN
30	Guharay A.	Reader	Atmospheric Physics	Ph.D. (2010)	SPASC
31	Gupta G. R.	Reader	Solar Astrophysics Region and Corona, Mhd Waves, Small-Scale Transients, Solar Spectroscopy	Ph.D. (2011)	USO
32	Jain N.	Scientist/Engineer-SD	Elect.& Comm. Engg.	(2002)	USO
33	Janardhan P.	Senior Professor	Solar Radio Astronomy &	Ph.D. (1991)	A&A

Sr. No.	Name	Designation	Specialization	Academic Qualification	Division
			Space Weather		
34	Jani R. A.	Scientist-SE(Tech.)	Paleoclimate and Application Of Stable Isotopes In Hydrology	M.Sc. (1988)	GSDN
35	Joshi B.	Asso. Professor	Solar Physics, Astronomy	Ph.D. (2007)	USO
36	Joshi V.	Scientist-SD	Observational Astronomy	Ph.D. (2014)	A&A
37	Konar P.	Asso. Professor	Particle Physics	Ph.D. (2005)	THEPH
38	Kumar B.	Asso. Professor	Solar Physics	Ph.D. (2007)	USO
39	Kumar P.	Scientist/Engineer-SD	Laser Matter Interactions, Spectroscopy & Payload Development	B.Tech. (2011)	AMOPH
40	Kumar S.	Asso. Professor	Aquatic and Terrestrial Biogeochemistry	Ph.D. (2004)	GSDN
41	Kumar V.	Scientist/Engineer-SD	Physical Science	B.Tech. (2013)	AMOPH
42	Kushawaha R. K.	Scientist-SD	Atomic Physics	Ph.D. (2009)	AMOPH
43	Louis R. E.	Reader	Sunspot Fine Structure, Photospheric-Chromospheric Coupling, Eruptive Phenomena, Post-Focus Instrumentation	Ph.D. (2011)	USO
44	Mahajan N.	Professor	Particle Physics	Ph.D. (2004)	THEPH
45	Mahajan R. R.	Scientist-SF(Tech.)	Noble Gas Isotopes, Meteorites	M.Tech. (1997)	PSDN
46	Manke A. A.	Scientist/Engineer-SD	Computer Science	M.Tech. (2013)	SPASC
47	Marhas K. K.	Asso. Professor	Solar System Studies	Ph.D. (2001)	PSDN
48	Mathew S. K.	Professor	Solar Magnetic & Velocity Fields	Ph.D. (1999)	USO
49	Mathur S. N.	Technical Officer-E	Mechanical Engineering	Dip. In Mech Engineering (1982)	A&A
50	Mehta D.	Scientist/Engineer-SD	Web Applications Development & Cyber Security	M.Tech. (2013)	ADMDN
51	Mishra H.	Senior Professor	Strong Interaction Physics & Nuclear Astrophysics	Ph.D. (1994)	THEPH
52	Mishra H. D.	Scientist/Engineer-SD	Computer Science and Applications	M.C.A (2003)	COMSR
53	Mishra S. K.	Reader	Complex (Dusty) Plasma Kinetics	Ph.D. (2009)	PSDN
54	Mithun Neelakandan Ps	Scientist/Engineer-SD	Physical Science	B.Tech. (2014)	A&A
55	Mohanty S.	Senior Professor	Astroparticle Physics	Ph.D. (1989)	THEPH
56	Naik S.	Asso. Professor	High Energy Astrophysics, X-Ray Binaries	Ph.D. (2003)	A&A
57	Nishtha A.	Librarian-SF	Library & Information Sciences	Ph.D. (2012)	LIBSR
58	Ojha N.	Scientist-SD	Tropospheric Chemistry and Climate Change	Ph.D. (2014)	SPASC
59	Pabari J. P.	Engineer-SF	Planetary and Interplanetary Dust	Ph.D. (2011)	PSDN
60	Padhya V. K.	Scientist/Engineer-SD	Computer Science	M.Tech. (2013)	GSDN
61	Pallamraju D.	Professor	Space Weather and Atmospheric Coupling Processes	Ph.D. (1997)	SPASC
62	Panda D. K.	Scientist-SE(Tech.)	Nuclear Instrumentation & Remote Sensing	Ph.D. (2019)	PSDN
63	Parmar V. M.	Scientist/Engineer-SE	Electrical Engineering	B.E. (2002)	CMDV
64	Patel A. R.	Scientist/Engineer-SD	Fpga, Payload Hardware Design and Testing	M.E. (2010)	PSDN
65	Patel K.	Reader	Physics Beyond The Standard Model	Ph.D. (2012)	THEPH
66	Patel S. H.	Medical Officer-SF	Medicine	M.D (1999)	DISSR
67	Rajesh T. A.	Scientist-SE(Tech.)	Aerosol Characterization	Ph.D. (2019)	SPASC

Sr. No.	Name	Designation	Specialization	Academic Qualification	Division
			and Instrumentation		
68	Rajpurohit A. S.	Scientist-SD	Astronomy & Astrophysics	Ph.D. (2013)	A&A
69	Ramachandran S.	Professor	Aerosols, Radiation & Chemistry- Climate Interactions	Ph.D. (1996)	SPASC
70	Rastogi N.	Asso. Professor	Atmospheric & Aerosol Chemistry	Ph.D. (2005)	GSDN
71	Raval J.	Scientist/Engineer-SF	IT/Cyber Security, Linux System Administration, Network Administration	M.Tech. (2006)	COMSR
72	Ray D.	Scientist-SD	Marine Geology & Igneous Petrology	Ph.D. (2009)	PSDN
73	Ray J. S.	Professor	Isotope Geochemistry	Ph.D. (1998)	GSDN
74	Sahoo B. K.	Professor	Atomic Physics	Ph.D. (2006)	AMOPH
75	Sahu L. K.	Asso. Professor	Atmospheric Science, Trace Gases	Ph.D. (2005)	SPASC
76	Samal M. R.	Reader	Massive Stars and Young Clusters: Formation, Evolution, Feedback Effects, and Associated Interstellar Medium	Ph.D. (2011)	A&A
77	Samanta G. K.	Asso. Professor	Laser and Nonlinear Optics	Ph.D. (2009)	AMOPH
78	Sarkar A.	Reader	Mhd Simulation & Solar Physics	Ph.D. (2005)	A&A
79	Sarvaiya T. N.	Scientist/Engineer-SE	IT Security Virtualization, Sys. Adm. & Networking	M.S. (2014)	COMSR
80	Shah A. B.	Engineer-SG	Automation, Robotics, Payload Development & Fpga	B.E. (1984)	A&A
81	Shah M.	Scientist/Engineer-SE	Automation, Robotics, Payload Development & Fpga	M.Sc. (2015)	GSDN
82	Shah R. R.	Engineer-SG	Instrumentation & Control, Data Acquisition, Telescope	B.E., M.B.A. (1997)	A&A
83	Shah V. M.	Technical Officer-E	Electronics	Dipl. In Electronics & Engineering (1982)	A&A
84	Shanmugam M.	Engineer-SF	Space Instrumentation and Study of Semi-Conductor Devices/Asics	Ph.D. (2017)	PSDN
85	Sharma S. K.	Asso. Professor	Middle Atmosphere & Long Term Atmospheric Changes	Ph.D. (2010)	SPASC
86	Sheel V.	Professor	Modelling of Lower Atmosphere	Ph.D. (1996)	PSDN
87	Shrivastava A.	Scientist/Engineer-SD	Cyber Security, Computer Networking and System Administration	M.Sc. (1998)	COMSR
88	Shukla A. D.	Scientist-SF	Geochemistry & Cosmochemistry	Ph.D. (2012)	GSDN
89	Singh A.	Reader	Ocean Biogeochemistry	Ph.D. (2011)	GSDN
90	Singh A. D.	Professor	Atomic Physics	Ph.D. (1998)	THEPH
91	Singh N.	Asso. Professor	Theoretical Condensed Matter and Statistical Physics	Ph.D. (2006)	THEPH
92	Singh R. P.	Professor	Laser Physics	Ph.D. (1994)	AMOPH
93	Singh R. P.	Scientist -SE(Tech.)	Mesosphere and Lower Thermosphere	Ph.D. (2018)	SPASC
94	Singh S. K.	Professor	Isotope Geochemistry	Ph.D. (1999)	GSDN
95	Singh V.	Scientist-SD	Active Galactic Nuclei and Evolution of Galaxies	Ph.D. (2011)	A&A
96	Sinha R. K.	Scientist/Engineer-SD	Planetary Remote Sensing, Glaciology & Impact Cratering	M.Tech. (2011)	PSDN
97	Sivaraman B.	Asso. Professor	Low Temperature Astrochemistry	Ph.D. (2008)	AMOPH

Sr. No.	Name	Designation	Specialization	Academic Qualification	Division
98	Srivastava M.	Reader	Astronomical Instrumentation	Ph.D. (2012)	A&A
99	Srivastava N and ita	Professor	Solar Physics	Ph.D. (1994)	USO
100	Srivastava Neeraj	Scientist - SE	Planetary Remote Sensing	Ph.D. (2014)	PSDN
101	Sudheer A. K.	Scientist -SE(Tech.)	Chemistry	Ph.D. (2018)	GSDN
102	Upadhyay N. K.	Scientist/Engineer-SE	Mechanical Engineering	M.Tech. (2008)	PSDN
103	Vadawale S. V.	Professor	High Energy Astrophysics and X-Ray Spectroscopy	Ph.D. (2003)	A&A
104	Vaghela H. R.	Engineer-SF	Mechanical Engineering and Finance	B.E. (1996), M.B.A. (2002)	WORSH
105	Vaishnav B. G.	Scientist/Engineer-SE	Atomic & Molecular Physics	Ph.D. (2008)	ADMDN
106	Venkataramani S.	Scientist-SG(Tech.)	Atmospheric Physics	M.Sc. (1986)	SPASC
107	Vijayan S.	Scientist-SD	Planetary Remote Sensing	Ph.D. (2013)	PSDN
108	Wairagade S. S.	Engineer-SE	Civil Engg.	B.E. (1993)	CMDV
109	Yadava M. G.	Scientist-SG	Palaeoclimate, Radiocarbon Dating and Stable Isotopes	Ph.D. (2003)	GSDN
110	Mahirale V.K.	Engineer-SG	Civil Engg.	B.E. (1982)	CMDV


भौतिक अनुसंधान प्रयोगशाला
पी.आर.एल. में गतिविधियां
Events at PRL
SEQUENCE AND SERIES IN NATURE
धरती, पानी, हवा, रखो साफ,
वरना आने वाली पीढ़ी नहीं करेगी माफ
जन जन का आज यही है नारा,
स्वच्छ भारत है लक्ष्य हमारा
स्वच्छ तन और स्वच्छ परिवेश,
बने निरोगी विकसित देश
भौतिक अनुसंधान प्रयोगशाला
Physical Research Laboratory
नवरंगपुरा, अहमदाबाद
विश्व अंतरिक्ष सप्ताह
4 अक्टूबर - 10 अक्टूबर
उदयपुर सौर वेधशाला






पी.आर.एल. में गतिविधियां
Events at PRL



































पी.आर.एल. में गतिविधियां
Events at PRL


































"He who can listen to the music in the midst of noise can achieve great things." - Dr. Vikram A. Sarabhai